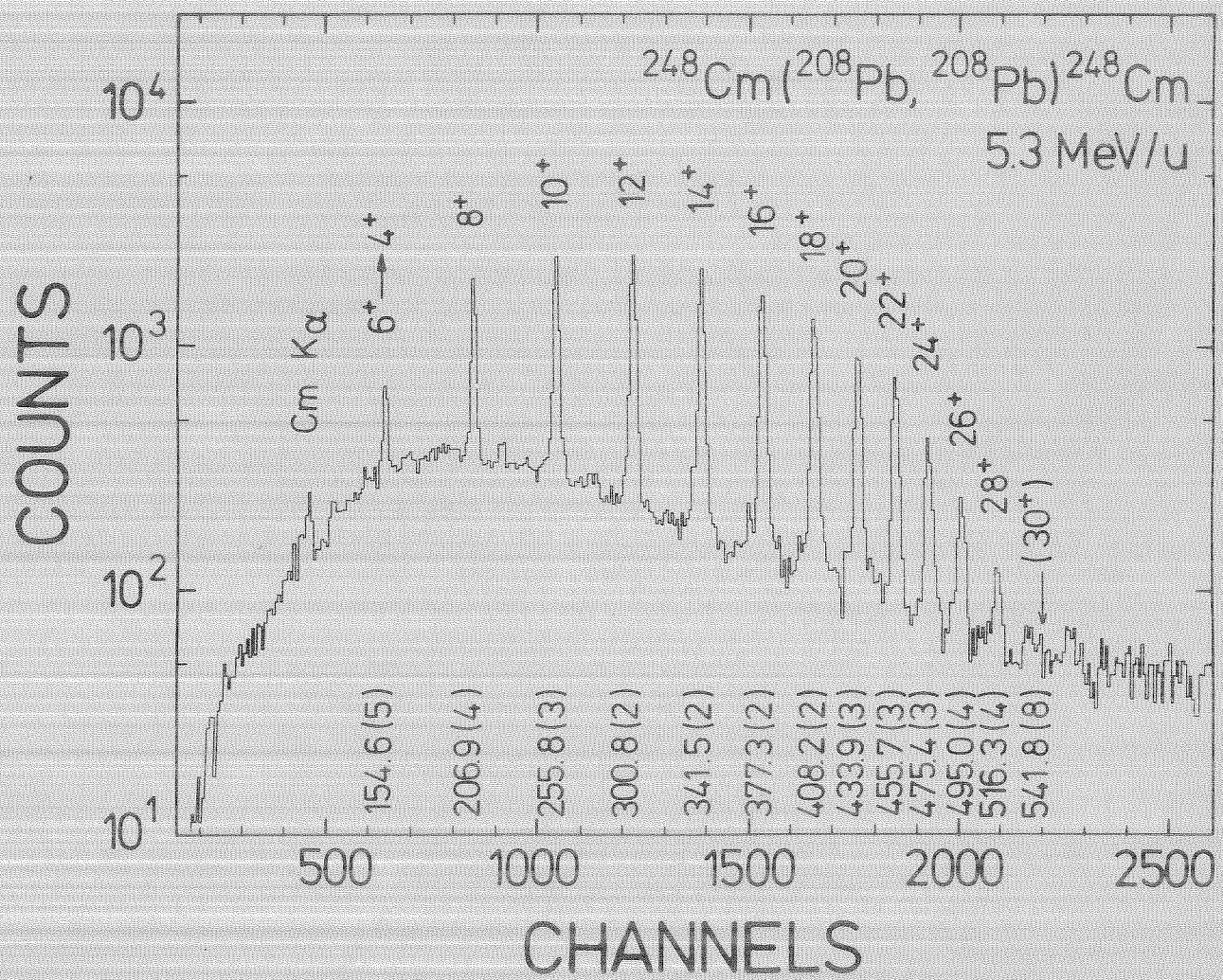
GSI

GSI 80-3
JULY 1980
ISSN 0174-0814

SCIENTIFIC REPORT 1979



GSI GESELLSCHAFT FÜR SCHWERIONENFORSCHUNG
DARMSTADT, MITGLIED DER AGF

FRONTCOVER

Doppler-corrected γ-spectrum resulting from Coulombexcitation of ^{248}Cm with 5.3 MeV/u ^{208}Pb-ions. The ground state band of ^{248}Cm was populated up to spin 28^+ (tentativeley 30^+). The de-excitation γ-rays from the $I \rightarrow I-2$ decays are labelled by the spin I of the initial state and the deduced transition energies are quoted in keV with the error of the least significant digit given in parenthesis (see report on page 47).

S C I E N T I F I C R E P O R T 1 9 7 9

Herausgeber: Gesellschaft für Schwerionenforschung mbH
Postfach 11 05 41
6100 Darmstadt

Redaktion: G. Siegert

ISSN 0174-0814

The year of 1979 marks the tenth anniversary of GSI - the Gesellschaft für Schwerionenforschung in Darmstadt - and the fourth year of operation of the universal heavy ion linear accelerator UNILAC. Beam statistics show a steady increase in target time with more than fifty percent devoted to experiments with lead and uranium projectiles.

The physics research program was carried out to a large extent at beam energies around the Coulomb barrier where a maximum use could be made of the variability and the high energy-resolution of the accelerator.

Highlights of the nuclear physics program included the observation of Coulomb fission, the study of reaction systems with a total nuclear charge as high as 188 and the observation of fissioning fragments with Z up to 115, the search for superheavy elements employing massive curium targets, and the excitation of states in uranium and curium with spins as high as 30 $\hbar$. New insight in the production of heavy nuclei by fusion has been obtained through experiments on the formation of nuclides around the double magic lead region. Investigations of nuclei far from stability were actively pursued around the shell closures Z=50, 82 and N=82, without revealing the exotic phenomenon of ground-state proton decay so far. The total number of new isotopes discovered so far at GSI exceeded sixty. New instruments went into operation like the large magnetic spectrometer and the doughnut spectrometer EPOS. Strong emphasis was given to the development of theories for the understanding of the different nuclear processes as well as the prediction of new phenomena. Future pathways for the GSI scientific program were extended through the joint research program of the GSI-LBL collaboration in experiments with heavy ions at relativistic energies as well as the promotion of theories to what might be expected in this exciting new domain of nuclear physics.

The atomic physics experiments made use of the availability of the heaviest projectile target systems where $Z \cdot \alpha$ exceeds unity significantly. The binding energies of electrons in the lowest molecular orbitals for small impact parameters measured in the experiments are still subject to further studies. The unambiguous identification of the different processes responsible for the creation of positrons in heavy ion collisions is underway

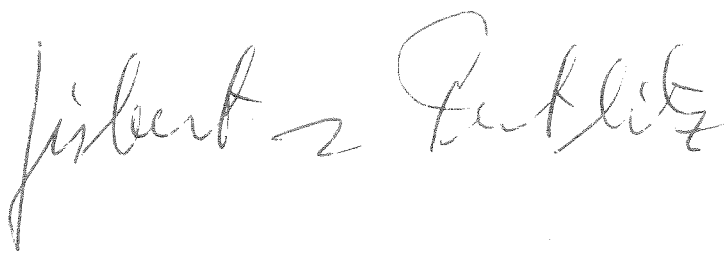
through the implementation of new sophisticated spectrometers. Molecular X-rays emerging from lead-on-lead collisions have been investigated for the first time. New possibilities for the spectroscopy of slowly moving highly charged light ions have been explored in collisions of uranium on neon.

Among the small but lively program for the application of heavy ions the development of methods for heavy ion lithography, for the structuring of material, for the production of holes and filters, and the influence of heavy ion radiation damage on magnetic memory materials should be mentioned. In addition, biological studies on the survival and mutation of cells have continued.

The accelerator UNILAC will undergo an upgrading program to increase the end energy by a factor of two. Because of the Coulomb barrier this amounts to an energy increase for the nuclear reactions of roughly a factor five for heavy collision systems. The upgrading is underway and will be completed by the end of 1981. For future options concerning heavy ion physics at very high energies up to 10 GeV/u GSI has described a scientific program and an accelerator facility, which can be utilized for such experiments.

The present report contains the names of 544 authors. More than 440 belong to universities and other research institutions, 100 are members of GSI. These numbers demonstrate the intense collaboration between scientists from GSI and those from outside institutions in Germany and abroad.

This scientific report from GSI is a supplement to the "Jahresbericht 1979" which contains general information about GSI and the different fields of research. Some scientific high-lights and developments regarding the accelerator are described there in more detail. The present report, however, should serve as up to date information on each of the ongoing scientific projects. It is published as a link to the international scientific community.



Some of the results included here are progress reports of research projects and therefore should be understood as preliminary communications.

Several University projects were financially promoted by the BMFT (Federal Ministry for Research and Technology); they are marked with a "B" after the title. In addition GSI supported external groups with certain resources for development of methods and appliances which are of general interest, this is indicated by a "G" in the title.

Die in diesem Bericht vorgelegten Ergebnisse stammen zum Teil aus noch nicht abgeschlossenen Arbeiten und sind daher als vorläufige Mitteilung zu bewerten.

Zahlreiche Arbeiten der Hochschulgruppen wurden durch das BMFT finanziell gefördert; sie sind in diesem Bericht durch ein "B" im Titel gekennzeichnet. Darüberhinaus konnte die GSI externen Gruppen gewisse Mittel für methodische und apparative Entwicklungen allgemeinen Interesses zur Verfügung stellen, worauf ein "G" im Titel hinweist.

CONTENTS PAGE

Survey of Experiments at GSI in 1979 XVI

1 NUCLEAR PHYSICS/NUCLEAR CHEMISTRY 1

1.1 Nuclear Reactions 2

1.1.1 Reactions Near the Coulomb-Barrier 2

Elastic and Quasielastic Scattering Observed with good Energy Resolution $^{86}Kr + ^{208}Pb$ 2
(P.R. Christensen, C.L. Viang, Ole Hansen, O. Nathan, S.P. Sørensen, F. Videbaek, D. Schüll, W.C. Shen, H. Freiesleben, F. Busch, F. Pühlhofer, F. Bond, F. Plasil)

Double Charge Exchange Reactions with Heavy Ion Beams 3
(F. Beck, G. Delic, H. Genz, A. Richter, G. Schrieder, P. Wastyn, D. Schüll, W. Shen, F. Busch, F. Pühlhofer)

Coulombfission 4
(H. Backe, F. Weik, P.A. Butler, V. Metag, J.B. Wilhelmy, D. Habs, G. Himmele, H.J. Specht)

Sub-Coulomb Fission and Transfer in Collisions of ^{208}Pb with ^{238}U 5
(W. Brüchle, H. Folger, B. Haefner, J.V. Kratz, G. Friedlander)

Cold Fragmentations of ^{234}U 6
(P. Armbruster, U. Quade, K. Rudolph, J. Weber, H. Schrader, F. Gönnenwein, H.J. Clerc, M. Mutterer, J. P. Theobald)

Fusion well below the Barrier 7
(R.G. Stokstad, W. Reisdorf, K.D. Hildenbrand, J.V. Kratz, G. Wirth, R. Lucas, J. Poitou)

Cross Sections of Argon Induced Fusion Reactions 8
(H. Schulte, H.G. Clerc, J. Keller, W. Land, C.C. Sahm, C. Schmitt, D. Vermeulen, K.H. Schmidt, F. Hessberger, G. Münzenberg, W. Reisdorf)

Fusion Reaction Studies of Transuranic Nuclei 9
(H. Sann, S. Björnholm, R. Bock, Y.T. Chu, A. Gobbi, E. Grosse, U. Lynen, W. Müller, A. Olmi, D. Schwalm)

Search for Delayed Fission of Heavy Nuclei 10
(Y.T. Chu, R. Bock, A. Gobbi, E. Grosse, U. Lynen, A. Olmi, E. Morenzoni, W. Müller, H. Sann, D. Schwalm, W. Wölfli)

Study of the Fusion Cross Section in the System $^{40}Ar + ^{40}Ca$ 11
(F. Beck, H. Feldmeier, H. Genz, M. Mutterer, A. Richter, G. Schrieder, J.P. Theobald, P. Wastyn)

Evaporation Residue Cross Sections at Bombarding Energies between 4.7 and 12 MeV/u 12
(B. Kohlmeyer, D. Bangert, F. Pühlhofer, W. Schneider, H. Freiesleben)

Influence of the Shell Structure of the Colliding Nuclei on the Energy and Charge Distributions in Dissipative Collisions 13
(M. Dakowski, P. Doll, A. Gobbi, G. Rudolf, H. Sann, R. Bock, U. Lynen, A. Olmi)

Shell Effects in the Deep Inelastic Reaction ^{154}Sm on ^{154}Sm 14
(E.C. Wu, K.D. Hildenbrand, H. Freiesleben, A. Gobbi, U. Lynen, A. Olmi, H. Sann)

The Significance of Rolling Friction in Classical Trajectory Calculations 15
(D. Bangert, H. Freiesleben)

Entrance Channel Effects in Dissipative Heavy Ion Reactions 16
(H. Essel, K. Hartel, P. Kienle, H.J. Körner, K.E. Rehm, P. Sperr, W. Wagner)

Observation of Inertia Effects in Dissipative Heavy Ion Reactions 17
(H. Essel, K. Hartel, P. Kienle, H.J. Körner, K. E. Rehm, P. Sperr, W. Wagner)

Mass and Charge Exchange in the Reactions ^{112}Sn + ^{208}Pb and ^{124}Sn + ^{208}Pb 18
(G. Beier, H.C. Britt, H. Essel, K. Hartel, H. Hopf, P. Kienle, H.J. Körner, W. Mayer, K.E. Rehm, P. Sperr, W. Wagner)

Investigation of the Reaction Mechanism for the Systems ^{208}Pb + ^{94}Zr and ^{208}Pb + ^{64}Ni at E_{LAB} = 1280 MeV 19
(G. Beier, H.C. Britt, K. Hartel, H. Hopf, P. Kienle, H.J. Körner, W. Mayer, K.E. Rehm, P. Sperr, W. Wagner)

Study of Charge- and Mass-transfer in Quasielastic Collisions 20
(D. Schüll, W.C. Shen, H. Freiesleben, D. Bangert, F. Busch, W. Pfeffer, F. Pühlhofer)

Scattering of ^{40}Ar from ^{208}Pb 21
(U. Artl, R. Bass, V. Hartmann, H. Noll, R. Renfordt, K. Sapotta, P. Fröbrich)

The Reactions ^{208}Pb + ^{58}Ni and ^{208}Pb + ^{64}Ni 22
(U. Artl, R. Bass, V. Hartmann, H. Noll, R. Renfordt, K. Sapotta)

Mass and Charge Transfer in ^{40}Ar + Ag Scattering 23
(U. Artl, R. Bass, V. Hartmann, H. Noll, R. Renfordt, K. Sapotta)

Search for Pre-equilibrium Neutron Emission Using 12 MeV /u Kr Projectiles 24
(I. Tserruya, A. Breskin, Z. Fraenkel, S. Wald, U. Artl, R. Bass, G. Kreyling, R. Renfordt, K. Stelzer, U. Lynen, M. Dakowski, P. Doll, A. Gobbi, H. Sann)

Gamma-ray Multiplicities from Deep Inelastic Collisions 25
(P.R. Christensen, F. Folkmann, O. Hansen, O. Nathan, N. Trautner, S.Y. van der Werf, F. Videbaek, H.C. Britt, H. Freiesleben, F. Pühlhofer)

Analyses of the Mass and Charge Yields for the System ^{132}Xe + ^{nat}Fe 26
(R.A. Esterlund, P. Patzelt, U. Reus, W. Wätzig, W. Westmeier)

Energy Dependence of the Mass Diffusion in ^{238}U + ^{238}U Collisions 27
(. J.V. Kratz, W. Brüchle, H. Gäggeler, H. Gäggeler-Koch, M. Schädel, G. Wirth, C. Riedel, M. Weis)

PAGE

Charge-, Mass-, and Energy Distributions in the ^{132}Xe + ^{197}Au Reaction 28
(J. Poitou, R. Lucas, J.V. Kratz, W. Brüchle, H. Gäggeler, M. Schädel, G. Wirth)

Charge-, Mass-, and Energy Distributions in the Reaction of 7.5 MeV/u ^{238}U-ions with ^{197}Au 29
(K. Sümmerer, W. Brüchle, H. Gäggeler, H. Gäggeler-Koch, J.V. Kratz, M. Schädel, G. Wirth, J. Poitou, R. Lucas, G. Kein, M. Weis)

Exclusive Three-Particle Measurement of the Reactions $^{238}U + ^{238}U$ and $^{238}U + ^{248}Cm$ 30
(Y. Civelekoglu, P. Glässel, D.v. Harrach, R. Männer, H.J. Specht, J.B. Wilhelmy, H. Freiesleben, K.D. Hildenbrand)

Mass-Determination in the Reaction $^{208}Pb \Longrightarrow {}^{nat}U$ 31
(P. Lemmertz, R. Faß, L. Alquist, F. Kassen, H. Wollnik, D. Hirdes, H. Jungclas, G. Dersch)

Study of the Reaction 2149 MeV $^{238}U + U_{nat}$ Using Special Glass Detectors 32
(G. Fiedler, R. Haag, R. Ulbrich, P.A. Gottschalk)

Double-sequential Fission in Heavy-ion Induced Reactions 33
(P. Vater, P.A. Gottschalk, R. Beckmann, R. Brandt, G. Grawert)

Study of Interaction ^{238}U on ^{238}U and ^{208}Pb at 9,1 MeV/n and 7.4 MeV/n with help of Polycarbonate Detector 34
(M. Debeauvais, S. Jokic, J. Tripier)

The Reaction Between Cu and 86 MeV/n ^{12}C 35
(T. Lund, D. Molzahn, D. Eriksen, E. Hagebø, I. Haldorsen, T. Bjørnstad, C. Serre)

1.1.3 Relativistic Nuclear Collisions

Energy Dissipation and Proton Emission in Central and Peripheral Relativistic Nuclear Collisions 36
(R. Stock, H.H. Gutbrod, W.G. Meyer, A.M. Poskanzer, A. Sandoval, C.H. King, G. King, N. Van Sen, K. Wolf)

Cluster Production in Relativistic Nuclear Collisions 37
(H.H. Gutbrod, W. G. Meyer, A.M. Poskanzer, A. Sandoval, R. Stock, J. Gosset, Ch. King, G. King, N. Van Sen, G. D. Westfall, K.L. Wolf)

Pion, Kaon and Λ-Particle Production in High Energy Nucleus-Nucleus Collisions 38
(A. Sandoval, J.P. Brannigan, J.V. Geaga, J. W. Harris, L.J. Rosenberg, L.S. Schroeder, H.E. Stelzer, R. Stock, K.L. Wolf)

1.2 Nuclear Sturcture

Multiple Coulomb Excitation of ^{104}Ru 39
(J. Stachel, N. Kaffrell, H. Emling, H. Folger, E. Grosse, R. Kulessa, D. Schwalm)

Coulomb Excitation and Recoil Distance Experiments in ^{156}Dy 40
(H. Emling, P. Fuchs, E. Grosse, R. Kulessa, D. Schwalm, R.S. Simon, H.J. Wollersheim)

PAGE

Measurements of Magnetic Moments of High Spin States 41
(G. Seiler-Clark, D. Pelte, A. Balanda, H. Emling, E. Grosse, R. Kulessa, D. Schwalm, H.J. Wollersheim, M. Hass, G. J. Kumbartzki, K.H. Speidel)

Collective Properties of ^{164}Dy 42
(H.J. Wollersheim, H. Emling, P. Fuchs, E. Grosse, D. Schwalm)

High Spin States in ^{160}Gd and ^{176}Yb 43
(H. Bohn, T. Faestermann, F.v.Feilitzsch, P. Kienle, H. Emling, P. Fuchs, E. Grosse, D. Schwalm, H. J. Wollersheim)

High Spin States and E2 Transition Strengths in ^{194,196}Pt 44
(J. Idzko, K. Stelzer, Th.W.Elze, H. Ower, H.J. Wollersheim, H. Emling, P. Fuchs, E. Grosse, R. Piercey, D. Schwalm)

Coulomb Excitation of ^{198}Hg and ^{200}Hg with ^{208}Pb Ions 45
(C. Günther, H. Hübel, A. Kleinrahm, J. Idzko, H. Ower, H. Emling, P. Fuchs, E. Grosse, D. Schwalm, H.J. Wollersheim)

High Spin States in ^{232}Th, ^{234}U and ^{236}U 46
(H. Ower, Th.W. Elze, J. Idzko, K. Stelzer, H. Emling, P. Fuchs, E. Grosse, D. Schwalm, H.J. Wollersheim, N. Kaffrell, N. Trautmann)

High Spin States in ^{248}Cm from Multiple Coulomb Excitation with ^{208}Pb Ions 47
(R.B. Piercey, H. Emling, P. Fuchs, E. Grosse, H.J. Hamilton, H. Ower, A.V. Ramayya, D. Schwalm, N. Trautmann, H.J. Wollersheim)

Search for Yrast Traps 48
(S. Bjørnholm, J. Borggreen, O. Christensen, A. Del Zoppo, B. Herskind, R.M. Lieder, J. Pedersen, G. Sletten, F. Folkmann, R.S. Simon)

Gamma-Spectroscopy within the Island of High-spin Isomers near N=82 49
(J. Borggreen, S. Bjørnholm, O. Christensen, A. Del Zoppo, B. Herskind, J. Pedersen, G. Sletten, F. Folkmann, R.S. Simon)

Spectroscopic Study of the High-spin Isomers in ^{152}Er 50
(C. Baba, S. Bjørnholm, O. Christensen, B. Herskind, R.M. Lieder, J. Pedersen, G. Sletten, F. Folkmann, R. S. Simon)

Investigation of High-Spinstates of ^{212m}Po in the Reaction ^{208}Pb $\rightarrow$ ^{nat}U 51
(P. Lemmertz, R. Faß, L. Alquist, F. Kassen, H. Wollnik, D. Hirdes, H. Jungclas, G. Dersch, R. Brandt)

Nuclear Charge Radius, Spin and Nuclear Moments of ^{45}Ca by Laserspectroscopy 52
(E. Bergmann, P. Bopp, J. Kowalski, F. Träger, G. zu Putlitz)

Gamma-Ray Catalog 53
(U. Reus, W. Westmeier, I. Warnecke)

PAGE

Beta-Delayed Proton and Alpha Decay of ^{114}Cs: Evidence for a Resonance in the Beta-Strength Function? 54
(E. Roeckl, G.M. Gowdy, R. Kirchner, O. Klepper, A. Piotrowski, A. Płochocki, W. Reisdorf, P. Tidemand-Peterson, J. Zylicy, D. Schardt, G. Nyman, W. Lindenzweig)

Identification of Two new Alpha Emitting Isomeric States 55
(S. Hofmann, G. Münzenberg, W. Faust, T. Kitahara, W. Reisdorf, F. Heßberger, H.J. Schött, P. Armbruster, K. Güttner, B. Thuma)

New Neutron Deficient Isotopes of Elements between Tm and Pt 56
(S. Hofmann, G. Münzenberg, W. Faust, T. Kitahara, W. Reisdorf, F. Heßberger, H.J. Schött, P. Armbruster, K. Güttner, B. Thuma)

Alpha Decay of Neutron-Deficient Isotopes with $78 \leq Z \leq 83$ Including the New Isotopes ^{183}, ^{184}Pb and ^{188}Bi 57
(U.J. Schrewe, P. Tidemand-Peterson, G.M. Gowdy, R. Kirchner, O. Klepper, A. Płochocki, W. Reisdorf, E. Roeckl, J.L. Wood, J. Zylicy, R. Fass, D. Schardt)

Decay of ^{189}Pb (51 s) and the Excited States of ^{189}Tl 58
(J.L. Wood, G.M. Gowdy, L.L. Riedinger, E.F. Zganjar, J.D. Cole)

Production of Isotopes of Element 104 by Fusion of $^{207, 208}$Pb with ^{50}Ti 59
(G. Münzenberg, S. Hofmann, F.-P. Hessberger, W. Reisdorf, K.H. Schmidt, H.J. Schött, P. Armbruster, B. Thuma, D. Vermeulen)

Search for Superheavy Elements in the ^{238}U + ^{238}U Reaction Using Gas-Phase and Solution Chemistry 60
(N. Trautmann, D. Gembalies, G. Herrmann, P. Peuser, G. Tittel, W. Brüchle, H. Gäggeler, J.V. Kratz, M. Schädel, W. Schorstein, K. Sümmerer, G. Wirth)

Search for Gaseous Superheavy Elements in ^{238}U on ^{238}U Collisions 61
(H. Gäggeler, B. Haefner, K. Sümmerer)

Search for Superheavy Elements with Half-Lives down to 1 msec in ^{238}U on ^{238}U Collisions 62
(H. Gäggeler, E. Schimpf, W. Weber, G. Wirth)

Search for Superheavy Elements and Heavy Actinides in the ^{238}U + ^{248}Cm Reaction 63
(M. Schädel, W. Brüchle, H. Gäggeler, J.V. Kratz, G. Wirth, G. Herrmann, G. Tittel, N. Trautmann, E.K. Hulet, R.W. Lougheed, A. Ghiorso, J.M. Nitschke, R.L. Hahn, R.L. Ferguson)

Search for SHE in the Reaction (^{nat}U + ^{208}Pb) Using the Gas Jet and Sulfide-Chemistry 64
(D. Hirdes, T. Lund, H. Jungclas, D. Molzahn, R. Brandt, P. Lemmertz, R. Faß, F. Kassen, H. Wollnik)

Search for SHE in the Atlantis II Hot Brine 65
(T. Lund, R. Brandt, D. Molzahn, G. Tress, P. Vater, A. Marinov, J. Halperin, R.W. Stoughton, B.H. Ketelle)

g-Factor Studies for Rare-Earth Deformed Nuclei 66
(M. Diebel, A.N. Mantri, U. Mosel)

Role of the Yrast Line in Heavy Ion Fusion Reactions 67
(M. Diebel, D. Glas, U. Mosel, H. Chandra)

Backbending Behaviour in the Actinides from Cranking Calculations 68
(S. Frauendorf, R.S. Simon)

Contributions to the Theory of Nuclear Structure 69
P.O. Hess, M. Seiwert, N. Abul-Naga, F. Margetan, J.A. Maruh, W. Greiner)

Contributions to the Theory of Nuclear Molecules 70
(R. Könnecke, J. Guirguis, J.A. Maruhn, W. Greiner)

Derivation of a Proximity Interaction between Nuclei from the Hartree-Fock Functional with Skyrme Interactions 71
(K. Pomorski, K. Dietrich)

Relaxation Times in Dissipative Heavy-Ion Collisions 72
(C. Riedel, G. Wolschin, W. Nörenberg)

Theoretical Estimates for the Production of Transuranium Elements in Heavy-Ion Collisions 73
(C. Riedel, W. Nörenberg)

Statistical Fluctuations in Dissipative Heavy-Ion Collisions 74
(C. Riedel, G. Wolschin)

Quantal Fluctuations in Inelastic Heavy Ion Collisions 75
(W. Cassing, H. Friedrich)

Shape Relaxation in Heavy-Ion Collisions 76
(G. Wolschin)

Mass Transport in Anharmonic Potentials 77
(R. Schmidt, G. Wolschin)

A Model Calculation for Mass Dispersion in a Fermion Gas 78
(H. Feldmeier, P. Buck)

Heavy-Ion Fusion Cross-Sections Calcualted with the One-Body Window-Friction and the Relaxed-Density Proximity-Potential 79
(H. Feldmeier, F. Beck)

On the Dynamics of Fission as a Dissipative Process 80
(K. Pomorski, H. Hofmann)

Initial Correlations in Dissipative Collisions and Compound-Nucleus Formation 81
(W. Nörenberg, C. Riedel)

Contributions to Fragmentation Theory 82
(J. Hahn, K.H. Ziegenhain, K. Depta, M. Uhlig, A. R. Degheidi, J.A. Maruhn, W. Greiner)

Study of the ^{238}U Reaction with ^{48}Ca and ^{238}U in TDHF and Fragmentation Theory 83
(R.Y. Cusson, J. Hahn, J.A. Maruhn, W. Greiner, H.J. Lustig, H. Stöcker)

TDHF Study of the ^{86}Kr (12.2 MeV/A + ^{166}Er Reaction 84
(R.Y. Cusson, H. Stöcker)

PAGE

Transport Theory of Heavy-Ion Collisions in the Adiabatic Representation 85
(S. Ayik)

Mean Field Theory and Statistical Treatment of Residual Interactions in Heavy-Ion Collisions 86
(S. Ayik)

A Nuclear Matter Approach to the Mean Free Path of a Nucleon in a System of Colliding Ions 87
(K. H. Müller)

Fermi Jets and Capture in TDHF-Calculations of Medium Energy Collisions of ^{12}C + ^{197}Au 88
(R.Y. Cusson, H. Stöcker, W. Greiner, J.A. Maruhn)

Medium Energy Collisions of Heavy Nuclei in the Three-Dimensional Nuclear Fluid Dynamical-(NFD) and Time-Dependent Hartree-Fock (TDHF) Models 89
(H. Stöcker, R.Y. Cusson, J.A. Maruhn, W. Greiner)

Collective Sideward Flow of Shocked Matter and the Highly Inelastic Bounce Off Event in Fast Nuclear Collisions 90
(H. Stöcker, J.A. Maruhn, W. Greiner)

Jets of Nuclear Matter in Relativistic Heavy Ion Collisions 91
(H. Stöcker, L.P. Csernai, R.Y. Cusson, J.A. Maruhn, W. Greiner)

Signatures of Phase Transitions in the Dense Matter in High Energy Heavy Ion Collisions 92
H. Stöcker, R.Y. Cusson, G. Buchwald, L.P. Csernai, G. Graebner, W. Greiner, J. Hofmann, H. Kruse, J.A. Maruhn, B. Müller, W. T. Pinkston, P.R. Subramanian, J. Theis, D. Vasak)

Percolation Phase of Hot, Dense Hadronic- and Quark Matter and Pulsating Quark Blobs in Relativistic Nuclear Collisions 93
(H. Stöcker, G. Graebner, J.A. Maruhn, W. Greiner)

Geometry and Dynamics in the Hot Spot Model 94
(N. Stelte, R. Weiner)

Drifting Hot Spots 95
(N. Stelte, M. Weström, R.M. Weiner)

Solution of the Diffusion Equation for Geometries of Interest in Nuclear Physics 96
(N. Stelte)

Contributions to the Field Theory of Spin 1 Bosons 97
(M. Riedel, W. Greiner)

Contributions to Theory of Strong Gravitational Fields 98
(M. Soffel, G. Schmidt, U. Heinz, A. Müller, B. Müller, W. Greiner)

2. Atomic Physics

2.1 Superheavy Quasi-Atoms and Inner Shell Excitation Mechanisms

Spectroscopy of High Energy δ-rays Emitted in Heavy-Ion Collisions 100
(E. Berdermann, F. Bosch, H. Bokemeyer, M. Clemente, F. Güttner, P. Kienle, W. Koenig, C. Kozhuharov, B. Martin, B. Povh, H. Tsertos, Th. Walcher)

PAGE

Positron Production in Heavy Ion Collisions 101
(H. Backe, W. Bonin, W. Engelhardt, E. Kankeleit, M. Mutterer, P. Senger, F. Weik, R. Willwater, V. Metag, J.B. Wilhelmy)

Differential Positron Production Probability in Quasi Atomic Systems 102
(A. Balanda, K. Bethge, H. Bokemeyer, H. Folger, J.S. Greenberg, H. Grein, A. Gruppe, S. Ito, R. Schule, D. Schwalm, J. Schweppe, N. Trautmann, P. Vincent, M. Waldschmidt)

Positrons from 1.4 GeV U-U Collisions 103
(E. Berdermann, F. Bosch, M. Clemente, F. Güttner, P. Kienle, W. Koenig, C. Kozhuharov, B. Martin, W. Potzel, B. Povh, H. Tsertos, W. Wagner, Th. Walcher)

MO X-Ray Angular Distribution for 1 GeV $^{208}Pb + ^{208}Pb$ and $^{209}Bi + ^{209}Bi$ 104
(Ch. Stoller, E. Morenzoni, W. Wölfli, W.E. Meyerhof, F. Folkmann, P. Vincent, P.H. Mokler, P. Armbruster)

A Coincidence Technique for the Measurement of Quasi-molecular X-rays from Superheavy Quasimolecules 105
(P. Vincent, D. Schwalm, H. Bokemeyer, H. Emling, E. Grosse, J.S. Greenberg)

A Scaling Law for the lsσ Excitation Probability in Collision Systems $\alpha\ (Z_1+Z_2) \gtrsim 1$ 106
(F. Bosch, P. Armbruster, D. Liesen, D. Maor, P.H. Mokler, H. Schmidt-Böcking, R. Schuch)

Excitation Probability of the Molecular lsσ Orbital in Collision Systems $\alpha(Z_1+Z_2) \gtrsim 1$ 107
(D. Liesen, P. Armbruster, F. Bosch, S. Hagmann, P.H. Mokler, H. Schmidt-Böcking, R. Schuch, J.B. Wilhelmy, H.J. Wollersheim)

Spectroscopy of the Molecular lsσ Orbital in Collision Systems $\alpha(Z_1+Z_2) \gtrsim 1$ 108
(P. Armbruster, F. Bosch, D. Liesen, D. Maor, P.H. Mokler, H. Schmidt-Böcking, R. Schuch)

lsσ Excitation Probability for Small Impact Parameter Xe+Pb Collisions 109
(P.H. Mokler, F. Bosch, D. Liesen, W.A. Schönfeldt, R. Schuch)

Inner Shell Excitation Mechanisms in Close Impact Parameter Collisions Between Ni Ions and Solid Targets 110
(D. Maor, B. Rosner, D. Liesen, P.H. Mokler, H. Schmidt-Böcking, R. Schuch)

Collision Broadening in MO-Electron Energy Spectra in Kr-Kr and Kr-Ar Collisions 111
(A.P. Shergin, R. Mann, H.F. Beyer, E. Pfeng)

2.2 Capture Processes, Few Electron Systems, and Metastable States

Capture of Electrons Into Swift Heavy Projectiles 112
(W.A. Schönfeldt, F. Bosch, D. Liesen, D. Maor, P.H. Mokler)

PAGE

Projectile Charge State Dependence of the Average L- and M-Shell Excitation in K-Shell Ionizing Collisions 113
(A. Warcyak, D. Liesen, P.H. Mokler)

Prompt and Delayed K-Auger Electron Emission from Slow Target Recoil Ions 114
(R. Mann, H.F. Beyer, F. Folkmann)

Investigation of Few Electron States in Target Molecules After Heavy Ion Impact 115
(R. Mann, H.F. Beyer, F. Folkmann)

Time Dependent X-Ray and Auger Electron Emission of Beam-Foil Excited Ions 116
(H.D. Dohmann, R. Mann, E. Pfeng)

Beamfoil-Spectroscopy on Hydrogenlike Oxygen 117
(P. v. Brentano, G. Dehmelt, A. Georgiadis, L. v. Gerdtell, H.D. Sträter)

Charge Transfer Involving Multiply Charged Ions 118
(A. Müller, Ch. Achenbach, P. Kester, K. Miethe, K. Rinn, W. Seim, I. Wirkner-Bott, E. Salzborn)

Ionisation of Argon Ions by Electron Impact 119
(R. Becker, R. Frodl, H. Klein, A. Müller, E. Salzborn, P. Varga, F.P. Viehböck, H. Winter)

2.3 Slowing Down of Heavy Ions in Matter

Stopping Power Measurements for 3-5 MeV/u ^{86}Kr, ^{136}Xe, ^{208}Pb and ^{238}U in Solids 120
(R. Bimbot, D. Gardes, H. Geißel, T. Kitahara, P. Armbruster, A. Fleury, F. Hubert)

Stopping Power Measurements with 10 MeV/u ^{238}U Ions 121
(W. Brüchle, H. Folger, J.V. Kratz)

Stopping Power Measurements of 0.2 - 1.4 MeV/u Heavy Ions in Solids 122
(H. Geissel, T. Kitahara, Y. Laichter, P. Armbruster)

Comparison of Stopping Powers Between Heavy Ions and Mean Fission Fragments 123
(Y. Laichter, H. Geissel, T. Kitahara, P. Armbruster, N.H. Shafrir)

Energy Loss Straggling of Heavy Ions and α Particles in Matter 124
(H. Geissel, Y. Laichter, P. Armbruster)

Limitation of the Z-Resolving Power Due to the Energy Straggling 125
(C.C. Sahm, K.H. Schmidt, H.G. Clerc, H. Schulte, D. Vermeulen)

2.4 Theory

Variable Binding of Electrons and Transfer of Polarization in Ion-Atom Collisions 126
(M. Kleber, K. Unterseer)

Solution of the Schrödinger Equation with a Trajectory Method in Atomic Collisions 127
(G. Terlecki, N. Grün, V. Maruhn-Rezwani, W. Scheid)

Charge Distributions after Ion-Atom Collisions 128
(K.H. Wietschorke, J. Reinhardt, W. Greiner, G. Soff)

Self-Consistent Determination of Critical Two-Centre Distances 129
(K.H. Wietschorke, B. Müller, W. Greiner, G. Soff)

PAGE

Multistep Processes for Electron Excitations in Superheavy Quasimolecules 130
(G. Soff, J. Reinhardt, B. Müller, W. Greiner)

Contributions to the Theory of Quasimolecular X-Rays 131
(W. Betz, H. Peitz, B. Müller, W. Greiner, J. Kirsch)

Contributions to the Spectroscopy of Electron States in Superheavy Quasimolecules 132
(J. Reinhardt, G. Soff, H. Peitz, W. Betz, K.H. Wietschorke, U. Müller, U. Heinz, J. Theis, T. de Reus, B. Müller, W. Greiner, J. Kirsch)

Contributions to the Emission of Positrons and δ-Electrons in Heavy Ion Collisions 133
(J. Reinhardt, G. Soff, B. Müller, W. Greiner)

An Atomic Clock for Deep-Inelastic Heavy-Ion Collisions 134
(G. Soff, J. Reinhardt, B. Müller, W. Greiner)

Test of Molecular Total Energy Calculations in an SCF Procedure 135
(R. Euler, B. Fricke, T. Morovit, W.D. Sepp, A. Rosen)

Relativistic Molecular Calculations of Superheavy Molecules 136
(T. Morovit, W.D. Sepp, B. Fricke, A. Rosen)

Spin Polarization of Electrons Induced by Strong Collisional Magnetic Fields 137
(G. Soff, J. Reinhardt, W. Greiner)

Heavy Ion Induced Mach-Shock Waves in the Electron Plasma of Solids 138
(W. Schäfer, B. Müller, W. Greiner, H. Stöcker)

3. Solid State Physics and Biology

Influence of Latent Nuclear Tracks on the Magnetic Properties of Ferrimagnetic Garnet Films 140
(H. Heitmann, P. Hansen, R. Spohr)

Heavy Ion Induced Sputtering of Glasses 141
(K. Thiel, H. Külzer, W. Herr)

In Search of Heavy Ion Induced Collective Electron Emission from Solids 142
(H.J. Frischkorn, K.O. Groeneveld, S. Schumann, R. Latz, G. Reichhardt, J. Schader, W. Kronast)

Radiation-Induced Defects in Type-II Superconductors 143
(V. Graeger, H.C. Freyhardt)

Heavy Ion Induced Thermoluminescence of Calcite and Fluorite 144
(U. Bangert, K. Thiel, W. Herr)

The Influence of Ion Bombardment on the Corrosion Behavior of Iron -Mechanistic Investigations- 145
(H. Ferber, G.K. Wolf)

The Electrocatalytic Activity of Iron Substrates Bombarded with Platinum Ions 146
(H. Kasten, G.K. Wolf, H. Folger)

Survival of Vegetative Yeast Cells after Irradiation with Heavy Ions 147
(F. Schöpfer, E. Schneider, J. Kiefer, G. Kraft)

Inactivation of Ribosomal RNA Synthesis in Vegetative Yeast Cells after Exposure to Heavy Ions 148
(K.J. Weber, E. Schneider, J. Kiefer, G. Kraft, H. Liesem)

PAGE

Mutation Induction by Heavy Ions 149
(S. Rase, E. Schneider, J. Kiefer, H. Liesem)

Inactivation Cross Sections of Bacillus Subtilis Spores for Very Heavy Ions 150
(M. Schäfer, K. Baltschukat, R. Facius, H. Bücker)

Determination of Passage Times of Red Blood Cells Through a Single Pore Membrane 151
(U. Dauer, H. Kiesewetter, K. Mussler, H. Schmid-Schönbein, R. Spohr)

4. Developments

4.1 Chemistry, Nuclear Track and Target Technology

Continuous Separations of Reaction Products in a Thermochromatographic Column with Various Halogenating Agents as Reactive Gases 154
(U. Hickmann, N. Greulich, N. Trautmann, H. Gäggeler)

Heavy Ion Lithography 155
(B.E. Fischer, R. Spohr)

Transmission Properties of Nuclear Track Filters 156
(C. Riedel, R. Spohr)

Production and Application of Molecular Filters 157
(A. Gerhard, A. Schempp, H. Klein)

Some further Properties of Mica Microfilters: Air Through-put up to 300 C 158
(G. Tress, P. Vater, D. Hirdes, R. Brandt, R. Spohr)

Determination of Light Contaminations in Heavy Targets 159
(F. Nickel, H. Geissel, D. Marx)

Measurements of the Density of a Gas Jet by Light Scattering 160
(P. Kreisler, W. Tietsch, K. Bethge)

4.2 Experimental Set-Ups

EPOS - a Flexible Solenoid-System for the Spectroscopy of Positrons in HI-Collisions 161
(A. Balanda, H.J. Beeskow, K. Bethge, H. Bokemeyer, H. Folger, J.S. Greenberg, H. Grein, A. Gruppe, S. Ito, S. Matsuki, R. Schule, R. Schultz, D. Schwalm, J. Schweppe, R. Steiner, P. Vincent, M. Waldschmidt)

Status of the NaI Crystal Ball Project 162
(R.S. Simon, R. Albrecht, D. Schwalm, V. Metag, H. Gräf, E. Jaeschke, R. Repnow, D. Habs, D. Pelte, W. Schneider, H. J. Specht, W. Weiter)

The Plastic Ball and Plastic Wall, A 4π Detector System for Relativistic Heavy Ion Reactions 163
(H.H. Gutbrod, M.R. Maier, J. Peter, A.M. Poskanzer, H.G. Ritter, H. Stelzer, R. Stock, A.I. Warwick, F. Weik, H. Wiemann)

A Multiparticle Detection System for High Energetic Projectiles (86 MeV/u ^{12}C) 164
(G. Augustinski, H.J. Beeskow, Y.T. Chu, H.W. Daues, P. Doll, A. Gobbi, K. Hildenbrand, M. Ludwig, U. Lynen, W. Müller, A. Olmi, H. Sann, R. Santo)

A Low Background Detection System for Fragments and Neutrons from Spontaneous Fission Sources 165
(U. Tharun, H.J. Keim, U. Knitz, P. Peuser, N. Trautmann, G. Herrmann, G. Wirth)

A Fast Detection System for Decaying Heavy Nuclei 166
(A. Marinov, W.F.W. Schneider, K.D. Hildenbrand, A. Gobbi, H. Freiesleben, R. Bock)

Tests of a Transmissionspectrometer for X-Ray Spectroscopy 167
(K.H. Schartner, H.J. Flaig, W. Spitz, A. Scharmann, H.F. Beyer)

A Si(Li)-Detector System for in Beam Positron Spectroscopy 168
(H. Backe, W. Bonin, E. Kankeleit, W. Patzner, P. Senger, F. Weik)

ISOL Ion Sources, Part 1: The FEBIAD Ion Source 169
(R. Kirchner, C. Bruske, K.H. Burkard, W. Hüller, O. Klepper)

ISOL Ion Sources, Part 2: The Thermal Ion Source 170
(R. Kirchner, K.H. Burkard, W. Hüller, O. Klepper)

Release Times and Separation Efficiencies of the GSI On-Line Separator 171
(O. Klepper, K.H. Burkard, W. Hüller, R. Kirchner, W. Reisdorf, E. Roeckl)

In-Beam Laser Fluorescence Spectrometer 172
(G. Huber, G. Ulm, D. Marx)

Optical Spectroscopy of Unstable Isotopes at the TRIGA-Reactor in Mainz 173
(J. Bonn, F. Jüttner, W. Klempt, T. Kühl, R. Neugart, E.W. Otten, W. Schinzler, K.P.C. Spath, K. Wendt)

Developmental Work on the HELIOS System 174
(A.K. Mayumdar, H. Wagner, W. Walcher, M. Brügger, N. Trautmann)

Microcomputer Control of the Velocity-Filter SHIP 175
(H.J. Schött, K. Poppensieker)

Calculation of a Dipole Magnet, Extending SHIP to a Mass Separator for Unslowed Fusion Reaction Products 176
(B. Thuma, H. Ewald, G. Münzenberg, S. Hofmann, F. Heßberger)

Computer Simulation of the Motion of Heavy Ions Passing Through Gas Filled Systems 177
(J. Zienert, K. Güttner, G. Münzenberg)

Preliminary Tests for an Experiment Searching for Shortlived Very Heavy Nuclei from Transfer Reactions 178
(J.B. Wilhelmy, Y. Civelekoglu, P. Glässel, D. v. Harrach, R. Männer, H.J. Specht)

4.3 Detectors

Development of the Big Position Sensitive Ionization Chamber 179
(G. Augustinski, H. Sann, A. Olmi)

Energy Loss of Very Heavy Ions in Si-Surface Barrier Detectors 180
(H. Essel, K. Hartel, P. Kienle, H.J. Körner, K.E. Rehm, P. Sperr, W. Wagner)

Rise Time Discrimination between Heavy Ions and α Particles with Seminconductor Detectors 181
(T. Kitahara, H. Geissel, S. Hofmann, Y. Laichter, G. Münzenberg, P. Armbruster)

PAGE

A Parallel Plate Ring Counter 182
(Y.T. Chu, H.W. Daues, H. Sann)

Test and Performance of a Position Sensitive Parallel Plate Avalanche Counter 183
(Ch. Schandera, C. Lauterbach, J. de Boer, H. Stelzer)

New Detector System for the 5m Time-of-Flight Spectrometer 184
(U. Arlt, R. Bass, V. Hartmann, H. Noll, R. Renfordt, K. Sapotta)

A Large-Area Scintillation Stop Detector for the Magnetic Spectrometer 185
(F. Busch, W. Pfeffer, F. Pühlhofer, D. Schüll)

Relation of Pulse Height and Absorbed Energy in Gas-Scintillation Heavy-Ion Detectors 186
(J. Pannicke, M. Mutterer, K. Scheele, J.P. Theobald, P. Zöller)

Recombination Luminescence in Heavy-Ion Excited Gas Scintillations 187
(W. Spreng, P. Brülls, H. Heckwolf, M. Mutterer, J. Pannicke, J.P. Theobald)

A Solid-Xenon Scintillation Detector for Heavy Ions 188
(H. Heckwolf, W. Spreng, M. Mutterer, J.P. Theobald, P. Zöller, J.C. van Staden)

Energy- and Time-Resolution Studies with Gas-Scintillation Heavy-Ion Detectors 189
(M. Mutterer, P. Brülls, J. Pannicke, W. Spreng, J.P. Theobald, P. Wastyn)

Track Profile Measurements for ^{132}Xe Tracks in Nuclear Track Emulsions 190
(N. Klein, E. Ganßauge, P. Vater)

Recording Properties of Plastic Track Detector CR-39 for Xe and Pb Ions 191
(B. Grabez, P. Vater, R. Brandt)

Study of Heavy Ion Tracks in Meteoritic Crystals 192
(C. Perron, P. Pellas, V.P. Perelygin, S.G. Stetsenko)

4.4 Electronics, Computing Center and Workshops

Experimental Electronics Department 193
(R. Albrecht, J. Dengler, J. Dusek, H. Hammal, H. Hardel, H.P. Liebold, K. Mömerzheim, K. Poppensieker, D. Quis, M. Richter, H.G. Schmidt, R. Schulze, H. Spieler, H. Wahl, W. Wißmann)

Microprocessor-Activities 196
(G. Englert, W. Dehnhardt, H. Groß, T. Györffy, P. Hahne, A. Huber, W. Weizel, M. Wiemers, V. Zelba)

Computing Center 197
(H. Hultzsch)

Engineering and Technology 202
(E. Malwitz, K. Blasche, W. Bleuel, H. Gaiser, K. Illert, H. Kiesewetter, U. Knopf, H. Kraus, F. Nöhmeyer, K. Wilhelm)

5. Accelerator PAGE

5.1 UNILAC Performance and Ameliorations

UNILAC-Operation 210
(N. Angert, J. Klabunde, M. Müller, P. Strehl)

Ions Source Development 211
(H. Schulte)

High Current Ion Source Development 212
(R. Keller)

300 kV Accelerator 213
(M. Müller, B.H. Wolf)

Process-Control 214
(M. Wiemers, F. Bock, R. Busch, A. Ehrich, B. Grasmück, I. Morrison, D. Rochna, E. Schaffner)

5.2 Accelerator - Projects

SIS - An Accelerator Facility for Relativistic Heavy Ions 215
(K. Blasche, D. Böhne, B. Franczak, B. Franzke, B. Langenbeck)

Injection System for the SIS 218
(B. Franczak, R. Steiner)

Extraction System for the SIS 219
(B. Franczak, R. Steiner)

Test Power Supply for Two SIS Dipole Magnets 220
(G. Breitenberger)

Amplitude, Frequency and Phase Control for the SIS Accelerating Cavaties 221
(M. Emmerling, K. Kaspar)

Prototype of a Synchrotron Accelerating Station 222
(K. Kaspar, M. Emmerling, A. Gasper)

Test-Cavity for Single SIS 100 Ferrite Rings 224
(K. Kaspar, G. Stubenrauch)

Charge Change Cross Sections for 1.4 MeV/u-Uranium in H_2 and N_2 225
(B. Franzke)

Test Program for an UHV-Section of the SIS 226
(P. Finke, B. Franzke, A. Kritzer)

RFQ Acceleration Structures 227
(R.W. Müller)

6. Annex 228

6.1 Scientific Activities Outside GSI 229

6.1.1 Publications 229

6.1.2 Conference Constributions

6.1.3 Seminars at other Instituts

6.1.4 Lectures and Courses

PAGE

6.2 Scientific Activities Within GSI

6.2.1 Conferences and Seminars on Research Proposals

6.2.2 Seminars at GSI

6.2.3 GSI-Berichte (Reports)

6.2.4 Visiting Groups at GSI

6.3 Scientific Committees, Guests, and Staff

6.4 Author Index

S U R V E Y

O F E X P E R I M E N T S A T G S I

I N 1 9 7 9

	Exp. Nr.	Authors	Affiliation	Title	Beam Position	Beam-time [h]	Ions	Energy [MeV/u]	Corresponding Article on Page
Nuclear Physics/ Nuclear Chemistry	4	Ahrens, Brüchle, Folger, Franz, Gäggeler, Herrmann, Kaffrell, Kratz, Peuser, Schädel, Stakemann, Tittel, Trautmann, Warnecke, Wirth, Weber, Zendel	Univ. Mainz GSI	Search for Superheavy Elements in the $^{238}U+^{238}U$ Reaction Using Gas-Phase and Solution Chemistry	T7	17,6	^{238}U	7,7-10	60
					Y3	7,2	^{208}Pb	10,5	
					Y3	104,0	^{238}U	8,35-8,7	
					Y3	2,1	^{238}U	8,3	
	14	Körner, Essel, Hartel, Henning, Kienle, Rehm, Sperr, Wagner	TU München GSI	Mass and Charge Exchange in the Reactions $^{112}Sn+^{208}Pb$ and $^{124}Sn+^{208}Pb$	X2	42,7	^{208}Pb	6,3	18
	18	Bass, Art, Hartmann, Noll, Renfordt, Sapotta, Zitzmann	Univ. Frankfurt	Scattering of ^{40}Ar from ^{208}Pb	Z3	8,0	^{238}U	5,9	21
	35	Freiesleben, Chestnut, Heusch, Hildenbrand, Pühlhofer, Schneider, Kohlmeyer, Pfeffer, Volant	Univ. Marburg GSI	Mass Distribution of Fragments from Deep Inelastic Reactions of ^{132}Xe with ^{56}Fe	Z3	21,0	^{132}Xe	5,0	---
					Z3	5,0	^{48}Ti	5,0	
	36	Pühlhofer, Freiesleben, Heusch, Schneider, Kohlmeyer, Pfeffer, Volant	Univ. Marburg GSI	Evaporation Residue cross Sections at Bombarding Energies between 4.7 and 12 Mev/u	Z3	63,7	^{48}Ti	12,0	12
					Z3	19,5	^{238}U	5,9	
	43	Clerc, Lang, Faust, Vermeulen, Münzenberg, Kitahara, Reisdorf, Schmidt	TH Darmstadt GSI	Production of Isotopes of Element 104 by Fusion of $^{207,208}Pb$ with ^{50}Ti	X0	41,8	^{40}Ar	4,7;5,0	59
					Y7	52,5	^{40}Ar	4,7-5,0	
	44	Schneider, Faust, Güttner, Münzenberg, Pühlhofer, Schüll	Univ. Gießen GSI	New Neutron Deficient Isotopes of Elements between Tm and Pt	Y7	33,7	^{58}Ni	4,7	56
	51	Kratz, Ahrens, Brüchle, Gäggeler, Schädel, Warnecke, Wirth, Klein, Weis, Trautmann	Univ. Mainz GSI	Charge-, Mass-, and Energy Distributions	T7	2,0	^{238}U	7,5	27, 28 + 29
					T7	16,3	^{238}U	7,5	
					T7	14,1	^{238}U	7,5	
	62	Kratz, Brüchle, Folger, Friedlander, Haefner	Univ. Mainz	Sub-Coulomb Fission and Transfer in Collisions of ^{208}Pb with ^{238}U	T7	11,3	^{208}Pb	4,8-5,1	5
					T7	16,8	^{208}Pb	4,8;5,1	
	91	Habs, Harrach, Metag, Specht	MPI Heidelberg	Coulombfission	X8	55,2	^{184}W	5,5-6,75	4
					X8	44,5	^{184}W	5,4-6,3	
					X8	47,7	^{152}Sm	4,8-6,6	
					X8	17,0	^{183}W	6,5	
	101	de Boer, Dünnweber, Graw, Hering, Lynen, Puchta, Schandera, Trautmann	TU München MPI Heidelberg	Test and Performance of a Position Sensitive Parallel Plate Avalanche Counter	Z5	83,6	^{86}Kr	9,4;7,5	183
					Z5	26,1	^{238}U	7,5	

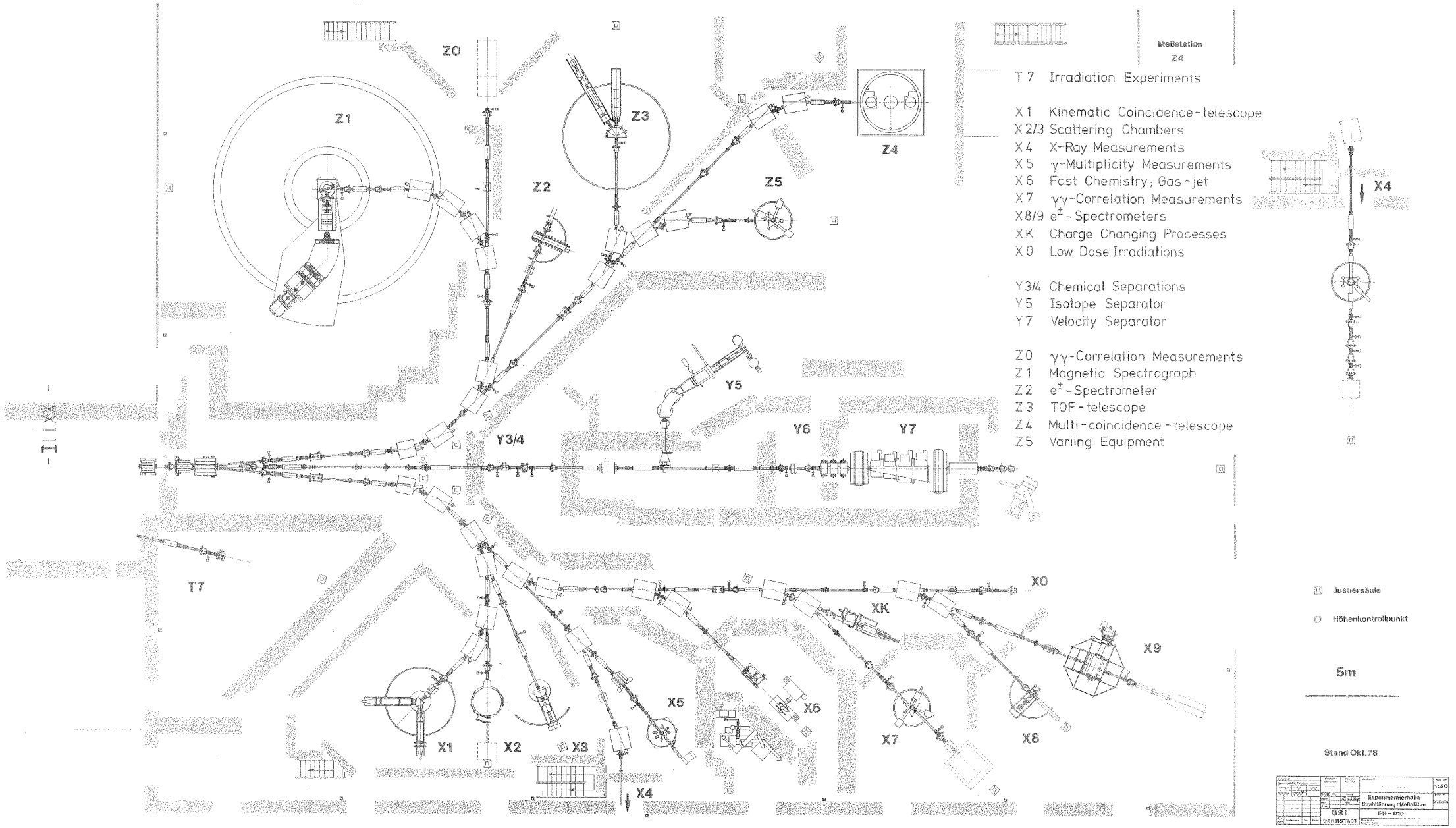
Exp. Nr.	Authors	Affiliation	Title	Beam Position	Beam-time[h]	Ions	Energy [MeV/u]	Corresponding Article on Page
104	Harrach, Civelekoglu, Glässel, Männer, Specht	Univ. Heidelberg	Exclusive Three-Particle Measurement of the Reactions $^{238}U+^{238}U$ and $^{238}U+^{248}Cm$	Z4	74,6	^{238}U	7,5	30
				Z4	17,0	^{129}Xe	6,0	
105	Pederson, Björnholm, Borggreen, Christensen, Folkmann, Herskind, Lieder, Simon, Sletten	NBI Kopenhagen Aarhus GSI	Studie of Yrast Traps	X5	32,0	^{132}Xe	4,6	48
				X5	5,0	^{136}Xe	4,6	
				X5	4,6	^{48}Ti	4,7	
				X4	45,8	^{50}Ti	4,74	
				X5	49,5	^{48}Ti	5,0	
117	Ahrens, Björnstad, Broden, Fischbach, Gäggeler, Georg, Jungclas, Kaffrell, Lemertz, Skarnemark, Stender, Trautmann, Weber, Zendel	Univ. Oslo, Univ. Göteborg, Univ. Mainz, Univ. Gießen, GSI	Continuous Separations of Reaction Products in a Thermochromatographic Column with Various Halogenating Agents as Reactive Gases	X6	9,1	^{238}U	7,7	154
124	Björnholm, Bock, Gobbi, Lynen, Olmi, Sann, Stelzer, Pelte, Specht	GSI, Univ. Heidelberg, MPI, Heidelberg	Low Energy Fissions of Heavy Compound Systems	X1	32,7	^{238}U	7,5	9, 10
				X1	3,0	^{238}U	5,9	
				X1	45,5	^{238}U	5,6-6,3	
				Z5	33,9	^{238}U	5,9	
128	Bohn, Festermann, Feilitzsch, Emling, Fuchs, Grosse, Schwalm, Kienle, Wollersheim	TU München GSI	High Sping States in ^{160}Gd and ^{176}Yb	X7	24,7	^{208}Pb	5,3	43
136	Simon, Emling, Grosse, Wollersheim, Folkmann, Garrett, Hagemann, Herskind, Hillis, Tjörn	NBI Kopenhagen Univ. Oslo GSI	Superdeformed Nuclei	Z0	2,9	^{238}U	5,9	--
138	Schrieder, Emling, Grosse, Richter, Staden, Wildenthal	GSI TH Darmstadt	Life Time of Excited Nuclear States in ^{137}Xe and ^{137}Cs	Z5	15,2	^{136}Xe	3-4	--
143	Specht, Glässel, Harrach	Univ. Heidelberg	Search for Very Heavy Elements from Collisions of Uranium on Uranium	Z4	21,9	^{238}U	7,5	--
				Z4	23,9	^{238}U	7,5	
147	Grant, Jonson, Kirchner, Klepper, Mattsson, Misaelides, Nyman, Peuser, Plochocki, Chardt, Schrewe, Tidemand-Peterson, Zylicz, Roeckl	CERN; GSI; TH Darmstadt; Univ. Göteborg, Göttingen, Mainz, Manchester, Warschau	Studies of Proton and Alpha Emission in the Tin Region	Y5	42,7	^{58}Ni	5,0	54
				Y5	46,0	^{58}Ni	4,5-5,0	
				Y5	7,6	^{58}Ni	4,5-5,0	
				Y5	15,0	^{58}Ni	5,0	

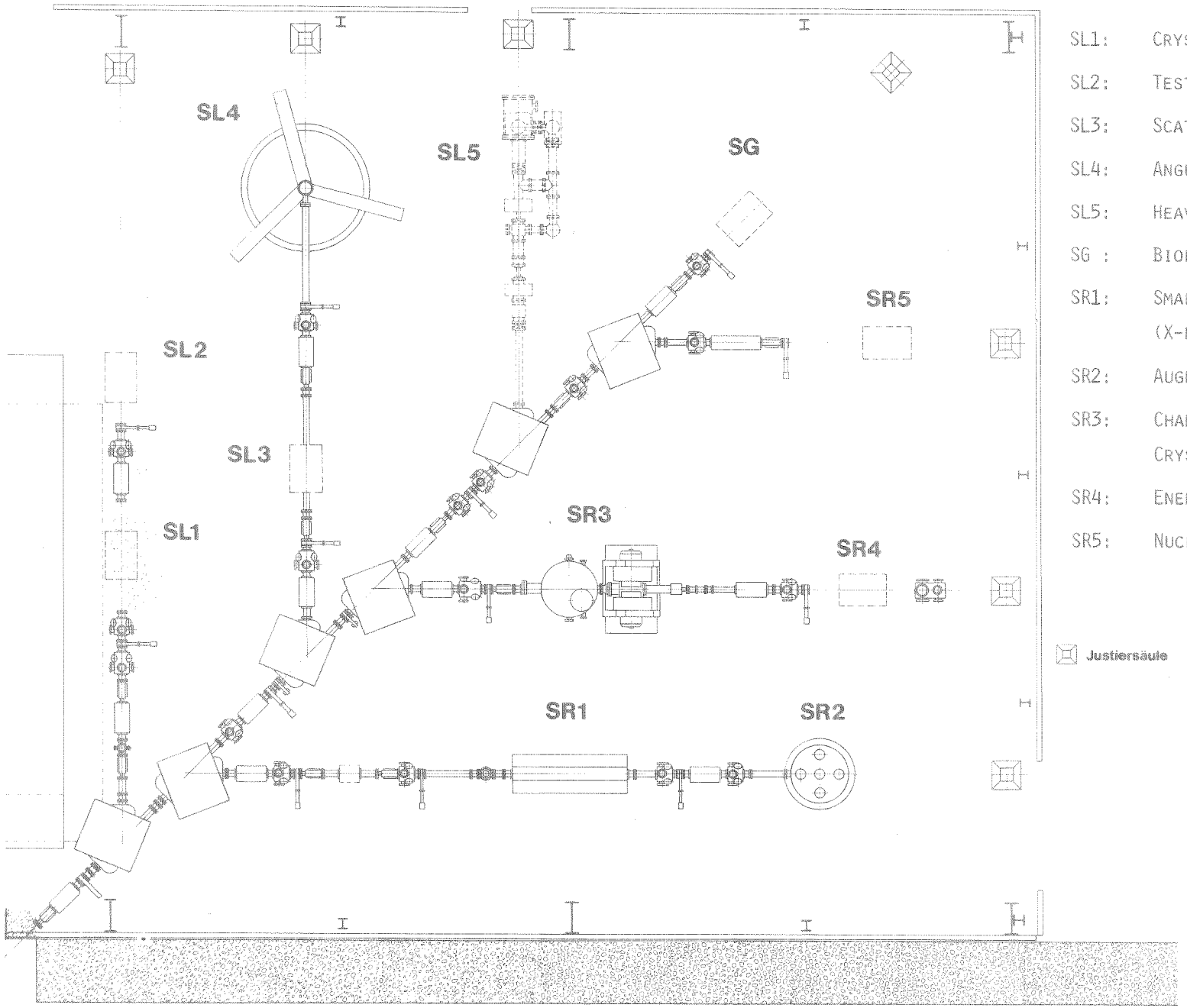
Exp. Nr.	Authors	Affiliation	Title	Beam Position	Beam-time [h]	Ions	Energy [MeV/u]	Corresponding Article on Page
150	Hofmann, Armbruster, Ewald, Faust, Güttner, Kitahara, Münzenberg, Reisdorf, Thuma	GSI Univ. Gießen	Identification of Two new Alpha Emitting Isomeric States	Y7	48,6	^{58}Ni	5,2-3,7	55
				X9	11,3	^{238}U	5,9	
				X9	40,1	^{238}U	5,9	
154	Stokstad, Hildenbrand, Kratz, Lucas, Poitou, Reisdorf, Wirth	ORNL Oak Ridge CEN Saclay; GSI	Nuclear Deformation and Heavy Ion Fusion	Z3	15,7	^{40}Ar	3,0-4,1	108
157	Junclas, Brandt, Goerg, Hirdes, Lemmertz, Wollnik	Univ. Marburg Univ. Gießen	Search for SHE in the Reaction (^{nat}U+ ^{208}Pb) Using the Gas Jet and Sulfide-Chemistry	X6	48,4	^{208}Pb	8,3	64
				X6	39,1	^{208}Pb	8,3	
159	Elze, Fuchs, Grosse, Idzko, Ower, Rauch, Schwalm, Simon, Stelzer, Wollersheim	Univ. Frankfurt GSI	High Spin States in ^{232}Th, ^{234}U and ^{236}U	X7	3,8	^{208}Pb	5,6	46
				Z5	3,8	^{208}Pb	5,6	
160	Schüll, Busch, Freiesleben, Pühlhofer, Langenbeck, Pfeffer	GSI Univ. Marburg	A Large-Area Scintillation Stop Detector for the Magnetic Spectrometer	Z1	14,9	^{208}Pb	5,9	185
164	Günther, Fuchs, Grosse, Hübel, Idzko, Kleinrahm, Schwalm, Wollersheim	Univ. Bonn, Univ. Frankfurt, GSI	Coulomb Excitation of ^{198}Hg and ^{200}Hg with ^{208}Pb Ions	X7	53,7	^{208}Pb	5,0-5,6	45
				Z5	26,6	^{208}Pb	5,6	
165	Hansen, Britt, Christensen, Flynn, Freiesleben, Nathan, Plasil, Videbaek	NBI Kopenhagen, ORNL Oak Ridge, LASL, GSI	Elastic, Inelastic, and Quasielastic Scattering of Medium Heavy Ions	Z1	14,7	^{86}Kr	8,1	2
				Z1	31,6	^{86}Kr	8,1	
168	Lynen, Gobbi, Natowitz, Olmi, Rode, Rudolf, Sann, Stelzer, Wurm	MPI Heidelberg, CRNS Strasbourg, GSI	Mass Drift Towards Asymmetry at High Incident Energies	X1	40,7	^{86}Kr	12,8-13,2	---
170	Schröder, Birkelund, Freiesleben, Hilder, Huizenga, Wilke	NSRL Rochester HMI Berlin, GSI	Study of the Bombarding Energy Dependence of Reaction Phenomena in Damped Collisions between ^{136}Xe and ^{209}Bi	Z3	2,6	^{208}Pb	7,5	---
				Z3	7,6	^{208}Pb	4,7	
				Z3	85,8	^{136}Xe	10,5-11,5	
171	Roeckl, Grant, Kirchner, Klepper, Misaelides, Nolan, Plochocki, Reisdorf, Riedlinger, Schrewe, Tidemand-Peterson, Wood, Zylicz	GSI; Univ. Göttingen; Univ. Tennessee; Univ. Warsaw; Univ. Manchester; Georgia Tech.	On-Line Mass Separation of Trans-Lead Isotopes	Y5	19,9	^{84}Kr	4,5-5	57
				Y5	20,7	^{48}Ti	5,1	
				Y5	13,3	^{48}Ti	5,4-6,6	
				Y5	44,4	^{48}Ti	5,1-5,3	
176	Schüll, Bangert, Busch, Freiesleben, Pühlhofer, Shen	GSI; Univ. Marburg, Univ. Bochum	Study of Charge- and Mass-Transfer in Quasielastic Collisior	Z1	29,5	^{129}Xe	5,99	20
				Z1	2,3	^{136}Xe	5,9	
				Z1	3,5	^{136}Xe	5,9	
				Z1	32,0	^{136}Xe	5,9	
				Z1	47,5	^{129}Xe	6,0	

	Exp. Nr.	Authors	Affiliation	Title	Beam Position	Beam-time [h]	Ions	Energy [MeV/u]	Corresponding Article on Page
	177	Bass, Artl, Hartmann, Noll, Renfordt, Sapotta	Univ. Frankfurt	The Reactions $^{208}Pb+^{58}Ni$ and $^{208}Pb+^{64}Ni$	Z3	34,1	^{208}Pb	5,4	22
	178	Wölfli, Bock, Chu, Gobbi, Grosse, Lynen, Morenzoni, Müller, Sann, Schwalm	ETH Zürich; MPI Heidelberg, GSI	Search for Delayed Fission of Heavy Nuclei	X7	11,7	^{136}Xe	5,9	10
					X7	0,8	^{136}Xe	5,9	
					X7	34,4	^{208}Pb	5,0-5,6	
					Z5	37,5	^{208}Pb	4,7-6,5	
	179	Lynen, Bock, Doll, Dakowski, Gobbi, Olmi, Pelte, Sann, Stelzer	MPI Heidelberg GSI	Pre-Equilibrium Effects of High Kinetic Energies	Z4	21,7	^{132}Xe	5,9	--
	180	Ngo, Gobbi, Gregoire, Kratz, Lucas, Lynen, Mazur, Olmi, Poitou, Ribrag, Sann, Signarbieux, Wirth	CEN Saclay, MPI Heidelberg, GSI	Study of Quantal Fluctuations	X1	8,6	^{208}Pb	8,0	--
					X1	44,4	^{208}Pb	4,7-8,0	
	181	Emling, Balanda, Grosse, Hass, Kumbartzki, Pelte, Schwalm, Seiler-Clark, Simon, Speidel, Wollersheim	GSI; Rehovot; Univ. Heidelberg, Univ. Bonn	Measurements of Magnetic Moments of High Spin States	Z5	20,5	^{208}Pb	5,3	41
					X7	20,5	^{208}Pb	5,6	
					Z5	58,2	^{208}Pb	4,7	
					Z5	27,5	^{208}Pb	4,7-7,0	
	189	Gäggeler, Brüchle, Ferguson, Hahn, Ghiorso, Herrmann, Hulet, Kratz, Lougheed, Nitschke, Schädel, Tittel, Trautmann	Livermore, Berkeley, Oak Ridge, Mainz, GSI	Search for Superheavy Elements in the Reaction of ^{238}U on ^{248}Cm	Y3	7,3	^{132}Xe	8,1	63
					Y3	26,9	^{238}U	10,0	
					Y3	148,1	^{238}U	10,0	
					T7	10,8	^{238}U	10,0	
	192	Fraenkel, Bass, Dakowski, Doll, Eyal, Gobbi, Kreyling, Renfordt, Shapira, Stelzer, Tserruya, Wald	Univ. Frankfurt, Rehovot, GSI	Neutron Emission in DIC at 12 MeV/u	Z6	80,7	^{86}Kr	12,0	24
					Z6	12,1	^{86}Kr	4,8-12,0	
	193	Stachel, Emling, Fuchs, Grosse, Kaffrell, Ower, Schwalm, Seiler-Clark, Sümmerer	Univ. Mainz, Univ. Frankfurt, GSI	Multiple Coulomb Excitation of ^{104}Ru	X7	27,0	^{208}Pb	4,9	39
Atomic Physics	15	Kienle, Jakubassa, Kleber, Martin, Kozhuharov, Schulze, Schwalm, Stettmeier	TU München, MPI Heidelberg, GSI	Spectroscopy of High Energy δ-Rays Emitted in Heavy-Ion Collisions	X9	20,3	^{238}U	5,9	100
					X9	71,1	^{208}Pb	4,7	

Exp. Nr.	Authors	Affiliation	Title	Beam Position	Beam-time [h]	Ions	Energy [MeV/u]	Corresponding Article on Page
15-1	Kienle, Bordermann, Kankeleit, Kozhuharov	TU München TH Darmstadt	Positrons from 1.4 GeV U-U Collisions	X9	28,0	^{208}Pb	5,9	103
50	Kraft, Armbruster, Geißel, Gattner, Kitahara	Univ. Gießen GSI	Stopping Powers of 0.2 - 1.4 MeV/u Heavy Ions in Solids	X8	32,5	^{184}W	5,3	122
55	Liesen, Armbruster, Behncke, Mokler, Schmidt-Böcking, Schuch	GSI Univ. Frankfurt	Excitation Probability of the Molecular 1sσ Orbital in Collision Systems $\propto (Z_1+Z_2) \gtrsim 1$	X4	21,8	^{132}Xe	3,6-6,3	107
				XK	24,3	^{208}Pb	8,2-8,5	
				X4	20,1	^{132}Xe	4,7	
86	Kankeleit, Backe, Bokemeyer, Gono, Handschug, Senger, Richter, Weik, Willwater, Vincent	TH Darmstadt GSI	Positron Production in Heavy Ion Collisions	X8	42,0	^{238}U	7,5	101
				X8	50,5	^{238}U	5,9	
				X8	24,4	^{238}U	5,2;5,9	
				X8	63,5	^{238}U	5,9	
87	Schartner, Beyer, Frekmann, Mann	Univ. Gießen; GSI	Tests of a Transmissionspectrometer for X-Ray Spectroscopy	SL1	17,0	^{238}U	1,4	167
95	Franzke, Erb, Steiner	GSI	Charge Change Cross Sections for 1,4 MeV/u-Uranium in H_2 and N_2	XK	24,3	^{238}U	8,2-8,5	225
				XK	14,0	^{238}U	5,9	
				XK	11,7	^{238}U	7,5	
				XK	1,4	^{136}Xe	5,9	
				XK	13,3	^{238}U	1,4	
137	Wölfli, Armbruster, Folkmann, Meyerhof, Mokler, Morenzoni, Stoller, Vincent	ETH Zürich; GSI	MO X-Ray Angular Distribution for 1 GeV ^{208}Pb+^{208}Pb and ^{209}Bi+^{209}Bi	X7	34,9	^{208}Pb	4,2	104
156	Bimbot, Armbruster, Gardes, Geissel, Fleury, Hubert	IPN Orsay; GSI CEN Bordeaux	Stopping Power Measurements	X3	20,1	^{132}Xe	5,0	120
				X3	11,2	^{208}Pb	3-5	
				X3	23,1	^{238}U	3,0;5,0	
158	Bethge, Hagmann, Liesen, Mokler, Schmidt-Böcking, Schuch, Stiebing	Univ. Frankfurt, Univ. Heidelberg, GSI	Spectroscopy of the Molecular 1sσ Orbital in Collision Systems $\alpha(Z_1+Z_2)\gtrsim 1$	X4	49,1	^{208}Pb	4,7	108
175	Schwalm, Balanda, Bethge, Bokemeyer, Folger, Greenberg, Gruppe, Kessel, Matsuki, Schule, Schweppe, Vincent Waldschmidt	GSI; IKF; Yale Univ.	Study of Positron Creation in Superheavy Quasiatomic Systems	Z2	34,1	^{208}Pb	5,87	102
				Z2	65,4	^{208}Pb	5,9	
				Z2	51,2	^{238}U	5,9	
				Z2	66,6	^{238}U	6,2	

		Exp. Nr.	Authors	Affiliation	Title	Beam Position	Beam-time [h]	Ions	Energy [MeV/u]	Corresponding Article on Page
Solid State and Biology	Physics	1	Thiel, Herr, Külzer, Spohr	Univ. Köln, GSI	Heavy Ion Induced Sputtering of Glasses	XO	17,1	^{132}Xe	8,5	141
						ZO	19,8	^{208}Pb	8,5	
						XO	17,0	^{129}Xe	6,0	
		3	Kiefer, Faber, Kraft, Koch, Schneider, Schöpfer, Weber	Univ. Gießen, GSI	Survival of Vegetative Yeast Cells after Irradiation with Heavy Ions	XO	10,0	^{238}U	7,5	147
		161	Dertinger, Weibezahn	KfK Karlsruhe	Biophysical Response of Mammal Cells to Heavy Ions	XO	13,0	^{129}Xe	6,5	—


Meßstation
Z4
T 7 Irradiation Experiments
X 1 Kinematic Coincidence-telescope
X 2/3 Scattering Chambers
X 4 X-Ray Measurements
X 5 γ-Multiplicity Measurements
X 6 Fast Chemistry; Gas-jet
X 7 γγ-Correlation Measurements
X 8/9 e± - Spectrometers
X K Charge Changing Processes
X 0 Low Dose Irradiations
Y 3/4 Chemical Separations
Y 5 Isotope Separator
Y 7 Velocity Separator
Z 0 γγ-Correlation Measurements
Z 1 Magnetic Spectrograph
Z 2 e± - Spectrometer
Z 3 TOF - telescope
Z 4 Multi - coincidence - telescope
Z 5 Variing Equipment
Z0
Z1
Z2
Z3
Z4
Z5
Y3/4
Y5
Y6
Y7
T7
X0
XK
X9
X5
X6
X7
X8
X1
X2
X3
X4
Justiersäule
Höhenkontrollpunkt
5m
Stand Okt. 78
1:50
Experimentierhalle
Strahlführung / Meßplätze
GSI
DARMSTADT
EH - 010



SL1: Crystal Spectrometer

SL2: Test Position

SL3: Scattering Chamber

SL4: Angular Correlation

SL5: Heavy Ion Microprobe

SG : Biological Experiments

SR1: Small Angle Scattering
(X-ray Particle Coincidence)

SR2: Auger Spectrometer

SR3: Charge Changing Collisions,
Crystal Spectrometer

SR4: Energyloss Experiments

SR5: Nuclear Track Experiments

Justiersäule

XXIX

1. Nuclear Physics/Nuclear Chemistry

		PAGE
1.1	Nuclear Reactions	2
1.1.1	Reactions Near the Coulomb-Barrier	2
1.1.2	Deep Inelastic Reactions	13
1.1.3	Relativistic Nuclear Collisions	36
1.2	Nuclear Structure	39
1.3	Exotic Nuclides	54
1.4	Theory	66

Elastic and quasielastic scattering observed with good energy resolution ^{86}Kr + ^{208}Pb

P.R. Christensen, C.L. Viang, Ole Hansen, O. Nathan, S.P. Sørensen and F. Videbaek
NBI, University of Copenhagen, Denmark

D. Schüll, W.C. Shen*and H. Freiesleben
GSI Darmstadt, *on leave from IMP, Academia Sinica, Lanchow, China

F. Busch and F. Pühlhofer
Fachbereich Physik, Universität Marburg

P. Bond
BNL, Upton, USA

F. Plasil
ORNL, Oak Ridge, Tennessee, USA

It has been proposed to study the elastic and quasielastic scattering with a ^{86}Kr beam of 8 MeV/u on a target of ^{208}Pb with an energy resolution of $\leq 10^{-3}$. The GSI magnetic spectrometer was used for the precision analysis of the reaction products.

One beam time was allocated during 1979, mainly for feasibility studies. ^{208}Pb targets, $\approx 40\ \mu g/cm^2$ thick, were bombarded with ^{86}Kr with beam intensity of 2 to 4 pnA. With a spectrometer solid angle of acceptance of ≈ 1.3 msr elastic and inelastic scattering could be measured at angles forward of grazing in runs from 2 to 6 hours. Data were obtained at 20, 25, 30 and 32.5 degrees, all forward of grazing. Transfer reactions were observed at the most backward angle.

The data analysis shows that the beam-target-spectrometer system is capable of an energy resolution of ≈700 keV at an incident energy of 700 MeV (see also the spectrum at fig. 1).

It was found that the settings of the beam line were very critical and the beam stability was not optimal. The observed variation of energy resolution over the acceptance angle of the spectrometer indicates that higher order contributions in the ion optics of the spectrometer were not corrected properly in this run.

In spite of these difficulties the spectrum of fig. 1 which shows the excitation of the first 2^+ state in ^{86}Kr and 3^- state in ^{208}Pb is encouraging and it is planned to measure elastic, inelastic and Q ≈ 0 transfer reactions from ^{86}Kr + ^{208}Pb in the near future.

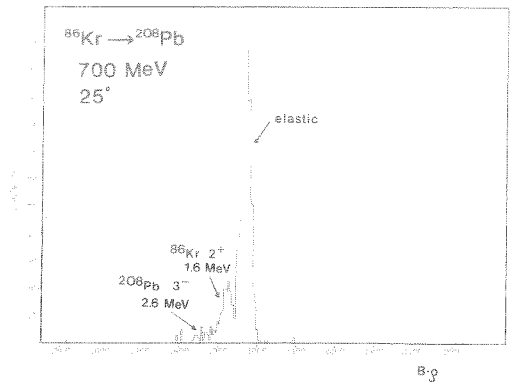


Fig. 1: Spectrum from ^{86}Kr + ^{208}Pb. The abszissa is in arbitrary units.

B

Double charge exchange reactions with heavy ion beams

F. Beck, G. Delic*, H. Genz, A. Richter, G. Schrieder and P. Wastyn
Institut für Kernphysik, Technische Hochschule Darmstadt

D. Schüll and W. Shen+
GSI Darmstadt

F. Busch and F. Pühlhofer
Fachbereich Physik der Universität Marburg

Recent results from the meson factories with pion beams have demonstrated the importance of the double charge exchange (DCE) reaction (π^+, π^-) in exploring fundamental nuclear properties. Experimental results are now available on target nuclei between ^{9}Be and ^{58}Ni but there exists presently no theoretical model which can provide consistent predictions for the observed cross sections. There seems, however, to be a strong dependence of the DCE cross section upon the particular nuclear structure involved. Since in DCE processes an isospin change of two units ($\Delta T_z = 2$) has to be accomplished, heavy ions are besides pions the only suitable particles by which DCE can be studied. Thus DCE forms a link between the fields of heavy ion and medium energy physics. It is our aim to investigate the DCE reaction together with single charge exchange (SCE) reactions with heavy ion beams at the GSI UNILAC and use it as a tool in the study of a wide range of nuclear properties.

Reported here are results from a test run using the reaction ^{48}Ti + ^{42}Ca. Reaction fragments produced with a Ti-beam of an energy E_{Lab} = 5 MeV/N were recorded at an angle $\Theta_{Lab} = 20^{\circ}$ with help of the GSI magnetic spectrometer. Figure 1 shows the nuclear charge and energy dependence of all detected events within 1.5h beam time.

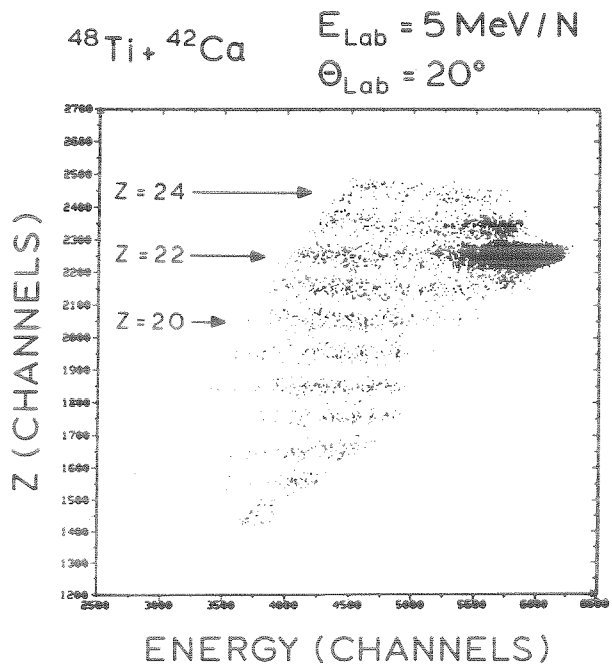


Fig. 1: Z-E plot of all interaction products

As seen in this figure, deep inelastic products with nuclear charges between Z = 14 and Z = 24 are produced as well as quasi-elastic events with Z = 22 ± 2. The masses of all these fragments are shown in fig. 2. The strongest populated channel is the elastic one with Z = 22 and M = 48. It is furthermore clear that the reaction channels with Z = 21, M = 47 (proton stripping) and with

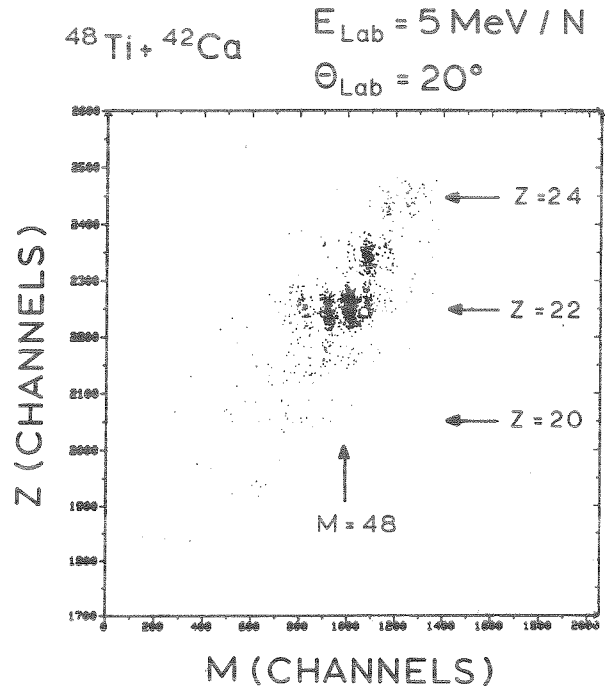


Fig. 2: Z-M plot of all interaction products

Z = 22, M = 49 (neutron pick-up) are not populated strongly enough so that sequential processes could lead to strong charge exchange channels. Altogether, about 10% of the events seen in the charge exchange channels are located in the quasi-elastic region of the energy spectrum. We have estimated the following cross sections

^{48}Ti + ^{42}Ca → ^{48}Sc + ^{42}Sc: $\frac{d\sigma}{d\Omega}_{CM}$ = 0.07±0.02 mb/sr (SCE)

^{48}Ti + ^{42}Ca → ^{48}Ca + ^{42}Ti: $\frac{d\sigma}{d\Omega}_{CM}$ < 58 μb/sr. (DCE)

*Perm. ad.: Nuclear Physics Dept., Univ. of the Witwatersrand, Johannesburg, South Africa

+Perm. ad.: Inst. of Modern Physics, Academia Sinica, Lanzhow, VR China

Coulombfission [B]

H. Backe, F. Weik
TH Darmstadt
P. A. Butler
University of Liverpool, England
V. Metag, J. B. Wilhelmy, D. Habs, G. Himmele, H. J. Specht
MPI and University Heidelberg

This year the first definite measurements of fission induced by inelastic scattering of heavy ions have been performed, showing the basic properties of Coulombfission [1].

The experimental set-up is shown in fig. 1. With a solenoid spectrometer the backscattered particles are identified via their emission of delayed conversion electrons. In a ring counter the fission fragments are detected in coincidence with the electrons.

Fig. 2 shows the fission probability of ^{238}U after inelastic backward scattering of ^{184}W and ^{152}Sm as a function of bombarding energy. For lower energies the fission probability increases by a factor between two and four when changing from ^{152}Sm to ^{184}W projectiles, corresponding to a projectile charge dependence of Z_p^n with $5 < n < 6{,}5$. This rather strong dependence points to a multiple excitation process. Fig. 2 also contains recent theoretical predictions by Oberacker et al [2]. The calculations using a pure Coulomb interaction roughly reproduce the experimental data. The predicted interference minimum between the attractive nuclear and repulsive Coulomb force is not observed. Besides inelastic scattering, also conversion electron lines from neutron transfer reactions followed by fission are found. Contribution to the inelastic scattering followed by fission therefore result from the to and fro transfer of nucleons. A comparison of the 2-n-transfer cross-section followed by fission for ^{182}W and ^{182}W shows, however, that the contribution of this transfer of a neutron below the Coulomb barrier contributes at most 20% of the observed cross-section in the system $^{184}W + ^{238}U$ and may only unsignificantly disturb the observed Z_p dependence. On the other hand, it may cover up the expected interference minimum.

Fig. 3 shows the targetdependence of Coulombfission for the irradiation of ^{232}Th, ^{238}U and ^{248}Cm with ^{184}W. Experimentally the fission cross-section for ^{232}Th is about 40 % lower than for ^{238}U, whereas theoretically [2] the opposite behaviour is calculated.

[1] H. Backe et al, Phys. Rev. Lett. 43, 1077 (1979)
[2] V. Oberacker, private communication and V. Oberacker et al, Phys. Rev. C. 20 (1979) 1453

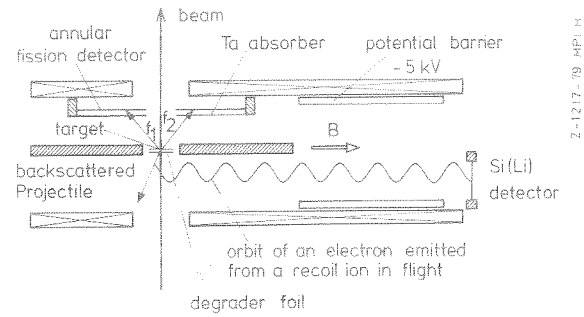


Fig. 1. Experimental configuration

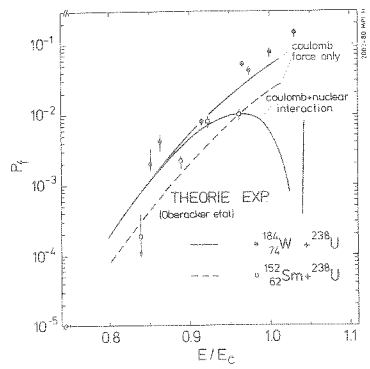


Fig. 2. Fission probability of ^{238}U after inelastic scattering of ^{184}W and ^{152}Sm.

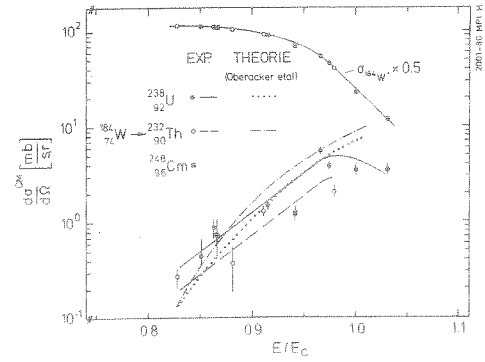


Fig. 3. Fission cross-sections of ^{238}U, ^{232}Th and ^{248}Cm in coincidence with the $2^+ \rightarrow 0^+$ ^{184}W transition.

Sub-Coulomb fission and transfer in collisions of ^{208}Pb with ^{238}U

W. Brüchle, H. Folger, B. Haefner, J.V. Kratz
GSI Darmstadt

G. Friedlander[+]
Institut für Kernchemie, Universität Mainz

In earlier experiments to detect Coulomb fission in bombardments of ^{238}U with Xe ions[1] sub-Coulomb transfer cross sections were found to exceed the fission cross sections by more than one order of magnitude even at the lowest energies of 0.7 E_C where E_C corresponds to the Coulomb barrier. Thus we could not clearly distinguish between pure Coulomb fission and sequential fission after quasi-elastic transfer. Theoretical calculations by Oberacker[2] predict a Z_p^6 dependence of the Coulomb fission cross sections on the charge of the projectile. This should enhance the cross section by about a factor of 15 when using ^{208}Pb instead of Xe ions. Therefore we bombarded ^{238}U with ^{208}Pb ions at energies of 0.85 E_C and 0.80 E_C. After passing through the 1.7 mg/cm^2 thick targets these energies are reduced to 0.80 E_C, and 0.75 E_C.

After irradiation the targets were assayed for uranium (transfer products), barium, and zirconium (fission products)[1]. For E_{IN} = 0.80 E_C a fission cross section of 3.2×10^{-28} cm^2 was obtained if we assume the fission mass distribution was the same as for neutron-induced fission of ^{235}U. Transfer cross sections for ^{237}U and ^{239}U were measured as 3.1×10^{-28} cm^2 and 5.2×10^{-28} cm^2, respectively. These transfer processes can partially contribute to the observed fission cross section with the tail of the associated Q-value distribution that extends up to excitation energies above the fission barrier. If we make the pessimistic assumption that all transfers are associated with excitation energies above B_f resulting in a fission probability $P_f \approx 0.2$, then the measured cross sections for the residual nuclei ^{237}U and ^{239}U indicate that at most 50% of the observed fission yield of 3.2×10^{-28} cm^2 can be due to sequential transfer-induced fission. Oberacker[2] predicted a Coulomb-fission cross section of 2.7×10^{-28} cm^2 for ^{208}Pb on ^{238}U at 0.8 E_C (for the moment of inertia Θ being proportional to the deformation parameter a_0).

This is in fairly good agreement with our measured value which corresponds to an effective energy of $\sim$ 0.78 E_C, see Fig. 1. Recent experiments with ^{184}W ions[3] where the backscattered excited ^{184}W-projectiles could be measured in coincidence with the fission fragments, were also consistent with the Coulomb-fission cross sections predicted by Oberacker et al.[2].

Our experiments at E_{IN} = 0.85 E_C did not yield valuable results because the beam energy was not constant over the whole irradiation times. These experiments are no being repeated.

[+]Holder of an Alexander von Humboldt-Award, on leave from Brookhaven National Laboratory

[1] G. Franz et al., Z. Physik A291. 167 (1979)
[2] V. Oberacker et al., Phys. Rev. C20, 1453 (1979) and V. Oberacker, private communication
[3] H. Backe et al., Phys. Rev. Lett. 43, 1077 (1979)

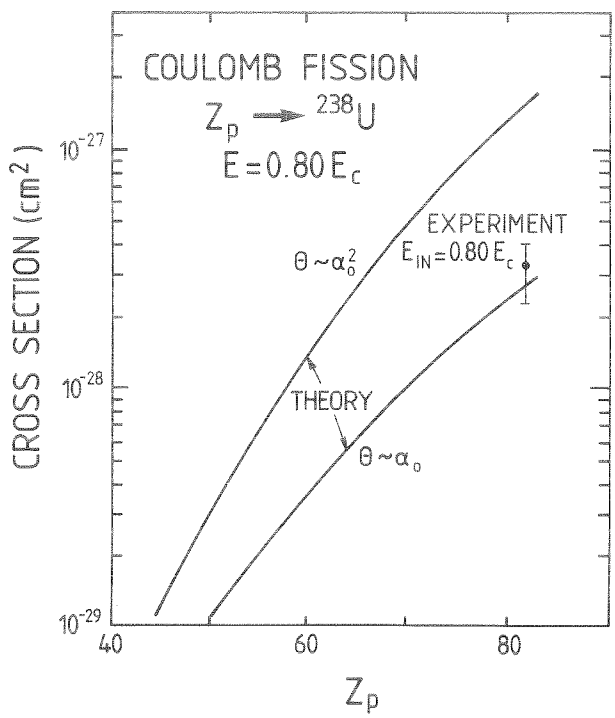


Fig. 1: Theoretical prediction of integral cross sections for Coulomb fission vs. projectile charge at 0.80 E_C by Oberacker et al.[2] The measured fission cross section in the $^{208}Pb+^{238}U$ system at an incident energy of 0.8 E_C is also indicated.

Cold Fragmentations of ^{234}U

P. Armbruster, Experiment at ILL, Grenoble, in collaboration with

U. Quade[1], K. Rudolph[1], J. Weber[1], H. Schrader[2], F. Gönnenwein[2], H.J. Clerc[3], M. Mutterer[3], J.P. Theobald[3]

[1]LMU München, [2]ILL Grenoble, [3]TH Darmstadt

The separator LOHENGRIN allows to separate fission products from thermal neutron fission according to their masses and secondary kinetic energies[1]. Their atomic numbers are determined by measuring the rest energy of the energy and mass selected products after passage through an absorber[2]. The small percentage of fission events ($\sim$ 2%) with excitation energies smaller than the energy necessary to evaporate a neutron ($E^X < 7$ MeV) has been investigated. For these events the separator gives primary fragments. Momentum conservation in the binary break-up allows to calculate the TKE of the primary fragments. Taking the Q-value of a given split from mass tables the excitation energy of the configuration $E^X = Q\text{-TKE}$ is calculated, as mass and atomic number conservation allow to identify the two fragments from the measurement of mass and atomic number of one fragment. The cold fragmentations of ^{234}U have been selected as light fission products with kinetic energies 110 MeV $< E_L <$ 117 MeV for the fission sources given in the experiment. Fig. 1 shows the calculated mass dependence of the kinetic energies corresponding to $E^X = 0$ and $E^X = \frac{1}{2}(S_{n1} + S_{n2}) \sim (6.5 - 7.5)$ MeV with S_{ni} the neutron binding energies. We define the region of cold fragmentation by these limits. Fission yields of 10^{-6} could be measured in the background free domain of high kinetic energies. In Fig. 1 the kinetic energies corresponding to a yield of $\sim 10^{-6}$ are given (x). The TKE approaches the Q-value within a few MeV for all masses, that is the excitation energy of the fragmented system for all mass splits may be smaller than the energy gained in the capture of the fission inducing neutron. Calculating from the TKE via Coulomb energy the distance between the charge centers gives for the most compact scission configurations $d \sim (15 \pm 0.5)$ fm, a distance which is (3 - 4) fm larger than the distance between undeformed touching spherical nuclei. Deformations with $b/a \sim 1.5$, if both the fragments are deformed or $b/a \sim 2.0$, if only one carries the deformation, have to be postulated for the scission configuration. The deformations fix part of the energy released in the process as deformation energy. Cold fragmentation demands deformation with the smallest possible amount of energy converted into deformation or intrinsic energy. A soft nucleus combined with a stiff one, or pairs of soft nuclei yield the lowest deformation energies, thus allowing for cold fragmentations. Fig. 2 shows the mass distribution of the light fission product group for E_L = 111 MeV and q = 21. The dependence of the independent yields of certain isotopes on the ionic charge state does not change the distribution shown essentially. An element analysis of the isobars has been performed with the final data evaluation in progress. The two peaks in Fig. 2 correspond to a breakage into a soft, ^{100}Zr, or ^{144}Ba, respectively, and a stiff nucleus, ^{134}Te, or ^{90}Kr, respectively. The intermediate range A = (90 - 100) corresponds to pairs, which cannot be created without appreciable conversion of energy into deformation energy. The peak at A = 100 shows a cold fragmentation into two closed shell nuclei, the deformed shell (N = 60) nucleus ^{100}Zr and the spherical shell (N = 82) nucleus ^{134}Te. It becomes dominant for $E^X < 10$ MeV. Shell effects govern the fragmentation at those low excitation energies, an encouraging lesson for those who discuss the production of SHE.

The preliminary analysis has lead to further remarkable findings a) for all masses below $E^X < 5$ MeV the yields follow a dependence $W(E^X)dE^X = P_0 \exp E^X/T_{eff} dE^X$ and not as for higher values of E_x a Gaussian distribution. The effective temperature is smallest ($\sim$ 0.9 MeV) in the range of high mass yields A_L = 91 - 99, and increases ($\sim$ 1.7 MeV) towards the masses $A_L < 91$ and $A_L > 99$. b) For comparable yields odd fragmentations have excitation energies which are on the average 1.1 MeV less than even mass fragmentations. They are colder than even pairs. Particles-hole excitation demands less energy in odd pairs than in even pairs. Non-collective intrinsic exciations seem to be of importance even for cold fragmentations. c) In the range $A_L > 100$ following the Q-values systematics the yields should drop drastically in the energy range investigated. This is not observed experimentally, Fig. 1. The negative excitation energy obtained in the evaluation points to an inadequacy of the shell energies in the domain Z > 50 and N > 60.

[1]E. Moll et al., Nucl. Instr. and Meth. 123 (1975) 615

[2]U. Quade et al., Nucl. Instr. and Meth. 164 (1979) 435

Fig. 1

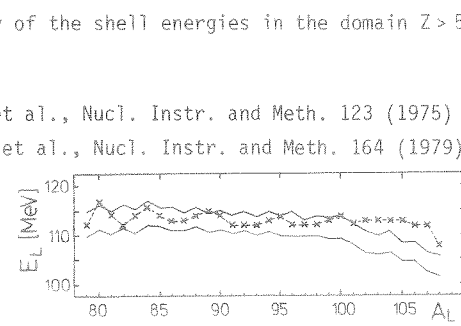
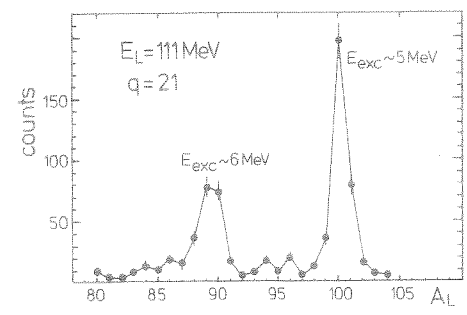


Fig. 2



Fusion well below the barrier

R.G. Stokstad, GSI Darmstadt and ORNL Oak Ridge
W. Reisdorf, K.D. Hildenbrand, J.V. Kratz, G. Wirth, GSI Darmstadt
R. Lucas, J. Poitou, CEN Saclay

Recently fusion cross sections spanning the range 400 mb down to 0.1 mb for ^{16}O + $^{148,150,152,154}Sm$ and ^{40}Ar + $^{144,148,154}Sm$ have become available[1]. The isotopes of Sm span the transition region from spherical (^{144}Sm) to strongly deformed (^{154}Sm) equilibrium shapes. The cross section for fusion, $\sigma_{fus} = \sigma_{er} + \sigma_{ff}$, was found to vary markedly at low energies with the isotope number and, hence, with the quadrupole collectivity of the target. As can be seen in fig. 1 the threshold for fusion of Ar with ^{148}Sm and ^{144}Sm are, respectively, about 3.5 MeV and 7 MeV (c.m.) higher than for fusion with ^{154}Sm at the 0.1 mb level. A comparative analysis for ^{16}O + Sm and ^{40}Ar + Sm in terms of static deformation using WKB transmission theory and proximity-like nucleus-nucleus potentials has been made. Fig. 2 shows the experimental fusion cross sections from reference 1. The solid curve in fig. 2a is a fit to the data using the experimentally known deformation of ^{154}Sm. Only the radius parameter of the proximity potential was adjusted. The dashed lines in fig. 2a and b represent the prediction for spherical nuclei. In fig. 2b the potential parameters were kept fixed (except for $A^{1/3}$ scaling) and the best apparent static quadrupole moment (Q_o) for ^{148}Sm was obtained (solid curve). Q_o was found to be larger than the value inferred from B(E2) values (dot-dashed line in fig. 2b). In fig. 2a the dot-dashed curve is obtained using the apparent Q_o of ^{148}Sm. The dashed lines in fig. 3 (^{40}Ar) represent calculations using the parametrisation found to fit the ^{16}O data.

These calculations fail to reproduce the Ar data below the 10 mb level. Acceptable fits (solid line) are obtained if the barrier curvatures are artificially increased by a factor 2.2. The calculations also fail to reproduce the cross section differences observed at high E_{cm} (fig. 1). Fig. 4 shows again the Ar + ^{154}Sm data together with the best fit as well as the corresponding best fits to Ar + ^{148}Sm (dot-dashed) and Ar + ^{144}Sm (dashed) all radii being scaled with $A^{1/3}$. In the absence of deformation effects all 3 curves should coincide.

[1] R.G. Stokstad et al., Phys. Rev. Lett. 47 (1975) 465 and Z. Physik (1980) to be published

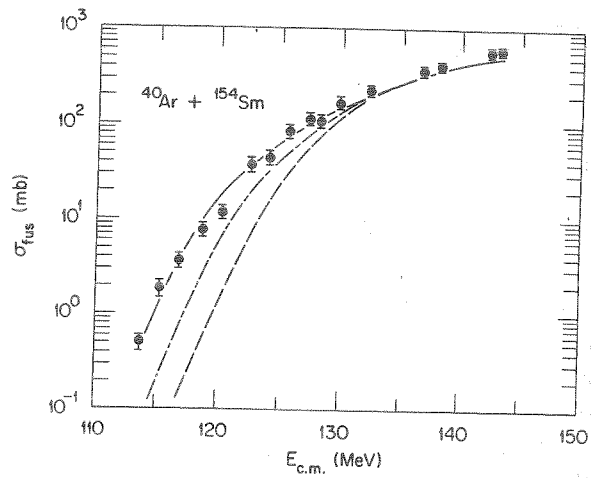


Fig. 4

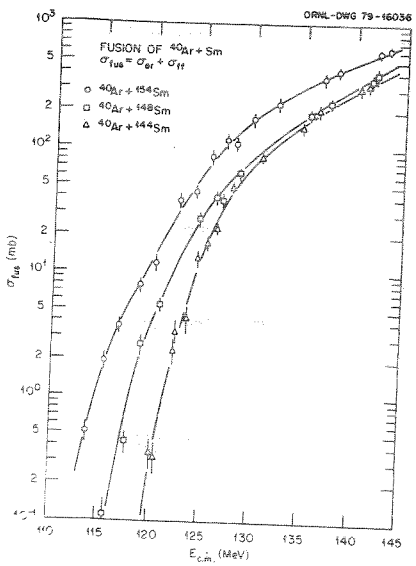


Fig. 1

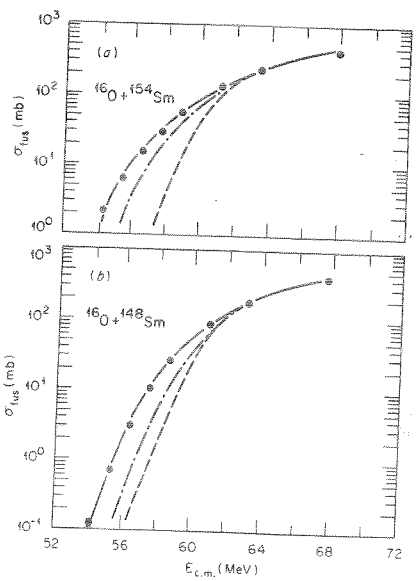


Fig. 2

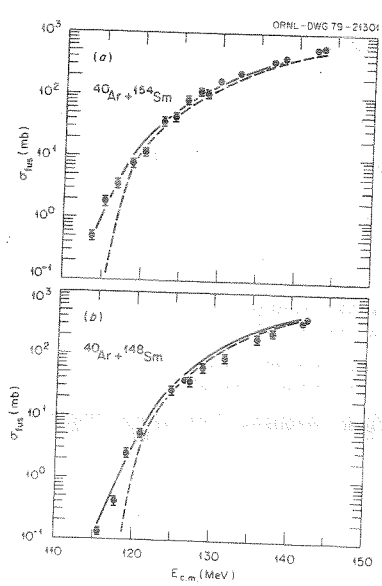


Fig. 3

Cross Sections of Argon Induced Fusion Reactions

H. Schulte, H.-G. Clerc, J. Keller, W. Lang, C.-C. Sahm, C. Schmitt, D. Vermeulen
Inst. für Kernphysik, TH Darmstadt

K.-H. Schmidt, F. Hessberger, G. Münzenberg, W. Reisdorf
GSI Darmstadt

Previously, in cross sections of evaporation residues, no influence of the N = 126 shell was found[1]. In order to exclude any possible structural effect of the fusion cross section which could alter this statement, the fission cross sections for the reactions ^{40}Ar on ^{144}Sm, ^{165}Ho, ^{169}Tm, ^{175}Lu, $^{176-180}Hf$, ^{181}Ta, and ^{208}Pb have been determined at different energies. The fission fragments were identified by measuring their kinetic energy and time of flight with a surface barrier detector, utilizing the micro pulse structure of the UNILAC. In order to check the angular distribution of the fission fragments, the laboratory angle was varied between 30 and 62 degrees. As for all systems, except ^{40}Ar + ^{144}Sm, fission is by far the most probable decay channel of the compound nucleus, the fusion cross sections were determined by normalizing the observed counts of the fission fragments to the elastic scattering. For evaluating the cross sections we assumed a symmetric fragmentation and that the angular distribution of the fission fragments is proportional to $1/\sin(\theta)$. This last assumption is compatible with the data.

In fig. 1, part of these data is compared with theoretical calculations. In these calculations, the Yukawa-plus-exponential potential, proposed by Krappe et al.[2] was used. Static deformations of the target were taken into account by using a procedure proposed by Alonso[3]. While one is able to describe the fusion cross sections of light systems[2] as well as the high energy data of this work in a very satisfactory way with this potential, obviously for these heavy systems, the model predictions are systematically below the data for energies near the barrier. Such a trend which may be related with the formation of a neck showed up already in the data, available previously[2].

Furthermore, no structural influence of the N = 126 shell is visible in these data. Thus, the conclusion of ref. 1, the independence of the fission probability on the N = 126 shell for Th compound nuclei, is confirmed.

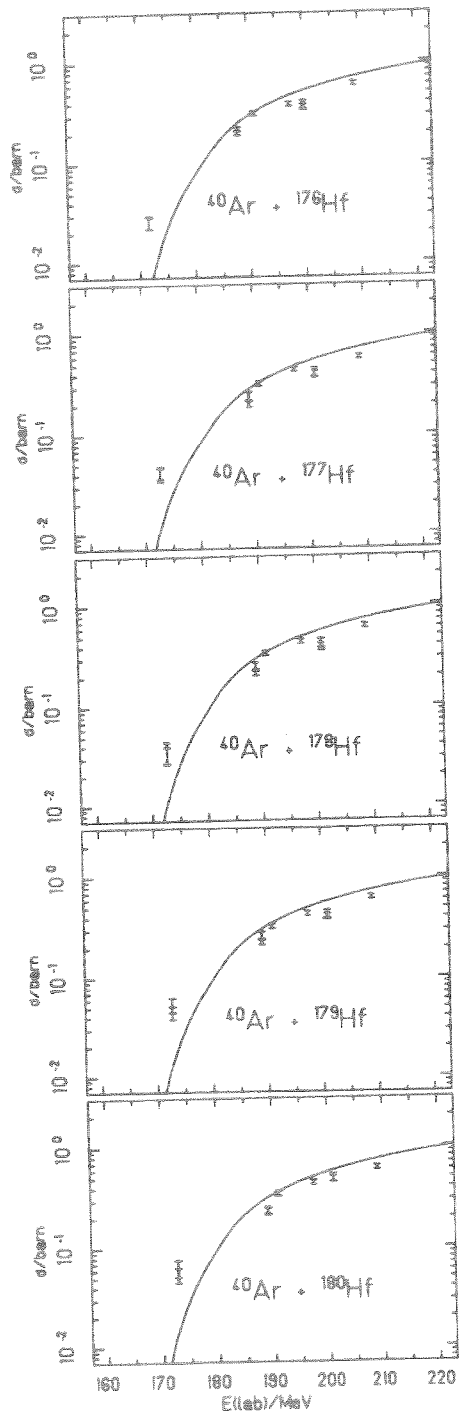


Fig. 1 : Experimental fusion cross sections for different systems (data points) in comparison with a model calculation (line).

[1] K.-H. Schmidt, et al., Contr. to the Int. Conf. on Phys. a. Chem. of fission IAEA, Jülich (1979)

[2] H.J. Krappe et al., Phys. Rev. C20 (1979) 99, R.G. Stockstad et al., this report

[3] J.R. Alonso, "Gmelin Handbuch der anorg. Chemie", 7b part A1, II, (G. Koch, Ed.), Springer (1974) 28

Fusion reaction studies of transuranic nuclei

H. Sann, S. Björnholm+, R. Bock, Y. T. Chu*, A. Gobbi, E. Grosse, U. Lynen", W. Müller", A. Olmi and D. Schwalm
GSI Darmstadt, +Niels Bohr Institute Copenhagen, "MPI Heidelberg
*Alexander von Humboldt-Fellow, on leave from Institute of Modern Physics, Academia Sinica, Lanshow, China

Reactions like U+Ca and Xe+Fe have indicated the presence of a mechanism intermediate between deep inelastic and fusion-fission reactions. So far the distributions measured as a function of mass-asymmetry, angle and energy display characteristics very similar to the fusion-fission process: a symmetric mass fragmentation, an almost isotropic angular distribution and total kinetic energy values satisfying the Viola systematics. The measured total reaction cross section is however considerably larger than the one predicted from the angular momentum limit of the liquid drop model. In order to investigate systematically the process as a function of system and bombarding energy we have bombarded targets of ^{26}Mg, ^{27}Al, ^{48}Ca, ^{50}Ti and ^{64}Ni with ^{208}Pb projectiles at 4.8 , 5.0, 5.2, 5.9 and 6.5 MeV/u. The measurements were achieved in two days of beam time, by using a position-sensitive ring counter described in details in a separated communication of this annual report. A monotonic evolution of the symmetric fragmentation as a function of system and bombarding energy is observed. For the light targets Mg and Al the observed mass distribution is narrow (FWHM ≃ 45 amu), as expected from the fission of the compound nucleus. The symmetric fragmentation appears already at bombarding energies close to the Coulomb barrier and is well separated from the deep inelastic products. In figure 1 and 2 we display the results gained for the heavier targets ^{50}Ti and ^{64}Ni.

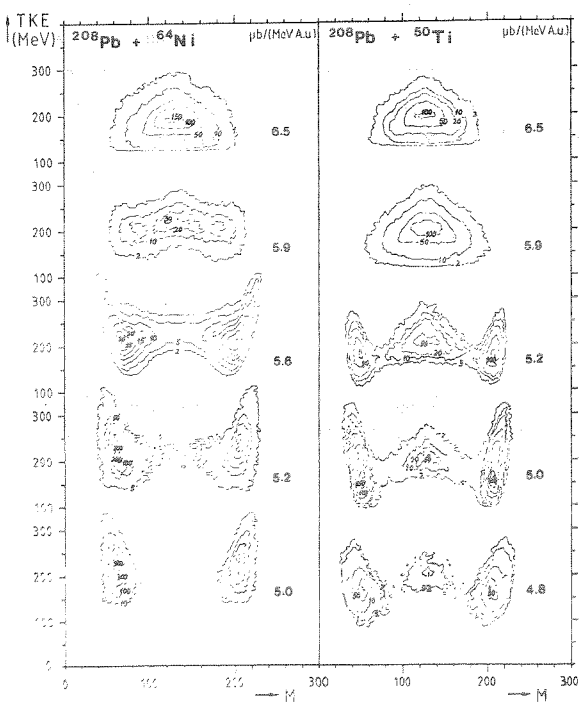


Fig. 1

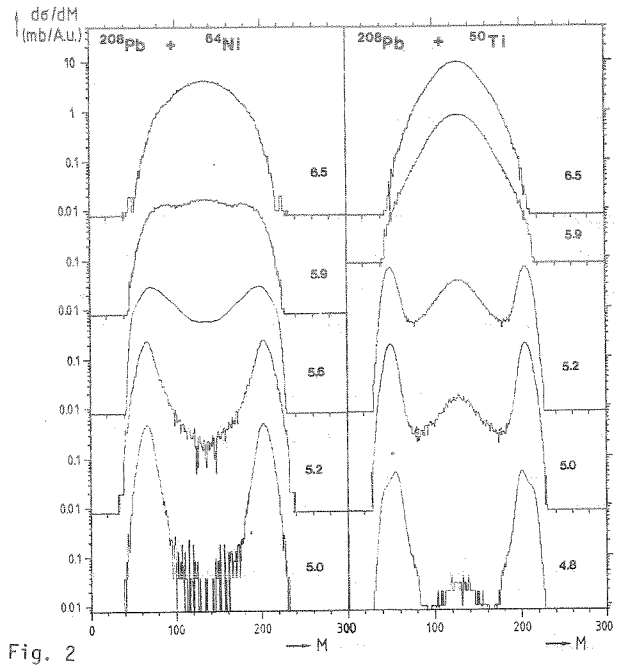


Fig. 2

Fig. 1 shows the double differential cross section as a function of mass asymmetry and total kinetic energy while fig. 2 shows the mass distributions observed at the measured bombarding energies. The symmetric mass distribution has a rather large width (FWHM ≃ 50-60 amu) and appears only at incident energies above the Coulomb barrier. The necessity to overshoot the barrier in order to reach a capture situation may be attributed to friction forces acting in the in oing channel. As shown in the case Pb+Ni at 5.9 MeV/u (fig. 1b) a distinction of the symmetric fragmentation from the deep inelastic products can be rather difficult. Nevertheless for a given system no drastic changes in the width of the mass distribution has been observed as a function of bombarding energy.
In fig. 3 is shown a preliminary result obtained for the angular distribution of the symmetric fragmentation in the $^{208}Pb+^{48}Ca$ reaction at 4.8 MeV/u. The observed angular dependence is intermediate between a constant $d\sigma/d\theta$ and a constant $d\sigma/d\Omega$-distribution. From the observed evolution of the distributions we expect to gain additional new insights when detailed comparisons to theoretical calculations will be available.

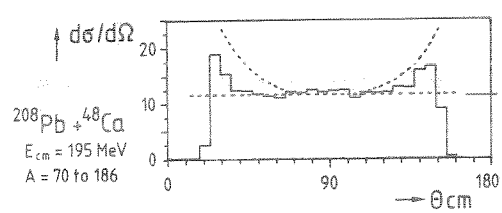


Fig. 3

Search for delayed fission of heavy nuclei

Y. T. Chu*, R. Bock, A. Gobbi, E. Grosse, U. Lynen", A. Olmi, E. Morenzoni+
W. Müller", H. Sann, D. Schwalm, W. Wölfli+

GSI Darmstadt, "MPI Heidelberg, +ETH Zürich

Studies of the symmetric mass fragmentation observed in reactions like $^{238}U+^{48}Ca$ and $^{208}Pb+^{48}Ca$ show that the memory of the ingoing channel configuration is completely lost and that the angular distribution of the products is nearly isotropic. This indicates the presence of a capture mechanism which leads to interaction times considerably longer than the collision time of the deep inelastic collision. It is therefore of great interest to find experimental techniques able to determine the survival probability of the heavy composite nuclei in a time interval between 10^{-20} and 10^{-16} s.

The method considered is based on an atomic process: during the compound nucleus formation K-vacancies of the united atoms are produced which have lifetimes of 10^{-18}-10^{-17} s for $Z_c \approx 100$. Thus a monoenergetic x-ray characteristic for the compound nucleus can be observed in coincidence with fission fragments if the lifetime of the compound nucleus is longer than 10^{-18}-10^{-17}s. The experimental set-up consists in a position sensitive ring counter positioned at forward angles for the detection of both fission fragments in coincidence with the x-rays to be detected in a Ge-ring counter at backward angles.

Up to now we have performed a survey experiment in order to choose the best conditions concerning bombarding energy and target-projectile combination to be selected for the final experiment. A Pb beam of 4.8, 5.0, 5.2, 5.9, and 6.5 MeV/u was used to bombard targets of ^{26}Mg, ^{27}Al, ^{48}Ca, ^{50}Ti and ^{64}Ni. The cross section for the symmetric mass fragmentation has been extracted under the assumption of an in-plane isotropic angular distribution ($d\sigma/d\Omega \approx 1/\sin\Theta$) and is plotted in fig. 1 as a function of excitation energy in the compound nucleus. In addition the average

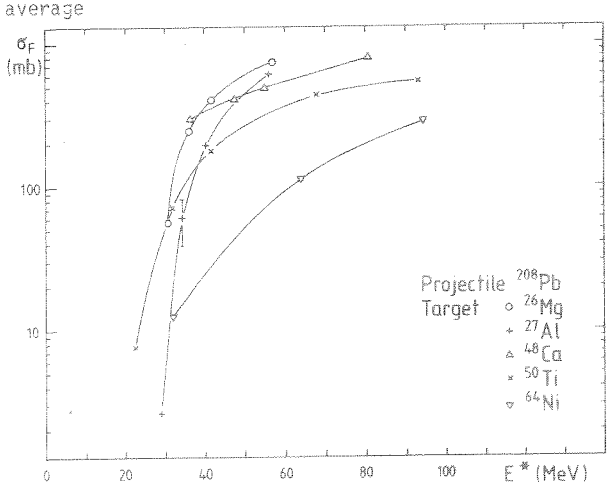


Fig. 1

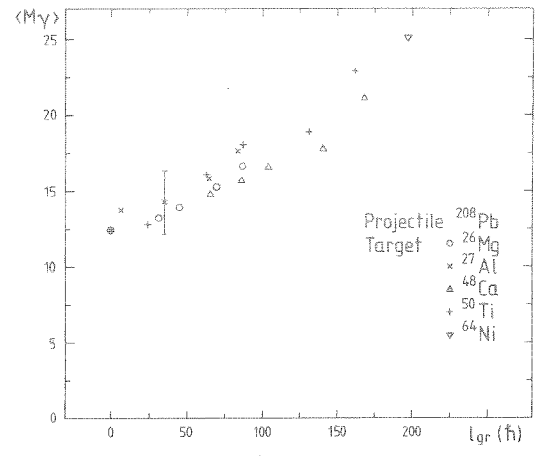


Fig. 2

gamma-multiplicity <Mγ> of the symmetric mass distribution was also measured using a 4" x 5.5" NaJ crystal. The results for <Mγ> are shown in fig. 2 as a function of the calculated grazing angular momentum of the ingoing channel. From the data of fig. 1 and 2, the $^{208}Pb+^{48}Ca$ reaction at sub-Coulomb energies displays the best conditions for the x-ray coincidence experiment since: (i) large cross sections are observed at relatively low excitation energies in the compound nucleus, (ii) the average number of gamma-rays emitted per fission-event (which is a measure of the background limiting the observation of a peak in the x-ray spectrum) is small and (iii) the K-vacancy production increases with the symmetry of the system and therefore Pb+Ca is preferable as compared to Pb+Mg (or Al). From the measured multiplicity one can estimate that an x-ray peak can be observed if more than 1 % of the composite system leading to a symmetric fragmentation lives longer than 10^{-18}-10^{-17} s.

*Alexander von Humboldt-Fellow, on leave from Institute of Modern Physics, Academia Sinica, Lanshow, China.

Study of the fusion cross section in the system $^{40}Ar + ^{40}Ca$ [B]

F. Beck, H. Feldmeier, H. Genz, M. Mutterer, A. Richter, G. Schrieder, J.P. Theobald and P. Wastyn
Institut für Kernphysik, Technische Hochschule Darmstadt

Cross sections for elastic[1], quasi-elastic and deep inelastic scattering[2] of ^{40}Ar projectiles on ^{40}Ca target nuclei have been measured at incident energies E_{Lab} = 191, 236 and 272 MeV. We report here about fusion cross sections extracted from these measurements with help of the relation

$$\sigma_R \cong \sigma_{DIC} + \sigma_{FF} + \sigma_{ER} + \sigma_{QE}, \qquad (1)$$

where σ_R is the reaction cross section and σ_{DIC} the cross section for the production of deep inelastic fragments. The sum of the cross section for fusion-fission products σ_{FF} and that for the production of evaporation residues σ_{ER} is equal to the fusion cross section σ_F. The quantity σ_{QE} denotes the cross section for quasi-elastic scattering.

The various cross sections in eq. (1) were obtained the following way:

(i) Elastic scattering. The comparison of experimental angular distributions with model calculations gives values for σ_R. The description of the data with help of the generalized Fresnel model (GFM) is of equal quality as that obtained in an optical model (OM) analysis. The corresponding values for σ_R obtained with these two models (σ_R^{GFM} and σ_R^{OM}) agree within 2%.

(ii) Quasi-elastic scattering. In all measurements at the three incident energies the cross section for the production of quasi-elastic events with a transfer of at least one charge unit was found to be smaller than 1 mb. For this reason σ_{QE} can be neglected in eq. (1).

(iii) Deep inelastic scattering. In the mass symmetric system $^{40}Ar + ^{40}Ca$ it is impossible (only on the basis of the fragment charge) to distinguish between deep inelastic and fusion-fission components in the measured cross section σ_{EXP}. Since (for technical reasons) data points at detection angles smaller than 10° could not be obtained, the following equation holds

$$\sigma_{EXP} < \sigma_{DIC} + \sigma_{FF}. \qquad (2)$$

With the help of eqs. (1) und (2), it is now possible to calculate upper limits for σ_{ER}, which are shown in the following table and figure. The most pronounced feature is the strongly decreasing σ_{ER} with increasing incident energy. A similar behaviour was observed[3] in the analogous system $^{40}Ca + ^{40}Ca$. The results of a calculation for the fusion cross section σ_F^{WF} in a one-body window-friction model[4] using a relaxed density proximity potential, which is describing the deep inelastic scattering data very well[1], and with inclusion of a neck formation, are shown in the table and on the figure. The main discrepancy found at the highest incident energy can be explained by a possible fusion-fission component. To evaluate this quantity and to study the exact energy dependence of σ_{ER}, we are planning direct measurements of σ_{ER} at different incident energies.

Table: Various cross sections used in eqs. (1) and (2)

E_{Lab}/MeV	σ_R^{OM}/mb	σ_{EXP}/mb	σ_{ER}/mb	σ_F^{WF}/mb
191	1736	609	< 1127	1327
236	2038	408	< 1630	1177
272	2202	2038	< 164	1021

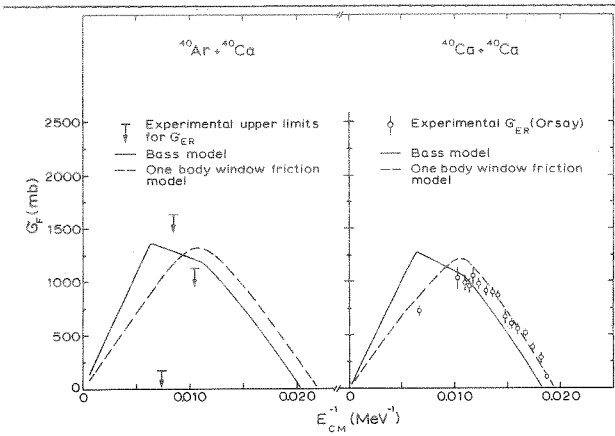


Figure: Energy dependence of the fusion cross section for the systems ^{40}Ar, ^{40}Ca on ^{40}Ca.

[1] P. Wastyn, H. Genz, M. Mutterer, A. Richter, G. Schrieder, J.C. van Staden and J.P. Theobald, Nucl. Phys. A320 (1979) 433.

[2] P. Wastyn, H. Feldmeier, F. Beck, M. Dworzecka, H. Genz, M. Mutterer, A. Richter, G. Schrieder and J.P. Theobald, Nucl. Phys. A332 (1979) 455.

[3] H. Doubre, A. Gamp, J.C. Jacmart, N. Poffé, J.C. Roynette and J. Wilczyński, Phys. Lett. 73B (1978) 135.

[4] F. Beck, J. Blocki, M. Dworzecka and G. Wolschin, Phys. Lett. 76B (1978) 35;

F. Beck, M. Dworzecka and H. Feldmeier, Z. Phys. A289 (1978) 113.

Evaporation residue cross sections at bombarding energies between 4.7 and 12 MeV/u [B]

B.Kohlmeyer,D.Bangert, F. Busch, F.Pühlhofer, Fachbereich Physik der Philipps-Universität Marburg*

W.Schneider, H. Freiesleben, GSI Darmstadt

In order to investigate the influence of pre-compound emission on the fusion probability total evaporation residue (ER) cross sections have been measured for various systems using beams between 4.7 and 12 MeV/u energy (tab.1). The ER were detected at forward angles between θ_{LAB}=1.5°and θ_{LAB}=12°(Fig.1)using the time-of-flight ΔE-E telescope at beam line Z3.

System	E(MeV/u)	CN	σ_{ER}(mb)	l_{ER}(ħ)
$^{58}Ni+^{12}C$	4.9	^{70}Se	1040	27
$^{46}Ti+^{24}Mg$	4.7	^{70}Se	1043	42
$^{46}Ti+^{24}Mg$	5.8	^{70}Se	983	45
$^{46}Ti+^{24}Mg$	8.5	^{70}Se	909	53
$^{46}Ti+^{26}Mg$	5.8	^{72}Se	1030	49
$^{48}Ti+^{24}Mg$	12.0	^{72}Se	801	60
$^{50}Ti+^{24}Mg$	5.9	^{74}Se	1040	48
$^{50}Ti+^{26}Mg$	5.9	^{76}Se	1078	52
$^{46}Ti+^{40}Ca$	8.5	^{86}Mo	670	62
$^{48}Ti+^{45}Sc$	12.0	^{93}Tc	656	79
$^{84}Kr+^{27}Al$	5.9	^{111}In	1070	62

Tab.1: Experimental ER cross sections σ_{ER}(± 7%) and corresponding angular momenta l_{ER}(± 4%).

Some of the measured ER cross sections are shown in Fig.2 leading to the excitation function of $^{46}Ti+^{24}Mg$ and $^{48}Ti+^{45}Sc$.It is seen from the two systems that σ_{ER} decreases with increasing energy,as is expected for the high-energy region of fusion excitation functions.The data are compared with theoretical predictions.The full curves indicate the total fusion cross sections σ_{CN} obtained from a trajectory calculation based on the proximity potential.The fission competition can be roughly estimated from the condition B_f=8 MeV.In order to adjust it more accurately calculations with the code ALICE were performed.The parameters in these calculations,the average amount of angular momentum removed by evaporated particles and the factor with which the liquid-drop fission barrier (B_f) has to be multiplied,were determined by fitting the ER mass distributions and cross sections.A constant amount of 0.8ħ/nucleon was found for all systems and energies.In the range of 4.7 to 6 MeV/u the experimental σ_{ER} would require a value of $0.6 \cdot B_f$,which is consistent with values found by Beckerman and Blann.It is remarkable to note that at the highest energies the measured σ_{ER} exceed these theoretical limits,in the case of $^{48}Ti+^{45}Sc$ even the l-value at which the fission barrier is assumed to vanish.

The relatively high values of the experimental ER cross sections are to be interpreted as a consequence of pre-equilibrium decays.Particle emission before complete fusion reduces the angular momentum in the system,which allow higher partial waves to contribute to fusion.Evidence for pre-equilibrium α-emission is also found in the mass distributions of the evaporation resid.

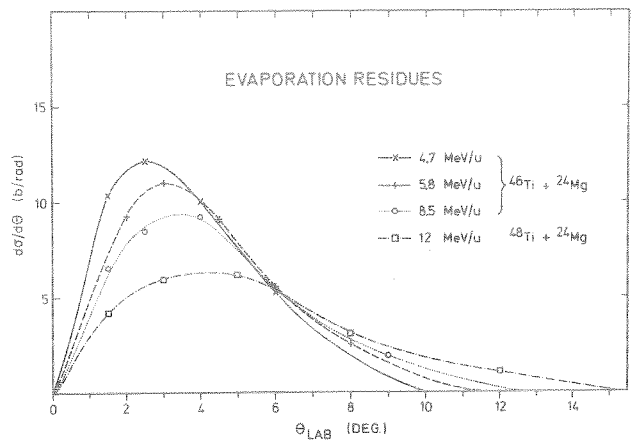


Fig.1: Experimental angular distributions of ER's for Ti+Mg.Due to the increasing number of α-particles the angular distributions shift to larger angles as the bombarding energy increases from 4.7 to 12 MeV/u.

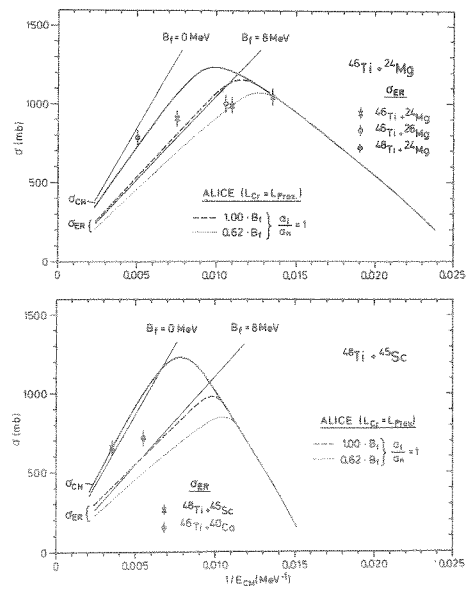


Fig.2: Excitation functions for $^{46}Ti+^{24}Mg$ and $^{48}Ti+^{45}Sc$.

Influence of the shell structure of the colliding nuclei on the energy and charge distributions in dissipative collisions

M. Dakowski, P. Doll, A. Gobbi, G. Rudolf, H. Sann, R. Bock, U. Lynen and A. Olmi
GSI Darmstadt and MPI Heidelberg

An ansatz representing a generalization of the one body recoil formula is proposed on the basis of the TKEL vs. σ^2_Z correlation systematics observed in collisions between very heavy nuclei. The predictions of calculations based on the one-body friction models have been seen to systematically underestimate the observed energy loss. The deviations are largest for low bombarding energies and for closed-shell nuclei. On the basis of these observations we propose a new ansatz which contains, besides the "one body" term E^*/μ depending on the relative velocity, an additive term DE depending on the excitation energy and on the nuclear structure of the nuclei involved:

$$-dE/d(\sigma^2) = E^*/\mu + DE(TKEL) \qquad \text{Eq. 1}$$

where:
$E^* = TKE - V$ is the available kinetic energy at each instant, V is the Coulomb potential energy of two touching spheres with initial masses, the nucleon mass is set to 1, and μ is the reduced mass of the system.

For simplicity we use the relation: $\sigma^2_A = (A/Z)^2 \cdot \sigma^2_Z$ between the measured σ^2_Z value and the deduced σ^2_A. The ansatz of Eq. 1 was verified for the system Kr-Er at three bombarding energies (6.0, 7.2 and 8.2 MeV/u). The derived histogram DE (TKEL) is, within the experimental uncertainties, the same for the three different bombarding energies. The dependence of the structure energy DE on the system is presented in fig. 1.

The DE values for the lowest TKEL bins, where the nuclei are not strongly excited, are called DE_0 (see fig. 1).

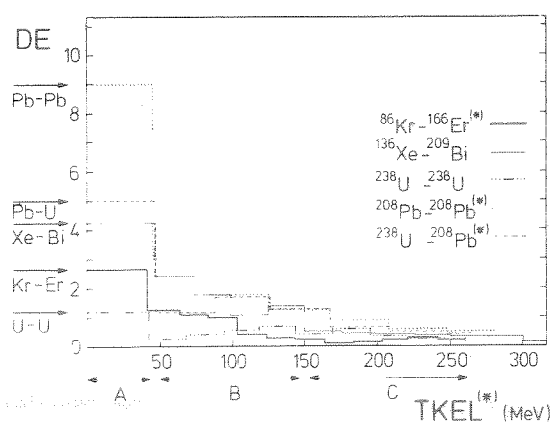


Fig. 1 Comparison of DE curves for different systems. The arrows on the ordinate show the position of DE values normalized to 5-45 MeV bins in the energy-loss.

As the "structure quantity" we consider the mean values of Q for two neutron and two proton transfers from target to projectile Q(1),Q(2) and vice versa Q(3),Q(4):

$$dS = \sum_i \frac{1}{4} Q^i_{gg} \qquad \text{Eq. 2}$$

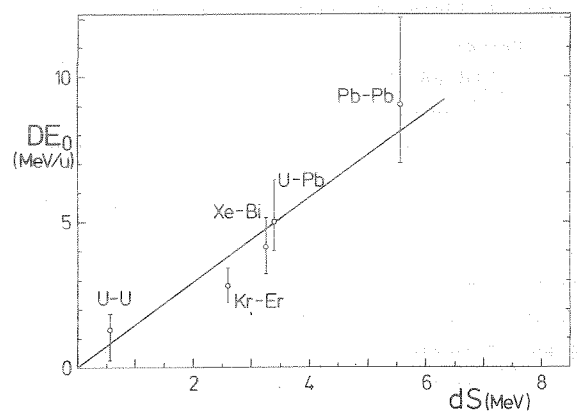


Fig. 2 Correlation between the DE values and dS. The line is to guide the eye.

Concluding, the presented ansatz is based on the separation of the rate of energy loss per exchange into two terms: one depending on the relative velocity and one depending on the dissipated energy. For small energy losses the dissipated energy depends strongly on the stiffness of the initial nuclei.

The ansatz is interpreted in terms of a direct reaction, where the identity of target and projectile is dissolved via both the pure inelastic and the nucleon exchange channel. The exchange between closed shell nuclei is restricted to the unpopulated higher orbits, what strongly increases the rate of energy loss per nucleon exchange. More details are presented in ref. 2.

[1] J. Blocki, Y. Boneh, J.R. Nix, J. Randrup, M. Robel, A.J. Sierk and W.J. Swiatecki, Annals of Phys., 113 (1978) 330

[2] M. Dakowski, P. Doll, A. Gobbi, G. Rudolf, H. Sann, R. Bock, U. Lynen, and A. Olmi, Phys. Lett. 90B (1980) No. 4.

Shell effects in the deep inelastic reaction ^{154}Sm on ^{154}Sm

E.C. Wu*, K.D. Hildenbrand, H. Freiesleben, A. Gobbi, U. Lynen", A. Olmi", H. Sann
GSI Darmstadt, "MPI Heidelberg, *A.v.H.-Fellow, on leave from IMP, Academia Sinica, Lanchow, China

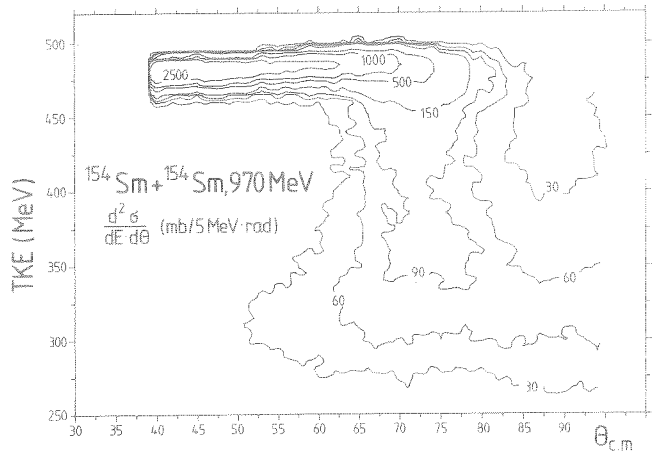
The reaction ^{154}Sm on ^{154}Sm has been studied at 6.3 MeV/u. The experiment, the motivation of which was discussed already in the last annual report[1], was carried out with two large double ionization chambers of 20^{o} acceptance angle at opposite sides of the beam direction, measuring ΔE, E and the scattering angle. Two parallel plate counters for timing masked one half of each chamber. Primary masses have been calculated from the relative time-of-flight and the scattering angle of two coincident binary fragments. The mass resolution obtained by this method was about 4 units (FWHM), the Z-resolution was 1.6 units.

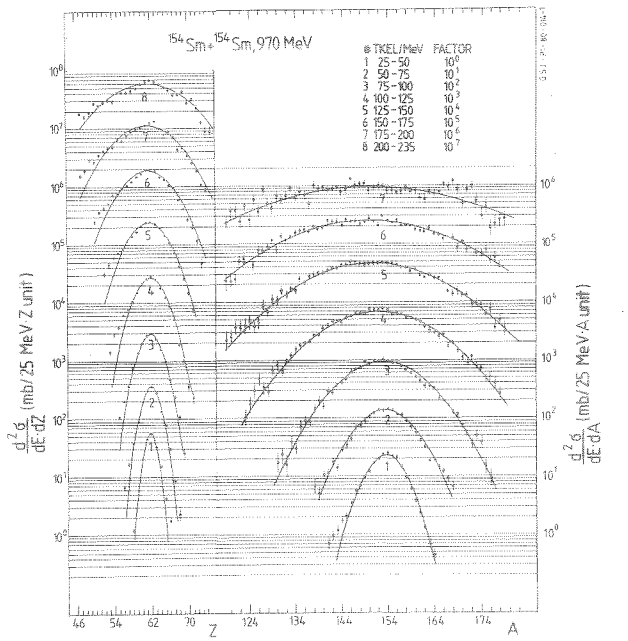
Fig. 1 displays the Wilczynski-plot of the reaction; it shows a well-focused deep inelastic component centered between 70^{o} and 75^{o} independent of kinetic energy loss, exhibiting a balanced influence between repulsive Coulomb and attractive nuclear forces. Fig. 2 shows the double-differential cross-sections $d^2\sigma/dE\cdot dZ$ and $d^2\sigma/dE\cdot dA$ for various bins of energy loss with least-square-fitted Gaussians. The corresponding variances σ_Z^2 and σ_A^2 are plotted in fig. 3 as function of the energy loss. σ_Z^2 exhibits a slope in the origin comparable to the Kr-Er system[2], but a factor of 2 smaller than in U+U-reaction. The mass variances, however, are surprisingly large (note the different scales in the figure). Below a TKEL of 125 MeV, the ratio σ_A^2/σ_Z^2 is constant (11.5 ± 1.0), a value significantly larger than $(A/Z)^2$=6.2 of the compound system.

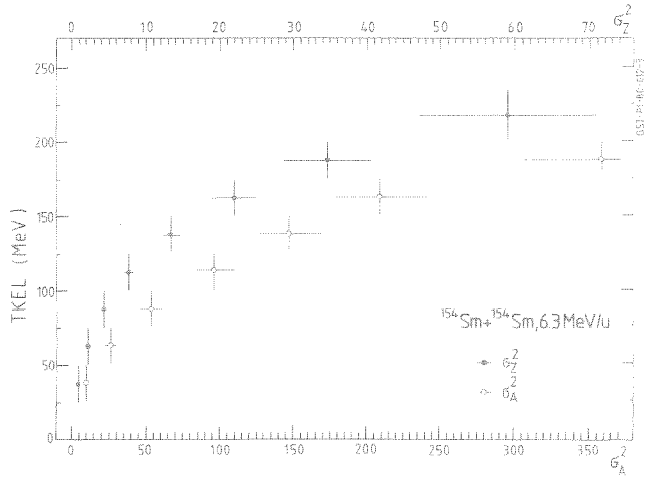
The rather large value may be explained by the Potential Energy Surface (PES) of the system: The experimental maximum reaction yields in the N-Z plane follow exactly the path of minimum potential in the PES. By means of an enhanced neutron transfer the system obviously tries to reach the N=82 shell as quickly as possible. The square of the large gradient $\Delta A/\Delta Z$=3.5 ($\Delta N/\Delta Z$ =2.5) in that region determines the ratio of mass and charge variances. Beyond the N=82 shell - a region only reached at high energy losses - the experimental gradient approaches the A/Z=2.48 of the combined system. But even in this case the ratio σ_A^2/σ_Z^2 is determined by the larger gradient near the injection point (A=154, Z=62) where the distributions are peaked because of the absence of any drift.

Therefore for energy losses up to 200 MeV the evolution of the deep inelastic component is determined by the PES. The ratio of mass and charge variances consequently reflects the shell structure in the vicinity of the starting point rather than the occurence of correlated or uncorrelated nucleon transfer.

[1] K.D. Hildenbrand et al., GSI-Jahresbericht 1979, p. 22
[2] G. Rudolf et al., Nucl. Physics A 330 (1979) 243







The significance of rolling friction in classical trajectory calculations

D.Bangert
Fachbereich Physik, Universität Marburg

H. Freiesleben
GSI Darmstadt und Institut für Experimentalphysik, Ruhr-Universität Bochum

Classical trajectory calculations with inclusion of friction as a method to consistently describe fusion and deep inelastic reactions have been performed. All trajectory calculations published so far utilize among a variety of different assumptions on potentials and dissipative forces one common supposition. It is argued that the friction force against rolling of the two nuclei around each other is negligible [1]. However, this kind of friction is necessary to prevent the unphysical case of rolling, where two unequal nuclei roll around each other undisturbedly. It adjusts the different angular velocities of the two reaction partners and finally enforces the sticking situation, where both nuclei rotate as a rigid dinuclear complex.

Hence, our objective was to study the influence of this additional dissipative force treating its strength as a free parameter. Details of the calculations can be found in ref.2.

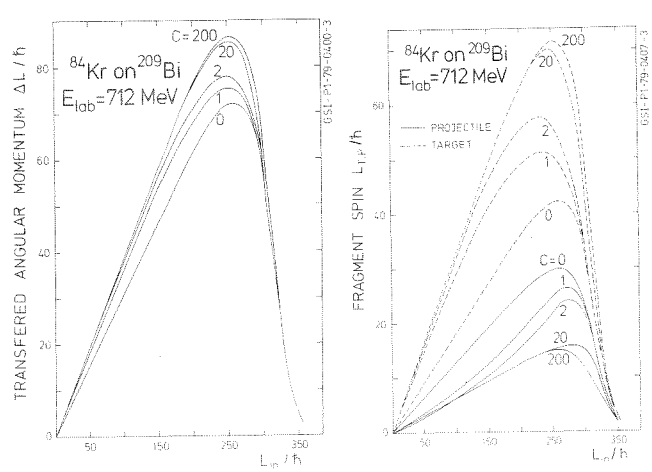


Fig. 1. Left frame: angular momentum, ΔL, transfered to the two fragments as function of entrance channel angular momentum.
Right frame: angular momentum sharing between the two fragments as function of entrance channel angular momentum.

Fig. 1 depicts the effect of the strength factor c of the friction against rolling on the angular momentum transfer ΔL and on the sharing of ΔL by the two outgoing fragments as function of incident angular momentum. The amount of dissipated angular momentum ΔL increases with increasing friction against rolling.

Another important quantity in trajectory calculations is the maximal partial wave, L_{cr}, which is trapped in the potential. This L_{cr} is often refered to as the critical angular momentum leading to fusion. Its dependence on the strength parameter c is shown in Fig. 2 for the $^{40}Ar + ^{208}Pb$-system. This leads to sizeable differences in the fusion cross section which can be operationally defined as $\sigma_F \sim L_{cr}^2$. Hence the incorporation of friction against rolling in trajectory calculations is essential and should not be neglected, since it determines the whole reaction dynamics.

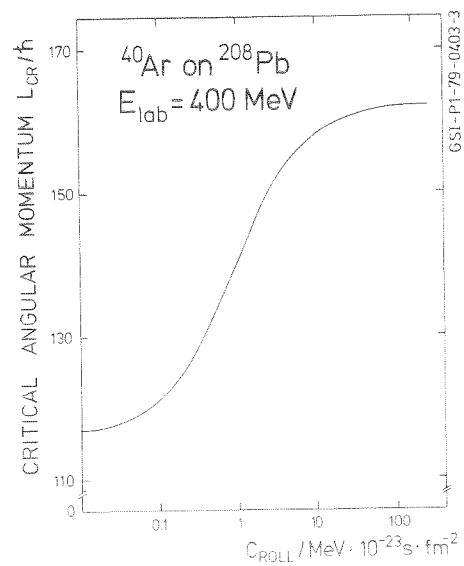


Fig. 2. Critical angular momentum L_{cr} as function of the strength factor c for friction against rolling.

[1] C. F. Tsang, Phys. Scr. 10A(1974)90

[2] D. Bangert, H. Freiesleben to be published in Nucl. Phys.

Entrance Channel Effects in Dissipative Heavy Ion Reactions [B]

H. Essel, K. Hartel, P. Kienle, H.J. Körner, K.E. Rehm, P. Sperr, and W. Wagner
Physik-Department, TU-München

Entrance channel effects on the charge and mass transfer in dissipative heavy ion reactions were investigated at incident energies close to the Coulomb barrier. Various targets between ^{94}Zr and ^{170}Er were bombarded with 6.27 MeV/u ^{208}Pb ions. The four-fold differential cross section $d^4\sigma/d\Omega dMdZdE$) was determined from the angular distribution of the target-like fragments measured with a Si detector ΔE-E time-of-flight telescope. The mass-charge distribution of the reaction products is spread out along the bottom of the mass valley; its width increases with increasing energy transfer. Thus a correlated exchange of protons and neutrons takes place, with an N/Z ratio corresponding to that of the Fermi surface of the interacting nuclei. Fig. 1 shows the variances of the charge (σ_Z^2) and the mass distribution (σ_A^2) as function of the energy transfer (TKEL). They exhibit a strong dependence on the entrance channel. The ^{208}Pb + ^{110}Pd system studied at 1280 MeV incident energy shows the largest values of σ_Z^2 and σ_A^2, respectively, for a given TKEL, even larger than the U-U case (Hildenbrand et al.[1]) which was considered to be anomalous as compared with those system investigated by Huizenga et al.[2]. The origin of this effect which is quite interesting for the synthesis of heavy elements is not yet understood. It was suggested that it may be related to the large deformability of Pd nuclei, as evidenced by exceptional soft surface vibrational modes.

A second interesting entrance channel effect is deduced from the bombarding energy dependence: When the incident energy is lowered from 6.27 MeV/u to 5.90 MeV/u the variance of the charge distribution is reduced by a factor two whereas the width of the mass distribution remains unaffected. This means that the reduced width of the charge distribution is compensated by an enhanced neutron transfer at the lower bombarding energy. This may be the first indication of the importance of pair correlations for the neutron transfer matrix elements at incident energies close to the Coulomb barrier.

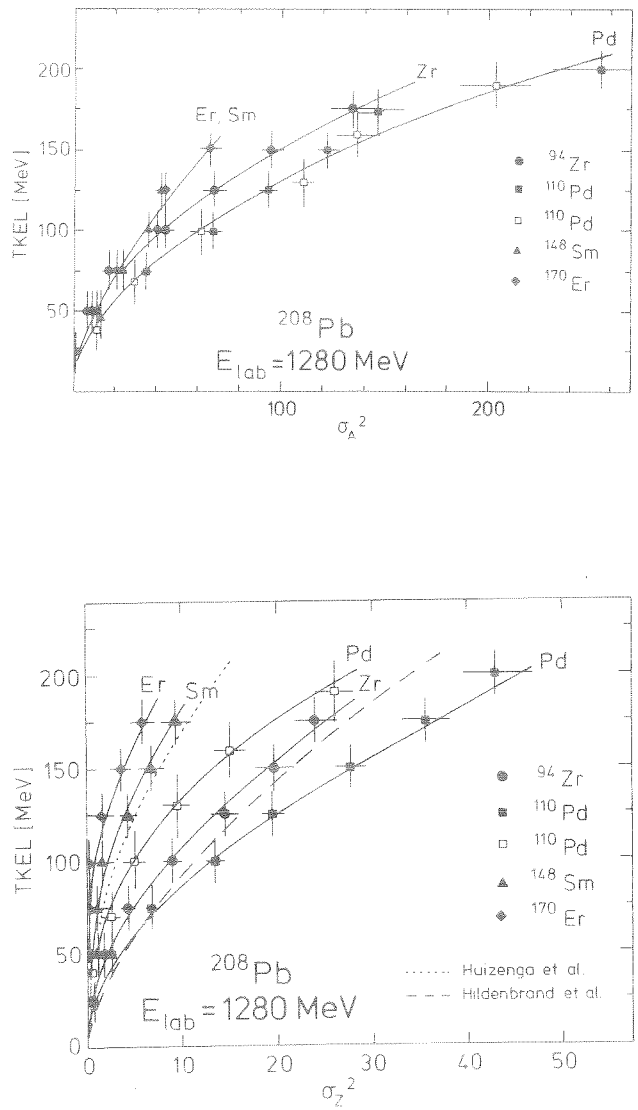


Fig. 1: Variances σ^2 of the mass and charge distributions as function of the energy loss (TKEL) for different systems. The open symbols correspond to an incident energy of 5.9 MeV/A.

[1] K.D. Hildenbrand et al., Phys. Rev. Lett. 39, 1065 (1977).

[2] J.P. Huizenga et al., Phys. Rev. Lett. 37, 885 (1976).

Observation of inertia effects in dissipative heavy ion reactions [B]

H. Essel, K. Hartel, P. Kienle, H.J. Körner, K.E. Rehm, P. Sperr, and W. Wagner
Physik-Department, TU-München

The investigation of deep inelastic collisions allows to study the time evolution of macroscopic quantities (energy, angular momentum, mass and charge exchange and the corresponding variances) in the time range 10^{-22} - 10^{-20} sec. At energies well above the Coulomb barrier the variances of the mass and charge distributions show a linear increase with interaction time, which is typical for diffusive phenomena. In contrast, at incident energies close to the Coulomb barrier we observe a nonlinear time dependence of the variances σ_A^2 and σ_Z^2 as shown in Fig. 1 for the system ^{208}Pb + ^{94}Zr at 6.27 MeV/nucleon. Such a behaviour is characteristic for the transition in a weakly damped system from an inertial to a diffusive motion. The solid lines in Fig. 1 are the result of theoretical calculations using Langevins theory for Brownian motion [1]. In this model the exchange of particles at short interaction times is governed by the transfer rates for mass, $\dot{A}_o$, and charge, $\dot{Z}_o$, respectively, which were found to depend on the structure of the interacting nuclei. The duration of this phase until diffusion processes set in, is of the order of 10^{-21} sec and is determined by the ratio of the inertia and the friction coefficients. For longer interaction times σ^2 shows a linear time dependence which allows to extract the relevant diffusion coefficients. The results for these parameters are summarized in Fig. 2, which shows that the large widths observed for mass and charge distribution for the system ^{208}Pb + ^{110}Pd are due a large transfer rate in the initial phase of the reaction. The calculations have also been extended to the angular and energy transfer in deep inelastic collisions.

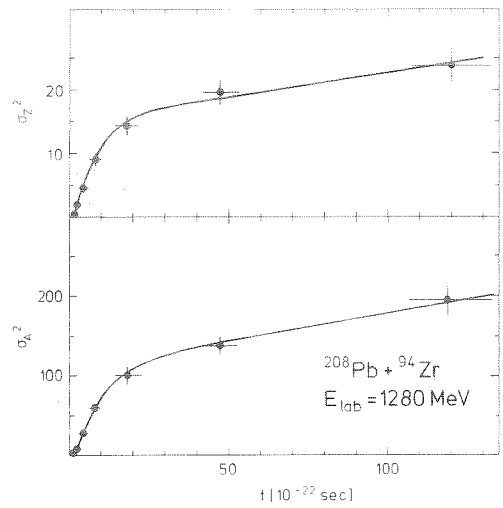


Fig. 1: Variances σ_A^2 and σ_Z^2 for mass and charge exchange, respectively as function of the interaction time for the system ^{208}Pb + ^{94}Zr

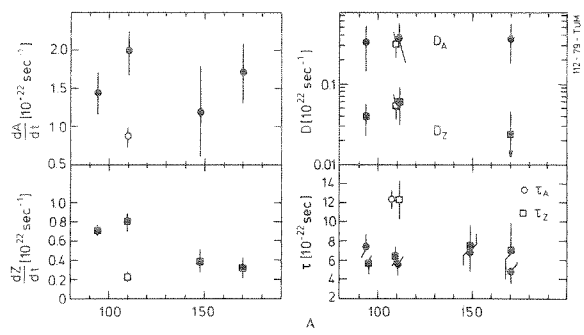


Fig. 2: Initial transfer rate $\dot{A}_o$ and $\dot{Z}_o$, relaxation time τ and diffusion coefficients D_A and D_Z obtained from ^{208}Pb induced reactions on ^{94}Zr, ^{110}Pd, ^{148}Sm and ^{170}Er at 6.27 MeV/N. The open symbols correspond to an incident energy of 5.9 MeV/N.

[1] K.E. Rehm et al., Phys. Lett. 86B, 256 (1979)

Mass and Charge Exchange in the Reactions $^{112}Sn + ^{208}Pb$ and $^{124}Sn + ^{208}Pb$ [B]

G.Beier, H.C.Britt, H.Essel, K.Hartel, H.Hopf, P.Kienle, H.J.Körner, W.Mayer, K.E.Rehm, P.Sperr, W.Wagner
Physik-Department, TU-München

As an extension of our studies on entrance channel effects in deeply inelastic collisions at incident energies close to the Coulomb barrier we have investigated the systems $^{208}Pb + ^{112,124}Sn$ at 6.27 MeV/u incident energy. These are similar to the $^{208}Pb + ^{110}Pd$ system which showed the largest mass and charge exchange observed in previous experiments. Furthermore we wanted to investigate whether the transfer of nucleons in deeply inelastic collisions is influenced by the neutron number of the target nucleus. Fig. 1 shows contour plots for the M - Z distributions obtained for energy losses exceeding 100 MeV in the systems $^{208}Pb + ^{112}Sn$ and $^{208}Pb + ^{124}Sn$. The reaction with the neutron-rich ^{124}Sn shows a considerably broader M - Z distribution. Fig. 2 shows the relation between the total kinetic energy loss (TKEL) and the variances σ_A^2 and σ_Z^2 for charge and mass exchange, respectively. We observe that the $^{208}Pb + ^{124}Sn$ system has the larger width, both in mass and charge exchange, for a given TKEL. The comparison with other systems reveals that the $^{208}Pb + ^{124}Sn$ data are similar to those for the $^{208}Pb + ^{94}Zr$ system which also has a closed proton shell in the projectile and the target. These variances are, however, smaller than for the $^{208}Pb + ^{110}Pd$ system. Thus neutrons near the Fermi surface do play an important role in the nucleon transfer process but other degrees of freedom like β- and γ stability of the potential energy surface appear to be of influence.

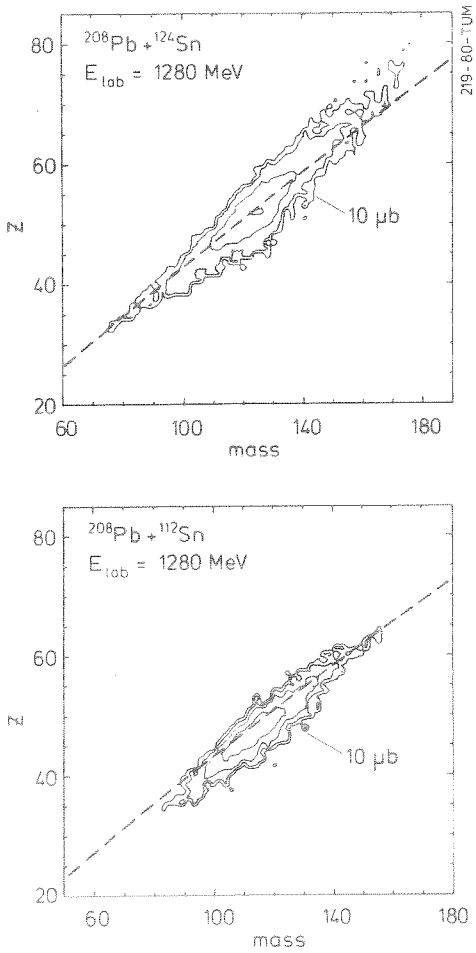


Fig. 1: Contourplots for the M-Z-distributions obtained in the reactions $^{208}Pb + ^{112}Sn$ and ^{124}Sn for energy losses exceeding 100 MeV.

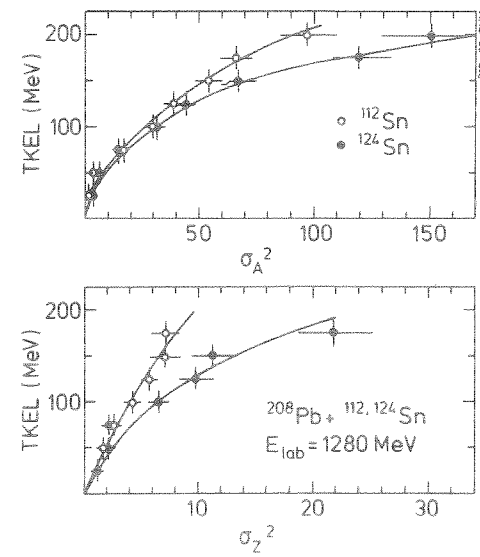


Fig. 2: TKEL as function of the variances σ_A^2 and σ_Z^2 for mass and charge exchange, respectively, observed in the reactions $^{208}Pb + ^{112,124}Sn$.

Investigation of the reaction mechanism for the systems $^{208}Pb + ^{94}Zr$ and $^{208}Pb + ^{64}Ni$ at E_{LAB} = 1280 MeV [B]

G.Beier, H.C.Britt, K.Hartel, H.Hopf, P.Kienle, H.J.Körner, W.Mayer, K.E.Rehm, P.Sperr, W.Wagner
Physik-Department, TU-München

We have studied the binary reaction mode in ^{208}Pb induced reactions on ^{64}Ni and ^{94}Zr target nuclei at energies close to the Coulomb barrier. The outgoing target-like fragments were detected by means of a ΔE-E time-of-flight telescope. The correlated projectile-like ejectiles were detected in coincidence with a position sensitive parallel plate avalanche counter, covering an angular range from 15° to 45°. With the time-of-flight difference method the mass and TKEL of the correlated projectile-like fragments could be determined independently. Three-fold overdetermination of the system together with double-readout of the position- and time signals of the PPAC allowed the elimination of sequential fission processes, target contamination and accidentals, and confirmed the binary character of the reaction. Fig. 1 and 2 show contour plots of the mass versus TKEL in the reaction $^{208}Pb + ^{94}Zr$ obtained $_{LAB}$ = 35° for the TOF-telescope. From the distribution in the time-of-flight telescope (Fig.1) we expect that at this angle 25 nucleons should be transferred from Zr to Pb. The independend measurement of the mass of the correlated particles (Fig.2) shows that nuclei with masses up to 232 are observed, which do not decay by sequentical fission.

The system $^{208}Pb + ^{64}Ni$ shows a totally different behaviour. The very broad mass distribution which is spread symmetrically between the projectile and the target mass together with the nearly isotopic angular distribution of the fragments in the center of mass system indicates a fission like splitting of the relatively long lived composite system formed in the reaction $^{208}Pb + ^{64}Ni$. Fig. 3 shows a M - Z distribution obtained with the time-of-flight telescope at 20°. The highest detected mass is determined by kinematic cut off.

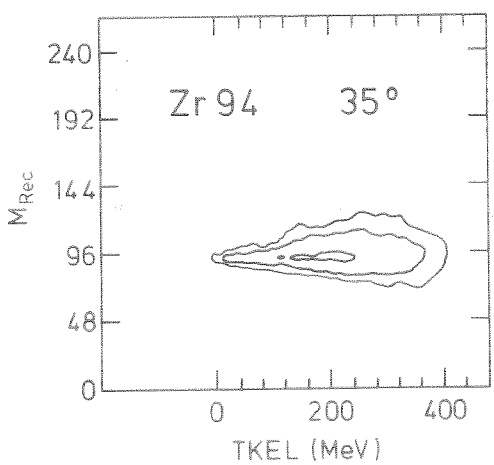


Fig. 1: Mass-TKEL distribution for the target-like particles, detected in the TOF-telescope.

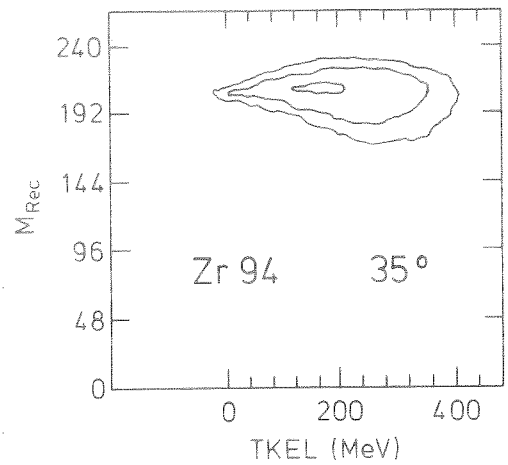


Fig. 2: Mass-TKEL distribution for the projectile-like particles, determined by the method of kinematic coincidences.

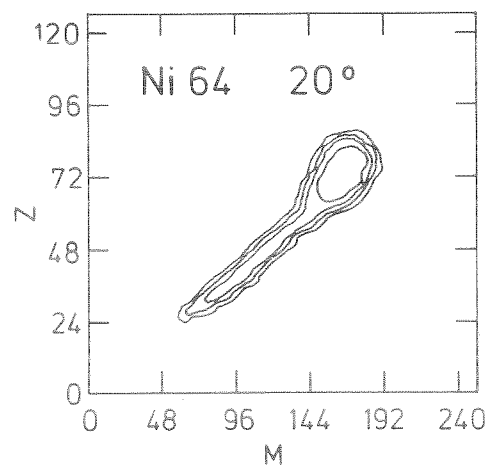


Fig. 3: Mass-charge-distribution for the system $^{208}Pb + ^{64}Ni$ as observed in the TOF-telescope at 20 degree.

Study of charge- and mass-transfer in quasielastic collisions[B]

D. Schüll, W.C. Shen*, H. Freiesleben
GSI Darmstadt, *on leave from IMP, Academia Sinica, Lanchow
D. Bangert, F. Busch, W. Pfeffer, F. Pühlhofer
Fachbereich Physik, Universität Marburg

During the initial phase of dissipative heavy-ion collisions the equilibration of the neutron excess mode, accompanied by some amount of energy dissipation, is the dominating process. It is known that the N/Z-ratio relaxes very quickly to a value, which minimizes the potential energy of the combined system. However, little is known about details of the interaction mechanism in the initial phase, in particular about the path on which the system reaches equilibrium, since previous experiments suffered from insufficient resolution in Z, A and energy.

Using our magnetic spectrometer[1] we studied quasielastic and deep inelastic reactions in the systems ^{129}Xe, ^{136}Xe + ^{56}Fe and ^{129}Xe + ^{116,124}Sn. The good mass- and Z-resolution obtained allows unique identification of the reaction products. Distributions of the Xe-like fragments could be measured as function of total excitation energy with an energy resolution of 5-10 MeV.

Fig. 1 shows a contour plot of the potential energy surface (PES) of the combined system ^{136}Xe on ^{56}Fe in the N-Z plane of the Xe-like products. In addition, the centroids of the measured N,Z-distributions are given (+). They start at the elastic channel and follow the gradient of the PES with increasing excitation energy. When the local minimum is reached the path bends towards mass symmetry. The deviation from the bottom of the PES-valley at higher excitation energies is due to evaporation of neutrons from the primary fragments. The secondary mass yields have to be corrected iteratively for sequential neutron emission (o).

While for low excitation energies single nucleon transfer channels are dominating, σ_Z^2 and σ_N^2 rise rapidly with increasing energy. It is found that a quantity $\sigma_\perp$ which characterizes the width of the distribution perpendicular to the slope of the PES-valley saturates at about 30 MeV energy loss, while $\sigma_\parallel$ along the valley increases further. Because of the (system dependent) slope of the PES-valley in the N-Z plane and the observed drift into different directions according to the PES gradient σ_Z^2 and σ_N^2 are correlated. Therefore neither σ_Z^2 integrated over all masses nor σ_Z^2 or σ_A^2 for fixed A or Z can be adequate parameters for the comparison of different systems.

The strong correlation of σ_Z^2 and σ_N^2 can also be inferred from fig. 2 where the fragment distribution for the nearly symmetric system ^{129}Xe on ^{124}Sn is shown. In this case the drifts are very small. But as can be seen qualitatively in the first steps transfer of neutrons is favoured in comparison with proton transfer which could be explained by the closed proton shell of the target nucleus or by a hindering by the Coulomb barrier[2]. With increasing excitation energy the distribution gets broader, rotates and follows the shape of the PES. A detailed analysis of the data and reconstruction of primary mass yields is under way.

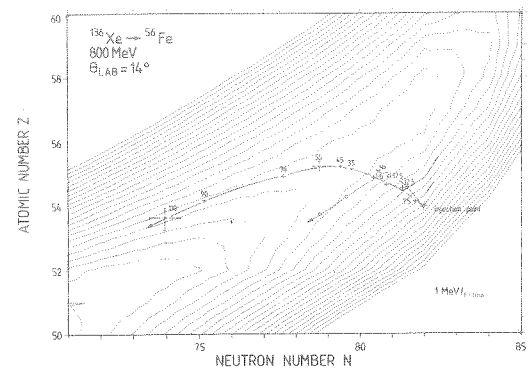


Fig. 1: Potential energy surface of the combined system
+ first moments of measured fragment distributions for marked total excitation energy
o corrected for neutron evaporation

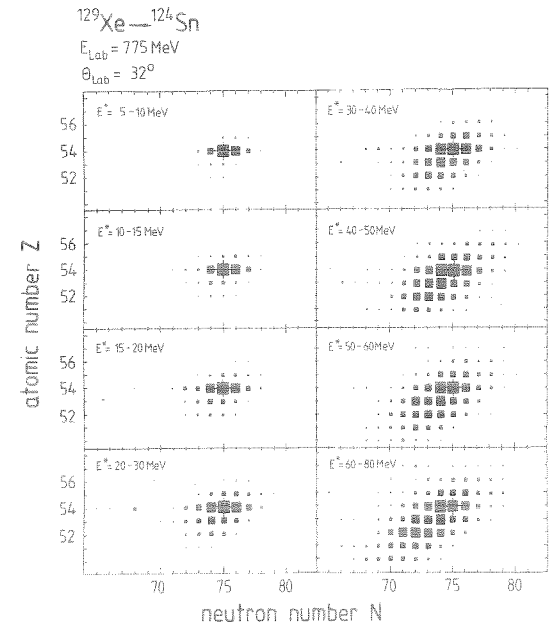


Fig. 2: Measured fragment yield of Xe-like products for different total excitation energy bins (normalized).

[1] F. Busch, W. Pfeffer, F. Pühlhofer, D. Schüll, this report and GSI annual report 1978, p. 165

[2] U. Brosa and D.H.E. Gross, to be published.

Scattering of ^{40}Ar from ^{208}Pb [B]

U.Arlt, R.Bass, V.Hartmann, H.Noll, R.Renfordt+, K.Sapotta
Institut für Kernphysik der Universität Frankfurt am Main
P. Fröbrich
Hahn-Meitner-Institut und Freie Universität Berlin

The investigation of the system $^{40}Ar+^{208}Pb(5.9\ MeV/u)$[1] was completed. One point of interest was the analysis of the elastic scattering and the comparison of the angular distribution with theoretical predictions. Fig.1 shows the measured differential cross sections divided by the corresponding Rutherford cross section of the elastic scattering (open diamonds) and the excitation of the 2^+ state in ^{40}Ar at 1.46 MeV (open circles). The elastic cross sections exhibit a conspicuous difference to the Fresnel pattern of previous heavy system scattering data. This deviation is explained by long range Coulomb absorption as verified by an extended optical model calculation. While curve 1 is computed with a standard Woods-Saxon potential, curves 2 and 3 show the effect of Coulomb excitation simulated by an additional "dynamical polarization potential"[2] which describes the monopole-multipole interaction between the two nuclei. Curve 2 represents the excitation of the 2^+(1.46 MeV) state in ^{40}Ar, curve 3 includes the 3^-(2.61 MeV) state in ^{208}Pb and four more low lying 2^+ and 3^- states in both nuclei.
The parameters of the real part of the nuclear potential were derived from a universal fusion potential[3] by requiring agreement with respect to strength and gradient at the interaction radius of 13.2 fm. The inelastic cross sections (curve 4) were obtained by multiplying the semiclassical Coulomb excitation probabilities by the elastic cross sections of the standard optical model.

Another important aspect was the analysis of the mass-, charge-, and energy-distributions of the quasi-elastic transfer. Efforts were made to correct the data with regard to neutron evaporation, using an iterative procedure and assuming the primary excitation energy to be divided between the products in proportion to their mass. The effect of neutron evaporation on the first and second moments of the overall A- and Z-distribution was found to be negligible for total energy losses up to about 60 MeV. The results (Fig.2) lead to the following conclusions: The average mass and charge evolve initially towards asymmetry in contrast to expectations based on potential energy arguments. The rate of change of σ_A^2 with energy loss is significantly smaller than expected for uncorrelated nucleon transfer as the dominating dissipative mechanism. This observation is consistent with the assumption of correlations induced by the Pauli principle ("Pauli blocking"). The ratio σ_A^2/σ_Z^2 tends towards $\bar{A}/\bar{Z}$ in the limit of small energy loss and approaches $(\bar{A}/\bar{Z})^2$ in the fully relaxed region, reflecting the different time scales of equilibration of the charge-to-mass ratio and the mass asymmetry, respectively.

+Now at University of Marburg and LBL Berkeley

[1] U.Arlt et al., GSI 79-11 (1979) p. 37
[2] W.G.Love, T.Terasawa, G.R.Satchler, NP A291 183(1977)
[3] R.Bass, PRL 39 265(1977)

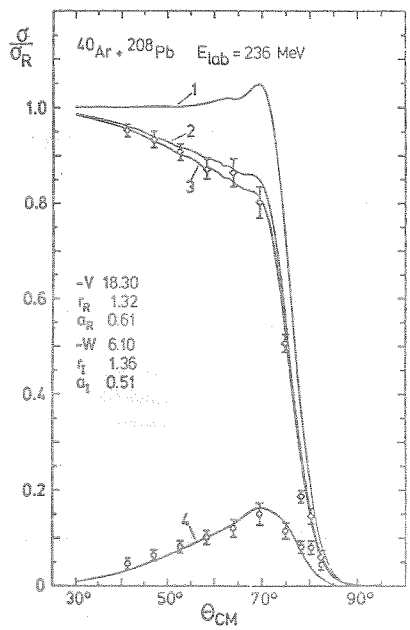


Fig.1 Angular distributions of elastic and inelastic scattering of ^{40}Ar from ^{208}Pb

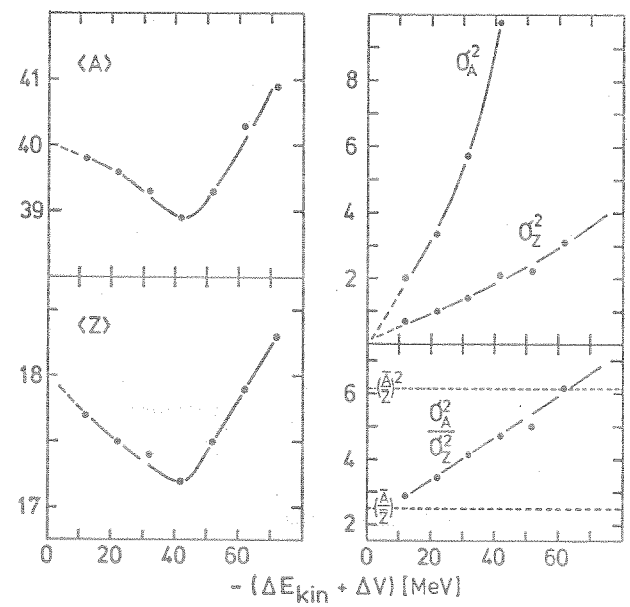


Fig.2 Mean values and variances of mass and charge distributions of projectile-like fragments as functions of reduced energy loss

The Reactions $^{208}Pb+^{58}Ni$ and $^{208}Pb+^{64}Ni$ [B]

U.Arlt, R.Bass, V.Hartmann, H.Noll, R.Renfordt*, K. Sapotta
Institut für Kernphysik der Universität Frankfurt am Main

The mass, charge, and energy distributions of the target-like products from the reactions $^{208}Pb+^{58}Ni$ and $^{208}Pb+^{64}Ni$ were studied at laboratory angles of 37.5^{0}(grazing angle), 40^{0} and 45^{0}. The beam energies (5.9 MeV/u and 5.4 MeV/u, respectively) were chosen to be 30 MeV above the interaction threshold$.

The measurements were performed at the focussing time-of-flight spectrometer at beam line Z3, using a newly installed detector setup which consists of two channel-plate time detectors and a ΔE-E ionization chamber.

One of the purposes of the investigation is a detailed study of the N/Z equilibration. The Z-distributions of the reaction products differ significantly due to the different N/Z ratios of the target nuclei (1.07 and 1.29, respectively).

Figure 1 shows energy- and mass-integrated Z-spectra at $\vartheta = 37{,}5^{0}$. There is a clear shift towards lower Z values in the case of the lighter target isotope (^{58}Ni).

The evolution of the Z-distributions with the laboratory energy of the products is demonstrated in Fig.2. The data are analyzed with the aim of extracting first and second moments of the A- and Z-distribution as functions of energy loss and angle.

*Now at University of Marburg and LBL Berkeley

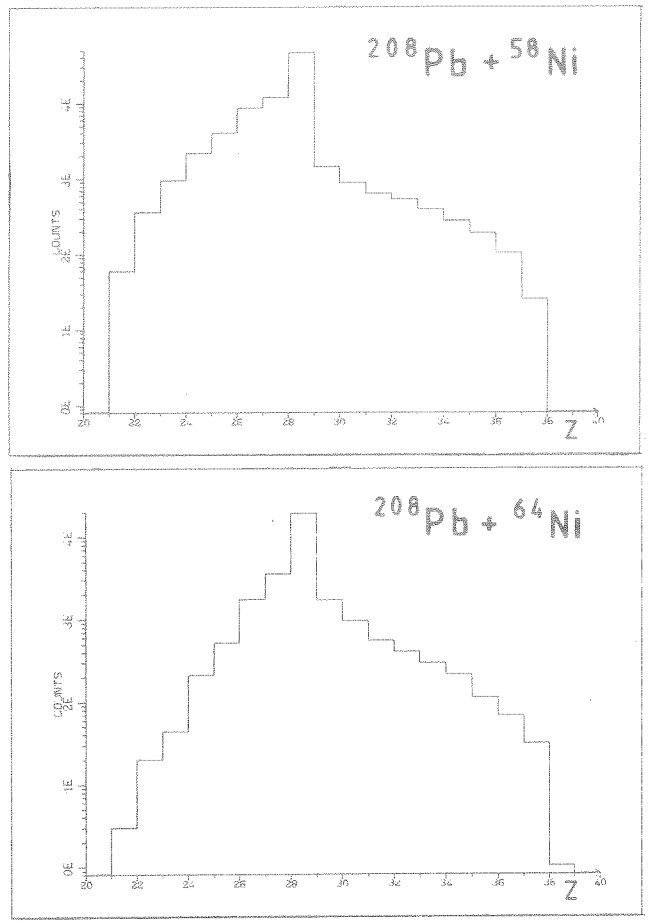


Fig.1 Z-spectra of the reaction products at $\vartheta = 37.5^{0}$

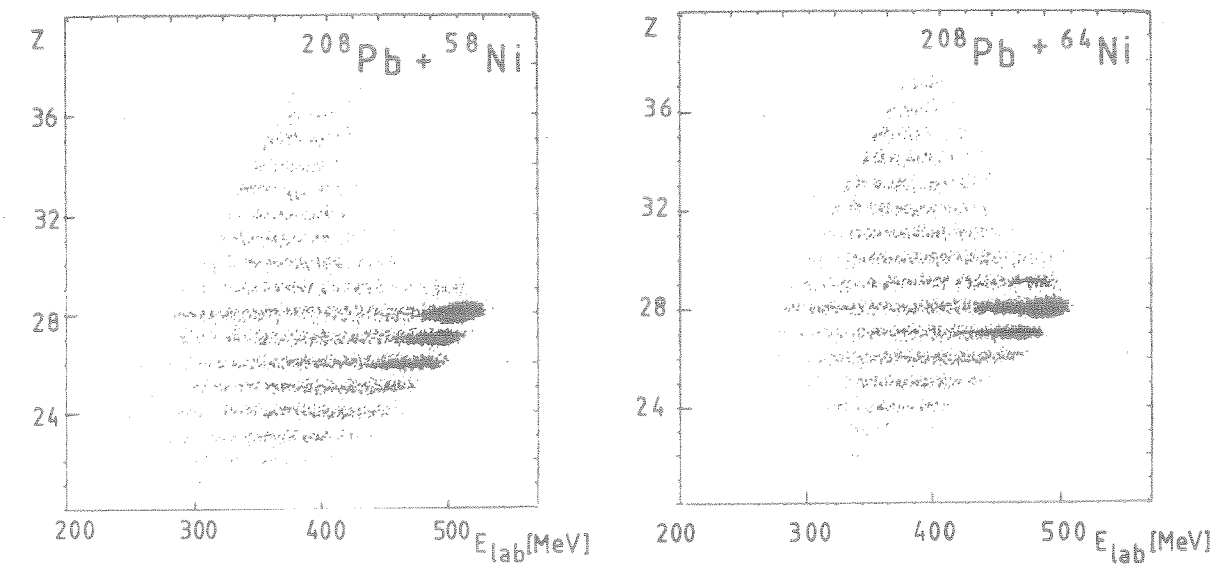


Fig.2 The evolution of the Z-distributions with the laboratory energy of the reaction products

Mass and Charge Transfer in ^{40}Ar + Ag Scattering [B]

U.Arlt, R.Bass, V.Hartmann, H.Noll, R.Renfordt[+] K.Sapotta
Institut für Kernphysik, University of Frankfurt

Projectile-like products emitted after scattering of 297 MeV ^{40}Ar projectiles from a natural Ag target were studied using the 5 m time-of-flight telescope. Mass and charge distributions of the products were measured with complete resolution in A and Z as a function of energy loss (Q value) at the laboratory angles 30^{o}, 35^{o}, 40^{o}, 45^{o}, 50^{o} and 60^{o}. The centre of mass bombarding energy was 40 MeV above the interaction barrier, resulting in a grazing angle of about 48^{o} in the laboratory system. The purpose of the investigation was to obtain information on the mechanism of energy dissipation and on the time scales of mass and charge equilibration in the region of small energy loss.

The observed A- and Z-distributions were corrected approximately for neutron evaporation by an iterative calculation, assuming the total excitation energy to be shared by the primary fragments in proportion to their mass. Results obtained at $\Theta_{lab}=50^{o}$ for the first and second moments of the A- and Z-distributions are given as functions of the reduced energy loss $-(Q+\Delta V)$ in Figs. 1 and 2. The uncorrected and evaporation-corrected data are shown as full points and open circles, respectively. The following conclusions can be drawn: 1) There is an initial mass drift towards asymmetry followed by an evolution towards symmetry as the relaxed region is approached. 2) The ratio of variances σ_A^2/σ_Z^2 is a function of energy loss, reflecting the different time scales of equilibration with respect to N/Z and the mass asymmetry degree of freedom. 3) The rate of change of σ_A^2 with energy loss is significantly smaller than would be expected if the energy loss was due to a completely statistical exchange of nucleons. Such a reduction of σ_A^2 can be attributed to "Pauli blocking". Similar results and conclusions were obtained also in a study of the system ^{40}Ar + ^{208}Pb.

[+] Now at University of Marburg and LBL Berkeley

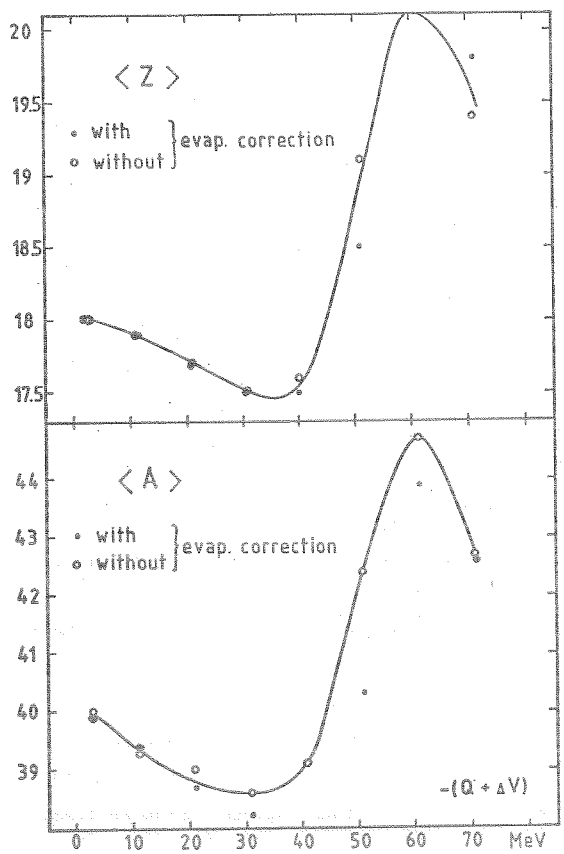


Fig. 1 Average values <A> and <Z> for projectile-like products as functions of the reduced energy loss (Θ_{lab} = 50^{o})

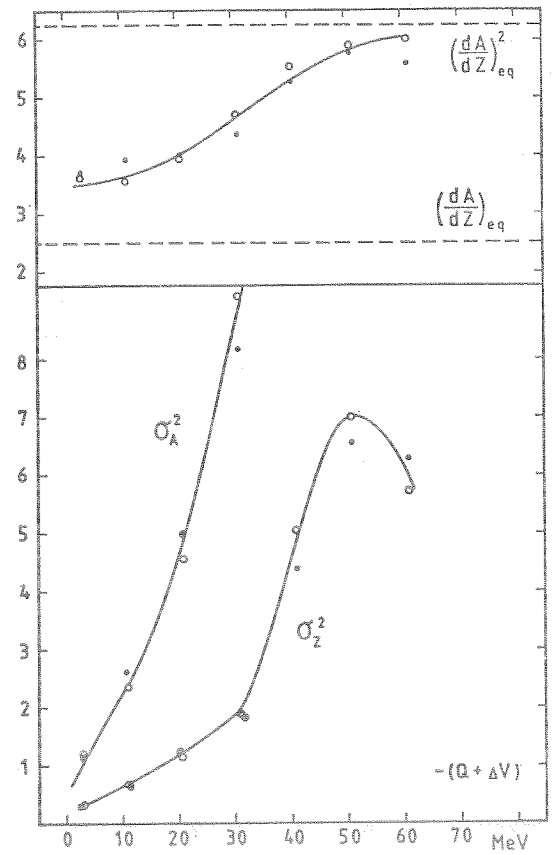


Fig. 2 Variances σ_A^2,σ_Z^2 and their ratio as functions of the reduced energy loss (Θ_{lab} = 50^{o})

Search for pre-equilibrium neutron emission using 12 MeV Kr projectiles [B]

I. Tserruya*, A. Breskin*, Z. Fraenkel*, S. Wald+, U. Arlt+, R. Bass+, G. Kreyling+, R. Renfordt+, K. Stelzer+, U. Lynen", M. Dakowski, P. Doll, A. Gobbi and H. Sann

*Weizmann Institute of Science Rehovot, +Institut für Kernphysik Universität Frankfurt, "MPI Heidelberg and GSI Darmstadt

The multiplicity of neutrons and their energy spectra were measured for the binary events in dissipative collisions for the Kr+Er reaction at 12 MeV/u.

The heavy fragment detection system consisted of two pairs of position sensitive (x,y) parallel plate counters. One pair was positioned in the direction of the projectile-like (PL) fragments (at Θ_{lab} = 14°, 17° and 20°) and the other in the direction of the very slow target-like (TL) fragments (Θ_{lab} = 29°, 50° and 71°). The time resolution between these counters and the bunched beam of the Unilac accelerator was about 300 ps; the mass resolution was ≈9 amu (FWHM).

As for this incident energy in few percent of events the projectile-like fragments split, these events were eliminated (and analysed separately) using kinematic considerations. The fragment detectors were operated in a spherical aluminium chamber of 1 m diameter with a 3 mm thick wall. The amount of matter around the experimental set-up was minimized to avoid the background from scattered neutrons and gamma-rays.

The neutrons were measured in eight liquid scintillators. Seven detectors were placed in the reaction plane and an additional one 45° out-of-plane. The flight path was 80 cm. The gamma-rays were rejected using pulse-shape discrimination and time-of-flight measurements.

The data are being analyzed. The preliminary results for one position of the fragment detectors (Θ_{lab} = 20°, Θ_{lab} = 71°) selecting mostly quasi-elastic events (TKEL = 100 MeV) are presented below.

Fig. 1 shows the measured neutron intensities for different lab angles of the n-detectors (full dots). These results are compared with the neutron intensities (open circles) calculated using the neutron data from only two detectors placed in the direction of projectile-like (PL) and target-like (TL) fragments. An isotropic emission of neutrons in the CM-frame of the appropriate fragments was assumed. The dots indicating the results for the out-of-plane n-detector are surrounded by a circle (fig. 1). A discrepancy between measured and reconstructed intensities is observed for the two n-detectors positioned close to the beam axis.

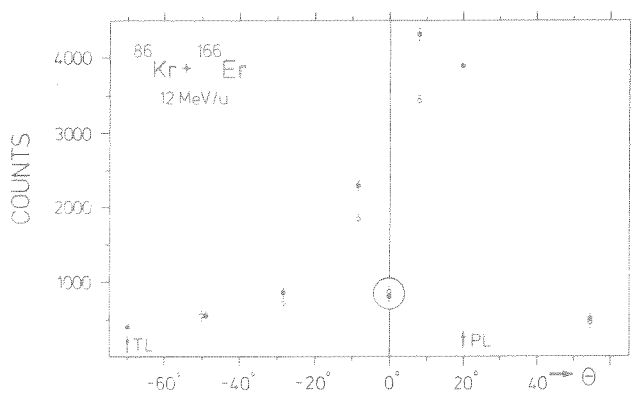


Fig. 1

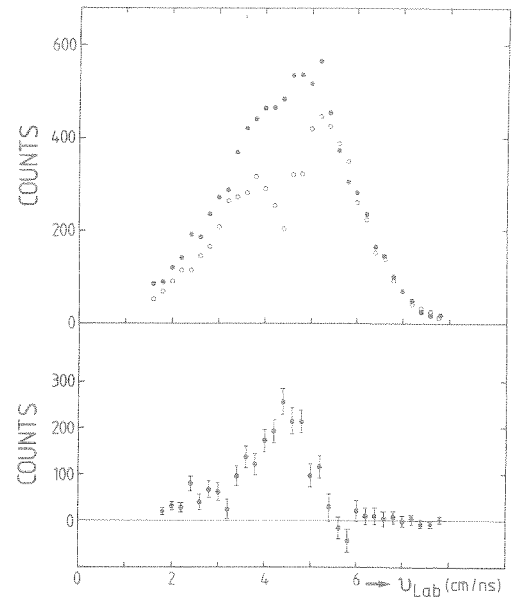


Fig. 2

Fig. 2a presents the comparison of measured (full dots) and calculated (open circles) neutron velocity spectra for the n-detector placed at Θ_{lab} = +8°, while fig. 2b displays the difference of these two curves. The neutron velocity in the maximum of distribution of fig. 2b is very near to the beam velocity.

The existence of the pre-equilibrium processes can be tentatively assumed on the basis of the presented results. The analysis of the other angular configurations, expecially that for DIC region, will furnish additional information.

Gamma-ray multiplicities from deep inelastic collisions

P.R. Christensen, F. Folkmann, Ole Hansen, O. Nathan, N. Trautner, S.Y. van der Werf, and F. Videbaek
NBI, University of Copenhagen, Denmark

H.C. Britt
LASL, Los Alamos, USA

H. Freiesleben
GSI Darmstadt

F. Pühlhofer
Fachbereich Physik, Universität Marburg

In previous years γ-ray multiplicities were measured for $^{86}Kr + ^{144}Sm$ at 490 MeV and for $^{86}Kr + ^{154}Sm$ at 490 and 610 MeV. At both bombarding energies neutrons are registered together with the gammas, but the neutron contamination is more serious at the higher energy than at the lower. In order to compare the data from ^{154}Sm at the two energies one must correct for the neutron sensitivity of the gamma counters in a consistent and reasonably precise fashion. Such a method was developed[1] and the entity of the data were reanalyzed using this new procedure. The old data on ^{144}Sm, published in ref. 2, were changed in detail, although the main conclusions remain the same. The typical numbers for deep inelastic collisions, uncorrected for neutron, were average multiplicity $\langle M\rangle=21$ and square root of second central moment $\sigma = 9$, i.e. $\sigma/\langle M\rangle = 0.43$. In the new analysis we find $\langle M\rangle = 19$, $\sigma = 7.5$ and $\sigma/\langle M\rangle = 0.39$. This still leads for very broad j-distributions for the deep inelastic collisions, in the old analysis with $\langle j\rangle/\sigma(j) = 0.62$ and now with $\langle j\rangle/\sigma(j) = 0.59$. Here $\langle j\rangle = \langle j_1\rangle + \langle j_2\rangle$ where $\langle j_1\rangle$ is the average angular momentum on reaction product 1 and $\langle j_2\rangle$ on product 2.

For ^{154}Sm the average multiplicity is $\langle M\rangle \simeq 22$ at the low bombarding energy and $\langle M\rangle \simeq 27$ at the high energy. Thus $\langle M\rangle$ increases and roughly proportional to $(E_{c.m.} - E_{coul.barrier})^{1/2}$. σ on the other hand is almost constant, 7.5 at 490 MeV and 8.0 at 610 MeV. These results point to a smaller importance of fluctuating components in the angular momentum transfer as the bombarding energy is increased.

We have also been trying to evaluate the angular momentum transfer in a statistical equilibration limit restrained to give an average transfer in agreement with the sticking limit. From such considerations the widths at the low bombarding energy must be termed large, while the high bombarding energy data largely agree with the statistical equilibrium picture.

An extensive paper has been proposed on the low energy data[1] while preliminary accounts have been given at conferences and seminars of the high bombarding energy results.

[1] P.R. Christensen et al., submitted to Nucl. Phys.
[2] P.R. Christensen et al., Phys. Rev. Lett. 40 (1978)1245

Analyses of the Mass and Charge Yields for the System $^{132}Xe + ^{nat}Fe$ [B]

R.A. Esterlund, P. Patzelt, U. Reus, W. Wätzig, and W. Westmeier
Institut für Kernchemie, Universität Marburg

Of utmost priority during 1979 in the analysis of mass-yield data previously reported here has been the understanding of the nature and origins of the various reaction components seen. A charge-yield curve has been constructed for the above system at $E_{lab} \leq 940$ MeV, and is shown in Fig. 1. It differs considerably from that curve for the same system (at a similar equivalent energy) reported by Heusch et al.[1], which exhibited only a very large symmetric component in addition to the quasi-elastic peaks. The deep-inelastic transfer

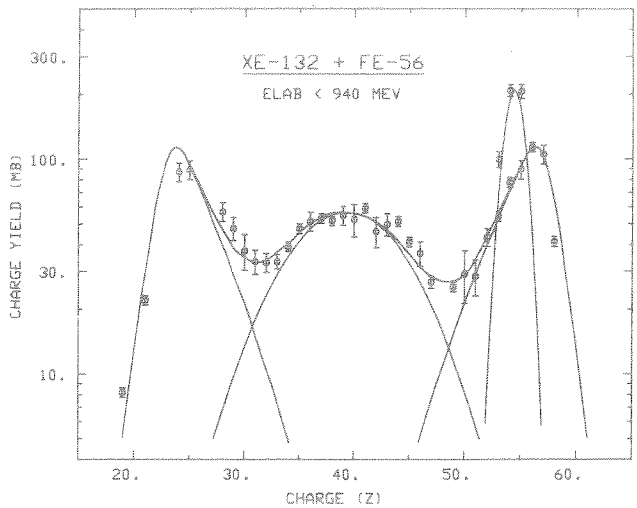


Fig. 1: Thick-target Charge Yields at 940 MeV.

(DIT) yields are centered at Z = 24 and 56, showing a shift of 2 charge units away from target and projectile and towards asymmetry in charge. The lines through the DIT data points are a diffusion-model fit, calculated with the inclusion of an initial fast step in which A and Z of the reaction partners adjust so as to minimize the contact potential between them (MPE assumption). This assumption yields better fits to the mass- and charge-yield data than the unchanged charge-density (UCD) assumption. In addition, the ratio of experimental variances in mass and charge, σ_A^2/σ_Z^2, is 5.44 ± 0.60, in good agreement with the MPE prediction that $\sigma_A^2/\sigma_Z^2 \triangleq (Acn/Zcn)^2 = 5.52$. The UCD assumption predicts $\sigma_A^2/\sigma_Z^2 = Acn/Zcn = 2.35$. The derived lifetime of the double nuclear system (DNS) was $\tau_{DNS} = 7.5 \times 10^{-22}$ sec, in good agreement with that predicted by the ansatz $\tau_{DNS} \triangleq \sqrt{2}\,\hbar\,\ell_{max}/B = 7.7 \times 10^{-22}$ sec. We also deduce a mass-diffusion constant $D_A = 1.51 \times 10^{22}$ amu^2/sec, in reasonable agreement with the simple approximation $D_A = Acn \times 10^{20} = 1.88 \times 10^{22}$ amu^2/sec.

Arguments previously presented here regarding the nature of the symmetric component (ie. observed FWHM, angular distributions, evaporation residues) have all been consistent with normal fusion-fission. The remaining quantity to be investigated is the magnitude of this yield. However, comparison of this yield (from a thick-target experiment) with the rotating liquid-drop limit (RLDM) is complicated by the fact that the angular momentum distribution in a thick target is different from that in a thin one. As a consequence, it is necessary to know the fraction of the reaction cross section which would go into fusion in the absence of an RLDM. We have fitted thick-target yields simultaneously at two energies, letting this fraction and the RLDM vary. The deduced excitation function is shown in Fig. 2. The resulting RLDM of 94 ± 4

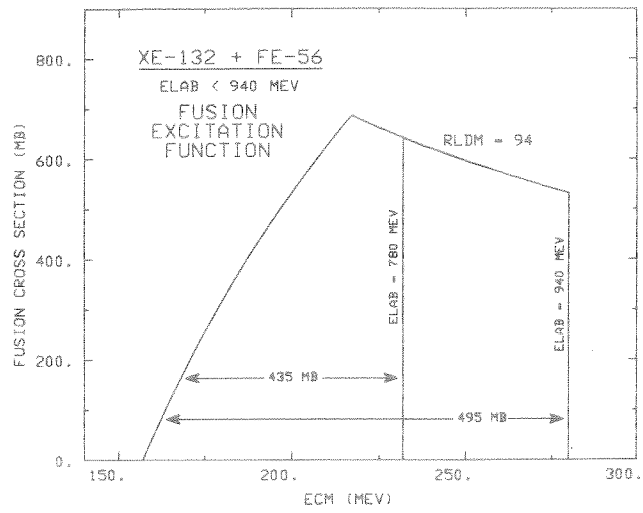


Fig. 2: Deduced Fusion Excitation Function.

$\hbar$ is considerably above the expected value of 72 $\hbar$. Further experimental investigations in pursuit of an explanation are planned for the near future.

[1] B. Heusch, et al., Z. Phys. A288, 391 (1978).

Energy dependence of the mass diffusion in $^{238}U+^{238}U$ collisions [B]

J.V. Kratz, W. Brüchle, H. Gäggeler, H. Gäggeler-Koch, M. Schädel, G. Wirth, C. Riedel
GSI Darmstadt

M. Weis
Institut für Kernchemie, Universität Mainz

Bombardments of thick ^{238}U targets with ^{238}U beams of 7.5 MeV/u incident energy have shown[1], that dissipative collisions between very heavy nuclei might be suitable for the production of superheavy elements. The diffusion model, generalized in order to take into account the superposition of different incident energies in the thick target, was used to extrapolate production rates into the region of superheavy fragments[2]. These calculations were based on a fit of an energy-independent, average diffusion coefficient ($D_Z=0.9\times10^{22}$ s^{-1}) to the reconstructed element yields[1] near Z=92. Folding of the predicted differential cross sections as a function of fragment charge and excitation energy ($d^2\sigma/dZdE$) with the relative width for neutron evaporation and spontaneous fission (Γ_n/Γ_f) as calculated by Moretto[3] yielded encouraging cross sections of the order of 10^{-34} cm^2 for Z=114. However, difficulties were encountered at the same time for Z=98,99 and 100, where folding of the predicted $d^2\sigma/dZdE$ with empirical Γ_n/Γ_f-values failed to reproduce the measured actinide cross sections. The discrepancies at Z=98-100 might be a shortcoming of the assumed[2] energy-independence of the diffusion coefficient. Therefore, we measured at several incident energies between 6.5 and 9.0 MeV/u cross sections for the production of transcurium elements[4] as well as for the production of their light complements. Fig. 1 shows as an example the energy dependence of the complementary Rn and Cf yields. It is evident that for the production of Cf only the lower incident energy bins contribute. Fig. 2 shows the measured element yields of residual products near Z=80 for three incident energies. The solid lines are predictions of the diffusion model where the theoretically predicted energy dependence of the diffusion coefficient, $D_Z \sim T$, was incorporated. While the model seems now to be capable of reproducing the data at the higher energies it clearly overestimates the cross sections for the near-barrier energies Since the production of surviving heavy products is mainly associated with the lowest bins of incident energy (see Fig. 1), the failure of the diffusion model to reproduce the cross sections in these bins casts some doubt on the relevance of previous predictions[2].

The problem is apparently connected with the fact that quasi-elastic few-nucleon transfer processes contribute a large fraction of the total reaction cross section, in particular at near-barrier energies. One is led to conclude that for dissipative collisions interaction radii considerably smaller than the quarterpoint radius (16.9 fm) are relevant. The data indicate that these interaction radii are somewhere between 15.4 and 16.0 fm.

[1] M. Schädel et al., Phys. Rev. Lett. 41, 469 (1978)
[2] C. Riedel et al., Z. Physik A290, 385 (1979)
[3] L. G. Moretto, Physics and Chemistry of Fission, I.A.E.A., Rochester, 1973
[4] M. Schädel, GSI-Report 79-8 (1979).

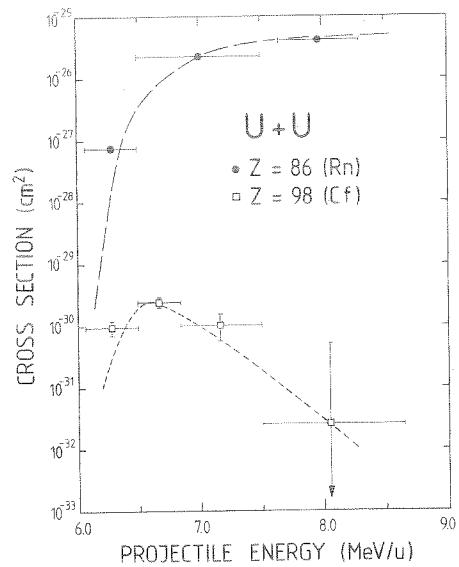


Fig. 1 Energy dependence of the complementary Rn and Cf yields.

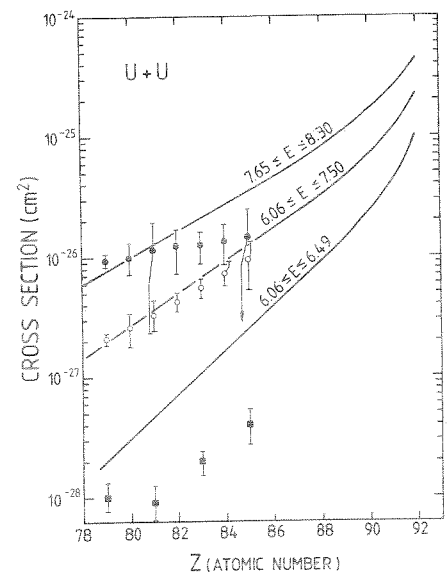


Fig. 2 Cross sections for ligh residual nuclei at different bins of projectile energies. The yields are increasingly depleted by sequential fission for the higher atomic numbers and for increasing incident energies. The curves are the results of the diffusion model.

Charge-, mass-, and energy distributions in the ^{132}Xe + ^{197}Au reaction

J. Poitou, R. Lucas
DPhN-MF, CEN Saclay

J. V. Kratz, W. Brüchle, H. Gäggeler, M. Schädel, G. Wirth
GSI Darmstadt

We have previously reported[1] on the variances of the charge distributions $(\sigma_Z^{A'})^2$ at fixed primary mass numbers A' in the ^{132}Xe + ^{197}Au system at 900 MeV. These data are based on the reconstruction[1] of the primary cross section surface P(Z,A',E) from radiochemical stacked-foil experiments. This surface can also be used to calculate other moments of the charge- (Z), mass- (A') and energy (E) distributions. As an example we show in Fig. 1 the centroid of the element distribution $\langle Z_h \rangle$ for the gold-like fragments as a function of the total excitation energy of the dinuclear system. $\langle Z_h \rangle$ seems to be stable at the entrance channel charge up to excitation energies of ∿ 100 MeV. Then a drift toward more symmetric fragmentations is visible. It is noteworthy that the drift occurs only for energy losses near or exceeding those given by the Coulomb barrier of two spherical fragments touching at R = $1.16\ (A_1^{1/3}+A_2^{1/3}+2)$ fm. Thus the drift seems to appear with the onset of deformation in the exit channel. Similar observations were reported for the ^{86}Kr + ^{166}Er system[2].

Another interesting result is concerned with the ratio σ_A^2/σ_Z^2 of the variances of the integral mass- and charge-distributions at fixed values of dissipated energy. The large ratios of σ_A^2/σ_Z^2 for relatively small energy losses, see Fig. 2, indicate that peripheral collisions enhance neutron exchange relative to proton exchange. Such a behaviour may be indicative of the existence of a larger barrier for proton exchanges than for neutron exchanges at large internuclear distances.[3] These differences should disappear for a deeper interpenetration of projectile and target,[3] in qualitative agreement with the results shown in Fig. 2.

For excitation energies exceeding about 70 MeV the experimental ratios of σ_A^2/σ_Z^2 are in line with the relation $\sigma_A^2/\sigma_Z^2 = (1 + dN/dZ)^2$ which holds for fully correlated exchange of neutrons and protons. Here, dN/dZ is the average slope of the potential energy valley in the N-Z-plane as calculated by minimization of the potential energy for two touching liquid drops. If shell effects are assumed to be washed out at these excitation energies values of $\sigma_A^2/\sigma_Z^2 \approx 6$ are to be expected. The apparent hindrance of proton exchanges relative to neutron exchanges might be seen as an explanation for the slow rise[1] of the width of the charge distributions $(\sigma_Z^{A'})^2$ at fixed mass asymmetry with increasing energy loss. Then, one might expect that at a higher bombarding energy, the rise of $(\sigma_Z^{A'})^2$ should be much faster.

[1] J. Poitou et al., Phys. Lett. 88B, 69 (1979)
[2] G. Rudolf et al., Nucl. Phys. A330, 243 (1979)
[3] D.H. E. Gross, private communication (1980)

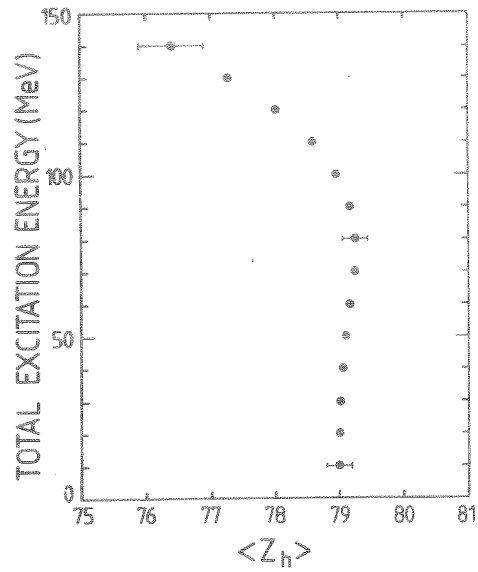


Fig. 1: Centroids of the heavy fragment charge distributions vs. total excitation energy in the dinuclear system.

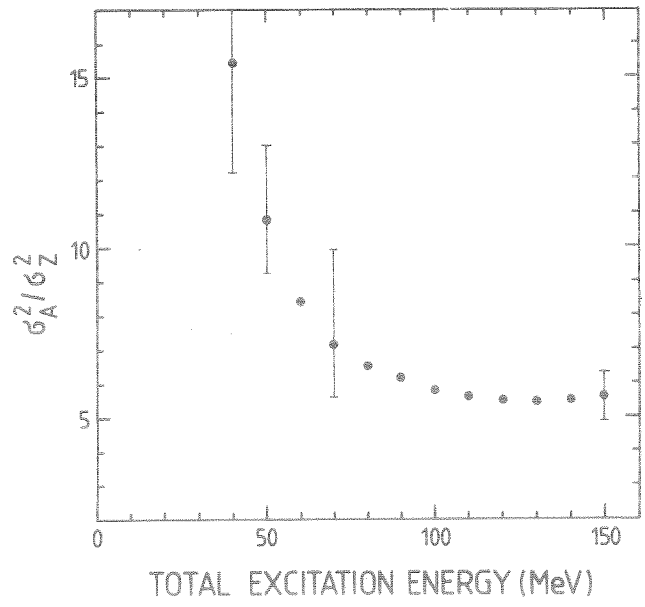


Fig. 2: Ratios of the variances of mass- and charge distributions σ_A^2/σ_Z^2 vs. total excitation energy of the dinuclear system.

Charge-, mass-, and energy distributions in the reaction of 7.5 MeV/u ^{238}U-ions with ^{197}Au B

K. Sümmerer, W. Brüchle, H. Gäggeler, H. Gäggeler-Koch, J.V. Kratz, M. Schädel, G. Wirth
GSI Darmstadt

J. Poitou, R. Lucas
DPhN/MF, CEN Saclay

G. Klein, M. Weis
Institut für Kernchemie, Universität Mainz

Radiochemical measurements of charge-, mass-, and energy distributions in damped collisions of ^{132}Xe-ions with ^{197}Au have provided evidence for very narrow variances of the charge distributions at fixed mass asymmetry[1]. These variances might be consistent with classical statistical fluctuations. Larger variances observed in the ^{86}Kr + ^{92,98}Mo system, on the other hand, were reported to present evidence for quantal fluctuations[2]. In order to find out whether light and heavy, symmetric and asymmetric systems behave in a different way, we have decided to investigate the ^{238}U + ^{197}Au system as an example for a very heavy asymmetric system.

Self-supporting targets of 520 µg/cm^2 ^{197}Au were bombarded with 7.5 MeV/u ^{238}U-ions and the target-like reaction products were stopped in stacks of thin mylar foils (6 µm) at several laboratory angles covering the range $22^o \leq \Theta_{lab} \leq 62.8^o$. After bombardment each foil, corresponding to a given range of angles and velocities of the Au-like products, was dissolved and chemically separated into fractions of the elements Hf, Ta, Ir, Pt, Au, Hg and Tl. Differential cross sections

$$\int_{R_1}^{R_2} \int_{\Theta_1}^{\Theta_2} (\delta^4\sigma/\delta Z \delta A \delta R \delta\Theta)\ \delta R \delta\Theta$$

for individual isotopes were then determined by γ-ray counting (R = range in mylar, Θ = laboratory angle).

Typical data for ^{196}Au in its 12$^-$ isomeric state are shown in Fig. 1. At each angle, the range distribution is indicated by the number of the mylar foil in the stack in which the Au fragment has been stopped. The maximum of the angular distribution is found near the grazing angle (48^o). Fig. 2 shows the isotope distributions for Au isotopes at four adjacent angular ranges. Similar to the ^{132}Xe + ^{197}Au system[1], the yield curves can be decomposed into a quasi-elastic and an inelastic component. While the quasi-elastic transfer dominates near the grazing angle, this component is essentially absent at smaller angles. The variances of the distributions for the damped compoment increase from $\sigma_A^2 = 2.2$ to $\sigma_A^2 = 5.5$ from the grazing angle to the smaller angles. Simultaneously their centroids are shifting continuously toward lower mass numbers.

Evaluation of similar data for Hf, Ta, Pt, Hg and Tl is in progress. Centre of mass transformation and the further data reduction in terms of the reconstruction of the primary cross section surface P(Z,A',E) will proceed in the same way as performed previously[1]. The magnitude of the charge variances σ_Z^2 at fixed mass asymmetry resulting from this analysis should allow to discern classical statistical fluctuations from quantal zero point oscillations[2].

[1] J. Poitou et al., Phys. Lett. 88B, 69 (1979)
[2] M. Berlanger et al., Z. Phys. A291, 133 (1979)

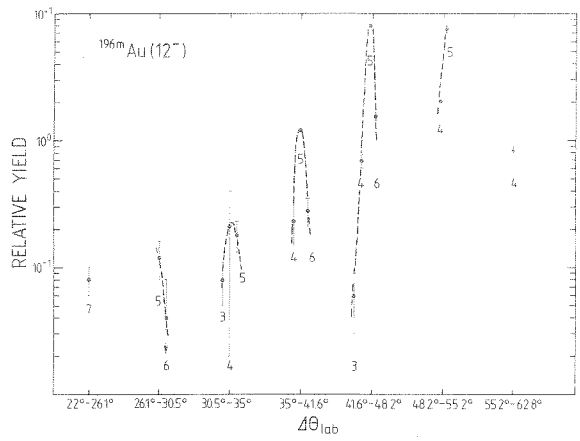


Fig. 1: Relative yields for ^{196m}Au at different laboratory angles. The numbers 3-7 denote the number of the mylar foil in the stack in which the Au fragment has been stopped.

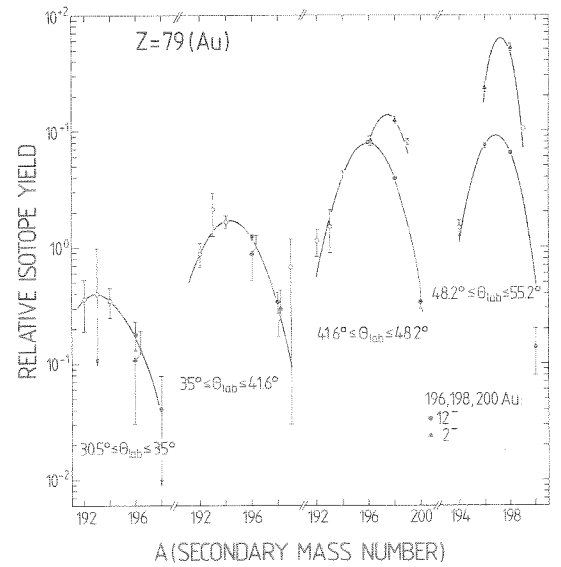


Fig. 2: Isotope distributions of Au isotopes at different laboratory angles. For ^{196,198,200}Au full circles denote the 12$^-$ isomeric states, while full triangles denote the 2$^-$ ground states.

EXCLUSIVE THREE-PARTICLE MEASUREMENT OF THE REACTIONS $^{238}U + ^{238}U$ AND $^{238}U + ^{248}Cm$

Y. Civelekoglu, P. Glässel, D. v. Harrach, R. Männer, H. J. Specht, J. B. Wilhelmy+
Universität Heidelberg
H. Freiesleben, K. D. Hildenbrand, GSI Darmstadt

Kinematically complete measurements of the three-particle exit channels of the very heavy collision systems of ^{238}U on ^{238}U and ^{248}Cm have been performed. The experimental set-up and data analysis have been presented in previous annual reports. The exclusive three-particle requirement selects large mass transfer of the first reaction step, producing a light fragment with low fissility. The dominant four-body channel was disregarded. Heavy fissioning transfer products up to $Z \sim 115$ were observed. The main question is whether thermal equilibrium is reached before fission or whether fast non-equilibrium processes set in.

As for lighter systems Pb, U+Ni, Zr, the distribution of separation velocities of the secondary fission fragments (Fig. 1) clearly demonstrates the existence of an intermediate fissioning nucleus, thus establishing a two-step mechanism even for the heaviest fissioning nuclei observed. Fig. 2a shows the total kinetic energy of fission vs atomic number of the intermediate nucleus, agreeing well with the semi-empiric Viola-systematics.

The angular distributions of fission, referred to the rest-frame of the fissioning nucleus, are isotropic in the scattering plane of the first step of the reaction to within 20%. The out-of-plane distributions are strongly concentrated in the reaction plane of the first step (Fig. 2b) as for the lighter systems. The surprising persistence of the strong out-of-plane anisotropy for the very heavy nuclei with vanishing liquid drop stability ($Z > 107$) cannot be understood in the equilibrium fission formalism using the saddle-point concept. It is conceivable that the fissioning system, being formed with a deformation beyond its saddle-point, starts the descent towards scission immediately after separation of the deep-inelastic complex. However, from the absence of coulomb-distortions of the kinetic energy of fission, a lower time-limit of $10 \cdot 10^{-21}$ s can be derived for the scission-to-scission time, long compared to most theoretical predictions. Independently, a similar time limit of $10\text{-}12 \cdot 10^{-21}$ sec follows from the absence of significant in-plane anisotropy.

In the region of nuclei with reasonable liquid drop stability (up to $Z \sim 104$) the analysis of the out-of-plane angular distributions of fission yields average oriented spins which vary as expected for a sticking model with respect to Z. At $Z = 100$, $J_Z \sim 50\ \hbar$ is found.
The widths of the fission fragment mass distribution show a considerable rise towards high Z's, doubling the relative width at $Z \sim 115$.

In summary, there are several indications for a relatively fast non-equilibrium process, but alternative explanations cannot be ruled out at present.

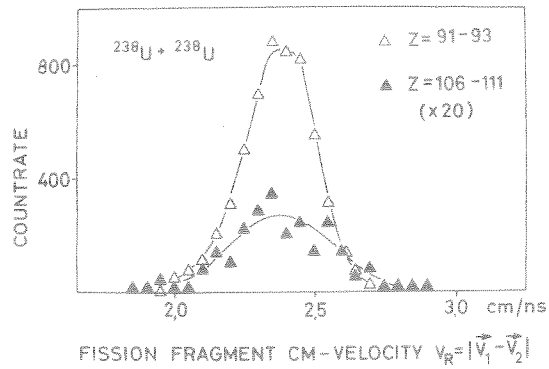


Fig. 1 Separation velocity of fission fragments for fissioning nuclei from two Z-bins.

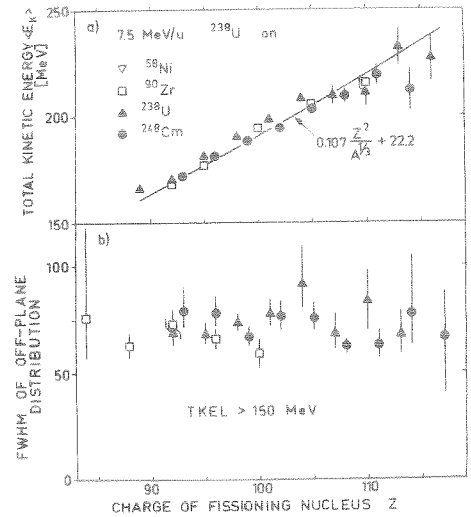


Fig. 2 Average total kinetic energy release of fission (a) and FWHW of the out-of-plane angular distribution of fission (b) vs. atomic number of fissioning nucleus.

+ Los Alamos Scientific Laboratory, N. M.

MASS-DETERMINATION IN THE REACTION $^{208}Pb \rightarrow ^{nat}U$ B

P. Lemmertz, R. Faß, L. Alquist, F. Kassen, H. Wollnik
II. Physikal. Institut Gießen
D. Hirdes, H. Jungclas, G. Dersch
Kernchemie Marburg

We performed a gas jet experiment on the ^{208}Pb ^{nat}U reaction and looked for SHE[1]. Simultaneously the mass of α-recoil nuclei was investigated via the time of flight spectrometer (TOF)[2].
It was possible by means of a 5-parameter experiment to identify most of the nuclei which contribute to the very complex α-spectrum.
The following parameters were recorded; α-energy, time-of-flight of the daughter nucleus and the x-ray and γ-events coincident with the α-events.
The halflives for α-decay were recorded independently at the α-wheel. Approximately 50 masses were determined with the TOF apparatus and about 40 isotopes identified. In some cases, α-γ-coincidences permitted the unequivocal identification of one isobar within a group with similar α-energies.

Figure 1 shows the results of the measurement. It can be seen that nearly all α-emitting nuclei between the Pb-projectile and the U-target are produced and, if their halflives are >1 sec, are detected by the gas-jet.
The most interesting features are the production of ^{192}Bi, which implies a loss of 16 neutrons from lead, and the production of the rare earth elements with high cross sections (o.5 mb). The production of the rare earth elements is highly correlated with the properties of the Pb nucleus because these elements were not observed in the reaction U → U. In addition this experiment established that the rare earth elements result from the reaction of Pb with either the Ti-window or the Ar-gas of the thermalizationchamber.

The production mechanism is not yet reproduced theoreticaly. The three different possible production modes are a.) inelastic transfer b.) sequential fission c.) long α- and $\beta^{\pm}$decay chaines of very neutron deficient Pb and Bi-Isotopes which can end in the rare earth region.

Calculations are now in progress to determine which mode of production is the most favorable.

Two (mass, α-energy) pairs which could not be assigned to known isotopes are (167, 4.231 MeV) and (164, 4.064 MeV). From the point of view of α-systematic these might be ^{165}Ta and ^{163}Hf, but because nothing is known about these isotopes this assignment is quite tentative.

1. D. Hirdes at al GSI Jahresbericht 1979
2. R. Faß et al. Nucl. Instr. Meth. 154, (1978), 233.

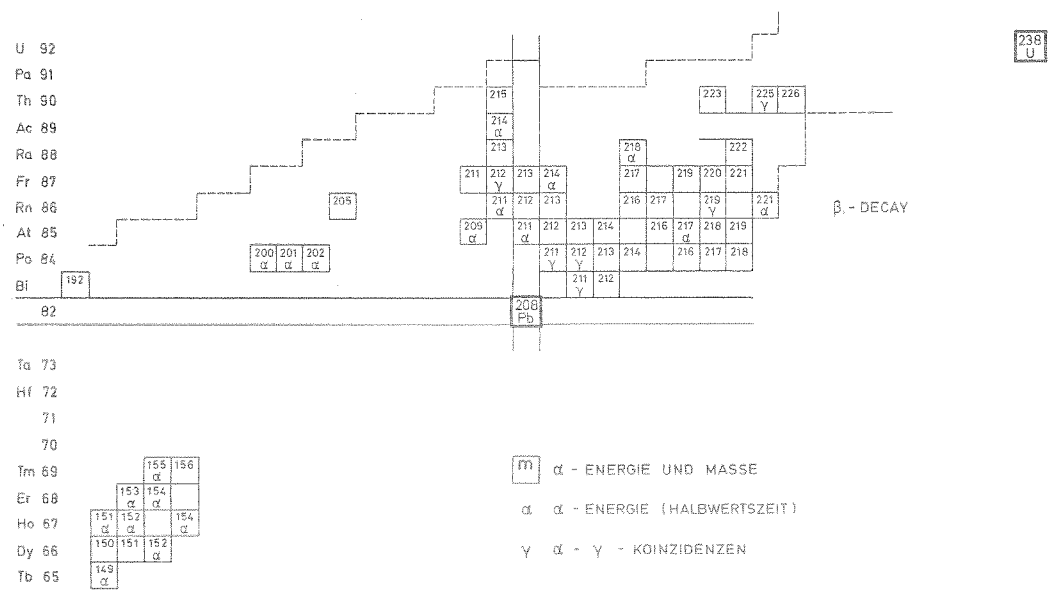


Fig. 1 Massdetermination with the TOF in the reaction $^{208}Pb \rightarrow ^{nat}U$. The mass number without additional letters means mass and α-energy are measured. The letter γ-denotes that in addition to the massdetermination α-γ-coincidences were measured. The letter α denotes that the assignment of mass is made only on the basis of α-energy and half-life.

Study of the Reaction 2149 MeV $^{238}U + U_{nat}$ Using Special Glass Detectors. [B]

G. Fiedler, R. Haag, R. Ulbrich
II. Physikalisches Institut, Universität Giessen

P.A. Gottschalk
Fachbereich Physik, Universität Marburg

A 2π-geometry technique (GSI-Report 1977) with meta-phosphate-glass detectors has been used in the last year for the study of the reaction 2149 MeV $^{238}U+U_{nat}$. In this reaction 137 three-pronged events, 205 four-pronged events and 1 five-pronged event have been found and measured event-by-event. Most of the events were analysed completely on the assumption of conservation of mass and momentum, and by employing an empirical velocity-range relation. So far, the three- and four-pronged events and the five-pronged event were associated with sequential fission. Four-pronged events can be interpreted as "double-sequential" fission. That means in a first step of the reaction two intermediate masses are formed in a deep inelastic process and both subsequently fission in a second step as isolated nuclei[1]. The intermediate masses, as well as the final fragment masses, the reaction Q-values and the angular distributions were determined.

The angular distribution of the final fragments of the four-pronged events observed in the intrinsic system of the prefissioning nuclei was found, within the statistics, to be isotropic in the reaction plane, (fig. 1a). The angular distribution with respect to the normal of the reaction plane shows strong enhancement at increasing angles (fig. 1b) i.a. the final fragmentations tend to occur at small angles with respect to the reaction plane[2].

In fig. 2a the track trajectories of the five-pronged event are plotted in detail (straight lines: projected track length with respect to the detector-surface; dotted lines: true track length). For this event one solution was found, which is due to a sequential fissioning process with three distinct reaction steps. In addition to the conservation of mass and momentum, the sum of the masses of two arbitrary fragments was held fixed. The decay chain is shown in fig. 2b. The Q-values measured for the intermediate fragments A = 203 amu and A = 159 amu are Q_f = 132 MeV and Q_f = 70 MeV, respectively.

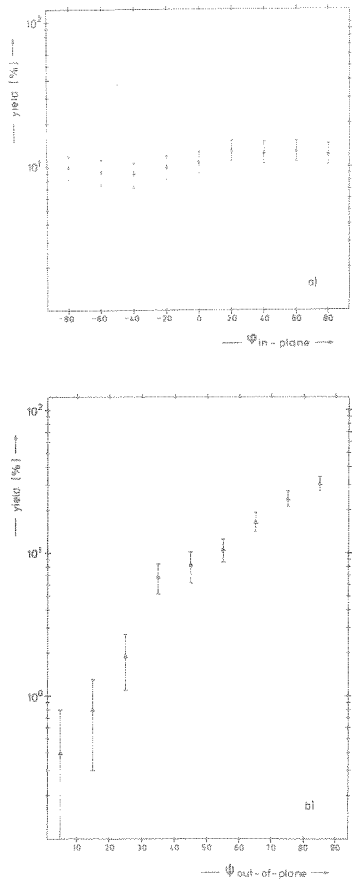


Fig. 1 Angular distributions
a) in plane, b) out of plane

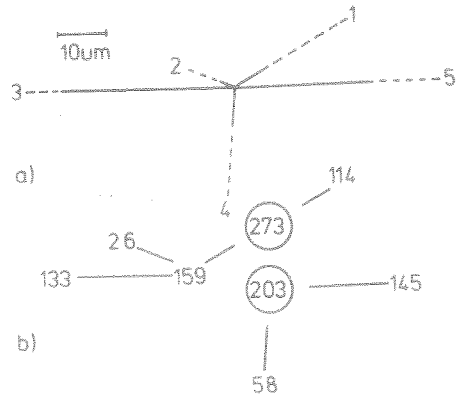


Fig. 2 Five-pronged event
a) plott of the track trajectories,
b) decay chain

[1] P.A. Gottschalk et al., Phys. Rev. Lett. 42 (1979)
[2] P. Haag et al., Proc. 10th Int. Conf. On SSNTD, Lyon (1979)

Double-sequential fission in heavy-ion induced reactions [B]

P. Vater, P.A. Gottschalk*, R. Beckmann, R. Brandt and G. Grawert
Kernchemie, FB 14, and FB Physik, Philipps-Universität Marburg

So far, nuclear reactions with heavy ions yielding 4 or 5 heavy fragments in the exit reaction channel can only be studied with solid state nuclear track detectors[1,2]. In this contribution we analyse in the frame-work of double-sequential fission[1-5] the first four-pronged event, ever seen with mica detectors[1] and then more recent experimental data from (U+U) studies.

1. ^{nat}U + 9.6 MeV/u ^{84}Kr. Using the 2π - geometry mica technique, in the interaction (U+Kr) we observed one four-pronged event ($\sigma_{4F} \simeq 20$mb)[1]. The four prongs are due to a double-sequential fission reaction after a deep-inelastic reaction with considerable mass transfer[2-5]:

U+Kr $\longrightarrow$ $A_1^*[=(132\pm7)] + A_2^*[=(190\pm7)]$ 1. step
TKEL = (202±42)MeV

$A_1^* \longrightarrow$ (86±10) + (46±15) 2. step

$A_2^* \longrightarrow$ (143± 8) + (47± 7)

The experimental fission Q-values of the second step agree with the expected values[6]:

Q_1 = (51±13)MeV, $Q_{1,expect}$ = 68 MeV

Q_2 = (118±12)MeV, $Q_{2,expect}$ = 124 MeV

In order to estimate the experimental errors due to inaccuracy in track-length ($\Delta l \simeq 1$ μm) and track-angle ($\Delta\phi \simeq 3^o$) measurements, we simulated artificially 189 "new" events with slightly different input values for the observed four prongs. These "new" events were analysed as usual. We obtained a complete set of "new" results. Fig. 1 gives -as an example- the distribution of the observed pre-fission masses after the first deep-inelastic collision. The width of the mass-distribution is a measure of the accuracy of our experimental method.

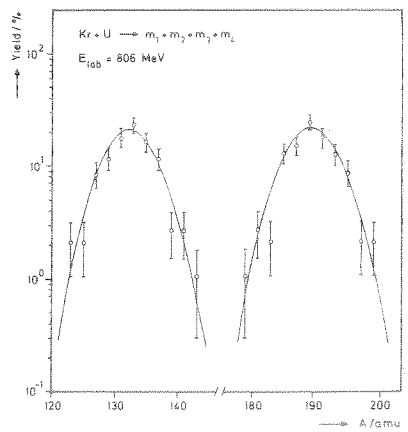


Fig. 1: Distribution of pre-fission masses after deep-inelastic collision

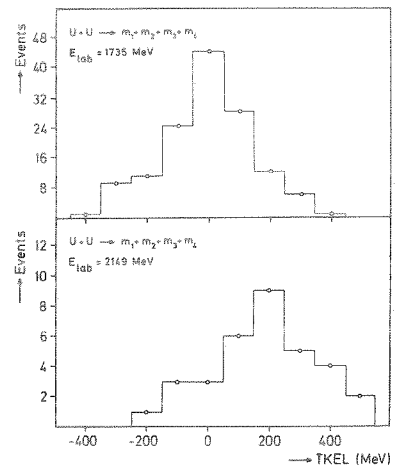


Fig. 2: Distribution of total kinetic energy loss in deep-inelastic collisions

2. Comparison of the interaction ^{nat}U + ^{238}U → 4 fragments at two bombarding energies (A: 7.5 MeV/u, B: 9.03 MeV/u). In continuation of the investigation of the above mentioned heavy ion reaction we studied the influence of the bombarding energy on the nature of the double-sequential fission process[4,5]. The most significant difference is observed in the damping of kinetic energy during the first reaction step (measured as increased TKEL with increasing U - energy). As shown in Fig. 2, in reaction A (close to the Coulomb-barrier) we observe $\langle TKEL \rangle \simeq 0$ MeV, however, at higher energies in reaction B we observe $\langle TKEL \rangle \simeq 200$ MeV.

[1] P. Vater et al., Phys.Rev.Lett. 39(1977)594
[2] P.A. Gottschalk et al., Phys.Rev.Lett. 42(1979)359
[3] R. Brandt et al., NIM (1980) in print
[4] P. Vater et al., GSI-J-1-78(1978)58
[5] P. Vater et al., GSI-79-11(1979)34
[6] V.E. Viola, Nucl.Data, Sec.A1(1966)391

*Reaktorsicherheitskommission, Köln

Study of Interaction ^{238}U on ^{238}U and ^{208}Pb at 9,1 MeV/n and 7.4 MeV/n with help of polycarbonate detector

M. Debeauvais, S. Jokic and J. Tripier
Centre de Recherches Nucléaires, Strasbourg, France

Makrofol E track detector has been used in 2π geometry for the study of the systems (U + U) at 9.1 and 7.4 MeV/AMU and (U + Pb) at 7.4 MeV/AMU. The target was evaporated directly on the polycarbonate sheet with a thickness of 1 mg/cm^2 and was irradiated perpendicularly to the beam by a flux of about 10^6 ions/cm^2. After etching, the detectors were scanned for binary, ternary and quaternary events. The binary events due to inelastic scattering permit us to determine experimentally the quater-point. As we can see on Fig. 1 the incident ions can be easely counted and we can measure the ternary and quaternary cross sections. The results are shown in Table 1.

In order to analyze in details the 4 prongs events we measure the track lengths and their geometry for the reaction U + U at 9.1 MeV and we use the range energy relation obtained previously for light particles and fitted experimentally for very heavy ions. The mass and impulsion (- 20 %) conservationsgive mass solutions and we conserve the only one corresponding to the minimum of the transverse momentum.

For every event we correlate the fragments pairwise ; we obtain also six possibilities. For each pair we determine the energy in the center of mass system. To consider a two prong event as fission, we assume that the energy in the CM system must be situated in the range of 60 to 260 MeV. 68 % of the 109 quaternary events give a convenient solution and thus can be considered as sequentially fission. Fig. 2 gives the mass distribution of compound nuclei just before fission and indicates that mostly, there is a nuclei exchange between the target ion and the incident one before fission.

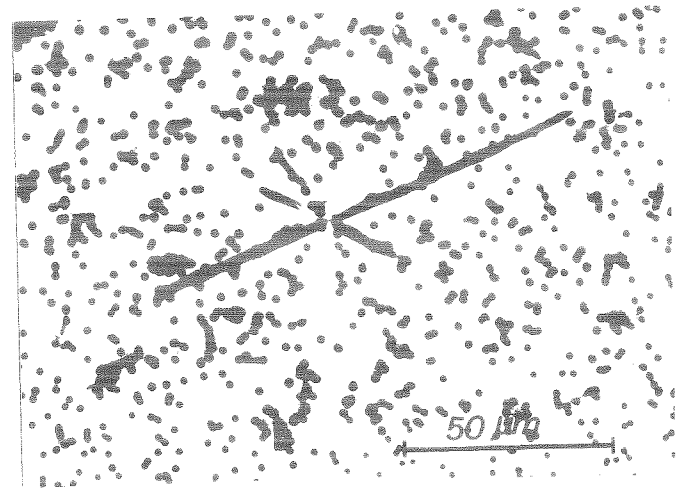


Fig.1

TABLE I - Cross sections of 3 and 4 prong events

	Reaction	3 prong events	4 prong events	5 prong events	σ_3	σ_4	σ_{3+4}	σ_{Th}
I	2156 MeV U + U	115 51 %	109 49 %	2 ∿ 0.9 %	1415 ±140	1360 ±139	2775 ±250	2800 ±300
II	1785 MeV U + U	49 58 %	36 42 %	-	941 ±90	693 ±70	1634 ±150	1600 ±150
III	1785 MeV U + Pb	182 92 %	15 8 %		1280 ±130	110 ±20	1390 ±140	1698 ±160



Fig.2

THE REACTION BETWEEN CU AND 86 MEV/N ^{12}C B

T.Lund and D.Molzahn
Kernchemie, F.B.14, Philipps-Universität, D-3550 Marburg
D.Eriksen, E.Hagebø and I.Haldorsen
Department of Chemistry, University of Oslo, Oslo, Norway
T.Bjørnstad and C.Serre
EP-Division, CERN, Geneva, Switzerland
and the ISOLDE Collaboration
CERN, Geneva, Switzerland

We report here on yields and thick target/thick catcher recoil properties of products in the reaction between Cu and 86 MeV/N ^{12}C.

We made four bombardments in the ISOLDE beam line at the SC, CERN. The typical beam intensity was $2 \cdot 10^{11}$ ions per second, and the bombardments lasted one to four hours. The target stack consisted of three 10 μ aluminium foils, the middle serving as monitor, a carbon guard foil, a carbon backward catcher foil, the Cu-target foil (~25 mg/cm^2) and a carbon forward catcher foil. After the bombardment the foils were mounted and measured for γ-activity. Absolute yields were determined by the reaction $^{27}Al(^{12}C,xp,yn)^{24}Na$, reported to have a cross section of 24.5 ± 3.0mb [1].

Yields of 34 nuclides could be determined, ranging from ^{22}Na to ^{65}Zn. The yields are shown in Fig.1. Curves are drawn to connect yields for one element. Where only one point is determined the trend of the curve is indicated.

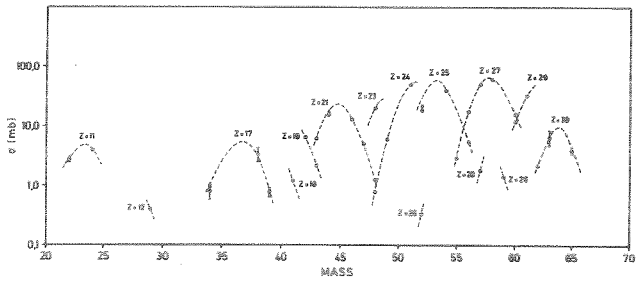


Fig.1 Isotopic yield distributions. The trend of curves through single points is found by interpolation.

The mean range of products R= 2W(F+B) in copper is shown in Fig.2. W is the target thickness in mg/cm^2 and F and B are the fractions of the total activity found in the forward and backward catcher foils, respectively. The ranges are in first order decreasing linearly with increasing mass number. Ranges of Sc-isotopes show a slightly stronger decrease with increasing mass than the all over trend, indicating an isotope effect.

The ratio of activity in the forward and backward catcher, F/B, is shown in Fig.3. The F/B-values go through a maximum about 20 mass units below target and reach a value of around 50.

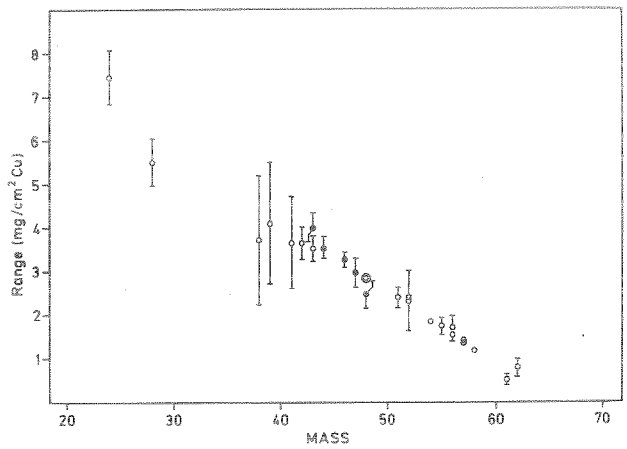


Fig.2 Ranges of products in mg/cm^2 Cu as a function of product mass number. The filled points are for Sc-isotopes.

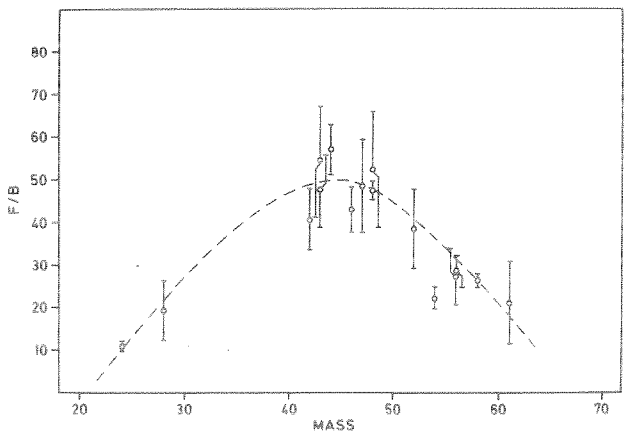


Fig.3 F/B-ratios as a function of mass number.

REFERENCES

1) J.W.N.Tuyn et al., Technical Memorandum, HS-RP/TM/80-5, CERN(Jan.1980)

ENERGY DISSIPATION AND PROTON EMISSION IN CENTRAL AND PERIPHERAL RELATIVISTIC NUCLEAR COLLISIONS [G]

R. Stock, H.H. Gutbrod, W.G. Meyer, A.M. Poskanzer, A. Sandoval, C.H. King, G. King, Nguyen Van Sen and K.L. Wolf

GSI Darmstadt and LBL Berkeley

In central collisions the disintegration of a large target nucleus by a light projectile should yield information on the energy dissipation from the incoming projectile to the target. If there is no transverse momentum transfer from the participants to the spectator a hole is punched into the target nucleus and little or no change in the decay pattern of the target spectator will be found as function of the projectile energy. However, a change will be seen with increase of the projectile size. On the other hand, if there is a strong and fast dissipation of the projectile's kinetic energy as it gets stopped in the target nucleus, the whole target nucleus will share the incident kinetic energy.

Uranium was bombarded with various projectiles from protons to ^{40}Ar at energies from 250 MeV/A to 2.1 GeV/A. A surprising result is observed in fig. 1 where the associated multiplicity for protons of 40 to 200 MeV at 90^0 lab (cf. ref. 1) is plotted vs. the total kinetic energy of the projectile. A smooth, nearly linear relationship between the mean associated multiplicity and the total kinetic energy is observed, regardless of the geometrical size of the projectile, or whether the incident energy is at the pion-threshold or way above it. In fact not only the means but also the observed multiplicity distributions are nearly the same as is shown for two projectiles with 42 GeV kinetic energy in fig. 2.

These observations support models where a high density is reached early in the diving stage, Then, in the expansion phase, the energy is spread over most of the nucleus. Transparency is therefore highly unlikely up to incident energies of 2.1 GeV/A.

Proton emission was studied with beams of p, He, Ne and Ar at 0.25 to 2.1 GeV/A on targets from Al to U. Central and peripheral reaction cross sections were obtained by high and low charged particle multiplicity selection. In central collisions of Ne and Ar with heavy targets, angular distributions show a forward emission suppression or even a sidewards enhancement from 150 to about 400 MeV/c proton laboratory system momenta (fig. 3), whereas peripheral collision exhibit 0^0 peaking at all proton momenta covered. Central collisions of equal size nuclei are dominated by fireball-type decay (fig. 4), plus a remaining spectator component because the yield is dominated by nonzero impact parameters even in the high multiplicity selection. In addition there should always be a direct component, from the interpenetration of the dilute nuclear surfaces of Ar and Ca.

On heavy targets, central collisions form a slow, non-isotropically decaying system heavier than the fireball or firestreak. The projectile seems to be "stopped down" inside the target nuclear matter, up to the highest Bevalac energies. This is expected because the momentum equilibration length should be much smaller than the U diameter even at 2 GeV/A. The emission patterns observed in central Ne+U reactions agree qualitatively with a recent hydrodynamical model calculation[2] for $b \leq 0.4\ b_{max}$.

[1] A. Sandoval et al., Phys. Rev. C, in press

[2] H. Stöcker et al., Phys. Rev. Lett. 44 (1980) 725

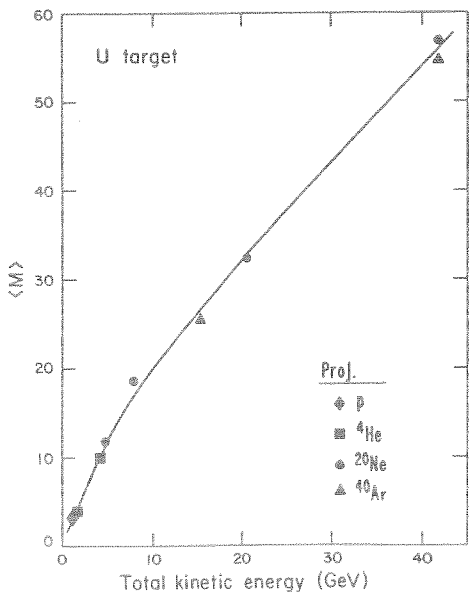


Fig. 1

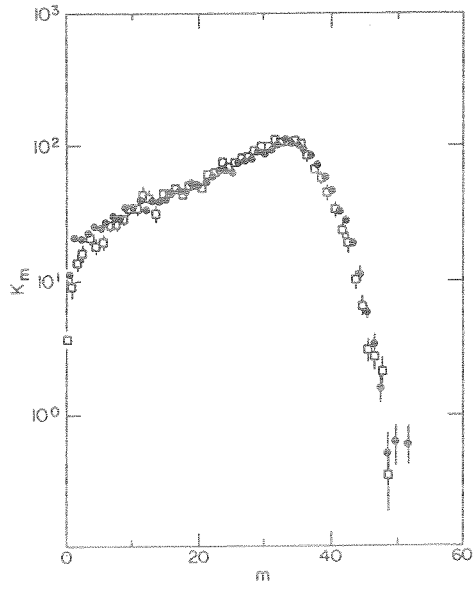


Fig. 2

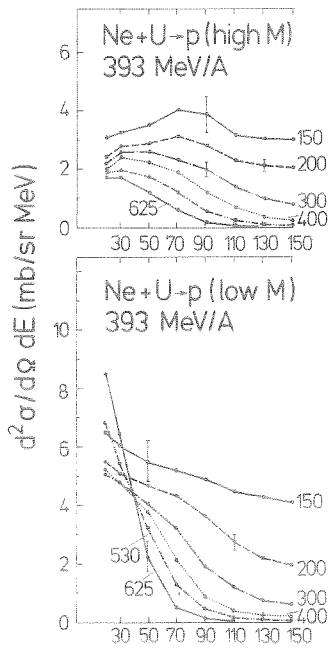
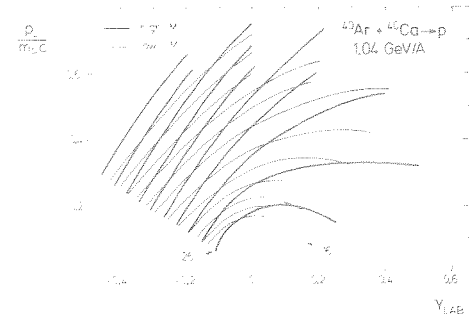


Fig. 3



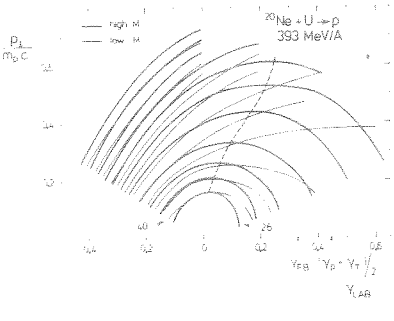


Fig. 4

CLUSTER PRODUCTION IN RELATIVISTIC NUCLEAR COLLISIONS [G]

H.H. Gutbrod, W.G. Meyer, A.M. Poskanzer, A. Sandoval, R. Stock, J. Gosset,
Ch. King, G. King, Nguyen Van Sen, G.D. Westfall and K.L. Wolf

GSI Darmstadt and LBL Berkeley

The emission of clusters (d, t, ^{3}He, ^{4}He) in heavy ion collisions at high energy has been measured, along with proton inclusive cross sections. Reactions with heavy target (Ne, Ar on U) show a higher cluster to proton yield ratio than equal mass systems like Ar+Ca, at fixed incident energy per nucleon. Thermal models make the same general prediction because Ar+U has more extended low temperature zones than Ar+Ca. Fig. 1 for Ne+U shows that deuteron formation dominates all the other composite products except for the "evaporation domain". The single proton yield amounts to only about 30 % (right hand vertical scale; left hand scale for cluster abundance) of the total emitted proton charges, at forward angles and for E/A ≤ 50 MeV. This may explain the observation[1] that single neutron yields far exceed single proton yields in Ne+U. The number of p and n bound up in clusters is about equal, thus enhancing dramatically the N over Z excess of U, as far as the remaining free nucleons are concerned. Ne+Al should thus not show such an enhancement in the single n: single p ratio.

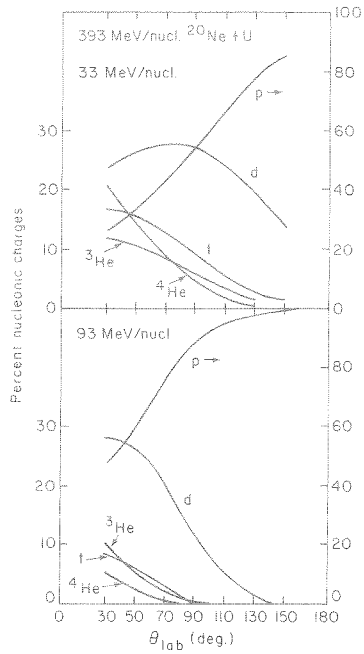


Fig. 1

Deuteron and triton emission from relativistic nuclear collisions has further been investigated, selecting for mostly central and mostly peripheral reactions by requiring a high and low associated multiplicity of charged particles. Fig. 2 shows the contour lines of constant invariant cross section in the plane of $p_\perp$ vs. y_{lab} for protons and deuterons from central Ne+U collisions. The set of deuteron lines exhibits a more pronounced asymmetry (deviation from approximate semi-circular shape). The cross section drops about twice as fast as for protons, both with increasing $p_\perp$ and y, when the same momentum per nucleon is considered. Fig. 3 shows that the asymmetry of the deuteron contour lines corresponds to sidewards peaking and forward suppression in the angular distributions for various bins of the laboratory momentum per nucleon. This effect is more pronounced than for protons, with the structures shifted forward in the lab. for d and t. The peaking cannot be reproduced in the firestreak model.

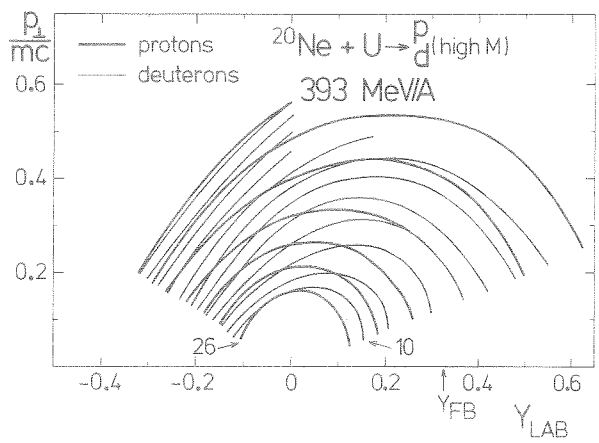


Fig. 2

The coalescence model has been applied successfully to the relative p-d inclusive cross sections[2,3]. The present data for Ne+U at 393 MeV/A are reproduced reasonably well with the ansatz $d^2\sigma(d)/d\Omega dE_d$ ($E_d=2E_p$) = $C(d^2\sigma(p)/d\Omega dE)^2$, with C = 0.14±0.045. The multiplicity cutoff, defining high multiplicity events, was the same for protons and deuterons. The measured proton cross sections were employed to determine C.

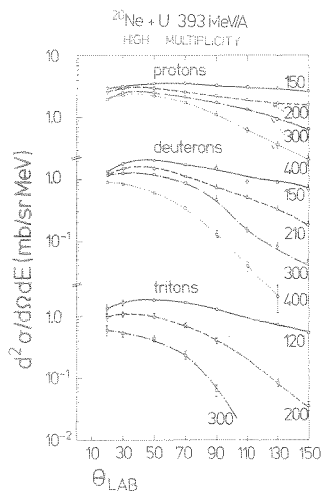


Fig. 3

[1] W. Schimmerling et al., Phys.Rev.Lett. 43(1979)1985

[2] H.H. Gutbrod et al., Phys.Rev.Lett. 37(1976) 667

[2] M.C. Lemaire et al., Phys. Lett. 85B(1979)38

PION, KAON AND Λ-PARTICLE PRODUCTION IN HIGH ENERGY NUCLEUS-NUCLEUS COLLISIONS [G]

A. Sandoval, J.P. Brannigan, J.V. Geaga, J.W. Harris, L.J. Rosenberg, L.S. Schroeder, H.E. Stelzer, R. Stock, K.L. Wolf

GSI Darmstadt, LBL Berkeley and ANL Argonne

There are many fundamental questions in the interaction of high energy heavy ions that have not had a definiteve experimental answer: is a fireball being formed? What is the pion production mechanism? What is the energy flux in pions and their multiplicities? Is there a signature of the first, most compressed state of the interaction? Answers to some of these questions can be given by exclusive measurements of the reaction products.

Exclusive π^- and charged-particle production in collisions of ^{40}Ar on KCl are studied at incident energies from 0.4 to 1.8 GeV/A using the Berkeley Streamer Chamber. The correlation between the π^- and the total charged particle multiplicity lies along a narrow ridge that reaches up to the total desintegration into singly charged fragments and pions (fig. 1). For central collisions the mean π^- multiplicity increases linearly with the bombarding energy with no marked discontinuities due to the Δ(3.3) resonance (fig. 2). Thermal models overestimate the observed pion production by a factor of 2.

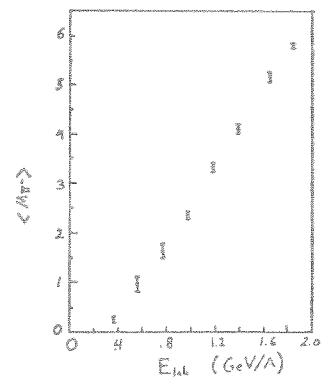


Fig. 2

The strange particle production is a unique probe in the study of high energy nucleus-nucleus interactions. The high production threshold due to associated production (Λ+K) and (Σ+K) leads at Bevalac energies to their production most probably only in the first stage of the collision, before a large energy degradation has set in. In contrast to pions and isobars, they cannot be reabsorbed, due to strangeness conservation, making them a more primordial probe. Their production in free NN interactions involves the strange quark-antiquark production from the vacuum. It is conceivable that this vertex is modified in a high density high temperature nuclear medium, making it very interesting to compare their production cross sections in different systems.

In our streamer chamber study of central collisions we should see the strange particle production at the higher bombarding energies. The charged kaons and sigmas, although detected, can not at present be identified from protons and pions. The neutral K^os and Λs can be readily identified if they decay by charged particles ($K^o \to \pi^+\pi^-$ with 68 %, $\Lambda \to p\pi^-$ with 64 % probability). Most of the identified neutral strange particle decays correspond to the invariant mass of a Λ (fig. 3). An independent particle model predicts a forward-backward c.m. Λ distribution but an almost isotropic kaon distribution. Fig. 4 shows that the presently available identified Λ's do indeed indicate a non-isotropic distribution of c.m. system momenta.

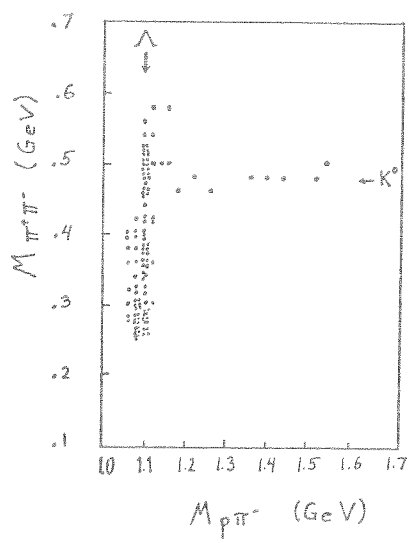


Fig. 3

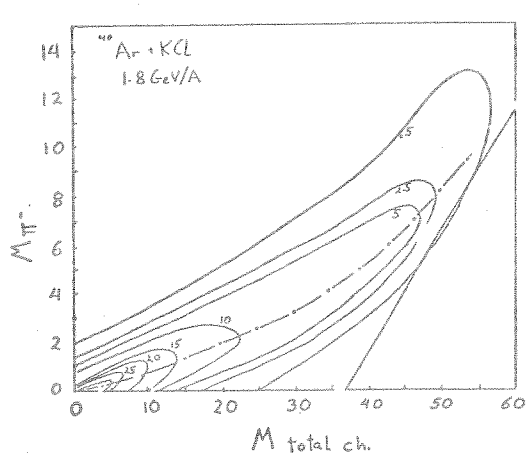


Fig. 1

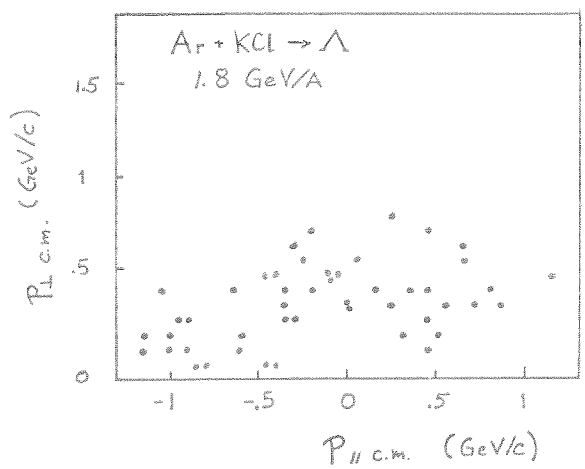


Fig. 4

Multiple Coulomb Excitation of ^{104}Ru

J. Stachel, N. Kaffrell, Institut für Kernchemie der Universität Mainz
H. Emling, H. Folger, E. Grosse, R. Kulessa*, D. Schwalm, GSI Darmstadt

Our systematic investigation of the neutron rich nuclei in the transitional region of A ~ 100 was continued by Coulomb exciting ^{104}Ru. Previous measurements of the γ-angular correlations following the β⁻-decay of 18.4 min ^{104}Tc[1] yielded spin-assignments for levels up to I = 4 and E2/M1-mixing ratios for the observed transitions; moreover in experiments with light projectiles ((d,d'), (α,α'), (^{16}O,^{16}O')) [2,3,7] rather high B(E2) values between the low lying levels of up to ~60 spu and the quadrupole moment of the 2_1^+ state of 0.70 eb were determined, indicative of the transitional character of this nucleus.

In the present experiments a thin ^{104}Ru target (520 µg/cm^2 on 35 µg/cm^2 C) was bombarded with ^{208}Pb projectiles (4.6 MeV/u). For the measurements a particle-gamma-coincidence set-up [4] was used, which allowed for the correction of the Doppler broadened gamma-spectra observed with 3 Ge(Li)-detectors. In addition 2 NaI-detectors were used as multiplicity filters. To obtain more accurate transition energies and to enable the placing of these transitions in the level scheme of ^{104}Ru, γ-singles and γγ-coincidences were measured using a thick target (~ 2 mg/cm^2 ^{104}Ru / 50 mg/cm^2 ^{208}Pb). The resulting scheme is shown in fig. 1. The ground-state-band (gsb) is observed up to the 10^+ level, the γ-band up to 8^+. The strong odd-even staggering of the γ-band predicted by the Interacting Boson Model (IBA-2)[5] and the Generalized Collective Model (GCM) of Gneuss and Greiner[6] is not observed. For the rather strongly excited level at 2232.4 keV previous experiments[1,7] allow $I^\pi = 4^+$. The possible interpretation of this state as a member of the β-band seems not likely, since the transitions to the 2_3^+ and 2_1^+ level are not observed.

The observed γ-yields in the thin target experiment were compared to those calculated using a modified De Boer-Winther-Code[8]. As input parameters we used sets of E2-matrix elements (ME) resulting from GCM-calculations[6] and from calculations within the Asymmetric-Rotor+VMI-Model (AR+VMI)[9]. The resulting γ-yields for the gsb are shown in fig. 2 together with the experimental ones. Multiplying the GCM E2-ME in the gsb by a constant factor to fit the known $B(E2,2_1^+\to0)$ and $Q_{2_1^+}$ values and taking into account the M1-radiation for the ΔI = 0,1 transitions the dashed curve results. The M1-ME were adjusted to the mixing ratio for the $2_2^+ \to 2_1^+$ transition[1] using the spin dependence proposed by Greiner[10]. Up to the 8^+ state the gsb-yields seem to be described rather well by this calculation, while the 10^+ state appears to be less collective. A more detailed comparison of all observed γ-yields with model-calculations is in progress.

* on leave from Jagiellonian University, Cracow, Poland

1 K.Sümmerer et al., Nucl. Phys. A 308, 1 (1978)
2 F.K.McGowan et al., Nucl. Phys. A 113, 529 (1968)
3 S.Landsberger et al., Phys. Rev. C 21, 588 (1980)
4 P.Fuchs et al., GSI Jahresbericht 1977, S. 195
5 K.Heyde, F.Iachello, P.van Isacker, private communication
6 G.Gneuss et al., Nucl. Phys. A 171, 449 (1971); P.Hess, J.A.Maruhn, private communication
7 J.Rekstad et al., J. Phys. G3, 411 (1977)
8 H.Ower, Jahresbericht 1979, Universität Frankfurt, IKF
9 H.Toki et al., Z. Phys. A 276, 35 (1976)
10 W.Greiner, Nucl. Phys. 80, 48 (1966)

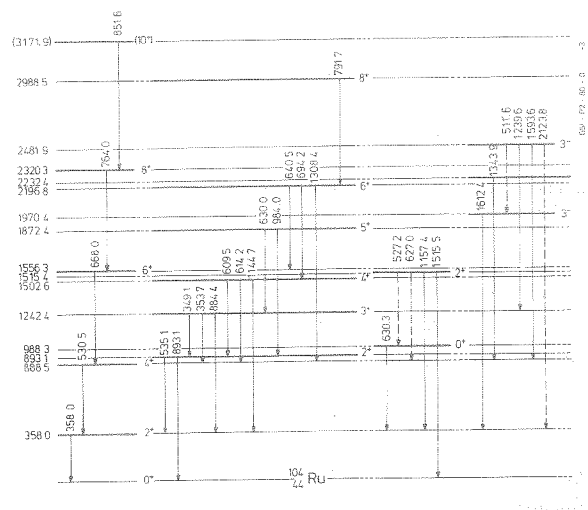


Fig 1. Level scheme of ^{104}Ru. The dashed lines indicate transitions only seen in the β⁻-decay of ^{104}Tc.

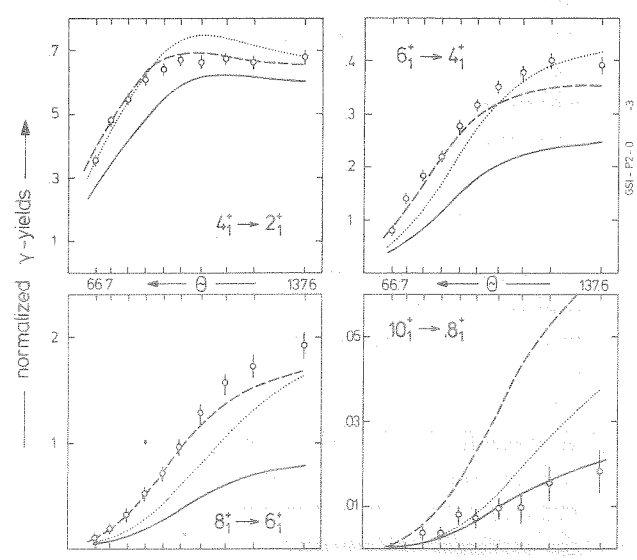


Fig 2. Angular dependence of the experimental and theoretical γ-yields for gsb transitions in ^{104}Ru (solid line: GCM, dotted line: AR+VMI, dashed line: modified GCM (see text)).

Coulomb Excitation and Recoil Distance Experiments in ^{156}Dy

H. Emling, P. Fuchs, E. Grosse, R. Kulessa[+], D. Schwalm, R.S. Simon, and H.J. Wollersheim
GSI Darmstadt

A remarkable result of our studies of the electromagnetic transition probabilities between high spin states in deformed rare earth nuclei is the observed reduction in collectivity of the rotational aligned band (s-band) in ^{158}Dy as compared to the ground state band (g-band) of this nucleus[1]. To further understand this result we have investigated also the collective behaviour of the s-band in ^{156}Dy for the following reasons: (i) In contrast to ^{158}Dy the interaction between ground band and s-band is very weak in ^{156}Dy and members pf both bands are known up to high spins[2] ($I^\pi = 26^+$ and 30^+, respectively). (ii) A much larger reduction of the B(E2)-values in the s-band of ^{156}Dy is expected assuming that its collective properties are mainly determined by a ^{154}Dy core with two aligned $i_{13/2}$ neutrons decoupled to it. (iii) The existence of low spin members of the s-band was established experimentally and a second crossing between s-band and β-band was found[3].

We performed two types of experiments, a recoil distance measurement using the reaction ^{25}Mg(^{136}Xe, 5n) at 4.7 MeV/u, and a Coulomb excitation measurement utilizing a highly enriched ^{156}Dy target and ^{208}Pb projectiles of 4.7 MeV/u. Both measurements, which are to some extent complementary, should allow for a rather complete determination of electromagnetic transition probabilities of the collective states in the vicinity of the Yrast line.

Recoil distance measurement. The experimental set up was improved over the one used in the previous investigation of ^{158}Dy.[1] By introducing a thin Au-foil (≈ 2.5 μm) instead of a thick ^{208}Pb-stopper we were able to avoid the large Doppler spread of the "stopped" components of transitions from shortlived high spin states; γ-rays from the Coulomb excitation of the Au foil were almost completely suppressed by the NaI multiplicity filter. Moreover, γ-spectra were recorded in a GeLi-detector located at 0^o and an annular Ge(Li)-detector at 180^o with respect to the beam thus exploiting both favourable γ-detection directions. Transitions from states $I^\pi = 8^+$ up to $I^\pi = 30^+$ in the β-band and up to $I^\pi = 24^+$ in the g-band could be observed. The decay curves were determined at 25 different target-plunger distances corresponding to decay times between 0.4 ps and 80 ps. As we are particularly interested in the faster transitions five of these runs were carried out for decay times below 1 ps and additionalmeasurements at decay times between .1 and .2 ps were obtained using ^{25}Mg targets evaporated on Au-foils of two different thicknesses.

Coulomb excitation. The particle-γ-coincidence set up used in the Coulomb excitation measurements has been described elsewhere[4]. In the Doppler shift corrected γ-spectra transitions from states up to $I^\pi = 18^+$ in the g-band, up to $I^\pi = 10^+$ in the β-band and up to $I^\pi = 12^+$ in the γ-band were observed. Of the s-band only the $I^\pi = 12^+$ state was observed; higher spin members of the s-band are not populated due to its weak interaction with the g-band. Several interband transitions between the β- and and g-band and the γ- and g-band were identified.

The data from both measurements are presently being analyzed together in order to obtain a consistent set of B(E2)-value for the low and high spin members of the g-, β-, γ- and s-band.

[+] on leave from Jagiellonian University, Cracow, Poland

[1] H.J. Wollersheim et al., GSI Jahresbericht 1978, p. 43, and H. Emling et al., GSI Jahresbericht 1977, p. 66.
[2] D. Ward et al., Nucl. Phys. A332 (1979) 433.
[3] H.R. Andrews et al., Nucl. Phys. A219 (1974) 141.
[4] P. Fuchs et al., GSI Jahresbericht 1977, p. 195.

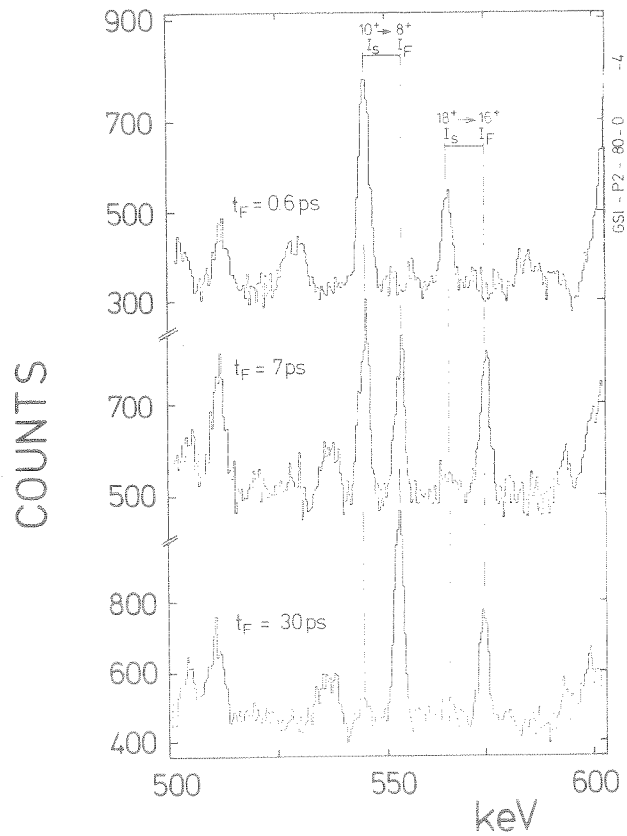


Fig. 1
A 100 keV wide section of γ-spectra observed at 0^o for three different distances between target and Au-foil. A coincidence with at least two NaI-detectors of the multiplicity filter was required. (I_F, I_S mark the γ-lines due to the decay of ^{156}Dy before and after the Au-foil, respectively).

Measurements of Magnetic Moments of High Spin States

G. Seiler-Clark, D. Pelte, Universität Heidelberg
A. Balanda+, H. Emling, E. Grosse, R. Kulessa*, D. Schwalm, H.J. Wollersheim, GSI Darmstadt
M. Hass, Weizmann Institute, Rehovot, Israel
G.J. Kumbartzki, K.H. Speidel, Universität Bonn

The backbending effect observed in the yrast-sequence of many rare earth nuclei is believed to result from the unpairing and alignment of a few nucleons along the axis of collective rotation. As the contribution of the aligned nucleons to the total magnetic moment is of the same order of magnitude as that caused by the core, a measurement of the g-factors of the yrast states in the backbending region should allow for a sensitive test of this picture. In particular, if the backbending observed for rare earth nuclei around spin 14 to 16 is caused by full alignment of two $i_{13/2}$ neutrons, a drastic reduction of the g-factors in the backbending region is expected, $g \sim 0.0$ as compared to the collective g-factor of $g_R \simeq +0.35$, while the g-factor is expected to be of the order of +1 in case the backbending is due to the alignment of two $h_{11/2}$ protons.

A first experimental attempt was made to measure the g-factors of the yrast states of ^{158}Dy in the backbending region by Coulomb exciting ^{158}Dy with ^{208}Pb projectiles of 4.7 MeV/u and employing the transient field effect. A large magnetic transient field is produced when a heavy ion passes through a magnetized iron foil at high velocity. This field leads to a precession of the magnetic moment of the moving nucleus, which in turn is reflected in a precession of the γ-angular correlation[1]. In the present experiment the recoil velocity of the Dy-nuclei is $v/c \sim .08$ and a transient field of 14 kTesla is expected[2]. Such a large field results in a measurable precession angle of $\sim 4^0$ (assuming $g = g_R = 0.35$) even for the short interaction time of .3 psec determined in the present experiment by the transit time of the Dy-nuclei through the iron foil.

The experimental set-up used is shown in fig. 1. The Coulomb excited Dy ions pass through an iron foil of 5 μm thickness magnetized by an external field of 250 G; its direction and thus the direction of the transient field was reversed every 30 seconds. The recoiling target nuclei were detected in two position-sensitive parallel plate counters[3] (I and II in fig. 1) each covering an angular range of $20^0 \leq \Theta_{Lab} \leq 40^0$ and $\Delta\phi_{Lab} = \pm 28^0$; they were identified using the measured kinematical correlation between flighttime and scattering angle. The γ-rays were observed approximately at the maximum logarithmic slopes of the angular γ-angular correlation. (viz. fig. 1)

By the coincident measurement of γ-rays and recoil particles the direct population of particular nuclear states can be optimized choosing appropriate recoil angle intervals. Moreover the Doppler spread of the γ-lines can be compensated. An example of the Doppler corrected particle-coincident γ-spectra is shown in fig. 2. The spectra are currently being analyzed to yield intensity ratios for the two magnetic field directions from which the precession of the angular correlation can be deduced.

+ present address: Jagiellonian University, Cracow
* on leave from Jagiellonian University, Cracow

1 see e.g. M. Hass et al., Phys.Rev. C14, 2119 (1976) and J.M. Brennan et al., Phys.Rev. C16, 899 (1977)
2 J.L. Eberhardt et al., Hyperfine Interact. 3, 195 (1977)
3 P. Fuchs et al., GSI annual report, p. 195 (1977)

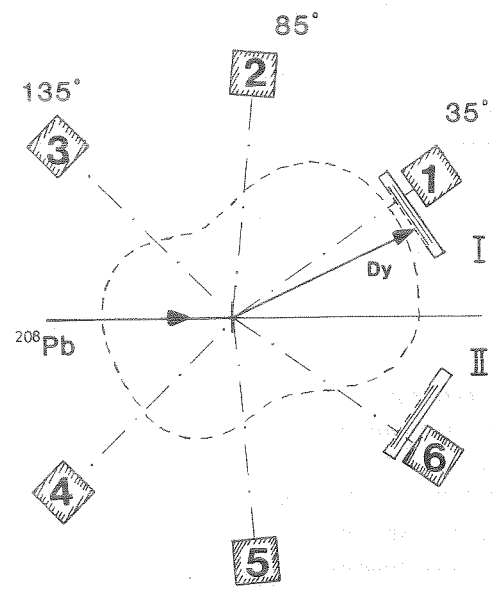


Fig. 1: The setup is symmetric about the beam axis. γ - detectors 2, 3, 5 and 6 and 1, 2, 4 and 5 are positioned at maximum slopes for correlations with counters I and II, respectively.

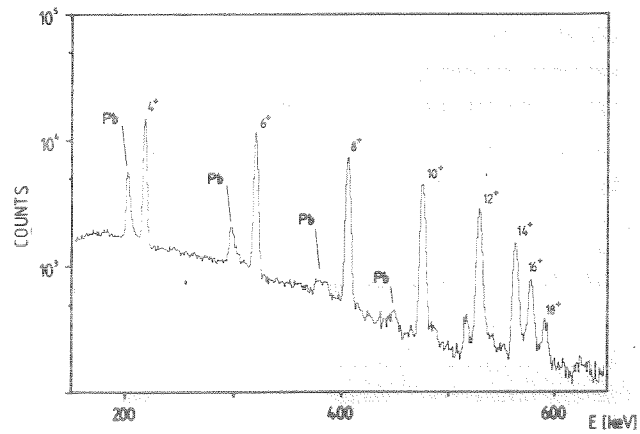


Fig. 2: Example of the corrected coincidence spectra. The lines marked Pb arise from incomplete suppression of projectile-coincident γ-rays.

Collective Properties of ^{164}Dy

H.J. Wollersheim, H. Emling, P. Fuchs, E. Grosse, and D. Schwalm
GSI Darmstadt

Rotational bands in strongly deformed n-rich nuclei such as ^{164}Dy and the coupling between these bands have been studies intensively[1] at low angular momenta with light ion induced Coulomb excitation. In an effort to determine the structure of these nuclei at high angular momenta we performed a Coulomb excitation experiment on ^{164}Dy using ^{208}Pb beams of 4.7 and 5.1 MeV/u.

The measurements were carried out using a coincidence arrangement between two position sensitive particle counters and three GeLi-detectors (for details see ref. 2). A Doppler-corrected γ-spectrum obtained at 4.7 MeV/u bombarding energy is shown in fig. 1

To extract B(E2)-values the γ-intensities were determined from the 4.7 MeV/u run as a function of the c.m. projectile scattering angle exploiting the full angular range ($35^{o} \leq \Theta \leq 150^{o}$). By comparing the observed intensities to those calculated using a semiclassical coupled channel code a step by step determination of the B(E2, I - 2 → I) values within the g-band was possible up to $I^{\pi} = 20^{+}$. These B(E2) values are in reasonable agreement with the rotational model predictions within the experimental errors.

This and the fact that the level energies in the g-band and the γ-band show only small deviations from the I(I+1) law, indicate that the rotational model is a good basis to discuss not only the low spin but also the high spin properties of ^{164}Dy. However, the intensities observed for transitions in the γ-band and between the γ- and g-band require a spin-dependent coupling between these bands which we treated in a modified RV-model. In the analysis of these transitions the ratio of the intrinsic quadrupole moments of the two bands as well as a factor reducing the interaction Hamiltonian of the original RV model[3] were adjusted to get agreement between calculated and observed yields for all transitions. The best fit was obtained for $Q_{0,\gamma} = 1.1\ Q_{0,g}$ and a reduction factor of 2.7, making use of the parametrization of ref. 4.

The magnitude of the band mixing is mainly determined by the E2 branching ratios of the $I_{\gamma} \rightarrow (I-2)_{g}$ - relative to the $I_{\gamma} \rightarrow (I-2)_{\gamma}$-transitions for I = 6,8,10, and 12. The deviation of the deduced inter-band E2-matrix elements from the Alaga-rule (which neglects the mixing between the K = 0 and the K = 2 band) is shown in fig. 2.

A first order perturbation treatment using an effective $\Delta K = 2$ interaction[5] predicts a straight line through the points at low spin and does not reproduce the high spin data. The solid line in fig. 2 shows the result of the calculation within the modified RV model. For the g-band B(E2)-values it predicts only small deviations from the rotational model in accordance with our experimental findings. Thus the renormalization in our RV-calculations yields a consistent description of the collective properties of ^{164}Dy for spins up to 20 ħ.

1 R.O. Sayer et al., Phys. Rev. C17 (1978) 1026; and references quoted therein
2 P. Fuchs et al., GSI-Jahresbericht 1977, p. 195
3 A. Faessler et al., Nucl. Phys. 70 (1965) 33
4 H.J. Wollersheim and Th.W. Elze, Nucl. Phys. A278 (1977)87
5 A. Bohr and B.R. Mottelson, Nuclear Structure, Vol. II (1975) 158 ff
6 R.N. Oehlberg et al., Nucl. Phys. A219 (1974) 543

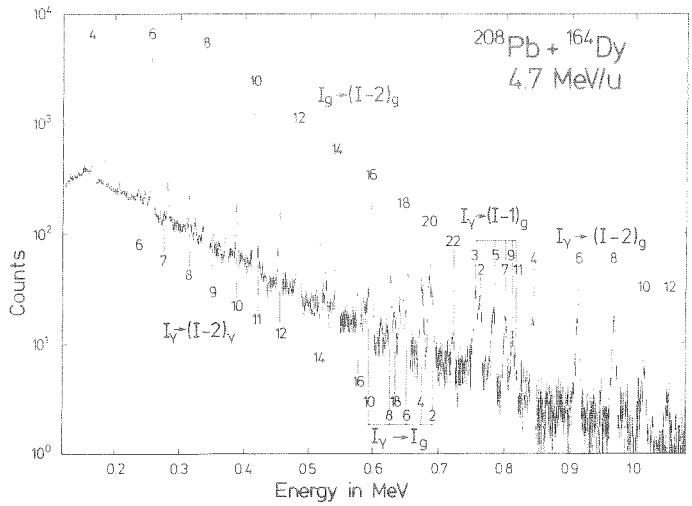


Fig. 1: Doppler-corrected γ-spectrum following Coulomb excitation of ^{164}Dy with 4.7 MeV/u ^{208}Pb-ions. (The unmarked γ-lines are due to the excitation of the target impurity ^{162}Dy.

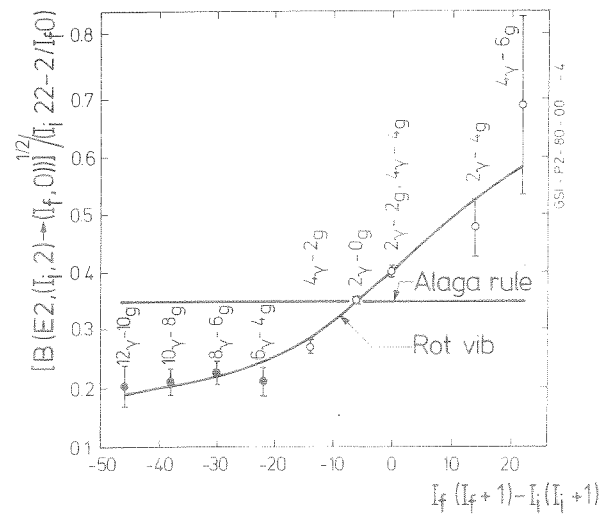


Fig. 2: Comparison of the interband E2-matrix elements with the modified rotational-vibrational (Rot.vib.) model (Φ see ref. 6)

High Spin States in ^{160}Gd and ^{176}Yb [B]

H.Bohn, T.Faestermann, F.v.Feilitzsch, P.Kienle
Physik-Department, TU-München

H.Emling, P.Fuchs, E.Grosse, D.Schwalm, H.J.Wollersheim
GSI Darmstadt

In continuing our systematic study of the behaviour at high angular momentum in neutron-rich nuclei throughout the rare earth region we investigated high spin states in ^{160}Gd and ^{176}Yb via multiple Coulomb excitation, employing a ^{208}Pb beam from the UNILAC. Thin (0.9 - 1.2 mg/cm^2), highly enriched (96.4 - 98.2%) ^{160}Gd and ^{176}Yb targets were bombarded at beam energies of 4.74 and 5.10 MeV/A. The γ-decay has been detected in coincidence with the scattered particles in a special set-up described previously.

As an example Fig.1 and Fig.2 show Ge(Li)-spectra corrected for the Dopplershift with respect to the recoils for the case of ^{160}Gd and ^{176}Yb, obtained at 5.10 and 4.74 MeV/A, respectively. These γ-spectra are in coincidence to recoils scattered into the total impact parameter range spanned by the particle detectors.

In the case of ^{160}Gd accurate energy information on the ground state band (g.s.b.) was known before only up to the 4^+ state from ß$^-$-decay data. Excitation of the g.s.b. up to the 8^+ state has been seen in older Coulomb excitation data. We observe (Fig.1) excitation of the g.s.b. up to the 22^+ state at 5.186 MeV excitation energy. The 22^+-20^+ transition is clearly visible in γ-spectra coincident to small impact parameter scattering. Concerning the excitation of side-bands up to now information about the location of the bandheads for the ß-, γ- and octupole-bands was available. We can easily interpret the γ-lines observed above ~ 800 keV (Fig.1) as transitions between members of the γ-band and g.s.b., i.e. we observe excitation of the γ-band up to $I^\pi = 12^+$, with the bandhead located at 988.5 ± 0.4 keV.

In the case of ^{176}Yb the g.s.b. has been excited in earlier Coulomb excitation experiments up to the 18^+ state, employing lighter projectiles (^{86}Kr, ^{136}Xe)[1]. We observe (Fig.2) excitation of the g.s.b. up to the 22^+ state located at 5.502 MeV. Recently information about the 2^+- and 4^+-members of the γ-band became available [2]. Analogous to the case of ^{160}Gd we interpret the γ-lines observed above ~ 1 MeV (Fig.2) as the transitions between γ-band and g.s.b., i.e. we observe excitation of the γ-band up to $I^\pi = 12^+$, with the bandhead located at 1261.4 ± 0.7 keV.

In the usual backbending plot the moment of inertia for the g.s.b. of both nuclei investigated rises only slowly with increasing rotational frequency. ^{160}Gd rotates most rigidly compared to all other stable even Gd isotopes, a behaviour similar to the one we have observed for other cases (^{170}Er, ^{180}Hf)[3]. In contrast, ^{176}Yb shows a stronger dependence compared to ^{174}Yb.

In ^{176}Yb we observe a delayed population of the 8^+ state in the g.s.b.. We interpret this as being due to the decay of the I^π, $K = 8^-$,8 isomer ($t_{1/2}$ = 11.7 s). This effect has also been observed for ^{176}Yb in other experiments, employing lighter projectiles (^{86}Kr, ^{136}Xe)[1] and is surprising because of the large K-difference between both bands.

[1] D.Ward et al., Nucl. Phys. A266, 194 (1976).

[2] L.L.Riedinger et al., Phys. Rev. C20, 2170 (1979).

[3] H.Bohn et al., Proc. Symp. High Spin Phenomena in Nuclei, 1979, Argonne National Laboratory.

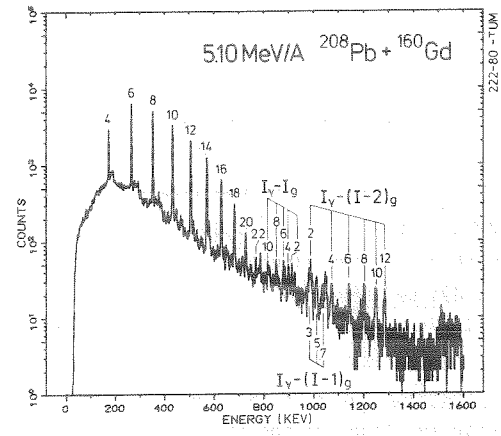


Fig. 1: Dopplershift corrected Ge(Li) spectrum for ^{160}Gd

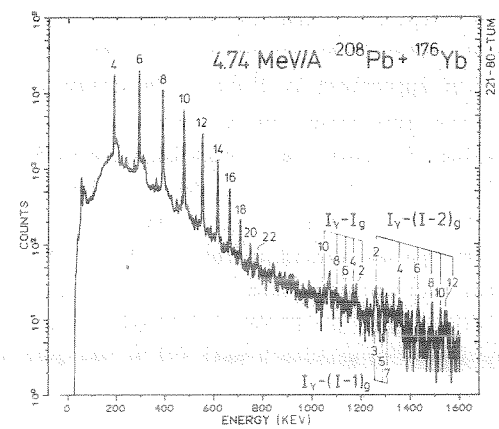


Fig. 2: Dopplershift corrected Ge(Li) spectrum for ^{176}Yb

High Spin States and E2 Transition Strengths in ^{194,196}Pt^{B}

J. Idzko, K. Stelzer, Th.W. Elze, H. Ower
Institut für Kernphysik, Universität Frankfurt am Main
H.J.Wollersheim, H. Emling, P. Fuchs, E. Grosse, R. Piercey, D. Schwalm
Gesellschaft für Schwerionenforschung, Darmstadt

The level structures of the shape transitional nuclei ^{194,196}Pt have been investigated by multiple Coulomb excitation with ^{208}Pb projectiles. The measurements included γ-ray singles and γ,γ-coincidences at a bombarding energy of 5.38 MeV/u and particle-γ-coincidences at 4.74 MeV/u, using the coincidence set-up developed at GSI[1]. Fig.1 shows the positive parity levels observed in our investigations.

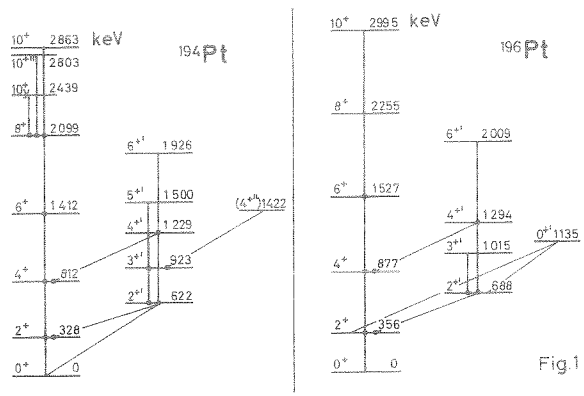


Fig.1

We observe the excitation of the ground state and γ-bands in the two nuclei up to 10^+ and $6^{+(}$ respectively. Excitation of levels in the negative parity bands was also identified. In ^{194}Pt the ground state band is excited with collective strength to a 10^+state at 2863 keV, which is 424 keV above the yrast 10^+ state known from (α,xn)-experiments[2]. In the γ,γ-experiments performed at the high bombarding energy we also observe the 10^+_y-8^+ yrast transition and a transition of 704 keV in coincidence with the lines of the ground state band. This transition shows a $0^0/90^0$ asymmetry in the coincidence intensities characteristic for a stretches E2-transition. We therefore postulate a third 10^+level at 2803 keV. From the intensity of the 704 keV line the transition can be estimated to be non-collective with an E2 strength of approximately 1 s.p.u. The situation is shown in the spin-transition energy-plot of Fig.2. B(E2) values for inter- and intra-band transitions were determined from a comparison of the experimental gamma yields observed in particle-γ-coincidence at the "safe" energy for Coulomb excitation of 4.74 MeV/u with semi-classical Coulomb excitation calculations. Starting with a preliminary set, the E2 matrix elements were systematically varied to achieve a best fit to the experimentally observed yields, and especially their impact parameter dependence. Fig.3 shows the results for the B(E2)-values in the ground state bands. The experimental values are compared with predictions of different models: the rigid symmetric rotor (SRM),the asymmetric rigid rotor with $\gamma_0=30^0$(ARM),the Interacting Boson Approximation in the O(6)limit and two calculations[3,4]on the basis of the Greiner-Gneuss model (GGM) starting from a general potential energy surface.

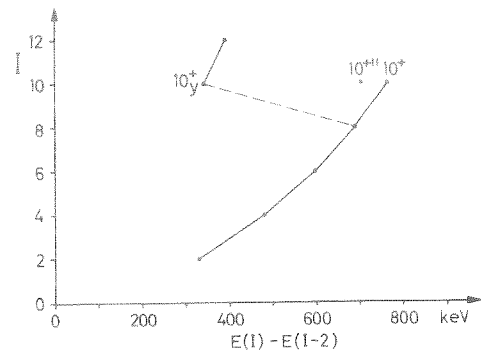


Fig.2 Spin-transition energy plot for the ground state and yrast transitions in ^{194}Pt.

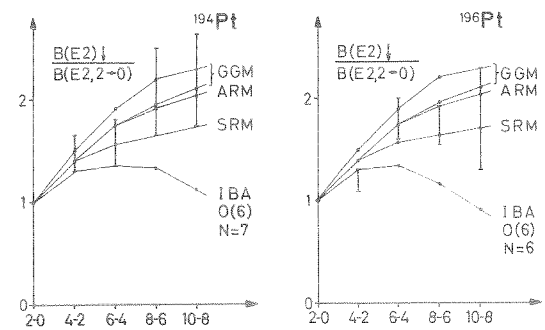


Fig.3 Experimental and theoretical B(E2)values for transitions in the ground state bands. The upper of the curves labelled GGM is for a triaxial($\gamma_0=30^0$) "γ-stiff" nucleus[3], and the lower corresponds to an oblate γ-soft nucleus[4].

The "geometrical" collective models can explain the experimentally observed B(E2)values within their errors. Because of the size of these errors and the small differences in the predictions of especially the more realistic models (GGM and ARM) a distinction between these models is not possible. On the other hand, the reduction of the B(E2)values for the transitions between states of higher spin as predicted by the IBA is not observed. The analysis of the transitions in the gamma band and between the gamma and ground state band depends more sensitively on the inclusion of additional bands and the sign[5] of inter-band E2 matrix elements. Calculations for the γ-band are in progress.

1. P.Fuchs et al., GSI Annual Report 1977,p.195
J.Idzko et al., GSI Annual Report 1978,p. 45
2. M.Piiparinen et al.,Phys. Rev. Lett.34(1975),1110
S.A.Hjorth et al., Nucl.Phys.A262(2976), 328
3. G.Leander, private communication
4. P.Hess, private communication
5. F.T.Baker et al.,Phys.Rev.Lett. 37(1976), 193

Coulomb excitation of ^{198}Hg and ^{200}Hg with ^{208}Pb ions [B]

C. Günther, H. Hübel, A. Kleinrahm
Institut für Strahlen- und Kernphysik, Univ. Bonn

J. Idzko, H. Ower, Univ. Frankfurt

H. Emling, P. Fuchs, E. Grosse, D. Schwalm, H.J. Wollersheim
GSI Darmstadt

The ground bands in the even $^{190-198}$Hg isotopes show irregularities at rather low spin values (8^+, 10^+, 12^+). This has been interpreted as a band crossing of the ground bands with aligned $(\nu i_{13/2})$- or $(\pi h_{11/2})$- bands. For ^{200}Hg the ground band is populated only up to the 6^+ state in (α,xn) reactions[1] which indicates a blocking of the alignment of the $i_{13/2}$ neutrons. Further information on the band structure of ^{198}Hg and ^{200}Hg can be obtained from multiple Coulomb excitation measurements. Previous Coulex work was carried out with light ions[2,3] and only states up to 4^+ were populated.

Targets of enriched $^{198,\ 200}$Hg with thicknesses of ~1mg/cm^2 were prepared by evaporation of HgS. For thermal stabilisation a 20 μg/cm^2 C film was evaporated onto both sides[4]. These targets showed no deterioration after several hours of bombardment with a ^{208}Pb beam of 15nA(charge) with an energy of 5MeV/A.

A particle-γ-coincidence arrangement[5] with two parallel plate avalange detectors which accepted recoil ions within a range of $15^o \leq \Theta_L \leq 60^o$ and with three Ge(Li) detectors was used. It allows the Doppler correction of the γ-energies for those events in the particle counters which correspond to the detection of a Hg ion (due to their proximity in A and Z the Pb and Hg ions cannot be separated in the particle detectors).

In order to deduce B(E2) values the observed intensities were compared to the results of DeBoer-Winther calculations. In these calculations the B(E2,2→0) and the Q(2^+) were taken from Refs.[2,3]. The quadrupole moments of the higher spin states were calculated within the rotational model. The transition matrix elements were then varied systematically until optimal agreement between the calculations and the experimental values was obtained. The results for the B(E2) values are shown in Fig.1. The most striking feature is the sharp reduction of the B(E2,8→6) in ^{198}Hg. Such a behaviour is expected for the crossing of two bands.

In ^{200}Hg the $8^+ \rightarrow 6^+$ transition could not be identified with certainty because no $\gamma\gamma$- coincidences could be measured. However, we found a transition of 973 keV which shows a dependence of the intensity on the impact parameter as calculated for a $8^+ \rightarrow 6^+$ transition. Under this assumption we obtain for its B(E2) = 0.325(43) e^{2}b^2. This value is consistent with the rotational model prediction and would indicate the absence of a band crossing in ^{200}Hg. This would explain the observed[1] unusual Yrast sequence in this nucleus: the 8^+ state would have an energy of 2.68 MeV which is much higher than that of the 5^-, 7^- members of the negative parity band. Therefore, the negative parity states become the Yrast sequence above the 6^+ state and the positive parity states with $I \geq 8$ are not populated in the compound reactions.

[1] C. Günther et al., Phys. Rev. C15, 1298 (1977)
[2] M.T. Esat et al., Phys. Letters 72B, 49 (1977)
[3] A. Bockisch et al., Z. Physik A291, 245 (1979)
[4] M.T. Esat et al., Nucl. Instr. Meth. 141, 405 (1977)
[5] P. Fuchs et al., GSI-Jahresbericht (1977), p. 195

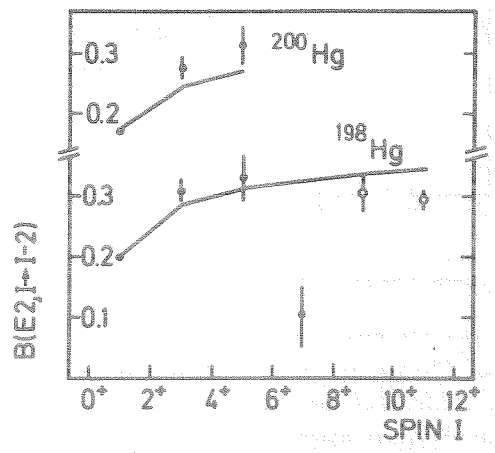


Fig. 1: B(E2) values for ^{198,200}Hg. The open circles are values derived from lifetime measurements. The solid lines are rotational model predictions.

High Spin States in ^{232}Th, ^{234}U and ^{236}U B

H. Ower, Th. W. Elze, J. Idzko, K. Stelzer, Universität Frankfurt
H. Emling, P. Fuchs, E. Grosse, D. Schwalm, H. J. Wollersheim, GSI Darmstadt
N. Kaffrell, N. Trautmann, Universität Mainz

The actinide nuclei ^{232}Th, ^{234}U and ^{236}U have been studied using multiple Coulomb excitation by 5.3 MeV/u ^{208}Pb ions obtained from the UNILAC. De-excitation gamma rays were observed with Ge(Li) detectors in coincidence with both the scattered projectile and recoil nucleus. These particles were detected by two position sensitive parallel plate counters developed at GSI[1]. By measuring time of flight and scattering angle of both particles it was possible to correct for the large Doppler shifts of the gamma rays and to determine the impact parameter dependence of the gamma yields. Representative corrected spectra are shown in Fig. 1.

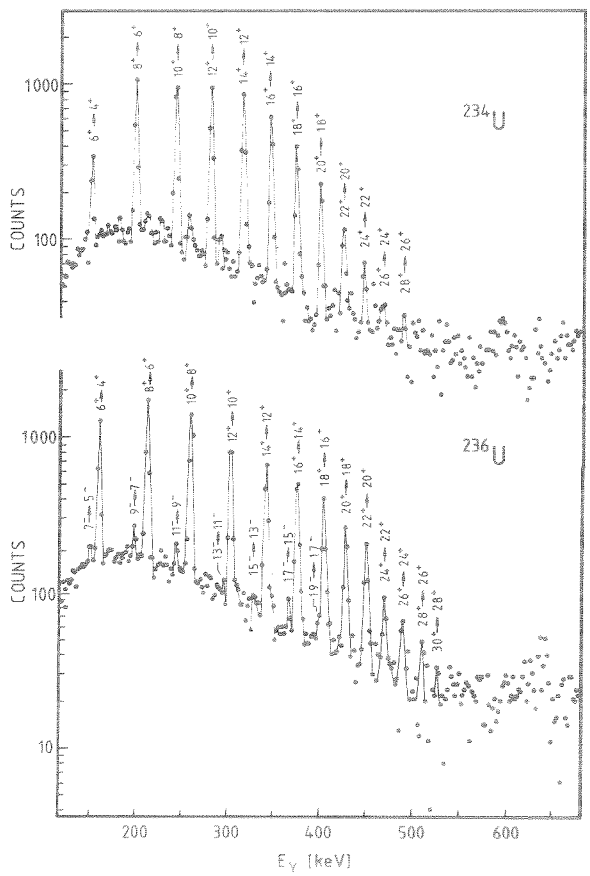


Fig. 1: Gamma spectra from Coulomb excitation of ^{234}U and ^{236}U

The ground state bands are observed up to spin 28^+ in ^{232}Th and ^{234}U and 30^+ in ^{236}U. Levels of the $K = 0^-$ octupole vibrational band were also identified. Fig. 2 shows the effective moment of inertia of the ground state band vs. rotational frequency. From the apparent upbending above spin 14 (e.g. ^{236}U) a rotation aligned angular momentum of 4 to 5 $\hbar$ at I = 26 can be deduced using the prescription of Bengtsson and Frauendorf[2]. The orbits responsible for this behaviour could be $\nu j15/2$ and/or $-i13/2$.

The experimentally determined gamma yields of the transitions within the ground state band are compared with results of semi-classical Coulomb excitation calculations based on the following nuclear models: rigid rotor, interacting-boson model[3], and rotation-vibration model[4]. Although this analysis has not been completed, preliminary results can be given. If only ground band levels are included in the calculation, the gamma yields are reproduced by the rigid-rotor model. The excitation of side bands, in particular the octupole vibrational band, cannot be neglected, however. Taking these side bands into account, the calculated gamma yields are found to become smaller than the measured values. The experimental uncertainties, however, make it difficult to decide to what extent the rigid-rotor model has to be modified. The interacting-boson model predicts a cut-off in the ground state rotational band at spin 24^+, 26^+ and 28^+ for ^{232}Th, ^{234}U and ^{236}U, respectively, and a strong reduction in the gamma yields in the high-spin region. This is in contrast to our data. Calculations employing the rotation-vibration model, which predicts larger gamma yields with increasing spin, are in progress.

1. P. Fuchs et al., GSI Annual Report 1977
2. R. Bengtsson and S. Frauendorf, Nucl. Phys. A327 (1979) 139; S. Frauendorf and R. S. Simon, GSI Annual Report 1979
3. A. Arima and F. Iachello, Ann. Phys. (N.Y.) 111 (1978) 201
4. M. Seiwert and P. Hess, private communication
5. R. Piercey et al., GSI Annual Report 1979

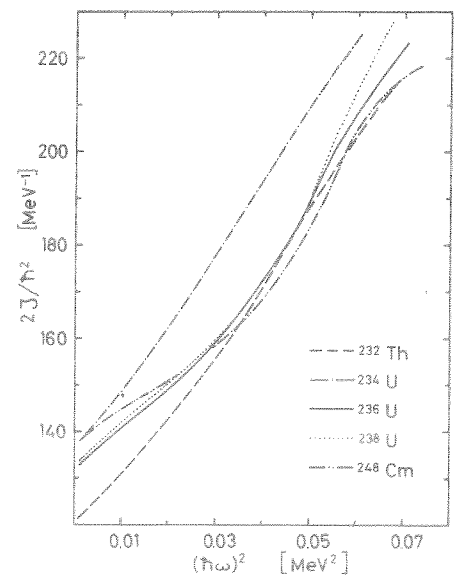


Fig. 2: Effective moment of inertia vs. rotational frequency. ^{238}U data from Ref.1, ^{248}Cm data from Ref.5

High Spin States in ^{248}Cm from Multiple Coulomb Excitation with ^{208}Pb Ions

R.B. Piercey[+*], H. Emling[+], P. Fuchs[+], E. Grosse[+], H.J. Hamilton[*▽], H. Ower[o], A.V. Ramayya[*], D. Schwalm[+], N. Trautmann[§], and H.J. Wollersheim[+]

[+] GSI Darmstadt; [*] Physics Dept., Vanderbilt University, Nashville, USA
[▽] Senior Alexander von Humboldt Fellow, Inst. for Theoretical Physics, University of Frankfurt
[o] Institute for Nuclear Physics, University of Frankfurt
[§] Institute for Nuclear Chemistry, University of Mainz

The ground state rotational band of ^{248}Cm has been studied up to spin 28^+ and tentatively to 30^+ by multiple Coulomb excitation using ^{208}Pb ions of 5.3 MeV/amu. The gamma-rays emitted from the recoiling curium nuclei were corrected for the strong Doppler broadening by detecting both the scattered Pb and the recoiling Cm particles in two gas detectors.[1] By measuring the time-of-flight difference of the kinematically coincident particles, it was possible to distinguish the scattered Pb ions from the recoiling Cm particles. A corrected gamma-ray spectrum is shown in fig. 1

A precise measurement of the transition energies was achieved by averaging the energies observed in two gamma detectors, one situated to detect gamma-rays emitted in the direction of the recoiling Cm nucleus and the other detector at 180^o to the Cm recoil direction. In this technique, errors associated with uncertainities in the recoil velocity and in the alignment are such that total errors in the transition energies are, for most of the transitions, less than 0.2 keV. The tentative identification of the $(30^+ \rightarrow 28^+)$ is based on the angular impact parameter dependence of the γ-ray yield.

The energy levels of ^{248}Cm determined in this way show an anomalous tendency at high spin to be too low as compared to the extrapolated level energies using the Harris-expression[2]. This trend corresponds to an upbending in an effective moment of inertia vs. rotational frequency plot and is illustrated in a more dramatic way in a plot[3] of Δ^2E vs I (fig. 2). It is not yet known exactly what causes this anomalous behaviour but a similar behaviour can be seen in the other actinides studies at GSI[4]; it might be due to a band crossing of the gs-band with a rotational aligned $\nu j_{15/2}$ or $\pi i_{13/2}$-band[5].

The experimentally determined γ-ray intensities are compared to semi-classical Coulomb excitation calculations for different scattering angles to get information about the B(E2)-values in the ground band. The observed yields are lower than the ones predicted by the simple rigid rotor model. Although the band heads of the γ, β and octopole bands are above 1 MeV, their influence on the observed yield in the gs-band can still be appreciable. The influence of these bands onto the determination of the B(E2)-values within the gs band is presently being investigated.

1 P. Fuchs, Ph.D. theses and P. Fuchs et al., GSI annual report 1977, 195
2 S.M. Harris, Phys. Rev. 138 (1965) B 509
3 L.K. Peker and J.H. Hamilton, Proc. Int. Conf. on Nuclear Structure, Contributed Paper, Tokyo, 1977, p. 110.
4 H. Ower et al., GSI annual report 1979,
5 S. Frauendorf and R.S. Simon, GSI report 1979.

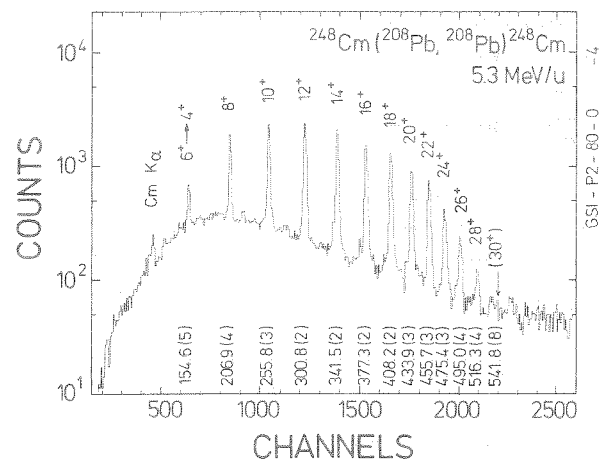


Fig. 1. A Doppler-shift corrected spectrum showing the gamma-rays observed for small impact parameters in ^{248}Cm (Transition energies in keV)

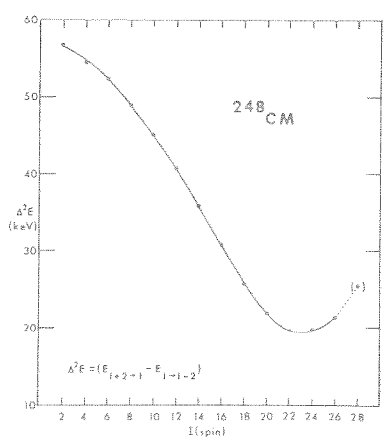


Fig. 2. Δ^2E plot of the level energies of the gs band members of ^{248}Cm showing the anomalous behaviour at high spin.

Search for Yrast traps

S. Bjørnholm, J.Borggreen, O. Christensen, A. Del Zoppo, B. Herskind, R.M. Lieder, J. Pedersen, and G. Sletten
The Niels Bohr Institute, University of Copenhagen

F. Folkmann, University of Arhus and R.S. Simon, GSI Darmstadt

High spin isomers identified during previous searches for yrast traps[1] have been explained as shell model states in spherical, or weakly oblate potentials with energies in the range 3-10 MeV and spins of 10-30 $\hbar$. Major shape changes are predicted to occur at even higher spins[2,3], and could lead to the formation of very high spin isomers. So far, these have not been found, but a lowering of the experimental detection limit from 10 ns to a few hundred picoseconds would perhaps make it possible. A search was therefore initiated with the new system described in ref.[4], and employing beams of ^{132,136}Xe and ^{48,50}Ti. The heaviest compound system populated was $^{198}_{82}$Pb and the lightest $^{144}_{60}$Nd. Between these extremes 24 different compound nuclei combining ^{136}Xe and the most neutron rich target isotope were investigated. Another 50 compound nuclei in the same Z range, but with lighter mass were formed by reactions with ^{132}Xe and ^{48,50}Ti.

Results obtained so far:

1) New isomeric species are detected with half lives in the range 0.2 ns $\lesssim T_{\frac{1}{2}} \lesssim$ 10 ns. The multiplicities are of the order of 12 or less.
2) As with the longer-lived isomers, the new ones are concentrated to the region around $Z \lesssim 68$, and $N \lesssim 86$. Below the N = 82 shell the isomers disappear.

The results do not exclude the existence of very high spin yrast traps for two reasons:

1) The apparent low multiplicity could result from short-lived isomeric states situated above known longer-lived $T_{\frac{1}{2}} \gtrsim 30$ ns isomers and therefore still represents decay of very high spins. Measurements of discrete Ge-spectra can in principle answer this question.
2) The sensitivity of the method with respect to cross section varies from 250 μb in the Er region (^{50}Ti bombardments) to about 10 mb in the Pt-Pb region (^{136}Xe beams). This is possibly insufficient to detect yrast traps.

Further improvements of the method are under consideration.

[1] J. Pedersen, B.B. Back, F.M. Bernthal, S. Bjørnholm, J. Borggreen, O. Christensen, F. Folkmann, B. Herskind, T.L. Khoo, M. Neiman, F. Pühlhofer, G. Sletten, Phys. Rev. Lett. 39, 990 (1977)

[2] A. Bohr and B.R. Mottelson, Physica Scripta 10A, 13 (1974)

[3] T. Døssing, K. Neergård, K. Matsuyanagi, Hsi-Chen Chang, Phys. Rev. Lett. 39, 1395 (1977)

[4] S. Bjørnholm et al., GSI Jahresbericht 1978, 52

Gamma-spectroscopy within the island of high-spin isomers near N=82

J. Borggreen, S. Bjørnholm, O. Christensen, A. Del Zoppo, B. Herskind, J. Pedersen and G. Sletten
The Niels Bohr Institute, University of Copenhagen

F. Folkmann, University of Arhus and R.S. Simon, GSI Darmstadt

A NaI sum-spectrometer combined with Ge-counters has been used to characterize the members of the island of high-spin isomers near N=82, ref.[1]. From the analysis of half lives, total γ-decay energies and discrete γ-lines it is found that 22 isomers, some previously known others unknown, are produced in the experiments.

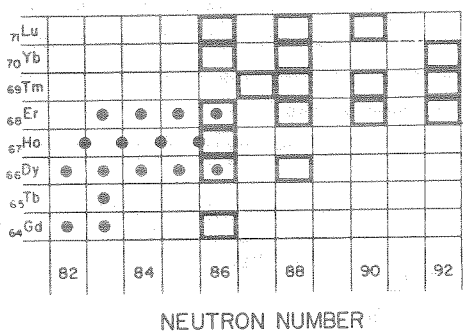


Fig.1

In fig.1 the location of the high-spin isomers is shown. Squares indicate compound nuclei formed (with ^{50}Ti and ^{65}Cu beams) and dots the nuclei where high-spin isomers are observed. In the Ho-isotopes the assignment is uncertain by one mass unit.

A characteristic feature is the sharp borderline at N=86. High-spin isomers disappear when N exceeds 86. This borderline reflects the onset of prolate deformations. The isomers are thought to be due to strong alignment of two to eight shell-model particles in a spherical or possibly weakly oblate potential.

In table 1 the major characteristics of the isomeric states are given. In most nuclei there is more than one isomeric state.

The most interesting case is ^{152}Er where isomers with excitation energies of ∿ 8.5±0.4 MeV and > 12.2 MeV, and half lives 32±3 ns and 4±2 ns, respectively, are found. From an empirical relation between spin and excitation energy we have estimated the isomeric spin values to be (25±2) ħ and > 33 ħ, respectively.

A more detailed spectroscopic study of this nucleus is in progress (see this report).

Table 1. Major associated γ-lines

Isomeric nucleus	$t_{\frac{1}{2}}$ upper / lower (ns)	E_γ (keV) and relative intensity	E_{exc} (MeV)
$^{148}Tb_{83}$	≳500	214(0.3),240(0.7),283(0.9),351(0.5),523(0.9),743(0.7),858(0.4), 1,335(1.0)	7.55±0.4
	22±2	1,006(1.0)	
$^{149,150}Ho_{82,83}$	≳100	337(0.5),436(0.6),636(1.0),648(0.7),671(0.9),777(0.9),896(0.6)	7.20±0.4
	45±20	305(0.9),727(1.0)	
$^{150,151}Ho_{83,84}$	1.500±500	191(0.4),350(0.8),363(1.0),1.060(0.9)	7.05±0.4
	50±5	225(0.5),263(0.6),280(0.4),313(0.6),630(0.5),887(0.2),1.098(1.0)	
$^{151,152}Ho_{84,85}$	≳500		7.3±0.8
	65±15	712(1.0)	
$^{152,153}Ho_{85,86}$	30±15		6.0±0.8
	≲400	605(1.0),712(1.0),734(1.0),760(0.9)	
$^{151}Er_{83}$	45±5	143(0.2),451(0.7),704(0.6),866(1.0)	3.4±0.2
	37±10	198(1.0)	
$^{152}Er_{84}$	<10		>12.2
	32±3	230(0.6),280(0.9),310(0.2),330(0.5),423(1.0),519(0.3),554(0.9), 562(0.5),564(0.6),673(0.9),731(0.3),765(0.9),787(1,1),809(1.1), 941(0.2),1.052(0.3),1.185(0.2),1.212(0.3),1.395(0.2)	8.5±0.4
$^{153}Er_{85}$	1.000±500	350(1.0),357(0.8),364(0.6),419(0.7),429(0.5),654(0.4),747(1.0), 911(0.9)	5.2±0.3
	300±100	300(0.8),341(1.0),588(0.7),713(0.7),812(0.7)	

[1] J. Borggreen, S. Bjørnholm, O. Christensen, A. Del Zoppo, B. Herskind, J. Pedersen, G. Sletten, F. Folkmann, R.S. Simon, Z. Physik A294, 113 (1980)

Spectroscopic study of the high-spin isomers in ^{152}Er

C. Baba, S. Bjørnholm, O. Christensen, B. Herskind, R.M. Lieder, J. Pedersen and G. Sletten
The Niels Bohr Institute, University of Copenhagen

F. Folkmann, University of Arhus and R.S. Simon, GSI Darmstadt

Two high spin isomers, with half lives $t_{\frac{1}{2}}$ = 32±3 ns and $t_{\frac{1}{2}}$ = 4±2 ns, are identified in ^{152}Er (ref.[1] and this report). From the measurement of their excitation energies the isomeric spin values are estimated to be 25±2 ħ and > 33 ħ, respectively. These isomers offer a unique possibility for a more detailed study of structural effects at high angular momenta. The present experiment is designed to study the decay and feeding of these isomers. The reaction is $^{48}Ti + ^{108}Pd \rightarrow ^{152}Er + 4n$, E(Ti) = 225 MeV with a beam duty-cycle of 50%. The set-up consists of five Ge-detectors, three 3"x3" NaI crystals and at large distance ($\Omega \times \varepsilon \simeq 0.2\%$ at $E_\gamma \sim 1$ MeV) one 5"x6" NaI crystal. For each of the detectors, both energy and time relation with respect to the beam burst are recorded.

The energy gain of the individual detectors is adjusted to allow a summation of the individual spectra. Thus, the five Ge-detectors offer 20 combinations of two-fold coincidences. The overall energy resolution after summation is 2.3 keV at $E_\gamma \sim 1.3$ MeV.

Only three-fold coincidences, where at least two Ge-detectors are triggered and where at least one of the three detectors is triggered delayed (>5 ns) with respect to the "earliest" detector, are recorded event-by-event. In a running time of 48 hours approximately 30 million events of this kind are recorded.

From the preliminary analysis of the data a decay-scheme for the 32±3 ns isomeric state is proposed, placing the isomeric level at 8.970 MeV excitation energy. The level scheme is showing an increased complexity above spin 16. Thus the decay from 16^+ to the ground state proceeds through eight E2 transitions whereas in the decay from the isomer ($I \gtrsim 26$ ħ) to the 16^+ state approximately 35 γ-lines are observed.

The level scheme between the two isomeric states is not yet established, but the data indicate a similarly complex pattern. In the proposed decay scheme no evidence for rotational structure is observed. The gamma spectrum obtained by the 5"x6" NaI crystal during the beam burst, with the requirement that the event is followed by doubly delayed events, the first one occurring within the time interval 5-25 ns and the latter one in the time interval from 40-70 ns after the beam burst, is shown in fig.1.

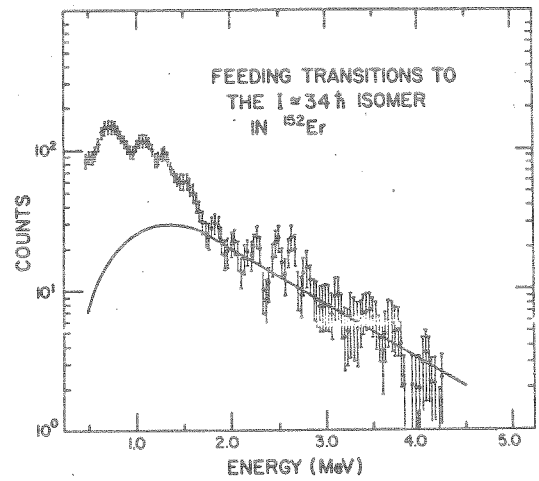


Fig. 1.

This spectrum is interpreted as feeding transitions to the upper of the two isomeric states (I > 33 ħ). The characteristic feature is the large amount of intensity around 750 keV presumably of dipole character. Assuming that the statistical part (drawn line) represents 4 transitions on the average, the dipole part is equivalent to 5 transitions, and the intensity in the energy interval from 1.0 to 1.6 MeV represents 7 transitions.

This observation does not indicate a rotational structure built on top of the isomeric state but rather that the nucleus stays spherical or weakly deformed up to even higher spin values (∿45 ħ).

[1] J. Borggreen, S. Bjørnholm, O. Christensen, A. Del Zoppo, B. Herskind, J. Pedersen, G. Sletten, F. Folkmann, R.S. Simon, Z. Physik A294, 113 (1980)

INVESTIGATION OF HIGH-SPINSTATES OF ^{212m}Po IN THE REACTION ^{208}Pb → ^{nat}U [B]

P. Lemmertz, R. Faß, L. Alquist, F. Kassen, H. Wollnik
II. Physikal. Institut, Universität Giessen
D. Hirdes, H. Jungclas, G. Dersch, R. Brandt
Kernchemie, Phillipsuniversität Marburg

During the search for superheavy elements[1] via the reaction ^{208}Pb → ^{nat}U we measured some new properties of the ^{212}Po level scheme, using the GSI gasjet system. α-γ-coincidences and time-of-flight measurements on α-recoils were performed.

The excited states of Po are populated from the β-decay of ^{212m}Bi. This was first described by Baisden[2] in a similar heavy ion experiment (Ar→U). Our results confirm that measurement and with the α-γ-coincidences we could obtain some more information. The $_{\beta}$-energies are in good agreement with the results of Lieder[3], who performed an in-beam experiment (α → ^{209}Bi).

Table 1 gives a comparison of relevant results from previous measurements and new information obtained in this experiment. The mass of the 11.6 MeV activity was determined to be 212.3±1.7 u. Despite the fact that only about 10 % of the activity belongs to the 9 min halflife this provides experimental confirmation of the interpretation of Baisden for that α-activity. The mass of the 10 MeV group is 216±6 u. The 121 keV γ-transition, which heretofore was not placed in the scheme, depopulates the 8^+ state. The α-energies fit well with the levels obtained from the γ-energies, the differences being within the error of the α-energies (5keV). Six new weak α-lines are seen. The 10.009 MeV line may belong to a level proposed by Bertolini[4]. The 10.302 MeV and 10.302 MeV lines may correspond to levels deduced by Faestermann[5]. The 10.5 MeV line fits with the γ-energy of 275 keV which fedds the 8^+ state. From these remarks we conclude that the β-decay of ^{212m}Bi not only populates the 8^+ level of Po but also some higher levels.

Fig. 1 shows a level scheme with all information about the relevant states.

1 D. Hirdes et. al. GSI-Jahresbericht 1979, S.
2 P. Baisden et. al. Phys. Rev. Lett. 41, (1978),738
3 R. Lieder et. al. Phys. Rev. Lett. 41, (1978), 742
4 G. Bertolini et. al. Nucl. Phys. 30 (1962) 599
5 T. Faestermann et. al. Frühjahrstagung der DPG Kernphysik, München 1980

This work		Baisden[2]	Lieder[3]
Eα MeV	9.896 *	9.890	
	10.009		
	10.110 *	10.105	
			10.187
	10.229 *	10.220	
	10.302		
	10.332		
	10.366		
	10.410		
	10.500		
Eγ keV	727		727.7
	404		405.2
	223	no gammas measured	222.9
	121		120.6
	275		
			375.7
			578.0

Table 1. Comparison of our results with ref1 and ref2. The three strongest lines are marked with an asterik, the error in energy is±5 keV for these lines and ±10 keV for the others.

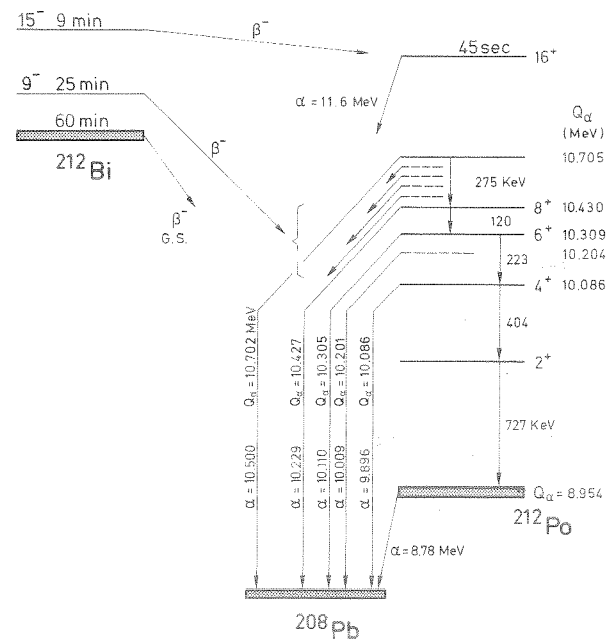


Fig. 1 Energies given to the right of the levels represent Q-values which were determined on the basis of ground state Q-value and the γ-energies; the Qα-values on the left hand side are from the experimental α-energies.

Nuclear Charge Radius, Spin and Nuclear Moments of ^{45}Ca by Laserspectroscopy

E. Bergmann, P. Bopp, J. Kowalski and F. Träger
Physikalisches Institut der Universität Heidelberg

G. zu Putlitz
Gesellschaft für Schwerionenforschung, Darmstadt
and Physikalisches Institut der Universität Heidelberg

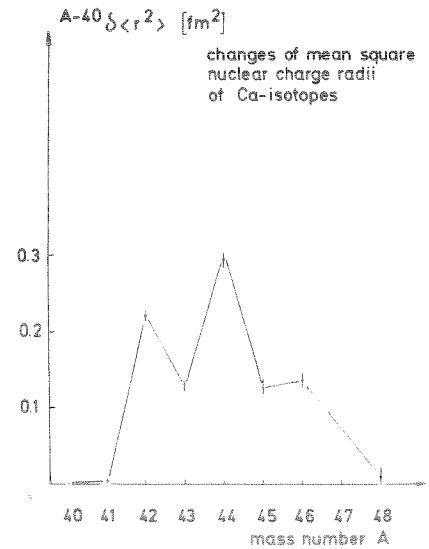
Extensive studies of the Ca-isotopes have revealed a rather peculiar change of the charge radii between double magic ^{40}Ca and double magic ^{48}Ca [1,2]. Whereas all the even isotopes with mass number 40-48 have been investigated, only little information on the charge radii of the odd isotopes was available. So far, only ^{43}Ca, which is stable and easily accessible to measurements, and radioactive ^{41}Ca could be studied. These odd mass nuclei exhibit some extraordinary features like the smaller charge radius of ^{43}Ca relative to its even neighbors of the charge radius of ^{41}Ca being equal to the one of ^{40}Ca.

In this paper measurements on a third odd mass isotope, ^{45}Ca, are reported [3]. ^{45}Ca was produced by neutron capture from isotopically enriched ^{44}Ca(98,55%) and evaporated to form a collimated atomic beam. The experimental technique applied here makes use of a frequency stabilized tunable dye laser to excite the different Ca-isotopes and hyperfine structure (hfs) components selectively from the $4s^2\ ^1S_0$ ground state to the long lived (τ=0.39 ms) $4s4p\ ^3P_1$ level by laser light of λ=6573 Å. The reemitted resonance fluorescence radiation is observed by a photomultiplier about 12 cm downstream the atomic beam. Details of the experimental technique and of the set-up have been described in previous publications. In order to keep the activity of the sample as low as possible only 60 mg of metallic Ca were used for the production of the atomic beam. Taking into account the low ^{45}Ca concentration of 0.018% this corresponds to an amount of this isotope as small as 10µg. This tiny quantity, however, is sufficient to observe ^{45}Ca with a good signal-to-noise ratio.

From the hfs measurements the following values for the spin, the magnetic moment and the quadrupole moment of the ^{45}Ca-nucleus have been obtained:

$$I = 7/2$$
$$\mu_I = -1{,}3278(9)\ \mu_N$$
$$Q = +0.043(9)\ b$$

In addition the isotope shift of ^{45}Ca relative to ^{40}Ca has been determined. The value of $^{40\text{-}45}\Delta\nu$=1259.6(9) MHz must be separated for the mass and field shift part of the total isotope shift $^{40\text{-}45}\Delta\nu$ in order to get information on the change of the mean square nuclear charge radius $^{40\text{-}45}\delta\langle r^2\rangle$. This separation is accomplished by means of a King-plot using $\delta\langle r^2\rangle$-values from isotope shifts in the K_α-line of muonic Ca-atoms [2] and isotope shift data of high accuracy in the intercombination line [1]. The figure shows how the value of $^{40\text{-}45}\delta\langle r^2\rangle$ = 0.127(10) fm^2 fits into the results for the other Ca-isotopes. This very peculiar change of the charge radii can be understood by different theoretical approaches and can be interpreted as a change of deformation in the $f_{7/2}$ neutron shell.



This work was sponsored by the Deutsche Forschungsgemeinschaft.

[1] E. Bergmann, P. Bopp, C. Dorsch, J. Kowalski, F. Träger, G. zu Putlitz, Z. Physik A294, 319 (1980)
[2] H. Wohlfahrt, E. Shera, M. Hoehn, Y. Yamazaki, G. Fricke, R. Steffen, Phys. Lett. 73B, 131 (1978)
[3] E. Bergmann, P. Bopp, J. Kowalski, F. Träger, G. zu Putlitz, Z. Physik A292, 401 (1979)

Gamma-Ray Catalog [G]

U. Reus and W. Westmeier
Institut für Kernchemie, Universität Marburg
I. Warnecke*
GSI Darmstadt

The objective of this project is the production and updating of a catalog comprising all available information on gamma-rays from the radioactive decay of nuclides which is useful for the identification of nuclides from gamma-ray spectra, for cross-section determinations, etc. Technical information about structure and layout of the catalog has been reported earlier[1,2].

In brief, Part I of the catalog is a listing of about 20,000 gamma-rays, ordered by increasing energy which is to be used for identification purposes. Part II of the catalog is ordered by mass number A and nuclear charge Z and contains the complete data sets for about 2,300 nuclides and isomers, i.e. about 35,000 gamma-energies, each data set including all important information on the decay of that nuclide, references, comments, etc.

The first complete version of the catalog has been printed at GSI and appeared as GSI-Report 79-2 in February 1979, with 240 copies in this first edition. Of these, about 90 copies were sent to people and institutions which were known to be interested or which were thought to be possible users. The remaining copies were distributed in fulfillment of requests arriving over the year from laboratories all over the world. Towards the end of the year, the stock had strongly diminished, and it will probably be exhausted sometime in 1980.

During the year, the preparations for a second edition of the catalog were started. A complete revision of the data will be performed, and the latest experimental results available from the literature will be included. The termination of these efforts is scheduled for the middle of 1980. Possibilities for a change in the publication modus to obtain a higher number of copies and thus be able to fulfill all demands are currently under discussion.

* Present address: Physikalisch-Technische Bundesanstalt, D-3300 Braunschweig.

[1] U. Reus and W. Westmeier, GSI-Report J-1-78 (1978), 184.

[2] U. Reus, W. Westmeier and I. Warnecke, GSI-Report 79-11 (1979), 54.

Beta-Delayed Proton and Alpha Decay of ^{114}Cs: Evidence for a Resonance in the Beta-Strength Function ?

E. Roeckl, G.M. Gowdy, R. Kirchner, O. Klepper, A. Piotrowski, A. Płochocki, W. Reisdorf, P. Tidemand-Petersson, J. Żylicz (GSI Darmstadt), D. Schardt (Institut für Kernphysik, Technische Hochschule Darmstadt), G. Nyman (Department of Physics, Chalmers University, Göteborg), W. Lindenzweig (Institut für Kernchemie, Universität Mainz)

Fusion reactions between 5.0 MeV/u ^{58}Ni projectiles and ^{58}Ni target nuclei were used to produce ^{114}Cs activity, which was studied by on-line mass separation and decay spectroscopy. The saturation source strength after mass separation amounted to about 300 s^{-1}, allowing first gamma-gamma coincidence measurements for the decay of this lightest known isotope of cesium. The following ^{114}Xe levels (excitation energy in keV) and spins/parities were identified: 449.7/2^+, 1068.0/4^+ (tentative assignment) and 1147.6/2^+. The beta-delayed proton and alpha spectra of ^{114}Cs were measured (see Fig. 1), yielding a branching ratio of 0.07(2) for proton decay and a probability ratio of 44(3) between proton and alpha emission.

Calculations of branching ratios and spectra of beta-delayed particles were carried out for ^{114}Cs using the approach outlined in ref. 1, which is based on a statistical model[2]. For the ^{114}Cs decay energy and the particle binding energies in ^{114}Xe we used the predicted values given in ref. 1. The low-energy levels of ^{113}I and ^{110}Te, which were assumed to be populated after particle emission, were taken from systematics. Assuming a spin/parity of 1^+ for ^{114}Cs, the calculations were based on two different shapes of the beta-strength function S_β (see Fig. 1). The "constant-plus-Gaussian" S_β yielded a probability ratio of 38 between beta-delayed proton and alpha decay in good agreement with experiment; the calculated branching ratio of 0.26 for beta-delayed proton emission appears to be too high. The latter effect might be reduced by taking into account a possible beta-feeding of ground and first excited state of ^{114}Xe, which is suggested by the above gamma-ray studies but not considered in the calculation. The most striking effect, however, is the comparison between experimental and calculated particle spectra (see Fig. 1): The assumption of a constant S_β result in a shift towards low energy, whereas good agreement is obtained by introducing a "bump" in S_β; this structure, which might be due to a $(\pi g_{9/2})^{-1}(\nu g_{7/2})^1$ resonance, is much more pronounced than those assumed earlier for ^{115}Xe (ref. 2), ^{109}Te (ref. 3) and the light barium isotopes (ref. 4).

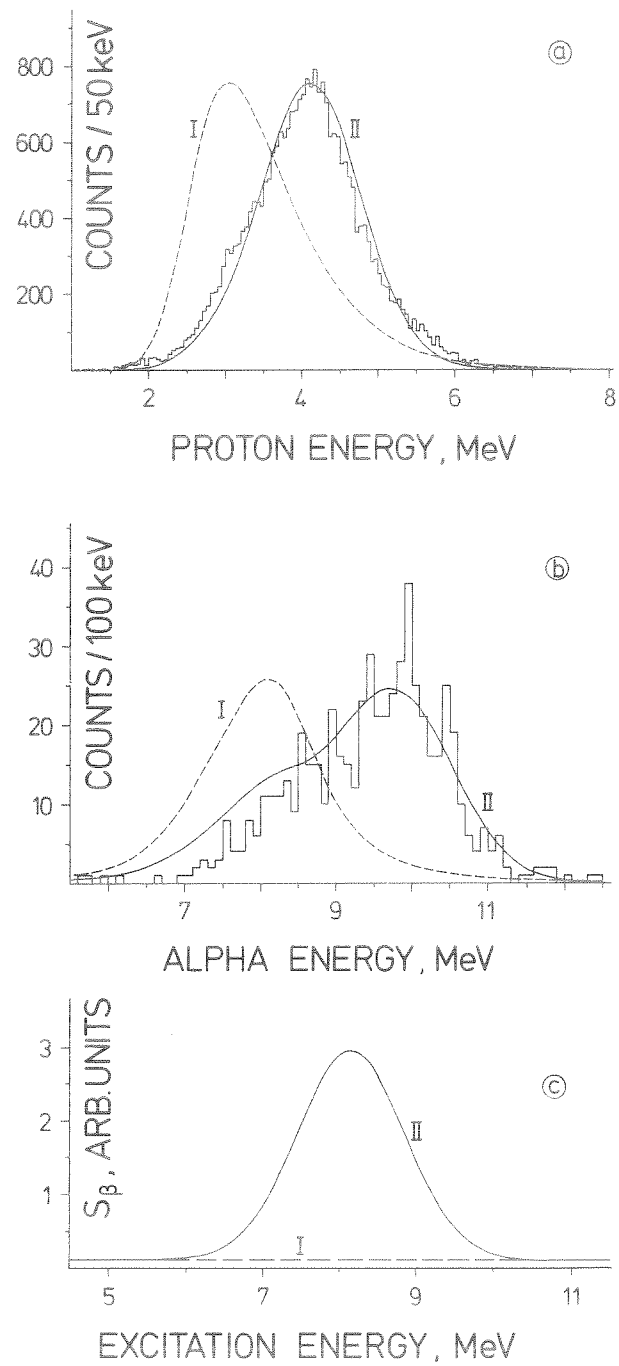


Fig. 1: Experimental (histograms) and theoretical (smooth curves) spectra of beta-delayed protons (a) and alpha particles (b). The theoretical spectra are based on the beta-strength functions S_β shown in part (c).

[1] B. Jonson et al., Proc. 3rd Int. Conf. on Nuclei far from stability, Cargèse, 1976, CERN 76-13, p.277

[2] P. Hornshøj et al., Nucl. Phys. A187, 609 (1972)

[3] D.D. Bogdanov et al., Sov. J. Nucl. Phys. 18, 1 (1974)

[4] D.D. Bogdanov et al., Nucl. Phys. A303, 145 (1978)

Identification of Two new Alpha Emitting Isomeric States

S. Hofmann, G. Münzenberg, W. Faust, T. Kitahara, W. Reisdorf, F. Heßberger, H.J. Schött, P. Armbruster, GSI Darmstadt

K. Güttner, B. Thuma, II. Phys. Inst. Universität Gießen

Further reactions were investigated to identify the earlier found two high energetic α lines (α_1 and α_2 in fig. 1). An identification with the newly developped technique of position and time correlations[1] was undertaken.

All compound nuclei where the high energetic α lines were observed are shown in the chart of nuclei (fig. 2). Signed with an "n" are those compound nuclei, where the α lines could not be found. The excitation energies of the compound nuclei were in the region between 40 MeV and 90 MeV. The highest measured cross section for the line α_1 was 1.1 mb in the reaction $^{58}Ni + ^{102}Ru \rightarrow ^{160}Hf$ ($E^* = 72$ MeV) and for the line α_2 it was 0.26 mb in the reaction $^{58}Ni + ^{102}Pd \rightarrow ^{160}W$ ($E^* = 57$ MeV) assuming a total efficiency of SHIP of 10 %.

A correlation was found between the line α_2 and the decay of ^{152}Er (fig. 3). Therefore, possible emitters of α_2 are the isobars A = 156. From those the isobars ^{156}Lu and ^{156}Yb can be excluded, because α_2 was not observed in reactions leading to ^{159}Lu as compound nucleus at excitation energies of 57, 61, and 68 MeV. The only possible decay chain left is drawn in fig. 2 and starts from the isotope ^{156}Hf identified as emitter of α_2.

A correlation of α_1 with daughter α lines could not be observed. The reactions leading to ^{159}Lu as compound nucleus show that one of the isotopes ^{155}Lu or ^{156}Lu is the emitter. From these two ^{156}Lu can be excluded because in this case a correlation with ^{152}Er would have been observed like in the former discussion of α_2. We conclude ^{155}Lu is the emitter of α_1.

The difference in the Q_α values between high energy transitions and ground state transitions give the excitation energies of the isomeric states of (1798 ± 12) keV and (1977 ± 18) keV for α_1 and α_2, respectively. Possible spin values of 10 ħ were already discussed in ref. [1]. Finally, we add that the two states belong to isotones with N = 84. The systematics of reduced α widths shows that these isotones two neutrons beyond the closed shell have an enhanced ground state transition probability. This may explain that especially for these isotones α decay becomes a competitive decay mode of isomeric states.

[1] S. Hofmann et al., Z. Physik A291, 53 (1979)

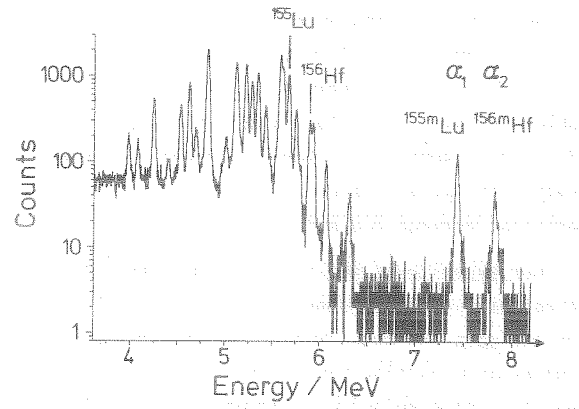


Fig. 1: α spectrum taken during the irradiation of ^{106}Cd with ^{58}Ni at excitation energies of the compound nucleus ^{164}Os of 64 MeV and 76 MeV.

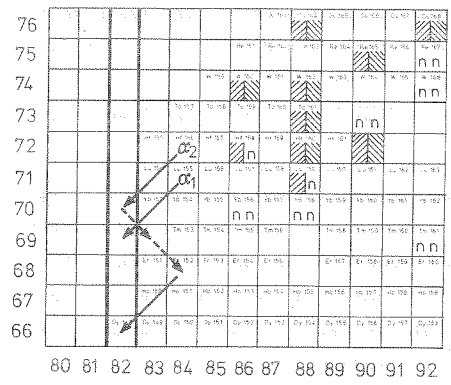


Fig. 2: Chart of nuclei with investigated compound nuclei. α_1 observed: ▨ ; α_2 observed: ▩ ; no high energetic α line observed: "n".

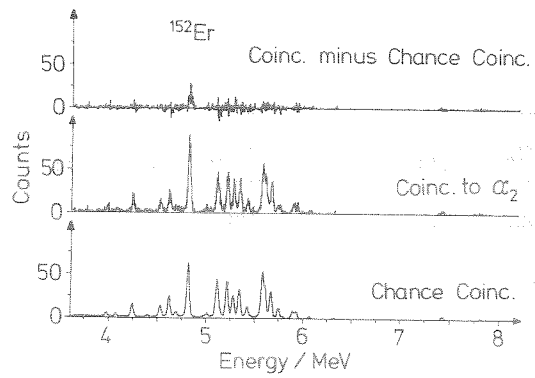


Fig. 3: Position-time coincidence spectrum to the high energetic line α_2.
Time window: 32 sec.
Position window: ± 0.6 mm.

New Neutron Deficient Isotopes of Elements between Tm and Pt

S. Hofmann, G. Münzenberg, W. Faust, T. Kitahara, W. Reisdorf, F. Heßberger, H.J.Schött, P. Armbruster, GSI Darmstadt

K. Güttner, B. Thuma, II. Phys. Inst. Universität Gießen

In our investigation of neutron deficient isotopes in the region between the elements Gd and Pb we have examined a variety of fusion reactions at the velocity filter SHIP. We have irradiated targets prepared from neutron deficient isotopes of elements between Mo-Sn and V-Ni, respectively, with beams of ^{58}Ni and ^{107}Ag with specific energies between 4.4 MeV/u and 5.9 MeV/u.

In our experiments we used a set-up consisting of an array of 7 position sensitive detectors[1]. The analysis of the data has been improved so that now all α-α decay chains of a reaction can be observed. Two dimensional position time coincidence spectra are compiled. An example is shown in fig. 1. In such a plot true parent daughter correlations can be found as an accumulation of points.

In the investigated reactions 10 new isotopes could be identified by their α decay. The measured energies are compiled in table 1 and presented in the systematics of α energies in fig. 2. The existence of 5 β decaying isotopes left from N = 84 could be shown by α-(β)-α correlation.

All newly found isotopes at SHIP in this region are shown in fig. 3. For some of the odd elements the proton drip line according to Ref.[2] is crossed by several isotopes. A proton decay of these isotopes could not be observed. The analysis of half-lives and α branching ratios of the new isotopes is in progress.

[1] S. Hofmann et al., GSI 79-11 (1979), p. 166

[2] K. Takahashi et al., IKDA 76/26, Inst. für Kernphysik, TH Darmstadt (1976)

Table 1: α energies of the newly found isotopes

Isotope	Energy/keV	Isotope	Energy/keV
^{171}Pt	6448 ± 5	^{164}Os	6320 ± 20
^{170}Pt	6545 ± 8	^{163}Os	6510 ± 30
^{169}Pt	6678 ± 15	^{165}Re	5506 ± 10
^{168}Pt	6824 ± 20	^{159}W	6299 ± 6
^{167}Ir	6386 ± 10		
^{166}Ir	6541 ± 20		

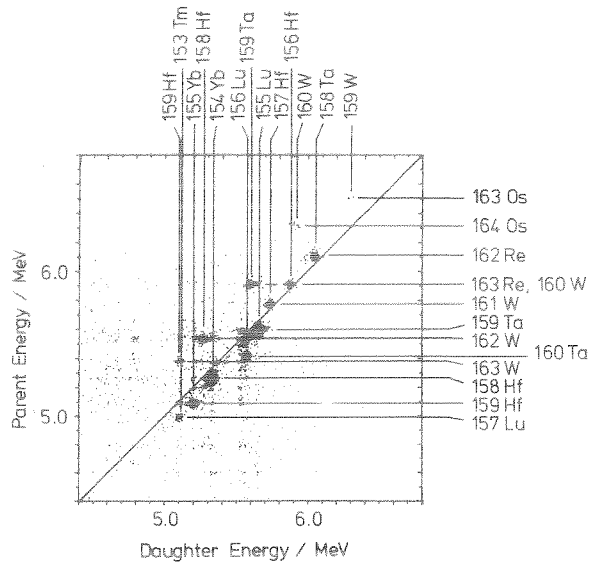


Fig. 1: α-α position-time coincidence spectrum.
Reaction: $^{58}Ni + ^{110}Cd \rightarrow ^{168}Os$ ($E^* = 83$ MeV).
Time window: 200 ms.
Position window: ± 0.5 mm.

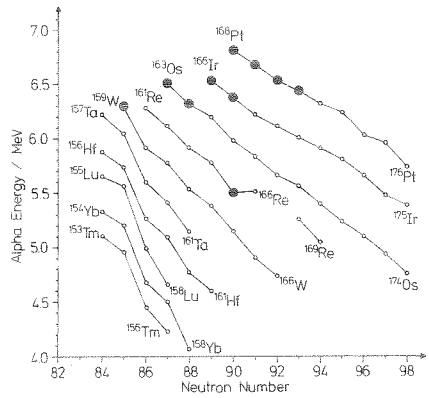


Fig. 2: α energy systematics.

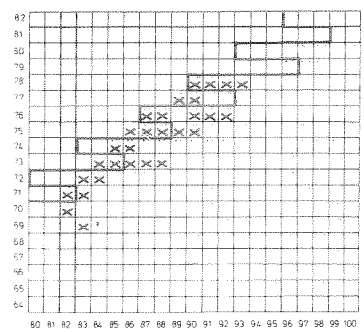


Fig. 3: Part of the neutron deficient region of the chart of nuclei between Gd and Pb. All newly identified nuclei are marked. The thick line is the proton drip line (1p for odd elements, 2p for even elements).

Alpha Decay of Neutron-Deficient Isotopes with $78 \leq Z \leq 83$ Including the New Isotopes ^{183,184}Pb and ^{188}Bi [B]

U.J. Schrewe (2. Physikalisches Institut, Universität Göttingen), P. Tidemand-Petersson, G.M. Gowdy, R. Kirchner, O. Klepper, A. Płochocki, W. Reisdorf, E. Roeckl, J.L. Wood, J. Żylicz (GSI Darmstadt), R. Fass (2. Physikalisches Institut, Universität Giessen), D. Schardt (Institut für Kernphysik, Technische Hochschule Darmstadt)

Alpha decay of very neutron-deficient nuclei in the lead region was studied applying on-line mass separation and subsequent alpha spectroscopy. The activity was produced by bombarding enriched targets of ^{142,146}Nd and ^{107}Ag with 4.6-6.3 MeV/u beams of ^{48}Ti and ^{84}Kr ions from the UNILAC. The following new isotopes were identified by their alpha decay (besides the isotope assignment, the alpha energies are given in keV together with the relative intensities): ^{188}Bi, 6820(20)/85(9), 7005(25)/15(9); ^{184}Pb, 6632(10); ^{183}Pb, 6715(20)/92(4), 6798(25)/8(4); ^{183}Tl, 6343(10)/83(4), 6378(15)/16(2), 6449(15)/1.0(3). The main alpha line assigned to ^{183}Tl confirms earlier unpublished data [1].

Half-lives were determined for ^{184}Pb, 0.55(6)s, ^{185}Pb, 4.1(3)s, and ^{183}Tl, 0.060(15)s (see Fig. 1). It is tempting to speculate about the surprisingly short half-life of ^{183}Tl. On the basis of the systematics of $3/2^+$ and $9/2^-$ levels in $^{185\text{-}201}$Tl, we expect the corresponding levels in ^{183}Tl to be at excitation energies of about 280 and 550 keV, respectively. We assume furthermore, that the 1.7s (Ref. 2) life-time of the 453 keV, $9/2^-$ isomer in ^{185}Tl (Ref. 3) is entirely determined by the E3 transition to the 284 keV, $3/2^+$ state. Applying this assumption also to ^{183}Tl, the life-time of the expected $9/2^-$ isomer if decaying predominantly by a 270 keV, E3 transition would indeed be of the order of the experimental value.

For $^{182\text{-}184}$Hg and ^{178,179}Pt, alpha branching ratios b_α were determined from comparison of the intensities of parent and daughter activities in the same spectrum (see Fig. 1). The results for ^{178,179}Pt and ^{184}Hg agree with the values given in Ref. 4, while we found substantially higher values - 0.152(8) and 0.232(14) - for ^{182,183}Hg. The literature values for platinum isotopes were derived from parent-daughter relationships as in our work, while for mercury isotopes b_α values were deduced from a comparison of K X-ray and alpha intensities. For nuclei such as $^{182\text{-}184}$Hg, the decays of which are not sufficiently known, this method includes an estimate of the contribution of K X-rays due to internal conversion, and is therefore uncertain. The measurement of b_α is of particular interest in this region in view of the anomalous behaviour of reduced alpha width observed around lead.

[1] S. Mattsson, Thesis, Göteborg 1978 (unpublished)
[2] K.S. Toth et al., Phys. Lett. 63B, 150 (1976)
[3] A.G. Schmidt et al., Phys. Lett. 66B, 133 (1977)
[4] P.G. Hansen et al., Nucl. Phys. A148, 249 (1970)

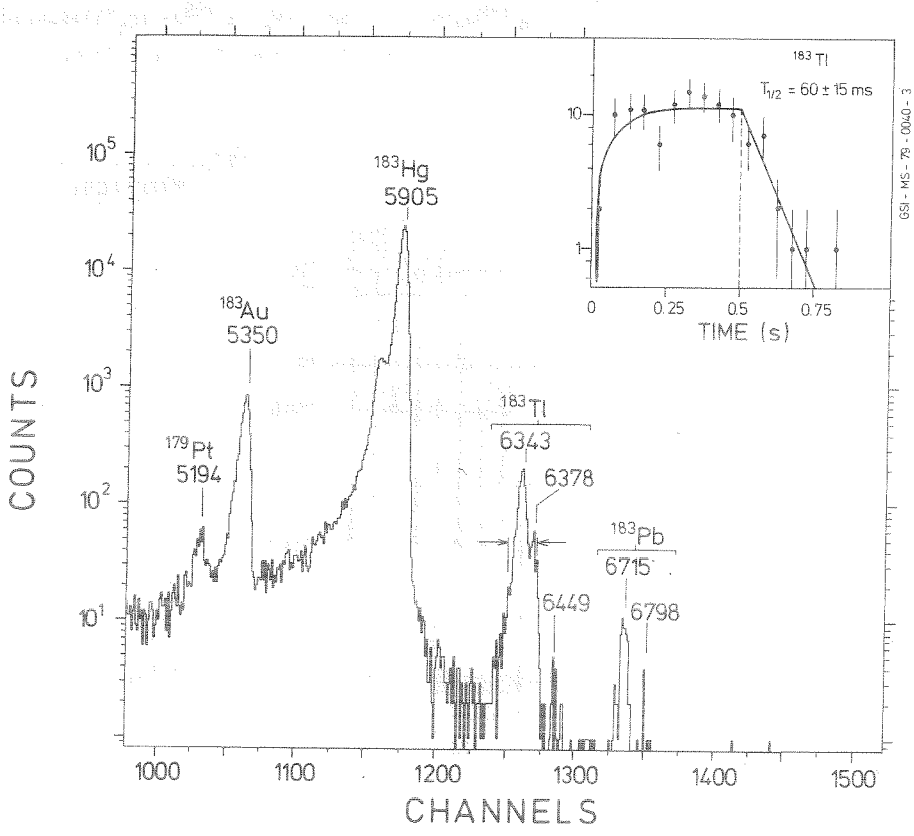


Fig. 1: Alpha particle spectrum measured with an "in beam" detector at mass number 183. Isotope assignments are given for the most prominent lines together with the corresponding alpha energies taken from this work and from the literature.

The insert shows the grow-in decay pattern measured by means of an electrostatic deflection device collecting the mass-183 beam alternatively in front of two detectors; only events corresponding to the ^{183}Tl alpha line (see arrows) are included.

Decay of ^{189}Pb (51 s) and the Excited States of ^{189}Tl

J.L. Wood
School of Physics, Georgia Institute of Technology

G.M. Gowdy[+]
GSI Darmstadt

L.L. Riedinger
Physics Department, University of Tennessee

E.F. Zganjar, J.D. Cole
Physics Department, Louisiana State University

The GSI on-line mass-separator facility and γ-ray spectroscopy techniques have been used to study the excited states of ^{189}Tl following the decay of ^{189}Pb (51 s). This work is in conjunction with studies made at the UNISOR isotope separator facility at Oak Ridge, where conversion electron spectroscopy has been conducted. The goal of this work is to determine whether or not the excited 0^+ state at 825 keV in ^{188}Hg is due to a $(\pi h_{9/2})^2$ pair excitation by studying the $^{188}\text{Hg} \otimes \pi h_{9/2}$ coupling scheme in ^{189}Tl. If the deformed 0^+ core state is due to a $(\pi h_{9/2})^2$ configuration, the presence of the unpaired proton in the $h_{9/2}$ orbital would block the formation of the state.

[+]Now at Physics Department, Brookhaven National Laboratory

The ^{189}Pb activities were produced at GSI by the $^{146}\text{Nd}(^{48}\text{Ti},5n)$ reaction. Both γ-γ coincidence and γ-multiscaling data were taken. Three coincident groups of γ rays were identified and using the systematic features of the heavier odd-Tl isotopes, two groups were identified as constituting the $h_{9/2}/i_{13/2}$ and $s_{1/2}/d_{3/2}$ bands, respectively (see fig. 1). The third group (see fig. 2) did not match any known band structure in $^{191\text{-}197}$Tl. The γ rays constituting this group are assigned to the $^{189}\text{Pb} \rightarrow {}^{189}$Tl decay scheme on the basis of half-life, γ ray-conversion electron energy differences (Z assignment) and mass separation (A assignment). We are in the process of analyzing the conversion electron data to determine multipolarities of transitions (and hence spins and parities of levels), and the weak coincidences to fully develop the level scheme. We believe this "extra" group of levels to be due to the ^{188}Hg (0_2^+, 825 keV) $\pi h_{9/2}$ coupling, the 781 keV transition being the $J^-\{\pi h_{9/2} \otimes {}^{188}\text{Hg}(0_2^+)\} \rightarrow 9/2^-\{\pi h_{9/2} \otimes {}^{188}\text{Hg}\ (0_1^+)\}$ transition: J depending on the coupling scheme for the deformed core state.

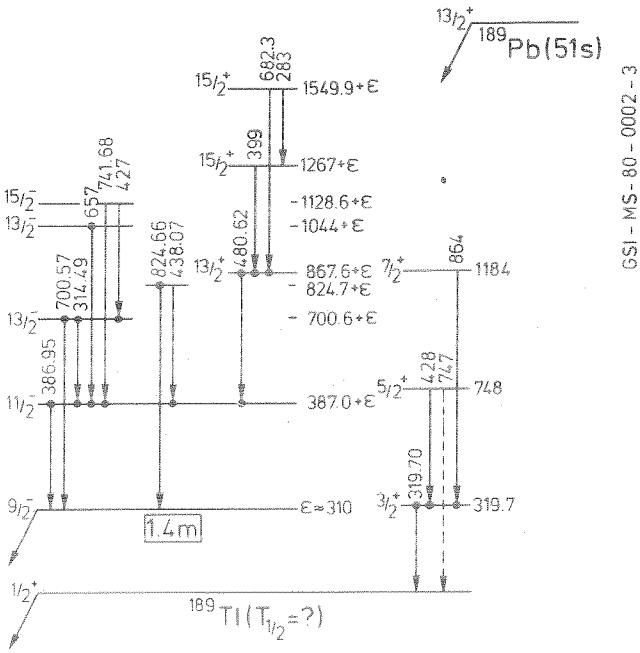


Fig. 1: The $h_{9/2}/i_{13/2}$ and $s_{1/2}/d_{3/2}$ bands in ^{189}Tl. All of these states are well-established from systematics in $^{191\text{-}197}$Tl. The half-life of the ^{189}Tl ground state is unknown.

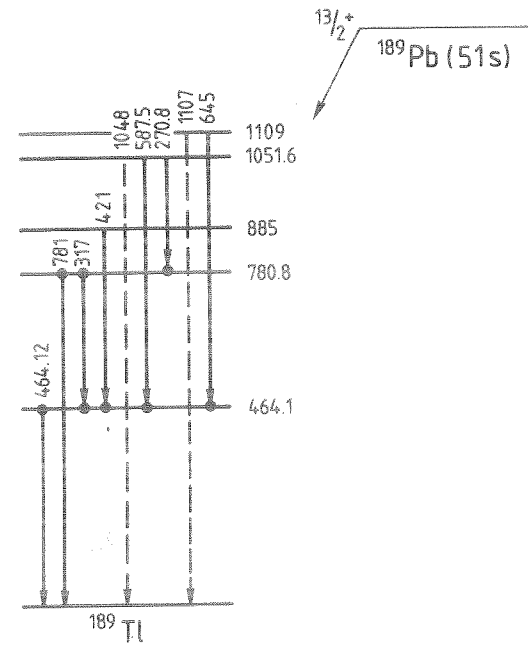


Fig. 2: New Band in ^{189}Tl.

Production of Isotopes of Element 104 by Fusion of ^{207,208}Pb with ^{50}Ti

G. Münzenberg, S. Hofmann, F.-P. Hessberger, W. Reisdorf, K.H. Schmidt, H.J. Schött, P. Armbruster
GSI Darmstadt

B. Thuma
II. Phys. Institut Univ. Giessen

D. Vermeulen
Inst. f. Kernphysik, TH Darmstadt

One interesting aspect to investigate element 104 is the systematics of spontaneous fission half-lives, which changes between element 102 and 104. Especially for the nucleus ^{256}104 the half-life is found to be shorter than expected taking into account the closed neutron shell at N = 152. Until now, using reactions with Pb-targets, the isotopes $^{253-256}$104 have been investigated in Dubna by observing spontaneous fission[1]. For the odd mass nuclei spontaneous fission half-lives are longer, therefore also α decay has been predicted.

At the velocity filter SHIP spontaneous fission as well as α decay can be observed down to half-lives of some microseconds, and nearly free from background of transfer products. If α decay occurs, an unambiguous assignment of nuclei establishing mother-daughter correlations is possible.

We bombarded ^{207}Pb and ^{208}Pb targets of 0.8 mg/cm^2 thickness covered with thin carbon layers and mounted on our rotating target wheel with ^{50}Ti beams of 70 - 100 particle nA at different energies. The evaporation residues were separated by SHIP and implanted into an array of position sensitive detectors to investigate spontaneous fission and α decay[2]. The calculated overall efficiency for spontaneously fissioning evaporation residues is 50 %. The total ion dose per irradiation was about 10^{16}.

In the ^{208}Pb irradiation at 4.75 MeV/u we observed correlated α decays fitting into the chain ^{257}104 - ^{253}No.

For example :

Typical decay chain (energy, time) :
mother (9.009 MeV, 2.8 s) -
daughter (8.015 MeV, 127 s)
Data from literature (most intense decay, half-life) :
^{257}104 (9.002 MeV, 4.5 s) -
^{253}No (8.013 MeV, 105 s)

This is the first observation of a 1n deexcitation channel for fusion of Ti and Pb.

At 4.85 MeV/u we observed spontaneous fission. Our preliminary data evaluation shows a half-life of (8.05^{+2}_{-1}) ms (Fig. 1). We collected about 40 events in a ten hours irradiation. The collected particle rate is in good agreement with the cross section of 6 nb as measured for the production of ^{256}104 by Oganessian and coworkers. With increasing irradiation energy spontaneous fission half-life exceeds the ms range. An exact half-life determination is in progress. The difficulties arising for long half-lives are due to the additional position-correlation between evaporation residue and spontaneous fission. With increasing projectile energy, up to 5.15 MeV/u the spontaneous fission counting rate decreases, whereas the α decay lines from transfer products become stronger.

In the ^{207}Pb irradiation also spontaneous fission is observed. Additionally, we observed some α decays, but until now we have difficulties to assign them. The same holds for the irradiation ^{50}Ti on ^{209}Bi to produce ^{257}105.

In a recent experiment on the reaction ^{40}Ar (^{206}Pb, 3n) ^{243}Fm we measured a decay energy of (8553 ± 10) keV and a half-life of (149^{+65}_{-25}) ms to confirm former experiments[3].

[1] Yu.Ts. Oganessian et al., Nucl. Phys. A239, 157 (1975)
[2] S. Hofmann et al., GSI Jahresbericht 79-11, 166 (1979)
[3] G. Münzenberg et al., GSI Jahresbericht 79-11, 68 (1979)

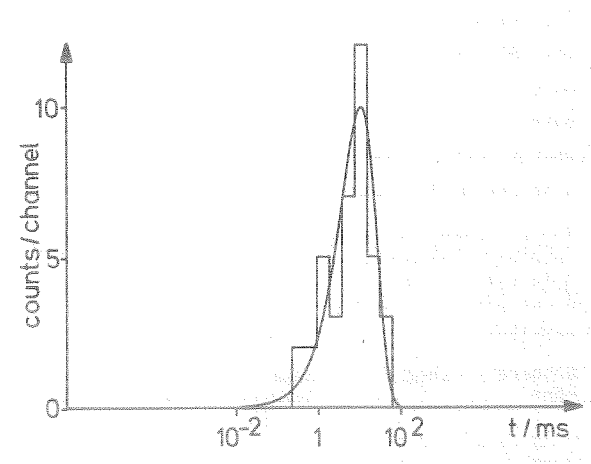


Fig. 1 : Correlation for the time distances between evaporation residue and spontaneous fission for ^{50}Ti on ^{208}Pb, 4.95 MeV/u.

Search for superheavy elements in the $^{238}U+^{238}U$ reaction using gas-phase and solution chemistry [B]

N. Trautmann, D. Gembalies, G. Herrmann+, P. Peuser, G. Tittel
Institut für Kernchemie, Universität Mainz

W. Brüchle, H. Gäggeler, J.V. Kratz, M. Schädel, W. Schorstein, K. Sümmerer, G. Wirth
GSI Darmstadt

Already the first experimental studies of damped collisions between two ^{238}U nuclei have indicated that this system may offer a novel approach to the synthesis of superheavy elements[1,2]. We have therefore performed during the past two years several attempts to identify superheavy elements in thick uranium-metal targets bombarded with 8.6 MeV/u ^{238}U beams. After bombardment the targets were processed with two chemical separation procedures based on entirely different principles with regard to the chemical behaviour of superheavy elements. One of these procedures, the gas-phase chemistry, is based on the predicted volatility of superheavy elements in their elementary state; it should cover elements 112 through 117. The other procedure, the solution chemistry which should cover elements 108 through 116, is based on the expected formation of strong anionic complexes with bromide ions and on the expected strong affinity to sulfur as is utilized in the solvent extraction with diethyldithiophosphate.

In 1979 we have continued this series of experiments[3] with two bombardments in which only the solution chemistry was applied. In addition, provisions were made to condense noble gases (element 118) and other species that are volatile at room temperature, as is described in a following contribution[4].

The two bombardments are listed under Nos. 5 and 6 in the Table which gives also the data for the preceding experiments[3] and the noble gas fraction[4]. 31 days after bombardment No. 6 a single fission fragment (23 MeV + energy loss in the 30 µg carbon foil) in coincidence with one neutron was observed. For this fraction a minor uranium contamination cannot absolutely be excluded.

Table: Summary of relevant quantities for searches for superheavy elements in bombardments of thick ^{238}U targets with 8.6 MeV/u ^{238}U ions. S=solution chemistry, G=gas phase chemistry, Gases=condensation of gaseous species.

Bombardment	Chemistry	Beam integral	Counting time [d]	Observed Sf-events
1	S	5×10^{15}	51	0[a]
2	G	7×10^{15}	275	2[a]
3	G+S	3.6×10^{16}	117	1[b]
4	G+S	4×10^{16}	220	0[b]
5	S	2.9×10^{16}	100	0[a]
6	S	2.8×10^{16}	160	1[b]
5+6	Gases	5.7×10^{16}	99	2[c]

[a] Counting samples placed between two opposed surface barrier detectors. Registered events are SF-coincidences, efficiency for detecting two fission fragments in coincidence 60%.

[b] Surface barrier detector-pair placed inside a neutron-multiplicity counter. Registered events are one or two detected fission fragments in coincidence with neutrons. Efficiency for the detection of one neutron 30%.

[c] Gaseous species condensed on a copper cryostat faced by one single surface barrier detector.

In order to estimate upper cross section limits for the production of spontaneously fissioning superheavy elements, we start with two observed events per 4×10^{16} particles which are still compatible with 6 events at 95 % confidence level. We assume 75 % chemical yield and a constant excitation function between 8.6 MeV/u and the interaction barrier. The results, denoted by "chemistry", are shown in the Figure as a function of the half-life of the superheavy nuclei. Also given are upper cross section limits reported by Hildenbrand et al.,[1] ("implanted recoils"), Junglcas et al.[6] ("gas-jet") and Gäggeler et al.[5] ("wheel").

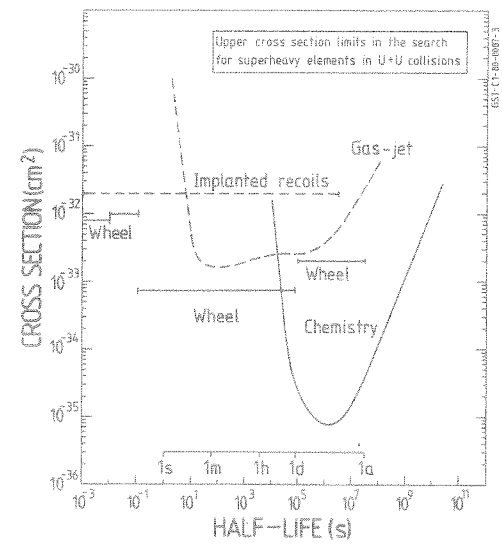


Figure
Upper cross section limits in the search for spontaneously fissioning superheavy elements in the $^{238}U+^{238}U$ reaction.

+Also at GSI Darmstadt

[1] K.D. Hildenbrand et al., Phys. Rev. Lett. 39, 1065 (1977)
[2] M. Schädel et al., Phys. Rev. Lett. 41, 469 (1978)
[3] N. Trautmann et al., GSI Annual Report 1978, p. 70
[4] H. Gäggeler et al., this Annual Report p. 61
[5] H. Gäggeler et al., this Annual Report p. 62
[6] H. Jungclas et al., Phys. Lett. 79B, 58 (1978).

Search for Gaseous Superheavy Elements in ^{238}U on ^{238}U Collisions

H. Gäggeler, B. Haefner, K. Sümmerer
GSI Darmstadt

Several authors, e.g. Pitzer[1], draw attention to the fact that due to closed electron shells and subshells, superheavy elements with Z ≈ 112, 114, 118 might be very inert and similar to noble gases. In the chemical procedures used in the experiments summarized in the preceding report[2], gaseous reaction products like radon were lost. The only experiment aimed at the search for gaseous superheavy elements in the U + U reaction was done by Aumann et al[3] using a gas jet system. It yielded an upper cross section limit of 1.5×10^{-33} cm^2 whereas values as low as 10^{-35} cm^2 are accessible with the uranium beam intensities now available at the UNILAC. Therefore, we extended our chemical experiments to search also for spontaneously fissioning gaseous reaction products. As an internal tracer the noble gas radon was assumed to show a representative behaviour for gaseous superheavy elements.

For these experiments, the targets from bombardments 5 and 6 listed in the Table in Ref.2 were dissolved in a closed apparatus and gaseous products were swept out of the reaction chamber using He as carrier gas. The gas was dried by H_2SO_4 and KOH and passed through a U-tube filled with quartz powder which was held at liquid N_2 temperature. This trap was connected to a counting chamber, evacuated to 10^{-2} Torr and then warmed up to room temperature.

Gaseous products were diffusing into the chamber and were adsorbed on the surface of a Cu rod immersed in liquid N_2. The deposition zone was faced by a surface barrier detector to count α-particles and fission fragments in 2π geometry. The condensation efficiency was measured using a ^{226}Ra (^{222}Rn) emanation source and was found to be ≥ 90 %.

Counting of gaseous reaction products was started 1.9 h after the end of the irradiations. Two spontaneous fission events (80 MeV and 103 MeV) have been observed during a counting time of 99 days. We do not attribute any significance to these single events since such a count-rate corresponds to the usual electronic background of our detectors. These two observed events correspond at a 95 % confidence level to the following production cross section limits: 2×10^{-35} cm^2 for half-lives from 2 to 100 d, and 1.6×10^{-34} cm^2 for 100 d.

The measured α-spectra can be explained by Rn isotopes and their daughter products. Deduced production cross sections for Rn isotopes are shown in the Figure. Due to their short half-lives the isotopes A = 212 - 220 were not accessible in these experiments. The cross sections are not corrected for growth from precursors and have therefore to be considered as cumulative values. For the neutron-rich isotope 1.9 h ^{224}Rn a remarkably high cross section of 20 μb was measured which demonstrates the possibility for producing new neutron-rich isotopes of Po and At in U + U collisions.

[1] K. S. Pitzer, J. Chem. Phys. 63, 1032 (1975).
[2] N. Trautmann et al., this Annual Report, preceding contribution
[3] D.C. Aumann et al., Phys. Lett., 82 B, 361 (1979)

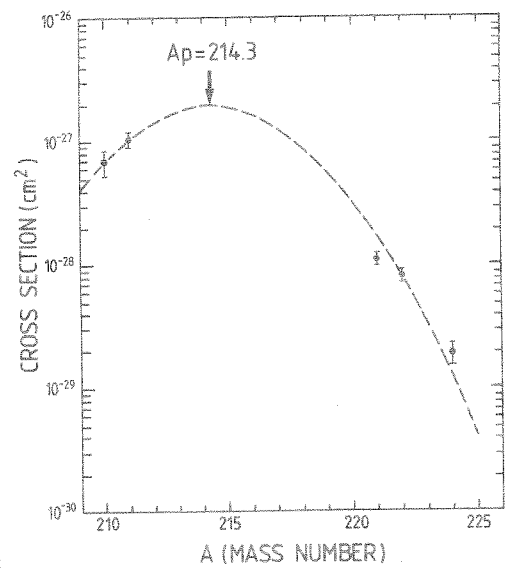


Figure Cumulative formation cross sections for radon isotopes in ^{238}U + ^{238}U collisions at ≤ 8.6 MeV/u bombarding energy.

Search for superheavy elements with half-lives down to 1 msec in ^{238}U on ^{238}U collisions

H. Gäggeler, E. Schimpf, W. Weber and G. Wirth

GSI Darmstadt

In order to improve the sensitivity in the search for short-lived spontaneously fissioning superheavy elements in uranium on uranium collisions, a rotating wheel system was developed. In this system products recoiling from a rotating uranium target are stopped in a stack of aluminium catcher foils covering an emission angle of $\pm$ 55° (lab)[1]. The stopped activities are continuously rotated out of the beam into shielded positions with static Macrofol fission track detectors positioned on either side of each rotating foil. After their on-line exposure, the fission track detectors are etched with KOH and the tracks are made visible by the spark technique. In order to search for long-lived superheavy elements which might have escaped radiochemical detection due to unexpected chemical behaviour, off line exposures of additional track detectors were performed. These detectors were exposed to the catcher foils after the end of bombardment for varying lengths of time. In a series of experiments, 11 mg/cm^2 thick metallic U-targets were bombarded with 7.6 to 8.3 MeV/u U-beams, while the catcher foils rotated at various velocities suitable for the detection of activities with half-lives of $\geq$ 1 msec. Due to the kinematics of damped reaction processes in the U+U interaction, the collected products are produced in the energy range from 7.4 MeV/u down to the interaction barrier. We observed four different spontaneous fission activities with half-lives of 1.1$\pm$0.1 msec and 13$\pm$5 msec, a product decaying largely during the irradiation time (100 msec $\leq$ T 1/2 $\leq$ 1 d) and a long-lived component with T 1/2 >> 1 d. Probable assignments of these activities, together with their production cross sections are summarized in the Table. Also listed are values from the literature. Due to the counting statistics and assumptions about the detection efficiency for fission fragments the reported cross sections are accurate within a factor of two. We attribute the long-lived spontaneously fissioning activities to ^{256}Fm and ^{254}Cf. Our cross sections are in good agreement with radiochemical data[2]. The msec-activities can most probably be assigned to the fission isomers $^{244mf}Am$ and $^{242mf}Am$. From the radiochemically determined Am yields listed in the Table, isomer to ground state ratios of 2.7×10^{-5} and 2×10^{-5} for ^{244}Am and ^{242}Am are deduced, respectively. These are lower than what is observed in light particle induced reactions, where ratios of the order of 10^{-4} are reported[3]. Note that the radiochemically determined Am yields have to be divided by a factor of two since target- and projectile-like fragments were not separated, whereas only target-like reaction products are detected with the rotating wheel system. From the observed range and angular distributions of the detected actinides within the foil stack their excitation functions can be deduced. They all show a similar shape with a maximum cross section at $E_U \approx 6.6$ MeV/u and a FWHM of 150$\pm$50 MeV (lab) in agreement with reported excitation functions for heavy actinides[2].

In conclusion, the sensitivity of the search for superheavy elements with this technique is limited by the production of spontaneously fissioning actinides. No evidence for the production of spontaneously fissioning acitivities with cross sections exceeding those for $^{242/244mf}Am$, ^{256}Fm and ^{254}Cf is found. Our upper cross section limits are included in the Figure of Ref. 4.

[1] W. Weber et al., GSI Annual Report 1978, p. 184

[2] M. Schädel et al., Phys. Rev. Lett. 41, 469 (1978) and GSI-Report 79-8 (1979)

[3] V.L. Kuznetsov et al., Nucl. Phys. A324, 29 (1979)

[4] N. Trautmann et al., this Annual Report, p. 60

Table

Nuclide	$T_{1/2}$	cross section	(Lit. (Ref. 2))
$^{244mf}Am$	1.1 msec	8×10^{-33} cm^2	6×10^{-28} cm^2 (^{244g}Am)
$^{242mf}Am$	14 msec	1×10^{-32} cm^2	1×10^{-27} cm^2 (^{242g}Am)
^{256}Fm	2.6 h	7.5×10^{-34} cm^2	6×10^{-34} cm^2
^{254}Cf	60.5 d	3.5×10^{-33} cm^2	2×10^{-33} cm^2

Search for superheavy elements and heavy actinides in the $^{238}U + ^{248}Cm$ reaction [B]

M. Schädel, W. Brüchle, H. Gäggeler, J.V. Kratz, G. Wirth
GSI Darmstadt

G. Herrmann+, G. Tittel, N. Trautmann
Institut für Kernchemie, Universität Mainz

E.K. Hulet, R.W. Lougheed
Lawrence Livermore Laboratory

A. Ghiorso, J.M. Nitschke
Lawrence Berkeley Laboratory

R.L. Hahn, R.L. Ferguson
Oak Ridge National Laboratory

Attempts of the GSI-Mainz collaboration to detect superheavy elements in damped collisions of two ^{238}U nuclei have failed[1], setting cross section limits of 10^{-32} cm^2 to 10^{-35} cm^2 for half-lives between 1 ms and 1 a. As we have demonstrated[1] it is most probably not reasonable to increase the bombarding energy in order to increase the production rates for superheavy elements because only the low-energy tails of the primary charge distributions contribute. Their enhancement is the essential problem. Riedel and Nörenberg[2], on the basis of an analysis of the $^{238}U + ^{238}U$ data[3] at $\leq$ 7.5 MeV/u, predicted for Z=114 an increase in the partial cross sections contained in the low energy tails ($E \leq 30$ MeV) by two orders of magnitude if a thick ^{248}Cm target is used instead of ^{238}U.

In October 1979 the first bombardments of 7 mg/cm^2 ^{248}Cm-metal targets with ^{238}U beams were performed. These targets contain a spontaneous fission activity of 2×10^9 events/day. The targets were previously tested with an electron beam gun and it was found that their thermal stability was excellent up to target temperatures $\geq 900^oC$. The target apparatus is schematically shown in Fig. 1. It served for two different experiments. Accelerator and beam line were protected against accidents with the highly active target by a Mo-window. Window and target were cooled by a fast nitrogen gas flow and the target itself by an additional He gas jet. Impurities in the gases were removed by a gas purification system. The target temperature was monitored online by an infrared thermometer. The outgoing He gas was assayed for nitrogen (M=28) by a quadrupole mass spectrometer (QMS). A sudden increase of the QMS signal for M=28 indicated that the target had developed a hole so that nitrogen entered the recoil chamber. Macropulses of the beam were spread over the target area by a beam wobbler. In case of a break of the target and the window a fast acting valve would be closed. To provide maximum protection, the wobbler, cooling gas flow, target temperature, accelerator vacuum, peak beam current etc. were interlocked to shut the beam off instantly if preset parameters were exceeded. The whole target apparatus was operated inside a glove box and all chemical separations were also carried out in glove boxes.

Counting of the isolated actinide and superheavy element fractions is still being continued. Qualitatively, we can state that the decrease in cross sections for the transuranium isotopes is as steep as the decrease for the transuranium nuclei in the $^{238}U + ^{238}U$ reaction. ^{259}No was possibly observed with an upper limit of 20 nb. ^{102} Preliminary upper limits for the production of superheavy elements are of the order of 10^{-33} cm^2. The lower sensitivity of these experiments as compared to the $^{238}U + ^{238}U$ experiments is due to the lower total beam intensity at which the bombardments had to be terminated because the targets developed stress cracks. It is not yet clear whether this cracking was caused by metallurgical, chemical, thermal, or radiation damage effects and whether the problem can be solved. This, however, is necessary in order to increase the sensitivity to $\leq 10^{-35}$ cm^2 in future experiments.

+Also at GSI Darmstadt

[1] J.V. Kratz, Paper presented at the Int. Conf. on Extreme States in Nuclear Systems, Dresden, Febr. 1980, GSI-Report 80-1; see also preceding contributions to this Annual Report.

[2] C. Riedel et al., Z. Physik A290, 385 (1979)

[3] M. Schädel et al., Phys. Rev. Lett. 41, 469 (1978

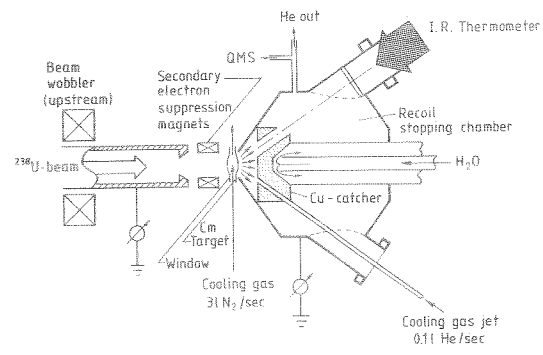


Fig. 1: Target apparatus for the $^{238}U + ^{248}Cm$ experiments

Search for SHE in the reaction ($^{nat.}U + ^{208}Pb$)^{B} using the gas jet and sulfide-chemistry

D.Hirdes, T.Lund, H.Jungclas, D.Molzahn, R.Brandt
Kernchemie, FB14, Philipps-Universität, Marburg

P.Lemmertz, R.Faß, F.Kassen and H.Wollnik
II.Phys. Institut, Liebig-Universität, Gießen

These experiments were performed to check up the possible production of SHE by the reaction ($^{nat.}U + ^{208}Pb$) via "instantaneous fission" [1]. We looked at spontaneous fission activities and high-energy alpha-emitters using our sulfide-chemistry [2] and the gas jet technique [3]. We used ^{208}Pb-ions with E/A=8.05MeV/u resp. 7MeV/u on thick $^{nat.}U$-targets. The energy of the beam leaving the target was always well below the reaction threshold (5.9MeV/u).

In the sulfide-chemistry experiment ($1.9\ 10^{16}$ Pb-ions) we obtained two fractions: the CdS-fraction carrying SHE and a transplutonium-fraction (TP) carrying Cm, Cf, etc. In the CdS-fraction we observed zero spontaneous fission events in the period 50 - 342 d after the bombardment, yielding the upper limits for spontaneous fission activities as shown in fig.1 In the TP-fraction we registered 4 spontaneous fission events (at energies of 110, 85, 100 & 69 MeV) during 164d of counting. This activity is assigned to ^{254}Cf (60.5d) produced with a cross-section of (0.20±0.09)nb.

During 36.4h of beam-time for the gas jet experiment we obtained $1.9\ 10^{15}$ Pb-ions (7.0MeV/u). The measurement of spontaneous fission activities was carried out during the beam-time with the same method as used for the (U+U) experiments [3,4] and extended up to 180d after the end of bombardment. One spontaneous fission event detected after 120d (energy 90MeV) yields a mean cross-section of ~0.2nb for ^{254}Cf, a result compatible with the above mentioned sulfide-experiment. Again the calculated upper limits are shown in fig.1. (As usual, we base the calculations on three events, giving a 95% confidence level to these upper limits.)
During the gas jet experiment we also looked with a dE-E counter telescope for alpha-particles with E> 11.5 MeV, as described previously [4,5]. Again, we saw no such activity.

Finally, the masses of the alpha-emitters, produced in this experiment and injected by the gas jet into our time-of-flight mass spectrometer, were analysed [6,7]. Once more, no indication of SHE was found.

We conclude, that these efforts to produce (non-volatile) SHE in the reaction ($U+^{208}Pb$) were limited by the cross-section as described in fig.1.

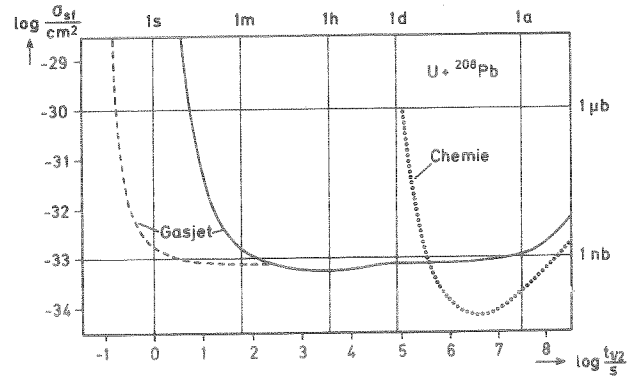


Fig.1: Upper limits for the production of SHE in the reaction ($U+^{208}Pb$) on a 95% confidence level: "Chemie": spontaneous fission in the CdS-fraction; "Gasjet": non-volatile spontaneous fission activities, based on longest transport time (56s ——) or shortest (1s - - -).

References:
1) H.H.Deubler and K.Dietrich, Phys.Lett.69B (1977)137
2) T.Lund et al., GSI-79/11, page 72
3) D.Hirdes, Dissertation, Univ.Marburg (1980)
4) D.Hirdes et al., GSI-79/11, page 71
5) H.Jungclas et al., Phys.Lett.79B(1978)58
6) R.Faß et al., this GSI report, page
7) P.Lemmertz, Dissertation, Univ.Gießen, in preparation.

SEARCH FOR SHE IN THE ATLANTIS II HOT BRINE B

T.Lund, R.Brandt, D.Molzahn, G.Tress, P.Vater and A.Marinov *
Kernchemie, F.B.14, Philipps-Universität, D-3550 Marburg
J.Halperin, R.W.Stoughton and B.H.Ketelle
Oak Ridge National Laboratory, Oak Ridge, U.S.A.

According to Flerov and coworkers, active hot brines as found on the Cheleken peninsula, in the Atlantis II deep and at the Solton Sea, should be promising sources for SHE: They have reported the observation of spontaneous fission activity in hydroxydes precipitated from the Cheleken geothermal water.[1] We are doing experiments using material from the Atlantis II deep. Our material is similiar in its chemical composition to the Cheleken hydroxydes, i.e. rich in typical "SHE-carriers" as Mn, Cd, Pb and Tl. We describe here three experiments:

1) Bulk measurements with the ^{3}He-counter in Oak Ridge.

2.36 kg deposits were measured for neutron-mutiplicities(for details see Ref.4) with the same type of counter as used in Ref.1, however with a higher background. No effect above background could be observed. The upper limits for the concentration of SHE in dependance of the average neutron number are shown in Fig.1, together with the results of Flerov et al.[1].

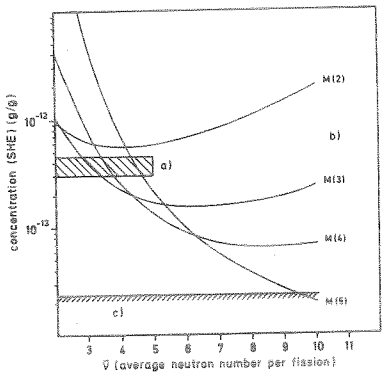


Fig.1 Comparison of SHE concentrations as a function of $\bar{\nu}$. a) Concentration of SHE in Cheleken material as quoted in Ref.1, b) Upper limits from ^{3}He-counter measurements of Atlantis II material and c) Upper limit based on measurements of volatile sulfidic elements prepared from Atlantis II

2) Search for SHE in a volatile fraction.

We heated repeatedly small charges(~50g) under oxydizing(air) and reducing(H_2) gas flow at 1050 °C. The volatile material(< 1000 °C) was dissolved and precipitated as sulfides from a weak acidic solution. We obtained a nearly quantitative separation of Pb and Cd, and assumed the same yield for SHE. The sulfides were prepared as thin layers on mica and covered with Makrofol[2,3]. In total we prepared ~250cm^2, and the foils were exposed for up to one year to the sulfides. After this the Makrofol foils were spark-jumped for vizualizing any fission track. The corresponding area on mica was scanned for fission tracks whenever a hole was observed. The counting efficiency of the set-up is 40%. We observed one track in mica, which could easily be due to background. We find an upper limit for the concentration of SHE (see Fig.1):

$$\text{SHE / Atlantis II} \leqslant 2.4\ 10^{-14}\ \text{g/g}$$

3) Search for transplutonium isotopes

Using conventional separation procedures (for details see Ref.5) we isolated from 106g deposit with 10% chemical yield (determined with ^{241}Am) a transplutonium fraction, electrodeposited on Ta. The sample is investigated for α- and fission activity. Results are shown in Fig.2 The α-activities are in general due to the natural decay chains (a few counts per day) and are too small to give observable fission rates of "man-made" transplutonium elements (with a few exceptions).

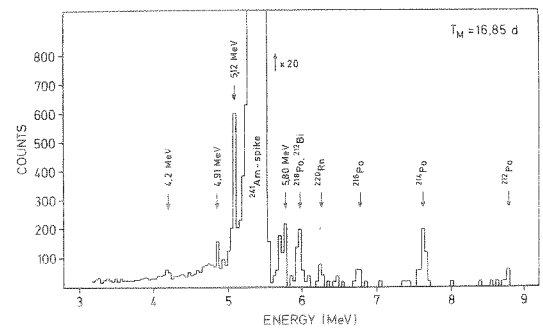


Fig.2 Alpha-spectrum of a transplutonium element sample prepared from 106 g Atlantis II deposit. The yield is determined to 10% with ^{241}Am.

REFERENCES

1) G.N.Flerov et al., Z.Physik A 292 (1979) 43
2) R.Brandt et al., GSI 79-11 (1979) 75
3) R.Brandt et al., Nucl.Instr.Meth., in print
4) J.Halperin et al., in preparation
5) T.Lund et al., in preparation

* GSI,Darmstadt and Hebrew University, Jerusalem

g-Factor Studies for Rare-Earth Deformed Nuclei [G]

M. Diebel, A. N. Mantri and U. Mosel
Institut für Theoretische Physik, Universität Giessen, Giessen

We have recently proposed a method[1] to include pairing correlations in Strutinsky type cranking calculations so as to make them more reliable in the well studied regions of low spins where these correlations play important role. Using this method we have carried out cranking HFB calculations for the four rare earth nuclei: ^{156,158,164}Dy and ^{164}Er. The results for yrast spectra are found to be in good agreement with experiments. The cranked HFB wavefunctions are then used for the calculations of the magnetic moments of high spin states and the results are presented here. We show in fig. 1 the spin variation of the g-factors for the four nuclei under study. We also show there the spin variation of the ratio of angular momentum of protons to total angular momentum. The g-factor equals this ratio if a part of the contribution coming from the intrinsic spin of neutrons and protons is neglected. It is clearly seen from Fig. (1) that this contribution is always negative.

The calculated systematics of spin variation of g-factors can be interpreted in terms of rotational alignment of $i_{13/2}$ neutrons. In ^{156}Dy (deformation $\varepsilon = 0.23$) there is one such orbital $[660\ \frac{1}{2}]$ occupied. The next neutron state $[651\ \frac{3}{2}]$ is filled up in ^{158}Dy ($\varepsilon = 0.25$) and in the cases of ^{164}Dy ($\varepsilon = 0.27$) and ^{164}Er ($\varepsilon = 0.265$) three such neutron orbitals are occupied. The expectation values of total angular momentum carried out by all the occupied $i_{13/2}$ neutrons are found to increase smoothly as a function of the total angular momentum except in the case of ^{156}Dy which shows a rather sudden alignment. Above $I = 10\hbar$ the single pair in ^{156}Dy carries more angular momentum than that carried by all the three pairs in ^{164}Dy. The variation of g-factor is found to be in direct correspondence to the extent of the alignment of $i_{13/2}$ neutron pairs. It is largest for ^{156}Dy, smaller for ^{158}Dy - smaller again for ^{164}Er and nearly absent for ^{164}Dy. Also, the difference between the g-factor and the angular momentum ratio at the minimum is found to decrease with increasing mass number. These results are direct manifestation of the decrease of Coriolis interaction strength as the $i_{13/2}$ neutron subshell fills up.

For ^{156}Dy, where single particle effects are most important, we also studied the sensitivity of g(I) due to changes in the sp level scheme as well as the pairing strength. A small increase in the deformation (from 0.23 to 0.25: characteristic of ^{158}Dy) which brings one more $i_{13/2}$ level below the Fermi surface has a substantial effect (Fig. 1) on g(I). The results for ^{156}Dy and ^{158}Dy become practically identical. A slightly lower choice of G_p/G_N which would not change the yrast spectrum causes an increase in g(I) for low spins whereas the high-spin behaviour is not changed.

1. M.Diebel and U.Mosel,Z.Physik A293,53(1979).

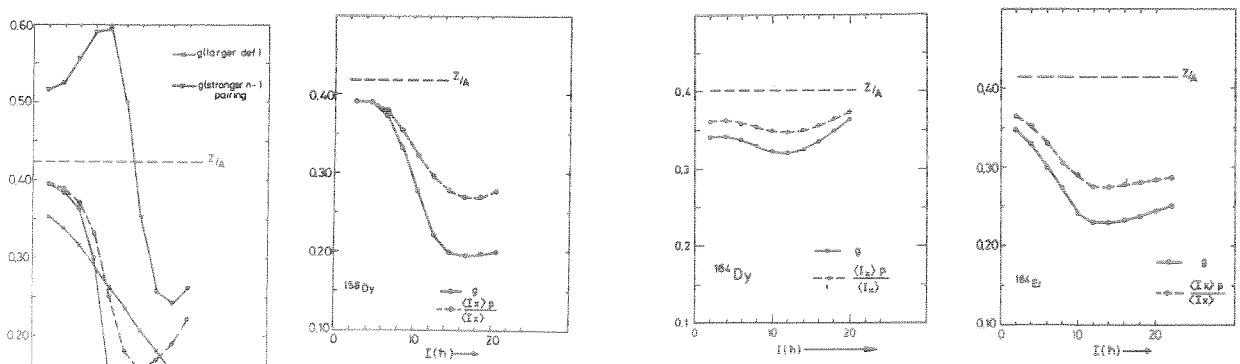


Fig. 1. Spin variation of gyromagnetic factors (points on full line) for the nuclei ^{156,158,164}Dy and ^{164}Er. For comparison, the variation of the ratio of proton spin to total spin is also shown (points on dashed line). For ^{156}Dy, the full triangles and crosses give respectively the gyrofactors for a stronger neutron pairing keeping same deformation and a bigger deformation with the same pairing strengths.

Role of the Yrast Line in Heavy Ion Fusion Reactions [G + B]

M. Diebel, D. Glas, U. Mosel and H. Chandra
Institut für Theoretische Physik, Universität Giessen

Yrast line limitations may be responsible for the observed limitation of the fusion cross section for light nuclei at high energies. Since the yrast lines are not known experimentally in the interesting spin range ($I \approx 10$-20) we have performed calculations of the yrast line by means of the cranked Strutinsky method. Details of the numerical method as well as an assessment of the accuracy of the calculations can be found in ref. 1.

Calculations along these lines do not include pairing, the calculated yrast line has thus to be identified with an unpaired band. In the high spin range ($I \gtrsim 10$) the true excitation energy is, therefore, higher than the calculated one just by the pairing correlation energy. For the case of ^{24}Mg there are indications that the pairing-type correlations disappear around $I \approx 8$-10 (see discussion in ref. 1). This is in line with observed moments of inertia that are essentially those of a rigid rotor at excitation energies $E^* \gtrsim 30$ MeV (ref. 2).

The figure shows as an example the calculated results for ^{24}Mg together with experimental fusion bands. These (full triangles and solid points) are obtained from the measured cross sections by means of the sharp-cut-off approximation. The lower solid line in the figure gives the result of a calculation without any pairing correlations, it lies obviously well below the fusion band for $^{12}C + ^{12}C$. If the pairing correlations are estimated as indicated above one obtains the dashed curve which at $I \approx 14$ comes quite close ($\Delta E \approx 8$ MeV or $\Delta I \approx 2$) to the empirical fusion band. Just at this point the empirical fusion cross section is found to bend upwards.

A possible explanation for the observed bend may, therefore, be the low number of levels available at the relatively low energies above the yrast lines that are reached in this process. Thus fusion in this case could be hindered by phase-space arguments. Fusion reactions may, therefore, be a valuable tool to explore the yrast line at high spins.

1. M.Diebel, D.Glas, U.Mosel and H.Chandra, Nucl. Phys. A333 (1980) 253
2. K.R.Cordell et al., ORNL preprint
3. J.J.Kolata et al., Phys.Rev.C21 (1980) 579

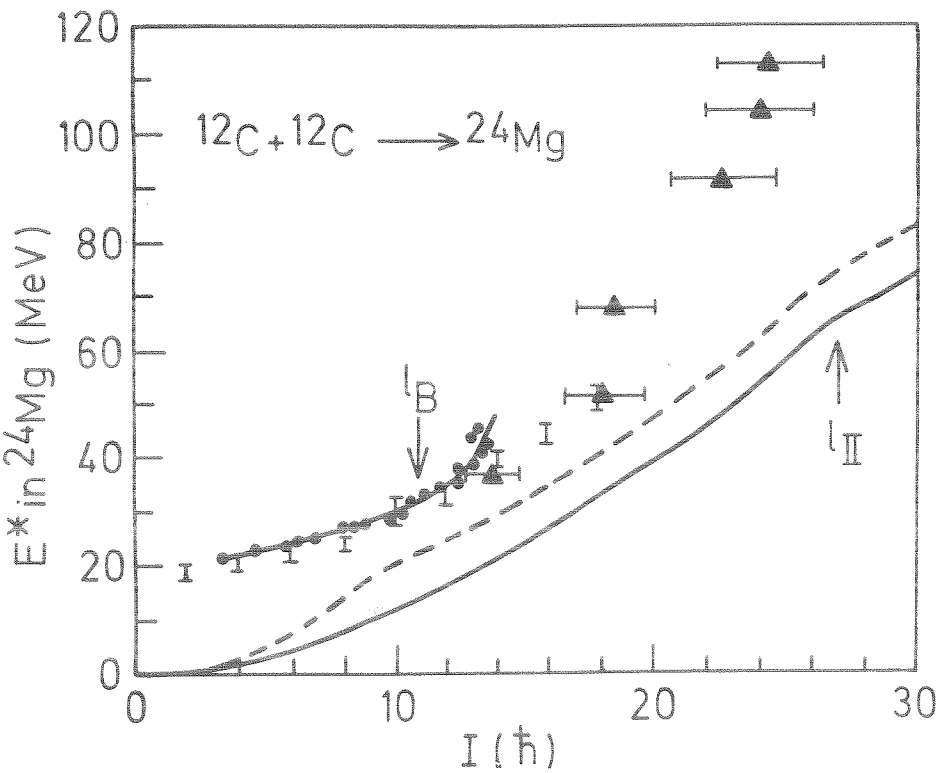


Figure:
Calculated yrast line and experimental fusion bands

Backbending Behaviour in the Actinides from Cranking Calculations

S. Frauendorf, NBI Copenhagen and Zentralinstitut für Kernforschung, Rossendorf, and R.S. Simon, GSI Darmstadt

In actinide nuclei both $i_{13/2}$ protons and $j_{15/2}$ neutrons are close to the Fermi surface. At rapid rotation these high-j particles will unpair and decouple from the rotating core giving rise to aligned or s-bands that cross the ground-state band. The crossing will cause an irregularity in the yrast sequence which may lead to pronounced backbending if the interaction between the two bands is small or cause only a gradual change in the character of the yrast levels in the other extreme.

In our calculations we followed the $i_{13/2}$ protons from Ra to Cf (Z = 88 to 98) and the $j_{15/2}$ neutrons from N = 138 to N = 152. Fig. 1 gives a summary for the neutron system. In the bottom part the rotational frequencies ω_c at the first two crossings are shown. Here the solid line corresponds to even nuclei with the crossing of the quasiparticle vacuum by a two-quasiparticle band (first crossing), while the two broken lines refer to odd-n cases where the two signatures $\alpha=\pm 1/2$ of the one-quasiparticle ground-state band are crossed by a three-quasiparticle configuration (second crossing). At least the first crossing is within reach of Coulomb excitation with ^{208}Pb.

The central part of the figure shows the aligned angular momenta at the first crossing: the contributions from the two signatures and the alignment i_s for the s-band which is very nearly the sum of the individual i-values. The interaction strengths V are given at the top of the figure. They show the oscillating behaviour known from the rare-earth region[1,2]. At the first crossing the diagram indicates vanishing interaction around N = 139, 145 and 151. If one varies the parameters that go into the cranking calculations these zeroes hardly shift more than one particle number.

It is interesting to compare the interaction V with the backbending limit $i_s^2/4J_c$, where the constant moment of inertia J_c corresponds to a linear approximation for the angular momentum of the ground-state band in the crossing region[2]. If the distance 2V between the two interacting bands is smaller than the recoil term $i_s^2/2J_c$ the nucleus backbends. The backbending limit given by the dotted curve in Fig. 1 is based on our cranking values for i_s. But since the calculations seem to overestimate i_s this limit is probably too high. For N = 142, 144 we obtain considerably lower thresholds if we use the experimental value i_s = 5.8 $\hbar$ deduced from the alignment of the odd neutron in ^{235}U. Therefore one expects a rather smooth behaviour for most of the neutron yrast lines. Exceptions are the neutron numbers N = 138, 140, 144 and probably N = 150 or 152 which should reveal a sharp upbending or might even show backbending.

In the proton system we find very similar crossing frequencies and have vanishing interaction for the first crossing around Z = 89 and 94. The backbending limit adjusted to i_s=6.6 $\hbar$ from ^{237}Np predicts a smooth upbending behaviour of the proton yrast lines in Th, U and Cm (Z = 90, 92, 96) while Ra and Pu (Z = 88, 94) might be backbenders.

There seems to be no backbending case among the actinide nuclei studied so far[3]. This is in agreement with the predictions in the proton system, but the smooth upbending observed does not disagree with the estimates for the neutrons, either. Here ^{236}U with N = 144 falls close to an interaction minimum as does ^{248}Cm with N = 152. The backbending in these nuclei, however, might be difficult to observe in Coulomb excitation, because the intensity will stay mainly in the neutron ground-state configuration up through the crossing region if the interaction with the s-band is small.

1 R. Bengtsson, I. Hamamoto and B. Mottelson, Phys. Lett. 73B (1978) 159

2 R. Bengtsson and S. Frauendorf, Nucl. Phys. A314 (1979) 27 and A327 (1979) 139

3 see contribution H. Ower et al., to this report

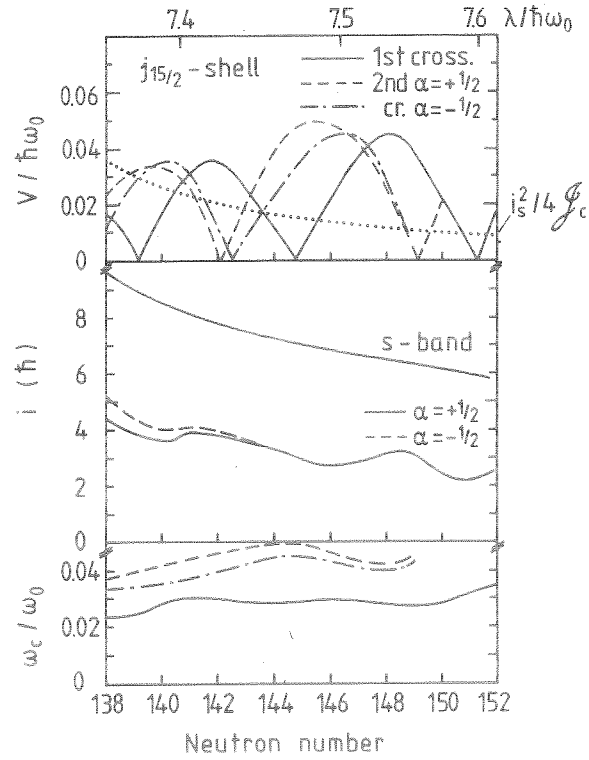


Fig. 1: Crossing frequencies, alignment and interaction strengths from HFB cranking calculations for bands built on $j_{15/2}$-orbitals, plotted as a function of neutron number and the position of the Fermi surface, respectively ($\hbar\omega_0$ = 41 $A^{-1/3}$MeV).

Contributions to the theory of nuclear structure [B]

P.O. Hess, M. Seiwert, N. Abul-Naga, F. Margetan, J.A. Maruhn, W..Greiner
Institut für Theoretische Physik der J.W.G.-Universität Frankfurt/Main

The work of Hess is a major step forward in the collective nuclear model of Gneuss and Greiner. He wrote the collective potential $V(\beta,\gamma)$ in the intrinsic system as a Taylor expansion in the collective coordinates β and γ. Thus, the whole potential energy surface can be described, and, contrary to the rotation-vibration model, one need not expand the Hamiltonian about a minimum in the β-γ-plane. The Moshinsky basis of the 5-dimensional oscillator was extended by the addition of a contrifugal term in the Hamiltonian. This gives a much better description of γ-instable nuclei than the original Moshinsky basis[4]. An atomatic, numerical fit-programme was established which allows an optimal adjustment of the potential to the transition energies and $\mathcal{B}(E2)$-values of the nuclei considered.
The physics of the nuclear structure will then be given by the general shape of the potential energy surface.
This new Frankfurt model yields a more physical picture , especially in the description of high-spin states, than the IBM (Interacting Boson Model) by Iacello et al, which has the same structure as our model. Nuclei, such as ^{238}U, Pt, Os and W, were investigated.[1-3]
The ordinary rotation-vibration model was extended by addition of a deformation-(α-) dependent term in the kinetic energy (Seiwert et al), which permits the description of two minima in the potential energy surface. This is of great importance for the treatment of fission isomers such as ^{238}U or ^{239}Pu.
By the coupling of a valence nucleon or a hole in the valence shell to the Hess-Greiner model one is now also able to describe the spectra of odd-even nuclei (Abul-Naga et al).
It was found that an interacting superposition of the core of an even-even nucleus with a valence nucleon or a hole gives the best description of odd-even spectra. An analytical basis for the harmonic oscillator in any dimension and the structure of the matrix elements was presented, too. This is important for the treatment of octupole and hexadecupole oscillations.[5]

[1] P.O. Hess, J.A. Maruhn, W. Greiner; Intern. Symposium on Future Directions in Studies of Nuclei far from Stability, Vanderbilt Univ., Nashville/Tenn.

[2] P.O. Hess, J.A. Maruhn, W. Greiner, XVIII Intern. Winter Meeting on Nuclear Physics Bormio/Italy

[3] P.O. Hess, M. Seiwert, J.A. Maruhn, W. Greiner; to be published

[4] P.O. Hess, F. Margetan; to be published

[5] S. Rohozinski, W. Greiner; to be published

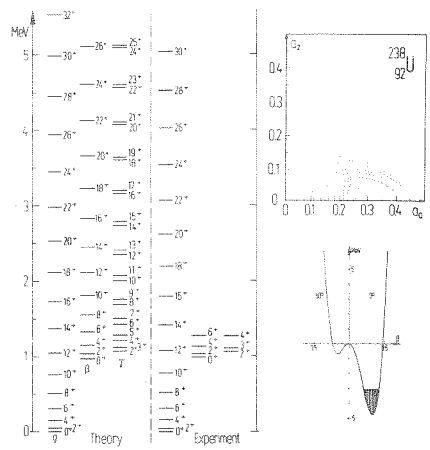


Fig.1 Potential-energy-surface and energy-levels for $^{238}_{92}$U, predicted by a general collective model.

Contributions to the theory of nuclear molecules [B]

R. Könnecke, J. Guirguis, J.A. Maruhn, W. Greiner
Institut für Theoretische Physik der J.W.G.-Universität Frankfurt/Main

Observations of the excitation spectrum of, for instance $^{12}C + ^{12}C$, show
a) broad structures of about 3 MeV width,
b) fine structures of about o,5 MeV, and
c) so called Ericson-fluctuations with a very small width.

A theory was developped for the description of such systems inhibiting a relative energy of the collision partners, intrinsic energy of both nuclei and an interaction term between both degrees of freedom.

The broad structures in the excitation spectrum are a consequence of the resonances on the relative nuclear potential above the Coulomb barrier. The fine structures in this model are related to a double-resonance mechanism: resonances above the Coulomb barrier are described by intrinsic degrees of freedom, forming - for a short time -nuclear molecules. This gives a good explanation of $^{12}C + ^{12}C$ excitation spectrum.[1]

[1] D. Hahn, G. Terlecki, W. Scheid, R. Könnecke, W. Greiner; in Lecture Notes in Physics 89, Microscopic Optical Potentials, ed.H.V.v. Geramb, Springer 79

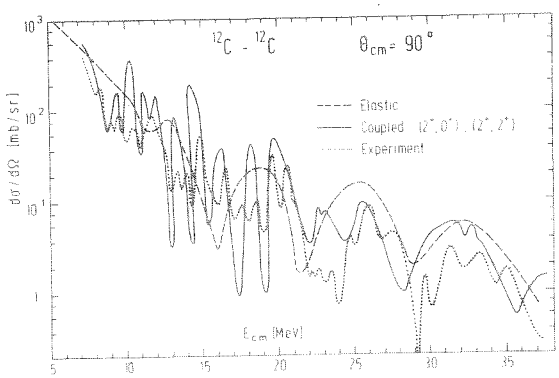


Fig.1 Comparison between the experimental and calculated 90° cross section for elastic $^{12}C - ^{12}C$ scattering. The theoretical curve was obtained using coupling potentials up to quadratic terms in the surface collective variables $\alpha_{\ell m}$.

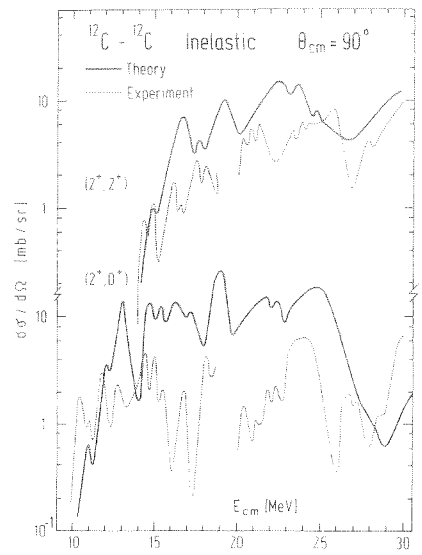


Fig.2 Comparison between the coupling (lower curve) of the excitation of a 2^+ state in one of the ^{12}C nuclei with the coupling of the excitation of the 2^+ state in one or simultaneously in both nuclei. The rich structure is obtained by the inclusion of quadratic coupling terms in the surface collective coordinates $\alpha_{\ell m}$.

G

Derivation of a proximity interaction between nuclei from the Hartree-Fock functional with Skyrme interactions

K.Pomorski and K.Dietrich,Phys.-Dept.,TUM and GSI Darmstadt

We derive a potential between heavy and medium heavy spherical nuclei on the basis of the proximity approximation and on the assumption of overlapping undisturbed spherical density distributions. The potential is written in the usual way in the form

$$V_{sudden}(R_{12}) = E[\rho_1 + \rho_2] - E[\rho_1] - E[\rho_2] \quad (1)$$

where $E[\rho]$ is taken to be the Hartree-Fock functional with Skyrme interactions. It is argued, that the ansatz (1) which is typical for the sudden approximation can also be interpreted in the adiabatic limit as long as the peripheral overlap is very small. The resulting proximity interaction consists of a isoscalar part which depends only on the mass numbers of the interacting nuclei and an "isovector" part which depends on the differences of neutron and proton numbers in the two interacting nuclei. Both parts depend on the distance s between the nuclear surfaces. The isoscalar as well as the isovector part are then written as a sum of products of a scaling factor depending on the mass numbers and charge and neutron number of the individual nuclei and universal functions of the distance s. It was shown that these universal functions of the distance s can be approximated with very good accuracy by simple analytical functions:

$$V = V_{isoscalar}(s) + V_{isovector}(s) \quad (2)$$

$$V_{isoscalar}(s) = \frac{R_1 R_2}{R_1+R_2} \cdot J_0(s) \quad (3)$$

$$V_{isovector}(s) = \frac{R_1 R_2}{R_1+R_2}\left\{J_{T_1T_1}(s)\left(\frac{N_1-Z_1}{A_1}\right)^2 + J_{T_1T_2}(s)\left(\frac{N_2-Z_2}{A_2}\right)^2 + J_{T_1T_2}(s)\left(\frac{N_1-Z_1}{A_1}\right)\left(\frac{N_2-Z_2}{A_2}\right)\right\} \quad (4)$$

The functions $J_{T_1T_1}(s)$, $J_{T_2T_2}(s)$, $J_{T_1T_2}(s)$ are defined in ref.1.

We draw attention to the existence of the third term in equation 4 which is proportional to the product of the neutron surplusses in the two interacting nuclei. Replacing the z-components of the isospin by the total isospin vectors one obtains a general iosopin dependent potential between heavy ions.

$$V_{isospin} = \frac{R_1 R_2}{R_1+R_2}\, 4\left\{J_{T_1T_1}(s)A_1^2\vec{T}_{(1)}^2 + J_{T_2T_2}(s)A_2^2\vec{T}_{(2)}^2 + J_{T_1T_2}(s)A_1A_2\vec{T}_{(1)}\cdot\vec{T}_{(2)}\right\} \quad (5)$$

which may be considered as a generalized Lane-potential.

We have calculated the proximity potential for various nuclear systems as a function of the Skyrme parameters (see fig.1 for the system ^{84}Kr on ^{208}Pb). Our results agree very well with microscopic calculations by Zint and Mosel. Because of the special interest in fusion reactions of the system ^{48}Ca on ^{248}Cm we show the sum of the nuclear and Coulomb potential as a function of the distance R_{12} between the nuclear centres in fig.2.

Careful experiments on elastic scattering of heavy ions can thus be used to select optimal sets of Skyrme parameters and to find an optimal nuclear interaction between heavy nuclei.

References:

K.Pomorski,K.Dietrich:"Derivation of a proximity interaction between nuclei from the Hartree-Fock functional with Skyrme interactions",preprint of the Physik-Department of the TUM, 8046 Garching, January 1980,submitted for publication to Zeitschrift für Physik.

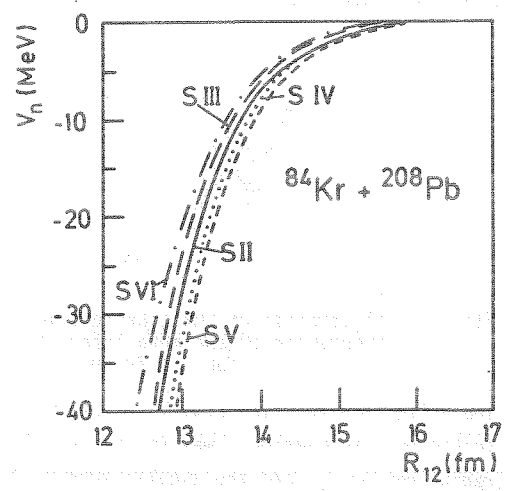


Fig.1

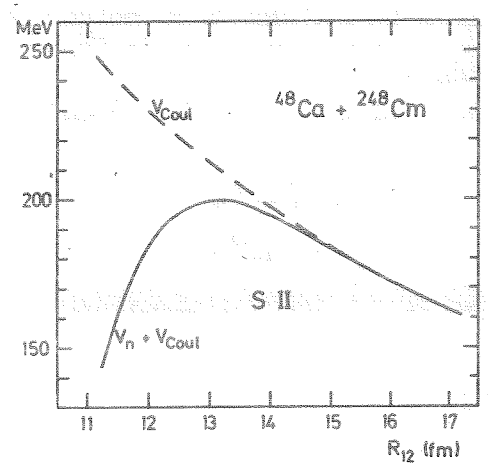


Fig.2

Relaxation Times in Dissipative Heavy-Ion Collisions [G]

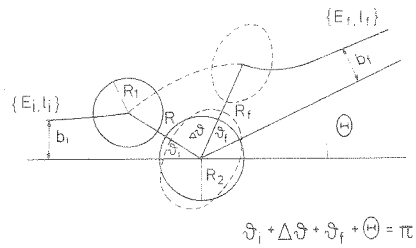
C. Riedel
GSI Darmstadt

G. Wolschin*
Institut für Theoretische Physik der Universität Heidelberg

W. Nörenberg
GSI Darmstadt

In this paper we improve and extend the analysis[1-3] of relaxation phenomena in dissipative (or deeply inelastic) heavy-ion collisions. The phenomenological classical model introduced in[1] avoids a complete dynamical calculation of the collision process which would suffer from the uncertainties of nuclear interaction potentials, mass parameters and friction coefficients. Instead we aim at the determination of a few parameters which characterize the observed relaxation processes and are as much as possible model independent. We generalize the considerations of[1] by including the gradual dissipation of radial kinetic energy and the development of fragment deformations during the collision.

The basis for the analysis of dissipative collisions is a classical model which is illustrated in Fig. 1.



$$\vartheta_1 + \Delta\vartheta + \vartheta_f + \Theta = \pi$$

Fig. 1. Illustration of the classical model for the calculation of the mean interaction time including the effect of fragment deformation

The deflection function $\Theta(\ell)$ is parametrized as described in[1]. Relaxation times for the dissipation of the radial energy τ_R and the angular momentum τ_ℓ as well as for the development of deformation τ_α are determined from an analysis of the reaction ^{86}Kr(8.18 MeV/u) + ^{166}Er [4].

The following set of relaxation times is used:

$$\tau_R = 0.3 \cdot 10^{-21}\,s,$$
$$\tau_\ell = 1.5 \cdot 10^{-21}\,s,$$
$$\tau_\alpha = 5 \cdot 10^{-21}\,s$$

The agreement with experimental data is illustrated in Fig. 2.

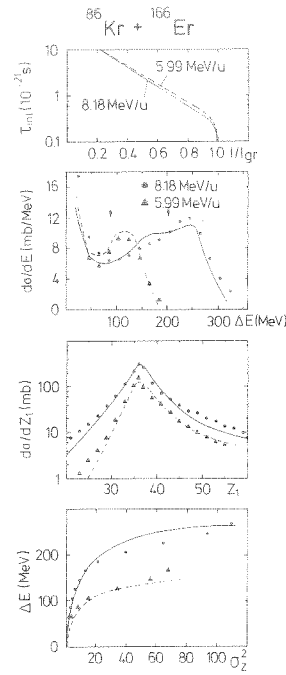


Fig. 2. Mean interaction times, energy and element distributions and correlation $\Delta E(\sigma_Z^2)$ for the reaction Kr+Er in comparison with the data of Rudolf et al.[4]

The same set of relaxation times can be used to analyze other reactions at various incident energies.

[1] Wolschin, G., Nörenberg, W.: Z. Physik A 284, 209 (1978)
[2] Wolschin, G.: Fizika 9, 513 (1977), Supplement 4 and Nukleonika 22, 1165 (1977)
[3] Wolschin, G., Nörenberg, W.: Phys. Rev. Lett. 41, 691 (1978)
[4] Rudolf, G. et al.: preprint GSI-VP-12-78 and submitted to Nucl. Phys. A

*supported by BMFT, Bonn and GSI, Darmstadt

Theoretical Estimates for the Production of Transuranium Elements in Heavy-Ion Collisions

C. Riedel and W. Nörenberg

GSI Darmstadt

Recent experiments[1] have shown that dissipative (or deeply inelastic) reactions between very heavy nuclei might provide the possibility for the production of superheavy elements. During the collision, projectile and target form a composite system which decays after times of the order of several 10^{-21}s. Experimental data of such collisions show strong dissipation of kinetic energy and angular momentum as well as large transfer of nucleons. The transfer of nucleons may lead for sufficiently heavy collision partners to a considerable probability for the primary formation of superheavy nuclei. Unfortunately, due to the large interaction time needed for such a far reaching diffusion, these primary heavy fragments are predominantly produced with large values of excitation energy and intrinsic spin. Under these conditions the branching ratio for neutron evaporation versus fission becomes very small and hence, the survival for superheavy isotopes might be suppressed.

In the experiment[1] a thick uranium target was used. As compared to the calculations for U + U presented in Ref.[3] we have to generalize our phenomenological classical model[2-6] to take into account the superposition of different incident energies in a thick target. Furthermore, we improve this model treating in a more rigorous way Q-value effects and variations in the value of the Coulomb barrier arising from the fragment charge distribution in the final channel.

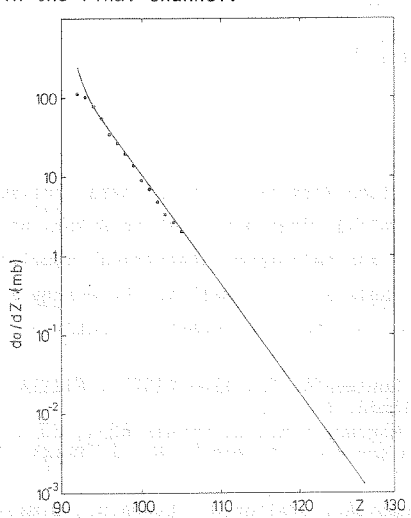
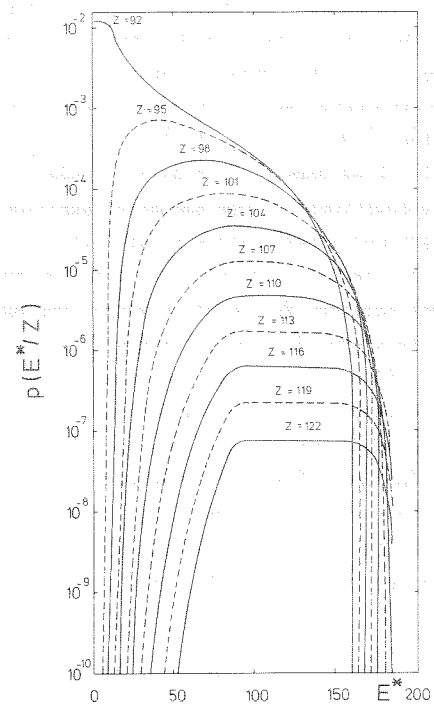


Fig. 1. Element distribution for U + U at 7.5 MeV/u in a fit of the diffusion coefficient to experimental data[1]

In Fig. 1 the calculated element distribution is compared with experimental data[1]. Here the theoretical results for $d\sigma/dZ$ have been normalized to $\bar{\sigma}_R \approx 1$b. Deviations from the experimental points in the region of the target charge 92 are due to the integration up to the grazing angular momentum.

For a more detailed discussion of the superheavy element production we consider the probability for various excitation energies E* and nuclear charges Z. In Fig. 2 the probability $p(E^*,Z)$ is plotted versus the excitation energy for different elements



Finally, we give some estimates for the changes of the formation probabilities for superheavy elements for different projectile-target combinations.

Reaction	Z =100	Z =114
$^{238}U + ^{238}U$	$2.7\cdot10^{-5}$	$1.4\cdot10^{-11}$
$^{238}U + ^{244}Pu$	$7.9\cdot10^{-5}$	$1.1\cdot10^{-10}$
$^{244}Pu + ^{244}Pu$	$8.0\cdot10^{-5}$	$1.0\cdot10^{-10}$
$^{238}U + ^{248}Cm$	$2.4\cdot10^{-4}$	$1.2\cdot10^{-9}$
$^{244}Pu + ^{248}Cm$	$2.3\cdot10^{-4}$	$9.0\cdot10^{-10}$
$^{238}U + ^{249}Cf$	$8.3\cdot10^{-4}$	$8.3\cdot10^{-9}$
$^{244}Pu + ^{249}Cf$	$8.4\cdot10^{-4}$	$7.0\cdot10^{-9}$

Table 1. Theoretical cross section $d^2\sigma/dZ\,dE$ in b/MeV for fragment formation with an excitation energy E^*=30 MeV

[1] Herrmann, G.: Invited Paper at the International Symposium on Superheavy Elements, Lubbock, USA, 1978
Schädel, M., Kratz, J.V., Ahrens, H., Brüchle, E., Franz, G., Gäggeler, H., Warnecke, I., Wirth, G., Herrmann, G., Trautmann, N., Weis, M.: Phys. Rev. Lett. 41, 469 (1978)
[2] Wolschin, G., Nörenberg, W.: Z. Physik A 284, 209 (1978)
[3] Wolschin, G.: Fizika 9, 513 (1977), Supplement A and Nukleonika 22, 1165 (1977)
[4] Wolschin, G., Nörenberg, W.: Phys. Rev. Lett. 41, 691 (1978)
[5] Ayik, S., Wolschin, G., Nörenberg, W.: Z. Physik A 286, 271 (1978)
[6] Riedel, C., Wolschin, G., Nörenberg, W.: Z. Physik A 290, 47 (1979)

B + G

Statistical Fluctuations in Dissipative Heavy-Ion Collisions

C. Riedel
GSI Darmstadt
G. Wolschin
Institut für Theoretische Physik der Universität and Max-Planck-Institut für Kernphysik, Heidelberg

In this paper we present an approximate analytical calculation of the statistical fluctuations in scattering angle, energy loss, and fragment charge number. To obtain the corresponding mean values $\langle\theta\rangle$, $\langle\Delta E\rangle$ as well as the mean interaction time τ_{int} as functions of the impact parameter b we employ our classical model[1] which successfully describes a large amount of experimental data. We start our investigation of statistical fluctuations in deeply inelastic heavy-ion collisions from a Fokker-Planck equation for relative motion and mass asymmetry. From this equation one can derive a set of coupled equations for first and second moments which determine the Gaussian distribution function. We do not solve the equations for the first moments but instead calculate the mean values for the relevant obervables $\langle\theta\rangle$, $\langle\Delta E\rangle$ as well as τ_{int} from our classical model[1] that includes fragment deformations. Neglecting higher-order derivatives of the potential and derivatives of the inertia tensor the coupled differential equations for the variances become

$$\frac{d}{dt}\sigma^2_{rr} = \frac{2}{\mu}\sigma^2_{rp} \qquad \frac{d}{dt}\sigma^2_{\theta\ell} = -\gamma_\ell\sigma^2_{\theta\ell} + \frac{1}{J_{rel}}\sigma^2_{\ell\ell}$$

$$\frac{d}{dt}\sigma^2_{rp} = -\gamma_p\sigma^2_{rp} + \frac{1}{\mu}\sigma^2_{pp} \qquad \frac{d}{dt}\sigma^2_{\ell\ell} = -2\gamma_\ell\sigma^2_{\ell\ell} + 2D_{\ell\ell}$$

$$\frac{d}{dt}\sigma^2_{pp} = -2\gamma_p\sigma^2_{pp} + 2D_{pp} \qquad \frac{d}{dt}\sigma^2_{AA} = -2\gamma_A\sigma^2_{AA} + 2D_{AA}.$$

$$\frac{d}{dt}\sigma^2_{\theta\theta} = \frac{2}{J_{rel}}\sigma^2_{\theta\ell}$$

It is our aim to calculate the statistical fluctuations in the observables total kinetic energy loss ΔE, scattering angle Θ and mass (charge) asymmetry measured by $A_1(Z_1)$. The transformation from the collective variables $x = (r, \theta, \ell, Z_1)$ with the corresponding covariance matrix

$$X = \{X_{ij}\} \equiv \begin{pmatrix} \sigma^2_{rr} & 0 & 0 & 0 \\ 0 & \sigma^2_{\theta\theta} & \sigma^2_{\theta\ell} & 0 \\ 0 & \sigma^2_{\theta\ell} & \sigma^2_{\ell\ell} & 0 \\ 0 & 0 & 0 & \sigma^2_{ZZ} \end{pmatrix}$$

to the covariance matrix of the observables $y = (\Delta E, \Theta, Z_1)$

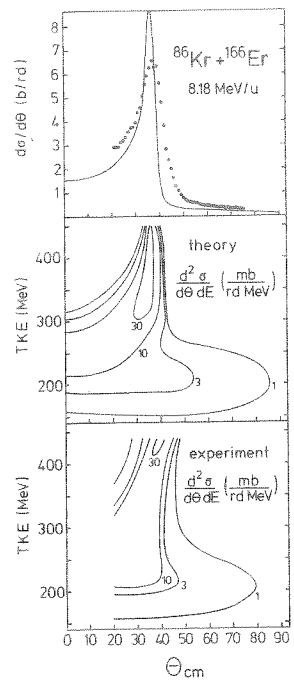
$$Y = \{Y_{ij}\} \equiv \begin{pmatrix} \sigma^2_{EE} & \sigma^2_{E\Theta} & \sigma^2_{EZ} \\ \sigma^2_{E\Theta} & \sigma^2_{\Theta\Theta} & \sigma^2_{\Theta Z} \\ \sigma^2_{EZ} & \sigma^2_{\Theta Z} & \sigma^2_{ZZ} \end{pmatrix}$$

is achieved by means of the transformation $Y = MXM^T$.

In accordance with the Fokker-Planck approximation to the transport problem it is consistent to keep only linear terms in the transformation of X. The transformation matrix M is composed of the partial derivatives

$M = \{M_{ij}\} \equiv \{\partial y_i/\partial x_j\}$

which have to be evaluated at the scission point. Multidifferential cross sections can now be calculated since the threedimensional Gaussian distribution function in the observables $\Delta E, \Theta, Z_1$ is completely determined by the mean values[1] and the covariance matrix.



Calculated angular distributions $d\sigma/d\theta$ and $d^2\sigma/(d\theta dE)$ for ^{86}Kr (8.18 MeV/u) + ^{166}Er in comparison with the data[2].

Detailed comparison with experimental data confirms a result that is familiar from numerical solutions of transport equations: the calculated statistical fluctuations in scattering angle are too small at low energy loss. This may hint at the importance of quantal fluctuations.

[1] Wolschin,G., Nukleonika 22, 1165 (1977); FIZIKA 9, 513 (1977), Supplement 4
Wolschin,G., Nörenberg,W., Z. Physik A284, 209 (1978)
Riedel,C., Wolschin,G., Nörenberg,W., Z. Physik A290 47 (1979)

[2] Rudolf,G., Gobbi,A., Stelzer,H., Lynen,U., Olmi,A., Sann,H., Stokstad,R.G., Pelte,D., preprint GSI-VP-12-78 and submitted to Nucl. Phys. A

Quantal Fluctuations in inelastic Heavy Ion Collisions

W. Cassing and H. Friedrich
Institut für Theoretische Physik I, Münster

In a collision of two heavy ions the finite spreading of the double differential cross section $d^2\sigma/d\theta dE$ for a given energy loss is usually attributed to statistical fluctuations as described by classical diffusion models. In the quasi-elastic region, where the collision time is very short, this classical interpretation always leads to fluctuations which are too small in comparison with experiment and in fact vanish in the limit of grazing collisions with zero energy loss.

In this contribution we present a quantum mechanically consistent calculation of $d^2\sigma/d\theta dE$ for the collision $^{40}Ar \rightarrow ^{232}Th$ at E_{CM} = 323 MeV. The description of the relative motion of the two nuclei is based on the Wigner transformed reduced von Neumann equation which can be regarded as a quantum mechanical generalization of the classical Fokker-Planck equation and has been discussed in ref.[1] for relative motion in one spatial dimension. The evaluation of the cross section from the asymptotic behaviour of quantal Wigner functions $\rho_\ell^\ell(R,P)$ makes use of a generalization of JWKB phase shifts to dissipative collisions.

In the present calculation, the dissipation of angular momentum was neglected and the radial motion was treated in the local harmonic approximation. This leads to Fokker-Planck equations for $\rho_\ell^\ell(R,P)$ which are correct in a quantal sense up to second moments with respect to the radial momentum P. Quantal effects associated with the coherent superposition of all partial waves were included without approximation.

Fig. 1 shows $d^2\sigma/d\theta dE$ for various values of the final kinetic energy of the projectile in comparison with the experimental data[2]. The discrepancy with respect to the absolute magnitude of the cross section is due to the restriction of the experimental data to the K-channel. The contour map of the double differential cross section obtained in the present calculation is displayed in fig. 2. Without any adjustable parameter the calculation reproduces the spreading of 10^0 to 20^0 for energy losses up to about 80 MeV. In contrast, calculations based on a classical Fokker-Planck equation[3] yield a spreading of less than 5^0 in this region of the Wilczynski plot.

We conclude that the large spreading of $d^2\sigma/d\theta dE$ for small energy losses can be accounted for in a natural way by quantal fluctuations arising from the interference of the various partial waves.

[1] W. Cassing and H. Friedrich, Z. Physik A291 (1979) 339
[2] J. Wilczynski, Phys. Lett. 47B (1973) 484
[3] M. Berlanger et al., Z. Physik A284 (1978) 61

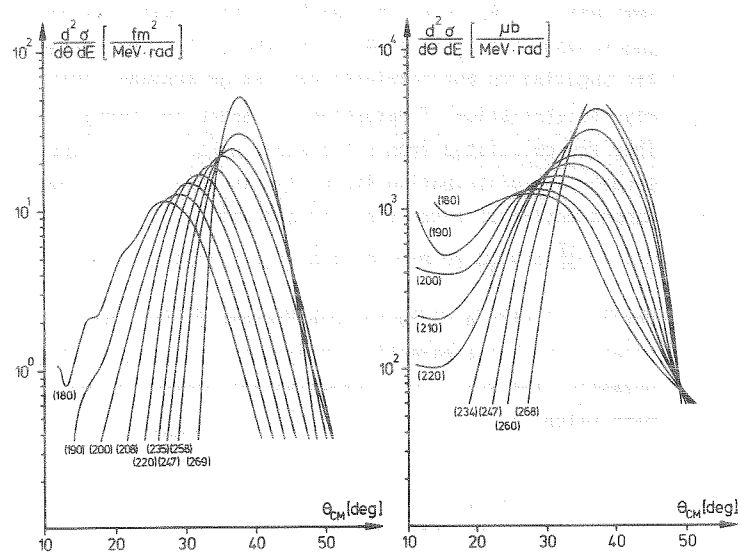


Fig. 1. The theoretical double differential cross section ($^{40}Ar \rightarrow ^{232}Th$ at E_{CM} = 323 MeV) for various final energies of the outgoing fragment (left) in comparison with the experimental data (right)

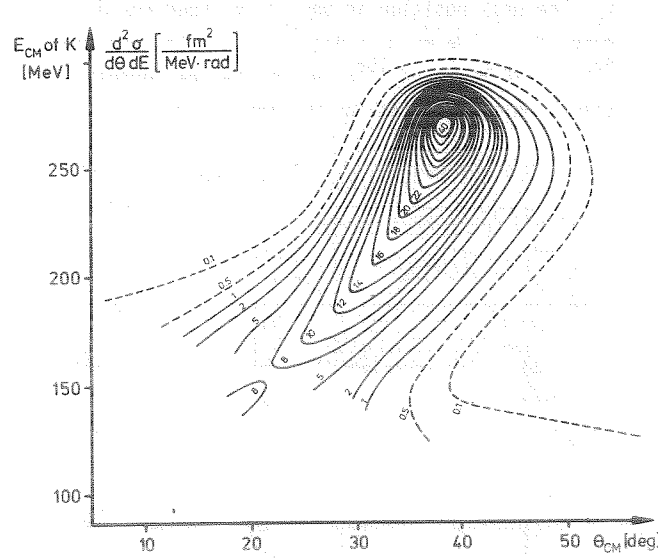


Fig. 2. Contour map of the double differential cross section $d^2\sigma/d\theta dE$ for $^{40}Ar \rightarrow ^{232}Th$ at E_{CM} = 232 MeV.

B + C

Shape Relaxation in Heavy-Ion Collisions

Georg Wolschin+

Institut für Theoretische Physik der Universität Heidelberg

Fragment kinetic energies in deeply inelastic collisions extend well below the interaction barrier. The corresponding relaxation of the fragment shape is treated in a transport model[1,2]. Spheroidal shapes are assumed with semi-axes $a = R(1 + \varepsilon)$, $b = R/\sqrt{1+\varepsilon}$, and ε with its conjugate momentum p_ε is taken to be the collective variable. Its coupling to the intrinsic degrees of freedom gives rise to statistical fluctuations in shape and energy loss. They are calculated from a transport equation[1] for the probability distribution $f(\varepsilon,p_\varepsilon;t)$. In the limit of overdamped motion it takes the simple form[2]

$$\frac{\partial P}{\partial t} = - \frac{\partial}{\partial \varepsilon} (v_\varepsilon P) + D_\varepsilon \frac{\partial^2 P}{\partial \varepsilon^2}$$

for $P(\varepsilon,t)$ with a diffusion coefficient D_ε for shape relaxation. For a harmonic approximation to the driving potential the solution is Gaussian and determined by mean value

$$\langle \varepsilon(t) \rangle = \varepsilon_0 \, [1 - \exp(-t/\tau_\varepsilon)]$$

and variance

$$\sigma^2_\varepsilon = \frac{T}{2k_\varepsilon} [1 - \exp(-2t/\tau_\varepsilon)]$$

with the stiffness k_ε of the potential and the characteristic time for shape relaxation[2]

$$\tau_\varepsilon = \tau/(2k_\varepsilon D_\varepsilon).$$

The calculated equilibrium deformation ε_0 is in good agreement with fit values. The only free parameter is τ_ε. The peak position in the energy spectrum determines its value as $\tau_\varepsilon = 4 \cdot 10^{-21}$s. For the reaction ^{86}Kr (5.99 MeV/u) + ^{166}Er we obtain the corresponding diffusion coefficient for the shape variable as

$$D_\varepsilon \approx 7.2 \cdot 10^{17} s^{-1}.$$

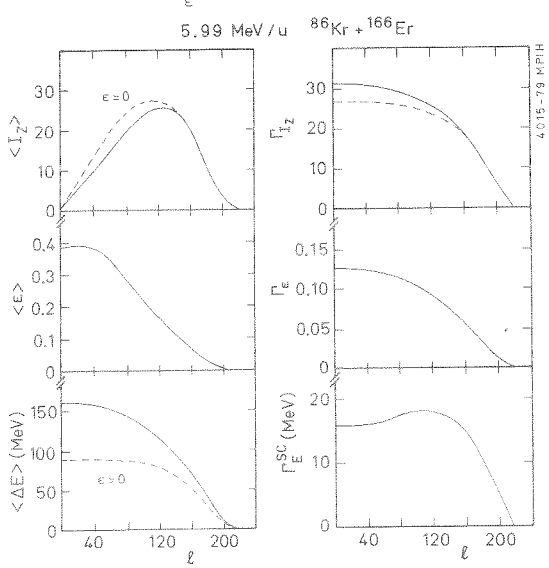


Fig. 1: Mean value and FWHM of intrinsic angular momentum, deformation and energy loss.

In a joint treatment of angular-momentum dissipation and shape relaxation we have calculated the dissipated angular momentum as a function of total kinetic energy loss[2]. The results are compared in Fig. 2 with data from the γ-multiplicity-experiment of Olmi et al.[3].

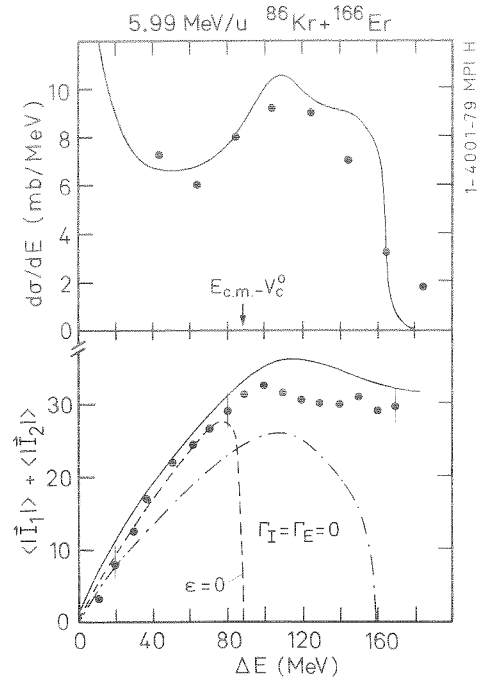


Fig. 2: Calculated energy spectrum and angular-momentum distribution in comparison with the data

[1] G. Wolschin, Proc. Int. School Physics Varenna 1979

[2] G. Wolschin, Phys. Lett. 88B (1979) 35

[3] A. Olmi et al., Phys. Rev. Lett. 41 (1978) 688

Mass Transport in Anharmonic Potentials [B]

R. Schmidt
Joint Institute for Nuclear Research, Dubna, USSR
G. Wolschin+
Institut für Theoretische Physik der Universität Heidelberg

The effect of nuclear structure on the mass transport in deeply inelastic collisions is investigated in a transport model[1,2]. As an example we consider the driving potentials of Fig. 1

$$U(x) = k \cdot x^2(1-\frac{1}{2}x^2) + C.$$

It approximates the shell-corrected driving potential for $^{238}U + ^{238}U$. The variable x is chosen to be ±1 at the Pb-minima. The transport equation for P(x,t) becomes

$$\frac{\partial}{\partial t}P = -\gamma \frac{\partial}{\partial x}[x(1-x^2)P] + D_x \frac{\partial^2}{\partial x^2} P.$$

The temperature-dependence of the structure effect on the driving potential is taken to be $f(T) = \exp[-(\frac{T}{T_0})^2]$ with a parameter T_0. Due to the nonlinear dependence of the drift coefficient on x the solutions of this equation are not Gaussian. Analytical solutions are obtained under suitable approximations. They are shown in Fig. 1 with full shell-structure effects ($T_0 \to \infty$) and for different values of relative angular momentum ℓ, or mean interaction time τ_{int}. For sufficiently long time, two asymmetric peaks develop in the nonlinear regime.

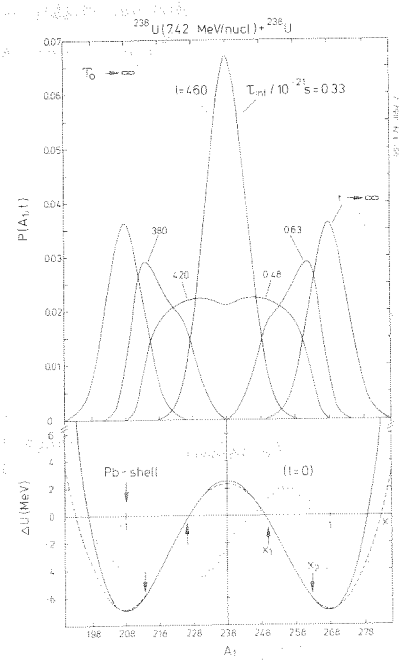


Fig. 1: Model potential and solutions of the transport equation

The corresponding mass distributions are obtained by integrating over impact parameter. They are shown in Fig. 2 (lower part). For smaller values of T_0 the structure effect on the mass distribution is damped out (upper part). Indeed the experimental element distributions do not reveal shoulders at the Pb-shell[3]. The surviving effect is a broadening of the variance σ_z^2 at fixed energy loss as compared to other systems[3]. In our calculation it is due to the drift towards the closed Pb-shell.

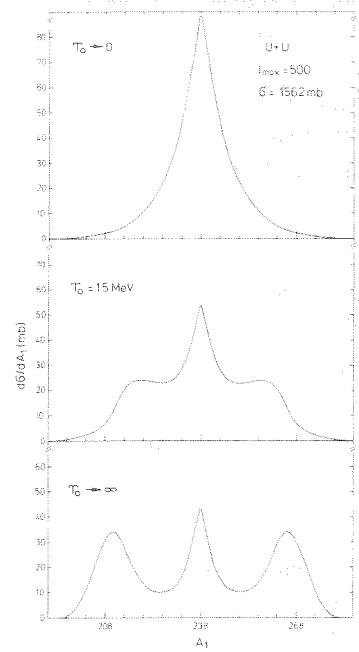


Fig. 2: Calculated mass distributions for fast ($T_0 \to 0$) and slow damping of the shell effect.

[1] G. Wolschin, Proc. Int. School Physics Varenna 1979
[2] R. Schmidt and G. Wolschin, MPI-H-1979-V22
[3] H. Freiesleben et al., Z. Physik A292 (1979) 171

B + G

A model calculation for mass dispersion in a fermion gas

H.Feldmeier and P.Buck
Institut für Kernphysik, Technische Hochschule Darmstadt, FRG

To gain better understanding of the mass distribution in heavy ion collisions we solve numerically the time dependent many body Schrödinger equation for a fermion system. The results are compared with different approximations.

The model consists of an infinite square well potential which contains $A=n_1+n_2$ identical fermions. For simplicity we treat only one dimension. The particles interact via a finite-range two-body interaction which can be varied in shape and strength. Initially a wall (strong delta-function) separates the container in two parts with sharp number of particles n_1, n_2 on each side. We start at time t=0 with an eigenstate of the separated system and remove the wall. The wavefunction evolves in time according the Hamiltonian H

$$H=\sum_{i=1}^{A}\{\frac{p_i^2}{2m}+V_{container}(x_i)\}+\sum_{i<j}V_{12}(|x_i-x_j|)$$

and describes the exchange of particles between the two sides. Due to the single particle motion and the two-body collisions the system heats up and reaches an equilibrated situation.

We'd like to concentrate on one macroscopic variable, namely the number of particles n_1 on one side of the container. The according operator is given by

$$N=\sum_{ij}\omega_{ij}\,a_i^+\,a_j\,;\quad \omega_{ij}=\int\phi_i^*(x)\,\theta(x)\,\phi_j(x)\,dx$$

The mean value and the variance

$$\langle N\rangle=\langle\psi(t)|N|\psi(t)\rangle\,;\quad \sigma^2=\langle\psi(t)|N^2|\psi(t)\rangle-\langle N\rangle^2$$

are calculated with the many body wavefunction $\psi(t)$ which is the solution of the time-dependent Schrödinger equation.

A typical result of the calculation is given in fig.1. The spread σ^2 is plotted versus time for a system with totally 16 fermions, 8 on each side. The upper-most curve shows σ^2 for distinguishable (classical) particles, where the transition probability for switching sides is given by the mean one-sided current of a fermi gas.[1] The other two curves are the exact results for fermions with an attractive and without any two-body interaction. The latter one corresponds to the TDHF case if one regards the container as the selfconsistent mean potential. Inclusion of the two-body interaction almost doubles the mass spread compared with the interaction free fermi gas.

Different conclusions have been drawn[2] about different approximations made in the literature. The model calculation provides the exact and the approximated answer thus being very helpful in understanding the approximations.

1. F.Beck, M.Dworzecka, H.Feldmeier; Z.Physik A289, 113 (1978)
2. H.Feldmeier, P.Buck; Proceedings of the "Winter Workshop on Nuclear Dynamics" March 1980, to be published by LBL

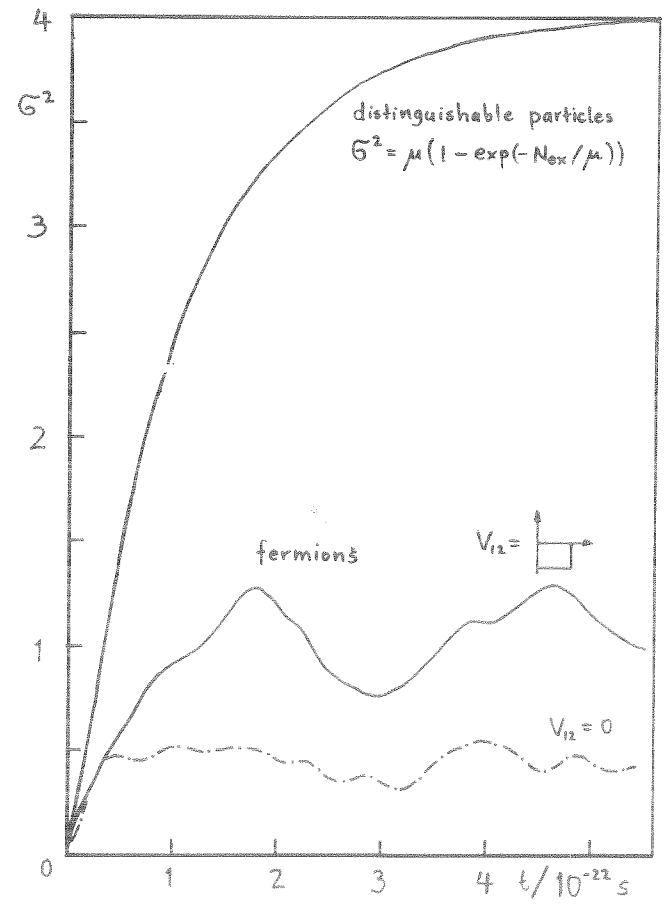


Fig.1: Mass spread for fermions and classical particles in a box of 2 times 15 fm length. Full line: attractive two-body interaction with strength V = 30 MeV and range 5 fm. Dash dotted line: interaction free Fermi gas.

B + G

Heavy-Ion Fusion Cross-Sections Calculated with the One-body Window-Friction and the Relaxed-Density Proximity-Potential

H.Feldmeier and F.Beck
Institut für Kernphysik, Technische Hochschule Darmstadt, FRG

To calculate fusion cross sections for a variety of projectile-target combinations we employ a classical trajectory model. The dissipative mechanism is the one-body window-friction. For the conservative nucleus-nucleus potential we use the "relaxed-density proximity-potential"[1] which is calculated by first defining a family of shapes and then calculating the liquid drop energy and the proximity contribution from the gap or crevice in the shape. The Coulomb potential is that of the uniformly charged system within the shape boundaries.

The resulting fusion cross sections for two typical systems are displayed. They are compared with the data and the cross sections calculated with the "modified proximity potential" published in ref.2). Figure 1 shows the systems $^{27}Al+^{12}C$. The two theoretical curves deviate from each other in the low energy region whereas they almost coincide for the high energy part. The experimental data are in between the two calculated curves.

In the other case $^{40}Ca+^{40}Ca$ (fig.2) the excitation function of the "relaxed-density proximity-potential" seems in better agreement with the data. Unlike in the previous case the two potentials give different cross sections also for the high energy part.

Assuming a critical-distance model for the low energy part one may extract a critical potential V_c at a critical radius R_c according to

$$\sigma_{fusion} = \pi R_c^2 (1 - V_c/E_{cm})$$

Approximating the theoretical curve by a straight line yields parameters of V_c which are within the uncertainties consistent with the "relaxed-density proximity-potential" (RDP):

$$V_c = V_{RDP}(R_c)$$

In the high energy regime the calculated fusion cross sections are consistent with a critical ℓ-value picture.

In conclusion the "relaxed-density proximity-potential" together with the one-body window-friction is able to reproduce a variety of fusion cross sections.

1. J.Blocki, F.Beck, M.Dworzecka, H.Feldmeier; Proceedings International Workshop on Gross Properties of Nuclei and Nuclear Excitations VIII 1980 ed. by H.Feldmeier, p.157
2. J.R.Birkelund, L.E.Tubbs, J.R.Huizenga, J.N.De and D.Sperber; Physics Reports 56, 107 (1979)

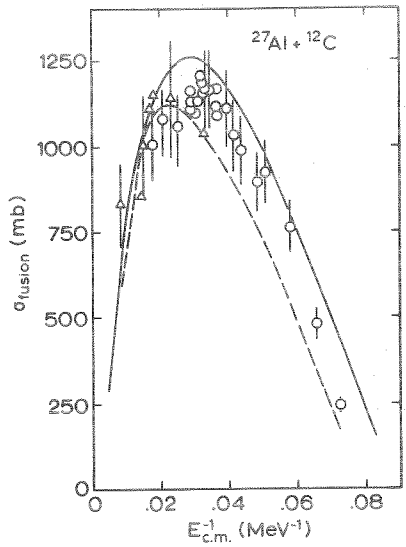


Fig.1

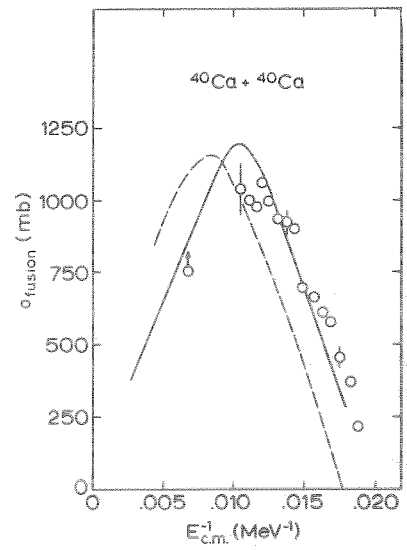


Fig.2

Fusion cross section. Full line: "relaxed density potential; dashed line: "modified proximity potential"

On the dynamics of fission as a dissipative process [G]

K. Pomorski, TU München and GSI Darmstadt and H. Hofmann, TU München

We studied the dynamics of fission from the region of the saddle point to that of scission. The shape of the fissioning nucleus was parametrized by three collective degrees of freedom. The dynamical evolution of the system was studied by means of the Wigner function of these variables and their conjugate momenta. The equation of motion for this d(t) is of a Fokker-Planck type, in which all nonlinear forces are linearized locally[1].

The input for this equation involves the knowledge of conservative forces on one hand and on dissipative and conservative ones on the other. As for the first type of force, we based our input on experience with cranking model type calculations (c.f.ref.2).For the second type of force we used phenomenological ansätze which were partly justified by microscopic studies, namely as far as the generalized relationship between the friction and the diffusion coefficients is concerned.

The quantities we were aiming at were the variances at scission of the total energy (σ_E^2) and of the mass asymmetry (σ_A^2). These quantities can be expected to be constant after scission and may thus be compared to experiment. We argue that the same will not be true for the prescission kinetic energy. This makes us believe that the latter is not a good measure of the importance of the statistical fluctuations.

Within our model we observe a large increase of σ_E^2 (see fig.1) and σ_A^2 on the way from saddle to scission. Furthermore, the final values of σ_E^2 and σ_A^2 depend strongly on the initial broadness of the distribution ,whereas only a moderate influence of the diffusion coefficient was found. Both questions are somewhat related, because, for high energy fission both the initial distribution as well as the diffusion coefficient will be governed by the large temperature of the fissioning system.

As far as a comparision with experiments is concerned our model may still be too crude. For instance, we did not take into account a temperature dependence of the conservative and frictional forces. Furthermore, the assumed independence of the mass parameter on the collective coordinates is a too strong assumption. An increase of the inertia in the scission region will certainly decrease the fluctuations. We have made a test by changing the collective inertia in the mass asymmetry direction. Then, indeed, the final value of σ_A^2 was reduced (see fig.2).

It is clear that a more quantitative calculation can be done only after microscopic inputs become available for the coefficients of the Fokker-Planck equation. We believe, however, that the features which we find and which were mentioned before are of somewhat more general nature. In particular, the strong dependence on the initial distribution certainly calls for a proper treatment of the problems of barrier penetration. It is here where, from a theoretical point of view, the interplay between quantal and dissipative phenomena is most stringent.

References:

1.H.Hofmann,P.J.Siemens,Nucl.Phys.A275(1977)464, H.Hofmann,A.S.Jensen,C.Ngô and P.J.Siemens,to be published see also:Proc.IVth Balaton Conference on Nucl.Phys.,Keszthely,Hungary,June 1979
2.A.Baran,K.Pomorski,S.E.Larsson,P.Möller,S.G. Nilsson,J.Randrup and A.Sobiczewski,Proc.3rd Int.Conf.on Nucl.far from Stability,Cargèse, France,1976,p.537

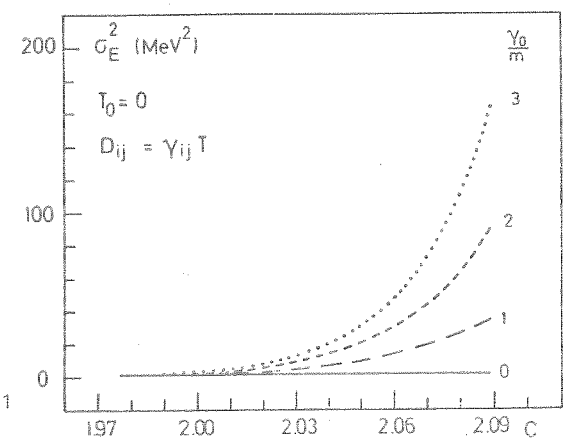


Fig.1

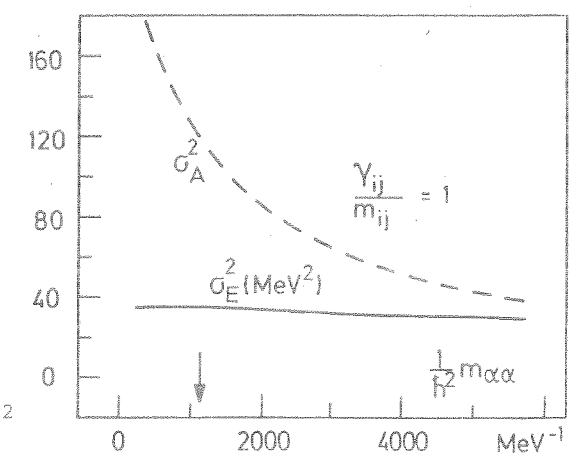


Fig.2

Initial correlations in dissipative collisions and compound-nucleus formation

W. Nörenberg and C. Riedel
GSI Darmstadt

During the fast approach of the nuclei the individual nucleons cannot follow the lowest possible (adiabatic) levels. The nucleonic wave functions stay essentially unchanged (conservation of number of nodes). Such a 'diabatic' behaviour is encountered also for electrons in atom-atom collisions. The motion of nucleons on diabatic levels gives rise to a large potential energy in addition to the adiabatic potential. The doorway configuration which is formed during the fast approach of the two nuclei can be considered as a highly correlated state of (n particle, n hole)-excitations with respect to the adiabatic configuration. This correlation is effectively lost by the decay via residual interactions. The time which is necessary to obtain local statistical equilibrium between all excited states at a given shape, is denoted by τ_{loc} and expected to be of the order 10^{-21}s. To take account of these initial correlations we have introduced a new concept in transport theories[1], the explicitly time-dependent dynamical potential which decays with time constant τ_{loc} from the initial diabatic value to the final adiabatic value.

A Fokker-Planck equation including the dynamical potential has been applied[1] to the compound nucleus ^{248}Fm. In general, the total cross-section consists of three components. For $0<\ell<\ell_{crit}$ or ℓ_{cap} there is compound-nucleus formation, for $\ell_{crit}<\ell<\ell_{cap}$ a slow component and for $\ell_{cap}<\ell<\ell_{gr}$ the familiar fast component of dissipative collision exist. Fig. 1 shows the angular and element distribution of the fast component for Kr (8.18 MeV/u) + Er together with the experimental results for energy losses < 160 MeV. Fig. 2 illustrates for Ar + Pb the calculated excitation functions for the capture cross-section σ_{cap}. For $\sigma_{cap}<\sigma(\ell_{crit})$ the capture leads to compound-nucleus formation. For small bombarding energies the compound-nucleus formation is strongly suppressed. It reaches the maximal value at the crossing point with the dashed line which corresponds to ℓ_{crit}. Above this cross-over a long-living component of dissipative collision occurs. The threshold for this component is well above the interaction barrier V_C. A significant dependence of the capture cross-section is roughly determined by an energy-independent upper limit ℓ_{cap} of relative angular momentum which depends on τ_{loc}. As a result of this, the capture cross-section exhibits a rather pronounced maximum as function of the bombarding energy. For more symmetric projectile-target combinations the depth of the pocket in the (adiabatic) potential is reduced and hence, the capture cross-section goes down correspondingly. Experimental evidence for the existence of the long-living dissipative component has been reported earlier[2].

We hope that the further study of excitation functions for various projectile-target combinations will reveal more about the role of the dynamical potential and hence, about the peculiar interplay between single-particle and collective degrees of freedom in nuclei.

[1] W. Nörenberg and C. Riedel, Z. Physik A 290, 335 (1979)
C. Riedel and W. Nörenberg, to be published (1980)

[2] H. Sann et al., GSI Annual Report 1977, GSI-J-1-78,p.30
B. Heusch et al., Z. Physik A 288 , 391 (1978)
C. Lebrun et al., Nucl. Phys. A 321, 207 (1979)

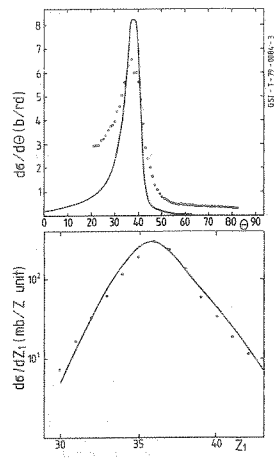


Fig. 1. Angular and element distribution for the fast component (energy loss < 160 MeV) of Kr (8.18 MeV/u) + Er

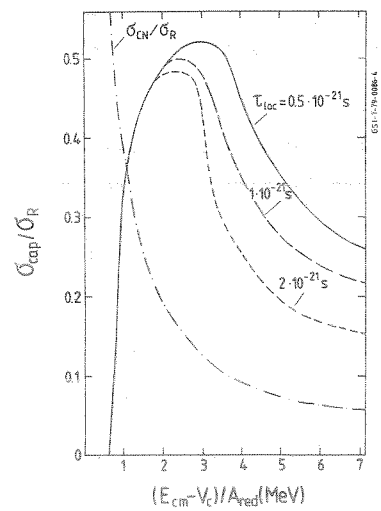


Fig. 2. Excitation functions of the capture cross-section in units of the reaction cross-section for Ar + Pb.

Contributions to fragmentation theory B

J. Hahn, K.H. Ziegenhain, K. Depta, M. Uhlig, A.R. Degheidi, J.A. Maruhn, W. Greiner
Institut für Theoretische Physik der J.W.G.-Universität Frankfurt/Main

The Frankfurt fragmentation theory describes the collective mass flow in fission processes by the dynamical variable of the mass asymmetry η. The potential $V(\eta, \alpha_i)$, where α_i are other collective coordinates, is determined from the liquid drop model including shell effects, which are calculated from the two-center shell model after Strutinsky.

The dissipation of energy from the relative motion of the nuclei can be considered by a phenomenological friction term.

For the first time a detailed dynamical investigation of medium-heavy systems, such as $^{86}Kr + ^{166}Er$, $^{132}Xe + ^{120}Sn$, leading to the same compound nucleus, was possible. The importnace of shell effects for the explanation of the experimental differential cross sections $d^2\sigma/dE\,dZ$ was shown, and good agreement with experimental data of G. Rudolf et al. (GSI-V8-12-78)[1,2] was found.

It could be shown that the measured widths of fragment-mass distributions in heavy ion reactions are the result of two different physical mechanisms, the quantum mechanical uncertainty in the collective motion in the mass-asymmetry degree of freedom and the width resulting from the thermal excitation energy in the system resp. statistical exchange of nucleons.

The discussion of the Fermium isotopes showed a markedly transition from asymmetric fission mass distribution with mass numbers growing from 254 to 258.

Additionally proposed was a strong asymmetric fragment distribution with mass numbers 60-65 and their complements. This new peak should be three orders of magnitude smaller than the main contribution from the (n,f) reaction.[3,4] Similar events had been found experimentally for the fission mass distribution of uranium (Carvalho, Epperson, Rao). A three-center shell model was developped for the description of ternary fission[5].

[1] J.A. Maruhn, H.J. Lustig, J. Hahn, W. Greiner; Proc. of the Int. Workshop on Gross Properties of Nuclei and Nuclear Excitations VII, Hirschegg

[2] J.A. Maruhn, J. Hahn, H.J. Lustig, K.H. Ziegenhain, W. Greiner; Proc. of the Erice School on Heavy Ion Interactions at High Energies, Erice/Italy

[3] J. Hahn, H.J. Lustig, K.H. Ziegenhain, J.A. Maruhn, W. Greiner; Proc. of the IAEA-Symposium on Physics and Chemistry of Fission, Jülich 1979

[4] H.J. Lustig, J.A. Maruhn, W. Greiner; J. Phys. G, Nucl. Phys. 6, L25 (1979)

[5] A.R. Degheidy, J.A. Maruhn; Z. Phys. A290 (1979) 205-212

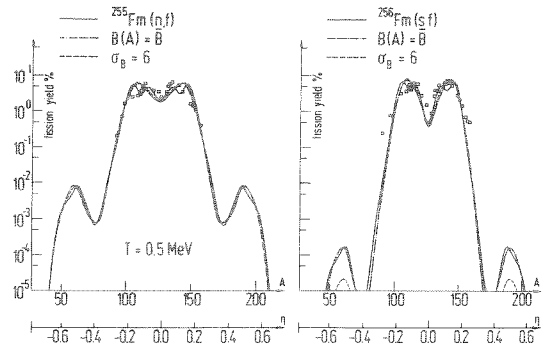


Fig.1 Calculated mass distributions for spontaneous fission of ^{256}Fm and neutron-induced fission of ^{255}Fm. Experimental data from Flynn (1972, 1975a).

Study of the ^{238}U reaction with ^{48}Ca and ^{238}U in TDHF and Fragmentation Theory

G

R.Y. Cusson, J. Hahn, J.A. Maruhn and W. Greiner, Inst. für Theor. Physik der J.W. Goethe Universität, Frankfurt/Main

and

H.J. Lustig, H. Stöcker, GSI Darmstadt

We have performed 3-D TDHF calculations[1] for the reaction U + Ca at 4.6,4.7,4.9,5.7 and 5.9 MeV/A, and U+U at 7.5 MeV/A and various impact parameters in order to obtain energy loss and deflection function curves vs impact parameters, which could be compared with recent GSI experimental results. We observed the formation of long lived nuclear molecules ($\tau_d >> 3\times10^{-21}$s) in the U+Ca reaction (Z united = 112) whose typical density contours are shown in fig. 1, for b = 3.13 fm.

The energy dependence of this nuclear molecule capture cross section is shown in fig. 2 and represents a large fraction of the total reaction cross section. In some cases a slow drift of the shape towards mass-symmetry is also observed. However, the system has too large an angular momentum to form a stable compound system, so it must decay to binary fragments. Whereas the classical decay path consists in a drift to symmetry followed by symmetric break up, there is a quantum mechanical amplitude for radial barrier penetration at all times during the drift to symmetry.This effect results in a reaction time $\tau_R \sim \exp[-(\ell-\ell_g)/\ell_0]$ and can not be reproduced by the TDHF method. Thus a fragmentation calculation[2] is superposed on the TDHF mean behaviour to determine the mass distributions vs impact parameter. After integrating over b this yields mass distributions with a broad symmetric component which grows with bombarding energy. This prediction is similar to the recent results[3] observed in $^{208}Pb+^{50}Ti$ and $^{208}Pb + ^{58}Ni$ at GSI. The U+U reaction does not show any molecular capture effect, probably because of the stronger Coulomb repulsion. Figure 3 shows the very long neck which forms before scission. We have observed that the pairing gap does not disappear even when the internal energy is above 125 MeV per U fragment. This indicates that the TDHF single-particle viscosity does not destroy the shell effects. We have followed a single U fragment after a collision and we have found that it does not fission in TDHF. This may be due to our wrong shell effects because we neglect the spin-orbit force. We note that all these TDHF calculations require large quantities of CPU time and therefore have benefited greatly from the recent addition of a Floating Point Corp. Array Processor to the GSI Computation Center.

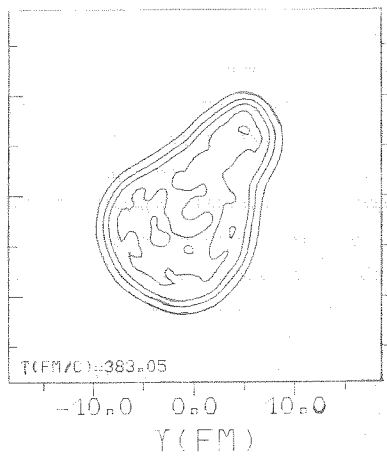


Fig. 1. Density contour at t=383fm/c (1fm/c = 3.3×10^{-24}s) in the Y-Z plane for the nuclear molecule formed in TDHF by the reaction ^{238}U (5.9 MeV/A) + ^{48}Ca at impact parameter b=3.13fm. The contour correspond to densities of 0.02, 0.06, 0.10 and 0.14 nucleons per fm^3.

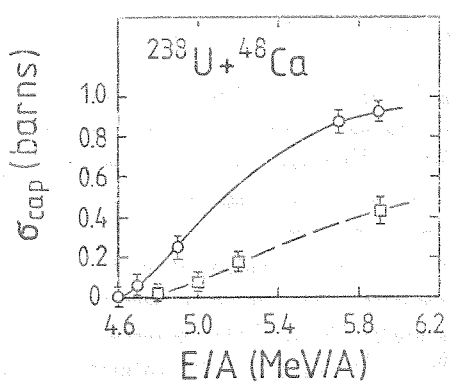


Fig. 2. Calculated (round points) Nuclear Molecule Capture cross-section in barns, vs bombarding energy per nucleon, for $^{238}U + ^{48}Ca$. The indicated error bars reflect the fact that long computing times require that only a few impact parameters for each bombarding energy be considered. The square points indicate recent measurements[3] at GSI for the corresponding symmetric break up cross section of $^{208}Pb+ ^{50}Ti$ which has a similar Coulomb energy.

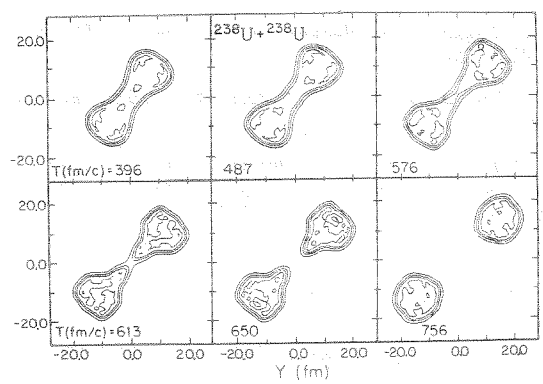


Fig. 3. ^{238}U (E/A = 7.5 MeV) + ^{238}U at impact parameter b = 4.18 fm, corresponding to ℓ_{in} = 300 $\hbar$. The outgoing orbital angular momentum is ℓ_{out} = 210 $\hbar$ only slightly larger than the rigid sphere clutching $\frac{5}{7}\ell_{in}$ = 124 $\hbar$.

[1] R.Y. Cusson, J.A. Maruhn, H. Stöcker, Z. Physik A214 (1980) 257

[2] J.A. Maruhn et al., Proc. of the Erice School on Heavy Ion Interactions at High Energies, Erice (Italy) 1979, in print in: Progress in Particles and Nuclear Physics

[3] H. Sann et al., Proc. Int. Conf., Hirschegg (1978) and contribution to this annual report

B + G

TDHF Study of the ^{86}Kr (12.2 MeV/A) + ^{166}Er Reaction

R.Y. Cusson and H. Stöcker, GSI Darmstadt

and

G. Buchwald, W. Greiner and J.A. Maruhn, Institut für Theoretische Physik der J.W. Goethe Universität, Frankfurt/Main

We have studied the above reaction by doing 3-D TDHF and 2-D NFD calculations at several impact parameters. The most remarkable result is the existence of a nuclear molecule capture window in ℓ_{in} and large angular momentum losses at other ℓ_{in}. A typical break up configuration is shown in fig. 1a. Nuclear Fluid dynamics suggest similar strongly deformed break up configurations as seen in fig. 1b. In order to study the life-time of the nuclear molecule we have studied its rms radius vs time (1 fm/c = 3.3×10^{-24}s). Vibrations of the molecule are observed. The configuration at ℓ_{in} = 215 $\hbar$ is seen to have $\tau_d >>$ 1500 fm/c in TDHF. However barrier penetration could shorten this considerably and cannot be computed in TDHF.

The large total angular momentum loss is seen in fig. 2. Assuming division among the fragments according to $A^{5/3}$ a mean value of 40 $\hbar$ can be imparted to the light fragment with an energy loss of 150 to 250 MeV. Such large angular momentum transfer result from non-rigid behaviour during the contact period. Corresponding to the momentum transfer fluctuation there is also an angular momentum transfer fluctuation for the light fragment which can not be obtained in TDHF. Experimental observations[2] on the ^{86}Kr + ^{144}Sm reaction have shown an rms ΔI spread of 20 $\hbar$ or more. This combined with our predicted mean of some 40 $\hbar$ suggest a non vanishing probability of bringing the light fragment above its critical fissionangular momentum. Thus one would have here an explanation of the projectile splitting observed recently[3] at GSI in the ^{86}Kr + ^{89}Y reaction. TDHF calculations for that reaction at 12 and 20 MeV/A show a similar behaviour to the present one. One of the intermediate configurations of the ^{85}Kr + ^{89}Y is shown in fig. 3.

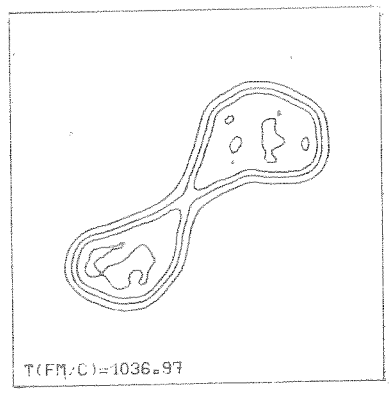


Fig. 1a: Break up of ^{86}Kr + ^{166}Er at 12.2 MeV/A and ℓ_{in} = 275 $\hbar$. At t=1037 fm/c the neck has just broken and large amounts of internal angular momentum is stored in the fragments. The mass of the light fragment has drifted towards symmetry by about 15 mass units.

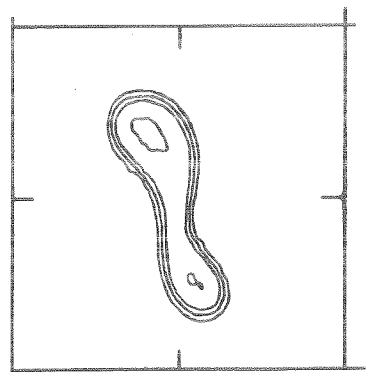


Fig. 1b: Break up of ^{86}Kr + ^{166}Er in a two dimensional nuclear fluid dynamics model analogous to fig. 1a.

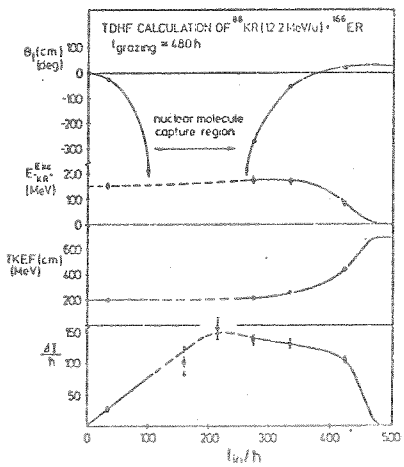


Fig. 2: Deflection angle, Kr-like fragment excitation energy, total kinetic energy and angular momentum loss vs incoming angular momentum ℓ_{in}. The $\Delta\ell$ is larger than the value given by rigid clutching. The Wilczynski plot is in reasonable agreement with experiment.

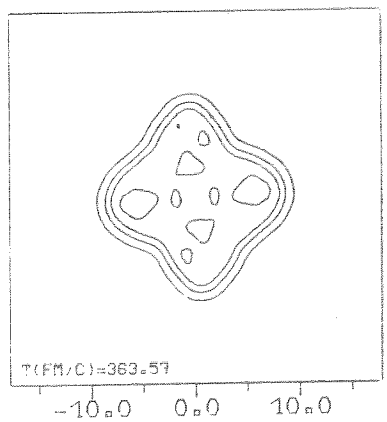


Fig. 3: Intermediate Configuration in the ^{86}Kr + ^{89}Y reaction at E/A = 20 MeV, b = 6.66 fm. The time is 364 fm/c. The diamond shape with four centers later reverts to a single elongated molecule which finally undergoes 2-body break up.

[1] R.Y. Cusson, J.A. Maruhn, H. Stöcker, Z. Physik A294 (1980) 257

[2] P.R. Christensen et al., Phys. Rev. Lett. 40 (1978) 1245

[3] A. Olmi, U. Lynen, J.B. Natowitz, M. Dakowski, P. Doll, A. Gobbi, H. Sann, H. Stelzer, R. Bock, D. Pelte, Phys. Rev. Lett. 44 (1980) 383

Transport theory of heavy-ion collisions in the adiabatic representation

S. Ayik
GSI Darmstadt

A transport equation is derived for dissipative heavy-ion collisions in the frame of an adiabatic representation[1]. The adiabatic basis of the intrinsic motion provides a convenient representation for the collision problem. In this representation the wave function $|\phi_n(r)>$ and the energies $\varepsilon(r)$ of the intrinsic degrees of freedom parametrically depend on the relative distance r between the colliding ions (and on the other collective variables as well). The transitions between the adiabatic levels are characterized by the dynamical coupling

$$V_{nm}(rp) = \frac{p}{\mu} \cdot <\phi_n(r)|\frac{\partial}{\partial r}|\phi_m(r)>. \qquad (1)$$

For slow collective motion (adiabatic limit) the coupling is weak and the dynamics can be described by the first order perturbation theory (linear response theory[2]). However, especially in the early stage of the collision the relative velocity is not slow. As a result, the dynamical coupling is large and the linear response theory is not applicable. In the present work we generalize the linear response theory by treating the coupling to all orders. We study the evaluation of the Wigner function $f_{nm}(rp,t)$ of the system. In the semi-classical limit of the relative motion, the Wigner function describes the joint probability distribution for finding the system in the adiabatic channel $|n>=|\phi_n(r)>$ with the relative distance r and the relative momentum p. Introducing the statistical properties for the dynamical coupling we obtain a non-perturbative transport equation for the Wigner functions. As a result of the fast approach of the two-ions, the initial stage of the collision is dominated by the coherent motion of the nucleons which is described by the inhomogeneity term in the transport equation. The inhomogeneity term is calculated using a two-centre diabatic slater determinantal representation. The inclusion of the initial correlations gives important modification in the transport equation[3]. For practical applications the transport equation can be converted into two-coupled equations. The first one is a master equation which determines the occupation probabilities $f_n(t)$ of the adiabatic channels. The second is a Fokker-Planck equation which gives the evaluation of the distribution function f(rp,t) of the relative motion,

$$(\frac{\partial}{\partial t} + \frac{p}{\mu}\frac{\partial}{\partial r} - \frac{\partial U}{\partial r}) f(rp,t) = \frac{\partial}{\partial p}(\gamma\frac{p}{\mu} + D\frac{\partial}{\partial p}) f(rp,t) \quad (2)$$

where U is the (dynamical) driving force.
In addition the usual adiabatic force, the driving force contains a dynamical contribution due to the initial channel correlations[3] which arises from the inhomgeneity term in the transport equation. The friction and diffusion coefficients are given as

$$\binom{\gamma}{D} = 2\pi\sum f_m(t)|<n|\frac{\partial H}{\partial r}|m>|^2 \xi_{nm}(rp) \binom{1/\omega_{nm}(r)}{1/2} \quad (3)$$

As a result of the non-perturbative treatment the transport coefficients are explicitly velocity dependent through the factor $\xi_{nm}(rp)$ which is determined by

$$\xi_{nm}(rp) = \frac{1}{\sqrt{2\pi}}\tau_{nm}(rp)\exp\{-\frac{1}{2}[\omega_{nm}(r)\tau_{nm}(rp)]^2\} \quad (4)$$

with

$$[\tau_{nm}(rp)]^{-2} = -\frac{p^2}{\mu}(<n|\frac{\partial^2}{\partial r^2}|n>_{ave} + <m|\frac{\partial^2}{\partial r^2}|m>_{ave}) \quad (4)$$

In the adiabatic limit of the relative motion ($p\to 0$, $\xi_{nm}(rp)\to\delta[\omega_{nm}(r)]$), from (3) we obtain the result of the linear response theory. The values of the transport coefficients decrease as the relative velocity increases. For a very fast relative motion the transport coefficients become much smaller than their adiabatic values. For the mass parameter and the mixed diffusion coefficient the similar expressions are obtained. In the limit of slow collective motion the adiabatic mass parameter comes out. The contribution of the mass parameter from the coupling decreases as the relative velocity increases and goes to zero for very large velocities. The present formulation is not restricted to the relative motion and it can be extended to the description of the other collective variables.

[1] S. Ayik, Z. Physik A 292, 257 (1979)

[2] H. Hofmann and J.P. Siemens, Nucl. Phys. A 275, 464 (1977)

[3] W. Nörenberg and C. Riedel, Z. Physik A 290, 335 (1979)
C. Riedel and W. Nörenberg, to be published (1980)

Mean field theory and statistical treatment of residual interactions in heavy-ion collisions

S. Ayik
GSI Darmstadt

The time-dependent Hartree-Fock theory (TDHF) is generalized in order to include the two-body collisions[1] (residual interactions). The density matrix $\rho^{(A)}(t)$ of an interacting many-particle system (A-particle system) can be considered as the sum of the uncorrelated part and the correlated part,

$$\rho^{(A)}(t) = \rho_o^{(A)}(t) + \rho_{cor}^{(A)}(t). \qquad (1)$$

The uncorrelated part of the A-particle density matrix is defined by

$$\rho_o^{(A)}(t) = \mathcal{A}\, \rho^{(1)}(11';t) \ldots \rho^{(1)}(AA';t) \qquad (2)$$

where $\rho^{(1)}(KK';t)$ is the one-particle density matrix corresponding to the K'th particle, K abbreviates the coordinates (including spin and isospin) of the particle, and $\mathcal{A}$ denotes the anti-symmetrization operator. The TDHF theory follows if we neglect the correlated part of the density matrix at all times. The restriction to the uncorrelated part (2) of the A-particle density matrix is equivalent to the single-determinantal description and eliminates the two-body collisions. At the present work we generalize the TDHF theory by replacing the factorization assumption (2) by a much less restrictive one. We assume that the correlated part $\rho_{cor}^{(A)}(t)$ of the A-particle density matrix vanishes only at an initial time $t=t_o$, but not at later times. This leads to a generalized equation for the one-particle density matrix which includes the residual interactions.

In order to derive an equation for the one-particle density matrix we use a procedure which is similar to the projection method of quantum-statistics. As a result of this procedure the correlated part of the A-particle density matrix can be expressed in terms of the uncorrelated part as (3)

$$\rho_{cor}^{(A)}(t) = G(t,t_o)\, \rho_{cor}^{(A)}(t_o) - i\int_{t_o}^{t} dt'\, G(t,t')L_1\, \rho_o^{(A)}(t')$$

where G(t,t') is a propagator expressed in terms of the total Liouville operator L. The Liouville operator L_1 corresponding to the residual interactions. In (3) the first term on the r.h.s. describes the propagation of the initial correlations whereas the second term determines the development of the correlations due to the two-body collisions. Assuming that the correlated part of the density matrix vanishes at the initial time $t=t_o$, we insert (1) together with (2) and (3) into the exact equation of motion. Taking trace over the (A-1)-particle space on both sides, we obtain a closed equation for the one-particle density matrix (4)

$$i\frac{\partial}{\partial t}\rho^{(1)}(t) = [\mathcal{H},\rho^{(1)}(t)] - i\int_{t_o}^{t} dt' \mathrm{Tr}\{L_1 G(t,t')L_1 \rho_o^{(A)}(t')\}_{A-1}$$

where $\mathcal{H}(t)$ denotes the mean-field Hamiltonian. The first term on the r.h.s. of (4) describes the changes in the one-particle density matrix due to the mean field. The second term, which is referred to as the collision term, describes the changes in $\rho^{(1)}(t)$ due to the residual interactions. The equation (4) provides a natural extention of the TDHF theory[2,3] and forms a basis for any further approximations. Here we simplify this equation by introducing some general statistical properties of the residual interactions. In the limit where the mean-free-path λ of the particles is larger than the correlation length σ of the residual interactions, $\lambda >> \sigma$, the collision term in (4) can be approximately evaluated. We consider the expansion

$$\rho^{(1)}(t) = \Sigma\, |\alpha(t)\rangle\, \rho_{\alpha\beta}(t) \langle\beta(t)| \qquad (5)$$

of $\rho^{(1)}(t)$ with respect to the single-particle eigenstates $|\alpha(t)\rangle$ of the mean-field Hamiltonian. Inserting the expansion (5) into (4) we obtain an equation for the matrix elements $\rho_{\alpha\beta}(t)$. We neglect the off-diagonal elements $\rho_{\alpha\beta}(t)$, $\alpha \neq \beta$. As a result of the statistical evaluation of the collision term in (4), the diagonal elements $\rho_{\alpha\alpha}(t) = \rho_\alpha(t)$ satisfy a master equation,

$$\frac{\partial}{\partial t}\rho_\alpha(t) = \sum_{\beta\gamma\delta} W_{\alpha\beta\gamma\delta}(t)\left[\rho_\gamma\rho_\delta(1-\rho_\alpha)(1-\rho_\beta) - \rho_\alpha\rho_\beta(1-\rho_\gamma)(1-\rho_\delta)\right] \qquad (6)$$

where $W_{\alpha\beta,\gamma\delta}(t)$ is the transition probability.

The knowledge about the one-particle density matrix is not sufficient for the description of heavy-ion collisions. In order to calculate the expectation value of an operator, in general, the knowledge about the A-particle density matrix is required. Using (1) and (3) the expectation value of an operator O can be expressed as

$$\langle O\rangle = \langle O\rangle_o - i\int_{t_o}^{t} dt' \langle O\, G(t,t')L_1\rangle_o \qquad (7)$$

where $\langle\cdots\rangle_o$ denotes the expectation value over the uncorrelated density matrix. The first term on the r.h.s. of (7) is the mean-field contribution to the expectation value whereas the second term arises from the correlations. From (7) an equation for the rate of the expectation value can be derived as

$$\frac{d}{dt}\langle O\rangle = \langle -i[O,\mathcal{H}]\rangle - \int_{t_o}^{t} dt' \langle O\, L_1 G(t,t')L_1\rangle_o. \qquad (8)$$

This equation determines the expectation value of the operator O taking full account of the A-particle density matrix. The second term on the r.h.s. of (8) has an analogous structure as the collision term in (4), and can be evaluated in a similar way by introducing the statistical properties of the residual interactions. The result (8) can be used to define the total conserved energy of the system and to calculate the variance of the observables of the system. The work along these lines is in progress.

[1] S. Ayik, to be published (1980)
[2] H. Orland and R. Schaeffer, Z. Physik A 290, 191 (1979)
[3] C.Y. Wong and H.F. Tang, Phys.Rev.Lett. 40, 1070 (1978)

A Nuclear Matter Approach to the Mean Free Path of a Nucleon in a System of Colliding Ions

K.-H. Müller
Institut für Kernphysik, Technische Hochschule Darmstadt, FRG

We calculated the mean free path of the projectile nucleons in a system of colliding ions in an energy domain between 70 MeV/A to 220 MeV/A[1]. For these relatively high energies we can describe the colliding ion-ion system in the sudden-approximation which is for lab. energies larger than about 70 MeV/A equivalent to the frozen density approach[2]. To describe the scattering process of two nucleons in the closer vicinity of a point $\vec{r}$ in the overlap region of the two ions a generalized local density approach is used; e.g. the influence on the scattering of two nucleons at $\vec{r}$ by the surrounding nucleons is assumed to be the same as in two colliding pieces of infinite nuclear matter with densities $\rho_T(\vec{r})$ and $\rho_P(\vec{r})$. This nuclear matter approach neglects effects due to the change of densities ρ_T and ρ_P in the neighbourhood of $\vec{r}$. ρ_T and ρ_P define the corresponding Fermi momenta K_{F_T} and K_{F_P}. The situation in momentum space for two not interacting extended Fermi systems is shown in fig.1. $2\vec{K}$ is the relative momentum per nucleon. We want to consider here only the case of not overlapping Fermi spheres. If we take into account the bare nucleon-nucleon interaction V, the two particle state $|\vec{K}_1\vec{K}_2\rangle$ is changed into a two particle correlated state $|\psi_{12}\rangle$. In the sense of the independent pair approach, this defines an effective interaction G_{T+P} which satisfies a Bethe-Goldstone equation. Here the Pauli-operator Q_{T+P} that projects on the unoccupied two particle states is included. Since the effective interaction G_{T+P} is non-Hermitian, the norm of the state $|\psi\rangle$ which describes the elastic channel, changes with time. In the sense of the optical model this leads to a probability that after the time t none of the nucleons has taken part in a real nucleon-nucleon scattering process. With this one gets for the mean free path λ of the projectile nucleons

$$\lambda = -\frac{\hbar^2}{m} K K_{F_P}^3 \left[\frac{3\Omega}{(4\pi)^4} \int_{F_{T+P}} \mathrm{Im} \langle \vec{K}_1\vec{K}_2 | G_{T+P} | \vec{K}_1\vec{K}_2 \rangle_A \, d^3K_1 d^3K_2\right]^{-1}$$

Ω is the volume in which the two matter systems are enclosed. For solving the Bethe-Goldstone equation we use a method similar to the extended Brückner-Gammel method developed by Jeukenne et al[3].

Fig.2 and fig.3 show λ in dependence of the Fermi momentum of the projectile system for different relative momenta above the Coulomb barrier. The target system density is of normal nuclear matter density ρ_o (K_{F_T} = 1.4 fm^{-1}) or of 0.4 ρ_o (K_{F_T} = 1 fm^{-1}).

For all the different momenta K shown, the mean free path of the projectile nucleons increases with increasing density of the projectile matter system. This is due to the enhanced Pauli blocking effect.

1. K.-H. Müller; Phys. Lett. B, accepted for publication
2. K.-H. Müller; Z. Physik A, 295, 79 (1980)
3. J.-P. Jeukenne, A. Lejeune and C. Mahaux; Phys. Rev. C10 (1974) 1391

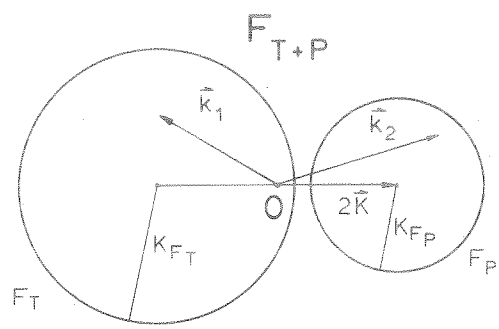


Fig.1 Momentum space

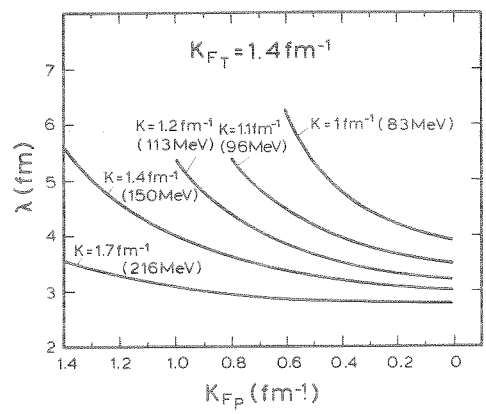


Fig.2 Mean free path λ for fixed K_{F_T} in dependence of K_{F_P} and K.

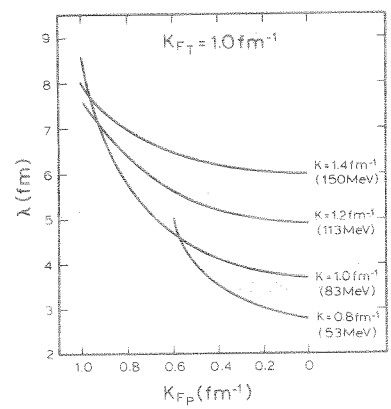


Fig.3 The same as in fig.2 but for a different fixed K_{F_T} value.

Fermi Jets and Capture in TDHF-calculations of medium energy collisions of $^{12}C + ^{197}Au$ G

R.Y. Cusson, H. Stöcker
GSI Darmstadt
and
W. Greiner and J.A. Maruhn
Institut für Theoretische Physik der Johann Wolfgang Goethe-Universität
6000 Frankfurt am Main, Germany

Using the 3-D TDHF method[1] we have calculated $^{12}C + ^{197}Au$ at E/A = 30, 42.5 and 85 MeV/A, as well as $^{12}C + ^{12}C$ at the same energies and for various impact parameter. Whereas the $^{12}C + ^{12}C$ reaction shows (see fig. 1) negative angle momentum transfer at low TKEL, the ^{12}C + Au show in addition the emission[2] of PEP's and Fermi jets for b ≤ 5 fm. Whereas the PEP (which moves with $v_f + v_{inc}$) is seen as soon as the ^{12}C hits the Au and contains only about 1 nucleon, the Fermi jet is delayed somewhat and is deflected sideways for noncentral collisions; it may hold up to 8-10 nucleons, which move with about $v_{incident}$. A typical jet event is shown in fig. 2. The jet angle grows to about 15^0 (cm) (E/A = 85) and 30^0 cm (E/A = 30) at b = 4.25 fm.

As the ^{12}C begins to stick out at higher impact parameter the scattering grows more complex. After an initial bounce-off the ^{12}C is quickly attracted right into the Au and later comes out on the bottom/left (see fig. 3 and 4). Some events show both jets and emitted particle (fig. 4) while others show a particle with a very diffuse surface (fig. 3). At still larger impact parameter (b = 8.5, E/A = 85 MeV) the ^{12}C is no longer absorbed and actually acquires a small additional mass in passing. These properties of the reaction are being compared with the results of recent GSI experiments[3]. At the lower energy (30 MeV/A) and b = 8.5 fm the ^{12}C is again captured and only about 1 jet particle comes out at about -90^0(c.m.)

[1] R.Y. Cusson, J.A. Maruhn, H. Stöcker, Z. Physik A294 (1980) 257

[2] D.H.E. Gross and J. Wilczynski, Phys. Lett. 67B (1977) 1

[3] Y. Chu, P. Doll, A. Gobbi, K. Hildenbrand, H. Ho, W. Kühn, H. Löhner, V. Lynen, W. Müller, A. Olmi, D. Pelte, H. Sann, R. Santo, V. Winkler
Collective Effects in ^{12}C Induced Reactions at 86 MeV/u, contribution to the Int. Conf. on Nucl. Phys., Berkeley 1980

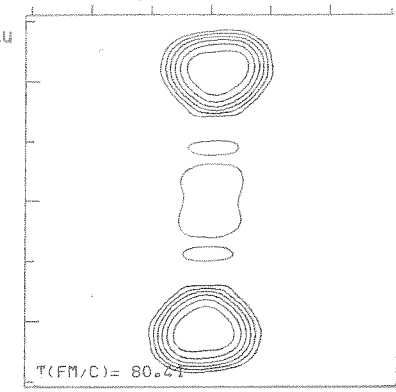


Fig. 1. Density Contours for ^{12}C (85 MeV/A) + ^{12}C at b=0.5 fm. No jets are seen but a low density cloud which breaks up into several pieces is left in between the fragments. The TDHF calculation predicts negative angle momentum transfer and small energy losses for this reaction.

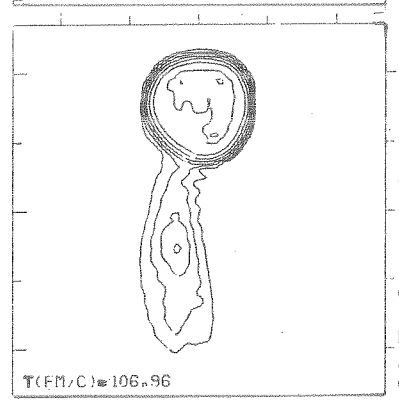


Fig. 2. Typical jet event at b=4.25 fm and E/A=85 MeV/A The outer contour represents 2^{-6} x 0.14 N/fm^3= 0.002 N/fm^3. The successive contours represent additional factors of 2 increases in density. The promptly emitted particle (PEP) is no longer visible at this time into the reaction. The direction of the jet is at about 15^0 from the vertical. The ^{12}C was incident on the right and was coming down parallel to the vertical axis. There are about 10 nucleons in the jet whose average velocity is that of the projectile.

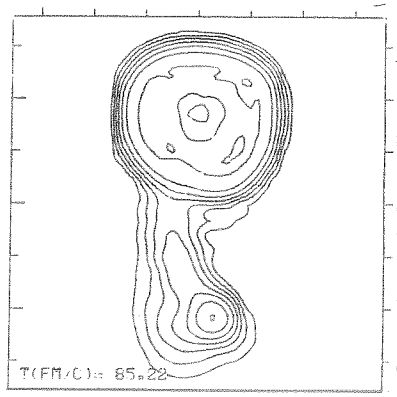


Fig. 3. Logarithmic density contours for ^{12}C (85 MeV/A) + 197Au at b=7 fm. The initial geometry is one where the ^{12}C was on top at the right of the Au and bearing down parallel to the axis, at 7 fm from the center of the Au. We are in the center of the velocity, and the light outgoing fragment is moving towards the lower left corner while the Au continues to move approximately parallel to the box. No jets are seen but a low density aura surrounds the light fragment.

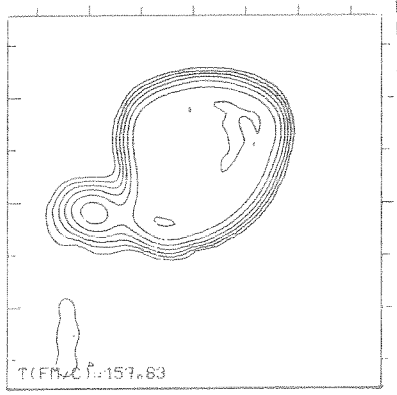


Fig. 4. Density contours for ^{12}C (30 MeV/A at b=6 fm. The initial geometry is similar to that of fig. 3. The emitted particle is moving to the left corner. At this time (158 fm/c) only an elongated low density (0.002 N/f^3) patch is seen at the jet location.

B + G

Medium Energy Collisions of Heavy Nuclei in the Three-Dimensional Nuclear Fluid Dynamical-(NFD) and Time-Dependent Hartree-Fock (TDHF) Models

H. Stöcker
GSI Darmstadt
and
R.Y. Cusson, J.A. Maruhn, and W. Greiner
Institut für Theoretische Physik der Johann Wolfgang Goethe-Universität
6000 Frankfurt am Main, Germany

We study heavy ion collisions at bombarding energies $E_{LAB}/n \sim 20$-200 MeV within the three-dimensional NFD- and TDHF-models[1]. The compression phenomena occuring at these bombarding energies are quantitatively similar as a function of the bombarding energy as well as for various impact parameters in the different models.

An important difference, however, of the two models is the strong transverse squeeze out of matter resulting in the NFD-calculation, which is not seen in the TDHF-model, even for b = 0 collisions[1] (see Fig. 1).

Furthermore, we investigate the possible formation of abnormal superdense nuclear matter ("density isomers") in a schematic model for the nuclear equation of state (i.e. with a secondary minimum in the binding energy $E_C L_D$). The cross sections for the formation of these abnormal matter can be $\gtrsim 100$ mb, if these secondary minima really exist. Again, however, we find a difference in the results of the two models (see Fig. 2).

Yet, both models predict a strong enhancement of the internal energy of the matter in the case that these abnormal states exist. Therefore, we propose to measure the excitation function of the excitation energy and search for threshold effects, which could indicate a phase transition of nuclear matter into an abnormal state.

[1] H. Stöcker, R.Y. Cusson, J.A. Maruhn, W. Greiner
Z. Physik A 294 (1980) 125

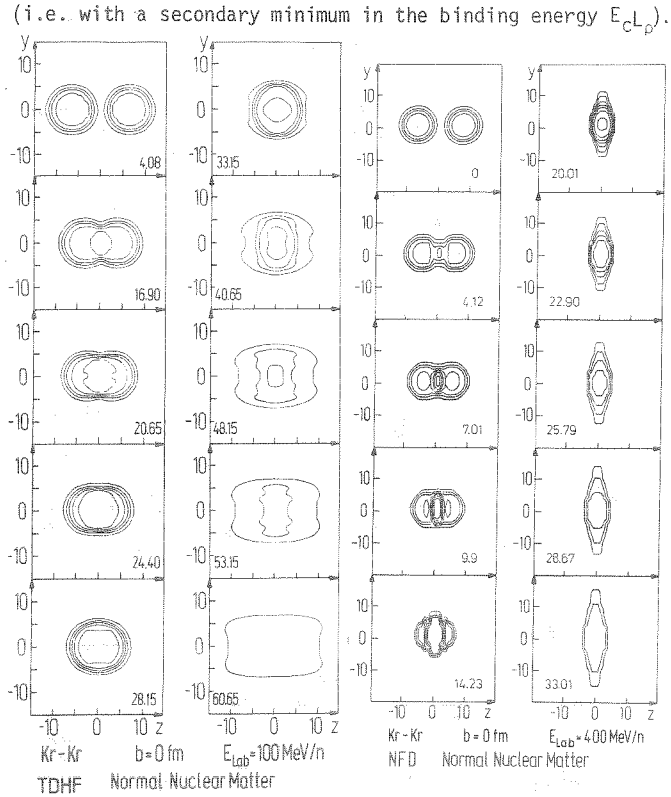


Fig. 1. Contour plots of the density in the scattering plane, the density increasing by 0.04 fm^{-3} from line to line. The outer lines represent 0.02 fm^{-3}, the collision time in fm/c is indicated by the numbers within each plot. Left: The TDHF calculations of the head-on collision of two Kr-nuclei at E_{LAB}=100 MeV/n. Right: The same for the NFD case at E_{LAB}=400 MeV/n. Notice that the matter is emitted to 90° compared to the left figure.

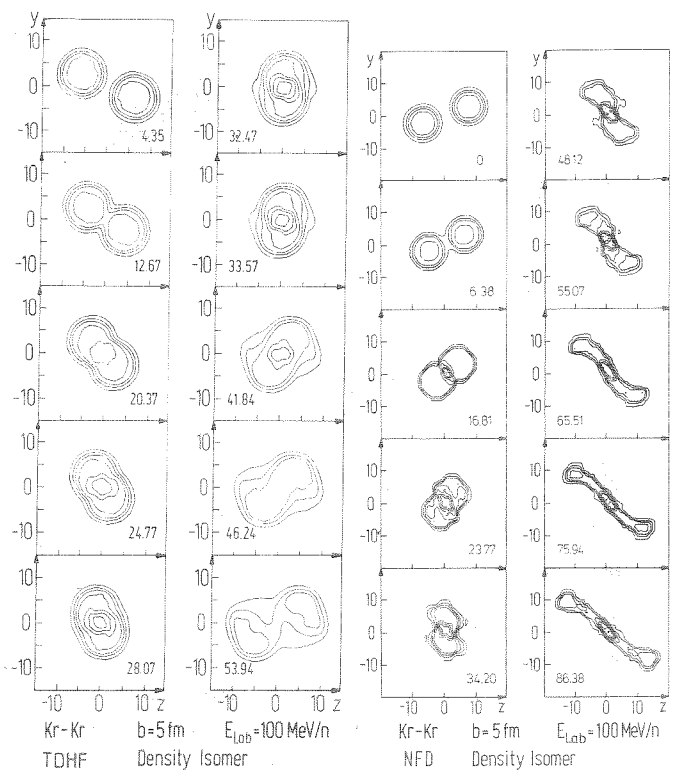


Fig. 2. The density contour plots for a finite impact parameter (b=5fm) collision of two Kr-nuclei using the abnormal nuclear equation of state (see Fig. 1). Left: The TDHF calculation leads to fission of the abnormal nuclear state into two normal nuclei. Right: For the NFD case a three-body break-up is observed, the metastable density isomer being at rest in the cm-frame. The residual projectile- and target-like nuclei are deflected to the side in analogy to the highly-inelastic bounce-off effect seen in asymmetric collisions (e.g. Ne→U).

G

Collective Sideward Flow of Shocked Matter and the Highly Inelastic Bounce Off Event in Fast Nuclear Collisions

H. Stöcker, GSI Darmstadt
and
J.A. Maruhn, W. Greiner
Institut für Theoretische Physik der Johann Wolfgang Goethe-Universität
6000 Frankfurt am Main, Germany

We have investigated high energy heavy ion collisions in the fluid dynamical model[1]. It was found that in violent collisions of nuclei one must distinguish between central collisions with a large multiplicity azimuthally symmetric fragment distributions (see Fig. 1), and non-central collisions with intermediate impact parameters and also with large multiplicities, but with azimuthally 180^0 correlated bounce off events.

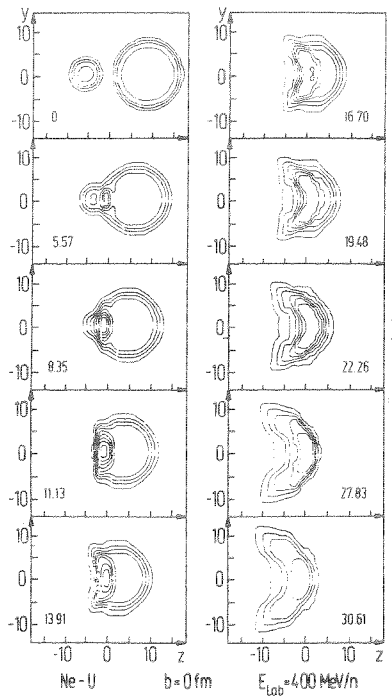


Fig. 1. The density contours are plotted for the reaction Ne → U at 400 MeV/n for b=0 fm. The time is given in units of fm/c. The formation of the head- and Mach shock waves can clearly be seen.

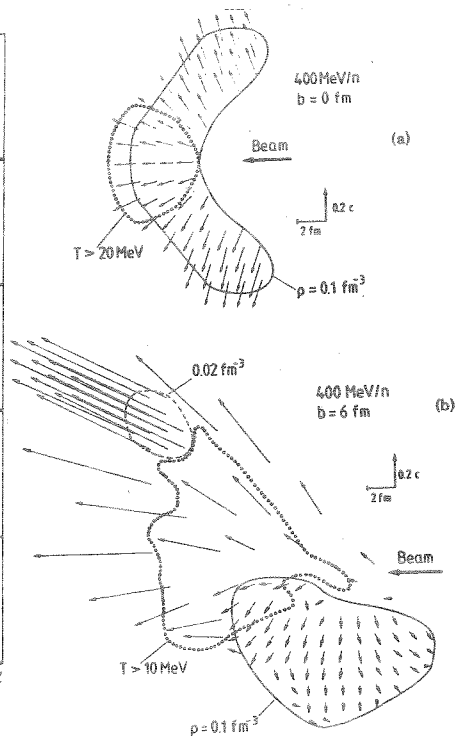


Fig. 2. Density and temperature contours and velocity field (arrows) in the scattering plane at a late stage of the reaction. (a) Central collision; (b) Intermediate impact parameter.

For very asymmetric collisions and small parameters the occurence of high density Mach shock waves leads to the predominant sideways flow of the compressed matter. Several experiments by Baumgardt and Schopper[2], by Stock, Gutbrod, Poskanzer, Sandoval, Meyer[3], and by Antonenko et al. present evidence for the predicted sideways flow in the form of maxima in the angular distributions of medium energy light nuclei and protons.

The peaks in the double differential cross sections measured by Stock et al. show the same dependence on the energy window as calculated in the fluid dynamical model. (See Fig. 2). As expected from fluid dynamics Sandoval et al. find that total momentum and energy transfer is observed in these collisions, indicating only little transparency. The experiments of Otterlund et al. also verify the strong transverse communication expected. In addition, they could not find indication for clear cut spectators, also in contradiction to cascade calculations.

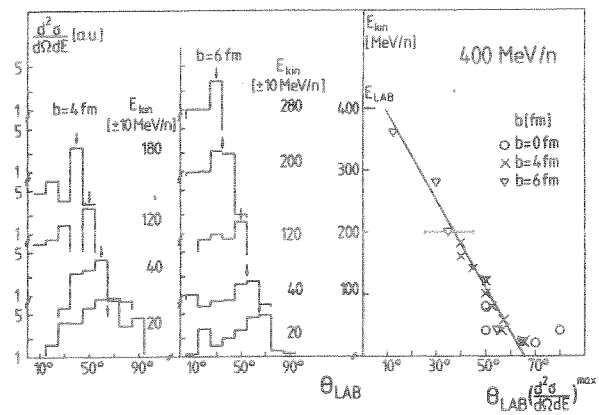
Meyer et al. have been succesfully looking for the bounce off effect- they find strong transverse momentum transfer to big target fragments and jets of exploding projectile particles emitted in opposite direction to these fragments. This is also of great importance as it may allow for the measurement of the compression achieved in fast nuclear collisions.

[1] H. Stöcker, J.A. Maruhn, W. Greiner, Z. Physik A293 (1979) 173 and Phys. Rev. Lett. 44 (1980) 725
H. Stöcker, B. Müller, GSI-preprint 4 (1980) submitted to Phys. Rev. Lett.

[2] H.G. Baumgardt, J.U. Schott, Y. Sakamoto, E. Schopper, H. Stöcker, J. Hofmann, W. Scheid, W. Greiner, Z. Physik A237 (1975) 359
H.G. Baumgardt, E. Schopper, J. Physics Letters G5 (1979) L 231

[3] R. Stock et al., GSI-preprint 22-79

Fig. 3 (see below) Double-differential cross section, plotted as angular distributions for different fragment kinetic energies, for 4- and 6-fm impact parameters. The right-hand-side plot shows the position of the maximum as a function of the laboratory angle.



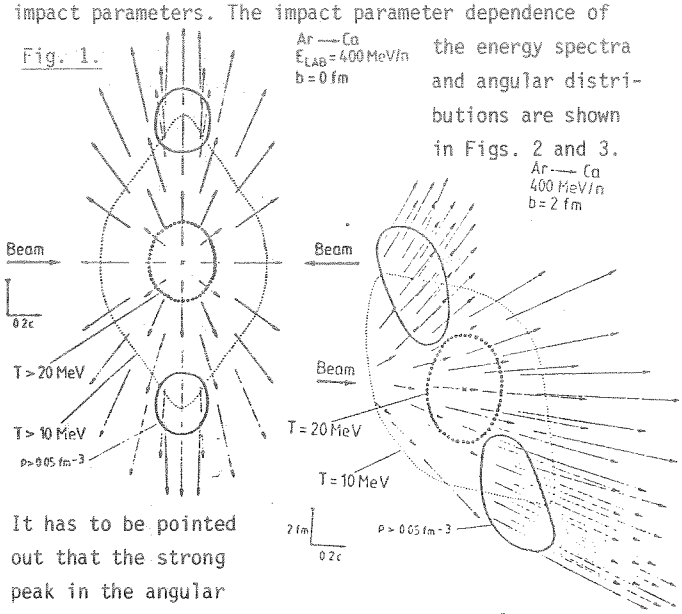
Jets of Nuclear Matter in Relativistic Heavy Ion Collisions [G]

H. Stöcker, GSI Darmstadt and

L.P. Csernai, R.Y. Cusson, J.A. Maruhn, W. Greiner, Inst. f. Theor. Physik der J.W. Goethe Universität, Frankfurt/Main

According to nuclear fluid dynamical calculations[1,2] central collisions of equal mass nuclei result in total desintegration of projectile and target, the matter is emitted predominantly perpendicular to the collision axis to 90° in the CM system. We investigated that phenomenon quantitatively in the reaction Ar → Ca at E_{LAB} = 400 MeV/n, which is shown in Fig. 1 for various impact parameters. The impact parameter dependence of the energy spectra and angular distributions are shown in Figs. 2 and 3.

Fig. 1.



It has to be pointed out that the strong peak in the angular distribution (Fig. 2) at 40° in the lab (90° in the cm) appears only for b=0. It is not seen at higher b. Also the peak in the energy distribution at E_{cm} = 200 MeV/n (Fig. 3) only shows up for b=0. Since b=0 has a vanishing geometrical cross section, this effect should not be observable. However, if one looks at b=2 in Figs. 2 and 3 one observes a remnant of this perpendicular explosion of the shocked matter, namely one can distinguish in dσ/dθ and dσ/dE three contributions, two stemming from projectile and target residues, for which a considerable parallel and transverse momentum transfer take place. The other contribution is located at exactly the same energy and emission angle as observed for the exploding shock zone at b=0. Since the expanding hot shock zone acts like a spring between the projectile and target residues, these residues are deflected to 180° azimuthally correlated. These bouncing-off fragments shadow the matter emission to 90° in the scattering plane. The shocked material will preferentially explode perpendicular to the scattering plane, however, still to 90° in the cm, only not azimuthally symmetric as for b=0. This is demonstrated also in Fig. 1, where the exploding shock zone and the shadowing fragments of projectile and target are clearly recognized. Therefore we predict the occurence of four jet events in fast nuclear collisions at small impact parameters: two stemming from the highly inelastic bouncing-off of projectile and target residues in the scattering plane, two broader out-of-plane jets due to the explosion of the hot compressed matter in the direct reaction zone. They are emitted with CM-energy at 90° in the cm. A recent experiment[3] of the GSI/LBL group at Berkeley seems to present evidence for a preferential outflow of π's (which by their relative abundance are already a trigger on nearly central reactions) at 90° in the cm-system. However, it is not completely clear to what extent the Coulomb distortion of the pions by the nuclear fragments may partially be responsible for this effect. More definitive experiments (e.g. look for π^-) with better impact parameter selection and heavier nuclei should be performed in order to clarify this point.

Fig. 2.

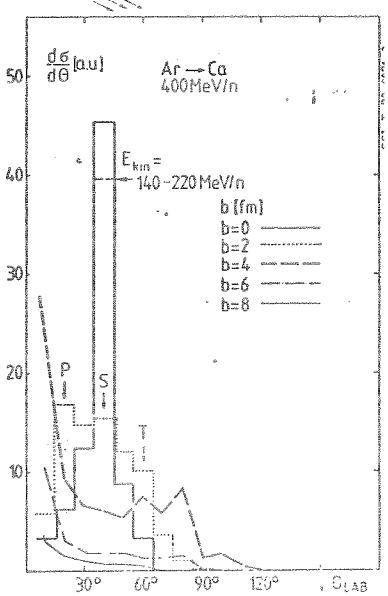
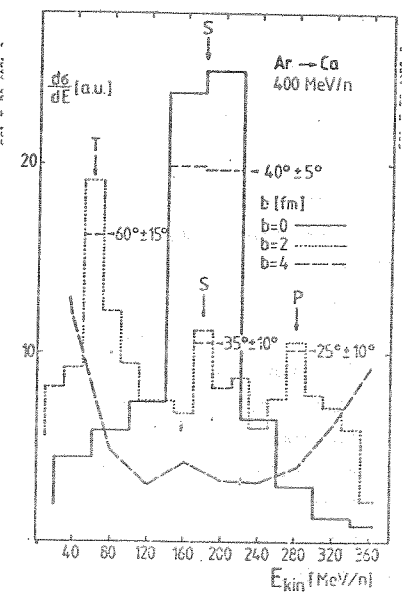


Fig. 3.



[1] W. Scheid, H. Müller, W. Greiner, Phys. Rev. Lett. 32 (1974) 741

[2] H. Stöcker, J. Hofmann, J.A. Maruhn, W. Greiner, to be published in: Progress in Particle and Nuclear Physics (1979), Z. Physik A290 (1979) 297, and A294 (1980) 125

[3] K. Wolf et al., Phys. Rev. Lett. 43 (1979) 1448

G

Signatures of Phase Transitions in Dense Matter in High Energy Heavy Ion Collisions

H. Stöcker, R.Y. Cusson, GSI Darmstadt, and

G. Buchwald, L.P. Csernai, G. Graebner, W. Greiner, J. Hofmann, H. Kruse, J.A. Maruhn, B. Müller, W.T. Pinkston, P.R. Subramanian, J. Theis, D. Vasak, Institut für Theoretische Physik der J.W. Goethe Universität, Frankfurt am Main

We have studied the influence of abnormal states of dense nuclear matter on the reaction dynamics of high energy heavy ion collisions in terms of the nuclear fluid dynamical model. We use in the hydrodynamical model an equation of state with a secondary minimum in the binding energy per nucleon $E_c(\rho)$. When the bombarding energy is large enough to overcome the barrier between the normal and abnormal states, the compressed matter collapses into the secondary minimum[1]. Owing to the sudden release of condensation energy[1], the temperature in the abnormal phase becomes considerably larger than in the normal nuclear matter. We proposed several methods to search for phase transitions and abnormal states in dense nuclear matter. The following signatures may be used for the detection of such phenomena if they exist. Density isomers would show up by a threshold increase of the excitation function of

1) the compression, detectable by the bounce-off effect[1] (see below); the matter may be trapped for a long time in the abnormal state ("fusion" into a density isomer)[1],
2) the temperature, which can be measured by the slope of the particle spectra or by secondary, high T_0 components in the energy spectra of light reaction fragments[1] ($p,\pi,\alpha,\ldots$).
3) The density isomer could also be detected by a threshold increase of the particle (pion) production excitation function, or by looking for secondary humps in the pion multiplicity distribution at small b.
4) The critical scattering near a phase transition point may be detected via threshold increase of the pion bremsstrahlung[1], i.e. a coherent pion radiation, also in peripheral collisions.
5) The shift of the Mach-shock angle predicted by fluid dynamical calculations[1] near a phase transition can be detected in the excitation function.
6) The bounce-off effect is sensitive[1] to changes in the compression. Therefore it enables the measurement of the compression excitation function, which may contain evidence for a soft nuclear equation of state, density isomers and quark matter for the following reasons[1]:

a) The density which is reached depends crucially on the nuclear equation of state. Accordingly, a soft equation of state would imply a rather abrupt increase in the density $\rho\ (E_{lab})$ attained at some threshold energy, and, therefore, a much stronger thermal pressure contrary to what one might have guessed. We conclude that a softer nuclear equation of state would result in higher transverse momenta transferred to the bounce-off fragments.

b) While the transfer of transverse momentum would be favoured by any kind of phase transition, dramatic effects would show up if a secondary minimum (density isomer) exists in the equation of state. Once the bombarding energy is sufficient to overcome the barrier ($E_{lab}(\rho_{crit}) \equiv E_{crit}$), the density $\rho\ (E_{lab})$ would jump suddenly from the threshold density ρ_{crit} to the density ρ_o' of the new phase. This, together with the accompanying increase in thermal energy due to the release of condensation energy, would cause an abrupt rise in the pressure exerted on the bounce-off fragments, i.e. the yield at large Δp would show a strong threshold enhancement above the critical bombarding energy.

c) A similar phenomen would be observable in the transverse momentum excitation function if quark matter is formed at a sufficiently high bombarding energy. In this case one has a transition from the hadronic Fermi gas with $P_T = \frac{2}{3}\rho E_T$ to the ultrarelativistic quark gas with $P_T = \frac{1}{3}\rho E^*$, where E^* contains also the rest energy of the nucleons in terms of kinetic energy of the quarks.

d) The thermodynamical model of Hagedorn predicts that most of the internal energy is transformed into excitation of hadronic resonances rather than into heat. This model would therefore predict for bombarding energies of several GeV/n a strongly reduced bounce-off effect. If eventually, at higher energies, the transition from hadronic to quark matter occurs, the enhancement of high transverse momenta would be even more pronounced. The slope of particle spectra can give additional information about the temperatures also making possible a search for a limiting temperature[1] ($T^{max} \sim 140$ MeV).

In conclusion, future experiments should measure the excitation functions of the various variables discussed above in small energy steps and look for threshold effects. The need for a good trigger of centrality (azimuthal symmetry of high multiplicity events) and exclusive experiments using 4π detectors must be clearly emphasized.

[1] H. Stöcker, B. Müller "The bounce-off effect as a barometer for hot, dense matter in fast nuclear collisions, GSI-preprint 80-4 (February 1980), submitted to Phys. Rev. Lett. and references therein and
H. Stöcker, G. Buchwald, R.Y. Cusson, G. Graebner, W. Greiner, J. Hofmann, H. Kruse, J.A. Maruhn, B. Müller, W.T. Pinkston, P.R. Subramanian, J.Theis, D. Vasak, H. Baumgardt, E. Schopper "Formation of hot, dense matter in fast nuclear collisions - theory and experiments", invited talk presented at the International Conference on Extreme States in Nuclear Systems, Dresden, February 4-8, 1980, submitted to Phys. Rev. Lett. 8.

G

Percolation Phase of Hot, Dense Hadronic- and Quark Matter and Pulsating Quark Blobs in Relativistic Nuclear Collisions.

H. Stöcker, GSI Darmstadt, and

G. Graebner, J.A. Maruhn, W. Greiner, Institut für Theoretische Physik der J.W. Goethe Universität, Frankfurt/Main

At very high energies, the compression of nuclear matter in nearly central heavy ion collisions may be so strong that the baryons lose their identity, amalgamating into blobs of hot, dense quark matter. We investigate some properties of such quark blobs and speculate on their consequences[1].

The quark matter is treated in the bag model. The quark matter energy is compared to nuclear matter in fig. 1.

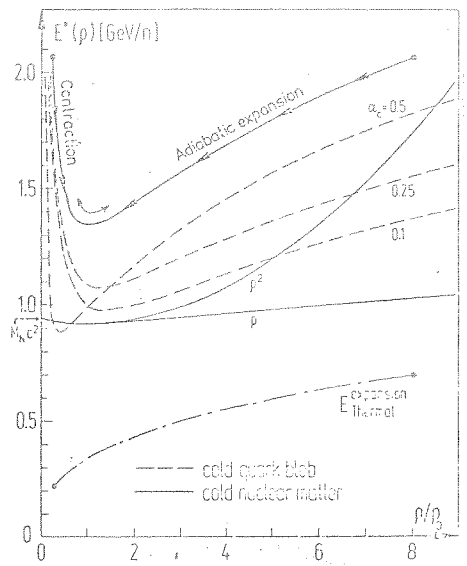


Fig. 1: The internal energy per baryon for cold (T=0) nuclear matter (solid lines: Model p linear density dependence and p^2 quadratic density dependence) and for cold quark matter with various quark-gluon coupling strength (dashed: α_c=0.1, 0.25, B=56 MeV-fm^{-3}; α_c=0.5, B=$\frac{1}{4}$ (56) MeV fm^{-3}), for which we want to point out that a temperature - and mass dependence of B can lead to strongly enhanced geometrical cross sections of the quark blob[2]. The upper most solid curve describes the density dependence of the internal energy of an expanding, hot blob of quark matter. The density dependence of the thermal energy (lower dashed dotted curve) of the quark matter during expansion is shown below.

The dependence of the quark matter compression on the bombarding energy per nucleon, E_{lab}, is studied in a relativistic hydrodynamical model (see fig. 2.)

A more detailed investigation[2], considering a mixture of quark - and excited nuclear matter, shows that pure quark matter may be produced at energies of several GeV/n, but that already at much lower bombarding energies a considerable fraction of the hadronic matter can be transformed into quark matter, making its production feasible with relativistic heavy ion accelerators. If such compressed, hot quark blobs can actually be formed, we may ask for their characteristic dynamical behaviour. Because of the large internal pressure, the metastable quark blob will expand isotropically from the initial compressed state. The internal energy E* (heat and compression) is transformed into kinetic energy (hydrodynamical outflow). E_{kin} increases drastically during the expansion and leads to an overshoot of the equilibrium density, where p=0. The radial motion stops at a minimum density where E_{kin} is changed into the potential energy of the confining vacuum pressure, which causes the blob to contract again. Therefore radial oscillations of the quark blob will appear, analogous to large amplitude giant monopole oscillations of nuclei.

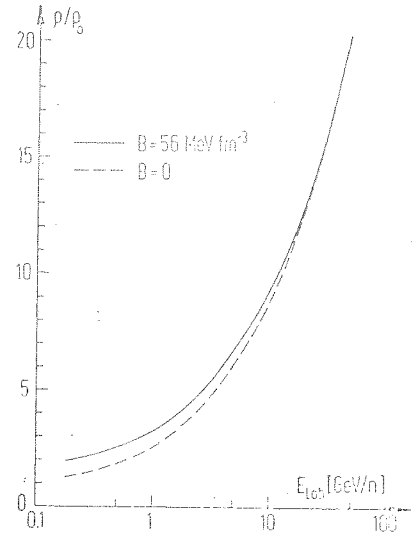


Fig. 2: The compression of quark matter as a function of bombarding energy for B=56 MeV-fm^{-3} and B=0.

The time dependence of the radius of a blob of quark matter R(t) is shown in fig. 3 for blobs produced at E_{lab}=2GeV/n containing 240 (e.g. $^{40}Ar \rightarrow ^{40}Ca$) and 15 quarks respectively. The short periods of τ = 14 fm/c and 5.5 fm/c ($\hbar\omega$ = 88 MeV and 225 MeV) have to be pointed out.

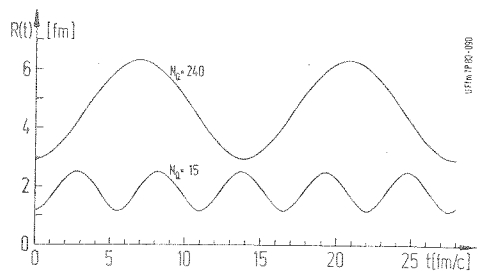


Fig. 3: Radial oscillations of a hot quark blob for E_{lab} = 2 GeV/n and N_Q = 15,240

If sufficiently long-lived, the oscillations may lead to radiation with energy $\hbar\omega$. Pulsed emission of matter will also occur owing to the inertia of the outer shells of the quark sphere. Higher multiple excitations should also be taken into account in a future investigation. The radial motion will be damped due to emission of hadrons (quark and gluon jets) from the surface of the quark blob. Such oscillating blobs of quark material may also be produced when the collapse of astronomical objects leads to sufficiently high densities for the phase transition to take place. This quark matter will (even for σ=0) expand again and start to oscillate. This would result in pulsating quark stars (pulsars?).

[1] H. Stöcker, G. Graebner, J.A. Maruhn, W. Greiner, GSI-preprint 80/7, submitted to Z. Physik

[2] H. Stöcker, G. Graebner, J.A. Maruhn, W. Greiner, submitted to Phys. Lett.

G

Geometry and Dynamics in the Hot Spot Model

N.Stelte and R.Weiner
Physics Dept., University of Marburg, 3550 Marburg

Projectile energies of a few MeV above the Coulomb barrier are expected to lead to grazing collisions with more or less pointlike excitations. For this purpose a delta-function was used as an initial condition [1] . It was applied to the reaction 96 MeV $^{16}O+^{58}Ni$. [2] . On the other hand higher energies well above the Coulomb barrier mean less peripheral reactions with a spatially extended excitation, which might resemble a spherical cap [3] (see fig.1). This geometry should be preferred with increasing mass number of the projectile if we look at hot spots in the target. As an example we show in fig.2 the temperature distribution at the nuclear surface for different times in the linear approximation. To get an impression of the importance of an "extended" initial condition several values of the cap parameter r_{in} are compared: large differencies in the maximum of the temperature at the early stage of preequilibrium are obtained. The application of the delta-function solution to nonperipheral collisions would thus lead to an overestimation of the observed asymmetry effect and an underestimation of the width of the temperature distribution as a function of the polar angle Θ . We expect the thermodynamical coefficients c_p, ρ and κ to be T-dependent and regard T-independent coefficients only as a linear approximation for regimes with small temperature gradients. In particular two cases of physical interest are considered in the following. A low energy regime corresponding to a Fermi gas, where

$$c_p \approx c_v = \frac{\pi^2}{2}\frac{k^2}{\varepsilon_F m}T$$

$$\kappa = \frac{7}{48\sqrt{2}\pi}\frac{\varepsilon_F^{3/2}}{\sqrt{m}\,Q}\frac{1}{T}$$

Here ε_F, k, m, Q are the Fermi energy, Boltzmann constant, nucleon mass, and the effective nucleon-nucleon cross section. For an intermediate energy regime (excitation energy up to few hundreds MeV/nucleon) corresponding to a Boltzmann gas one has

$$c_p = \frac{5}{2}\frac{k}{m}$$

$$\kappa = \frac{1}{\sqrt{\pi}}\frac{k^{3/2}}{\sqrt{m}\,Q}\sqrt{T}$$

In fig.3a and b we compare the results of a numerical integration of the diffusion equation for these two cases for a cap parameter r_{in}=0.7R. The t and z=cos Θ dependence of T shows that for a Fermi gas high temperatures are to be found in the system for a rather long time ($t=10^{-22}$s). At the very end of the diffusion process the temperature falls down quickly, so that there should be essentially only one high temperature observed in the experiment besides the equilibrium temperature. This means that in a first approximation for a Fermi gas regime a hot spot picture with fixed geometry can be used without considering heat diffusion. The situation is quite different for a Boltzmann type gas where the temperature shows a smooth behaviour in space and time which is similar to that of T-independent coefficients. In this case the whole continuum of temperatures is relevant for the description of the process. These results have important implications for the investigation of the equation of state via the hot spot effect.

1) R.Weiner, M.Weström, Nucl.Phys. A286, 282 (1977)
2) P.Gottschalk, M.Weström, Nucl.Phys. A314, 232 (1979)
3) N.Stelte, to be published

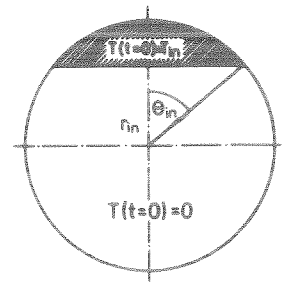


Fig.1 Spherical cap with temperature T_{in} as initial condition on a sphere. The parameter r_{in} = R cos Θ_{in}, determines the size of the cap.

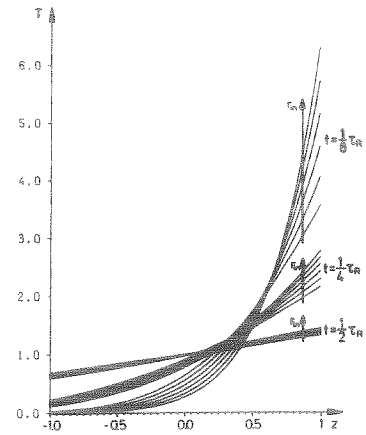


Fig.2 Temperature distribution at the nuclear surface as function of Z = cos Θ (Θ polar angle) for three times and cap parameter r_{in} =0.5, 0.6, 0.7, 0.8, 0.9, 1. R (fig.1). The excitation energies are the same for all cap parameters.

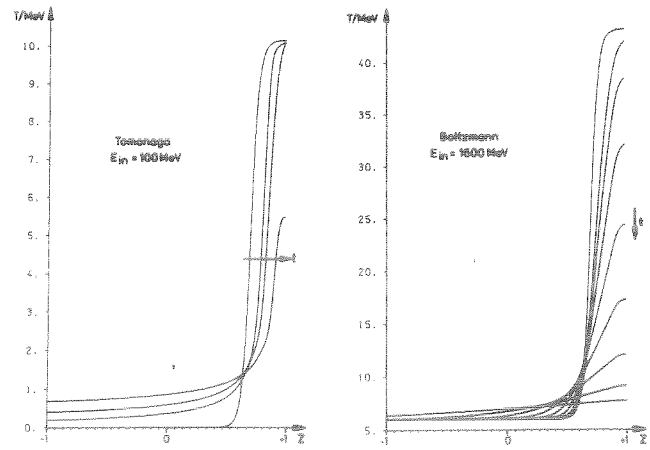


Fig.3a,b Temperature distribution at the nuclear surface as function of Z=cos Θ at different times $t = 2^n \cdot 10^{-23}$s, n = 0,1,2,... E_{in} is the initial excitation energy.

G

Drifting Hot Spots

N.Stelte, M.Weström and R.M.Weiner

Physics Dept., University of Marburg, 3550 Marburg

Inclusive reactions N + A→N' + X where N is a light nucleus or an elementary particle and A a nucleus are analyzed in terms of a drifting hot spot. The model describes the space time evolution of the excited system in the preequilibrium stage. An approximate simple analytical formula for the forward hemisphere is derived which describes angular and energy distribution of the high energy spectrum; qualitative agreement with data at E = 100 MeV is found with a Fermi-gas equation of state. We limit the discussion here to the non-relativistic case. We assume that in the interaction of the incident particle with the nucleus there exists a class of events (as will turn out from the comparison with experiment, this is an important class indeed) in which a few nucleons share the momentum (energy) transfer so that a local excitation takes place which we call a hot spot. Beginning with the moment τ_0 at which the hot spot can be defined [1] we assume that the system can be treated by non-equilibrium thermodynamics. Taking into account that the hot spot is moving, the differential cross section for nucleon emission in the solid angle $\Omega, \Omega + d\Omega$ with kinetic energy $\varepsilon, \varepsilon + d\varepsilon$ is

$$\frac{d^2\sigma}{d\Omega\, d\varepsilon} \sim \varepsilon\, \sigma_{inv}(\varepsilon) \int\int\int_{V}\int_{\tau_0}^{\tau_R} d\vec{r}_e\, d\vec{r}_f\, dt\; e^{-\frac{\varepsilon - \vec{p}\,\vec{v} + S}{T(\vec{r}_e, \vec{r}_f, t)}}\, f_e(\vec{r}_e, \Theta)\, W_f(\vec{r}_f)$$

Here, $\sigma_{inv}(\varepsilon)$ is the inverse cross section, $f_e(\vec{r}_e, \Theta)$ is a function which describes the emission from a volume element at $\vec{r}_e$ into the direction of experimental observation Θ; in general, it will depend on the type of particles emitted. $W_{form}(\vec{r}_f)$ is the formation probability of the hot spot at a point $\vec{r}_f$, $\vec{p}$ the momentum of the emitted nucleon; S is the energy needed for separation of the particle. Its actual value is not important for the high energy tail we are interested in. The temperature $T(t, \vec{r}_f, \vec{r}_e)$ is the temperature at time t and at the emission point $\vec{r}_e$ of the hot spot which originally was created at $\vec{r}_f$. $\vec{v}$ is the instantaneous velocity of the volume element at the position $\vec{r}_e$. The $\vec{p}\,\vec{v}$ term corresponds to the Galilei transformation of the moving hot spot. It is this term which in our approach is responsible for the "memory effect" i.e. for the fact that the spectrum remembers the direction of the incident particle. Since we are interested only in preequilibrium emission we limit the time integral only up to τ_R = relaxation time. Both, energy and momentum conservation have to be observed during the relaxation process of the temperature and the velocity. This couples the space-time evolution of both fields. We assume that the collective motion can be separated from the dissipation of the thermal energy. While the former is approximated by a mean drift length, the latter is treated by the diffusion equation

$$\partial T/\partial t = \chi\, \Delta T$$

which describes the dissipation of momentum as well, if T and χ are replaced by $\vec{v}$ and ν respectively. We get eventually for the preequilibrium spectrum in the forward hemisphere for $\varepsilon \gg T_{preeq}$.

$$\frac{d^2\sigma}{d\Omega\, d\varepsilon} \sim \varepsilon\, \sigma_{inv}(\varepsilon)\, e^{-\frac{\varepsilon}{T_{preeq}}} + \alpha \sqrt{\varepsilon} \cos\Theta \sum_{\nu=0}^{\infty} a_\nu(\Theta)\, \Gamma\left(\frac{\nu+4}{2}\right)$$

$$\times \left(\frac{4\tau_0}{\tau_R}\right)^{\frac{\nu+2}{2}} \left(\frac{T_{preeq}}{\varepsilon}\right)^{\frac{\nu+4}{3}} P\left(\frac{2\varepsilon}{T_{eq}} - \frac{2\varepsilon}{T_{preeq}}\,(\nu+4)\right)$$

Here P is the chi-square function. If we are dealing with a system with a known equation of state (e.g. a Fermi gas) and a given theory of transport coefficients (e.g. that of Tomonaga [2]) χ and τ_R are determined. For τ_0 a value of $3 \cdot 10^{-23}$ s was guessed [1] from kinematical considerations. The number of nucleons n is related to τ_0 through the equation of state and the solution of the diffusion equation at $t = \tau_0$. At 90° the $\vec{p}\,\vec{v}$ term vanishes. Since the spectrum is dominated by one temperature $T_{preeq} = T(\tau_0)$ which corresponds to the inverse slope, this temperature can be read off direcly from experiment. We get thus independent information about τ_0 and n. As an application of our formalism we consider a reaction at an energy E=100 MeV for incoming protons on ^{58}Ni and compute the differential cross section in the angular range $15° \leq \Theta \leq 80°$ for 20 MeV $\leq \varepsilon \leq$ 50 MeV assuming an equation of state of a Fermi gas and using the corresponding T dependence for the transport coefficients [2]. Within our model this leads to $T_{preeq} \approx 17$ MeV and $n \approx 3$ which suggests that we are at the limits of applicability of thermodynamics. The results of our calculations are given in Fig.1 where they are compared with the data of ref.3.

1. R.Weiner and M.Weström, Phys.Rev.Lett. 34 (1975), 1523
2. S.Tomonaga, Z.Phys. 110, (1938), 573
3. J.R.Wu, C.C.Chang and H.D.Holmgren, Phys.Rev. C19, (1979), 659, 698

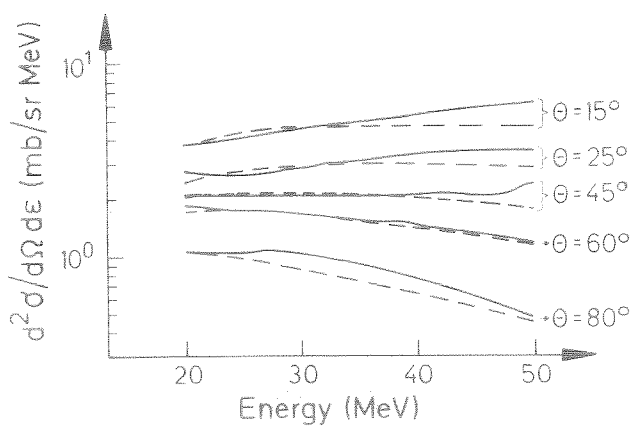


Fig.1 Reaction p+A p+x at 100 MeV. The continuous curves are experimental data from ref.3.

Solution of the Diffusion Equation for Geometries of Interest in Nuclear Physics

N. Stelte

Physics Dept., University of Marburg, 3550 Marburg

The solution of the diffusion equation for an extended spatial excitation on a sphere is given and applied within the hot spot model to heavy ion reactions. For applications in nuclear problems the only geometrical configuration for which an analytical solution is known and which has some resemblance to what one would expect in an actual collision, is that of a delta function excitation on a sphere [1]. While such a configuration might be a crude first approximation for a peripheral reaction between a light projectile and a heavy target it is clear that in a "deep inelastic" collision the initial excitation is not expected to be localized in a point but rather in a region of appreciable volume. Since reactions of this last type are of considerable experimental (and theoretical) interest the diffusion equation has to be solved for a more realistic geometrical configuration. In the following we consider excitations on a sphere with an initial configuration corresponding to a spherical cap (see Fig.1) given by

$$T(z=\cos\vartheta, r, t=0) = \begin{cases} T_{in} & \text{for } R\,z_{in}/z \le r \le R \\ & \text{and } z_{in} \le z \le 1 \\ 0 & \text{elsewhere} \end{cases}$$

The linear diffusion equation for the temperature T

$$\frac{\partial T}{\partial t} = \chi\,\Delta T$$

can be solved analytically with a linear boundary condition

$$\left.\frac{\partial T}{\partial r}\right|_{r=R} = \lambda T\big|_{r=R}$$

where χ is the thermal conductivity, λ is the radiation constant and R is the radius of the sphere. After separation of variables the solution in sperical coordinates is found to be

$$T(z,r,t) = \sum_{n=0}^{\infty}\sum_{m=0}^{\infty} c_{nm}\, e^{-\alpha_{nm}^2 \chi t}\, r^{-\frac{1}{2}}\, J_{n+\frac{1}{2}}(\alpha_{nm} r)\, P_n(z)$$

where $z = \cos\vartheta$, $J_{n+\frac{1}{2}}$ and P_n are Bessel functions and Legendre polynomials respectively. α_{nm} is determined from the boundary condition which can be written in the form

$$\alpha_{nm} J_{n+\frac{1}{2}}(\alpha_{nm}R) + \left(\lambda - \frac{1}{2R}\right) J_{n+\frac{1}{2}}(\alpha_{nm}R) = 0 \quad .$$

c_{nm} is determined from the initial condition

$$c_{nm} = \frac{(2n+1)\,\alpha_{nm}^{\frac{1}{2}}\, T_{in} \int_{z_{in}}^{1} dz\, P_n(z) \int_{R z_{in}/z}^{R} dr\, r^{\frac{1}{2}} J_{n+\frac{1}{2}}(\alpha_{nm} r)}{\left(R^2(\lambda - \frac{1}{2R})^2 + R^2\alpha_{nm}^2 - (\ell+\frac{1}{2})^2\right) J_{n+\frac{1}{2}}^2(\alpha_{nm}R)} \quad .$$

An example of a reaction which could lead to an extended spatial excitation is shown in Fig.2. Here we assume straight line trajectories. Then the geometrical overlap region of each nucleus corresponds to the intersection of a cylinder with a sphere. At high energies it is assumed within the fireball model that the nucleons in the overlap region are swept out of the nucleus. At intermediate energies, however, the momentum transferred between projectile and target can be small and the two nuclei should penetrate each other without a violent disturbance of their original configuration. We assume that the overlap region is heated and can be regarded as an initial condition for the heat diffusion process after the reaction partners have separated. For impact parameter $b=R_{target}$ the symmetry axis of the cylinder which is parallel to the beam direction goes through the point ($\vartheta=0, r=R$). As the delta-function excitation at this point shows for early times approximately spherical symmetry, it is clear that delta-function and cap describe the shape of the excitation region equally well. For $b > R_{target}$ the inner boundary of the excited region approaches a plane, so that the cap is the most natural description. In those cases where the delta-function initial condition can be applied further simplifications are often possible. The preequilibrium component of the particle spectrum is essentially determined by the highest temperatures. As these temperatures are restricted to a small area in space and time around the initial configuration, only the local geometry, which is quite different from the geometry of the whole system, is of interest. If the local geometry is that of

a) infinite matter, the delta-function solution is a Gaussian

$$T(\vec{r},t) = T_{norm}\,(6\sqrt{\pi})^{-1}\,(t/\tau_R)^{-3/2}\, exp\left(-\frac{\tau_R\,\vec{r}^{\,2}}{t\,4R^2}\right)$$

with the delta-function at the origin of the coordinate system. This is a good description for a pointlike excitation far from the nuclear surface or just on the surface.

b) semiinfinite matter, $\lambda = 0$ and the delta-function does not lie on the boundary, the solution is not a Gaussian but obeys a simple transformation law, so that the knowledge of the solution for one distance s between boundary and delta-function determines the solution for other distances s'. The weight function for the temperature at the nuclear surface for s=0.3R is

$$g(T,s) = \frac{\int_0^{t_0}\int_0^{\ell_0} dt\, d\ell\, (2\pi\ell)\, \delta(T(t,\vec{r}(\ell),s) - T)}{\int_0^{t_0}\int_0^{\ell_0} dt\, d\ell\, (2\pi\ell)} \approx \frac{467}{T_{eq}} \cdot \left(\frac{T}{T_{eq}}\right)^{-4} .$$

1) R.Weiner: Phys.Rev.D13, 1363 (1976)

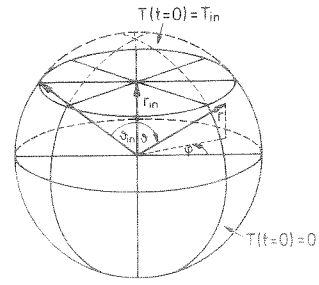


Fig.1 Spherical cap as geometry for the initial excitation in the nucleus.

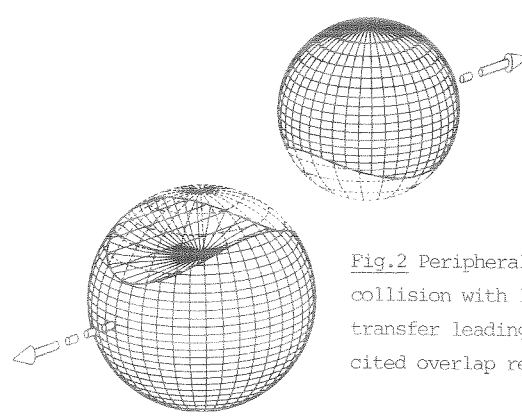


Fig.2 Peripheral heavy ion collision with low momentum transfer leading to an excited overlap region (cap).

Contributions to the field theory of spin 1 bosons [B]

M. Riedel, W. Greiner
Institut für Theoretische Physik der J.W.G.-Universität Frankfurt/Main

The theories of Kemmer, Proca and Shay-Good for the description of spin-1-bosons have been considered. It was well known that the free theories without interaction coupling are equivalent. Now Riedel[1] has shown the equivalence of the theories taking into account three general coupling schemes as a) minimal coupling 2) dipole coupling and c) quadrupole coupling.
It was possible to show the reversibility of the transformation scheme for the Proca- and Kemmer-equations. Taking into account anomalous magnetic moments it could be shown the equivalence of Proca- and Shay-Good equations.
A two-particle potential describing the interaction of spin 0 and spin 1 particles was derived, following the ideas of Bethe and Salpeter. The outcome is consistent with former results by Bethe and Salpeter (1957).

[1] M. Riedel, W. Greiner, in print

B + G

Contributions to theory of strong gravitational fields

M. Soffel, G. Schmidt, U. Heinz, A. Müller, B. Müller, W. Greiner
Institut für Theoretische Physik der J.W.G.-Universität Frankfurt/Main

The interaction between the expanding universe and quantum fields was studied, using the WKB approximation. This allows one to derive a total particle production rate from the path integral formulation of quantum field dynamics in the expanding universe.
The number of created particles is then given by the path integral over the classical action in the complex time plane. A comparison with the exact calculations of particle production rates in the de-Sitter universe (Thesis Rumpf Vienna 1978) shows that the approximation method for gravitational fields gives a good description for the dominant contributions of the particle production rate.
The development of approximation methods for these kinds of quantum field theoretical processes is important because of the non-existence of analytical solutions in all realistic problems[1].
The investigation of the stability of heavy astrophysical objects after thermal formation has been done within a new scalar-tensor theory of the gravitational field where a scalar field ϕ is coupled selfconsistently to the normal metrical gravitational field.
This leads to a space dependence of either the gravitational constant or the heavy masses. A stabilising effect up to 40 % was proposed for incompressible matter, but using realistic equations of state give only a minor change in the Chandrasekkar mass aroused by the influence of those ϕ fields[2].
The phenomenon of the overcritical vacuum in static gauge fields of U(1), Poincaré-group P and SU(3) was studied in general by Soffel et al[3] - with the following main results:

a) The Dirac vacuum is stable in any, static magnetic fields,
b) the Dirac vacuum is stable in global, static Einstein-fields without an event horizon,
c) the Dirac vacuum decays in ECSK-theory of gravitation - because of a torsion of space induced by the spin of matter.

If strong enough, this leads to the destruction of spontaneous pairs by spin interaction and to the spontaneous creation of pairs from the vacuum.
This new ground state - the vacuum with spin - was described for the first time by Soffel, Müller and Greiner[3]. The quantum field theory of a uniform accelerated spectator was discussed and the related visibility of a thermal distribution of fermions in the Minkowski vacuum was shown for the first time.[4,5]
Additionally the problem of classical brems-strahlung of a uniform accelerated charge in Minkowski space was investigated[6].

[1] A. Müller, B. Müller, W. Greiner; Phys.Lett. 74A, 281 (1979)

[2] G. Schmidt, W. Greiner, U. Heinz, B. Müller, to be published

[3] M. Soffel, J. Theis, B. Müller; 4th EPS Gen. Conf., Chapter 4, 262 (1979)

[4] M. Soffel, B. Müller, W. Greiner; to be publ. in Proc. 2nd Marcel Grossmann Meeting on General Relativity and Gravitation, ed. by Hawking, Ruffini et. al

[5] M. Soffel, B. Müller, W. Greiner; Phys. Rev.D in print

[6] M. Soffel, B. Müller, W. Greiner; GRG in print
M. Soffel, B. Müller, W. Greiner; Phys. Lett. 70A, 167 (1979)

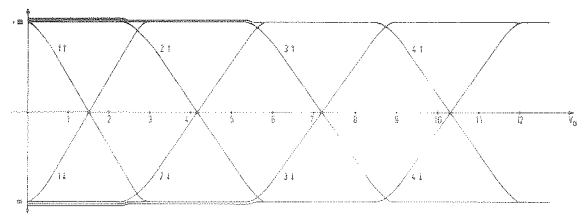


Fig.1 The first four bound states of the two dimensional Dirac equation in a square well torsion background are shown. (The U_4 geometry was taken to be flat.)

2. Atomic Physics

		PAGE
2.1	Superheavy Quasi-Atoms and Inner Shell Excitation Mechanisms	100
2.2	Capture Processes, Few Electron Systems and Metastable States	112
2.3	Slowing Down of Heavy Ions in Matter	120
2.4	Theory	126

B

Spectroscopy of high energy δ-rays emitted in heavy-ion collisions

E. Berdermann[3], F. Bosch[1], H. Bokemeyer[1], M. Clemente[3], F. Güttner[2], P. Kienle[3], W. Koenig[2], C. Kozhuharov[1], B. Martin[2], B. Povh[2], H. Tsertos[3], Th. Walcher[2]

[1]GSI-Darmstadt - [2]MPI Heidelberg - [3]TU München

The experiments reported previously[1] have been extended further. Spectra of δ-rays, emitted in the collisions of 4.7 MeV/u ^{208}Pb ions with ^{120}Sn, ^{197}Au, ^{208}Pb, ^{232}Th and ^{208}U-targets have been measured. Both cross sections ($d^2\sigma/d\Omega_\delta dE_\delta$) and δ-ray production probabilities per collision ($d^2P/d\Omega_\delta dE$) have been investigated as a function of the impact parameter and δ-electron kinetic energy. Coincidences between the δ-electrons and the characteristic K X-rays of the projectile were also carried out, thus allowing a preferential observation of contributions from particular quasiatomic bound states.

The experimental arrangement[1] has been optimized by increasing the X-ray detection efficiency and by selecting the heavy-ion scattering events in an angular range between 17° and 45° by an annular parallel-plate counter whose sensitive area is divided into 8 rings.

The principal features reflected in the data of fig. 1 are the high kinetic energy of the δ-rays observed, the large difference in the intensities of the (Pb+Pb) and (Pb-Sn) spectra and the steeper fall-off of the (Pb-Sn)-spectrum. All of these imply that the electrons have been emitted from bound quasiatomic states, where, due to the Z-dependent relativistic contraction of the wave functions, large momentum transfers to strongly localized bound electrons become possible.

In fig. 2 the measured spectrum for the Pb-Sn system, selected by the δ-X-ray coincident requirement is displayed, showing good agreement with the calculated distribution[2]. Thus the expectation to exploit in this way the characteristic behaviour of the innermost bound state in the Pb-Cm or Th-Cm quasi-atoms has been corroborated, since the contribution from the 1sσ bound state dominates the spectrum. However, double ionization in the same collision of the K- and higher shell with additional detection of the higher shell electron produces a prompt background, not negligible at low δ-ray energies.

The impact parameter dependence of the δ-ray production has been studied for following reasons: i) the binding energy of the electrons in a quasi-atom is expected to depend on the internuclear separation, ii) a possible deduction of the energy and momentum transfer dependence on the impact parameter or the distance of closest approach is a sensitive test for scaling laws not only for δ-ray emission but also for X-ray and induced non-nuclear positron emission. A part of the experimental results is shown in fig. 3 compared with the theoretical calculations[2]. The latter exhibit a somewhat steeper fall-off with the increasing kinetic energy. An additional X-ray coincidence requirement should provide more detailed information. The data are being currently analyzed.

[1]GSI Annual Report 1978, p. 95

[2]G. Soff et al., Z. Physik A294, 137 (1980)

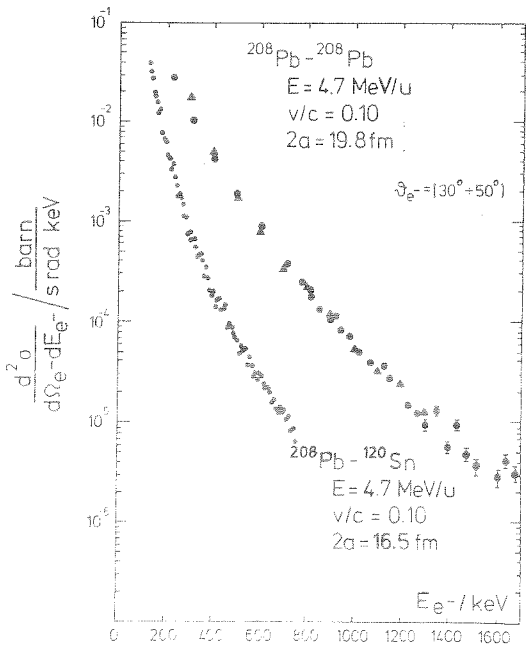


Fig. 1: Cross section for δ-ray emission from the systems Pb+Pb (Z_U = 164) and Pb+Sn (Z_U = 132) measured at the same relative velocity.

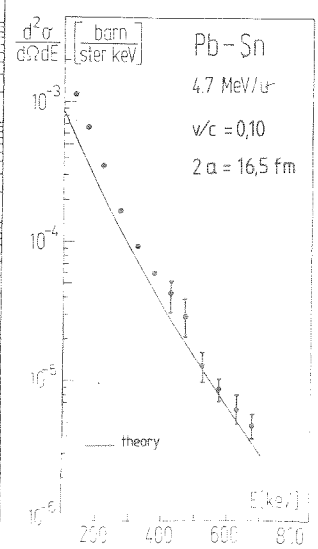


Fig. 2: Cross section for δ-ray emission from the (Pb+Sn) system with a δ-(Pb-K-X)-coincidence requirement.

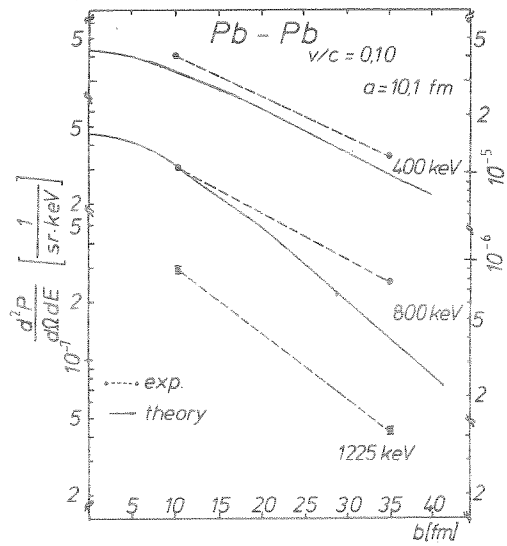


Fig. 3: δ-ray production probability as a function of the impact parameter.

B

Positron Production in Heavy Ion Collisions

H. Backe, W. Bonin, W. Engelhardt, E. Kankeleit, M. Mutterer, P. Senger, F. Weik, R. Willwater
Institut für Kernphysik der TH Darmstadt
V. Metag, J.B. Wilhelmy
Max-Planck-Institut für Kernphysik, Heidelberg

In a first generation of experiments the atomic positron production in HI collision was established[1,2]. The dependence on the kinematical conditions and on the combined charge Z of projectile and target nucleus turned out to be well described in the model[3] of dynamically induced pair production. We report here on a next step of experiments, the search for signatures in the "supercritical" domain for which the "diving" of the $1s_\sigma$ quasimolecular level into the Dirac sea is predicted. Such a situation arises if the heaviest systems like U-U or better U-Cm come as close as to their reaction distances. Depending of how well the adiabatic picture does apply deviations from the trend for undercritical systems are to be expected. An experimental search for these signatures was performed by 1. a study of the total positron production as a function of total charge and on minimum distance R_m or characteristic time $2\hat{t}$, the distance between extrema of $\dot{R}/R$, 2. by measuring the positron spectra in the supercritical domain and comparing them with undercritical ones and 3. by searching for effects in deep inelastic collisions when reaction times are lengthened (increase of $2\hat{t}$) and "spontaneous" processes are predicted to participate more strongly[3].

As in earlier measurements with the solenoidal spectrometer[1] the scattered particle was detected at $45^\circ \pm 10^\circ$, thus defining R_m or $2\hat{t}$ uniquely in (nearly) symmetric systems. A new positron detector with much improved efficiency was installed (part of the Torispectrometer in construction) with a four sector NaI ring and a pair of Si detectors arranged such that the δ electrons are rejected . In Fig. 1 the new results on the high energy U-U and U-Cm systems are included. The exponential scaling behavior[4] as function of $2\hat{t}$, expected for undercritical systems, seems to prevail also for the supercritical high energy (low $2\hat{t}$) U-U and U-Cm systems.

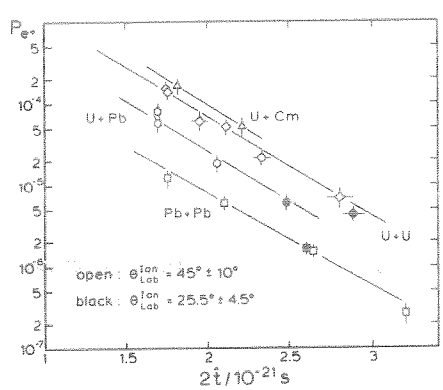


Fig. 1: Atomic positron yield as a function of $2\hat{t}$, the distance between extrema of $\dot{R}/R$. The U-Cm and the low $2\hat{t}$ U-U data are expected to result from supercritical systems.

The Z dependence at given $2\hat{t}$ also follows the $Z^{\sim 17}$ trend of the lighter systems. The positron spectra are shown in Fig. 2. For the U-Pb system (R_m = 21 fm, E_{1s} = 89o keV) good agreement with theory[3] is obtained, while for U-U (R_m = 21 fm, E_{1s} = 115o keV, diving 124 keV) some deviations are seen. But additional systematic studies are required to verify that these can be related to the diving process.

The time delay effect was studied on U-U and U-Cm systems at 7.5 MeV/u projectile energy using fission fragments as signature for deep inelastic collisions. The data with large errors suggest a lowering of the yield compared to the trend from elastic events. This may be explained[4] by a near cancellation of the incoming positron production amplitude by the phase delayed outgoing one.

[1] H. Backe, L. Handschug, F. Hessberger, E. Kankeleit, L. Richter, F. Weik, R. Willwater, H. Bokemeyer, P. Vincent, Y. Nakayama and J.S. Greenberg, Phys. Rev. Letters 4o, 1443 (1978).

[2] L. Kozhuharov, P. Kienle, E. Berdermann, H. Bokemeyer, J.S. Greenberg, Y. Nakayama, P. Vincent, H. Backe, L. Handschug and E. Kankeleit, Phys. Rev. Letters 42, 376 (1979).

[3] J. Reinhardt, W. Greiner, B. Müller and G. Soff, XI Int. Conf. on Physics of Electronic and Atomic Collisions, Kyoto 1979 and references.

[4] E. Kankeleit, 12. Summer School Mikolajki, Poland 1979, IKDA 79.

[5] P. Schlüter, G. Soff and W. Greiner, Z. Phys. A286, 149 (1978).

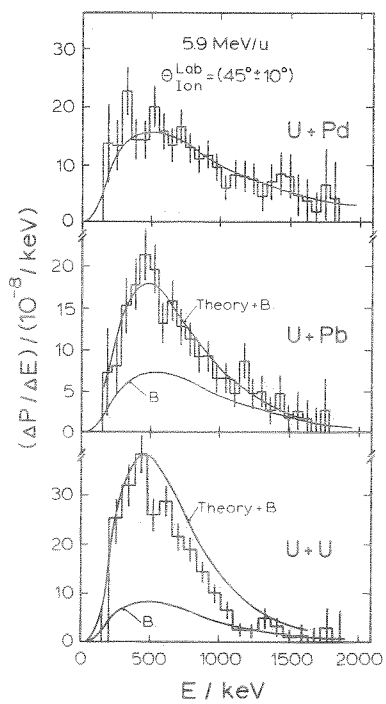


Fig. 2: Positron spectra. The solid curve in U-Pd was derived from γ spectrum assuming E1 multipolarity[5]. Using this procedure the nuclear background curve B has been obtained, to which theoretical[3] values have been added.

Differential Positron Production Probability in Quasi Atomic Systems [B]

A. Bałanda[+], K. Bethge[Δ], H. Bokemeyer, H. Folger, J.S. Greenberg[*], H. Grein, A. Gruppe[Δ], S. Ito[§], S. Matsuki[§], R. Schulé[Δ], D. Schwalm, J. Schweppe, N. Trautmann[▽], P. Vincent, M. Waldschmidt[Δ]

GSI Darmstadt, [Δ]University Frankfurt, [*]Yale University, [§]Kyoto University, [▽]University Mainz

Theoretical descriptions of the evolution of inner shell electron orbitals in superheavy collision systems predict a rapid increase in the binding energies of the quasimolecular orbitals with decreasing internuclear separation. For a sufficiently high combined nuclear charge these binding energies can exceed the "overcritical" value of 2 mc^2, and thus such systems may provide the necessary vehicle for observing the predicted instability of the vacuum state of QED in "overcritical" fields via a spontaneous positron decay of a hole state produced in the collision. The search for this process is complicated by dynamic positron creation processes and by comparably intense sources of e^+-production originating from the internal pair-conversion decay of the highly excited nuclei. The latter processes must be quantitatively understood if the spontaneous component is to be uniquely identified. Such studies have been the object of intense experimental investigations at GSI during the past few years[2,3].

To extend these studies to include a more detailed analysis of the differential positron-yields with respect to the impact parameter of the collision and the e^+-energy distribution, a high efficiency magnetic solenoid system (EPOS)[4] has been designed and constructed at GSI. In a first series of experiments, collisions between 5.9 MeV/u ^{238}U-ions with ^{208}Pb, ^{238}U, and ^{248}Cm targets have been carried out. All data were taken in coincidence with both scattered particles. This kinematic coincidence, on the one hand, defines the scattering trajectory and thus provides a crutial selection between distant and close collisions in asymetric collision-systems such as U-Pb; on the other hand it discriminates elastic scattering from other reaction channels.

An example of recent results is shown in the accompanying fig. where the e^+-production probabilities, averaged over E^{e+} from 0.1 to 1 MeV, for ^{238}U + ^{208}Pb collisions are plotted as a function of R_{min}. These observations, for the first time, include data with unambiguous R_{min} values and backward scattering events. In this collision system no spontaneous positron production is expected and the measurement therefore serves as a study of the other positron producing processes. The contribution of the nuclear e^+-production can be derived from the measured γ-ray spectra. Although this procedure introduces uncertainties - due to the unknown multipolarity of the observed γ-decays (E1, E2) and the possible contributions from E0 transitions, it is clear that a e^+-production probability due to atomic processes remains after subtraction of the nuclear contribution. This remainder is drawn in the fig. as a crossed hatched region; the border lines correspond (without considering statistical errors) to the assumption of pure E2- (upper line) and pure E1-multipolarity (lower line). A comparison to the theoretical prediction seems to indicate that the experimental atomic e^+-production probability decreases faster with increasing R_{min}. A similar result is obtained when considering the energy differential atomic e^+-production probability at E^{e+} = 480 ± 60 keV, where our data can be compared to results obtained previously[3] at $R_{min}/2a$-values > 1.4. After correcting the latter data for contributions from small impact parameters (not distinguished in ref. 3), the slopes of the two measurements agree and indicate again a steeper fall-off than predicted by theory.

Before drawing any further conclusions the analysis of other collision systems (including the e^+-energy spectra) must be completed and a more detailed estimate of the nuclear e^+-contribution has to be made.

[1] J. Reinhardt et al., in Electronic and Atomic Collisions, N. Oda et al., ed. North Holland (1980) 369
[2] H. Backe et al., Phys. Rev. Lett. 40 (1978) 1443
[3] C. Kozhuharov et al., Phys. Rev. Lett. 42 (1979) 376
[4] A. Bałanda et al., contributions to this report
[5] P. Schlüter et al., Z. Phys. A 286 (1978) 149

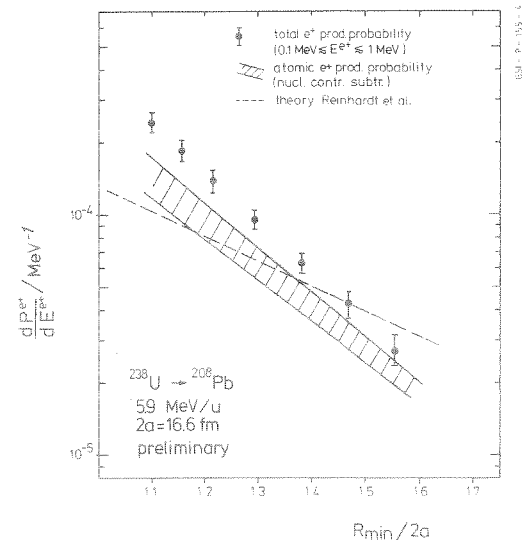


Fig. 1: The energy differential e^+-production probability for the ^{238}U + ^{208}Pb system at 5.9 MeV/u averaged over E^{e+} from 0.1 MeV to 1 MeV as a function of the distance of closest approach R_{min}. (R_{min} = 2a for a head-on collision). Also shown is the expected atomic e^+-production according to the theory of Reinhardt et al.[1].

[+] on leave from Jagellonian University, Crakow

B

Positrons from 1.4 GeV U-U collisions

E.Berdermann[3], F.Bosch[1], M.Clemente[3], F.Güttner[2], P.Kienle[3], W.Koenig[2], C.Kozhuharov[1], B.Martin[2], W.Potzel[3], B.Povh[2], H.Tsertos[3], W.Wagner[3], Th.Walcher[2] ([1]GSI-Darmstadt, [2]MPI-Heidelberg, [3]TU-München)

A series of measurements on pair creation in the collision of very heavy ions have been pursued, utilizing an improved experimental arrangement, which prosesses a high detection efficiency both for positrons and particles and particulary optimizes the determination of positron production probabilities per collision (dP/dE) as a function of the positron energy and of the impact parameter. Fig.1 shows a schematical view of the experimental set-up. The positrons emitted between 30° and 70° to the beam (and spectrometer)-axis and within a momentum range $\Delta p/p = 0.17$, are focused by the spectrometer field on the coaxial proportional gas counter-plastic scintillator combination. The outer anode foil of the gas counter, mounted in the focal area of the spectrometer, is position-sensitive, which allows an additional determination of the e^{+}-momentum. In order to minimize the background due to scattered electrons, the 12 cm long, slightly cone-shaped plastic scintillator (12-16 mm Ø) is placed on the spectrometer axis (note the absence of a counter for annihilation quanta). The positron detection efficiency runs to 15.5% within the focused momentum compared with 2.6% for the previous set-up. All particles scattered in the angular range between 25° and 70° to the beam axis are detected by an annular parallel plate avalanche counter whose sensitive area is divided into 16 rings and whose anode and cathode foils are transparent to positrons with kinetic energies in the region of interest. A kinematic coincidence between particular rings gives a sufficient identification of projectile and recoil nuclei for asymmetric colliding systems, thus allowing one to measure the positron production probabilities, even at small impact parameters.

Fig.2 shows preliminary data for the production of 500 keV positrons, in 5.9 MeV/u U + U collisions, measured with the new set-up. The positron production probability as a function of the impact parameter is well described by an exponentially decaying function: $P(b) = P(o)e^{-b/a}$. The fall off constant a is correlated with the average impact parameter $\bar{b}$ by $\bar{b} = 2a$. Using energy and momentum conservation the energy transfer ΔE in the collision gives $\Delta E = \frac{K v}{\bar{b}}$. C with $C \approx 1$. From Fig. 2 one gets a fall off constant a = 7.7 fm, leading to a ΔE of 1.41 MeV in good agreement with an expected energy transfer of 1.5 MeV. This shows that the behaviour of P(b) is determined by the dynamics of the collision process. A resonance in the negative energy continuum however should produce a deviation from the above described exponential dependence of P(b) at small impact parameters. With the new experimental set-up the positron production probabilities could be measured with statistical errors in the order of a few precent. Therefore the experimental method turns out to be very suitable for precise measurements of positron energy spectra as a function of the impact parameter in order to detect small deviations induced by a resonance in the negative energy continuum.

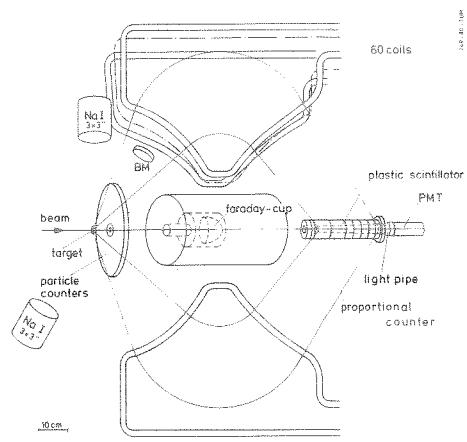


Fig. 1: A schematic view of the experimental set-up

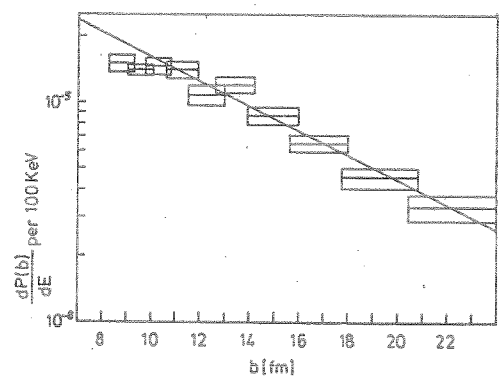


Fig. 2: Preliminary data of P(b) at an average positron energy of 500 keV. The positrons of nuclear origin are not subtracted.

MO X-Ray Angular Distribution for 1 GeV $^{208}Pb + ^{208}Pb$ and $^{209}Bi + ^{209}Bi$

Ch. Stoller, E. Morenzoni, W. Wölfli, ETH Zürich, W.E. Meyerhof, Stanford University
F. Folkmann, P. Vincent, P.H. Mokler, P. Armbruster, GSI Darmstadt

The shape and the anisotropy of the quasi-molecular orbital (MO) X-ray spectra above the separated-atom K-lines emitted in $^{208}Pb + ^{208}Pb$ and $^{209}Bi + ^{209}Bi$ collisions have been measured at beam energies between 4.2 and 4.8 MeV/u. The highly enriched ^{208}Pb (99.0% and 99.968%) and 99.9% pure ^{209}Bi-targets were oriented at 45° to the beam axis and thick enough to stop the beam. The spectra were measured with two Ge(Li)-detectors (86 and 109 cm^3), which could be placed at arbitrary angles between 0° and 140°. Absorbers of Ta (0.25 - 0.35 mm) Sn or Cd (2 or 3 mm) and Cu or Al (1 mm) were used to reduce the intensity of the low-energy radiation in order to avoid pulse pile up and large dead times in the data acquisition system. A Si(Li)-detector mounted above the beam axis at a backward angle of 135° was used as a monitor to normalize the spectra. In order to determine the pure photon spectra, the ambient background measured between the beam pulses, the spurious γ-lines observed at 511 keV (positron annihilation), 570 and 803 keV (Coulomb excitation in ^{207}Pb and ^{206}Pb respectively) or at 896 keV (^{209}Bi) as well as the Compton contribution from the continuum were subtracted from the measured pulse high spectra. Finally the unfolded spectra were corrected for absorption and detector efficiency. The upper part of fig. 1 shows, as an example, the thick target photon yield obtained in Pb-Pb collisions at 4.2 MeV/u. The solid line indicates the predicted spectrum, if nucleon-nucleon Bremsstrahlung (NNB) and radiative transitions into the $1s\sigma$-molecular orbital are taken into account[1]. The agreement is satisfactory only in the energy range between 400 and 550 keV. Transitions into the next higher lying MO's ($2s_{\sigma}$, $2p_{\sigma,\pi}$), not yet included in the theory, may explain the discrepancy below 400 keV. Recently it has been shown[2] that much better agreement between theory and experiment can be achieved above 600 keV, if rotationally coupling and multistep excitation to higher lying empty bound and unbound states are taken into account. The anisotropy of the MO X-ray radiation was derived from the corrected c.m. spectra observed at 0° and 90°, using the formula $A(E_x) = N(E_x,\Delta E_x,90^{\circ})/N(E_x,\Delta E_x,0^{\circ})-1$, where the number of counts N were obtained from variable energy windows ΔE_x between 10 and 75 keV wide. The lower part of fig.1 shows the result obtained in 4.2 MeV/u Pb - Pb collisions. It is interesting to note that only one distinct peak around 140 keV can be seen in the energy range above the Pb K-lines. In contrast to the prediction of Hartung and Fricke[3] and Kirsch[2] no significant effect has been found neither around 400 keV (UA L_{α}-transition) nor at 750 keV (UA K_{α}-transition). This result indicates, that relativistic effects strongly suppress the anisotropy, as has been predicted by Anholt[4].

1 J. Kirsch et al., Z. Phys. A292, 257 (1978)
2 J. Kirsch, Diss. Univ. Frankfurt, 1980
3 H. Hartung et al., Z. Phys. A288, 345 (1978)
4 R. Anholt, Z. Phys. A289, 257 (1979)

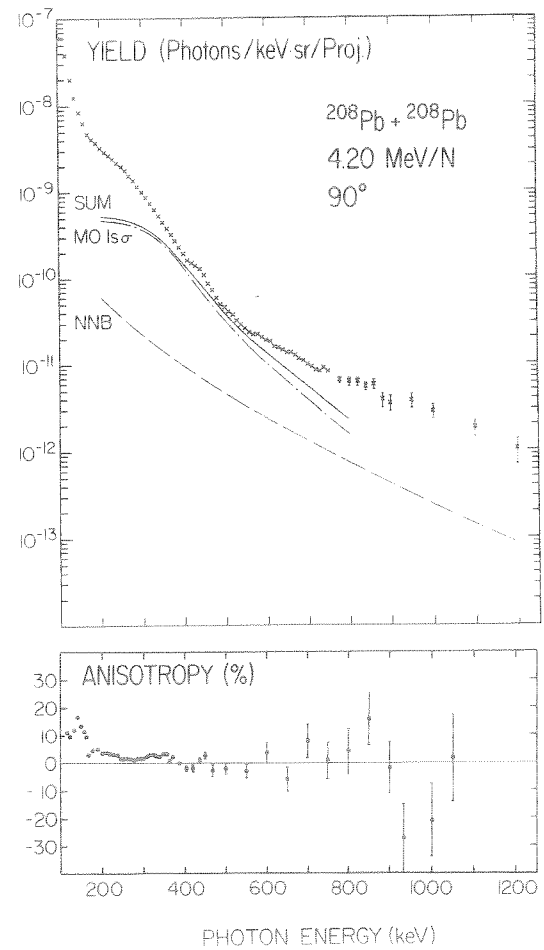


Fig. 1: Thick target photon yield and anisotropy for 4.2 MeV/u $^{208}Pb + ^{208}Pb$.

A Coincidence Technique for the Measurement of Quasimolecular X-rays from Superheavy Quasimolecules

P. Vincent, D. Schwalm, H. Bokemeyer, H. Emling, and E. Grosse, GSI Darmstadt
J.S. Greenberg, Yale University

Theoretical descriptions of the evolution of molecular orbitals during collisions of heavy ions with heavy target atoms predict maximum binding energies for inner shell electrons which approach or exceed twice their rest mass energy. Direct evidence for such large binding can in principle be gained through observations of the molecular orbital X-ray transitions between the transiently formed quasimolecular shells. However, extraction of spectroscopic information from such measurements is complicated by the continuous nature of the resulting spectra, the overlap of K-like, L-like, and M-like transitions in the quasiatom, and by dynamic collision broadening effects. As is illustrated in Fig. 1, requirement of a coincidence between high energy molecular orbital X-ray transitions and separated atom K X-rays exploits the cascade relationship between $2p_{1/2}\sigma \rightarrow 1s_{1/2}\sigma$ molecular X-rays and the K X-rays to discriminate against other continuum transitions in the quasimolecule, thereby simplifying the comparison between experiment and theory.

Such K X-ray, molecular orbital X-ray coincidence measurements have been carried out using the $^{208}Pb + ^{208}Pb$ collision system at 4.8 MeV/u[1]. The cross sections for production of a continuum X-ray with and without an accompanying K X-ray are shown in Fig. 2. A detailed analysis of the experimental results indicates that a substantial fraction of the coincidence events are due to double vacancy production in a single collision which therefore represent a background to the desired $2p_{1/2}\sigma \rightarrow 1s_{1/2}\sigma$ K X-ray cascade coincidence. The contribution of such events can be calculated on the basis of a simple model which assumes that the excitation of the second vacancy is only statistically correlated with that of the first. The validity of this description was tested for the case of double K X-ray excitation, where the measured double to single K X-ray cross section ratio of .033 ± .004 compare favourably to the model calculation result of 05 ± .015. The solid line in Fig. 2 below the coincidence data at low energies represents the calculated contribution of double vacancy events to the data. Extension of the calculation to higher energies is not straight forward, but estimates show that up to 50 % of the high energy coincidence yield could come from double vacancy production.

We conclude, on the basis of this coincidence study, that the radiation observed is quasimolecular in origin and that the continuum yield below 200 keV is dominated by transitions to vacancies in that orbital which leads to separated atom K X-rays ($2p_{1/2}\sigma$). The results and interpretation of the measured cross sections show that similar measurements, carried out as a function of projectile energy, will allow for quantitative understanding of double vacancy and other dynamic effects and thereby allow for a more unique assignment of the high energy continuum yield to $2p_{1/2}\sigma \rightarrow 1s_{1/2}\sigma$ molecular transitions only. Furthermore, if in addition to the K X-ray coincidence a coincidence with the scattered projectile is demanded, the resulting reduction in otherwise prohibitive backgrounds from nuclear excitation could allow for the observation of molecular orbital radiation from U + U or U + Cm collisions. Such measurements would complement current experimental and theoretical understanding of the behaviour of electrons under the highest of achieveable binding energies.

[1] P. Vincent et al., GSI annual report 1978, p. 99

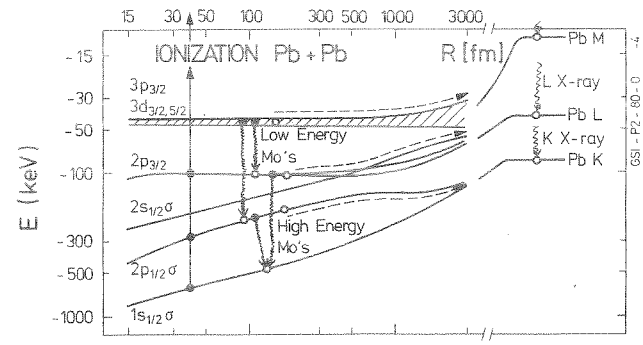


Fig. 1: Evolution of molecular binding energies in Pb+Pb collisions as a function of internuclear separation R. The figure illustrates that only $2p_{1/2}\sigma \rightarrow 1s_{1/2}\sigma$ molecular orbital (Mo) transitions directly result in a cascade K X-ray.

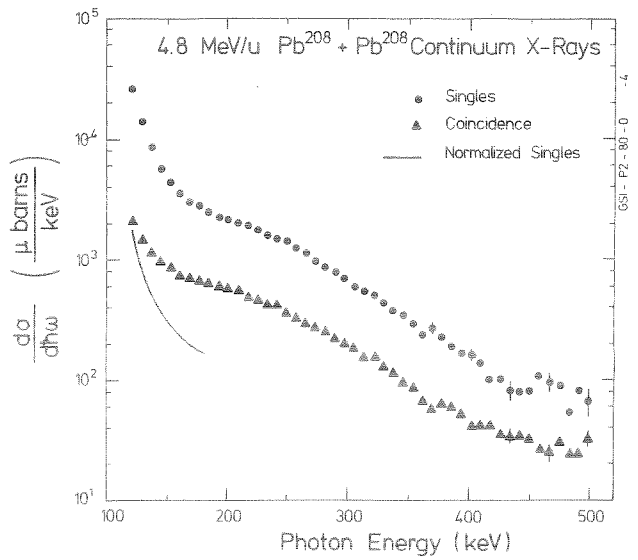


Fig. 2: Production cross section for continuum singles and coincidence X-rays. The absolute error is ± 30 % and relative error between the two curves is ±15%. The solid line indicates the two-vacancy background contribution to the coincidence low energy yield.

A scaling law for the 1sσ excitation probability in collision systems $\alpha(Z_1+Z_2) \gtrsim 1$

F. Bosch[1], P. Armbruster[1], D. Liesen[1], D. Maor[1], P.H. Mokler[1], H. Schmidt-Böcking[2], R. Schuch[3]
[1]GSI Darmstadt - [2]IKF Frankfurt - [3]Univ. Heidelberg

In adiabatic collisions between very heavy ions Z_1 and atoms Z_2 with $\alpha(Z_1+Z_2) = \alpha Z \gtrsim 1$ quasimolecules or quasi-atoms are formed with combined nuclear charges Z far exceeding those of the heaviest available elements. Due to the strong, extended Coulomb field of both nuclei the binding energy of the innermost electrons drastically increases as a function of the nuclear charge. At Z=173 the 1s-state is predicted to be bound with twice the electron rest mass and to dive for still higher nuclear charges into the negative continuum. In collision systems with $\alpha Z \gtrsim 1$ the innermost electrons represent thus highly relativistic systems. They exhibit one characteristic feature which makes an experimental investigation feasible, namely a tremendous shrinking of their spatial wavefunctions and a corresponding increase of their high momentum components. The consequence important for experiments is a high excitation probability for 1sσ electrons in collisions at those impact parameters which are comparable to the region of the enhanced spatial distribution. On the other hand, the 1sσ *excitation probability*, when restricted to a very small interaction region in such superheavy systems, must be directly connected with the *binding energy* of the 1sσ orbital. We derived a simple analytical formula, which demonstrates this dependence for systems $\alpha Z \gtrsim 1$.

During a collision, excitation of electrons is caused by the time changing two center Coulomb potential of both nuclei. Using first order perturbation theory one gets for the transition amplitude $a(E_f)$ of an electron from the initial 1sσ-state with an energy $E_i(t)$ to a final state with energy E_f:

$$(1)\quad a(E_f) = -\int_{-\infty}^{\infty} dt \langle \psi_{E_f} | \partial/\partial t | \psi_{E_i} \rangle \exp\left\{ i/\hbar \int_{-\infty}^{t} dt' (E_f - E_i) \right\}$$

Evaluating Eq. (1) we benefit from the experimentally proved fact that the 1sσ excitation in systems $\alpha Z \gtrsim 1$ is confined to very small internuclear distances R. Thereby, only the radial part $\dot{R}\,\partial/\partial R$ of the $\partial/\partial t$ operator has to be taken into account, because the rotational coupling is negligible at those small distances. Thus

$$(2)\quad a(E_f) = -\int_{-\infty}^{\infty} dt\, \dot{R}(t) \langle \psi_{E_f} | \partial/\partial R | \psi_{E_i} \rangle \exp\left\{ i/\hbar \int_{-\infty}^{t} dt' (E_f - E_i) \right\}$$

with $\dot{R}(t)$ the radial collision velocity.
It was shown[1] that the coupling matrix element in Eq. (2) can be well parametrized for $\alpha Z \gtrsim 1$ as:

$$(3)\quad \langle \psi_{E_f} | \partial/\partial R | \psi_{E_i} \rangle = \left(\frac{D(Z)}{4\pi^2 mc^2} \right)^{1/2} \cdot \left(\frac{mc^2}{E_f} \right)^{\frac{\eta(Z)}{2}} \cdot \frac{1}{R}$$

where mc^2 is the electron rest mass, D(Z) and η(Z) are slowly varying functions of Z alone. With Eq. (3) we can calculate from Eq. (2) the 1sσ excitation probability $P_{1s\sigma}$ by summing over all final electron energies:

$$(4)\quad P_{1s\sigma} = 2 \int_{mc^2}^{\infty} |a(E_f)|^2 dE_f + 2 \sum_{k}^{E_k < mc^2} |a(E_{fk})|^2$$

The first term in Eq. (4) gives the continuum final states states, whereas the second denotes the sum over all unoccupied bound states. Now, it has been proved experimentally[2] that the average kinetic energy of the electron emitted into the continuum is very small compared to its rest mass. Hence, it seems to be reasonable to fix the total electron energy in the final state as $E_f = mc^2$, thus compensating the excitations into weakly bound state states ($E_f < mc^2$) with ionization into continuum states ($E_f > mc^2$). With this premise we obtain after some approximations an analytical expression for the 1sσ excitation probability as a function of the united charge Z and the impact parameter b:

$$(5)\quad P_{1s\sigma}(b) = \tfrac{1}{2} D(Z) \left| \exp(-\gamma) + \sqrt{\frac{2\gamma}{\pi}} \sum_{n=1}^{\infty} (-i)^n \left(\frac{\gamma}{2}\right)^{n/2} \frac{K_{n/2-1/2}(\gamma)}{\Gamma(n/2+1)} \right|^2$$

with

$$\varepsilon = \frac{R_0 - a}{a}, \qquad \gamma = \frac{E_{1s\sigma}(R_0)\,(R_0 - a)}{\hbar v}$$

and $K_\nu(\gamma)$ the modified Bessel functions, whereby R_0 is the distance of closest approach in an encounter with impact parameter b, 2a is the minimum distance in a head-on collision and $-E_{1s\sigma}(R_0)$ is the 1sσ binding energy at the internuclear distance R_0. Whenever b is not too small and therefore $\varepsilon \gg 1$ Eq. (5) reduces to the simple expression:

$$(6)\quad P_{1s\sigma}(b) = \tfrac{1}{2} D(Z) \cdot \exp\left\{ -2R_0 \frac{E_{1s\sigma}(R_0)}{\hbar v} \right\}$$

Eq. (6) which differs both in slope and in the prefactor from a previously derived formula[3] contains a basic relation between the 1sσ excitation probability and the 1sσ binding energy as a function of R_0. The range of applicability of this scaling law, however, is restricted to collision systems $\alpha Z \gtrsim 1$ and to impact parameters $b \gg a$.

[1] G. Soff et al., Phys. Rev. A20, 169 (1979)
[2] C. Kozhuharov et al., Phys. Rev. Lett. 39, 540 (1977)
F. Bosch et al., Phys. Lett. 78B, 568 (1978)
[3] B. Müller et al., Z. Physik A285, 27 (1978)

B

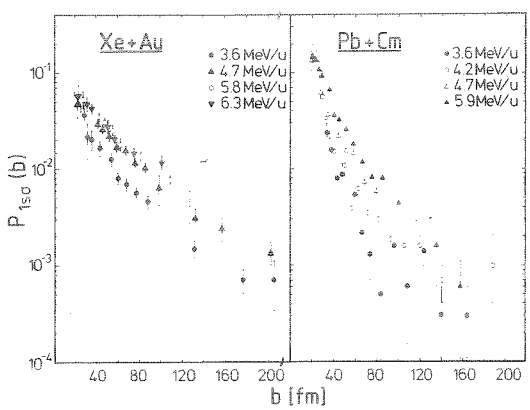
Excitation Probability of the Molecular 1sσ Orbital in Collision Systems $\alpha(Z_1+Z_2) \gtrsim 1$

D.Liesen[1], P.Armbruster[1], F.Bosch[1], S.Hagmann[1], P.H.Mokler[1], H.Schmidt-Böcking[2], R.Schuch[3], J.B.Wilhelmy[4], H.J.Wollersheim[1]

[1]GSI Darmstadt - [2]IKF Frankfurt - [3]Univ. Heidelberg - [4]Los Alamos, USA

In many experiments, performed within the last few years, the excitation probability P(b) as a function of the impact parameter b for the K-shell of both collision partners has been determined from measurements of coincidences between scattered primary particles and K X-rays emitted with the decay of the inner shell vacancies.

Especially the data for the excitation probability $P_{1s\sigma}(b)$ of the molecular 1sσ orbital in systems with $\alpha(Z_1+Z_2)=\alpha Z \gtrsim 1$ have shown quantitatively that excitation of the 1sσ orbital is restricted to impact parameters small compared to the K-shell radius of the <u>united</u> atom. This is demonstrated in fig.1, where $P_{1s\sigma}(b)$ for Xe+Au and Pb+Cm at different projectile energies is shown. Both measurements clearly demonstrate that 1sσ excitation in these heavy systems takes place predominantly at very small b.



<u>Fig.1</u> 1sσ excitation probability $P_{1s\sigma}(b)$ for the systems Xe+Au (Z=133) and Pb+Cm (Z=178), measured at several projectile energies.

It has been shown in the foregoing contribution that for $Z_1+Z_2 \gtrsim 130$ the excitation probability $P_{1s\sigma}(b)$ is given by the scaling law:

$$(1) \quad P_{1s\sigma}(b) = \tfrac{1}{2}\, D(Z) \cdot \exp\{-2R_0 q_0\}$$

where D(Z) is a function only of Z, R_0 is the distance of closest approach in a collision with impact parameter b and $q_0 = \frac{E_{1s\sigma}(R_0)}{\hbar v}$

Eq.(1) predicts that a plot of $\ln\{P_{1s\sigma}(b)/\tfrac{1}{2}D(Z)\}$ vs. $R_0 q_0$ gives one projectile velocity independent universal straight line with a slope 2 for all collision systems $Z \gtrsim 130$. Fig.2 shows this plot for Xe+Au, Pb+Cm from fig.1 and all other available coincidence data, at different projectile energies. Static binding energies $E_{1s\sigma}(R_0)$ from Ref.1 were used to calculate q_0. The values of D(Z) for the 7 different systems have been determined by a fit of Eq.1 to the $P_{1s\sigma}(b)$ data for each collision system separately.

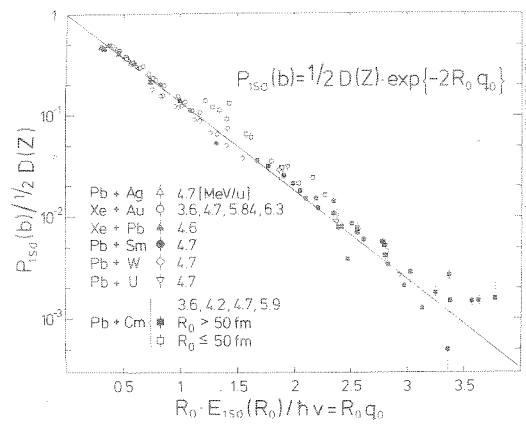


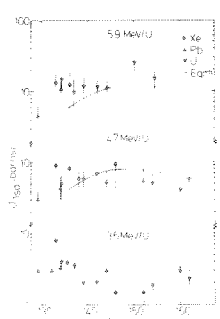
Fig.2 Normalized 1sσ excitation probability vs. $R_0 q_0$ for <u>all</u> systems $\alpha Z \gtrsim 1$ measured up to now. The full line gives the prediction acc. to Eq.(1).

Obviously, the experimental data are consistent with Eq.(1) if static binding energies from Ref.1 are used, except the Pb+Cm system for $R_0 \lesssim 50$ fm. These data will be discussed in more detail in the following contribution. Thus, the scaling law (Eq.(1)) may be considered as a possible basis in order to calculate important quantities like the total 1sσ excitation cross section $\sigma_{1s\sigma}$. Using Eq.(1) we obtain the expression:

$$(2) \quad \sigma_{1s\sigma} = \pi/4 \cdot D(Z) \cdot \langle q_0 \rangle^{-2} (1+\xi) \cdot \exp(-2\xi)$$

with $\xi = 2a\langle q_0 \rangle$ and the mean momentum transfer $\langle q_0 \rangle = \frac{E_{1s\sigma}(R_0)}{\hbar v}$

In fig.3 we compare the calculated with measured 1sσ-cross sections. The possibility, to extract 1sσ binding energies from measured $P_{1s\sigma}$-values acc. to Eq.(1) will be discussed in the following contribution.



<u>Fig.3</u> Measured total 1sσ excitation cross sections for Xe-, Pb- and U-projectiles vs. $Z_u = Z_1+Z_2$, compared with the theoretical values from Eq.(2) (full lines).

[1]G. Soff et al., Phys. Rev. <u>A20</u>, 169 (1979)
[2]H.H. Behncke et al., Z. Physik <u>A289</u>, 333 (1979)
R. Anholt et al., Z. Physik <u>A289</u>, 349 (1979)

Spectroscopy of the Molecular 1sσ Orbital in Collision Systems $\alpha(Z_1+Z_2) \gtrsim 1$ [B]

P. Armbruster[1], F. Bosch[1], D. Liesen[1], D. Maor[1], P.H. Mokler[1], H. Schmidt-Böcking[2], R. Schuch[3]

[1]GSI Darmstadt - [2]IKF Frankfurt - [3]Universität Heidelberg

The analytical formula for the 1sσ excitation probability derived in the foregoing contribution for collision systems $\alpha(Z_1+Z_2) = \alpha Z \gtrsim 1$:

$$(1) \quad P_{1s\sigma}(b) = \tfrac{1}{2} D(Z) \cdot \exp\left\{-2R_0 \frac{E_{1s\sigma}(R_0)}{\hbar v}\right\}$$

connects the 1sσ excitation, measured at an impact parameter b with the binding energy of the molecular 1sσ orbital at an internuclear distance R_0. Thus, according to Eq. (1), 1sσ binding energies could be extracted from measured $P_{1s\sigma}(b)$-values, provided D(Z) would be known very accurately. This method of a spectroscopy of the 1sσ orbital, proposed first by B. Müller et al.[1], has been applied by H.H. Behncke et al.[2] However, the thereby used scaling law of Ref. 1 and the absolute values of D(Z) are not in agreement with the meanwile measured $P_{1s\sigma}$-data (cf. the foregoing contribution). Even now, having a scaling law (Eq.(1)) which describes satisfactory both the absolute values and the impact parameter dependence of $P_{1s\sigma}$, we are far from the accuracy needed to determine binding energies by methods which make use of the absolute values of D(Z).

On the other hand, when measuring $P_{1s\sigma}(b)$ at different projectile velocities v_i, one can calculate the ratio of those $P_{1s\sigma}(b_i)$-data which correspond to the same R_0 - thus cancelling D(Z). This procedure is based only on the assumption - selfevident for adiabatic collisions - that for a given system the binding energy $E_{1s\sigma}(R_0)$ depends only on R_0 and not on the projectile velocity. We then obtain:

$$(2) \quad E_{1s\sigma}(R_0) = \frac{\hbar v_i v_j \ln\{P_{1s\sigma}(b_i)/P_{1s\sigma}(b_j)\}}{2R_0(v_i - v_j)}$$

with

$$R_0 = a_i + \sqrt{a_i^2 + b_i^2} = a_j + \sqrt{a_j^2 + b_j^2}$$

Up to now $P_{1s\sigma}(b)$ has been measured at several projectile velocities only for two systems: Xe+Au (Z=133) and Pb+Cm (Z=178) . In fig. 1 we show the values for $E_{1s\sigma}(R_0)$ extracted from the experiments according to Eq. (2), whereby the full curve gives the calculated values according to Ref. 3.

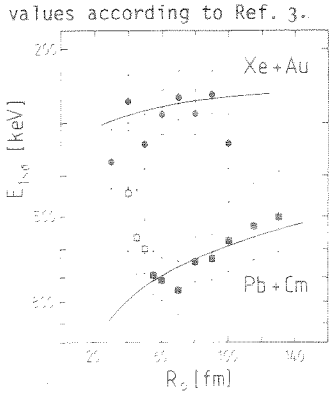


Fig. 1: 1sσ binding energies as function of R_0 extracted according to Eq. (2) from measured $P_{1s\sigma}(b)$-data. The full line gives the theoretical values from Ref. 3.

For Xe+Au the binding energies obtained from Eq. (2) agree fairly well with those from theory. Certainly, the variation of the theoretical energies within the whole covered R_0-range amounts only to ≈ 40 keV and is even smaller than the statistical errors of the "measured" binding energies. Nevertheless, we find here 1sσ binding energies for a very heavy system, directly extracted from experiment, and they coincide within ≈ 10 % with the theoretical values.

In the Pb+Cm system the change in the binding energies as a function of R_0 is much more drastic - due to the very large Z. As for Xe+Au, the agreement with theory is quite satisfactory - but only down to $R_0 \approx 50$ fm (black rectangles in fig. 1). However, conclusions on the 1sσ binding energy in the Pb+Cm system below 50 fm should not be drawn. Probably the premises made in deriving Eq. (1) (cf. the foregoing contribution) are here no longer fulfilled. Looking at these premises one can speculate that the coupling matrix element differs from the expected behaviour ($^1/_R$) for $R_0 \lesssim 50$ fm. Further systematic measurements in the region $Z \gtrsim 150$ are needed.

Another way to gain spectroscopic information - at least in form of a lower bound to the 1sσ binding energy - is possible. Differentiating Eq. (1) with respect to R_0 one obtains:

$$(3) \quad -\frac{d}{dR_0}\left(\ln P_{1s\sigma}(b)\right) = \frac{2}{\hbar v} E_{1s\sigma}(R_0) + \frac{2R_0}{\hbar v} \cdot \frac{d}{dR_0}\left(E_{1s\sigma}(R_0)\right)$$

Now, if both $P_{1s\sigma}(b)$ and $E_{1s\sigma}(R_0)$ monotonically decrease as functions of R_0, Eq. (3) leads immediately to

$$(4) \quad E_{1s\sigma}(R_0) > \frac{\hbar v}{2} \left| \frac{d}{dR_0} \ln P_{1s\sigma}(b) \right|$$

In fig. 2 these lower bounds are shown for Xe+Au together with the theoretical values according to Ref.3. . In this system, the lower bounds coincide nearly with the calculated binding energies, because for small R_0 $E_{1s\sigma}(R_0)$ is practically constant - i.e. the second term of the right side in Eq. (3) remains very small.

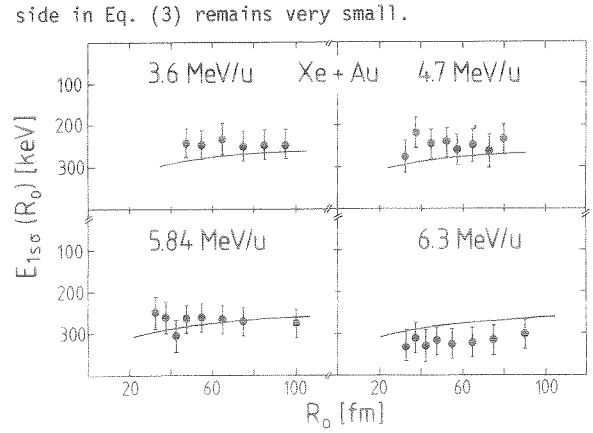


Fig. 2: Lower bounds for the 1sσ binding energy as function of R_0 according to Eq. (4). The full line gives the theoretical energies according to Ref.3.

[1]B.Müller et al. Z. Physik A285, 27(1978)

[2]H.H.Behncke et al. Z. Physik A288, 35(1978)

[3]G.Soff et al. Phys. Scripta, 17, 417(1978)

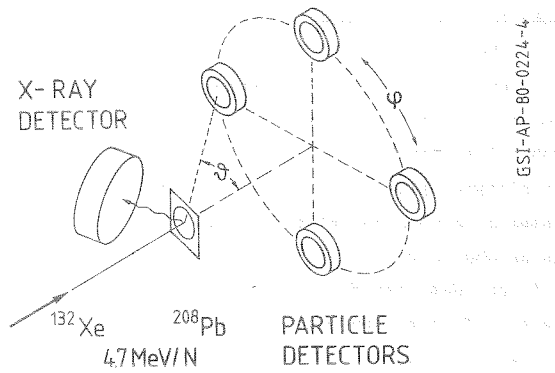
1sσ Excitation Probability for Small Impact Parameter Xe+Pb Collisions [B]

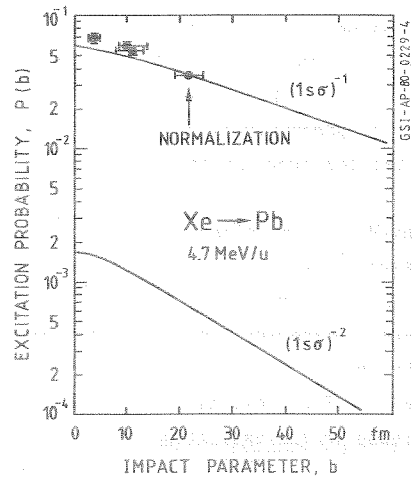
P.H. Mokler, F. Bosch, D. Liesen, W.A. Schönfeldt
GSI Darmstadt

R. Schuch
I. Phys. Inst. Univ. Heidelberg

For 4.6 to 4.7 MeV/amu $^{132}Xe \rightarrow {}^{208}Pb$ collisions contradicting dependences of the 1sσ-excitation probability, $P_{1s\sigma}(b)$, as a function of the impact parameter, b, are found for small b ($\lesssim$ 40 fm) by different authors[1,2]. For b values around 40 fm both measurements agree within the normalization errors and fit closely to the $P_{1s\sigma}(b)$ data for 4.7 MeV/amu Xe → Au collisions at larger internuclear distances[3]. The contradicting small impact parameter results are gained using different experimental methods : The line-shape method of Greenberg et al.[1] integrates over all azimuth angles ∅, whereas the coincidence method used by Anholt et al.[2] yields only $P_{1s\sigma}(b)$ values for one fixed azimuth angle. Hence, we studied experimentally the ∅ dependence of the 1sσ excitation using the particle x-ray coincidence method. In fig. 1 a sketch of the used set up is shown. For the detection of scattered ions two sets of four identical surface barrier detectors were mounted at a fixed laboratory angle, Θ_{LAB}, of 27.5° (± 2.5°) and 50° (±8°) at four different azimuth angles ∅ = 0°, 180°, and 90°, -90° (∅ = 0° corresponds to the x-ray detection direction). The particle detectors allow via energy discrimination to distinguish between scattered ^{132}Xe ions and ^{208}Pb recoils. Hence, four impact parameters could be measured with the two sets of particle detectors.
For all measured impact parameters no ∅ dependence was observed within the statistical uncertainty. In fig. 2 our $P_{1s\sigma}(b)$ values integrated over all measured ∅ angles are shown together the prediction of Ref. 4 ($P_{1s\sigma}(b) = 1/2\ D(Z)\{\exp -2R_0 q_0\}$). The data are normalized to the prediction at b = 22 fm ($\Theta^{Xe}_{LAB} = 27.5° \pm 2.5°$). The $P_{1s\sigma}$ values increase for decreasing impact parameter. This is in clear contrast to the line shape analysis data showing a maximum for the excitation probability around 15 fm. But we are also not in agreement with the coincidence data of Anholt et al. which show a plateau in the excitation at small impact parameters. We cannot give an explanation for this last discrepancy. For the line shape analysis data we point out, that hypersatellite contributions are not considered in the original data evaluation. Looking on the steep dependence of $P_{1s\sigma}$ one expects an even steeper dependence on b for double hole excitation, $P_{(1s\sigma)^2} = 2 \times (1/2\ P_{1s\sigma})^2$. Due to this steep dependence hypersatellite contributions will not show up as a peak in the x-ray spectra observed at 0°, but will contribute widely to the important high energy tail of the K x-ray spectra. This fact will possibly be responsible for the peak in the $P_{1s\sigma}(b)$ data extracted via line shape analysis. Additionally, we mention that the underlying MO contributions have also to be subtracted correctly during the line shape analysis.

[1] J.S. Greenberg, H. Bokemeyer, H. Emling, E. Grosse, D. Schwalm, F. Bosch, Phys. Rev. Lett. 39 (1977) 1404.
[2] R. Anholt, W.E. Meyerhof, Ch. Stoller, Z. Phys. A291 (1979) 287.
[3] D. Liesen, P. Armbruster, H.-H. Behncke, S. Hagmann, Z. Phys. A289 (1979) 333.
[4] D. Liesen, P. Armbruster, F. Bosch, S. Hagmann, H. Schmidt-Böcking, P.H. Mokler, H.J. Wollersheim, R. Schuch, J.B. Wilhelmy, Phys. Rev. Lett. (1980) to be published.





Inner Shell Excitation Mechanisms in Close Impact Parameter Collisions Between Ni Ions and Solid Targets [B]

D. Maor, B. Rosner
Technion, Haifa, Israel

D. Liesen, P.H. Mokler
GSI Darmstadt

H. Schmidt-Böcking
Universität Frankfurt

R. Schuch
Universität Heidelberg

Thin solid targets of Ni, Zr, Ag, Te, and Au were bombarded by Ni ions at 1.4 MeV/u. Ni- and Zr-K shell, as well as Te- and Au-L shell excitation probabilities as a function of impact parameter (P(b)) below 0.1 a.u. were determined by coincidence measurements between scattered particles and characteristic x rays.

The K-shell excitation probability in all asymmetric systems increases monotonically with decreasing impact parameter and flattens out at the smallest impact parameters. The impact parameter for which the differential cross-section $d\sigma = 2\pi bP(b)db$ reaches its maximum is found to be almost equal to the adiabatic radius, $r_{ad.} = \hbar v/E_B^{u.a.}$, (v the projectile velocity, $E_B^{u.a.}$ the electron binding energy in the united atom). This is demonstrated in fig. 1 where the K-shell excitation probability for Ni on different targets, normalized to its plateau value at low impact parameters (P*) is presented as a function of the impact parameter scaled to the adiabatic radius. In this presentation the different data are found to fall on one common curve. The Ni → Te data are not included in fig. 1; they contain a contribution from vacancy sharing with higher lying orbitals. After its subtraction, they fall on the common curve, too.

This behaviour indicates that at these impact parameters the dominating mechanism for K-shell vacancy production is direct ionization out of the united atom orbitals. The plateau value for the K-shell vacancy production probability is between 10 % and 45 % for Ni in the different systems and about 0.6 % for Zr. These values are found to be proportional to $(E_B^{u.a.})^{-2}$. Using this dependence and the curve of fig. 1, one can evaluate the contribution of direct ionization to P(b) for the symmetric Ni-Ni system. After subtracting this from the measured values, one is left with a curve typical for rotational coupling. However, the adiabatic peak appears at lower impact parameters and with a height less than predicted by the scaling law of Taulbjerg et al.[1].

Fig. 2 shows the P(b) results for Te-L. One notices a strong increase in the excitation probability at small impact parameters. This increase is interpreted as a "kinematic peak", which originates from the spatial overlap between molecular wave functions upon a sudden turning of the internuclear axis. In this case, it is a $3d\sigma$-$3d\pi$ coupling and quantum-mechanical calculations show the excitation probability to be proportional to $\sin^2 2\Theta_{c.m.}$. The solid line in fig. 2 represents this function and the agreement with the data seems satisfactory although an additional measurement with better statistics and extended to even higher scattering angles would be desirable.

[1] K. Taulbjerg, J.S. Briggs, and J.S. Vaaben, J. of Phys. B9, 1351-1370 (1976).

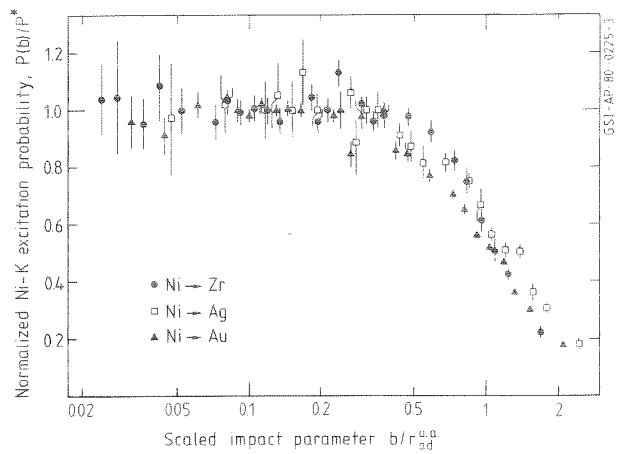


Fig. 1

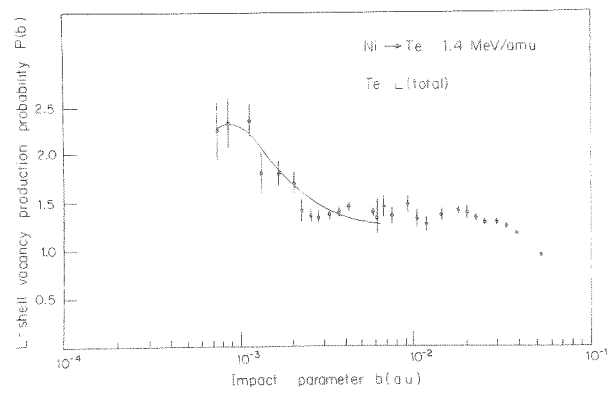


Fig. 2

Collision Broadening in MO-Electron Energy Spectra in Kr-Kr and Kr-Ar Collisions

A.P. Shergin
on leave from A.F. Ioffe Physical-Technical Inst., Leningrad
R. Mann, H.F. Beyer, and E. Pfeng
GSI Darmstadt

Electron energy spectra produced in $Kr^+ \rightarrow Ne$, Ar, Kr collisions at projectile energies 50 keV $\leq E_p \leq$ 400 keV have been measured under an observation angle $\theta = 90^0$ with respect to the projectile impact. In the Kr → Kr and Kr → Ar spectra broad bands distributed between 100 and 500 keV are observed (fig. 1). Such bands were found earlier[1,2] and attributed to Auger transitions in quasimolecules at small internuclear distances, showing a characteristic long exponential fall off in the high energy region. These tails were studied now in dependence on the projectile velocity v_p and target atomic number Z_t. From MO x-ray experiments the existence of high energy photons above the transition energy $E_x(R_0)$ at the turning point R_0 are shown and explained by the nuclear motion[3]. Obviously, the same collision broadening (cb) mechanism contributes to the MO-electron spectra. The exponential slope of cb is characterized by a width Γ corresponding to an energy interval within which the cross section is reduced by a factor of two[3]. Different authors give different dependences of Γ on v_p ($\Gamma \sim v_p^{1/2}$)[3,4], ($\Gamma \sim v_p$)[5], ($\Gamma \sim v_p^{2/3}$)[6,7] for collisions with specified impact parameters b. Electrons with largest energies are assumed to be produced in head on collisions which may select $b \sim 0$ although in the experiment we do not discriminate between impact parameters. Fig. 2 shows the experimental values Γ for Kr^+-Ar, Ar^+-Kr, and Kr^+-Kr collisions at different v_p together with data of other authors[1]. The experimental results are fitted by $\Gamma \sim v_p^{2/3}$, agreeing with predictions of Nikulin[6] and Fritsch[7]. Finally, a Z-dependence of cb expected to follow a $Z^{4/3}$ law[6,7] was tested in this experiment. Assuming screened $Z_{eff} = 44$ and 26 for 4p electrons in Hf (Kr-Kr case) and Xe (Kr-Ar case) according to Slater rules, a ratio $\Gamma(44)/\Gamma(26) = 2$ results which is close to the experimental value of 1.5.

From these experimental results it is conclusive that qualitative features of MO-electron spectra in the classically forbidden region can be described by theoretical models.

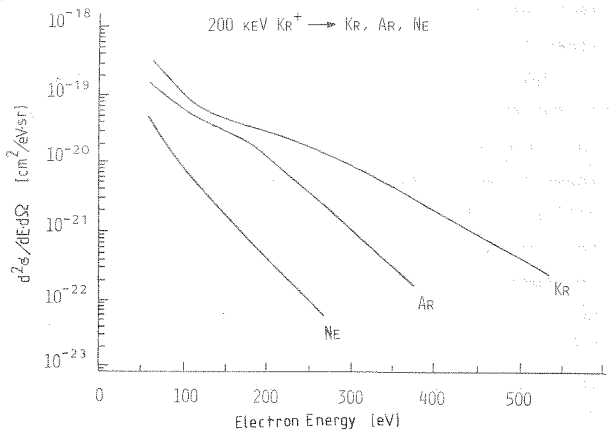


Fig. 1: Electron energy distribution from 200 keV $Kr^+ \rightarrow$ Kr, Ar, Ne collisions.

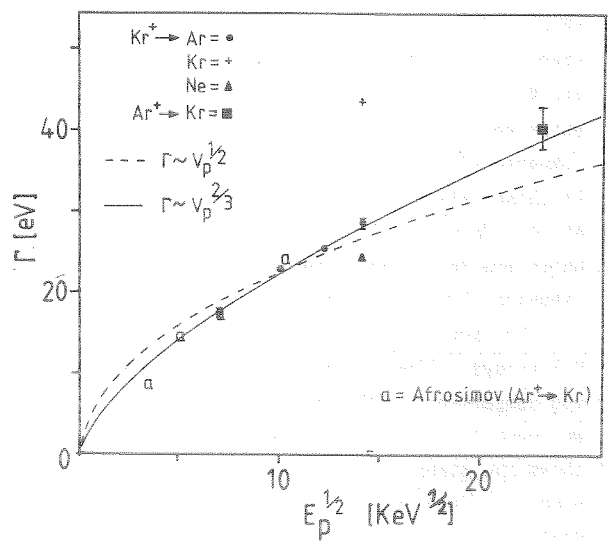


Fig. 2: Width Γ of collision broadening of continuous electron energy distributions versus square root of projectile energy. The Ar^+ projectile energies are multiplied by a factor 2,1 corresponding to the ratio of Kr and Ar masses.

[1] V.V. Afrosimov, Yu.S. Gordeev, A.N. Zinoviev, A.A. Korotkov, A.P. Shergin, X ICPEAC 1977 (p. 924)
[2] Yu.S. Gordeev, P.H. Woerlee, H. de Waard, and F.W. Saris XI ICPEAC 1979 (p. 746)
[3] J.H. Macek and J.S. Briggs, J. Phys. B. 7 1312 (1974)
[4] H.D. Betz, F. Bell, H. Panke, W. Stehling, E. Spindler, and M. Kleber, P.R.L. 34 1256 (1975)
[5] B. Müller, Proc. IX ICPEAC 1975 (p. 481)
[6] V.K. Nikulin, Abstr. VI ICAP 1978 (p. 379)
[7] W. Fritsch, U. Wille, J. Phys. B 12 L335 (1979)

Capture of Electrons Into Swift Heavy Projectiles

W.A. Schönfeldt, F. Bosch, D. Liesen, D. Maor, P.H. Mokler
GSI Darmstadt

The capture of electrons into heavy highly ionized projectiles at 1.4 MeV/u was investigated via x-ray emission after heavy ion collisions. Such measurement can be studied for charge-state dependent x-ray emission of projectiles under single collision conditions. Charge-state dependent x-ray emission is well known e.g. for 1.4 MeV/u Cu^{q+} → Kr collisions (Ref. 1) : L-vacancies of the projectile are transferred via radial and $2p\pi$-$2p\sigma$ rotational couplings into the K shell of the projectile. There is an increase in K x-ray emission observed after collisions for increasing incoming L-vacancy numbers in the projectile. Preceeding distant collisions decrease the number of projectile L vacancies via electron capture. Changing the pressure p in our gas cell and/or the length l in front of the observation region we increase the number of distant collisions. Hence, preceeding distant charge changing collisions can be studied from the dependence of the x-ray yield on the product p · l. (This is an analogy to the decay laws of radioactivity).

In this sense we have measured Ni^{q+} → Kr with zero to four incoming L vacancies in the projectile. The results are shown in fig. 1.

If the atomic numbers of projectile and target are too different, K x-ray emission after close collisions are too insensitive to the incoming number of L vacancies. However, we may use also L x rays with energies larger than ≳ 1 keV as an indicator for the incoming charge state. For 1.4 MeV/u Kr^{q+} → Ar collision we measured the Kr-L x-ray emission up to one incoming L vacancy. Our extracted electron capture cross section for Kr^{27+} is compared with the cross sections via magnetic selection of charge states behind gas targets (Ref. 2). The step at q = 26 (fig. 2) is interpreted as shell effects, which are not incorporated in the theory of Bohr and Lindhard. The large energy shifts observed up to $\Delta E \gtrsim 1.2$ keV for 1.4 MeV/u projectiles (Kr-L, Sm-M, and U-N x-rays) allow an identification of the transitions via comparison to HFS calculation.

We found evidence for the capture of electrons. Fig. 3 shows the strong increase in x-ray yield ($I \sim q^{18}$) if the number of incoming vacancies is enlarged for Sm^{q+} → Ar collision. However, a detailed interpretation is not yet available.

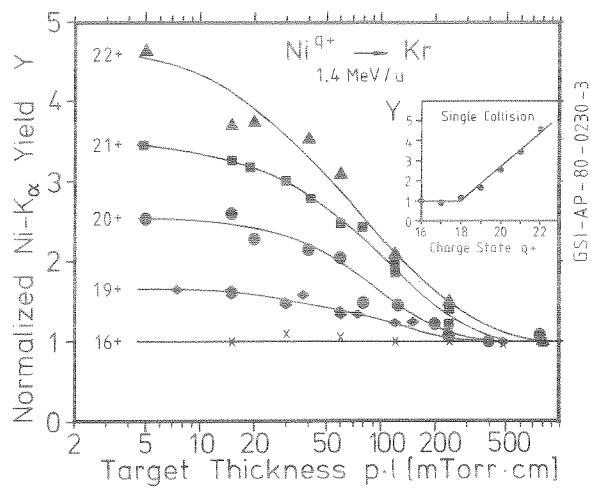


Fig. 1

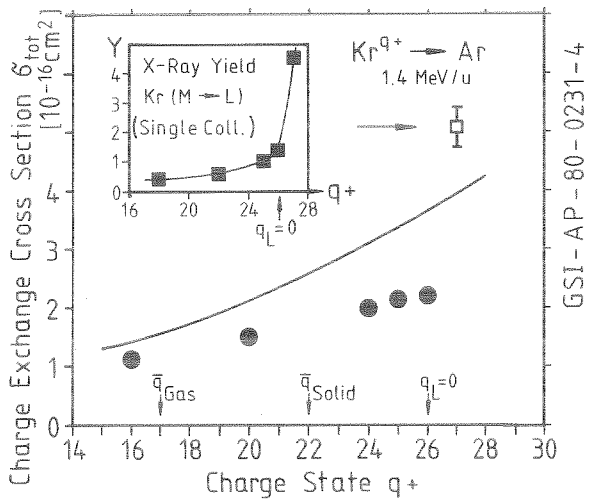


Fig. 2

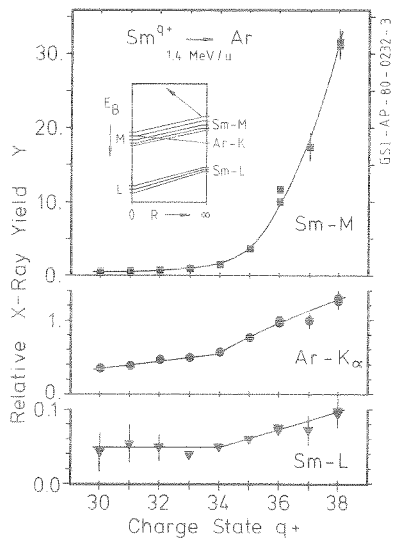


Fig. 3

[1] A. Warczak et al., Z. Phys. A285 (78) 235
[2] W. Erb, GSI-Bericht P-7-78

Projectile Charge State Dependence of the Average L- and M-Shell Excitation in K-Shell Ionizing Collisions

A. Warczak
On leave from the Jagellonian University, Cracow, Poland
D. Liesen, P.H. Mokler
GSI Darmstadt

The analysis of the energy shift and intensity of characteristic K x-rays emitted after heavy ion-atom collisions allows an estimation of the simultaneous L- and M-shell ionization. The influence of the projectile charge state on this simultaneous target atom ionization was investigated. 1.4 MeV/amu Xe ions from UNILAC bombarded thin Ar and Kr gas targets under single collision conditions. The target K radiation was recorded with a Si(Li) detector. The charge state q of the incoming projectile was varied between 24 and 32 using a stripper foil and magnetic charge state selection[1]. The energy shift of the target K_α line and the target K_β/K_α ratio were analysed as a function of the charge state q of the incoming Xe ions.

In fig. 1 the results for Ar K-radiation are shown. According to calculations of Bhalla[2] and Burch et al.[3] it is possible to estimate simultaneous L- and M-shell ionization of Ar. For the lowest charge state q=24 we found 2-3 L and about 5 M electrons are removed together with an electron from the K-shell. For higher q (29-32) a saturation state in the L and M ionization is reached (see fig. 1). This state is related to about 5 L and 6 M vacancies. Such a saturation effect of target atom ionization was also observed by Beyer[4] for collisions of heavy highly-ionized ions with Ne atoms. Increasing the atomic number of the target (Kr) such an equilibrium is not reached anymore in the range of projectile charge states under consideration (see fig. 2). From the analysis presented above we deduce that for suitably high projectile charge states we produce few electron Ar systems with cross sections at least as high as the cross section for the K-shell excitation.

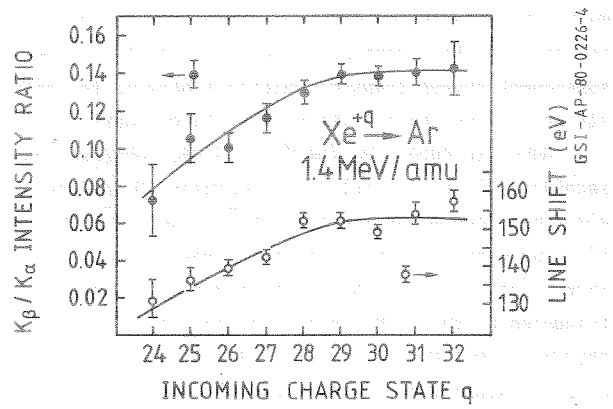


Fig. 1: The charge state dependence of the Ar K_α line shift and Ar K_β/K_α ratio for Xe+Ar collisions; Solid line serves as eyeguide.

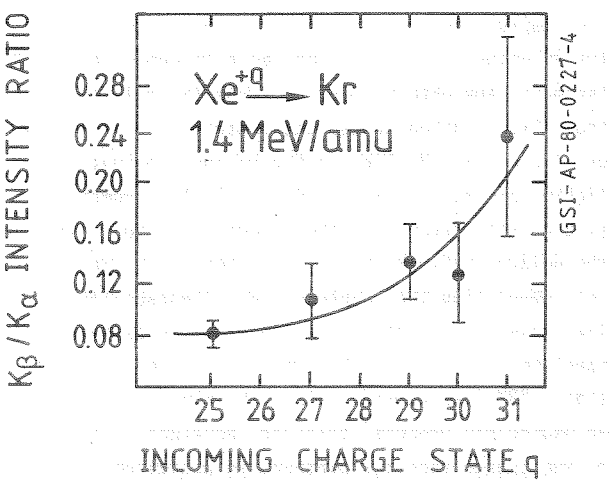


Fig. 2: The charge state dependence of Kr K_β/K_α ratio for Xe+Kr collisions.

[1] A. Warczak et al., Z. Phys. A285, 235 (1978).
[2] C.P. Bhalla, Phys. Rev. A8, 2877 (1973).
[3] D. Burch et al., Phys. Rev. A9, 1007 (1974).
[4] H.F. Beyer, GSI-Report 79-6.

Prompt and Delayed K-Auger Electron Emission from Slow Target Recoil Ions

R. Mann, H.F. Beyer
GSI Darmstadt

F. Folkmann
Universität Aarhus

The most important property of a heavy ion light target atom collision is the high degree of target ionization combined with a small recoil energy $E_r \lesssim 5$ eV. Thereby, mainly metastable few electron states are excited being the base for the creation of specific spectral lines by subsequent charge transfer reactions between the highly stripped target recoil and neutral target particles[1].

Here, we report on the first direct observation of secondary electron population processes. Ne K-Auger electrons induced by 1.4 MeV/u Kr^{18+} and Ar^{12+} projectiles were measured at different target pressures and target constituents. The electron detection was triggered by the 27 MHz pulsed projectile signal, thereby prompt and delayed ($t \gtrsim 8$ ns) electron emission could be separated. Figure 1 exhibits total and delayed spectra from Kr^{18+} impact illustrating that most lines are secondarily excited, only the $^4p^o$ line from the metastable $(1s2s2p)^4P^o_{5/2}$ ($T \approx 9$ ns) state may arise from direct excitation appearing also in the delayed. The occurance of the "capture lines" $^3S4$, $^3P4$, $^3S5^{1,2}$ in the delayed spectrum gives evidence for a selective capture process. Moreover, cascade contributions from the "capture shells" (n = 4,5) to the L shell producing the $^4p^e$-line ($T \lesssim 0.2$ ns) and an enhancement of the $^4p^o$ intensity are obtained as well from the delayed spectrum. Fig. 2 demonstrates the contribution of directly excited Li- and Be-like configurations dominating for lighter projectile impact (Ar^{12+}) in the prompt spectrum (± 5 ns with respect to the target collision), whereas the delayed reflects the minor intensity of He-like core ions generating the "capture"- and "cascade-lines". At low pressure secondarily excited lines disappear in the spectrum, only the primary contribution of the metastable $^4p^o$ line remains. Since the electron capture is an exothermic process[3] transferring kinetic energy to the charge exchange partner, an additional kinematic line broadening of certain Auger lines are expected. This was found from the $^4p^o$ and $^4p^e$ lines, being systematically broader in the delayed spectra (except at 1 mTorr) in comparison to the prompt (table).

ΔE [eV]	$^4p^o$	$^4p^e$	
	1.7±0.2	2.2±0.2	50 mTorr Ne (prompt)
	2.4±0.2	3.2±0.2	50 mTorr Ne (delayed)
	1.8±0.2	-	1 mTorr Ne (delayed)

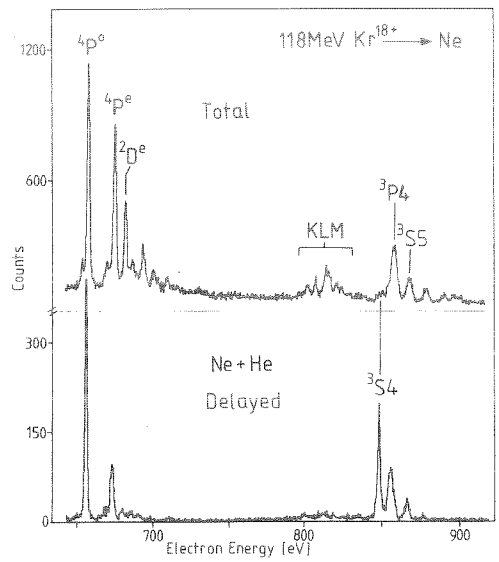


Fig. 1: Total and delayed ($t \geq 10$ ns) Ne K-Auger spectra from (1.4 MeV/u Kr^{18+}) impact on pure Ne and Ne-He (50 %) mixture.

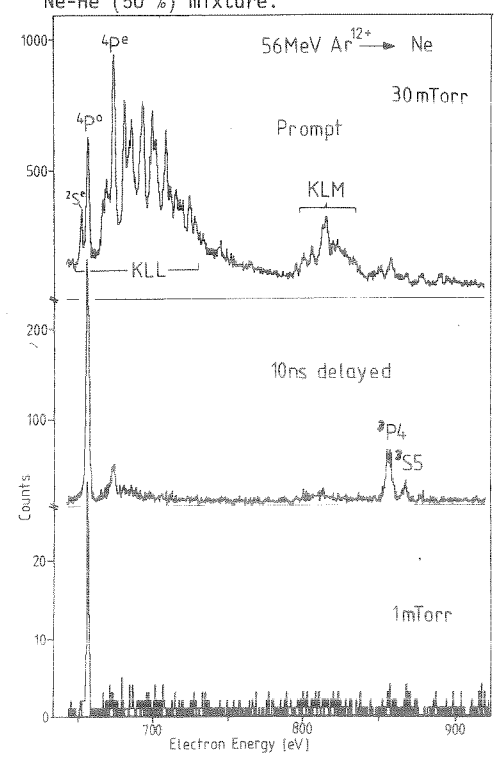


Fig. 2: Prompt (± 5 ns) and delayed (≥ 10 ns) Ne K-Auger spectra from Ar^{12+} impact.

[1] R. Mann, F. Folkmann, J. de Physique, C1-236 (1979)

[2] Annual Report GSI 79-11 p. 112-114

[3] A. Salop, R.E. Olson, Phys. Rev. A13 1312 (1976)

Investigation of Few Electron States in Target Molecules After Heavy Ion Impact

R. Mann, H.F. Beyer
GSI Darmstadt

F. Folkmann
Institute of Physics, University of Aarhus

It was pointed out recently[1,2] that in heavy ion light target atom encounters few electron states are excited dominantly, arising from direct and secondary electron populations. The degree of both contributions depend on the "ionization power" of the heavy ion impact. However, for molecular targets the multiple ionization of single atoms may be covered by a fast electron redistribution[3] of the dissociating molecule.

CH_4, NH_3, H_2O, CO_2, and SF_6 gas targets were bombarded with 1.4 MeV/u Kr^{18+} and Ar^{12+} projectiles. The K-Auger electron emission from highly stripped molecular atoms measured in time relation to the exciting beam bunches (27 MHz) allows to distinguish between direct excitation (including a fast electronic rearrangement during the molecular dissociation) and a delayed population of high Rydberg states due to secondary electron capture processes. The spectra from light molecules (CH_4,NH_3 H_2O) containing 10 electrons are quite similar to that of a monoatomic Ne target[2] and are dominated by the secondary excitation. Heavier target molecules change the excitation processes because of two facts: 1) The contribution of highly stripped, metastable core ions is lowered as the number of electrons increases, indicating limits of the excitation of few electron states in molecular atoms by heavy ion projectiles. 2) The kinetic energy $E_K \approx 100$ eV of molecular fragments, inferred by the Coulomb explosion[5], opens the study of electron capture processes at somewhat higher collision energies in contrast to low energy ($E_r \lesssim 5$ eV) target recoil ions[2] (fig. 1). A strong line broadening[5] reflects the kinematics of the Coulomb explosion, appearing for the metastable $^4P^o$ line more precisely in the delayed spectrum at low target pressure because of drastic suppression of continuous electron background and secondary cascade populations[2]. The delayed spectrum of fig. 1 arises predominantly from Li-like configurations, indicating still a remarkable intensity of He-like collector ions produced in the primary collision. Furthermore, a small contribution of He-like hypersatellits LN is noticed, attributed to a selective electron capture into the n=4 shell of a 2s core ion. Quite different spectra are obtained from fluorine, bombarding SF_6 molecules with Ar^{12+} ions (fig. 2). Many blending lines of multiple electron configurations dominate the total spectrum. A fast rearrangement of molecular electrons[6] into highly stripped F atoms may respond a multistate population. A small remainder of metastable components as $(1s2s2p)^4P^o_{5/2}$ is found in the delayed spectrum demonstrating that only a small fraction of highly stripped F ions escape from the molecule prior to an electronic recombination.

[1] R. Mann, F. Folkmann, and H.F. Beyer, J. Phys. B to be published.
[2] This report, 1 page before.
[3] Physics News in 1977, p. 18.
[4] R. Mann, F. Folkmann, R.S. Peterson, Gy. Szabó, and K.O. Groeneveld, J. Phys. B11 3045 (1978).

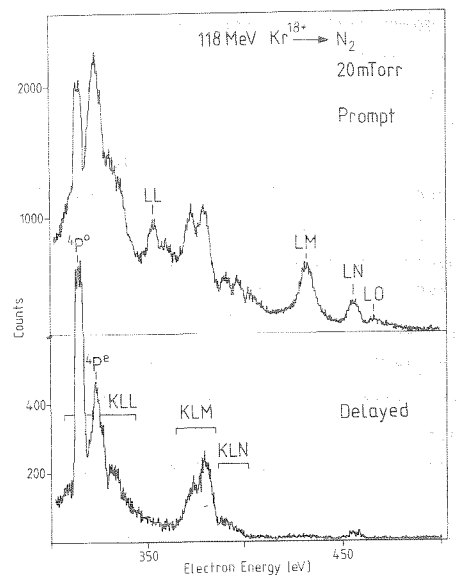


Fig. 1: Prompt and delayed ($t \geq 10$ ns) Auger electron emission from N_2 target after Kr^{18+} (1.4 MeV/u) impact.

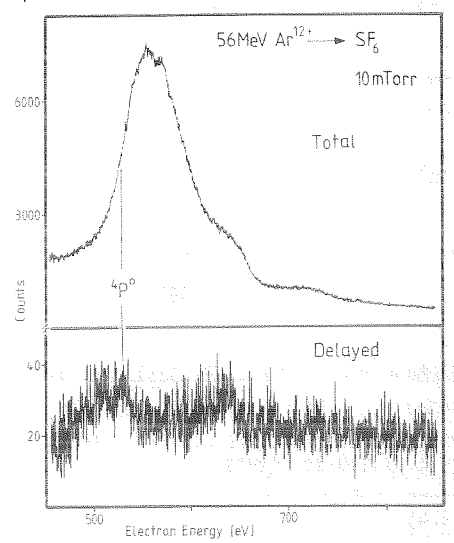


Fig. 2: Total and delayed fluorine Auger electron spectra from SF_6 molecules after Ar^{12+} bombardment.

Time Dependent X-Ray and Auger Electron Emission of Beam-Foil Excited Ions

H.D. Dohmann, R. Mann, E. Pfeng
GSI Darmstadt

The K-x-ray and K-Auger electron emission from Ar^{12+} projectiles (1.4 MeV/u) penetrating thin carbon foils (40 µg/cm^2) was studied behind the foil. At short distances (X ≤ 5 mm) behind the foil many overlapping lines dominate the spectra (fig. 1 and fig. 2) attributable mainly to promptly decaying Li-, Be-, and B-like configurations. They originate from various cascade feedings[1] from high lying orbits (principal quantum number n ≥ 12, orbital quantum number l ≳ n-1) into metastable core states. At larger foil distances (X ≥ 10 mm) only lines from metastable $(1s2p)^3P^o_2$ and $(1s2s2p)^4P^o_{5/2}$ terms arise. This is demonstrated in the contour plots of fig. 1 for the x-ray spectra, in fig. 2 for the Auger electrons, respectively. In order to extract accurate lifetimes T from the observed time behaviour of the metastable states, it is necessary, to take into account all cascade processes[3], which populate and depopulate these states[1]. In the x-ray measurements using a crystal spectrometer[2] in first order resolution, the $(1s2p^2)^4P^e_{5/2} \rightarrow (1s^22p)^2P^o_{3/2}$ transition and transitions from Be-like configurations $(1s2s2p^2)$ are not separated from the $(1s2s2p)^4P^o_{5/2} \rightarrow (1s^22s)^2S^e_{1/2}$ transition, however, the corresponding Auger transition $(1s2s2p)^4P^o_{5/2} \rightarrow (1s^2)^1S_o + e^-$ (fig. 2) is free of line blending. Therefore, and due to high intensities in the Auger channel, an accurate lifetime $T(^4P^o_{5/2})=(585 \pm 4)$ps was obtained, agreeing well with theoretical predictions[6] (Table).

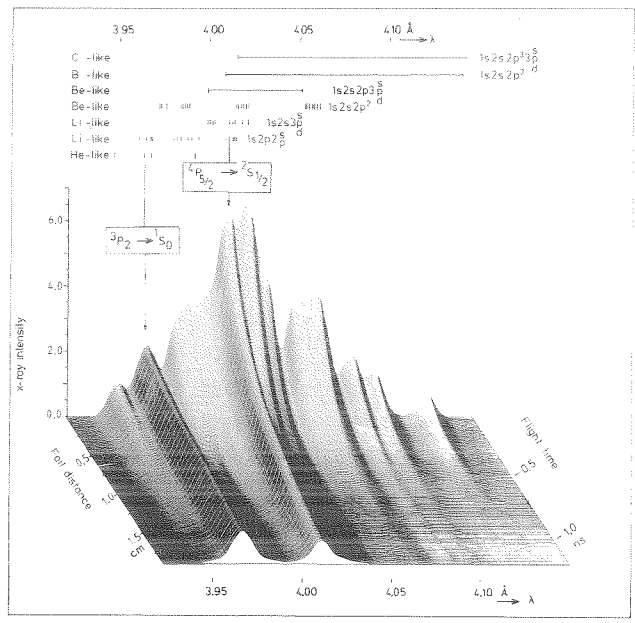


Fig. 1: Contour plot of delayed observed x-ray spectra from 1.4 MeV/u Ar^{q+} projectiles after penetrating a carbon foil (40 µg/cm^2).

Table Theoretically predicted values of transition probabilities P(M2), and the lifetimes $T_1 = (P(M2)+P_1(\text{Auger}))^{-1}$ and T_2 for the $^4P^o_{5/2}$ term of Ar^{15+}, corresponding to $P_1(\text{Auger}) = 1.554 \times 10^9$/s and $P_2(\text{Auger}) = 1.463 \times 10^9$/s of references 5 and 4, respectively.

P(M2) [10^9/s]	T_1 [ps]	T_2 [ps]
0.3138[4]	535	563
0.285 [5]	544	572
0.24 [6]	557	587

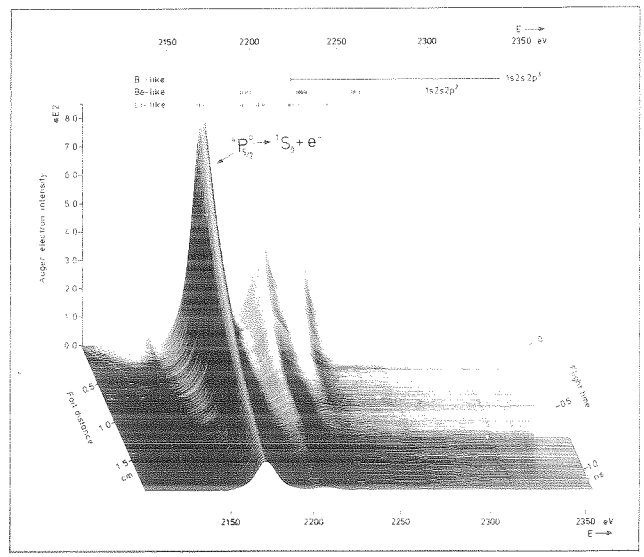


Fig. 2: Contour plot of delayed Auger electron spectra from 1.4 MeV/u Ar^{q+} projectiles, observed behind a carbon exciting foil.

[1] H.D. Dohmann and R. Mann Z.P. A291, 15 (1979)
[2] H.D. Dohmann, E. Pfeng Z.P. A288 29 (1978)
[3] H.D. Dohmann, R. Mann, and E. Pfeng, Annual Report GSI 79-11 p. 110-111 (1979)
[4] K.T. Cheng, C.P. Lin, W.R. Johnson, Phys. Lett. 48A 437 (1974)
[5] U.I. Safranova, V.S. Senashuko, I.A. Shavtralishvili, IZV VUZ FIZ (USSR) no. 12, 13 (1977) Translation Sov. Phys. J. (USA) (1978)
[6] Interpolated by a $(Z-0.61)^8$ scaling from C.D. Lin, W.R. Johnson, A. Dalgarno, Phys. Rev. A15 154 (1977)

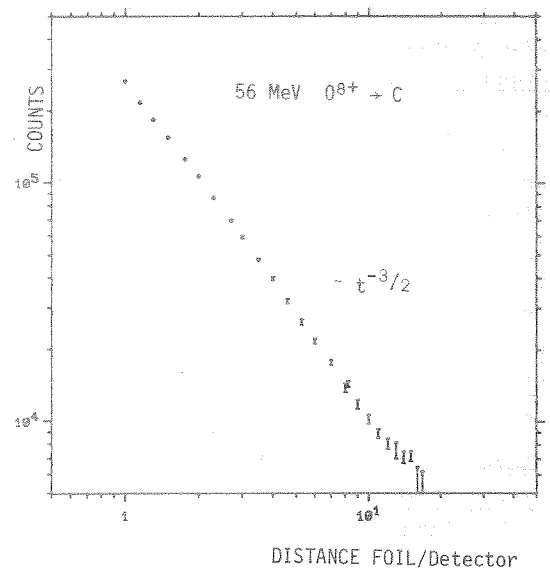
Beamfoil-Spectroscopy on Hydrogenlike Oxygen

P. von Brentano, G. Dehmelt, A. Georgiadis, L. von Gerdtell, H. D. Sträter
Institut für Kernphysik der Universität zu Köln

At the Cologne tandem accelerator we prepared a 56 MeV, 200 nA O^{8+} beam with a two-foil technique. 20 % of the completely ionized O^{8+} beam is converted to an excited H-like O^{7+} beam with a thin (6 $\mu g/cm^2$) pick-up foil in our apparatus.

The decay (2p→1s, E = 653 eV) of the H-like O^{7+} ions was measured over a length of 50 cm with an argon-methan proportional counter. The decay shows a power law ($t^{-\alpha}$,α = 3/2) time function [1].

With a photomultiplier we observed the transitions n = 9→8 (λ = 4345 Å). The time dependence of this decay is also disturbed by cascading effects. We intend to make further measurements in this subject.



Decay of the H-like Oxygen

1) Multiply Excited States in the Two and Three Electron Oxygen Ion,
D. L. Matthews, W. J. Braithwaite,
H. H. Walter, C. F. Moore,
Phys. Rev. A, Vol. 8, 1397-1402 (1973)

Konferenzbeiträge:

Verh. DPG 9, München, Germany, March 1980
A. Georgiadis, G. Dehmelt, L. von Gerdtell,
H. D. Sträter, P. von Brentano:
Beamfoil Spectroskopie am Wasserstoffähnlichen Sauerstoff

G

Charge transfer involving multiply charged ions

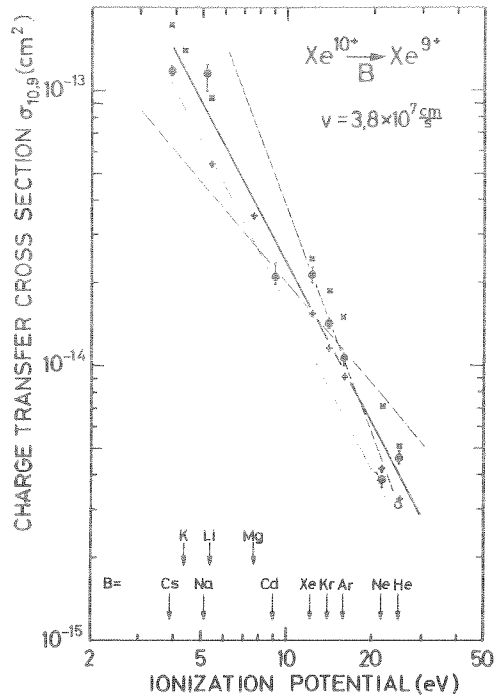
A. Müller, Ch. Achenbach, P. Kester, K. Miethe,
K. Rinn, W. Seim, I. Wirkner-Bott and E. Salzborn
Institut für Kernphysik, Strahlenzentrum, Universität Giessen

The research program on electron capture by multiply charged ions included three main topics:

1. Investigation of systematic dependences of charge transfer in collisions of highly charged ions and neutral particles.
Cross sections $\sigma_{10,9}$ for the capture of one electron by 100 keV Xe^{10+} ions from atoms B with a maximum range of ionization potentials I_B have been measured in order to clarify the validity of scaling laws and theoretical predictions[1]. The results are shown in Fig. 1. Cross sections larger than 10^{-13} cm^2 have been observed for Cs as a target. On the whole, $\sigma_{10,9}$ shows approximately a quadratic decrease with increasing I_B.

2. Development and calibration of single particle detectors for ions with keV energies.
For the measurement of small cross sections respectively low ion fluxes detectors have been constructed which are based on the production of secondary electrons by ions incident on a metal surface. A channeltron serves for the multiplication of these electrons and provides nano-second pulses with a charge of about 10^{-11} Cb which can be counted by conventional techniques. The obtained results are so encouraging that a further improvement in respect to a larger detector area with uniform counting efficiency and higher counting dynamics seems possible.

3. Preparation of special projectile ions and targets for atomic collision experiments.
Working conditions have been found for the electron beam ion source to produce beams of Xe^{12+} ions . Pure beams of Xe^{10+} ions (isotope 132) have been used for the measurements described in section 1. A further aim is the production of heavy metal ions in high charge states and high specific charges for light ions. For this purpose an oven has been built which can be heated up to 800° C. First tests included the evaporation of lithium and bismuth. Furthermore, a target of atomic hydrogen based on the dissociation of H_2 molecules in a hot furnace has been constructed and will soon be used in charge transfer experiments.



Cross sections $\sigma_{10,9}$ for one-electron capture by 100 keV Xe^{10+} ions from various target atoms B as a function of the ionization potential I_B of the atoms. ● Müller et al.[1] (the targets B used are indicated by the lower row of elements B); —— least square fit of the experimental data points with a power function of I_B; ----scaling law[2]; ....theory of Presnyakov and Ulantsev[3]; × theory of Grozdanov and Janev[4]; + theory of Chibisov[5]; ○ classical trajectory Monte-Carlo calculation of Olson[6]; -·-·-·absorbing sphere model of Olson and Salop[7].

[1] A.Müller, Ch.Achenbach and E.Salzborn, Phys.Lett. 70 A, 410 (1979)

[2] A.Müller and E.Salzborn, Phys.Lett. 62 A, 391 (1977)

[3] L.P.Presnyakov and A.D.Ulantsev, Sov.J.Quant. Electronics 4, 1320 (1975)

[4] T.P.Grozdanov and R.K.Janev, Phys.Rev. A 17, 880 (1978)

[5] M.I.Chibisov, JETP Lett. 24, 46 (1976)

[6] R.E.Olson, Phys.Rev. A 18, 2464 (1978)

[7] R.E.Olson and A.Salop, Phys.Rev.A14,579 (1976)

Ionisation of Argon Ions by Electron Impact [G]

R. Becker, R. Frodl, H. Klein, Institut für Angewandte Physik, Universität Frankfurt/Main

A. Müller, E. Salzborn, Institut für Kernphysik, Universität Gießen

P. Varga, F. P. Viehböck, H. Winter, Institut für allgemeine Physik, Technische Universität Wien

In a crossed beam experiment[1,2] cross sections for multiple ionisation of singly (fig. 1) and multiply ionised (fig. 2) argon ions have been measured[3]. In general, with increasing number of electrons being removed the cross sections decrease considerably; but at electron energies above the threshold for L-shell ionisation I_i^L the curves show a remarkable step. This suggests that besides the simultaneous removal of outer electrons, which is more unlike with increasing numbers of electrons involved, the production of inner shell vacancies by electron impact is important for multiple ionisation of multiply charged ions.

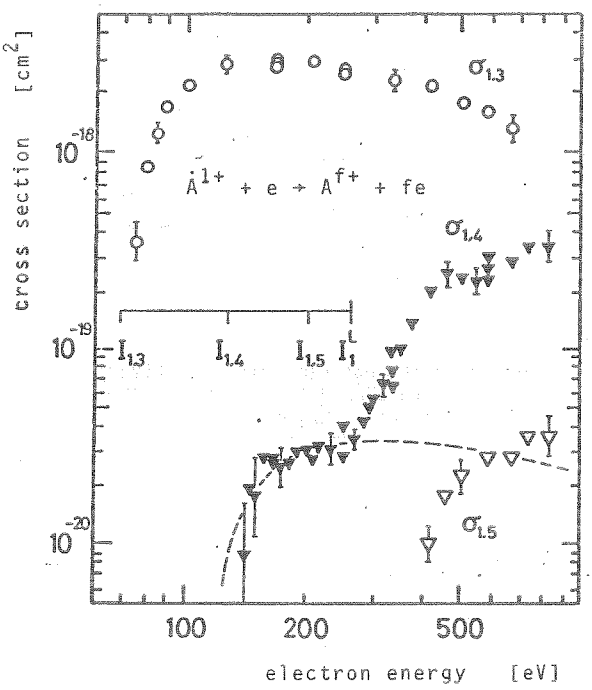


Fig. 1 Measured cross sections for multiple ionisation of singly charged argon

In a separate experiment* the production of metastable ions by electron impact on noble gases has been studied[4]. The strong decrease of the portion of metastable ions with increasing electron energies (measured now up to 300 eV) gives confidence that the ion beams used in the crossed beam experiment have negligible metastable content. This is due to their production at much higher electron energy under low vacuum conditions. Therefore the cross sections reported here can be ascribed to ground state ions only.

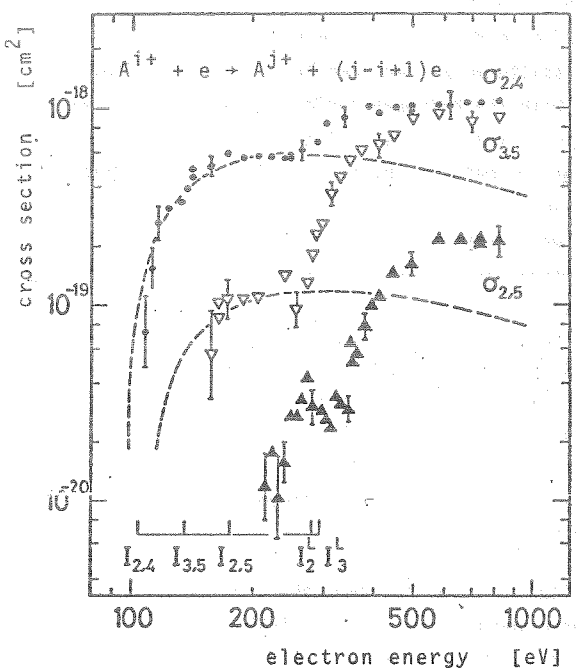


Fig. 2 Measured cross sections for multiple ionisation of multiply charged argon

The investigation of secondary electron emission by slow ions in DIAZ[1,5] from gas covered surfaces (e. g. O_2 on W) revealed a considerable relative detection sensitivity for metastable ions, even at ion energies as high as 500 eV. This will allow a much simpler construction of the metastable ion detector. From preliminary results of producing metastable ions by charge exchange, especially $Ar^{+,m}$ and $Ne^{+,m}$, one can expect higher fractions of metastables compared to production by electron impact.

* The authors are indebted to W. Hofer for improving the DIAZ facility by computer control and data acquisition

[1] R. Becker, R. Frodl, H. Klein, G. Clausnitzer, A. Müller, E. Salzborn, P. Varga, F. Viehböck, H. Winter, GSI 79-11 (1979) 121
[2] A. Müller, E. Salzborn, R. Frodl, R. Becker, H. Klein, H. Winter, J. Phys. B 13 (1980)
[3] A. Müller and R. Frodl, Phys. Rev. Lett. 44 (1980) 29
[4] H. Winter and P. Varga, Proc. XI ICPEAC Kyoto 1979, p. 204
[5] P. Varga and H. Winter, Phys. Rev. A 18 (1978) 2453

Stopping Power Measurements for 3-5 MeV/u ^{86}Kr, ^{136}Xe, ^{208}Pb and ^{238}U in Solids

R. Bimbot, D. Gardes
Orsay, France

H. Geißel, T. Kitahara, P. Armbruster
GSI Darmstadt

A. Fleury, F. Hubert
Bordeaux-Gradignan, France

The energy loss measurements were performed at GSI using the recoil proton technique[1]. The principle of this method is to measure the energy of the proton elastically scattered at zero degree in heavy ion collisions with the hydrogen nuclei of a formvar target. A gold foil stops the heavy ion beam while the recoiling protons are detected by a Si-surface barrier detector. Using such a device, absolute energies of Kr, Xe, Pb and U were measured with an accuracy better than ± 0.4%. The energy loss is obtained from the energy difference with and without absorber.

The mean thicknesses of the absorber foils were determined by weighing, whereas the homogeneity was checked by measuring the energy loss of 8.785 MeV alpha particles. The uncertainties in the thickness determination, combined with inhomogeneity effects, are estimated to be ± 4%.

The stopping power has been obtained by dividing the measured energy loss by the thickness of the target. In order to compare the experimental stopping powers (S_{exp}) with the values tabulated by Northcliffe and Schilling (S_{NS}), the relative deviations $(S_{exp}-S_{NS})/S_{NS}$ have been plotted in Fig. 1 versus the atomic number Z_2 of the stopping medium. The comparison of these data with N.S. values indicates strong deviations, mostly for light stopping media. A further comparison, Fig. 2, demonstrates the deviations from the N.S. values for O, Ar, Cu, Kr, Xe, Pb and U projectiles at 4.5 MeV/u in C, Al, Ni, Ag and Au media. Results of Ref. 2 from light projectiles are included.

[1] R. Bimbot, S. Della Negra, D. Gardes, H. Gauvin and B. Tamain, Rev. Phys. Appl. 13, 393 (1978)

[2] R. Bimbot, S. Della Negra, D. Gardes, H. Gauvin, A. Fleury and F. Hubert, NIM 153, 161 (1978)

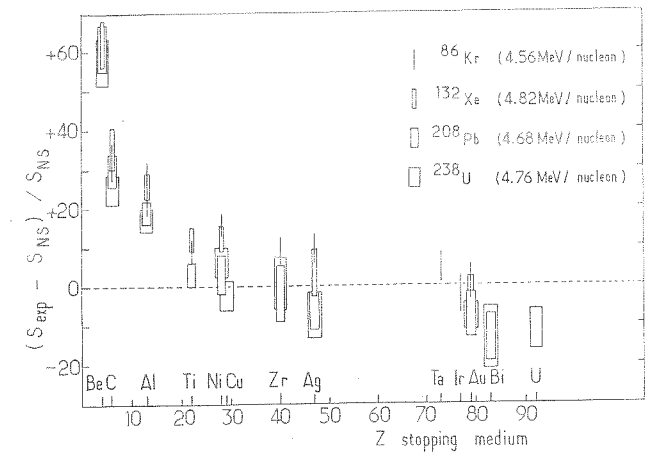


Fig. 1: Comparison between experimental stopping powers and the calculated values from N.S. table. The relative deviation has been plotted versus the atomic number of the stopping medium.

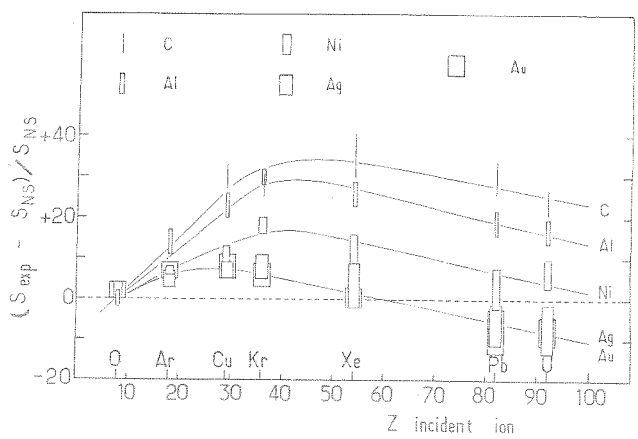


Fig. 2: The relative deviations from N.S. are plotted versus the atomic number of the incident ion at fixed energy of 4.5 MeV/u.

Stopping power measurements with 10 MeV/u ^{238}U ions

W. Brüchle, H. Folger, J.V. Kratz
GSI Darmstadt

For the design of the $^{238}U+^{248}Cm$ experiment[1] and of $^{238}U+^{238}U$ experiments using a wheel system[2] it was necessary to measure the energy loss of ^{238}U projectiles in thick ^{238}U targets and in Al, Mo, Ta, and W metal foils. The foils were prepared by rolling. In the case of ^{238}U oxidation of the surface layer was prevented by evaporation of thin Ni layers onto the uranium foil which had previously been cleaned by sputtering. After rolling the thickness of the Ni layer was reduced to 34-63 µg/cm^2. The targets were transported and inserted into the beam line under Ar atmosphere. The thicknesses of the foils were determined by weighing. Several energies of the primary ^{238}U beam between 5.9 and 10.0 MeV/u as determined by the UNILAC time-of-flight system were used to calibrate a surface barrier detector which was inserted directly into the reduced beam. The same detector was then used to determine the degradation of the incident beam energy in a given metal foil.

Projectile energies after transversing different foil thicknesses were calculated by the use of the Northcliffe and Schilling tables.[3] The figure shows for uranium foils the deviations between calculated (E_{NS}) and measured values (E_{OUT}) for three different incident energies (E_{IN}) of 10.0, 8.6, and 5.9 MeV/u. For the energy range of interest in the $^{238}U+^{238}U/^{248}Cm$ experiments,[1,2] i.e. 6 to 10 MeV/u, the differences between measured and tabulated values are below 3 %. The table shows that, except for Al, there is no dramatic deviation from the Northcliffe and Schilling tables. In this table the stopping power values are compared after averaging different foil thicknesses. For ^{238}U-energies around 5 MeV/u our data for Al and U are in agreement with those of Bimbot et al.,[4] who report a deviation ε = + 17±3% for Al and ε = -11±5% for U.

Table: Deviations of experimental average stopping powers S_{exp} from Northcliffe-Schilling stopping powers S_{NS} for ^{238}U ions:

$$\varepsilon = \frac{S_{exp} - S_{NS}}{S_{NS}} \times 100 \quad [\%]$$

E_{IN}	5.9 [MeV/u]	8.5 [MeV/u]	10.0 [MeV/u]
Al	+18.1±2.5		+22.0±5.0
Mo	+ 6.6±2.5		+ 3.7±2.5
Ta	+ 0.5±2.0	- 5.0±5.0	- 0.8±2.5
W	+ 4.2±4.0		- 1.5±2.5
U	-12.0±5.0	- 4.0±2.5	- 2.4±3.2

[1] M. Schädel et al., this report p.
[2] H. Gäggeler et al., this report p.
[3] L.C. Northcliffe, R.F. Schilling, Nucl. Data Tables A7 233 (1970)
[4] R. Bimbot et al., Report IPNO-RC-80-0a, (1980)

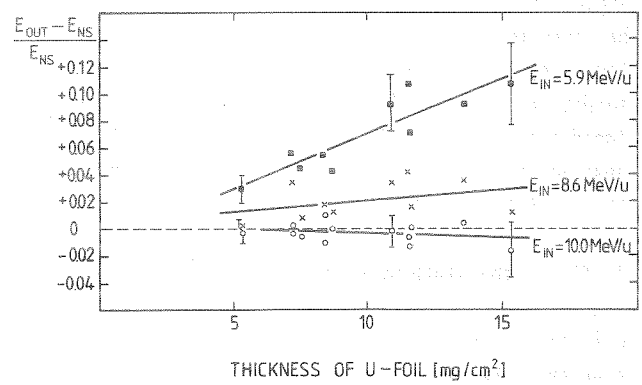


Fig. 1: Relative deviation of the energy E_{OUT} of ^{238}U-ions (after passing various ^{238}U-metal foils) from the predicted[3] energy E_{NS}.

Stopping Powers of 0.2 - 1.4 MeV/u Heavy Ions in Solids

H. Geissel, T. Kitahara, Y. Laichter and P. Armbruster
GSI Darmstadt

The stopping powers of 0.2 - 1.4 MeV/u Ar, Ti, Cu, Kr, Xe, W, Pb, Bi, and U projectiles in various solids ($6 \leq Z_2 \leq 92$) have been measured. The kinetic energy of the projectiles was determined by time of flight spectrometry, thus avoiding uncertainties due to pulse-height defects in surface barrier detectors frequently used in such experiments. Adequate counting rates have been achieved by reducing the beam intensity by Rutherford-scattering. The energy was varied by reducing the original fixed 1.4 MeV/u beam by the aid of homogeneous carbon stacks and plastic foils. The thickness of the targets has been deduced from energy loss measurements of α particles by using up-to-date stopping power tables[1]. All targets were produced by the staff of the GSI-target lab. Inhomogeneity of the foils, uncertainties in the thickness and target oxidation are the main contribution to the 5 % estimated total error of the measured stopping powers.

In fig. 1 the stopping cross sections of 0.5 and 1 MeV/u Ti, Xe, and Pb projectiles in solids are given together with the relevant data for α particles[1]. It is clearly seen that the heavy ions demonstrate the same structure of the Z_2 dependence measured and calculated for α particles (Z_2-oscillation)[2]. This has already been suggested from a smaller set of measured projectile-target combinations[3]. The same structure has been shown for 0.32 MeV/u ^{35}Cl ions for $20 \leq Z_2 \leq 40$[4] and for ^{252}Cf fission fragments[5]. The amplitude of the Z_2-oscillations is dependent on the velocity and mass of the projectile. The larger the velocity the smaller are the oscillations and they disappear for light ions at velocities smaller than for heavy ones. In the same figure we represent also the calculated results obtained by Lindhard and Scharff using the Thomas-Fermi model[6]. In the calculations we replace the Z_1 by our experimental Z_{eff} values. It is clear that a more realistic atomic model taking into account the shell structure of the atom is needed to describe the oscillating structure. In fig. 2 the dependence of the stopping power on Z_1 is presented for 1 MeV/u, U, Bi, Pb, W, Xe, Kr, Cu, Ti, and Ar ions in C, Al, Zr, and Au. For this limited number of projectiles no Z_1-oscillation is observed.

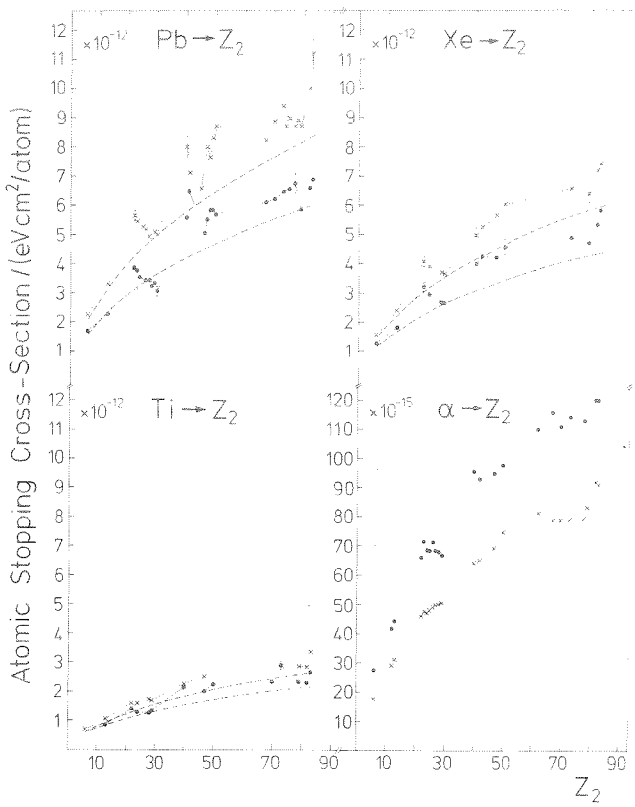


Fig. 1: Stopping cross sections of 0.5 and 1 MeV/u Pb, Xe, Ti, and α projectiles vs. Z_2 of the stopping media. Theoretical curves according Lindhard[6].

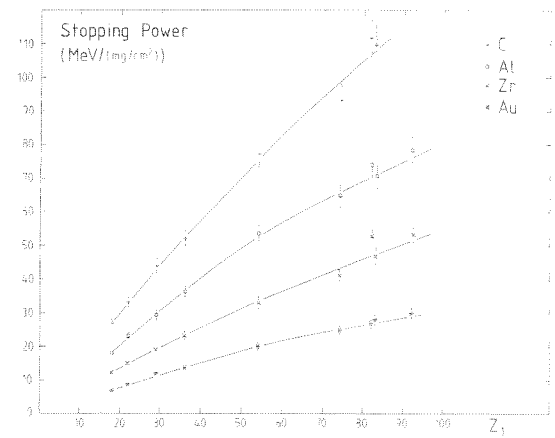


Fig. 2: Stopping powers measured in C, Al, Zr, and Au vs. atomic number of 1 MeV/u projectiles.

[1] J.F. Ziegler, Helium Stopping Power and Ranges in all Elements (Plenum Press; New York, 1977)
[2] W.C. Chu and D. Powers, Physics Letters 38A, 267 (1972)
[3] H. Geissel et al., GSI Annual Report 1978, p. 115
[4] J.S. Forster et al., Nucl. Instr. and Meth. 136, 349 (1976)
[5] Y. Laichter and N.H. Shafrir, to be published
[6] J. Lindhard and M. Scharff, Mat. Fys. Medd. Dan. Vid. Selsk. 27, No 15 (1953)

Comparison of Stopping Powers Between Heavy Ions and Mean Fission Fragments

Y. Laichter, H. Geissel, T. Kitahara, and P. Armbruster

GSI Darmstadt

N.H. Shafrir

Department of Nuclear Engineering, Technion, Haifa, Israel

The existing published data concerning heavy-ion energy losses in matter have been derived from two sources, namely accelerated heavy ions and fission fragments. The latter usually have been measured by a heavy ion surface barrier detector and the results are represented for the "mean light" M_L and "mean heavy" M_H fission fragments located at the centers of the two peaks of the fission fragment energy spectrum. Stopping power tables usually omit the fission fragment data because they represent a collection of many fragments having a composition that is varying during the slowing down process due to an exchange of particles between M_L and M_H [1]. In order to investigate this phenomenon, the $^{252}C_f$ fission fragment spectra as expected to be measured by a surface barrier detector was composed from elementary data and compared to the measured ones. The calculated spectra were adjusted to the measured by varying the free parameter of the LSS stopping power formula [2]. The Z and A content of the channels representing the M_L and M_H fission fragments were analyzed. In Fig. 1 representative results are shown for the unattenuated spectrum and for one attenuated in 1.0 mg/cm^2 nitrogen. The change in composition due to the transfer from peak to peak is clearly seen. It has been found that energy losses as high as 50 MeV cause the attenuated mean Z and A values to deviate by up to 1 unit from the unattenuated ones. Such deviations cause a change of up to 3 % in the energy loss calculations of the mean fission fragments, which typically is smaller than the uncertainties quoted for stopping power measurements. To check this result, experimental stopping powers of M_H for ^{252}Cf (Ref. 3) (A_H = 141.7 Z_H = 55.4) and ^{235}U (Ref. 4) (A_H = 138.1 Z_H = 53.4) are compared with stopping powers of ^{136}Xe in solids as measured with the UNILAC. The small differences between the Z and A values were corrected and an uncertainty of 5 % was assumed for the stopping powers. In Fig. 2 it can be seen that the heavy ions and fission fragment data overlap, suggesting that fission fragment energy loss data can be incorporated into heavy-ion stopping power tables.

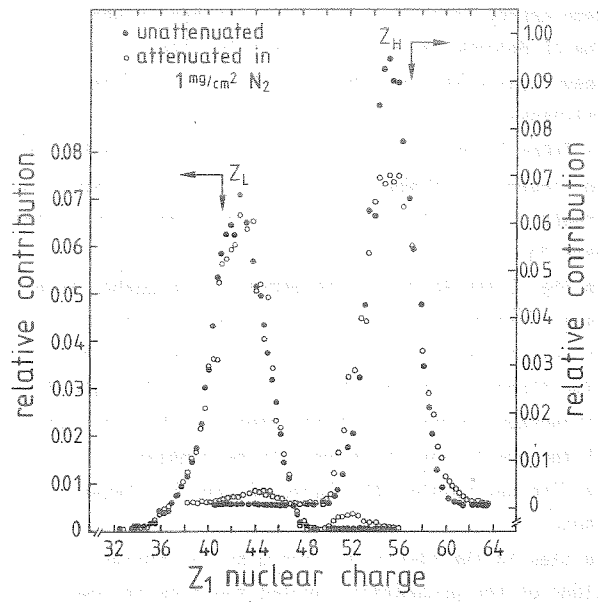


Fig. 1: The contribution of fission fragment charges to the mean charge of the unattenuated and attenuated mean fission fragments.

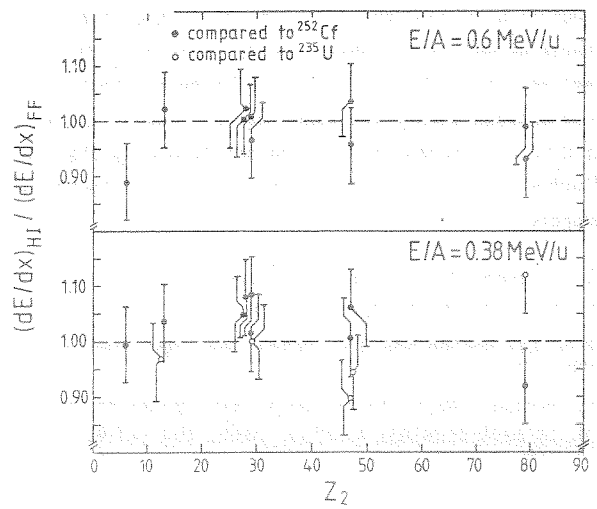


Fig. 2: Measured ^{136}Xe stopping powers divided by the mean heavy fission fragment stopping power for ^{235}U and ^{252}Cf vs. atomic number of the stopping medium.

[1] M. Hakim and N.H. Shafrir, Can. J. Phys. 49, 3038 (1971)

[2] J. Lindhard, M. Scharff and H.E. Schiøtt, Kgl. Danske Vidensk. Selsk, Mat. Fys. Medd. 33, No. 14 (1963)

[3] R. Müller and F. Gönnenwein, Nucl. Instr. and Meth. 91, 357 (1971)

[4] S. Kahn and V. Forgue, Phys. Rev. 163, 290 (1967)

Energy Loss Straggling of Heavy Ions and α Particles in Matter

H. Geissel, Y. Laichter, and P. Armbruster
GSI Darmstadt

It was shown previously that for the same energy loss (ΔE) of 1.4 MeV/u ^{238}U projectiles in carbon stacks, the energy loss straggling (δE = FWHM) is strongly dependent on the number of foils constituting the stacks. A minimum was found for stacks having n ≈ 10 foils[1]. In Fig. 1 we represent δE of ^{241}Am α-particles in carbon stacks having different numbers of foils and causing the same energy loss (ΔE = 417 keV). It can be seen that the δE dependence on n has a similar trend as for the heavy ions with a minimum at n ≈ 7. The variance of the thickness fluctuations of a small number of foils, n < 5, is found to be larger than for an optimum stack of n ≈ 7. For increasing number of foil n > 7, the variance increases with n. For further δE measurements represented here for carbon, stacks with 10 ≤ n ≤ 14 were used.
In Fig. 2 the δE of U ions versus ΔE in carbon is given as a representative result for heavy ions together with calculated results from the Tschalär theory[2] and the same theory including shell corrections from the Bethe-Livingston theory[3]. In these theories the ionic charge of the projectile is assumed to be constant. In order to find out whether the large discrepancy between the theory and the experimental results is due to inhomogeneities in the stacks or caused by the charge fluctuations of the projectiles during the slowing down process[4], the δE of the 5486 keV Am α particles in the same stacks and in He, Ne, Ar, Kr, and Xe were measured. The charge fluctuations of these α-particles are negligible. In Fig. 3 representative results are given together with the theoretical calculations. It can be seen that the Tschalär theory, together with the shell corrections, predicts with good precision the δE in the carbon stacks as well as in gases. It is therefore concluded that the stacks have a high uniformity and that difference between theory and experimental results for δE of U ions in carbon stacks are mainly due to the charge fluctuations of the projectiles during the slowing down process.

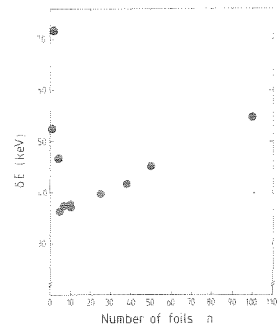


Fig. 1 Energy loss straggling of ^{241}Am α particles in carbon stacks of the same total thickness as a function of the number of foils constituting the stacks.

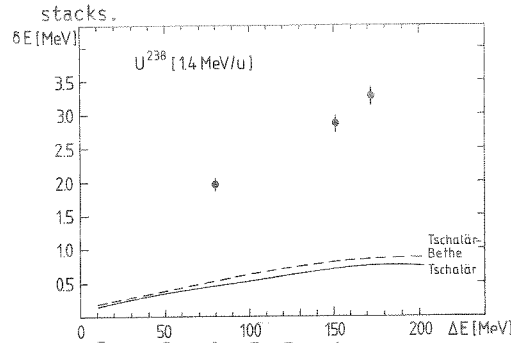


Fig. 2 Experimental and calculated energy loss straggling of ^{238}U ions versus energy loss in carbon

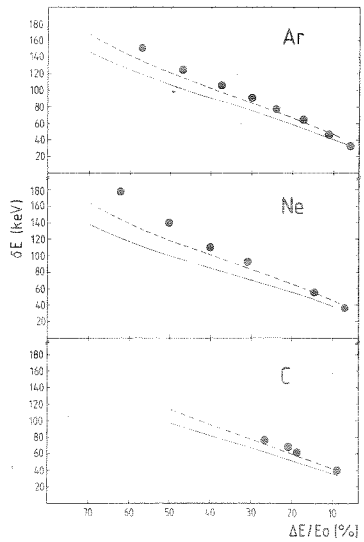


Fig. 3 Experimental and calculated energy loss straggling of ^{241}Am α particles in C, Ne and Ar. ——— Tschalär[2], – – – Tschalär-Bethe[3] theories.

[1] T. Kitahara et al., GSI annual report 1978
[2] C. Tschalär, Nucl. Instr. and Meth. 61, 141 (1978)
[3] M.S. Livingston and H.A. Bethe, Rev. Mod. Phys. 9, 245 (1937)
[4] O. Vollmer, Nucl. Instr. Meth. 121 (1974) 373
H. Schmidt-Böcking, Z. Phys. A286, 253 (1978)

Limitation of the Z-Resolving Power Due to the Energy Straggling

C.C. Sahm, K.H. Schmidt+, H.-G. Clerc, H. Schulte, D. Vermeulen
Inst. für Kernphysik, TH Darmstadt, +GSI Darmstadt

The nuclear charge Z of heavy ions can be determined by means of the Z dispersion of the energy loss in a homogeneous absorber. In order to estimate the optimum Z resolution obtainable, the width of the energy distribution of ^{208}Pb ions and α-particles having passed different absorbers (see table 1) was measured.

Table 1 :

abs.	material	number of foils	thickness (mg/cm^2)
a	C	1	.12
b	C	10	1.20
c	C	160	1.30
d	$(CH_2)_n$	1	.77
e	$(CH_2)_n$	1	1.02

The energy loss ΔE and the energy straggling δE of the Pb ions were determined by measuring the time of flight before and after passing the absorber. The α-particles were detected in a surface barrier detector. The values of the experimentally determined energy straggling are shown in fig. 1 in a reduced representation which was derived by Schmidt-Böcking et al.[1] for the energy straggling due to charge-change processes :

$$\delta E_{red} = \delta E \cdot \frac{S(E_0)}{S(E_0-\Delta E)} \cdot (Z_T^{1/3} + Z_r^{1/3}) \cdot Z_p^{-1/2} \qquad (a)$$

The stopping power S was computed with a code written by Braune et al.[2]

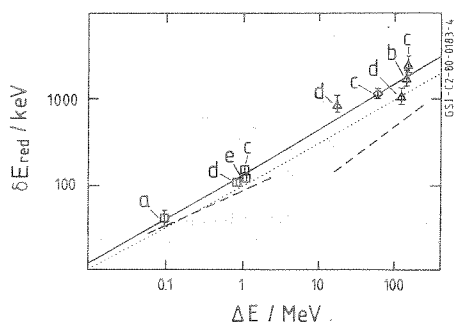


Fig. 1 : Experimental reduced energy straggling (see text).

□ : α-particles (5.48 MeV); ◇ : ^{90}Zr-projectiles (92.3 MeV)[3]; △ : ^{208}Pb-projectiles (291 MeV). The different absorbers (a-e) are listed in table 1.

The straight line in fig. 1 is a fit to straggling data of Cl ions in a Ar-CH_4 target according to[1]. The dashed lines show the calculated collision straggling[4] for α-particles and Pb ions, respectively, with an initial energy 1.4 MeV/u.

Obviously, the collision straggling cannot account for the observed values of the straggling of Pb ions in contrast to the straggling of α-particles, whereas Schmidt-Böcking's empirical description of the straggling due to charge fluctuations[1] agrees approximately with the data. Even the straggling of α-particles is well represented by this description although it should not be applicable in this case.

Inhomogenities, especially of solid targets, may influence appreciably the measured energy width. The systematic differences between the data may be explained by this fact. E.g. the plastic foil (absorber d) apparently is much more homogeneous than the carbon foils. We tried to get an estimation for a large range of projectiles by adjusting the theoretically expected dependence[1] of the reduced energy straggling $\delta E_{red} \sim \sqrt{\Delta E}$ to the measured energy straggling of Pb ions in the absorber d. This leads to the following empirical expression

$$\delta E = \sqrt{1.67\ keV \cdot \Delta E} \cdot \frac{S(E_0-\Delta E)}{S(E_0)} \cdot Z_p^{1/2} \cdot Z_T^{1/2} / (Z_p^{1/3}+Z_T^{1/3}) \qquad (b)$$

for the straggling represented in fig. 1 by the dotted lines.

Relation (b) was used for estimating the Z-resolving power of a detector utilizing the Z-dispersion of the energy loss in a solid absorber. In fig. 2, the greatest nuclear charge Z_{max} for which the energy

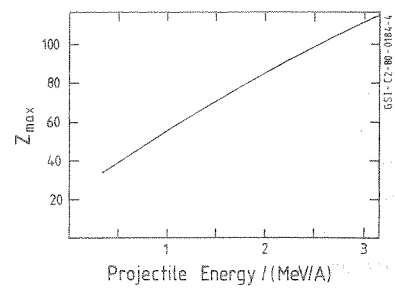


Fig. 2 : Estimated limitation of the Z-resolution due to the energy straggling for ΔE/E = 60 %.

width is smaller than the Z dispersion (the difference between the energy losses of neighbouring elements) is shown. This curve agrees well with the actually reached Z-resolution of Z/ΔZ = 58 for Y ions with E/A = 1 MeV[5]. According to fig. 2, for E/A > 3 MeV it should be possible to separate all elements. This still holds for higher velocities when the straggling is dominated by the collision processes. Until now, for higher velocities this extrapolated Z-resolving power has not yet been achieved, e.g. Z/ΔZ = 80 was reached for Xe-ions with 4.4 MeV/nucleon by an ionization chamber[6]. Probably gaseous and solid absorbers behave differently. Experimental straggling values in this range are highly needed.

[1] H. Schmidt-Böcking, H. Hornung, Z. Phys. A286, 253 (1978) and private communication
[2] K. Braune, D. Schwalm, GSI-report J1-77, 117 (1977)
[3] K.-H. Schmidt et al., NUM 134 (1976) 157
[4] C. Tschalär, Nucl. Instr. Meth. 61 (1968) 141
[5] U. Quade, K. Rudolph, G. Siegert, NIM 164 (1979) 435
[6] D. Schüll, private communication

Variable binding of electrons and transfer of polarization in ion-atom collisions [G]

M. Kleber and K. Unterseer

Theoretische Physik, Universität zu Köln

In slow atomic collisions transient molecules are formed. This means that inner-shell electrons experience a collision-induced, temporarily enhanced binding (monopole polarization). With increasing impact velocity the electrons are less able to follow the adiabatic levels. Binding corrections vanish for impact velocities which are large compared to the orbital velocity of the electron. In fast collisions it is mainly dipole polarization which leads to excitation and ionization.

We calculated monopole and dipole excitation within the self-consistent variational method[1]. As usual the internuclear motion is treated classically whereas the electron motion is described quantum mechanically. For K-shell excitation we used a variational wave function of the type

$$\langle \vec{r} | \psi \rangle \sim \exp(i\vec{p}\vec{r}) \exp(-\alpha r).$$

Both α and $\vec{p}$ are time-dependent complex variational parameters; their time dependence follows the corresponding self-consistent equations of motion[2]. For $\vec{p} = 0$ the real part of α is the inverse of the Bohr radius and the imaginary part the radial velocity. Prior to the collision this velocity is zero. Due to the lack of adiabaticity in the electron motion near the united atom configuration there will be a non-vanishing radial velocity at the end of the collision. The corresponding monopole excitation was calculated. Similarily, real and imaginary part of $\vec{p}$ account for dipole polarization in momentum and configuration space. From the collision-induced transfer of dipole polarization we determined the dipole excitation. It is obvious that transfer of polarization occurs in longitudinal and transverse direction (relative to the beam axis).

In Fig. 1 we compare our calculations (full curve) with experimental data[3] for proton impact on copper. The theory underestimates slightly the experiment. Relativistic effects and contributions of higher order multipoles, $\ell \geq 2$, will account for the small deviations.

For very small impact parameters recoil makes its appearance: In asymmetric collisions it is natural to calculate Coulomb excitation of target electrons in the target system. This is a non-inertial system. Therefore the target Hamiltonian must be modified

$$H \to H + m\ddot{\vec{d}}\vec{r}$$

with $\ddot{\vec{d}}$ the acceleration of the target system relative to the center of mass, m the electron mass and $\vec{r}$ the electron coordinate. Due to recoil Coulomb ionization will be reduced in close collisions but enhanced in distant collisions. The magnitude of the effect depends on the specific reaction but it is clear that recoil becomes more important for deuteron projectiles than for protons. This fact is displayed in Fig. 2.

[1] M. Kleber and J. Zwiegel, Phys. Rev. A19, 579 (1979)
[2] M. Kleber and K. Unterseer, Z. Physik A292, 311 (1979)
[3] J.U. Andersen et al., Nucl. Instrum. Meth. 132, 507 (1976)

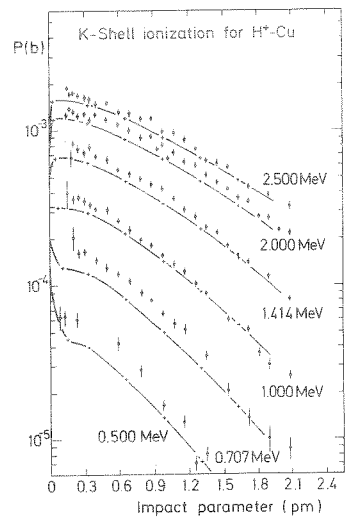


Fig. 1. Impact-parameter dependence of K-shell ionization probabilities of Cu by protons with variable energies.

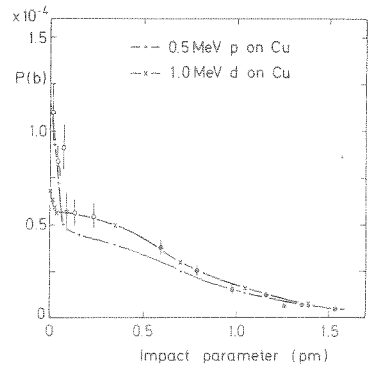


Fig. 2. K-shell ionization probabilities for proton and deuteron impact. Proton data (0.5 MeV) from Ref.3

Solution of the Schrödinger Equation with a Trajectory Method in Atomic Collisions [G]

Georg Terlecki, Norbert Grün, Vida Maruhn-Rezwani and Werner Scheid
Institut für Theoretische Physik der Justus-Liebig-Universität Gießen

For H^+-H collisions at energies, where the velocities of the projectile and electron are of the same order of magnitude, we propose a trajectory method for solving the time-dependent Schrödinger equation. Within this method we calculate trajectories of the probability density up to large distances from the protons. Therefore, the trajectory method is especially suitable for studying the ionization process, whereas the direct numerical integration of the time-dependent Schrödinger equation[1] has been found advantageous for the calculation of probabilities for excitation and charge exchange.

The trajectory method starts from the Schrödinger equation for the electron moving in the time-dependent Coulomb field of the protons:

$$i\hbar\frac{\partial}{\partial t}\psi = (-\frac{\hbar^2}{2m}\Delta + V(\vec{r},t))\psi \qquad (1)$$

With the ansatz $\psi(\vec{r},t)=A(\vec{r},t)\exp(iS(\vec{r},t)/\hbar)$ (A,S real) one obtains the equation of continuity and the Hamilton-Jacobi equation

$$\frac{\partial\rho}{\partial t} + \operatorname{div}\vec{j} = 0 \qquad (2)$$

$$\frac{\partial S}{\partial t} + \frac{(\vec{\nabla}S)^2}{2m} + V_{eff} = 0 \qquad (3)$$

$$V_{eff} = V(\vec{r},t) - \frac{\hbar^2}{2m}\frac{\Delta\sqrt{\rho}}{\sqrt{\rho}} \qquad (4)$$

Here, $\rho=A^2$ is the density and $\vec{j}=\rho\vec{\nabla}S/m$ the current density. Eqs.(2) and (3) describe a fluid of interacting classical particles with mass m and are subject to the effective density dependent potential V_{eff}. The assembly of these classical particles ("probability" particles) is a representation of the probability distribution of the electron.

By solving the equations of motion, which follow from Eqs.(3) and (4), we obtain the time-dependence of the density ρ and the current density $\vec{j}$. The initial distribution of the "probability" particles is proportional to the exact 1s-density of hydrogen. First calculations have been carried out for an energy of E_p=200 keV and impact parameter b=0.5 a_0.

Fig.1 shows the time evolution of the "probability" particles. The electron density is indicated by points, the proton position by crosses. From this figure we conclude that the ionization process becomes more and more isotropic with increasing time. Fig.2 shows the time-development of the ionization rate as a function of the energy of the emitted electron. The predominant part of the ionization rate is concentrated at low energy values.

In conclusion the trajectory method is a complementary method to the direct numerical integration of the time-dependent Schrödinger equation[1].

[1] V. Maruhn-Rezwani, N. Grün and W. Scheid, Phys. Rev. Lett. 43, 512 (1979)

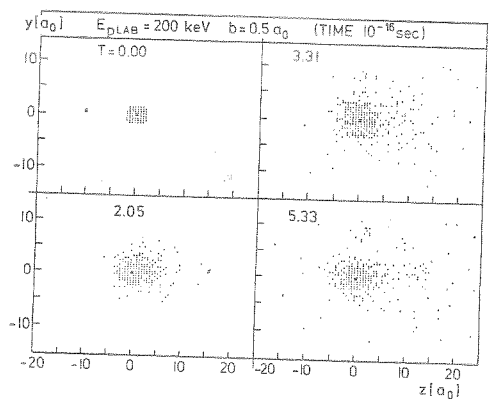


Fig.1: Time evolution of the "probability" particles

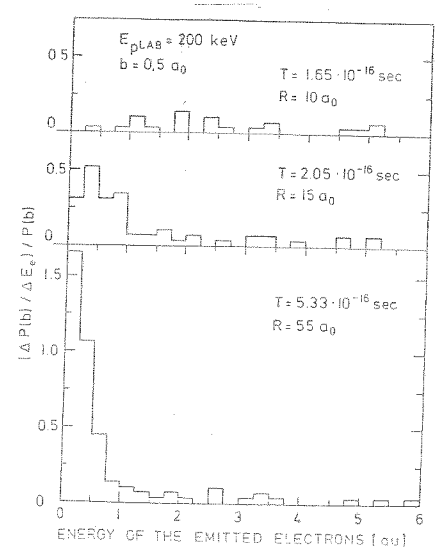


Fig.2: Time evolution of the ionization rate versus the energy of the ionized electrons

Charge distributions after ion-atom collisions [G]

Karl-Heinz Wietschorke, Joachim Reinhardt and Walter Greiner
Institut für Theoretische Physik, Universität, 6000 Frankfurt am Main

and

Gerhard Soff
GSI Darmstadt

For the description of the charge distribution of an ion passing through a gas or a solid target usually the semiempirical relations of Betz[1] and Dmitriev[2] are applied. Good estimates for the mean equilibrium charge can also be obtained by employing the Bohr criterion[3]. Theoretically more detailed informations about the charge state probability distribution Y can be taken from the solution of the differential equation

$$\frac{dY_f(x)}{dx} = \sum_{i \neq f} \sigma(f,i)\, Y_i - \sum_{i \neq f} \sigma(i,f)\, Y_f \qquad (1)$$

where σ denotes the corresponding charge exchange cross section. σ is determined by the impact parameter integration of the independent probabilities of ionization and electron capture in the various shells of the ions. For a first application ionization and capture has been calculated within the binary encounter approximation. We solved the differential equation (1) with constant, position independent coefficients σ which is a reasonable approximation only for thin target materials. In fig. 1 we show the calculated equilibrium charge distribution G(q)[4] for the stripping of Argon ions with 0.217 MeV/u in a gas target (N_2) in comparison with the experimental data of Franzke et al.[5].

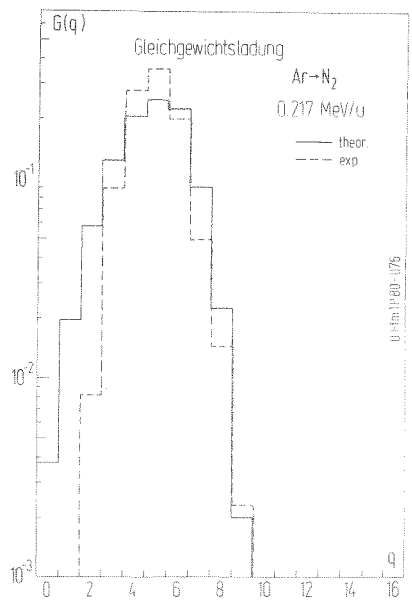


Fig. 1: Equilibrium charge distributions after $Ar \rightarrow N_2$ collisions

In fig. 2 the relaxation to equilibirum as function of the target thickness is displayed for the same system. The discrepancy between the theoretical (dashed lines) and experimental[5] (solid lines) target thickness dependence of the charge state probability distribution results from an overestimate of the electron capture contribution within the binary encounter approximation.

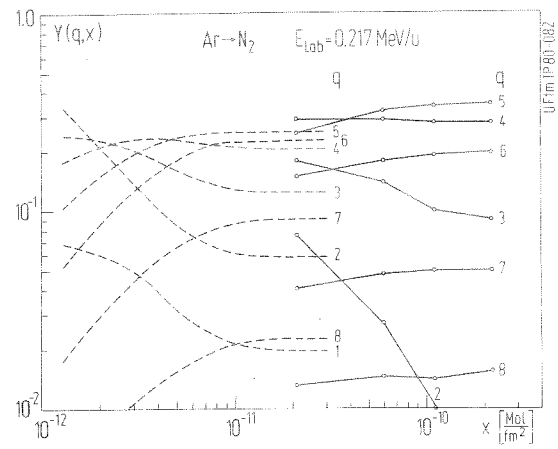


Fig. 2: Target thickness dependence of the charge state probability distribution. Experimental data (solid lines) from ref. 5.

[1] H.D. Betz, L. Grodzins, Phys. Rev. Lett. 25 (1970) 211

[2] I.S. Dmitriev, V.P. Zaikov, Y.U.A. Tashev, Nucl. Instr. Meth. 164 (1979) 329

[3] N. Bohr, Dan. Math. Fys. Medd. 18-8 (1948)

[4] K.-H. Wietschorke, diploma thesis, Frankfurt, 1980

[5] B. Franzke, GSI-PB-4-75

Self-consistent determination of critical two-centre distances [G]

Karl-Heinz Wietschorke, Berndt Müller and Walter Greiner
Institut für Theoretische Physik, Universität, 6000 Frankfurt am Main
and
Gerhard Soff
GSI Darmstadt

In collisions of very heavy ions ($Z_1 + Z_2 > 173$) below the Coulomb barrier, adiabatic two-centre orbitals are formed. The internuclear separation R where the binding energy of the quasimolecular 1sσ electron exceeds twice the electron rest mass $E_{1s\sigma} = 2m_e c^2 \sim 1$ MeV is called critical. For R less than R_{cr} the 1sσ electron dives into the negative-energy continuum of the Dirac equation. Provided that the 1sσ state is not completely occupied, this opens the channel of spontaneous positron emission.

For a comparison with the measured impact parameter dependence of 1sσ-vacancy formation or δ-electron emission in overcritical systems it is desirable to evaluate the critical two-centre distance as accurately as possible. For that purpose we take into account the electron-electron interaction described within the relativistic Hartree-Fock-Slater model.

Only the dominant monopole term in the multipole expansion of the two-centre potential has been retained in the numerical calculations. Non-overlapping homogeneously charged spheres have been used for the finite size nuclear charge distributions.

The critical internuclear separation R_{cr} is displayed in the figure[1)] for different degrees of ionisation d as a function of the combined nuclear charge. For d less than 100, R_{cr} is obviously only negligibly influenced by ionisation. For the almost neutral U-U system, we found R_{cr} = 26 fm which is far below the values of R_{cr} = 33 fm computed in the one-electron approximation. For the system Z = 190 (U + Cf), we obtained R_{cr} = 35,5 fm.

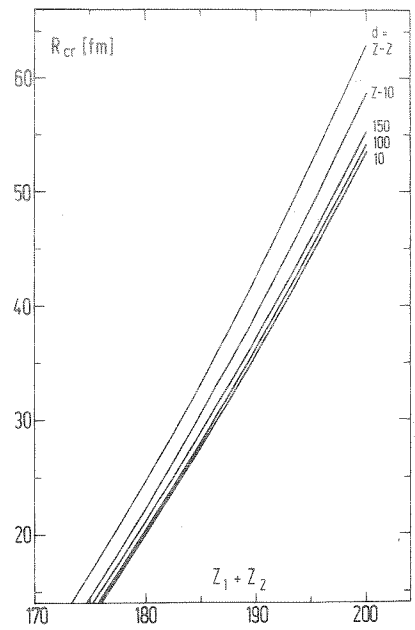


Figure caption: Critical two-centre distances as a function of combined nuclear charge for the 1sσ state. The electron-electron interaction has been calculated within the relativistic Hartree-Fock-Slater model. Different curves belong to different degrees of ionisation.

[1] K.-H. Wietschorke, B. Müller, W. Greiner, G. Soff
J. Phys. B 12 (1979) L 31

Multistep processes for electron excitations in superheavy quasimolecules B + G

Gerhard Soff
GSI Darmstadt
and
Joachim Reinhardt, Berndt Müller, and Walter Greiner
Institut für Theoretische Physik, Universität, 6000 Frankfurt am Main

The collision of very heavy ions with bombarding energies below the Coulomb barrier provides a powerful tool for a spectroscopy of electronic states in transient superheavy systems with $Z_1 + Z_2 > 107$. The excitations of inner-shell electrons in collisions of heavy ions at energies up to the nuclear Coulomb barrier is best described in the quasimolecular model. Here one starts from the solution of the stationary two-center Dirac equation and treats the excitations as being caused by the explicit time dependence of the electronic Hamiltonian.
The multistep excitation processes[1,2] of a single electron are properly described by the solutions of the coupled differential equations

$$\dot{a}_{ij}(t) = - \sum_k a_{ik}(t) \langle \phi_j | \partial/\partial t | \phi_k \rangle \exp[-i(\chi_k - \chi_j)] \qquad (1)$$

with the phase $\chi_j = \int_t dt' E_j(R(t'))$. a_{ij} denotes the occupation amplitude for a state j by the electron i and ϕ_k are solutions of the two-centre Dirac equation. The solution of the many electron problem can be reduced completely to single electron coupled channel integrations provided that the two-body electron-electron interaction is neglected. For instance if one is interested in the vacancy production probability of the 1sσ-state only, one finds

$$N_{1s\sigma} = 1 - \sum_{r<F} |a_{1s\sigma,r}|^2 \qquad (2)$$

where F denotes the Fermi surface of occupied states. The differential probability for the emission of a Esσ-δ-electron with energy E and one definite spin projection measured in coincidence with a 1sσ-vacancy with the same spin projection is given by

$$\frac{dP_{1s\sigma}}{dE} = \sum_{r<F} |a_{r,Es\sigma}|^2 \left(1 - \sum_{r'<F} |a_{r',1s\sigma}|^2\right) + \left|\sum_{r<F} a^*_{r,Es\sigma} a_{r,1s\sigma}\right|^2 \qquad (3)$$

Using eq. (2) we calculated the number of created 1sσ-vacancies P(b) per collision as function of the classical impact parameter for one of the heaviest systems which can be investigated experimentally, namely Pb + Cm with a total charge $Z_1 + Z_2 = 178$. For 5.9 MeV/u bombarding energy the results are shown in fig. 1. In addition we show the experimental data[3], which agree satisfactory with the calculation including electron screening corrections. No agreement is found for a smaller bombarding energy of 3.6 MeV/u. According to eq. (3) we calculated the δ-electron distribution for the Pb + Sn-system. In fig. 2 we compare our results with the experimental data of Kozhuharov et al.[4]. The theoretical cross sections are found to be slighthly below the measured data which might be caused by the neglection of electron screening effects.

[1] J. Reinhardt, B. Müller, W. Greiner, G. Soff, Phys. Rev. Lett. 43 (1979) 1307
[2] G. Soff, J. Reinhardt, B. Müller, W. Greiner, Z. Physik A294 (1980) 137
[3] D. Liesen, P. Armbruster, F. Bosch, S. Hagmann, P.H. Mokler, H. Schmidt-Böcking, R. Schuch, J.B. Wilhelmy, H.J. Wollersheim, Phys. Rev. Lett. (1980)
[4] Ch. Kozhuharov, P. Kienle, Th. Walcher, F. Bosch, H. Bokemeyer, private communication

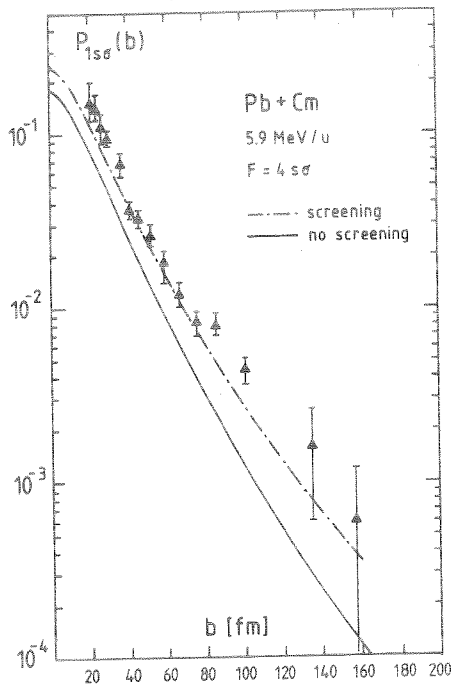


Fig. 1: 1sσ ionization probability for Pb + Cm collisions at 5.9 MeV/u lab energy compared with experimental data.[3]

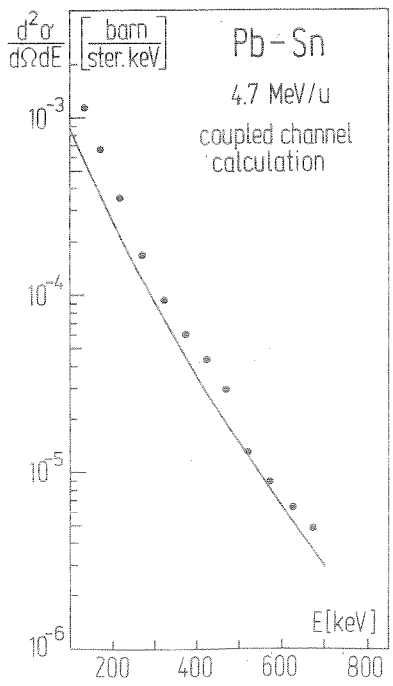


Fig. 2: δ-ray spectrum for the Pb + Sn system which should be measured in coincidence with 1sσ vacancy formation devided by 4π in comparison with experimental data[4].

Contributions to the theory of quasimolecular X-rays [B]

W. Betz, H. Peitz, B. Müller, W. Greiner
Institut für Theoretische Physik der J.W.G.-Universität Frankfurt/Main

J. Kirsch
GSI Darmstadt

The coupled channel equations can be used to derive an electron current density operator. With the help of Maxwell's equation the photon spectrum in heavy ion collisions can be calculated in second quantization (see figure). This method has been chosen to replace intensive calculations of configurations resp. Slater determinants. One has to use the two-center basis to describe phenomena such as alignment (different population of magnetic substates) and the anisotropy of the photon spectrum.[1,2,3] Calculations with light systems, such as Ni + Ni show good agreement with experiments.
The electron-electron interaction is taken into account by considering an effective (Hartree-Fock) correction for the electron binding energies and the coupling matrix elements in those calculations.

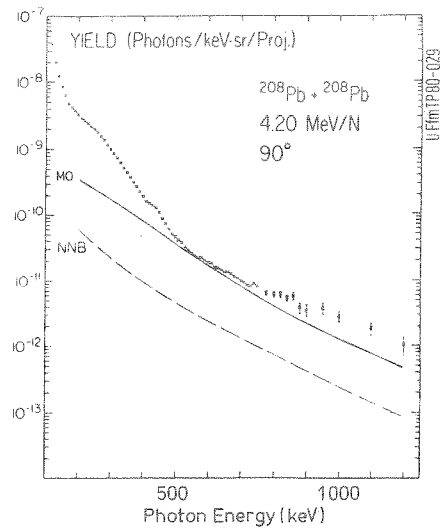


Fig. 1:
Comparison of the theoretical MO-X-ray spectrum of Pb+Pb with the experimental data of W.B. Meyerhoff and W. Wöfli et al.

[1] J. Kirsch, W. Betz, J. Reinhardt, B. Müller, W. Greiner, G. Soff; Z. Physik A292, 227-34 (1979)

[2] J. Kirsch, W. Betz, B. Müller, J. Reinhardt, G. Soff; Proc. of the ISIAC VI, Tokio, 1979, p. 79

[3] J. Kirsch, W. Betz, B. Müller, W. Greiner, G. Soff, XVIIth International Winter Meeting, Bormio/Italy

[4] W.E. Meyerhoff, W. Wölfli, et al, to be published

Contributions to the spectroscopy of electron states in superheavy quasimolecules [B]

J. Reinhardt, G. Soff, H. Peitz, W. Betz, K.H. Wietschorke, U. Müller, U. Heinz, J. Theis, T. de Reus, B. Müller, W. Greiner
Institut für Theoretische Physik der J.W.G.-Universität Frankfurt/Main

J. Kirsch
GSI Darmstadt

The following processesplay an important role in heavy ion collisions.

a) K-hole probabilities, which experimentally can be detected by the intensity of the characteristic X-rays emitted,
b) creation of positrons and electrons
c) quasimolecular X-rays and the anisotropy in the angular distribution of the emitted rays.

The calculations where the nuclear motion is described classically and the quantum mechanical motion of the electrons treated in a coupled channel code, have been continued. The coupled channel equations are the result of an expansion of the exact, time-dependent electron wave functions in the adiabatic basis. Extensive calculations have been done approximating the Coulomb potential of the nuclei in the collision process by the monopole term.

A problem arises in the overcritical case where the adiabatic electron states dive into the lower continuum. It was solved by Reinhardt within a projection method where the resonance in the lower continuum is split into a bound and a scattering state. The elegance of this method is demonstrated in the appearance of anadditional term in the modified coupled channel equations describing the spontaneous decay of the Dirac vaccum in overcritical Coulomb fields.[1-11]

The calculations with the adiabatic two-centre Dirac-wave functions for the electrons was extended. It is now possible to calculate the rotational coupling during the collision, which does not contribute in the monopole approximation. The quality of the basis used for the electron wave functions has been discussed, and it was found that a suitably chosen adiabatic basis will be ideal for the description of heavy ion collisions.

(On the other hand an adiabatic basis is very bad for the description of a gravitating collapsing mass distribution.[12,13]

In all calculations the coupling matrix elements don't fall off rapidly enough at large internuclear distances, because the asymptotic translational velocity of the electrons, following the nuclear centre - of - mass, has not been considered.

Within the new calculations the translational effects of the electronic motion are now considered in the coupled channel equations.[14]

[1] J. Reinhardt, B. Müller, W. Greiner, G. Soff Z.Physik A292, 211-2 (1979)

[2] J. Reinhardt, B. Müller, W. Greiner, G. Soff Phys.Rev.Lett. 43, 1307-10 (1979)

[3] G. Soff, J. Reinhardt, B. Müller, W. Greiner in print in Z. Physik A

[4] G. Soff, J. Reinhardt, B. Müller, W. Greiner Phys. Rev. Lett. 43, 1981 (1979)

[5] J. Reinhardt, B. Müller, W. Greiner Plenum Press, New York, 1979, p. 331-59

[6] J. Reinhardt, B. Müller, W. Greiner, G. Soff, Proc. of the XVIIth Intern. Winter Meeting on Nuclear Physics, Bormio/Italy, 1979, p.1-67

[7] J. Reinhardt, B. Müller, W. Greiner Proc. of the Erice School on Heavy Ion Interactions at High Energies, Erice/Italy, March 1979

[8] J. Reinhardt, G. Soff, B. Müller, W. Greiner Dynamical Aspects: Coherent Production of Positrons in Heavy Ion Collisions, ibid

[9] G. Soff, J. Reinhardt, W. Betz, J. Kirsch, B. Müller, W. Greiner, ibid 1979

[10] J. Reinhardt, W. Betz, J. Kirsch, B. Müller, W. Greiner, G. Soff, Proc. of the XIIth Summer School of Nucl.Phys. Mikolajki/Pol.79

[11] G.Soff, W. Greiner, W. Betz, B. Müller; Phys.Rev. A20, 169 (1979)

[12] J. Theis, J. Reinhardt, B. Müller; J.Phys.B: Atom.Mole.Phys.12, L479-83 (1979)

[13] J. Theis, B. Müller; 1980 to be published

[14] U. Heinz, Dissertation 1980

B

Contributions to the emission of positrons and δ -electrons in heavy ion collisions

J. Reinhardt, G. Soff, B. Müller, W. Greiner
Institut für Theoretische Physik der J.W.G.-Universität Frankfurt/Main

It is proposed that the positrons created in heavy ion collisions result from three processes. There are

a) a strong increasing rate ($\sigma \sim (Z_1+Z_2)^{20}$) of direct created electron-positron pairs, - known as the shake-off of the vacuum polarization,
b) the induced positron emission, which results from the filling of the inner electron shells,
c) the spontaneous decay of the vacuum.

The comparison of the positron cross sections for under and overcritical systems showed no qualitative differences. Therefore it was suggested to study deep inelastic reactions, where the nuclei stick together for about 10^{-20} sec. In these reactions the decay of the vacuum in overcritical fields should be indicated By an intensive positron line in the spectrum. In this connection the exciting discovery has been made that a certain sticking time Δt of the colliding nuclei is connected with an interference pattern in the energy width $\Delta E = \hbar/\Delta t$ for the positron - and δ -electron-spectra. This gives a method for the experimental verification of very short reaction times ($\Delta t \approx 10^{-20}$ sec) and has been called "atomic-clock".[1,2]

The energy dependence of measured δ -electron spectra, for instance Pb + Sn(Kozhuharov et al) can be well reproduced theoretically.

[1] J. Reinhardt, B. Müller, W. Greiner, G. Soff; Z.Physik A292, 211-2 (1979)

[2] G. Soff, J. Reinhardt, B. Müller, W. Greiner Phys.Rev.Lett. 43, 1981 (1979)

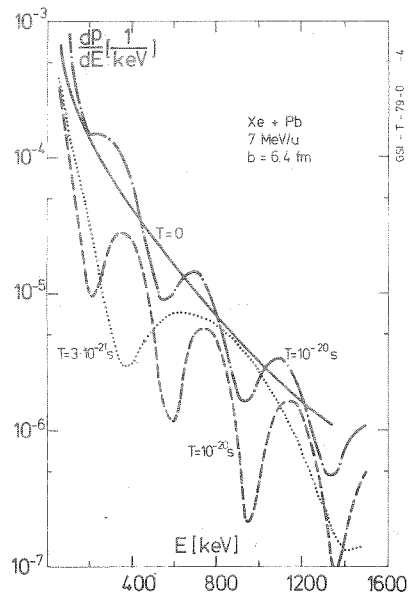


Fig. 1:
Differential emission probability with respect to kinetic delta-electron energy. A coincidence with created 1sσ-formation is required. The nuclear delay times T = 0, $3\cdot10^{-21}$s and 10^{-20}s are considered. The dashed-dotted line represents the total delta - electron spectrum ($T = 10^{-20}$s) originating from 1sσ, 2sσ and 3sσ -ionization.

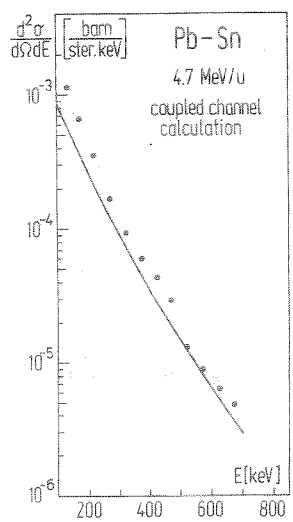


Fig. 2:
Delta electron spectrum in Pb-Sn collisions in coincidence with Pb K-Xrays. Data from Kozhuharov et al.

An atomic clock for deep-inelastic heavy-ion collisions [G]

Gerhard Soff
GSI Darmstadt

and

Joachim Reinhardt, Berndt Müller, and Walter Greiner
Institut für Theoretische Physik, Universität, 6000 Frankfurt am Main

One of the central questions in deep inelastic heavy ion scattering is the determination of the sticking time of superheavy nuclear composite system. We calculate the δ-electron distribution resulting from heavy ion collisions with projectile energies above the Coulomb barrier. It is shown[1,2] that the life time ($T \gtrsim 10^{-21}$s) of superheavy composite systems causes pronounced oscillations in the electron spectrum. The width of the oscillations is found to be $\varepsilon = h/T$. This effect can be used to measure sticking times quite accurately.

We have considered as an example the systems ^{136}Xe + ^{208}Pb with E_{LAB} = 7 MeV/u and grazing impact parameter because it allows for measurements in coincidence with a K-X-ray from the target-like fragment. Our conclusions hold qualitatively for any other superheavy system. The principal mechanism how a nuclear time delay influences the excitation amplitude becomes most transparent in time-dependent perturbation theory for electron excitation. In this approximation we find that the probability of ionizing an electron from state i into the continuum state j for a fixed delay time T is given by

$$dP_i(\Delta E,T)/dE_j = 4|a'|^2 \sin^2[(T/2)\Delta E + \arg(a')].$$

Here a' is the amplitude after the incoming branch of the trajectory, $\Delta E = E_i - E_j$ is the energy difference between states i and j in the nuclear compound configuration. Obviously, dP_i/dE_j exhibits regular oscillations in the δ-electron energy E_j. These oscillations became slightly damped if higher-order and many-electron effects are included. The electron spectra resulting from corresponding coupled-channels calculations is shown in the figure. Without nuclear reaction time the spectrum is a smoothly falling function, while a sticking time $T = 10^{-20}$s produces oscillations with a period of 400 KeV.

Taking into account energy dissipation which destroys the symmetry between the incoming and outgoing branches of the Coulomb trajectory we find that the spectrum as a whole is lowered, but the oscillations remain qualitatively unchanged.

The nuclear reaction may not be sharp but distributed over a certain range. Assuming a Gaussian distribution function of T centered at T_0 it results that in principle only a few oscillations can be observed. For increasing electron energy, the oscillations become more and more damped.

[1] J. Reinhardt, B. Müller, W. Greiner, G. Soff
Z. Physik A292 (1979) 211

[2] G. Soff, J. Reinhardt, B. Müller, W. Greiner,
Phys. Rev. Lett. 43 (1979) 1981

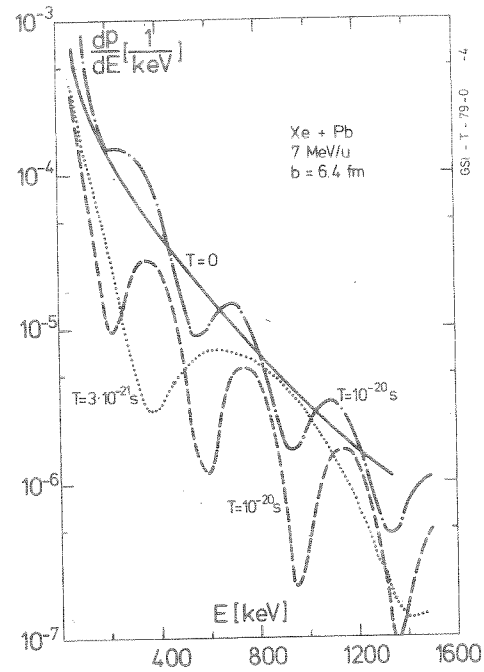


Figure caption

Differential emission probability versus kinetic δ-electron energy. A coincidence with created 1sσ vacancy formation is required. The dash-dotted line represents the total δ-ray spectrum ($T = 10^{-20}$s).

Test of molecular total energy calculations in an SCF procedure [G]

R. Euler, B. Fricke, T. Morović, W.-D. Sepp
Physics Department, University of Kassel

A. Rosén
Physics Department, Chalmers University of Technology, Göteborg, Sweden

The development of a relativistic Dirac-Slater code which is reviewed in earlier works [1] now makes it possible to calculate wavefunctions and energy eigenvalues of small molecules including heavy atoms.

Up to now, all interpretations of relativistic calculations have been made only within the so-called transition state procedure [2]. Due to the numerical inaccuracy of the method involved, only one attempt has been undertaken earlier to calculate directly total energies for a low Z molecule [3]. Here we present our first attempt to achieve ab initio relativistic potential energy curves for a heavy system. As examples we have chosen various noble gas difluorides. The reason for this choice is the theoretical importance of these compounds which did not exist until the early 60's. Furthermore, there exist very elaborate non-relativistic calculations [4,5]. The only noble gas difluorides which are known are KrF_2 [6] and XeF_2 [7,8] with a bond length of 3.5 and 3.8 a.u., respectively, and bond energies of 1.01 and 2.08 eV.

The basis set for the noble gas has been generated in the $n\,p^6$ configuration for the free atom problem. The molecular potential was determined in the successive iterations, from Mulliken gross orbital populations for the basis functions. The total energy in an actual numerical calculation using this method is not achieved easily, because the convergence of the SCF procedure still is very slow.

The result presented in Fig. 1 for the potential energy curve of KrF_2 shows a rather smooth behaviour. In this calculation we use the basis set, enlarged by 4d, 5s and 5p wavefunctions of atomic Kr. The comparison with the minimum basis set calculation shows that the result is basis set dependent, but the trend goes into the right direction. So we can expect that the inclusion of a few additional atomic wavefunctions leads to the correct behaviour of the potential energy curve for large distances. The main discrepancy up to now is that the absolute minimum is by far too deep. Table 1 presents the results of the calculated binding energies and bond distances for NeF_2, ArF_2, KrF_2 and XeF_2 to compare with the experimental results of KrF_2 and XeF_2. This allows us to extrapolate an "experimental" value for the binding energy E_B for ArF_2, which is expected to be ≈ 0.5 eV. The theoretical potential energy curve for NeF_2 does not show a clear minimum, so that it cannot be expected that NeF_2 may exist.

Summary: This work for chemical distances is necessary in order to improve the accuracy of the calculations for the scattering potential in heavy ion collisions for small internuclear distances.

TABLE 1

		NeF_2	ArF_2	KrF_2		XeF_2	
		rel	rel	rel	nonrel	rel	nonrel
Calc.	R_B/a.u.	3.0	3.50	3.45	3.40	3.61	3.52
	E_B/eV	0.3	2.95	6.60	7.10	12.20	13.10
Exp.	R_B/a.u.	-	-	3.54 Ref. 6		3.8 Ref. 7	
	E_B/eV	-	-	1.01 Ref. 6		2.8 Ref. 8	

[1] A. Rosén et al., Chem. Phys. Lett. 27, 595 (1974); J. Chem. Phys. 62, 3039 (1975)

[2] A. Rosén et al., J. Physique C4, 218 (1979)

[3] T. Ziegler et al., Theor. Chim. Acta 46, 1 (1977)

[4] P.S. Bagus et al., J. Am. Chem. Soc. 94, 6635 (1972); ibid, 97 7216 (1975)

[5] H. Basch et al., J. Chem. Phys. 55 1922 (1971)

[6] C.R. Brundle et al., J. Chem. Soc. Faraday 68, 959 (1972)

[7] J.G. Malm et al., Chem. Rev. 65, 199 (1965)

[8] J. Berkowitz et al., J. Phys. Chem. 75, 1461 (1971)

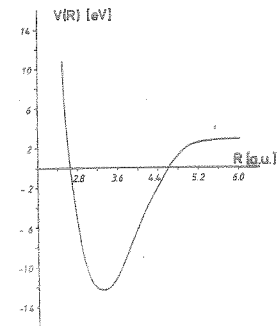


Fig. 1
Potential energy curve for KrF_2 with extended basis.

Relativistic molecular calculations of superheavy molecules [G]

T. Morović, W.-D. Sepp, B. Fricke
Physics Department, University of Kassel

A. Rosén
Physics Department, Chalmers University of Technology, Göteborg, Sweden

In the recent years a number of atomic calculations have been carried out in the region of superheavy elements. With sophisticated interpretations of these results one was able to get a first idea of the physical and chemical properties of the still unknown superheavy elements. These results have been reviewed by Hermann [1] and Fricke [2]. Many authors [1-3] also have emphasized that further development in this field is dependent on realistic (which in this case means relativistic) calculations for molecules containing superheavy elements. A better knowledge of their chemical and physical properties is the condition for the successful extraction and identification of possibly artificially generated superheavy atoms. Calculations have been performed for $(E106)F_6$ and its 4d and 5d elements analogous to MoF_6 and WF_6 for comparison. This also has to be compared with our results [4] for $(E110)F_6$, the analogy to the 5d element PtF_6.

The calculation procedure which is based on the relativistic self-consistent Dirac-Slater model is given elsewhere [5,6].

In Fig. 1 we present the outer electron structure resulting from relativistic calculations of $(E106)F_6$, WF_6 and MoF_6 as well as a non-relativistic calculation of MoF_6. The composition and relative ordering of the molecular levels depend on the relative level positions for the constituent atoms, the crystal-field splitting and covalency effects. The experimental bond length of

$$R_{Mo-F} = 1.82 \text{ Å}, \quad R_{W-f} = 1.83 \text{ Å}$$

have been used; R_{E106-F} was estimated as 1.84 Å. Extended calculations [4] of $(E110)F_6$ have shown that the positions of the levels are very insensitive to changes even of 0.1 Å of the relative distance between the metal and the fluor atoms. For the valence electron levels at about - 10 eV, a more detailed analysis shows that there is a reordering of the valence levels for $(E106)F_6$, so that a γ_8^- level becomes the last occupied state, whereas in all lighter systems this is a γ_6^+ level.

The first excited states for these molecules (dashed levels in Fig. 1) are the crystal-field split t_{2g} and e_g molecular levels derived from the nd atomic level. Experimentally, the t_{2g} spin-orbit splitting for the 5d metal hexafluorides has been measured to be ≈ 0.6 eV [7], which is in good agreement with the relativistic result of (0.5 ± 0.1) eV. The corresponding spin-orbit splitting for $(E106)F_6$ is ≈ 1.2 eV. First ionization energies have been calculated by performing transition state calculations for the last occupied valence level with the results 14.4 eV, 14.5 eV and 14.4 eV for the MoF_6, WF_6 and $(E106)F_6$, respectively. This should be compared with the experimental values of 15.1 eV, 15.5 eV for MoF_6 and WF_6. Assuming the same discrepancy for $(E106)F_6$, we predict its first ionization energy to be 15.4 eV.

[1] G. Hermann, MTP International Review of Science, Series 2. Radiochemistry (Butterworth, London) 1975, p. 221

[2] B. Fricke, in Structure and Bonding (Springer Verlag, Heidelberg) 1975, Vol. 21

[3] I.P. Grant et al., Nature (London) 265, 715 (1977)

[4] A. Rosén et al., Phys. Rev. Lett. 40, 856 (1978)

[5] A. Rosén et al., Chem. Phys. Lett. 27. 595 (1974) and J. Chem. Phys. 62, 3039 (1975)

[6] D.E. Ellis et al., Z. Phys. A 283, 3 (1977)

[7] W. Moffit et al., Mol. Phys. 2, 109 (1959)

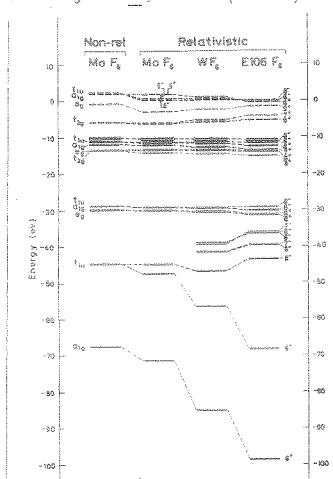


Fig. 1

Energy eigenvalues of the outer electrons for MoF_6, WF_6 and $(E106)F_6$.

Spin polarization of electrons induced by strong collisional magnetic fields [G]

Gerhard Soff
GSI Darmstadt

Joachim Reinhardt and Walter Greiner
Institut für Theoretische Physik, Universität, Frankfurt am Main

We calculated the spin polarization of 1sσ-vacancies and emitted δ-electrons induced by the strong magnetic field ($|\vec{B}_{max}| \sim 10^{16}$G) in collisions of very heavy ions ($Z_1 + Z_2 = 178$). Within the adiabatic, quasimolecular picture we solved for the first time the coupled channel equations for the electron occupation amplitudes $a_{ij}(t)$ with inclusion of the scalar and vector potentials in the transverse Coulomb gauge

$$\dot{a}_{ij}(t) = -\sum_{K=1}^{\infty} a_{iK}(t)[\langle\phi_j|\frac{\partial}{\partial t}|\phi_K\rangle + i\langle\phi_j|H'(t)|\phi_K\rangle] \cdot \exp\{ i\chi_{jK} \}_t \qquad (1)$$

with the phases $\chi_{jK} = \chi_j - \chi_K$ and $\chi_j(t) = \int^t E_j(t')dt'$. The basis states ϕ_j are determined as solutions of the stationary two centre Dirac equation.
The magnetic interaction is given by $H' = \vec{\alpha} \cdot \vec{A}$ with $\vec{\alpha}$ being the Dirac matrices. For the vector potential in the Coulomb gauge it results

$$\vec{A}_c(\vec{r},t) = -\sum_{i=1,2} \frac{Z_i e^2 \vec{v}_i(t)}{2|\vec{r}-\vec{R}_i(t)|} - \sum_{i=1,2} \frac{Z_i e^2 \vec{v}_i(t)\cdot(\vec{r}-\vec{R}_i(t))}{2|\vec{r}-\vec{R}_i(t)|^3}(\vec{r}-\vec{R}_i(t)) \qquad (2)$$

where $\vec{v}_i$ denotes the individual heavy ion velocity. Retardation, electron screening effects and the two body electron-electron interaction are neglected in our calculations. The solution of the many electron problem has been performed by the reduction to single electron occupation amplitudes.
As a main result we found that the additional magnetic interaction does not change the total ionization probabilities in collisions of very heavy ions below the Coulomb barrier but leads to spin polarizations of electron states. As dominant effect the Zeeman splitting of the 1sσ state gives rise to a stronger ionization of one of the usually degenerated spin states, whereas the other becomes less ionized. However, the total sum remains almost exactly the same as obtained with the Coulomb interaction only. The spin polarization of holes q is defined by

$$\eta_q = (N^y_{q+} - N^y_{q-}) / (N^y_{q+} + N^y_{q-}) \qquad (3)$$

where N^y_{q+} denotes the number of created holes with positive spin projection along the y-axis perpendicular to the scattering plane. The dependence of $\eta_{1s\sigma}$ on impact parameter b is shown in fig. 1. Its maximum value is obtained for medium impact parameters between b = 30 and 80 fm. The spin polarization η_p of δ-electrons versus kinetic electron energy E stemming directly from ionization of the 1sσ-state is presented in fig. 2 for b=20 fm. Larger polarizations are found for increasing δ-electron energy.

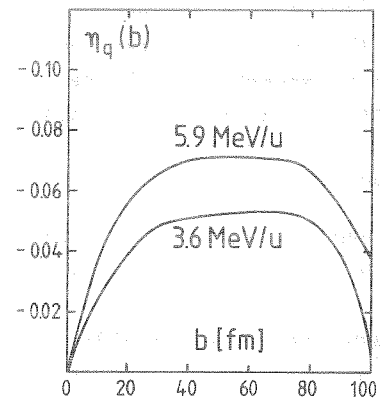


Fig. 1: Spin polarizations of 1sσ-vacancies versus impact parameter.

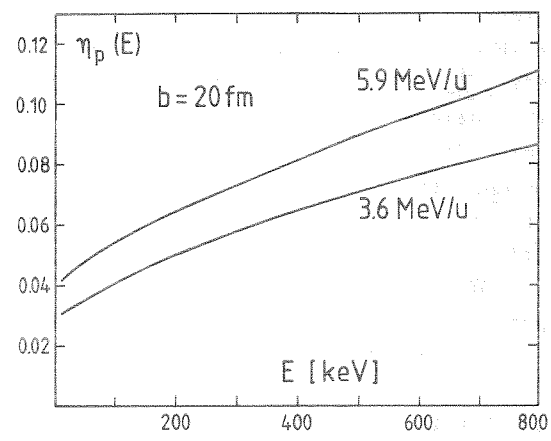


Fig. 2: Spin polarizations of emitted δ-electrons stemming directly from the 1sσ-state versus kinetic electron energy.

Heavy Ion Induced Mach-shock Waves in the Electron Plasma of Solids [G]

W. Schäfer, B. Müller, W. Greiner
Institut für Theoretische Physik der J.W.G.-Universität Frankfurt/Main

H. Stöcker
GSI Darmstadt

We demonstrate that heavy ion induced density fluctuations in the electron plasma of solids, called wakes[1], show the characteristic features of Mach-shock waves.

Treating the solid as a homogeneous electron plasma with the nuclear charges forming a rigid positive background, the response of the system to an external perturbation consists in oscillations around the equlibrium density ρ_0 of the medium.

If the perturbing particle has a velocity v_0 which exceeds the Fermi velocity v_F of the plasma electrons ($v_0 > v_F$) the oscillations manifest themselves in an axially symetrical wake behind the penetrating charge (see Fig.1)[2]. We interpret these collective density fluctuations, consisting of regions of enhanced and depleted electron density, as Mach-shock waves, which should lead to the directed emission of electrons from the solid. Considering the continuity equation we are then able to obtain the induced current density $\vec{j}_{ind}$ and the velocity of the electrons in the regions of enhanced density by dividing through the total charge density $\rho = \rho_0 + \rho_{ind}$ at eack grid point in the $\bar{z}$-r-plane. The emission angle is obtained from the relation

$$\Theta_{em}(\bar{z},r) = \arccos\left(j_0^2 / j_{ind}^2\right)^{1/2}$$

We propose to detect the electron wake in solid state materials by measuring the angular distribution of the emitted shock electrons, which show up as distinct maxima at certain angles (see Fig. 2).

We find that the emission angles increase with bombarding energy, following approximately the Mach relation $\cos\Theta_{em} = v_0/v_0$. First experimental results by K.O. Groeneveld et al[4] (1979) show qualitatively good agreement with our theoretical results.

1. J. Neufeld, R.H. Ritchie,
Phys.Rev. 98, 1632 (1955)

2. W. Schäfer, H. Stöcker, B. Müller, W. Greiner
Z.Phys. A288, 349 (1978)

3. W. Schäfer, H. Stöcker, B. Müller, W. Greiner
Z.Phys. B36, 319 (1980)

4. H.J. Frischkorn, K.O. Groeneveld, R. Latz, G. Reichhardt, J. Schader, S. Schumann, R. Mann,
Phys.Lett. (in print)

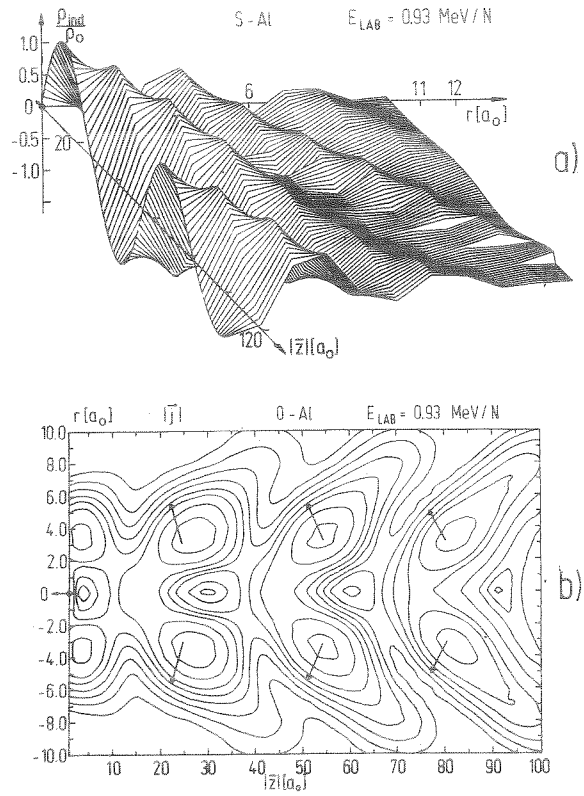


Fig.1a
A 3-dimensional plot of $n_{ind}(\bar{z},r)$ for the system ^{16}S-^{13}Al at E_{lab}=0.93 MeV/N is depicted as a function of the coordinates $\bar{z},r$. The formation of a cone structure in the charge density oscillations behind the projectile is clearly visible. b A contour-plot of the induced current density $\vec{j}_{ind}$ for the system ^{8}O-^{13}Al at E_{lab} =0.93 MeV/N. Lines of equal current density are plotted as function of the coordinates $\bar{z},r$ behind the projectile, marked as a black dot. Observe again the formation of conic structures. The direction and modulus of the current density is shown at several points by arrows.

PAGE

3. Solid States Physics and Biology 139

Influence of Latent Nuclear Tracks on the Magnetic Properties of Ferrimagnetic Garnet Films

H. Heitmann, P. Hansen
Philips GmbH Forschungslaboratorium Hamburg

R. Spohr
GSI Darmstadt

Ferrigmagnetic garnet films of composition $(Gd,Bi)_3(Fe,Ga)_5O_{12}$ have received considerable attention owing to their large magneto-optic effect allowing for application as a combined storage and display medium[1]. For optimization of the magneto-optic efficiency a film thickness of about 8 µm is required. A proper materials quality has been achieved using single crystalline films prepared by liquid phase epitaxy. In storage applications the stability of the magnetic domain pattern has to be increased by the introduction of pinning centers for magnetic domain walls. This can be achieved by irradiation with high energy heavy ions, e.g. ^{132}Xe of 1.4 MeV/u penetrating 10 µm into the garnet material. In order to understand the wall pinning effects the magnetic structure of the material within a nuclear track in its surrounding has to be investigated. We studied the effect of irradiation with 1.4 MeV/u ^{132}Xe ions on the saturation magnetization M_s and Faraday rotation θ_F of a garnet film with composition $Gd_{2.3}Bi_{0.7}Fe_{4.5}Ga_{0.5}O_{12}$. The sample of 2.5 cm diameter has been irradiated in 0.2 cm x 0.5 cm areas with 3 doses in the range from 10^{11} up to 13 x 10^{11} cm^{-2}. It has been found that the change of magnetic properties is proportional to the ratio of nuclear track area to the undistorted area. For reliable measurements ratios close to 100 % are required corresponding to an estimated dose of 10^{12} cm^{-2}.

We measured the temperature dependence of the saturation magnetization[2] and the Faraday rotation[3] in the temperature range from 4.2 K up to the Curie temperature T_C. T_C decreases with increasing dose while the compensation temperature remains nearly unchanged. The dose dependence of the saturation magnetization and the Faraday rotation at T = 4.2 K are displayed in fig. 1. Both exhibit essentially the same reduction with increasing dose. These experimental results can be interpreted in terms of a simple model as follows:

The longe-range order in the nuclear track volume is completely destroyed. The average ion distances in the track are increased causing a compressive stress onto the surrounding material[4]. Magnetic coupling is strongly perturbed and magnetic ordering has disappeared.

The boundary between the amorphous and the undamaged volume seems sharply defined because the shape of the temperature dependences of M_s and θ_F is not changed even in the areas irradiated with the highest doses. Therefore, the dependence on dose d can be described by the simple exponential law $M_s(T,d)/M_s(T,0) = \theta_F(T,d)/\theta_F(T,0) = \exp(-\sigma d)$ where σ is the effective cross-section of the track. The track diameter evaluated from fig. 1 is about 15 nm.

[1] B. Hill and K.P. Schmidt, Philips J. Res. 33, 211 (1978)
[2] P. Hansen and H. Heitmann, Phys. Rev. Lett. 43, 1444 (1979)
[3] H. Heitmann, P. Hansen, and R. Spohr, J. Magn. Magn. Mat. to be published 1980
[4] B. Strocka, G. Bartels, and R. Spohr, Appl. Phys. 21, 141 (1979)

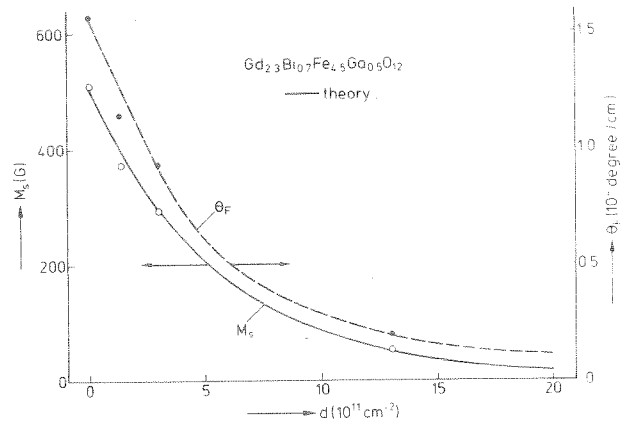


Fig. 1: Dose dependence of the saturation magnetization and the Faraday rotation (λ = 633 nm) at T = 4.2 K.

The described work was sponsored by the German Federal Ministry of Research and Technology (BMFT) under Grant No. NT 2007/3.

B

HEAVY ION INDUCED SPUTTERING OF GLASSES

K.Thiel, H.Külzer, W.Herr
Institut für Kernchemie der Universität Köln

U- and Th-containing silicate and phosphate glasses and vitreous lithium tetrabarate were irradiated with ^{40}Ar-, ^{56}Fe- and Xe-ions (nat.abundance) in the energy range of 50 to 130 keV to study heavy ion induced sputtering. Angular distributions of sputtered target atoms and total sputter yields were measured using a special nuclear track technique [1-2].

The sputtered U-,Th-,B- and Li-tracer atoms were collected in 2π-geometry on a teflon catcher foil and by n-induced autoradiography recorded on a suitable nuclear track detector. To get convenient track densities (~10^5...10^6 cm^{-2}) heavy ion doses of $10^{16}cm^{-2}$ and subsequent thermal or fast neutron fluences of approx. $10^{16}cm^{-2}$ were chosen.

To avoid surface charges on the target due to the ion bombardment charge compensation was provided using specially designed "electron showers".

A total of 29 targets were ion irradiated under polar angles of 0°, 45° and 60° and the resulting track signals semi-automatically scanned and counted. Sputter yields as derived from the number of tracer atoms on the catcher foils were checked independently by interferometry of the target area in reflected light, proving that no preferential sputtering occured in the ion dose range chosen. Expecially no dose-dependent effects were observed for ion doses from $5x10^{16}$ to $5x10^{17}cm^{-2}$ in the case of U-phosphate glass.

From the track autoradiographs of the catcher foils in most cases of oblique ion incidence, differential sputter yields for 126 different solid angles were calculated. For vertical ion incidence the angular distribution of sputtered tracer atoms was fitted by the expression $a \cdot \cos^b$ revealing a so-called "overcosine" distribution (b>1) of sputtered atoms ejected preferentially perpendicular to the target surface. This type of angular distribution indicates an energy transfer originating from deeper regions of the collision cascade. For oblique ion bombardment a distinct forward-backward asymmetry in the plane of incidence was observed. The intensity of sputtered atoms has a maximum in forward directions. An example for forward-backward asymmetry is shown in fig 1 giving the azimuthal variation of sputter yields at constant polar angles for a ^{56}Fe-irradiation of phosphate glass under 60° ion incidence.

An important feature in view of the surface erosion of extraterrestrial samples and the corrosion of fusion reactor walls is the ejection of so-called "chunks". Their emission and size distribution was found to depend on surface charging and was effectively supressed by charge compensation.

In fig 2 the track density and the "chunk" frequency as a function of polar angle is plotted for $Li_2B_4O_7$. Single atom sputtering and "chunk" emission are anticorrelated for $Li_2B_4O_7$ (fig 2) but show positive correlation in the case of silicate and phosphate glasses. At oblique ion incidence chunk emission was found to occur mainly in forward directions. Experiments to study the sputtering of rock-forming minerals are in preparation.

[1] K.Thiel, H.Külzer, W.Herr, GSI 79-11(1979) p 140
[2] K.Thiel, H.Külzer, W.Herr, Nuclear Tracks 3(1979) (in press)

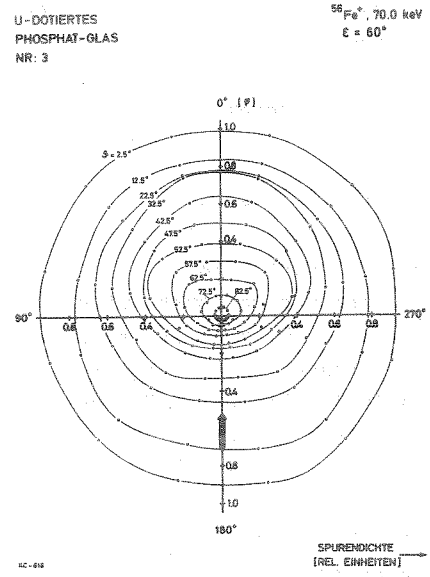


Fig 1: Sputter yield (rel.units) as a function of azimuth angle for various polar angles
Target: U-phosphate glass. Ion: 70 keV ^{56}Fe.
Angle of incidence: 60°.

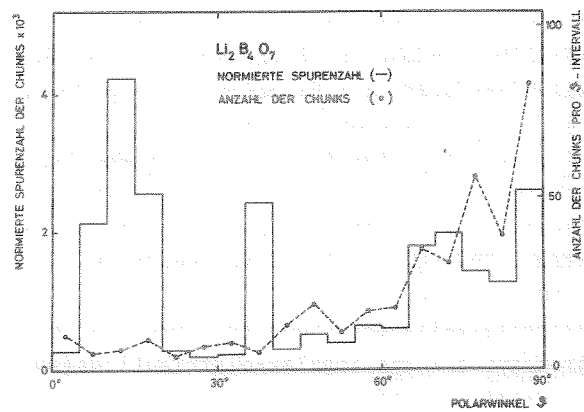


Fig 2: Track density normalized to unity ion dose and unity neutron fluence (solid bars) and chunk frequency (dashed line) as a function of polar angle.
Target: $Li_2B_4O_7$. Ion: 70-100 keV Xe.
Angle of incidence: 45°.

IN SEARCH OF HEAVY ION INDUCED COLLECTIVE ELECTRON EMISSION FROM SOLIDS [B]

H.J.Frischkorn, K.O.Groeneveld, S.Schumann, R.Latz, G.Reichhardt, and J. Schader
Institut für Kernphysik der J.W.Goethe-Universität,Frankfurt/M,Germany
W.Kronast
Gesellschaft für Schwerionenforschung, Darmstadt/Germany

Energetic (~ MeV/N)ions penetrating solids induce electron density fluctuations behind the projectile. These fluctuations can be represented by the wake potential[1,2], which is characterized a) by the charge and velocity of the projectile v_p and b) by the plasma properties of the solid. Phenomenologically, the wake potential can be compared to water surface waves (velocity v_s) produced by a ship which moves on the water with a velocity $v_p > v_s$. Experimental evidence for the wake potential properties can be found in the stirring force exerted on the internuclear direction of energetic (MeV/N) diatomic molecular projectiles penetrating the solid (kinematic experiments[2,3], electronic deexcitation[4]).

It has been predicted by Schäfer et al.[5] that such electron density fluctuations cause the directed, collective emission of electrons from solids. Signatures of these electrons are:

1. Energies $1 < E_e < 10$ eV depending mostly on the projectile velocity v_p.
2. The emission direction follows the Mach relation $v_s/v_p = \cos \vartheta_e$.
3. The angular distribution peak at ϑ_e has a half width of ca 10 to 20^0 depending on E_p and the collision system.

Possible evidence for electrons with these characteristics have been found in the C-C-collision system at $3 < E_p < 20$ MeV[6,7], and in the Pb-C-collision system at $E_p = 290$ MeV. The conclusiveness of this experiment is hindered by a number of experimental problems which are difficult to control. In particular, the exit surface of the solid is not microscopically plane; the surface can change its properties (e.g. work function) by the heavy ion impact or by contamination with residual gas atoms. However, a surprising agreement is found between the predicted "fingerprints" and the experimentally observed structures in the electron energy- and angular-distributions (see Fig.1) Systematic studies of different collision systems as a function of E_p are needed to verify this interesting new type of electrons.

Additional support for the concept of collective electron emission stems from a recent experiment[8] from Uppsala; macro-molecules are detached from solid surfaces by heavy ion impact, a mechanism which is explained by the wake potential.

1. V.N.Neelavathie, R.H.Ritchie, W.Brandt,Phys.Rev.Lett. 33, 302 (1974)
2. Z.Vager, D.S.Gemmell, Phys.Rev.Lett.37 1352 (1976)
3. E.P.Kanter, P.J.Cooney, P.S.Gemmell, K.O.Groeneveld, J.W.Pietsch, A.J.Ratkowski, Z.Vager,B.J.Zabransky, Phys.Rev. A20, 834 (1979)
4. S.Schumann, H.J.Frischkorn, R.Kluge, D.Rosich, J.Schader, I.O.Groeneveld, J.de physique 40,C1-354 (1979)
5. W.Schäfer, H.Stöcker, B.Müller, W.Greiner, Z.Phys.A288 349 (1979) and Z.Phys.(1980), to be published
6. H.J.Frischkorn, K.O.Groeneveld, S.Schumann, R.Latz, G.Reichhardt, J.Schader, W.Kronast, R.Mann, Phys.Lett (1980) to be published
7. H.J.Frischkorn, K.O.Groeneveld, S.Schumann, J.Schader, G.Astner, S.Hultberg,L.Lundin, R.Ramanujam,R.Didriksson, B.Sundqvist, P.Håkansson, Verhandl.DPG(VI)15(1980)
8. S.Sundqvist, P.Håkansson, A.Johansson, J.Fohlman, P.Peterson, Univ.of Uppsala, to be published

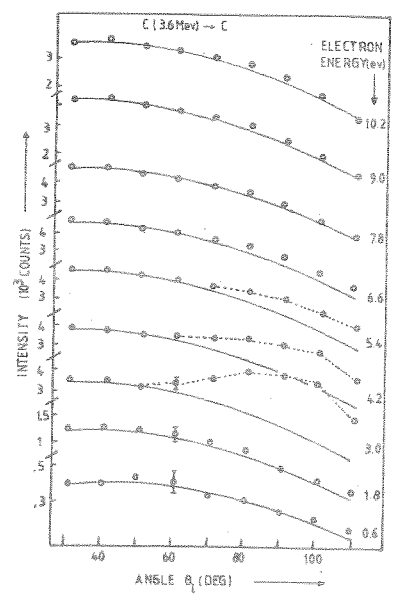


Fig.1: Angular distributions of electrons emitted from C(3.6MeV) → C collisions with different electron energies Ee[5].

Radiation-Induced Defects in Type-II Superconductors

V. Graeger, H.C. Freyhardt
Institut für Metallphysik, Universität Göttingen

A type-II superconductor in the mixed state can carry (large) lossless transport currents only if the flux lines become pinned; i.e. its current density is determined by the micromechanics of pinning forces. To investigate the fundamental pinning problem - the summation problem - model systems are required with geometrically simple obstacle structures. Radiation induced lattice defects, in particular voids in niobium, are well suited for this purpose. Their size distribution and density can be varied by changing the impurity concentration of the niobium and the irradiation conditions.

In earlier experiments[1,2] various void distributions were created during high-temperature irradiation (500-1000°C) of niobium foils with 3.4-MeV Ni^+ ions (up to 6×10^{16} Ni^+/cm^2). It became desirable to extend these investigations to irradiations (a) with (very) high-energy particles (to achieve a homogeneous damage or void distribution in a thin niobium foil, (b) with rare-gas ions and self ions ($Nb^+ \rightarrow Nb$). Irradiations with a 1.4 MeV/nucleon $^{136}Xe^{33+}$ beam yielded indeed the desired homogeneous damage in thin foils, however, the beam current was too small. Much higher particle currents (1.2×10^{13} $Ne^{2+}cm^{-2}sec^{-1}$, 1.6×10^{12} $Nb^{2+}cm^{-2}sec^{-1}$) became available by using the Unilac test-injector. Thus displacement rates larger than 200 dpa (displacements per atom) could be achieved. However, at an energy of 480 KeV Ne^{2+} ions penetrate the niobium only to an average distance of ~ 500 nm (~ 100 nm for 480-KeV Nb^{2+}) and voids are formed in thin layers near the surface. A systematic variation of the irradiation temperature and particle dose allowed the introduction of different void size distributions (an example is given in Fig. 1) leading to volume increases ("void swelling") up to $\Delta V/V = 8{,}5\%$.

The (overall) critical current density at 4.2 K, which gives a measure for the pinning of flux lines by voids, increases with irradiation temperature for fixed Ne^{2+} dose (Fig. 2). After the irradiation the upper critical field is enhanced to 0.85 T due to the contamination of the foil with interstitial impurities (irradiation vacuum ~5×10^{-7} Torr). Self-ion irradiations were performed in improved vacua (differential pumping) and no impurity pick-up was observed.

The measured critical current densities are compared to recent summation theories[3] for irreversible type-II superconductors and to calculations of the elementary interaction forces between voids (bubbles) and flux lines.

[1] H.C. Freyhardt, J. Low Temp. Phys. 32, 101 (1978); Phil. Mag. B38, 15 (1978)

[2] H.C. Freyhardt, V. Graeger, J. Nucl. Materials 72, 34, (1978)

[3] E.J. Kramer, J. Nucl. Materials 72, 5 (1978)

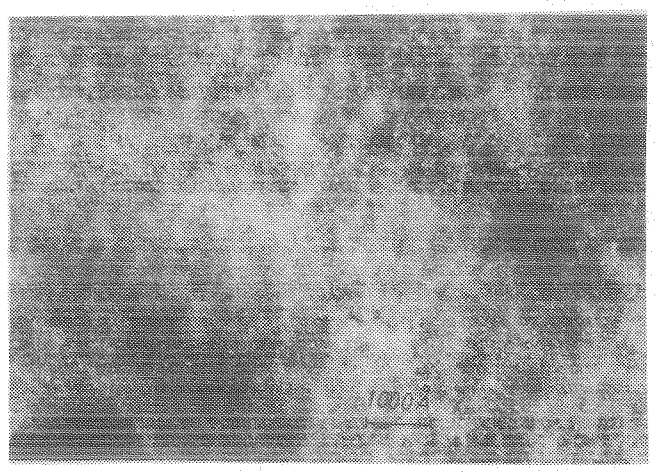


Fig. 1: Voids in niobium introduced by a 480-KeV Ne^{2+} irradiation (T_{irr} = 980°C, 170 dpa). Average void diameter = 7,5 nm, $\Delta V/V$ = 1.3 %

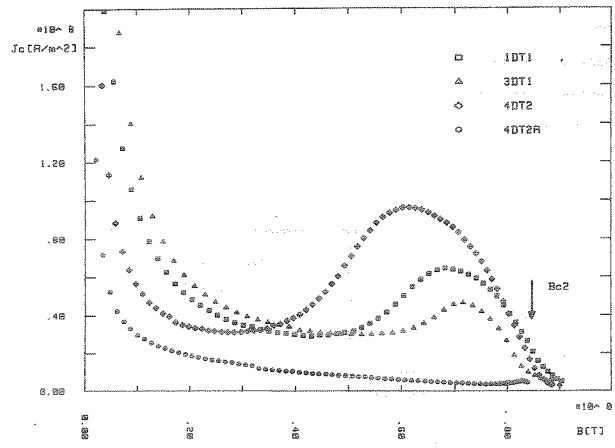


Fig. 2: Overall critical current density J_c vs magnetic field B for different irradiation temperatures (Δ: 780°C, ▭ : 920°C, ◇ : 980°C). 480-KeV Ne^{2+}/170 dpa. ⊙ : damaged layers is etched away.

HEAVY ION INDUCED THERMOLUMINESCENCE OF CALCITE AND FLUORITE [B]

U.Bangert, K.Thiel, W.Herr

Institut für Kernchemie der Universität Köln

High temperature thermoluminescence (TL) of artificial $CaCO_3$ and CaF_2 is studied in order to examine the applicability of TL-dating to naturally occurring calcite and fluorite deposits.

A detailed knowledge of the influence of certain impurities acting as luminescence centres and/or trapping sites in these crystals should improve our understanding of the TL-process and contribute to better defined TL-ages of natural $CaCO_3$- and CaF_2-containing samples.

The implantation technique was used to dope high purity artifical crystals with well-defined amounts of "Impurities" which are thought to affect the TL-signal [1-2].

Particularly Fe-,Mn-,Y-, and Dy-ions were implanted in the dose range of ~$5x10^{14}$ - ~$5x10^{15}$ cm^{-2} and in the energy range of 80-160 keV.

The measured glow curves of $CaCO_3$ indicate that the 200°C-TL-peak which normally is used for the dating [3-4] of calcite deposits can be induced by Dy as well as by combined implantation of Mn and Y (cf fig 1). In this case Mn obviously acts as luminescence centre and Y as trapping site, whereas Dy acts in a bimodal way as luminescence and trapping centre.

The TL-responce of the targets strongly varies with the concentration of the implanted "impurity". In the case of Dy-ions the TL-sensitivity of calcite increases with increasing ion dose up to $2.5x10^{15}$ cm^{-2} whereas the TL-sensitivity of fluorite in this dose range already starts to decrease due to "concentration quenching".Additional ESR-measurements of the irradiated targets shall give information about the change of lattice symmetry in the vicinity of the implanted ions due to the damage of the latent ion tracks.

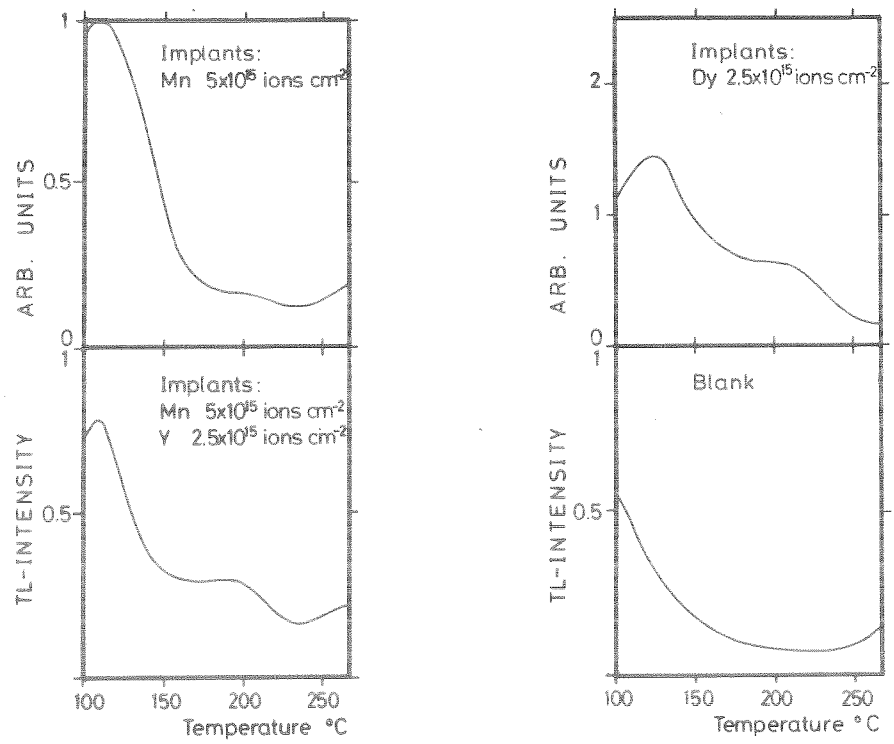
First measurements on CaF_2:Mn give evidence for the occurrence of Mn in the bivalent state in a rather undisturbed cubic symmetry.

1 S.A.Marshall, J.A.Mc Millan, J.Chem.Phys., 48,5131. (1968)

2 W.L.Medlin, Thermoluminescence of Geological Materials, Academic Press, London and New York, 193,(1968)

3 A.G.Wintle, Can.J.Earth Sci., 15,1977,(1978)

4 G.J.Hennig, U.Bangert, W.Herr, A.N.Poulianos, Anthropos, 7,172,(1980)



Tl-glow curves of $CaCO_3$ doped with Mn, Y and Dy. Signals are induced by a ß-dose of 480 krad.

The Influence of Ion Bombardment on the Corrosion Behaviour of Iron [B]

-Mechanistic Investigatons-

H.Ferber, G.K.Wolf, Institut für Physikalische Chemie der Universität Heidelberg

In a number of recent publications[1,2] we have reported on the modification of the corrosion properties of iron in aqueous solutions by means of ion bombardment. The corrosion current density of iron in sulfuric acid which is proportional to the corrosion rate could be enhanced by a factor of 10-100 implanting platinum or gold, and reduced by a factor of $\geq$10 implanting lead. The amount of material necessary for these modifications was less than 10$\mu g/cm^2$. The effect of gold and lead was especially interesting because of their insolubility in iron under equilibrium conditions.

The present study is concerned with the mechanism causing the phenomenon of increased or lowered corrosion rate. In this connection it has to be noticed that the effects due to the implanted elements are orders of magnitude higher than one would expect from their fraction of the surface area, and their contribution to the electrochemical properties of the resulting alloy system.

The following explanations of the mechanism have to be discussed:

1. Lattice defects produced during the bombardment.
2. Enrichment of implanted elements at the surface during the implantation or analysis procedure.
3. Changes of the surface area and structure due to selective dissolution reactions in the corrosion solution.
4. Precipitation of active clusters caused by the implantation process.

Experimental tests were performed in order to understand the importance of the different possible explanations. They yielded the following results:

1. Irradiations of iron with self ions and rare gases proved that pure lattice defects lead only to slightly increased corrosion rates.

2. From electrochemical measurements and depth profiling with Rutherford backscattering no enrichment of lead on iron surfaces could be deducted. On the other hand, gold was found to be enriched to a certain extent. But, since the effect of implanted gold is even higher than the one of smooth gold the enrichment allone can not account for the measured current densities.

3. In the lead case a major increase in surface area from selective dissolution is impossible because no selective iron corrosion takes place. Again for gold this reaction is possible. Inspection of the resulting surface with the microscope, and a comparison with experiments on sputtered foreign atom layers on the iron surface led to the conclusion that this process can not account for the magnitude of the effect.

4. Lattice location studies of our system with Rutherford backscattering at single crystals* showed the presence of a certain persentage of gold and lead clusters of unknown sice in the substrate lattice. Also microscopic investigations led to the conclusion that Pb forms during the course of the experiment clusters at grain boundaries of polycristallyne iron.

Thus at present the effect of gold and lead implantation on the corrosion behaviour of iron is explained as being partly caused by the formation of local elements with successive selective dissolution of iron and partly by the precipitation of highly reactive clusters of the elements in the substrate.

[1] H. Ferber, H.Kasten, G.K.Wolf, W.J.Lorenz, H.Schweickert and H.Folger, Corr. Science 20,117(1980)

[2] G.K.Wolf, Werkstoffe und Korrosion 30,853(1979)

* In collaboration with O.Meyer and W.A.Alberts, IAK, GfK-Karlsruhe.

The Electrocatalytic Activity of Iron Substrates bombarded with Platinum Ions

H.Kasten, G.K.Wolf, Institut für Physikalische Chemie der Universität Heidelberg

H.Folger, GSI Darmstadt

Recent Experiments dealing with the effects of ion bombardment (Au,Cu,Pb) on the corrosion properties of iron[1,2] showed a considerable difference of the corrosion rates in aqueous solution resulting from the novel surface layers. Mainly the cathodic hydrogen reduction reaction was strongly affected by the chemical nature of the implanted elements. Therefore the conclusion could be drawn that ion bombardment may improve considerably the electrocatalytic behaviour of certain materials.

Platinum is known hitherto to be the best electrocatalyst for the hydrogen redox reaction which is important in fuel cell and hydrogen technology. Consequently a study of the electrocatalytic activity of platinum implanted in iron substrates was undertaken.

The carefully pretreated iron samples were bombarded with Pt^{++} ions from the 300 kV accelerator of GSI. The ion energy was 400 keV and the dose varied from 10^{16} to $5x10^{16}$ ions/cm^2. The resulting surface layers are 500-1000 Å thick and contain 2-10 at% platinum. The electrocatalytic effect was measured by recording the potentiostatic current-density potential curves in 1N H_2SO_4 in the potential range of hydrogen evolution . Experimental details are reportet elsewhere[3]. The results are summarized in figure 1. Here the current density potential curves for implanted substrates are reproduced in comparison with untreated iron and smooth platinum. In addition a curve resulting from sputtering one monolayer platinum onto iron is plotted. There is clear evidence of implantation of 10^{16} Pt ions/cm^2 leading to an increase of the catalytic activity of iron for the hydrogen evolutin reaction by several orders of magnitude. The activity approaches easily the one of smooth platinum, even thoug the platinum content in the surface layer is only 2 at%. A bombardment with $5x10^{16}$ ions/cm^2 corresponding to 10 at% Pt shifts the activity well above the one of smooth platinum. In addition one realizes a change in the slope of the Tafel line in direction of the one of platinized platinum. The behaviour of the sputtered samples is different. Their activity is also higher than in the case of untreated iron but it does not reach the values for the implanted specimen or the smooth platinum.

Even more striking is a comparison of the different samples at a fixed negative polarization $\eta = \xi - \xi_{corr}$ or $\eta = \xi - \xi_{oH_2/H^+}$. For η = -50mV the current density of iron implanted with $5x10^{16}$ Pt ions/cm^2 is three orders of magnitude higher than iron, and two orders of magnitude than smooth platinum or platinum sputtered on iron substrates.

The conclusion of these findings is that one is able by bombarding iron with platinum ions to produce a very good catalyst for the hydrogen redox reaction. It acts in a completely different electrochemical potential region than normal platinum catalysts do. With commercial platinum catalysts of high surface area one is able to obtain even higher catalytic activity but, at the expense of consuming more platinum per unit surface. For implanted samples 1-2% of the platinum content of the commercial ones are sufficiant (10-20 µg/cm^2)

[1] H.Ferber, H.Kasten,G.K.Wolf,H.Folger GSI 79-11, 139

[2] G.K.Wolf, Werkstoffe und Korrosion 30,836 (1979)

[3] H.Ferber,H.Kasten,G.K.Wolf,W.J.Lorenz,H.Schweickert, H.Folger, Corr.Science 2),117 (1980)

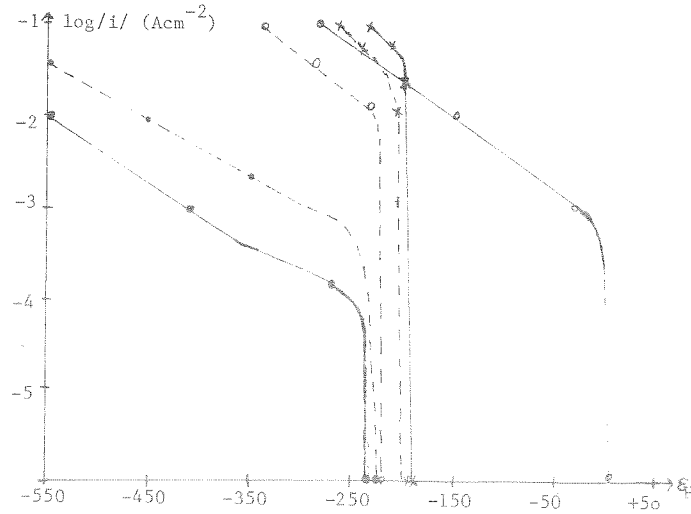


Fig. 1: Cathodic current-density potential curves in 1N H_2SO_4 of iron samples, bombarded with platinum (10^{16}/cm^2 ⊖---⊖, $2x10^{16}$/cm^2 ×---×, $5x10^{16}$/cm^2 ×—×) in comparison with untreated iron (⊖—⊖), smooth platinum (○—○) and one monolayer platinum sputtered onto iron (⊖-·-⊖).

G

Survival of vegetative yeast cells after irradiation with heavy ions

F. Schöpfer, E. Schneider, J. Kiefer, Strahlenzentrum der Universität Giessen
G. Kraft, GSI Darmstadt

Survival of wet yeast cells S. cerevisiae was determined as a function of the heavy ion fluence. From the exponential parts of the survival curves, effective inactivation cross sections were determined. The influence of different gaseous environments, of the ion velocity, of the post-irradiation treatment, and of genetic differences on the radiation sensitivity of the cells was also studied.

The following results were obtained:

1. The different sensitivities of the three strains to X-rays persist also for radiations of extremely high ionisation densities. The sensitivities, therefore, appear to be not or only partially determined by the intracellular geometry.

2. For radiations of low and high relatively ionization density, the survival curves of strain 211 have an initial shoulder. This shoulder is missing for irradiation with Pb and U ions which means that there is no accumulation of sublethal damage for these radiations.
For U ions, the survival curves for both immediate and delayed plating (IP and DP) are practically identical, i.e. no delayed plating recovery occurs, in contrast to the response to less densely ionizing radiations. It had been stated by others that delayed plating-recovery in diploid yeast is independent of LET[1]. This general statement does obviously not hold true for very high LET.

3. Sensitization by O_2 was observed for irradiations with Kr ions of 7 MeV/u. The extent of the sensitization is twice as much as observed for α-rays of 2.6 MeV.

4. The particle velocity and, therefore, the δ-ray range influences the radiation sensitivity of the yeast cells to a similar extent as the energy loss does. This is indicated for example by the effective cross sections of strain 211 for Kr, Xe and Pb ions (see table).

[1] T. Alper: Cellular Radiobiology, Cambridge University Press 1979, p. 238

Ions	E/m MeV/u	dE/dx keV/µm	r(δ) µm	σ/µm² 211	211-1a	rad52a
^{84}Kr	7	3800	4	1.5	2.6	3.9
	4.4	4400	2	1.4	2.5	3.2
^{129}Xe	3.9	7400	2	1.4	3.6	3.8
	1.4	8200	0.3	1.0		
^{208}Pb	0.5	4400 to 9400	0.06	0.9	1.3	1.6
^{238}U	6	14100	3	2.0	4.3	

Table 1: Effective inactivation cross sections σ for the strains 211, 211-1a and rad52a. r(δ) = δ-ray range.

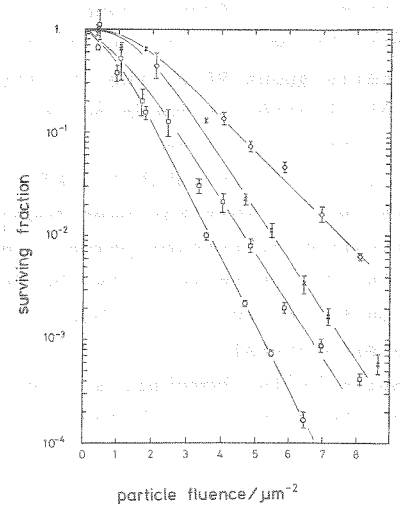


Fig. 1: Survival of diploid yeast cells (strain 211) after irradiation with Kr ions of 7 MeV/u in different atmospheres
○: air, IP; □: anoxic, IP; X: air, DP;
◇: anoxic, DP

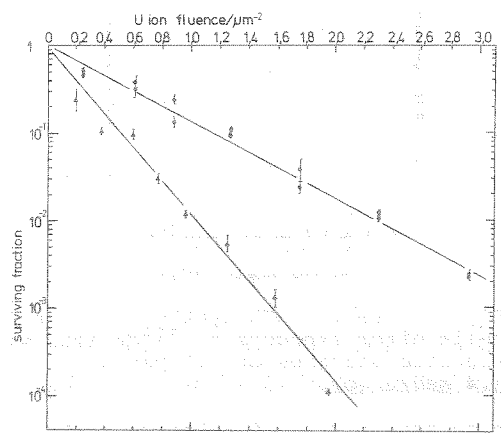


Fig. 2: Survival of differently sensitive yeast cells after irradiation with U ions of 6 MeV/u.
●: strain 211, IP; ○: strain 211, DP;
△: strain 211-1a, IP

G

Inactivation of ribosomal RNA synthesis in vegetative yeast cells after exposure to heavy ions

K.J. Weber, E. Schneider and J. Kiefer
Strahlenzentrum der Universität Giessen

G. Kraft and H. Liesem
GSI Darmstadt

The loss of colony forming ability (cfa-test) of yeast cells after exposure to heavy ions has been determined (1).
To investigate the effect of heavy ion irradiation on the function of important subcellular targets, we measured the template activity of DNA for transcription of ribosomal ribonucleic acid (r-RNA).
Our special assay was to measure the synthesis of r-RNA after irradiation.
r-RNA is transcribed from a gene - a scripton with a molecular weight of 3×10^6 Dalton.
In yeast cells about 90 of the 140 scriptons per cell are located as repeated sequences on a single chromosome (chromosome I).
The r-RNA synthesis is inhibited after particle irradiation. This has been found for the inactivation of transcription in dried yeast cells (2). In these cells the dependence on particle fluence has been found to be purely exponential.
In vegetative cells, however, a "resistant tail" could be measured at higher fluences (Fig. 1).

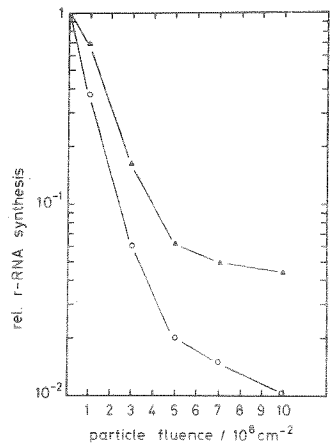


Fig. 1: rel. r-RNA synthesis in yeast cells after exposure to ^{129}Xe ions with specific energies of 3.9 MeV/u ( ) and 1.4 MeV/u (o).

The high sensitivity of relative r-RNA synthesis in the lower exposure region may be correlated with the inactivation of the large target - the gene cluster on chromosome I.

Additionally the remaining single genes contribute to total r-RNA synthesis with low sensitivity to the irradiation.
Apparent inactivation cross sections derived from initial slopes are presented in table 1.

ions	^{40}Ar	^{84}Kr		^{129}Xe		^{238}U	
spec. energy MeV/u	3.8	7.0	4.4	3.9	1.4	6.0	3.0
energy loss keV/µm	1800	3800	4400	7400	8200	14100	14800
inactivation cross-section ($\times 10^{-9}$ cm^2)	1.25	2.5	3.5	5.5	10	(~4)	(~5)

Table 1: formal cross sections for the inactivation of ribosomal RNA synthesis in yeast cells after exposure to heavy ions.

It can be seen from the table that σ increases if particle energy is lowered by an absorber foil.
With the experimental data available, however, no obvious functional dependence of cross section on energy loss could be found.

[1] GSI-Jahresbericht 1979, this issue

[2] GSI-Jahresbericht 1978, S.

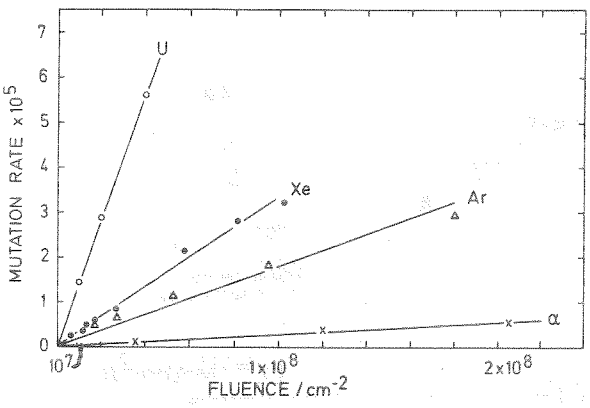
Mutation induction by heavy ions [G]

S. Rase, E. Schneider, J. Kiefer
Strahlenzentrum der Universität Gießen

H. Liesem, GSI Darmstadt

Wild type haploid yeast, Saccharomyces cerevisiae strain 211-1a, was exposed to heavy ions and for comparison also to ^{241}Am-α-particles and 80 kV-X-rays. Mutation was studied by the appearance of cells resistent to the arginine-analogue canavanine. Mutation rates are given as number of mutants per number of cells surviving. Fig. 1 shows mutation rates as a function of particle fluence for several ions; a relation either to LET or specific ion energy cannot yet be verified. From the linear part of the curves mutation cross sections may be calculated which are given in table 1.

U : $\sigma = 1.4 \cdot 10^{-12}$ cm²
Xe: $\sigma = 3.3 \cdot 10^{-13}$ cm²
Ar: $\sigma = 1.8 \cdot 10^{-13}$ cm²
α : $\sigma = 2.6 \cdot 10^{-14}$ cm²



The data are still preliminary. The interpretation is complicated by the fact that surviving cells form a heterogeneous population in terms of exposure experience. They consist on one hand of cells which were not hit even by a single particle and on the other hand of those which survived one or more particle hits. Induced mutants, however, are only formed in the latter subpopulation. This means that on an average surviving mutants received a higher dose than the whole population[1]. A detailed analysis is only possible when more data are available. Further experiments using other heavy ions with different energies.

[1] D.T. Goodhead, R.J. Munson, J. Thacker, and R. Cox, Int. J. Radiat. Biol. 37, 2, Feb.1980, S. 135

Fig. 1: Radiation induced mutation rates as a function of ion fluence.

^{241}Am-α-particles: LET_∞ = 160 keV/µm
Ar-ions: 4 MeV/u, LET_∞ = 1930 keV/µm
Xe-ions: 4,9 MeV/u, LET_∞ = 7300 keV/µm
U-ions : 7 MeV/u, LET_∞ = 13900 keV/µm

Inactivation cross sections of Bacillus subtilis spores for very heavy ions

M. Schäfer, K. Baltschukat, R. Facius, H. Bücker

DFVLR - Abt. Biophysik, Frankfurt/M.

Irradiation experiments with heavy ions are continued to investigate the inactivation of Bacillus subtilis spores. The experimental details and the procedures of evaluation have been described in an earlier report[1]. The particles used in these experiments ranged from Argon to Uranium. The energies lay between about 0.4 MeV/n and 8 MeV/n. The so far highest energies at the GSI of about 10 MeV/n could not yet be exploited, since experiments could only be performed at the parasite beam.

Within the experimental errors, no deviation of the survival curves from an exponential behaviour could be observed, e.g. $S = \exp(-\sigma\Phi)$, where S is survival (e.g. the colony forming ability), σ is the formal inactivation cross section and Φ is the particle fluence. The inactivation cross sections of these experiments together with results from some earlier measurements are presented in Fig. 1a as a function of $(Z_{eff}/\beta)^2$, where at lower energies Z_{eff} was determined from dE/dx measurements. If plotted against the LET this dependence shows a double-valued nature which is demonstrated in Fig. 1b, a feature which has been discussed from radiobiological viewpoints by Katz[2], Turner and Hollister[3] or from physical aspects by Muga and Griffith[4].

Two results can be drawn from Fig. 1a. For a constant β the inactivation cross section increases with the increasing atomic number of the particles as found earlier[1]. It is difficult to explain this increase in terms of the action of secondary electrons, especially for lower energies, where e.g. for 1.4 MeV/n their maximum effective range is about 0.1 μm, whereas the effective cross section increases by about a factor of two, above the geometrical cross section of the sensitive spore core. Another result is the fact that the inactivation cross section for the same particle increases with increasing energy and that the rate of increase is larger for higher atomic numbers. While these features agree in principal with particle track models, the experimental results are about a factor 10 higher than predictions from the model of Katz[5].

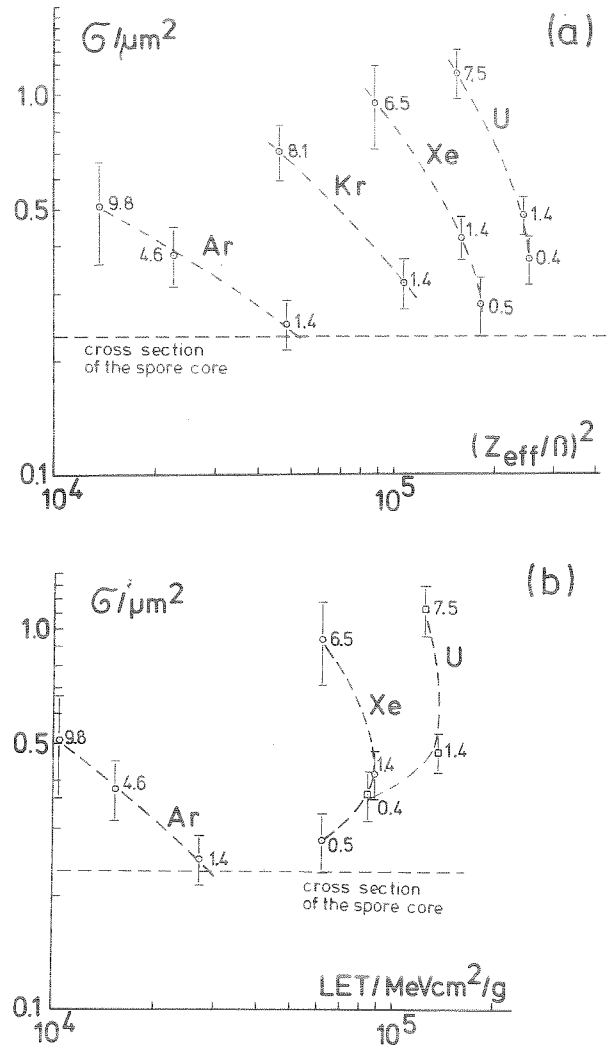


Fig. 1 Inactivation cross sections as a function of (a) $(Z_{eff}/\beta)^2$ and (b) LET. The numbers beside the measured points are the energies in MeV/n.

[1] M. Schäfer et al., GSI-79-11 (1979), p. 148

[2] R. Katz, Health Phys. 18, 175 (1970)

[3] J. E. Turner, H. Hollister, Health Phys. 17, 356 (1969)

[4] L. Muga, G. Griffith, Phys. Rev. 8, 4069 (1973)

[5] J. J. Butts, R. Katz, Rad. Res. 30, 855 (1967)

Determination of Passage Times of Red Blood Cells Through a Single Pore Membrane

U. Dauer, H. Kiesewetter, K. Mussler, H. Schmid-Schönbein
Department of Physiology, RWTH Aachen

R. Spohr
GSI Darmstadt

In the living microcirculation, the erythrocyte has to pass through capillary vessels of only 3 - 5 µm diameter, while its own diameter at rest is 7 - 8 µm. It is obvious that the ability to deform is the limiting factor in this case. From 1977 - 1979, a measuring method for the determination of a parameter for the deformability of red blood cells has been developed.
Hereby, the passage times of single cells traversing a measuring capillary of 3 - 5 µm diameter and 10 - 50 µm length is determined. The capillary is formed by the pore of a single pore membrane, which is produced by irradiation of a suited organic foil with a heavy ion beam of extremely low particle density. When one particle has passed the target, the beam is shut off. The so formed nuclear track is etched up to the desired pore diameter.
During the report period, a new microcomputer (Type AIM 65) has been employed for the determination of the passage times. After 10^3 passages, the measurement is terminated, the passage times are statistically processed and put out in form of a histogram.
With the help of this measuring device, the influence of the ionic concentration of Ca^{++} and several pharmaca upon the deformability of erythrocytes were investigated. When suspended in isotonic, phosphate-buffered saline (ph = 7.4) containing 200 mg/l Ca^{++}, the passage times of red blood cells from a healthy person are markedly prolonged compared with homologous erythrocytes suspended in isotonic saline. The detrimental influence of a high Ca^{++} concentration could be partially reversed by addition of pentoxifylline (0.1 mg/l). Restoration of the normal erythrocyte fluidity, however, was not obtained.

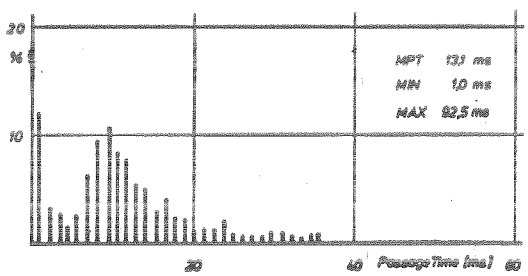


Fig. 1: Normal Erythrocytes

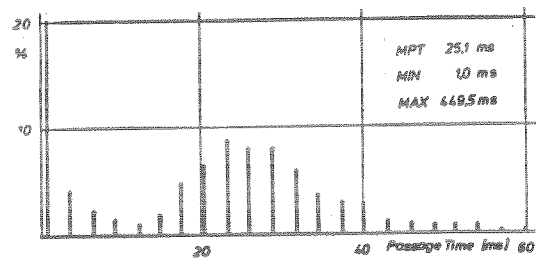


Fig. 2: Erythrocytes under influence of high Ca^{++} concentration
(MPT = Mean Passage Time)

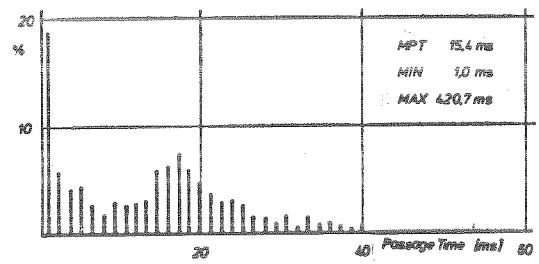


Fig. 3: Addition of pentoxifylline improves red blood cells deformability (30 min. incubation at 37° C)

For the first time, a great number of single pore membranes could be manufactured at GSI during the report period. In measuring the pores of a series of membranes type Triafol BN, we noticed a deviation of pore diameters of ± 15 % etched under the same conditions. Obviously, this is due to the inhomogeneity of the foil material. As the diamter of the pores decisively influences the passage times, a more homogenous foil material has to be found. Preliminary etching experiments with Hostaphan BN 50 showed positive results.

4. Developments

		PAGE
4.1	Chemistry, Nuclear Track and Target Technology	154
4.2	Experimental Set-Ups	161
4.3	Detectors	179
4.4	Electronics, Computing Center and Workshops	193

G

Continuous separations of reaction products in a thermochromatographic column with various halogenating agents as reactive gases

U. Hickmann, N. Greulich, N. Trautmann
Institut für Kernchemie, Universität Mainz
H. Gäggeler
GSI Darmstadt

The combination of a gas-jet recoil-transport system with a thermochromatographic column[1] has been applied for continuous chemical separations of fission products in form of volatile chlorides, bromides and iodides. A nitrogen gas-jet containing potassium chloride clusters was used to transport the fission products produced in the Mainz reactor from the target area to the thermochromatographic column. The clusters were stopped in a quartz-wool plug located in a quartz column with an inner diameter of 4 mm which was filled with quartz powder. The plug was heated to 960°C in order to destroy the clusters and to enable a complete halogenation. The first 8 cm of the column were kept at a constant temperature of 960°C; along the other part of the column a negative temperature gradient of ≈18°/cm was established. For halogenation of the fission products a mixture of the reactive gas with nitrogen was fed into the column through a by-pass. The element distribution along the thermochromatographic column was measured after removal of the column from the oven by γ-ray spectroscopy using a lead collimator.

In an earlier report[2] the element distribution of the volatile chlorides was given. With HBr and HI (8 vol% in the gas stream) quite similar thermochromatograms were obtained. As an example the Figure shows the element distribution with HI in the carrier gas at a flow rate of 1.3 l/min and after an exposure time of 15 min.

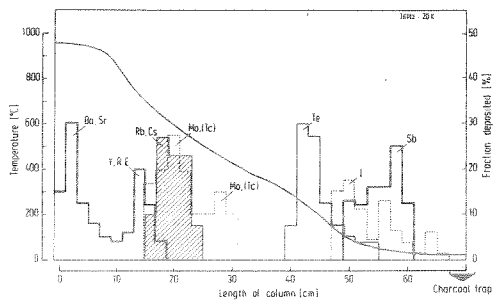


Fig. 1: Element distribution in the thermochromatographic column with 8 vol-% of hydrogen iodide in the N_2 carrier gas

With both agents the alkaline earth elements were found in the isothermic part of the column adjacent to the quartz-wool plug. The lanthanides are deposited at lower temperature with HI than with HBr. Rb and Cs appear at around 660°C and Mo forms a rather broad peak centered at 570°C. With HBr molybdenum is deposited at a lower temperature. Technetium is found in the same zone as molybdenum and therefore no clear statement on its behaviour can be made since the technetium nuclides measured after exposure are formed exclusively in the β^--decay of Mo. Proceeding to lower temperature regions tellurium is found at 210°C and antimony in a region between 100°C and room temperature. Iodine activity is deposited together with iodine from decomposition of HI in a visible adsorption zone between 150°C and room temperature.

The deposition temperatures of the elements in the thermochromatographic column and in the following charcoal trap as obtained with HCl, HBr and HI are summarized in the Table. In general one can say that the deposition temperatures for the chlorides and iodides are lower than for the bromides.

Table: Deposition temperatures of fission product halides in a thermochromatographic column

Element	Deposition temperatures in °C with		
	HCl	HBr	HI
Rb	650	730	660
Cs	630	730	660
Sr,Ba	960	960	960
Y,R.E.	780	850	760
Mo	20	140	590;410
Tc	50;ch.	160	590;430
Sb	30;ch.	100	35
Te	180	290	210
Br,I	ch.	ch.	150 - ch.

ch. = charcoal trap

Elementary bromine and iodine are only applicable up to a concentration of 12 vol%; at higher concentrations the column is plugged by these agents within a very short time. With Br_2 and I_2 as reactive gases the alkaline earth elements and the lanthanides are not volatilized. The other elements are found at higher temperatures than with hydrogen halides.

On the other hand, with a mixture of BBr_3+Br_2+N_2 the alkaline earth and lanthanide elements could be volatilized almost completely and were found in a broad zone between 500 and 600°C. The other fission products were deposited in the cold part of the column and the charcoal trap without further separations.

[1] U. Hickmann et al., Nucl. Instr. Meth., in press
[2] N. Greulich et al., GSI-Bericht 79-11, 154 (1979)

Heavy Ion Lithography

B.E. Fischer, R. Spohr
GSI Darmstadt

One measure for the rapid pace of technological advancement is the steady refinement of our machining tools. In solid state technology this rule applies directly, where components have to be packed onto smaller and smaller areas. Conventional planar technology is approaching 1 µm line width. Maintaining simultaneously conductor cross sections requires a better control over depth profiling. Therefore, high lateral resolution is not anymore a sufficient condition. Any further progress will depend on the capability of the applied tool to stop at a precisely defined depth.

In contrast to irradiation with x-rays or electrons, heavy ions possess this feature. Only heavy particles are subject to a continuous energy loss on their trajectories and thus, come to a hold at precisely defined depth. Range and angular straggling are of the order of a few percent. Therefore, very deep structures with very high aspect ratios can be achieved. Profiling depth is independent of particle dose and time of development, up to 10^{12} particles per cm^2.

Application of heavy particles has another inherent advantage over x rays and electrons. Due to the very high specific energy loss of heavy ions an almost unlimited number of different materials can be used quasi as photoresists. Therefore, the resist coating step in silicon technology can be replaced by an oxidizing step using a silicon dioxide layer of much better defined thickness. Even pure silicon can be track sensitized using heavy ion irradiation and transforming the inscribed information into structure during a later selective etching process.

A final virtue of heavy ions as a structuring tool in comparison to x-ray sources resides in the existence of very bright ion sources. Parallel heavy ion beams of high intensity can be achieved using conventional ion optical systems. Heavy ion lithography can be directly applied to small accelerators and low energy implanters. At one milliampère beam current a sample throughput of one m^2/sec. can be achieved.

[1] B.E. Fischer, R. Spohr, Heavy Ion Microlithography - A New Tool to Generate and Investigate Submicroscopic Structures, Nucl. Instr. and Meth. 168, 241-246 (1980)

[2] B.E. Fischer, R. Spohr, Heavy Ion Lithography, Contribution to "Microcircuit Engineering '79 - Microstructure Fabrication", 25.-27. September 1979, RWTH Aachen; Proceedings: Inst. of Semiconductor Electronics, p. 349-357 (Nov. 1979).

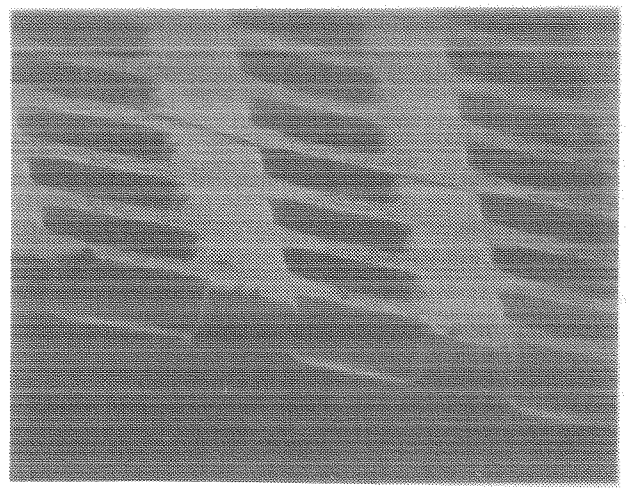


Fig. 1: Heavy ion lithogram of metal mask* inscribed into high resolution photoresist.
Material: Polymethyl metacrylate (PMMA) layer on silicon substrate*.
Irradiation: 3 x 10^{12} argon ions per cm^2 at 720 keV particle energy. Distance between metal mask and photoresist was approximately 1 mm.
Development: 10 min methyl isobutyl keton plus isopropanol 1:3.
Observation: Scanning electron micrograph of cross section.

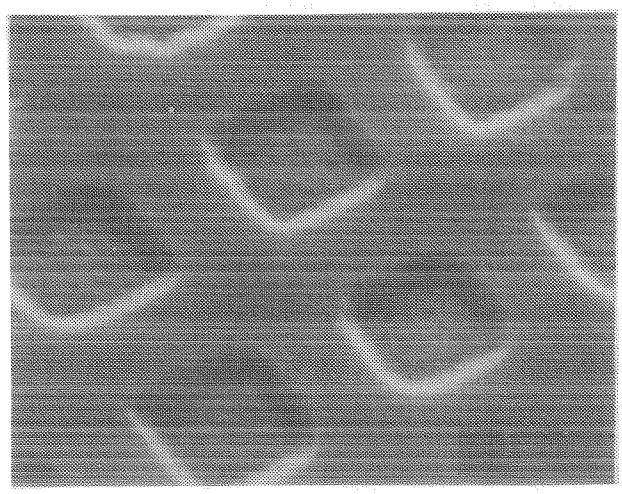


Fig. 2: Bare silicon - a resist material for heavy ion lithography. Mask*: Self-supporting metal mask.
Resist*: Bare silicon, (111) orientation.
Irradiation: 7 x 10^{13} argon ions / cm^2 at 720 keV particle energy. The distance between the mask and the silicon was approximately 1 mm.
Development: 10 sec Sirtl etch (CrO_3-HF-H_2O), a dislocation sensitive etching medium.
Observation: Scanning electron microscopy.

*Courtesy: P. Tischer, Siemens AG, Munich

Transmission Properties of Nuclear Track Filters

C. Riedel, R. Spohr
GSI Darmstadt

Nuclear tracks are a unique tool for manufacturing statistically distributed holes of predictable size and areal density[1]. Sieves of this kind are essentially controlled by only three parameters : (1) hole diameter, (2) areal density of the holes, and (3) hole length. Due to the statistical distribution of the holes, multiple holes with larger areas occur, deteriorating the selectivity in comparison to a regular array of holes. This has been studied in a two-dimensional model, introducing an upper limit, T_s, and a lower limit, T_r for the filter transmission as function of particle size. Main parameter used hereby is the term nominal porosity, P, defined as product of single hole area, S_1, and areal density of original tracks, N.

The "areal transmission function" T_s (upper limit) was determined by computer simulation[2] using square holes of identical size and compared to image analysis[3] using etched nuclear track holes in mica of rhombic shape. An excellent agreement between theory and experiment has been achieved (fig. 1).

The "particle transmission function" T_r (lower limit) was determined by image analysis using etched nuclear tracks in mica (fig. 2). It corresponds to the total cross section for transmission of rigid spherical test particles of radius r, whereby r_m is the maximum radius of an inscribed circle for a single hole[4].

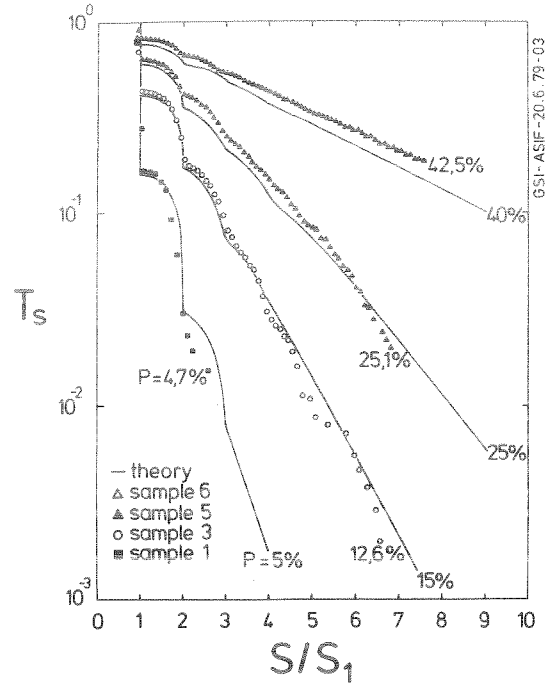


Fig. 1: Areal transmission function T_s, defined as fraction of holes with larger area than S, representing an upper limit for the actual transmission function. Points: Image analysis[3]; Lines: Computer simulation[2].

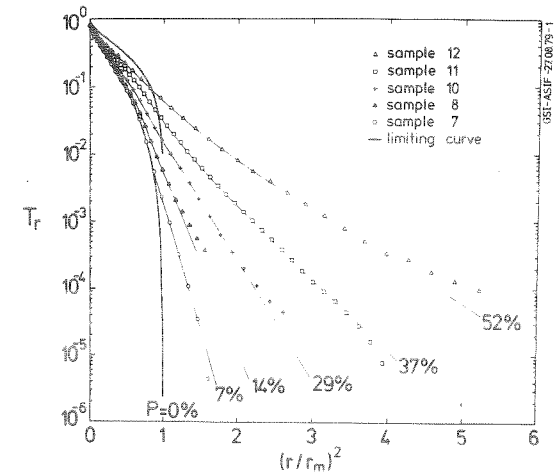


Fig. 2: Particle transmission function T_r for rigid spheres of radius r, defined as that fraction of the filter area which enables a straight-through transmission of the spheres. T_r represents a lower limit for the actual transmission function. Points: Image analysis[4]; Thin lines: Computer simulation[2].

[1] C. Riedel, R. Spohr, Möglichkeiten und Grenzen bei der Herstellung von Kernspurfiltern aus Glimmer, Ber. der Bunsenges. Phys. Chem. 83, 1165-1168 (1979).

[2] C. Riedel, R. Spohr, Statistical Properties of Etched Nuclear Tracks I. Analytical Theory and Computer Simulation, Radiation Effects 42, 69-75 (1979).

[3] C. Riedel, R. Spohr, Statistical Properties of Etched Nuclear Tracks II. Experiment and Filter Design, Radiation Effects (accepted July 27, 1979).

[4] C. Riedel, R. Spohr, Statistical Properties of Etched Nuclear Tracks. Contribution to Second Symposium on Synthetic Membranes in Science and Industry, Tübingen, BRD, 17.-19. September 1979.

Production and Application of Molecular Filters

A. Gerhard, A. Schempp, H. Klein
Institut für Angewandte Physik, Universität Frankfurt/Main

Plastic foils have been irradiated with heavy ions and the tracks have been etched to produce small uniform pores. Different ions with energies from 1.4 to 8.5 MeV/N and foils of thickness between 12 and 50 µm were used. Pores between 0.06 and 5 µm had been produced by etching of the foils with hot NaOH for 10 - 60 minutes. Pore detection was done by an electrochemical method and by both transmission and scanning electron microscopy.

Properties of such a filter with micropores are determined by size and shape of the individual holes as well as by the distribution of the pores (porosity, multiple holes). In the last year mainly the shape of the individual pores has been investigated. Irradiation with heavy ions produces a damaged region of about 110 Å diameter by primary and multiple scattered electrons. The etching velocities v_t along this track and v_s in the undamaged region e. g. at the surface have different values and determine the shape of the pore, which is in general of conical form (fig. 1). Obviously a high value of track etching velocity v_t is necessary for an approximately "cylindrical" form of the pores. This is of importance especially for submicropores smaller than 0.1 µm in diameter. The etching velocity v_t is increasing with higher ion energy and ion mass and can be varied to some extend by use of special etching fluids, mixtures and additives. We irradiated the foils with UV-light of wavelengths between 185 and 320 nm. This increases the etching sensibility of the damaged region by excitation of chemical bonds of the polymeres.

Fig. 2 shows the track etching velocity v_t as function of UV-light irradiation time T.

The ratio of v_t to surface etching velocity v_s can be increased by a factor of six.

Fig. 3 shows a scanning electron micrograph of Hostaphan®NN12 irradiated with 4.7 MeV/N Xe ions. After this irradiation the foil was exposed to UV-light for 120 minutes and etched in 5 N NaOH at 39 °C for 15 minutes. Pore density has to be less than 0.5 % for proper measurements of the etching velocities.

Further plans of our investigations are to produce nuclear track filter membrans with pores of diameters less than 500 Å.

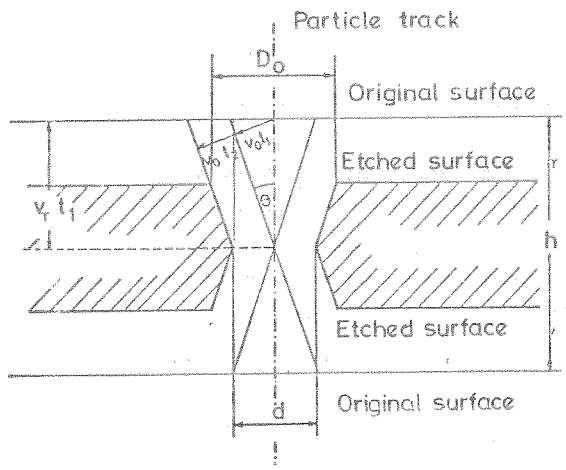


Fig. 1 Schematic drawing of micropore growth

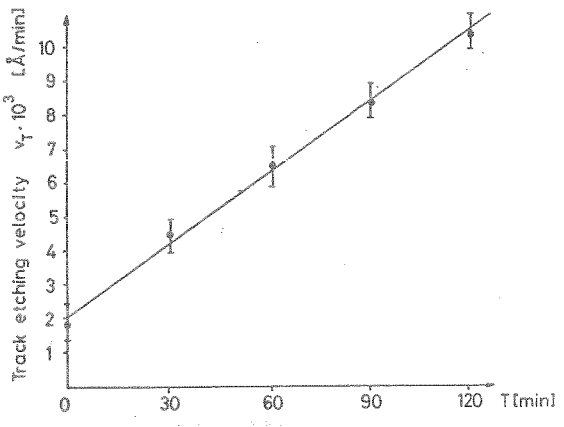


Fig. 2 Track etching velocity v_t as function of UV-irradiation time T

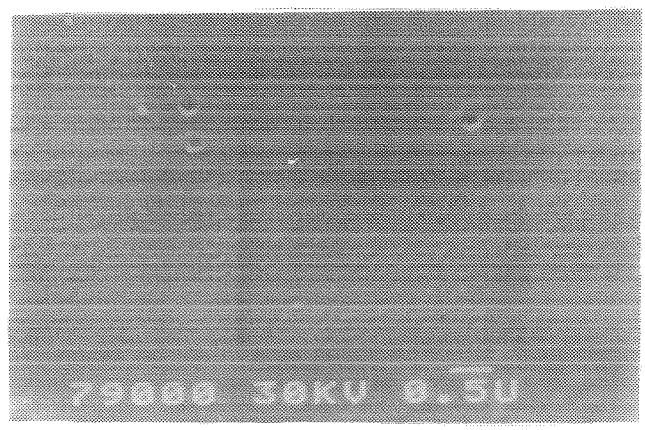


Fig. 3 Micropores with 680 Å diameter

Some further properties of mica microfilters: air through-put up to 300 °C [B]

G. Tress, P. Vater, D. Hirdes, R. Brandt, Kernchemie, FB 14, Uni Marburg
R. Spohr, GSI, Darmstadt

We produced a new set of mica microfilters: 5 cm diameter, 50 µm thick mica plates with 4 cm "effective" sieve diameter, $(0{,}8\text{-}1{,}4)\cdot 10^6$ holes/cm² and edge lengthes k with $0{,}35\ \mu m \leq k \leq 1{,}8\ \mu m$. These microfilters were obtained through heavy ion bombardment ($E > 7{,}5$ MeV/u) and consecutive etching with HF [1,2].
The air through-put Q was measured within the following ranges:

$0 \leq \Delta p \leq 200$ cm H_2O (pressure difference)
$25\ °C \leq T \leq 300\ °C$ (temperature range)
$0{,}35\ \mu m \leq k \leq 1{,}8\ \mu m$ (edge length of single hole)

The results are shown in Fig. 1.
We observe an increase of Q with the edge length k at a given temperature T and a decrease of Q with the temperature T for a given edge length k.
The quantitative analysis of the air through-put Q as a function of k, T and other parameters is carried out in the same frame-work, as we understand the air through-put in the gas-jet system of the GSI.
The result of this analysis is given below [3]:

(1) $Q = L\cdot\Delta p$; $Q = \dot{V}\cdot p$

L - conductance
Δp - pressure difference between both sides of the microfilter
p - total mean pressure
$\dot{V}$ - gas flow

(2) $$L \simeq 480\cdot\frac{\sqrt{293}}{T}\cdot\frac{k^4}{X}\cdot p\cdot(N_1+3.3\ N_2+5{,}3\ N_3)$$

X - hole length, i.e. mica plate thickness
N_1 - number of single holes
$N_{2,3}$ - number of double and triple holes

A quantitative comparison of measured and calculated values of Q gives a ratio of $(0{,}20\pm0{,}04)$, independent of the wide range in T, Δp, and k investigated.
The major emphasis of further work will be primarily on practical applications of mica microfilters. Experiments for cleaning hot air at some ovens at the NUKEM, Hanau, are under preparation.

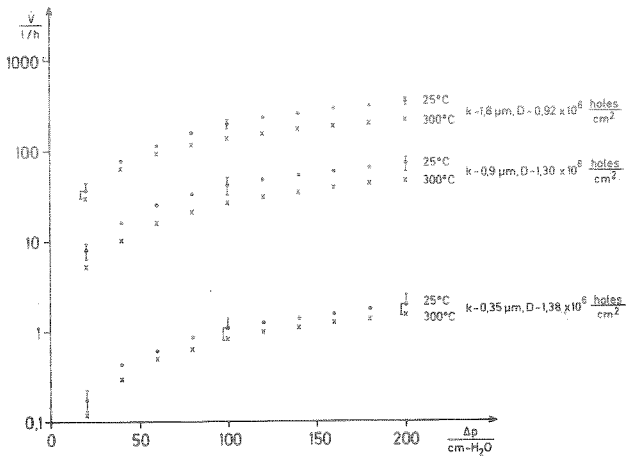


Fig. 1: Air through-put Q, measured as gas flow $\dot{V}$ at atmospheric pressure p, through mica microfilters. We used 5 cm Ø mica plates of thickness 50 µm with an effective filter diameter of 4 cm and appr. 10^6 holes per cm². Different edge lengths k were employed. Given is $\dot{V}$ as a function of Δp, the pressure difference between both sides of the filter, for two temperatures 25 °C and 300 °C.

References

1) G. Tress, et al. GSI 79-11(1979)136
2) P. Vater, et al. Nucl.Instr.Meth.(in print)
3) G. Tress, et al. Nuclear Tracks (in print)

Determination of Light Contaminations in Heavy Targets

F. Nickel, H. Geissel, D. Marx
GSI Darmstadt

The contamination of thin self-supporting targets of heavy material by light elements as carbon (or oxygen) can be determined quantitatively by Rutherford scattering of heavy ions. In test experiments this well known method allowed to detect small contaminations with a sensitivity of a few per cent, even in the most unfavourable case of light contaminations as carbon in heavy targets as gold. The accuracy is limited by the background due to multiple scattering, especially at low energies. These measurements can be performed simultaneously during the main experiment in order to get information about the instantaneous state of the target (degree of oxidation, surface contamination by carbon-hydrogen compounds etc.).

Atoms of the target material and of target contaminations recoiling in forward direction ($\Theta_{lab} \geq 60^0$) are of sufficient intensity for measurements of their intensity as a function of their energy. We have used a 1.4 MeV/u Xe^{136}-beam of 10^9 to 10^{10} ions/sec, collimated to an area of 4 mm^2 at the target. At an angle of $\Theta_{lab} = 60^0$ a surface barrier detector ($\Delta\Theta = 1^0$, $\Delta\varphi = 1^0$) measured the energy of the scattered atoms.

As an example fig. 1 shows the spectrum of a target of 500 $\mu g/cm^2$ Au, fig. 2 of 500 $\mu g/cm^2$ Au + 23 $\mu g/cm^2$ C, fig. 3 of 260 $\mu g/cm^2$ Au + 23 $\mu g/cm^2$ C.

Taking into account the energy loss in the target and the pulse height defect of the surface barrier detector, the calculated and measured energies of the scattered atoms agree within a few per cent (E_{Xe} = 95 MeV, E_{Au} = 46 MeV, E_C = 11 MeV). The line widths of the energy spectra are broadened due to multiple scattering and the finite size of the detector.

The relation of the intensities N_C/N_{Au} of the scattered C and Au atoms is given by

$$\frac{N_C}{N_{Au}} = \frac{Z_C^2 \, M_{Au}^3 \, (M_{Xe} + M_C)^2}{Z_{Au}^2 \, M_C^3 \, (M_{Xe} + M_{Au})^2} \cdot \frac{(\rho d)_C}{(\rho d)_{Au}} = 5 \cdot \frac{(\rho d)_C}{(\rho d)_{Au}} \, .$$

Z and M are atomic number and mass of the involved atoms, ρd is the thickness (mass per target area).

The calculated and measured intensity relations agree within the experimental errors due to poor counting rate statistics and errors of target thickness:

$(N_{Au}/N_{Xe})_{calc} = 6.1$ $\quad (N_{Au}/N_{Xe})_{exp} \approx 8$ $\quad$ (fig. 1)

$(N_C/N_{Au})_{calc} = 0.24$ $\quad (N_C/N_{Au})_{exp} \approx 0.2$ $\quad$ (fig. 2)

$(N_C/N_{Au})_{calc} = 0.46$ $\quad (N_C/N_{Au})_{exp} \approx 0.3$ $\quad$ (fig. 3)

A carbon contamination of one per cent of the gold target results in a C peak of an intensity of 1/20 of the intensity of the Au peak in the energy spectrum.

These test experiments show that Rutherford scattering of target atoms in forward direction induced by the UNILAC heavy ion beam can be used to detect quantitatively small target contaminations of a few per cent.

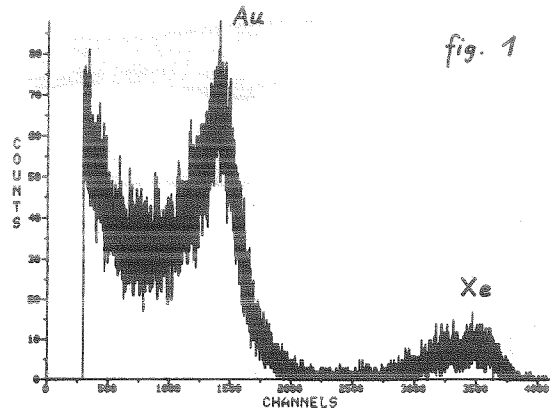


fig. 1

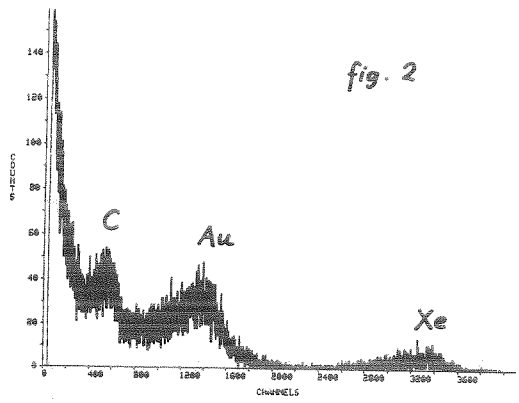


fig. 2

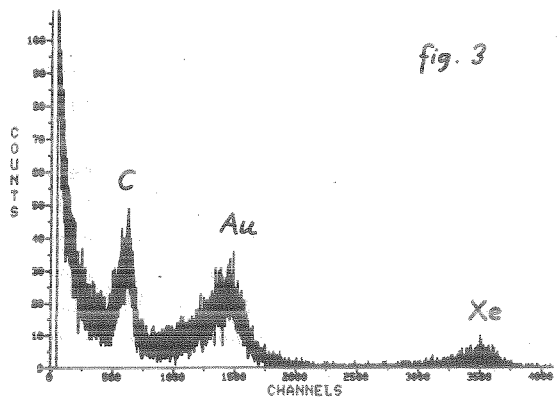


fig. 3

Energy spectra of scattered Xe projectiles and target atoms: fig. 1: 500 $\mu g/cm^2$ Au,
fig. 2: 500 $\mu g/cm^2$ Au + 23 $\mu g/cm^2$ C,
fig. 3: 260 $\mu g/cm^2$ Au + 23 $\mu g/cm^2$ C.

Measurements of the Density of a Gas Jet by Light Scattering [G]

P. Kreisler, W. Tietsch+, K. Bethge
Institut für Kernphysik, Frankfurt am Main

The density of the windowless gas jet target[1,2] has been measured at high mass flows[1]. Rayleigh scattering of light from a He Ne laser was used at Argon and Nitrogen jets. The results obtained by this method can be summarized as follows:

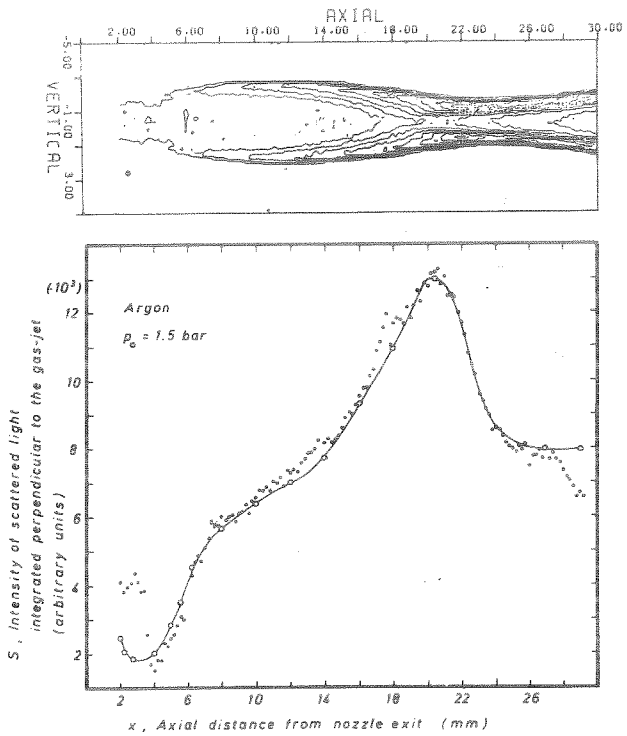


Fig. 1 (p_o = pressure at nozzle entrance)

a) The intensity of light scattered at Argon is three orders of magnitude larger than the one at Nitrogen, although one expects a somewhat larger intensity for N_2 than for Argon at the same particle density. This expectation follows from the theory of Rayleigh scattering and from calibration measurements (at a static gas target).

b) The integrated intensities S increase with the distance from the nozzle-exit. This increase is also observed in areas where the gas jet diverges and thus the density decreases (Fig. 1).

c) The density-knot (described in [1,2]) or a Mach-disc[2] cannot be observed in the contour-line plots.

These effects can be explained under the assumption, that the gas in the jet is partly condensed.

+Present address: Babcock Brown Boveri Reaktorbau, Mannheim

The effect has been verified by measuring the temperature dependence of the intensity profiles of the scattered light. The results are shown in Fig. 2.

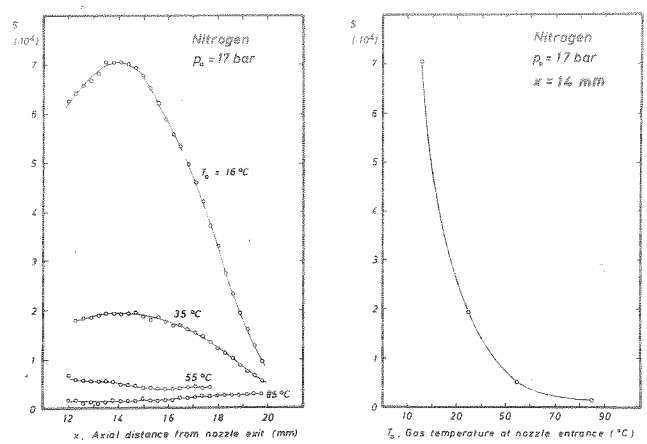


Fig. 2

The result of the measurement at Nitrogen (17 bar, 95° C) is shown in Fig. 3, where a density knot is observable according to earlier experiments. Assuming that there is no effect of condensation at this temperature, the target thickness has been determined to 102 µg/cm^2 in the density-knot.

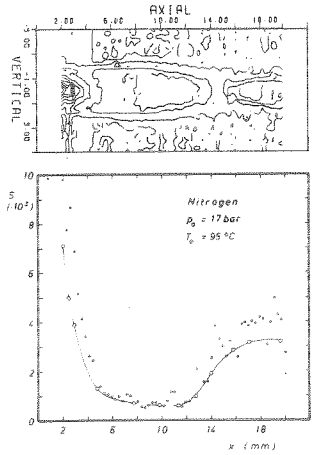


Fig. 3

The experimental results show that densimetry at supersonic gas-jets is possible only under certain conditions: If there are droplets in the jet due to condensation, which are not small compared to the wavelength of the incident light, it is not possible to determine the gas density by measuring the scattered light without knowing the particle size. The scattering characteristic is no longer the one of Rayleigh scattering, it changes to Mie-scattering.

[1] Jahresbericht 77, GSI-J-1-78, S. 175

[2] W. Tietsch, K. Bethge, H. Feist, E. Schopper Nucl. Instr. and Meth. 158 (1979) 41

EPOS - a Flexible Solenoid-System for the Spectroscopy of Positrons in HI-Collisions[B]

A. Balanda[†], H.J. Beeskow, K. Bethge[†], H. Bokemeyer, H. Folger, J.S. Greenberg*, H. Grein, A. Gruppe[+], S. Ito", S. Matsuki", R. Schule[+], R. Schultz, D. Schwalm, J. Schweppe*, R. Steiner, P. Vincent, M. Waldschmidt[+]

GSI Darmstadt, [+]Universität Frankfurt, *Yale University, "Kyoto University

The variable, two arm solenoid system for the detection of electrons and positrons, already described in the last annual report[1], has been completed and tested successfully in various configurations with radioactive sources and under beam conditions. The set-up used in a first series of experiments[2] performed for further investigation of positron production in very heavy quasi-atomic systems is shown schematically in fig. 1.

The magnetic guiding field produced by adjusting the spacings of the pancake-coils and the sign and magnitude of the electric current ($\leq$ 1000 A), has the following properties: It creates a magnetic mirror on the target side opposite to the e^+-detector, a field dip at the spiral baffle, and is decreasing very fast over the light guides of the e^+-detector system. In order to reduce the e^--singles counting rate in the e^+-detector and suppress sum-coincidences between positrons and electrons due to intense δ-electron yields a spiral baffle is installed which makes use of the different helicity of the electrons and positrons in a solenoid field. The length of the spiral baffle, the inclination angle of the baffle plates, and the field dip are optimized for highest e^+-transmission and minimal limitation of the momentum band pass. The thickness of the baffle plates increases radially to prevent high-energy electrons from passing through the blades. The probability of detecting electrons scattered by the baffle is reduced strongly by using a pencil-like e^+-detector of 1 cm^{ϕ} positioned along the axis of the spectrometer. The detector is made from NE 104 A scintillation material and has a length of 10 cm necessary to accumulate all positrons; its energy resolution is $\leq$ 30 %. The transport efficiency of the solenoid has been measured with several e^--sources and different reversed current settings. The efficiency is plotted in fig. 2 vs. the scaling parameter B_t/η; it is in qualitative agreement with trajectory calculations. The measured suppression factor of the baffle (relative to its transmission) is given in the insert.

An e^+-signal in the scintillation detector is identified by its annihilation radiation, which is detected by 8 wedge shaped NaI detectors in a cylindrical arrangement. By requiring a total γ-sum energy of $\geq$ 450 keV, a background free signature (efficiency $\cong$65%) for an e^+-event is obtained even in U+U collisions. The maximum e^+-detection efficiency of the total set-up amounts to 13 %.

Positrons are measured in coincidence with the scattered projectile as well as the recoiling target nucleus with the aid of two position sensitive parallel plate avalanche detectors with delay line readout[3]. The angular acceptance of each of the particle counters is $15^0 \leq \theta \leq 80^0$ at constant $\Delta\phi = 36^0$. The angular resolution is better than 1^0 and allows e.g. for separation of close and distant collisions in the U→Pb system. Moreover, unwanted reaction channels can be suppressed, which is important in the use of targets with backing or covering foils.

The photon spectrum is measured from ~50 keV up to ~10 MeV with a set of 3 detectors, a Ge(i), Ge(Li), and a 3"x3"-NaI counter, operated in coincidence with the HI-counters. The experimental data are fed via an event-type oriented electronic set-up to the GSI online data accumulation system.

[1] A. Bałanda et al., GSI-annual report (1978) 163
[2] A. Bałanda et al., this report
[3] P. Fuchs, Ph.D. thesis, GSI, to be published

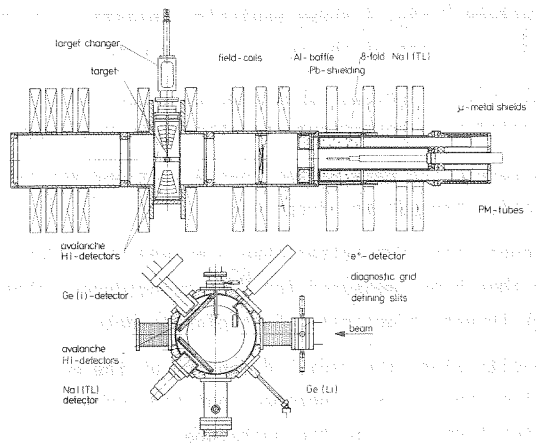


Fig. 1: A schematic view of EPOS

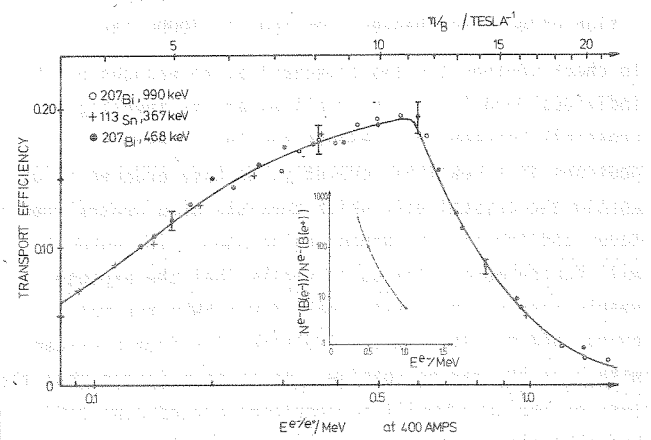


Fig. 2: Transport efficiency of the solenoid-system as a function of the electron/positron kinetic energy $E^{e+/e-}$ and the scaling parameter B_t/η, the magnetic field at the target and the e^+/e^--momentum in units of m_0c. Insert: e^--suppression factor (ratio of total e^--transmission for opposite field settings) as a function of initial kinetic e^--energy.

[†] on leave from Jagellonian Univ., Cracow

Status of the NaI Crystal Ball Project

R.S. Simon, R. Albrecht and D. Schwalm, GSI Darmstadt
V. Metag, H. Gräf, E. Jaeschke and R. Repnow, MPI Heidelberg
D. Habs, D. Pelte, W. Schneider, H.J. Specht and W. Weiter, University Heidelberg

A modularized NaI detector with close to 4π geometry - the crystal ball - can provide unique information on the decay γ-radiation following heavy-ion reactions.[1] GSI, the Max-Planck-Institute (MPI) and the University of Heidelberg have joined in a collaboration to develop and realize such a detector. The system will be first set up at the postaccelerator of the MPI.

The detector has the shape of a spherical shell of NaI with a free inner radius of 25 cm and a thickness of 20 cm. This shell comprises 162 individual modules of equal solid angle which have pentagonal or hexagonal cross section in order to perfectly tile the full sphere. Only four basic types of modules are required. The individual segments - each an independent γ-detector of its own - will be supported by a large spherical honeycomb structure.[2] Fig. 1 shows equivalent plastic dummies mounted in a section of the supporting structure.

From tests with a pentagon prototype we expect the following scintillation performance for the individual modules:

- energy resolution FWHM better than 8 % at 662 keV for irradiation through the front end;
- time resolution FWHM better than 3 ns and FW 1/10 M better than 6 ns, measured for ^{60}Co coincidences above 200 keV threshold against a fast plastic detector;
- homogeneity along the radial dimension of the module ± 1.5 % of the 662 keV photopeak position except for the outer 4 cm close to the phototube;
- stability within ± 1 % of the 662 keV photopeak position under rate changes from 1000 to 70000 cts/s.

To check whether the tight mechanical tolerances of the individual modules can be realized and to investigate crosstalk between the elements and their response to neutrons in a realistic geometry, we have ordered a subunit of the crystal ball which consists of a central pentagon and the five neighbouring hexagons. The subunit will furthermore allow us to verify that the expected resolutions of the crystal ball (20 % FWHM for total energy and multiplicity, 4 isolated hits from a cascade with $M_\gamma = 30$) can be obtained. It is anticipated that the test of the subunit will be completed around June 1980 and that all modules can be ordered immediately thereafter.

The data acquisition system for the crystal ball has to handle high event rates together with a large number of parameters per event, since we obtain an energy signal plus the corresponding time information from each participating module. Both energy and time will be digitized by charge sensitive ADC's. Successive events will be sorted with respect to multiplicity and total energy and may be analyzed online in more detail by a subsequent array of parallel microprocessors to yield for instance spatial patterns and transition energy correlations. The development of the necessary electronics and programs has been started.

[1] R.S. Simon, D. Schwalm, V. Metag, R. Repnow, D. Habs, GSI Jahresbericht 1979, page 164

[2] see contribution from engineering and construction division, E. Malwitz et al., to this report.

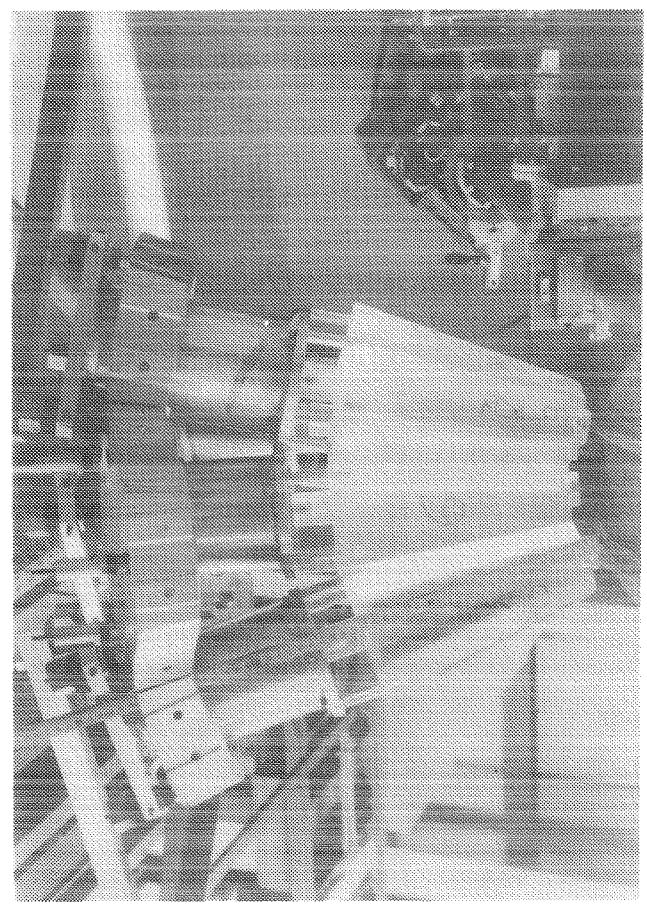


Fig. 1: Plastic dummies of crystal ball modules mounted in a section of the sperical honeycomb supporting structure. The spherical scattering chamber has an outer diameter of 50 cm.

G

THE PLASTIC BALL AND PLASTIC WALL, A 4π DETECTOR SYSTEM FOR RELATIVISTIC HEAVY ION REACTIONS

H.H. Gutbrod, M.R. Maier, J. Péter, A.M. Poskanzer, H.G. Ritter
H. Stelzer, R. Stock, A.I. Warwick, F. Weik, H. Wiemann

GSI Darmstadt, LBL Berkeley and Universität Marburg

Single particle inclusive data from high multiplicity events tend to indicate strong thermalization in relativistic heavy ion reactions. However, Bevalac and similar high energy accelerator research has passed from the stage where only one particle from each event is measured and has advanced to attempts to measure many or all of the charged particles produced in each event in order to look for collective effects that are predicted by different theories and indicated by latest experiment.

The GSI-LBL collaboration at the Bevalac is currently engaged in the design and fabrication of a spectrometer having nearly 98 % of 4π solid angle acceptance. The spectrometer consists of two systems: the Plastic Ball and the Plastic Wall (fig. 1).

The Plastic Ball is a multidetector system covering a solid angle of 96 % of 4π. Each element is a ΔE-E-detector where the ΔE counter is a 4 mm thick CaF_2 crystal and the E detector is a 36 cm long plastic scintillator. Both are optically coupled and read out by one photomultiplier. The ΔE and E signals are separated by puls shape analysis (phoswich idea). The shape and the geometrical arrangement of the counters was adopted from the SLAC Crystal Ball detector. In order to take into account the strongly forward peaked particle distribution a finer division was necessary in the region between 10^0 and 30^0. This region contains 160 modules. 655 counters cover the angular range from 30^0 to 160^0. Each detector provides particle identification and measures the particle energy in the range from 30 to 210 MeV for protons, from 45 to 330 MeV for deuterons, from 55-390 MeV for tritons, from 124 to 880 MeV for ^{3}He and from 135 to 980 MeV for ^{4}He. For slower or faster particles only a multiplicity information is obtained. Positive pions from 15 to 120 MeV are in addition to the ΔE-E identification detected by their delayed decay.

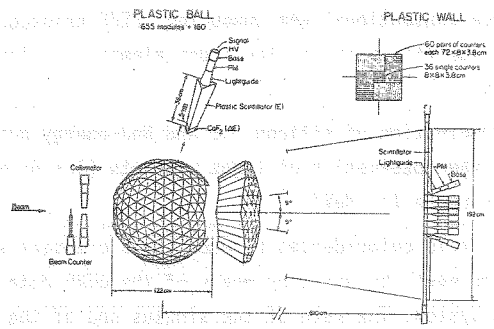


Fig. 1

The Plastic Wall is a multisegmented TOF detector to measure at small angles the shower of reaction products from relativistic nuclear collisions. It covers an area of 192 x 192 cm^2 and consists of scintillators arranged in an inner and an outer area. The inner one is a square of 48 x 48 cm^2 consisting of 36 individual counters each 4 cm thick. At a distance of 600 cm from the target this area covers an angular region of about 0^0 to 2.5^0. The outer region extends to 9^0 and consists of 60 pairs of position-sensitive scintillation detectors. The Wall can be moved on rails and comparison of the time of flight at two different known distances allows an absolute time calibration if the mass of the detected fragment, e.g., the beam particle, is known. The distance of 6 m corresponds to flight times varying from 24 ns at 800 MeV/n to 65 ns at 50 MeV/n. The width of the scintillators of 8 cm results in an angular resolution of 0.75^0.

The inner region of the Plastic Wall will provide the event trigger for both the Plastic Ball and the Wall. For high intensity experiments the inner part is removed.

The purpose of the Wall's outer region is to detect the reaction products of projectile fragments at angles between 2^0 and 9^0 with sufficient angular resolution and sufficient multiparticle detection capability. It is made of 60 position-sensitive double modules, each consisting of two scintillator rods with dimensions of 72 x 8 x 4 cm^3. Each scintillator of the double module is viewed by one photomultiplier at different ends (fig. 2). The time difference between the two photomultiplier signals gives the longitudinal position of the particle, the mean time gives the flight time from the upstream detector.

For high energy charged particles the dE/dx in one or both scintillators combined with time-of-flight determines Z and E/n. For energies below 120 MeV/n, particles are stopped in the wall. Thus the velocity measurement and the E information determines the mass of the stopped particles. The double coincident dE/dx information for particles above 80 MeV/n, furthermore, allows one to discriminate against neutron and γ-response in the scintillators, which is rather important since as many neutrons as protons are expected for light projectiles at forward angles. In tests with beam particles, a time resolution in a double module of 350 ps (FWHM) was obtained without any off-line walk correction.

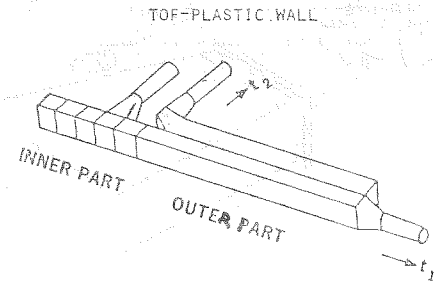


Fig. 2

Since the detection scheme is based on stopping the particles, the main domain of the spectrometer is the investigation of central collisions at low and intermediate Bevalac energies. The initial experiment, scheduled for the fall of 1980 will use a ^{40}Ca and ^{208}Pb targets.

A multiparticle detection system for high energetic projectiles (86 MeV/u ^{12}C)

G. Augustinski, H.J. Beeskow, Y. T. Chu*, H.W. Daues, P. Doll, A. Gobbi, K. Hildenbrand, M. Ludwig
U. Lynen", W. Müller", A. Olmi, H. Sann, R. Santo+

GSI Darmstadt, "MPI Heidelberg, +Universität Münster
*Alexander von Humboldt-Fellow, on leave from Institute of Modern Physics, Academia Sinica, Lanshow, China

The availability of a high-intensity (>10^{10} particles/s) 86 MeV/u ^{12}C-beam at CERN, offered the possibility of studying heavy ion reactions with thin targets (<500 µg/cm^2). So, besides the projectile-like fragments also the very low energetic target-like reaction products could be studied. The main interest of the experiment consists in the registration of multiple heavy fragments with Z > 4. Five different types of coincident counters are used in the experiment (fig. 1):

1. A position sensitive ionization chamber with a depth of 120 cm to measure E, M, Z, Θ, φ for elements Z > 4 (see separate report in this annual report). As start detector a thin parallel plate avalanche counter is used.

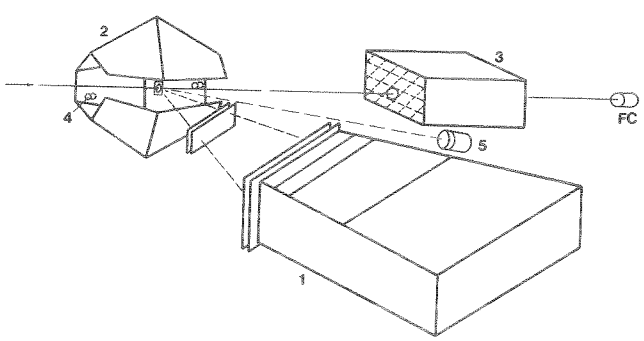


Fig. 1

2. A heavy-ion hodoscope to detect the multiplicity of heavy products, consisting in 10 position sensitive parallel plate detectors (fig. 2). The 10 counters are arranged symmetrically around the beam axis and target at a distance of 15 cm; they cover a solid angle of more than 2π. Each module allows the measurement of time of flight, Θ and φ position and an approximate energy-loss. The shape of each counter is trapezoidal and the active area is 230 cm^2. The counter gas was isobutylen at a pressure of 8 Torr. The particles have to pass through a 2 µ Hostaphan window and a 0.8 µ metallized Polypropylen foil (Cathode) before reaching the 3 mm wide amplification zone. The timing signal was taken from the cathode. The anode is subdivided in 20 strips for the read out of the φ-signal. A Θ-grid (20 µφ wires) is placed halfway between cathode and anode. Both position coordinates are read out by delay lines at both ends. So recognition of double hits is possible.

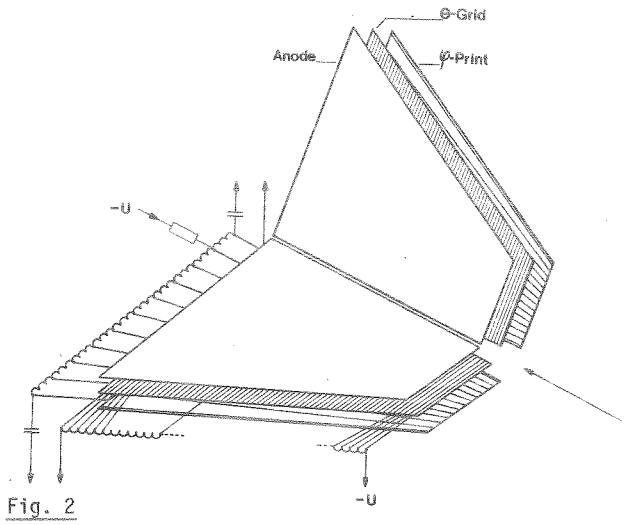


Fig. 2

3. A $A0^0$-hodoscope to detect the multiplicity of the light fragments emitted at forward angles between 1.5^0 and 10^0. It consists of 27 hexagonal NE 102A scintillators (fig. 3) with a thickness of 5 mm, and a 3/4" photomultiplier tube (RCA 4516). At beam velocities protons and ^{12}C-particles loose 4.5 to 160 MeV in the scintillator. It was possible to separate all elements up to carbon by means of their energy-loss and time of flight.

4. Three conventional semiconductor ΔE/E-telescopes for the identification of the light elements at low energies.

5. A combination of silicon ΔE and NaJ-energy detectors for the observation of light elements (Z < 6) at energies up to 150 MeV/u.

All possible coincidences between the 5 counters were recorded event by event by means of the JUHU data acquisition system. The rate of the singles and of the most frequent coincidences was strongly reduced. Preliminary results using this set-up are reported separately in this annual report.

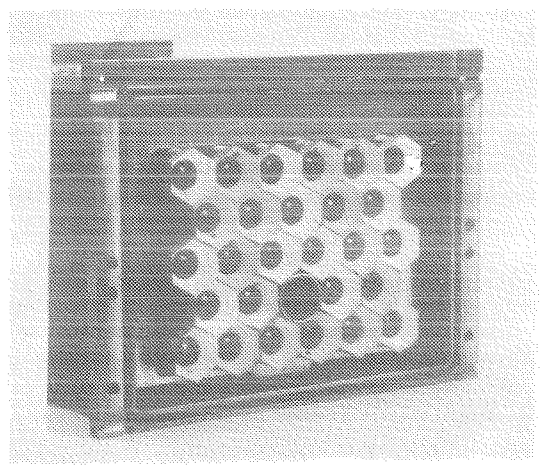


Fig. 3

A low background detection system for fragments and neutrons from spontaneous fission sources

U. Tharun, H.J. Keim, U. Knitz, P. Peuser, N. Trautmann, G. Herrmann
Institut für Kernchemie, Universität Mainz
G. Wirth
GSI Darmstadt

Detection of spontaneous fission events provides the most sensitive and specific method in the search for superheavy elements. Measurements of the fission-fragment kinetic energies and average neutron numbers per fission are important in order to distinguish between spontaneously fissioning activities of superheavy and of ordinary elements. Since the rate of fission events in typical samples is expected to be very low, a low background detection system is desirable which can record these quantities simultaneously.

We have developed a system which registers single and coincident fission fragments, their kinetic energies and the number of neutrons emitted per fission along with the time intervals between fission-fragment and neutron pulses. The system consists of 12 surface-barrier detectors which are surrounded by 30 ^{3}He-filled neutron counters as it is shown in the Figure.

The surface-barrier detectors (900 mm^2) are arranged horizontally in a vacuum chamber in a compact array of 2x3 detector pairs. The source position is equidistant between the detectors giving a 50% detection efficiency for coincident fission fragments for a 10 mm diameter sample as measured by thermal-neutron-induced fission of ^{235}U. With a ^{241}Am point source the efficiency for detecting α-particles with a single detector was measured to be ≈35%. The design of the neutron detector is similar to the one assembled at Oak Ridge[1]. The neutron counters are embedded in paraffin and are arrayed on two cylindrical surfaces with diameters of 24.2 and 31.4 cm, respectively. The efficiency for detecting a single neutron is 25±1 % as determined with a calibrated Am-Li source. The background rate for single neutron events is about 4 neutrons/min.

The electronics, designed to a large extend specifically for this system, is outlined in the lower part of the Figure. To achieve a compact assembly of the fission-fragment detectors, miniaturized preamplifiers are used. For registration of the neutron-multiplicity distribution doublets of close lying counters are coupled electronically. The multiplicity unit is triggered by the first detected neutron. The gate remains open for a preset time interval (normally 300 µs) to permit registration of coincident neutron events. The number of events accumulated for different multiplicities are printed out in 500 min intervals. Fission-start events are recorded event-by-event by printing (i) the energies of the singles or coincident fission fragments and the positions of the corresponding surface-barrier detectors, and (ii) for each neutron the time of detection after the fission-fragment pulse (in µs) and the number of the counter doublet in which the event was detected. In addition, α-spectra from 4 of the samples can be recorded simultaneously.

This system has first been used in the search for superheavy elements in the ^{238}U+^{248}Cm reaction[2]. Counting of various chemically isolated fractions was started in October 1979 and is still being continued. As an internal standard, a sample of ^{254}Cf is being measured. No event with fragment energies between 15 and 200 MeV occured within five months in one detector pair. This indicates the low background achieved with the system.

[1] R.L. Macklin et al., Nucl. Instr. Meth., 102, 181 (1972)
[2] M. Schädel et al., this Annual Report, p.

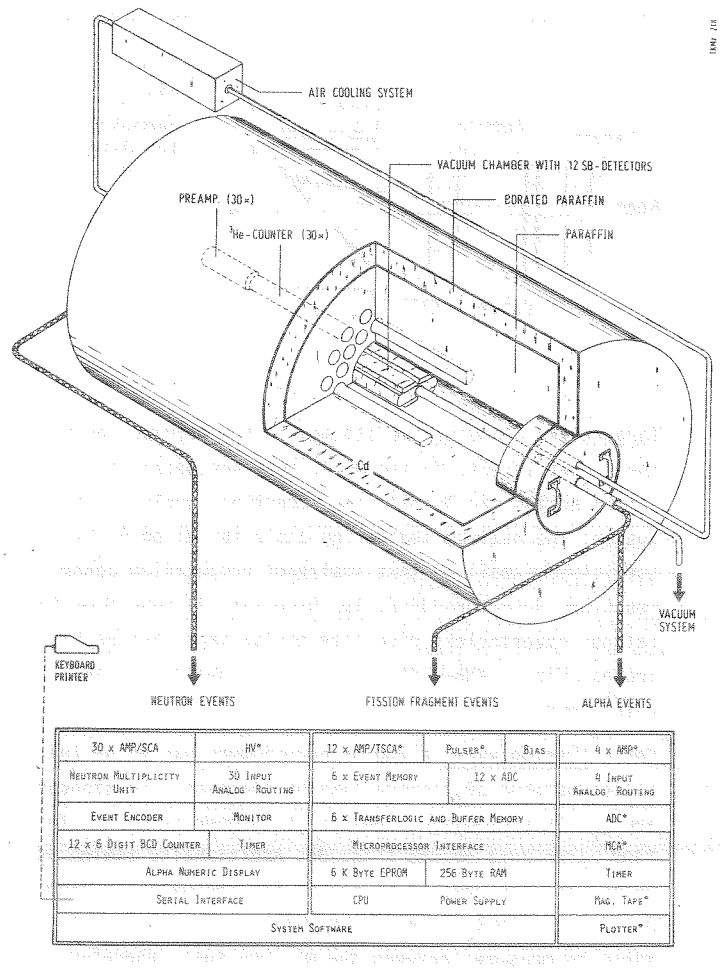


Fig. 1: Schematic drawing of the low background detection system (*commercially available parts)

A fast detection system for decaying heavy nuclei

A. Marinov
GSI Darmstadt and The Hebrew University of Jerusalem
W.F.W. Schneider, K.D. Hildenbrand, A. Gobbi, H. Freiesleben, R. Bock
GSI Darmstadt

A detector arrangement (Fig. 1) has been developed for a survey of fusion experiments, which uses the degrader-catcher technique in order to study the decay of products with lifetimes down to the ns range. Heavy evaporation residues, as for example formed by a ^{58}Ni beam in a ^{150}Nd target of 2.7 mg/cm^2 are slowed down in a degrader of 1.3 mg/cm^2 Al and finally stopped in the 0.7 mg/cm^2 Al catcher. Degrader and catcher are made of ultrapure Al (impurities <10^{-5}). The direct beam passes the catcher through a hole. A subsequent decay (α-decay or fission) can be measured with a ΔE-E telescope and a single detector. The two E-detectors are 400 mm^2 silicon counters of 250 μ thickness, the ΔE counter has 19.5 μ at 300 mm^2 thickness. The total efficiency of the system is 10-20 %. Possible particle/x-ray coincidences can be analyzed by means of an intrinsic Ge detector close to the catcher. Targets in the mg/cm^2 region allow to study a certain range of the compound nucleus excitation energy.

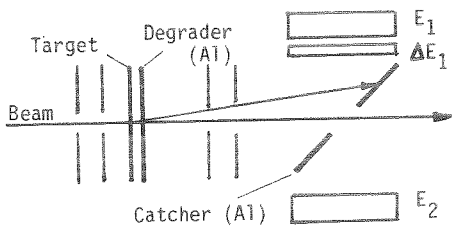


Fig. 1 Geometry of the detection system.

Target-like products are stopped in the degrader or in the target itself; furthermore, they are peaked at reaction angles far outside the acceptance angle of the system. The maximum scattering angle for Ni on Al is sufficiently small so that scattered projectiles cannot reach the detectors directly. Recoiling Al ions from the catcher nevertheless give rise for an important background. Fig. 2 shows the free energy spectrum of ΔE_1 (~10^6 counts).

For a fission event a 200 ns coincidence has to be fulfilled between ΔE_1 (where fission fragments are stopped) and E_2. This condition reduces the number of counts to 1400 coincident events (Fig. 3). Additionally timing is performed with respect to the rf and the macrostructure. As timing with E_2 is accurate within 1 ns, it is possible to measure 'between the micropulses'; therefore real binary events during the pulse or shortly after can be eliminated. If a time window is set which accepts events only during a 25 ns interval out of 37 ns between the micro-bunches only 4 coincidences with low energy are left in the spectrum of Fig. 3.

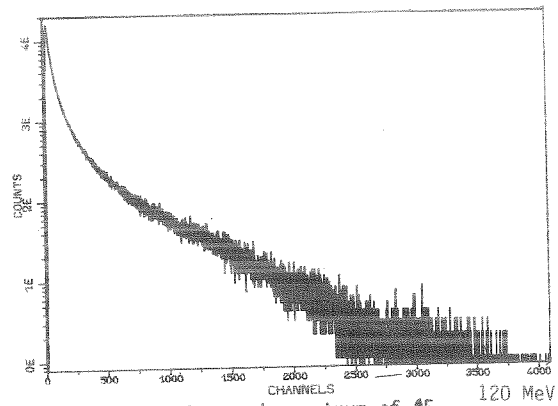


Fig. 2 Background spectrum of ΔE_1

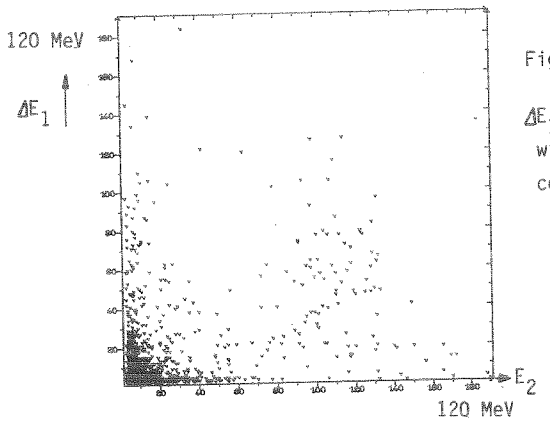


Fig. 3 ΔE_1 vs. E_2 with 200ns coinc.time

In a similar way α-decay is measured. The energy resolution is limited to ~500 keV due to the catcher thickness. Exact timing (ns) including particle identification is only possible for $E_\alpha \geq 5.5$ MeV.

In summary fission and α-decay with $E_\alpha \geq 5.5$ MeV can be measured with lifetimes down to ~5 ns using the microstructure of the UNILAC beam. Similarly, slow timing is done with respect to the macropulses (~5 ms out of 20 ms). Decays in the ms region can be analyzed with negligible background between the macropulses. Additionally x-ray spectra are recorded when an x-ray and a particle arrive within 1 μs.

The system was tested with a nickel beam and different targets (Ag, ^{150}Nd, ^{164}Dy, Pt). For Ag and ^{150}Nd α-groups of decaying fusion products could be identified.

Tests of a Transmissionspectrometer for X-Ray Spectroscopy [G]

K.-H. Schartner, H.J. Flaig, W. Spitz, A. Scharmann
I. Physikalisches Institut der Justus-Liebig-Universität Giessen

H.F. Beyer
GSI Darmstadt

A transmissionspectrometer is suitable for high-resolution spectroscopy of harder x rays ($Z \gtrsim 40$) (fig. 1)[1]. An experimental set-up[2] has been tested for first experiments with lighter targets, to be bombarded with projectiles of 1.4 MeV/amu impact energy, applying a Cu-x-ray tube as source and a 0.2 mm thin SiO_2-crystal in Cauchois geometry. The [1011] planes (2d = 6.71 Å) have been selected for dispersion of the x rays. A Xe-filled proportional counter serves as detector.

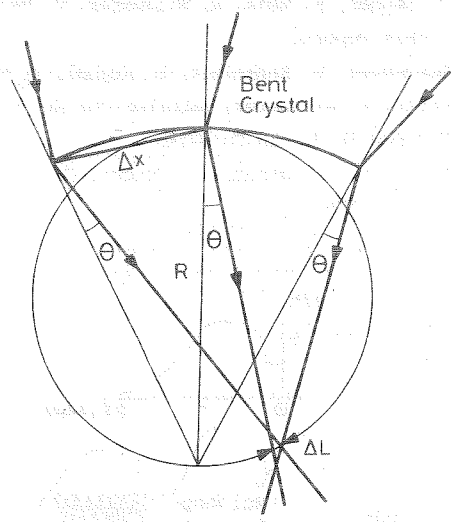


Fig. 1: Bent crystal focussing in Cauchois geometry.

Fig. 2 shows in a) the pulse height spectrum of the x-ray source and in b) the pulse height spectrum of the diffracted radiation. In the last case Cu-K_α radiation is diffracted in first order while parts of the continuous bremsstrahlung are diffracted in second and third order. By scanning the diffraction pattern in the calculated position on the focal circle, the Cu-$K_{\alpha 1}$- and $K_{\alpha 2}$-lines are resolved (fig. 2c) with a resolution $\lambda/d\lambda$ of 700. For obtaining the result of fig. 1c, only one third of the crystal was illuminated. By shifting the spectrometer set-up, the position and width of the e.g. $K_{\alpha 1}$-line could be measured as function of the illuminated part of the bent crystal.

It was found that position and resolution depend systematically on the transmitted part of the crystal. The position of the $K_{\alpha 1}$-line varies 1 mm for the extreme parts of the crystal, in comparison with a 0.5 mm separation of the peaks in fig. 1c. This result can be compared with calculations of the width ΔL of the diffracted pattern of the focal circle (fig. 1)

$$\Delta L = R\Omega + (\Delta x^2/2R)\tan\theta + (h^2/2R)\sin\theta \qquad (1)$$

wherein the second and third term are due to the linear opening Δx and height h of the crystal, while Ω represents the width of the diffraction pattern of the crystal, including bending effects.

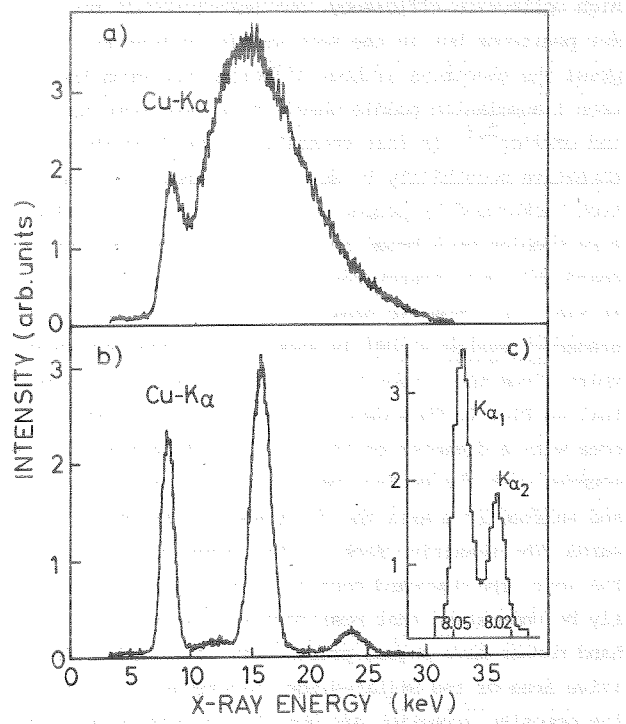


Fig. 2: a) Proportional counter spectrum of Cu-x-ray tube and
b) proportional counter spectrum of diffracted x rays,
c) scan of the $K_{\alpha 1}$- and $K_{\alpha 2}$-intensity on the focal circle.

For the present case the geometrical effects are negligible in comparison with 1 mm. In conclusion, the used crystal and bending device have to be investigated to decrease Ω which at present seems to amount to 0.06°.

[1] Y. Cauchois and C. Bonnelle in Atomic Innter-Shell Processes II (B. Crasemann ed.), Academic Press (1975), p. 84.
[2] A. Scharmann, K.-H. Schartner, N. Stiller, GSI-11-79 (1979), p. 172.

G

A Si(Li)-Detector System for in Beam Positron Spectroscopy

H. Backe, W. Bonin, E. Kankeleit, W. Patzner, P. Senger, F. Weik
Institut für Kernphysik der TH Darmstadt

In experiments dealing with atomic positron emission in collisions of very heavy ions[1] (e.g. U+U at E_{Lab}=5.9 MeV/u) the kinetic energy of a few positrons has to be measured in presence of a large amount of δ-electrons. The solenoidal positron transport system with a Si(Li)-detector as energy dispersive element has the virtue of high collection efficiency, but unfortunately not only for positrons but in the same way for electrons. To suppress the electrons without affecting too much the positron transmission paddle wheels have been used as reported earlier[2,3]. In this contribution we describe an alternative possibility to suppress strongly the δ electron background by proper mounting of two Si(Li)-detectors keeping up a broad range energy acceptance and a reasonable good energy resolution of about 1o keV.

In Fig. 1 a schematic drawing of the solenoidal positron transport system at GSI is shown. Positrons and electrons spiral from the target to the detector shown in more detail in Fig. 2. This detector consists of two Si(Li) diodes with a diameter of 19.5 mm and a thickness of 3 mm mounted with the surface parallel to the solenoid axis and shifted from axis the one upwards, the other downwards. The sensitive face of the upward counter looks to the left, the downward counter to the right. It can easily be understood that positrons spiraling in a right hand manner have a good probability of entering the sensitive area of the Si(Li)-diode. Electrons spiraling in the opposite direction are absorbed or scattered in the 3 mm thick Aluminum back cover of the detector. Only the very few electrons with an energy greater than about 1.4 MeV can penetrate the Al-absorber. A serious problem arises from electrons not following the usual trajectories from the reaction zone but suffered scattering in the target or its frame or from backscattering from the Al absorber behind the Si(Li) detectors. The probability for such a process was determined with 365 keV conversion electrons from a ^{113}Sn source, off line, and turned out to be about o.7%. Because the positrons are detected in coincidence with the annihilation radiation by help of a NaI ring detector the suppression of electrons was sufficient to avoid electron positron sum coincidences. For instance in a U+U experiment at 5.9 MeV/u and a scattering angle $\theta^{Ion}_{Lab} = 45^{o}\pm 1o^{o}$ sum coincidences contribute to less than 2% in the positron spectrum.

The positron detection efficiency as shown in the insert of Fig. 1 was measured with intensity calibrated ^{22}Na and ^{68}Ge/Ga sources. As in the beam experiment the 511 keV full energy peak was selected for one of the NaI counters and the total energy spectrum in the opposite NaI counter. By this procedure the detection efficiency was increased by a factor of two. No deterioration of the positron spectrum was observed due to sum coincidences with Compton scattered annihilation radiation in the Si(Li) detector. About 3o% of the impinging positrons were analysed in energy. The efficiency may be increased appreciably by using two or three rectangular Si(Li) detectors instead of the circular ones.

[1] H. Backe, W. Bonin, W. Engelhardt, E. Kankeleit, M. Mutterer, P. Senger, F. Weik, R. Willwater, V. Metag, J.B. Wilhelmy, this report.

[2] H. Backe, H. Bokemeyer, E. Kankeleit, E. Kuphal, Y. Nakayama, L. Richter, R. Willwater, Laborbericht Nr. 67, Institut für Kernphysik der TH Darmstadt.

[3] H. Backe, M. Mutterer, W. Patzner, P. Senger, GSI Jahresbericht 79-11, p. 175.

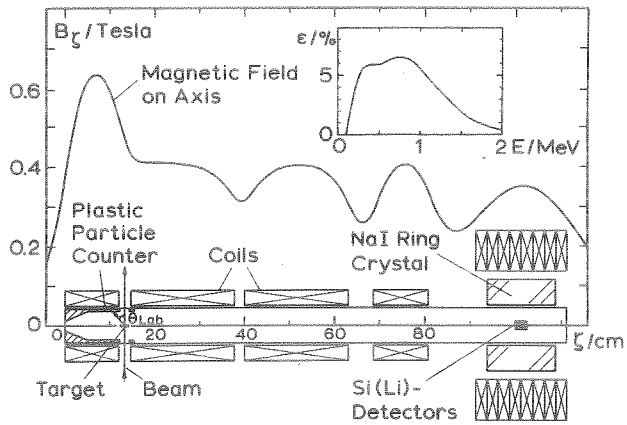


Fig. 1: Schematic view of the Solenoid with detection efficiency ε of the Si(Li) detector

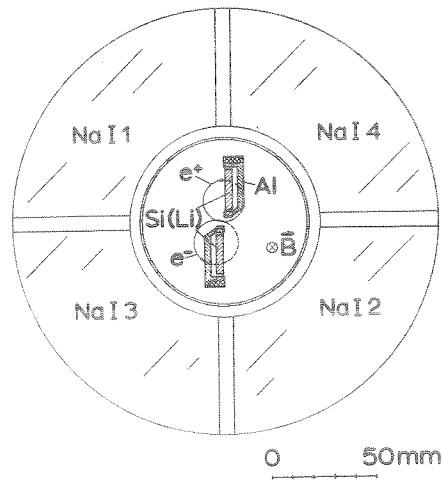


Fig. 2: The positron detector assembly

ISOL Ion Sources. Part 1: The FEBIAD Ion Source

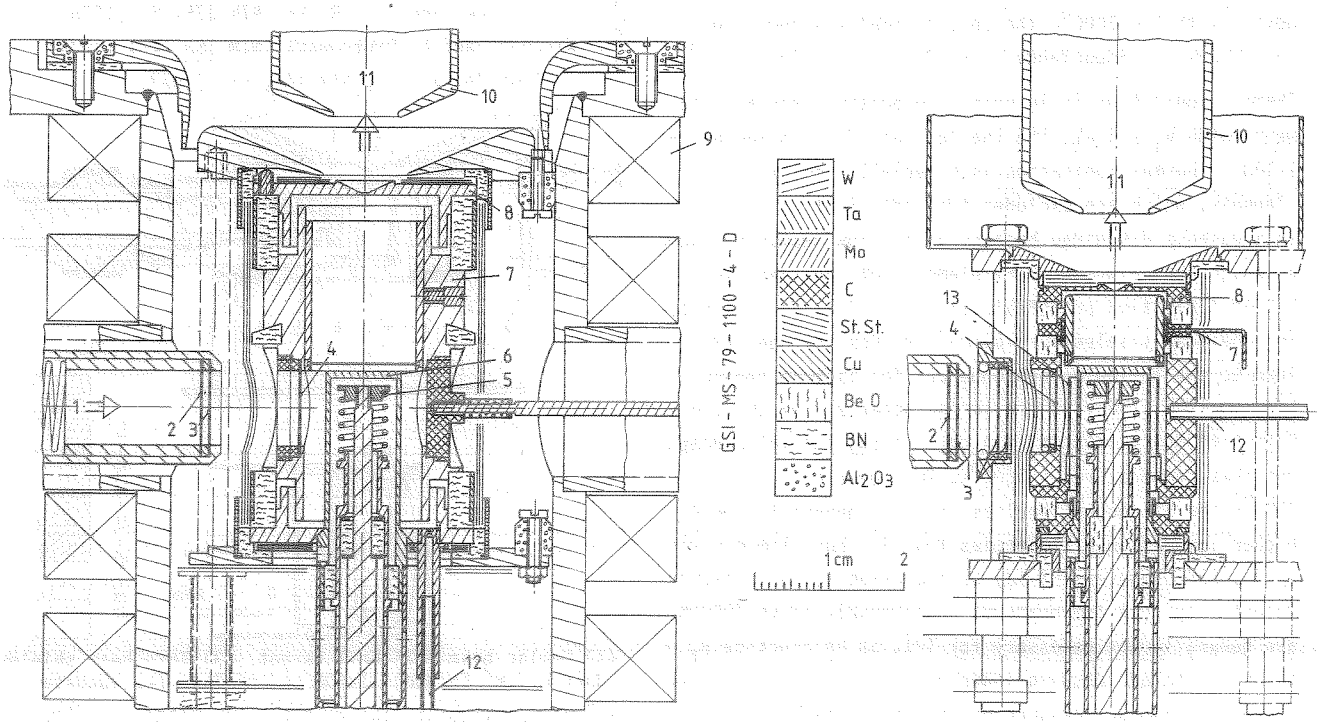
R. Kirchner, C. Bruske, K.H. Burkard, W. Hüller, O. Klepper
GSI Darmstadt

Gaseous discharges are in principle universal ion sources for isotope separation on-line (ISOL). Their application is, however, in general restricted to elements with a sufficiently high vapour pressure at the temperature of the discharge chamber. The natural aim - the design of a gaseous discharge source for the utmost temperature - is limited by the necessity for electrical insulators, the thermal, electrical, chemical and mechanical properties of which cause increasing problems above 1600°C.

Below two versions of the FEBIAD (forced electron beam induced arc discharge) ion source[1] are shown. Type A has been used successfully on-line for many years. Type B represents the result of a development versus higher temperature, greater flexibility and utility. The change to BeO-insulators and a more compact design in connection with the very effective 6-fold heat-shielding raises the "cold spot"-temperature from ∿ 1500°C to 1900°C. Two additional thin carbon heat shields close to the entrance window eliminate the window as a "cold spot" and reduce the thermal radiation to the target considerably. Another major improvement is the introduction of a catcher electrode at separate potential enabling electron bombardment heating. The initially combined functions of the tantalum capsule as cathode for the discharge and as catcher for the nuclear reaction products are thus decoupled. In addition, materials other than tantalum, especially materials excluded for thermionic cathodes (e.g. graphite) become available as catcher materials (tested are C, Nb). For the reaction products (In-Xe) so far investigated, Nb (at ∿ 2200°C) turned out to be inferior compared to Ta (∿ 2400°C), whereas graphite (∿ 2200°C) shows equal or considerably better results: e.g. ^{106}Sn(126s/3.6x/6%), ^{108}Sb(7s/4x/≳3%), ^{108}Te(2s/2x/0.3%), ^{110}I(0.7s/4x/0.6%). Numbers in brackets denote halflife, gain of efficiency with source B (graphite catcher) compared to version A, and estimated total separation efficiency. So far, the most short-lived isotope separated with source B is 60 ms-^{183}Tl.

The graphite catcher offers another (unexpected) advantage: The long lifetime of source A of several hundred hours turned out to be restricted to 20-50 h under on-line conditions due to the fact that the window (thickness initially 1 mg/cm^2) gradually lost the transparency for the reaction products. This was caused by the evaporation of tantalum from the cathode (=catcher) onto the window at a rate of 0.2 mg/cm^{2}h. In version B, where the window is faced by the graphite catcher cylinder, only a total conversion of the window into TaC is noticed without any thickness increase worth mentioning.

[1] R. Kirchner and E. Roeckl, NIM 133, 187 (1976)



(1) Unilac beam. (2) Foil target (2-5 mg/cm^2). (3) Thin carbon heat shields (∿ 20 µg/cm^2). (4) Tantalum window (∿ 1 mg/cm^2). (5) Filament for electron bombardment heating of the (6) tantalum cathode. (7) Anode with grid for primary electron extraction. (8) Outlet plate. (9) Source magnet. (10) Extraction electrode. (11) Separator beam. (12) Gas line; in version B used also as electrical support for the (13) catcher electrode (graphite ∿ 0.1 mm)

ISOL Ion Sources. Part 2: The Thermal Ion Source

R. Kirchner, K.H. Burkard, W. Hüller, O. Klepper
GSI Darmstadt

For the degree of ionization in a thermally equilibrated system of temperature T, Nernst's heat theorem yields

$$n_e n_i/n_o = \text{const.}(2\sigma_i/\sigma_o)(kT)^{3/2}\exp(-W_i/kT). \quad (1)$$

$n_{e,i,o}$ denote the densities of electrons, ions and neutrals, W_i the first ionization potential and $\sigma_{i,o}$ the statistical weights for ions and neutrals, respectively. Eq. (1) suggests two practicable ion source concepts:

- The surface ionization (SI-)concept supposing that the density n_e is given by Richardson's law as for a metal surface of work function Φ. Eq. (1) then reduces to the Saha-Langmuir equation for the ionization efficiency per surface collision $\beta_S = n_i/(n_i+n_o)$:

$$\beta_S = \alpha/(1+\alpha) \quad \text{with } \alpha = (\sigma_i/\sigma_o)\exp\{(\Phi-W_i)/kT\}. \quad (2)$$

- The thermal plasma ionization (TPI-)concept[1,2] in case of a quasi-neutral ($n_e \approx n_i$) ensemble of neutral particles, ions and electrons. Then the ionization efficiency β_T is described by the Eggert-Saha-equation:

$$\beta_T^2/(1-\beta_T^2) = \text{const.}(2\sigma_i/\sigma_o)P^{-1}(kT)^{5/2}\exp(-W_i/kT) \quad (3)$$

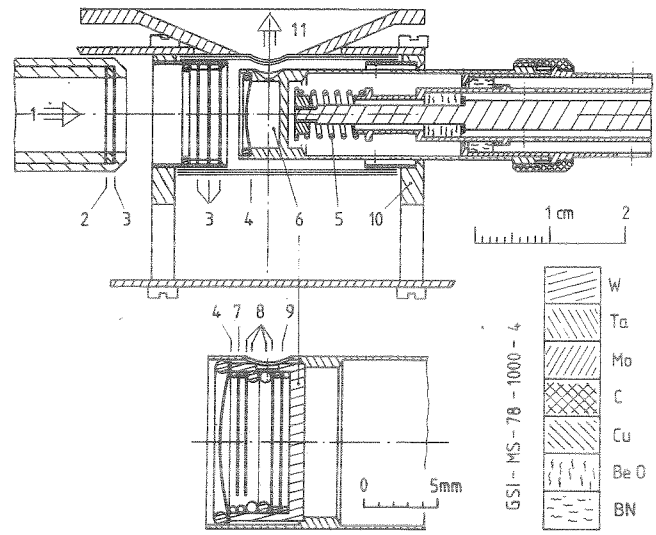
To create a thermal plasma in a real cavity two boundary conditions have to be satisfied. Firstly the condition $\lambda_D \ll l$ (λ_D Debye-length, l linear dimension of the cavity) to enforce quasi-neutrality and secondly $\beta_T/\beta_S < k$ (k mean number of collisions of neutrals with the cavity walls) to guarantee thermal equilibrium[3], as in a laboratory device with $T \lesssim 3000^oC$ the only thermally induced ionizing process of importance is surface ionization.

Thermal ionization is in principle possible for all elements with $W_i \lesssim 8$ eV, the theoretical efficiencies being 1-100%. Thermal ionization is especially indicated for elements, which are excluded from efficient ionization in a gaseous discharge because of too low vapour pressure or which are neighboured by elements of considerably higher ionization potentials (e.g. In, Tl), thus permitting chemically selective ionization. Eqs. (2) and (3) lead to the following consequences for isotope separation-on-line (ISOL), which is characterized by the ionization of trace amounts in a cavity: (a) The TPI-concept requires temperatures $\gtrsim 2800^oK$, for temperatures below 2500^oK the SI-concept applies. (b) TPI generally yields higher ionization efficiencies than SI. For elements with $W_i \lesssim 5.5$eV, however, SI may be indicated to reach higher selectivity. (c) Temperatures considerably above 2800^oK are generally not necessary for TPI, as in practice β_T turns out to be pressure-independent because of strongly increasing vapour pressure of the cavity material with increasing temperature (pressure dependence in eq. (3)!). (d) From vapour pressure considerations tungsten is the optimum cavity material, though elements with $W_i > 6.5$eV may indicate the use of rhenium to circumvent the need for excessively high wall collision rates.

The figure below shows the technical design of the ion source. Tungsten source body and heater are one unit which can be exchanged through an airlock without breaking vacuum. The complex set-up of foils follows from the problems associated with high temperature for efficient ionization on the one hand and the need for entrance window and catcher on the other hand. So far only tungsten windows in dished shape withstand both temperature and thermal stress. To reduce the vapour pressure of the catcher material, the catcher is mounted on the "low" temperature end of the source close to the window. The actual ionizing cavity is formed by the tungsten or rhenium foils and spacer rings placed in the hotter zone. The electron bombardment power is set such that the temperature of graphite catchers is $\lesssim 2200^oC$ and is not exceeding $\approx 2400^oC$ for Ta catchers to prevent a too fast thickness increase of the window.

Graphite catchers were used for the on-line production of cesium, the total efficiencies being estimated to 20% for ^{118}Cs (16s) and 9% for ^{114}Cs (0.6s). With the Ta-catcher the efficiencies were 25-50% for ^{117}Ba (1.9s), about 10% for ^{153}Er (40s), ^{153}Tm (1.6s) and ^{157}Lu (5.5s), 1.3% for ^{154}Yb (0.4s) and $\gtrsim$0.7% for ^{81}Y (300s).

[1] A. Latuszynski and V.I. Raiko, NIM 125, 61 (1975)
[2] R. Kirchner and A. Piotrowski, NIM 153, 291 (1978)
[3] V.P. Afanas'ev et al., NIM 145, 533 (1977)



(1) Unilac beam. (2) Foil target. (3) Thin heat shields (3x20 µg/cm^2 Carbon), 1x700 µg/cm^2 Ta). (4) Tungsten window (1.5-2 mg/cm^2). (5) Filament for electron bombardment heating of the (6) tungsten source body (see inset). (7) Catcher (15 µm Ta or 0.2 mm graphite). (8) Ionizer foils and rings (W or Re). (9) Tungsten heat shield (only for Re ionizer foils). (10) Housing for radiation shielding and alignment. (11) Separator beam.

Release Times and Separation Efficiencies of the GSI On-line Separator

O. Klepper, K. H. Burkard, W. Müller, R. Kirchner, W. Reisdorf, E. Roeckl
GSI Darmstadt

Separator parameters such as release time and efficiency have been investigated in order to correct, for instance, measured isotopic distributions of reaction products for the individual decay loss of the isotopes within the ion source due to their different half-lives. Generally release time distributions for a given isotope of half-life $T^*_{1/2}$ are obtained by collecting and measuring mass-separated samples for consecutive intervals Δt, after the accelerator beam has been turned off[1]. However, this technique becomes very inefficient for $\Delta t \ll T^*_{1/2}$. This is circumvented by a method sketched in fig. 1. Using a pulsed accelerator beam (50% duty cycle) and a synchronized deflection system in the separator the isotope under investigation can be alternately collected at two positions: at one while the beam is on target (during the time T_{pulse}), and at the other, while it is turned off (during T_{pause}). From the ratio of the two source strengths measured for various pulse frequencies, the release-time function for times $\lesssim T^*_{1/2}$ and relative separation efficiencies for isotopes with half-lives $\lesssim T^*_{1/2}$ can be deduced.

As an example fig. 1 shows the release-time measurement for mercury from a FEBIAD ion source (version A)[2] employing the α decay of 48s-^{185}Hg. In fig. 2 separation efficiencies relative to the efficiency for a (fictitious) isotope with half-life $T_{1/2}$=40s are shown for mercury, polonium and iodine from the FEBIAD ion source (catcher: Ta cathode) and for cesium and erbium from thermal ion sources[3]. In the cesium case a graphite catcher inside a tantalum cavity was employed. The erbium nuclei, on the other hand, were stopped in a 10 mg/cm^2 tantalum window of a tungsten cavity.

Absolute separation efficiencies η(40s)=20(6) and 21(8)% for mercury and polonium, respectively, have been derived by measuring production yields in the target with a catcher technique.

[1] K. H. Burkard et al., GSI Annual Report 1977, GSI-J-1-78, p. 191

[2] R. Kirchner et al., contribution to this annual report

[3] R. Kirchner et al., contribution to this annual report

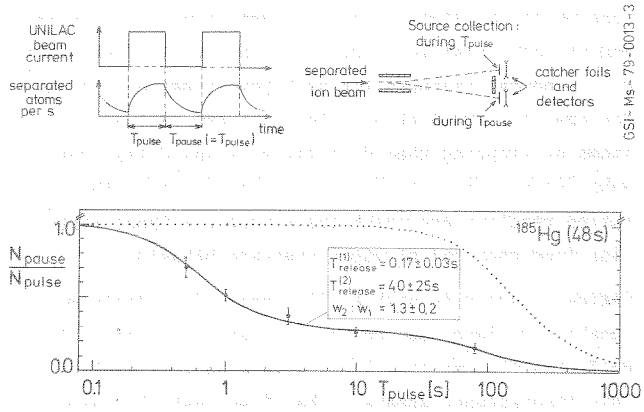


Fig. 1, upper part: scheme of release time measurement with a pulsed accelerator beam
lower part: ratio of the ^{185}Hg α-activities of the two sources collected during T_{pause} and T_{pulse} (reaction: ^{148}Sm(^{40}Ar,3n)). The full curve represents a fit assuming a superposition of two exponential release-time functions with half-time components $T_{release}$ and weights w. The dotted line illustrates the case $T_{release} \gg T^*_{1/2}$.

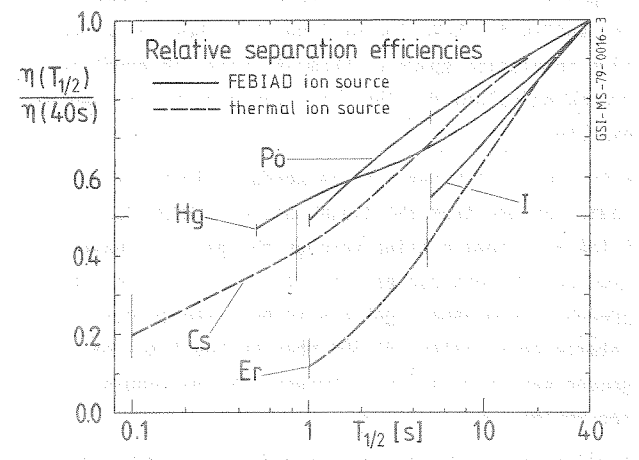


Fig. 2: Relative separation efficiencies as function of the half-life for isotopes of the indicated elements. The curves are calculated from fitted release-time distributions and normalized to a half-life of 40 s. The vertical bars display the accuracy of the results.

In-beam laser fluorescence spectrometer

G. Huber, G. Ulm, D. Marx

Several recent laser spectroscopy experiments on radioactive isotopes[1] have used hyperfine structure and isotope shifts in atomic lines for determination of spins, moments and relative charge radii of nuclei. The use of H.I. produced isotopes for such investigations allows for specific preparation methods of the radioactive atoms by stopping them directly in a gas filled resonance vessel. Selectivity is provided by both the H.I. fusion reaction and laser spectrsocopy without restriction from chemical or vapor pressure behaviour.

Optical resonances with a light beam of a single mode tunable dye laser can be observed via the wide angle collected fluorescence light with a photomultiplier. This fluorescence apparatus has been installed at GSI in the experimental area X6. In the neighbouring laboratory a laser spectrometer including a single mode dye laser and a reference atomic beam fluorescence set up has been installed.

Fig. 1 shows fluorescence signals of the λ = 451 nm line in natural indium from the reference atomic beam. Similar curves have been obtained with the λ = 410 nm line in indium using a different laser dye. With these lines optical pumping has been observed in the fluorescence apparatus at various neon and nitrogen gas pressures. From the saturation of the fluorescence the maximum excitation rate of indium could be determined to $\sim 10^4$/s at pressures > 100 mbar. Moreover pressure broadening and shifts in these indium lines have been observed in high resolution spectra. From all these observations promising values for the detection sensitivity can be expected.

With a beam of 6 MeV/u Ti background signals from nuclear radiation and from the plasma and afterglow due to a 8 TnA H.I. beam passing through the gas cell have been studied. Whereas nuclear radiation gives a minor background, the plasma light has to be filtered out by an interference filter. At 300 mbar Ne the total background was below 10^4/s in between the macropulses of the Unilac.

A pilot experiment on neutron deficient indium isotopes is planned to demonstrate feasibility and sensitivity also for short lived isotopes.

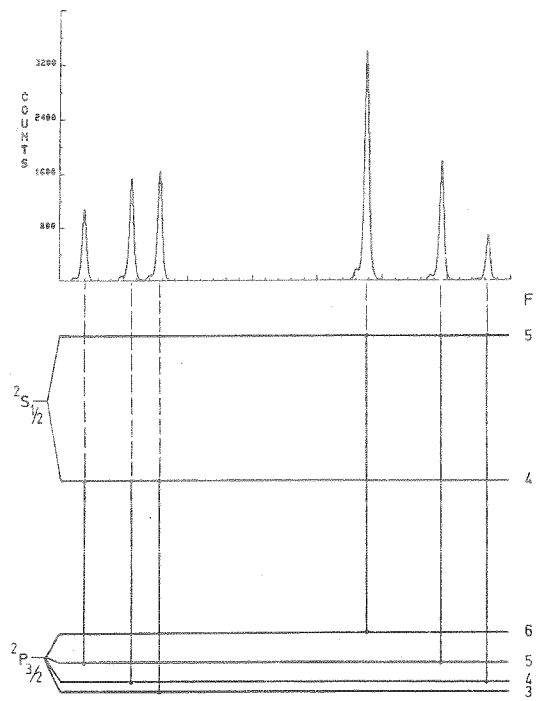


Fig. 1: Top: atomic beam laser resonance in λ = 451 nm with natural indium;
bottom: hyperfine structure of the corresponding atomic levels schematically.

[1] H.J. Kluge et al., Laser Spectroscopy IV, Rottach-Egern, June 11-15 (1979) ed. H. Walther and K.W. Rothe Springer 1979 p. 517

S. Liberman et al., ibid. p. 527

G. Schatz ibid. p. 534

G. Huber et al., GSI Annual Report 1978 p. 60

Optical Spectroscopy of Unstable Isotopes at the TRIGA-Reactor in Mainz [G]

J. Bonn, F. Jüttner, W. Klempt, T. Kühl, R. Neugart, E.W. Otten, W. Schinzler, K.P.C.Spath, K. Wendt
Universität Mainz

After successful laser-spectroscopic and RADOP-measurement of Rubidium and Caesium Isotope-shifts in 1978, work during the last year was dedicated to efforts to improve i) the efficiency and diffusion time of the target-ion source system and ii) the detection probability of the laser-optical experiment.
As to i) two new target types have been develloped, both using internal heating of the target vessel. This is necessary to provide the higher target temperatures essential for a faster release of alkali and alkali earth isotopes without overheating the walls of the vacuum enclosure in the vicinity of the reactor's core. Test running in the reactor proved the feasability of much higher target temperatures but also showed severe lifetime and outgasing problems. This resulted in a new design of the heater coil and the attempt to use graphite cloth discs as matrix for the uranium, which seemed to be promising in off-line tests.

The redesign ii) of the optical detection system should result in a lowering of the detection limit. The light collecting arrangement for the fluorescence photons was completely changed to yield a geometric detection angle of nearly 4 π. Test measurements demonstrated an increase in detection probability by 500 %.
The expected increase of collected stray light was tried to be reduced by fast chopping of the laser-beam using an acousto-optical deflector. The most likely application of the new system will be in cases, where detection of a secondary transition is possible.

G

Developmental work on the HELIOS system

A.K. Mazumdar, H. Wagner, W. Walcher
FB Physik, Marburg

M. Brügger, N. Trautmann
Institut für Kernchemie, Universität Mainz

By technical improvements and with a new ion source the overall efficiency of the HELIOS system at the Mainz reactor has been increased in particular for the Rare Earth elements.

1. A high temperature surface ion source has been developed by modification of the integrated skimmer ion source. The new ion source can be operated in two modes: a) elements with lower ionisation energies E_i are ionized by thermal surface[1] ionisation in the hot hollow cathode of the ion source, b) elements with high ionisation energies E_i are ionized by an arc discharge[2] by applying an additional voltage of 150-200 V to the ion source between the hollow cathode and skimmer anode. The measured ionisation efficiencies for fission products are given in Table 1 for both operating modes. Mode 1 is suited for the ionisation of lanthanides and alkaline earth elements with source efficiencies of about 4%. Mode 2 allows ionisation of many elements, but with lower ionisation efficiencies.

2. The transfer time from the target to the measuring position at the collector of the separator has been determined by operating the TRIGA reactor in the pulse mode. The growth and decay curve of mass separated ^{142}Cs ($T_{1/2}$ = 1.6 s) measured at the collector plane of the separator is shown in Figure 1. The first activity arrives about 1 s after the neutron pulse, whereas the total activity was found within 3.7 s[2].

3. Using another target chamber and a gas pressure of 4 bar an almost mass independent jet transmission of about 60% was obtained[2] without using any foils on the target[3].

4. The ion optical imaging system equipped with rotatable poletips at the entrance and the exit of the magnetic sector field achieves two directional focussing of the ion beam without electrostatic einzellenses. The mass dispersion is $\frac{\Delta x}{\Delta M} = \frac{190}{M}$ cm, the mass resolving power $(\frac{M}{\Delta M})_{1/2} \approx 600$.

5. For laser fluorescence measurements on the mass separated ion beam a laser set-up has been intalled at HELIOS by the optical group of the Marburg Physics department. In continuation of their work on stable isotopes[4,5] measurements on short lived neutron-rich alkaline earth and lanthanide nuclides are in preparation.

[1] G.J. Beyer et al., Nucl. Instr. Meth., 96 457 (1971)
[2] A.K. Mazumdar et al., Nucl. Instr. Meth., in press
[3] A.K. Mazumdar et al., GSI-Report 79-11, 170 (1979)
[4] Th. Meier et al., Opt. Comm., 20, 397 (1977)
[5] C. Höhle et al. Z. Physik, in press

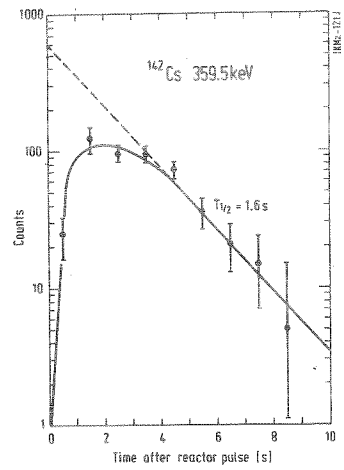


Fig. 1: The growth and decay curve of ^{142}Cs measured at the collector as a function of the time after the reactor pulse.

Nuclide recorded	Mode 1: Thermal plasma		Mode 2: Arc plasma	
	η	η_I	η	η_I
^{93}Sr	2,3 %	11,5 %	0,6 %	2,4 %
^{95}Y	1,4 %	7,0 %	0,3 %	1,2 %
^{141}Ba	6,0 %	30,0 %	1,2 %	4,8 %
^{146}Ce	3,9 %	19,5 %	0,2 %	0,8 %
^{151}Nd	4,4 %	22,0 %	0,2 %	0,8 %

Table 1: Efficiency of the integrated skimmer ion source $\eta = \eta_I \cdot T_{sk}$, the product of ionization efficiency η_I in the source times the transmission T_{sk} of the skimmer. T_{sk} is ≈0,20.

G

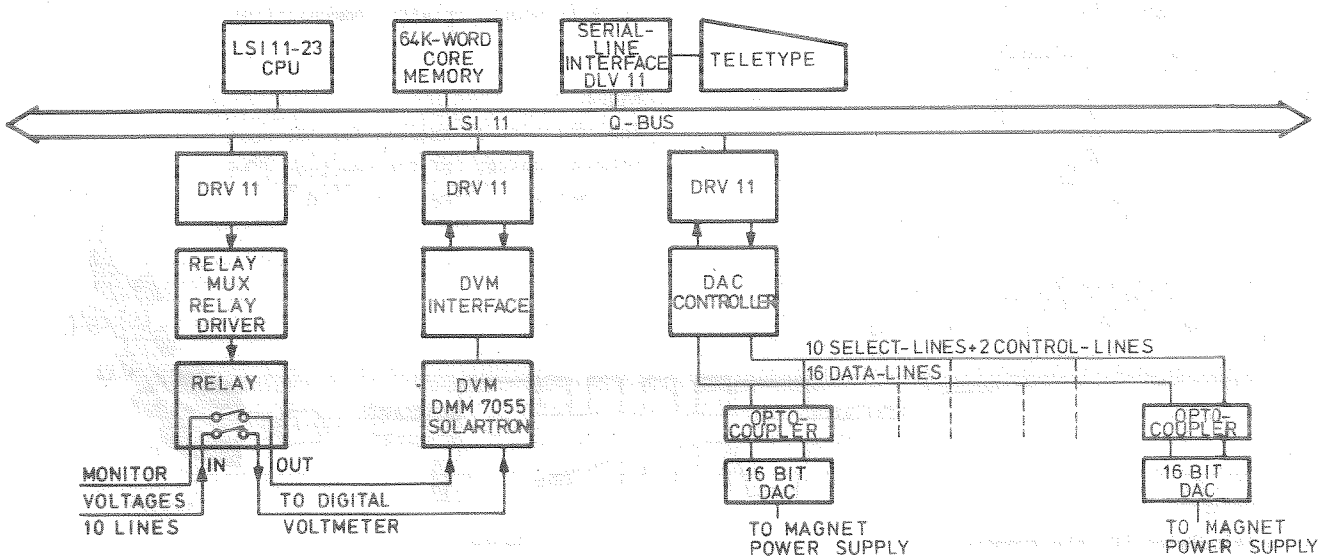
Microcomputer Control of the Velocity-Filter SHIP

H.-J. Schött, K. Poppensieker
GSI Darmstadt

Setup of the velocity separator SHIP for a specific experiment involves adjustment of ten individual field parameters. These are determined by calculations on the IBM 370 system in the computer center and heretofore were transferred manually (required accuracy 10^{-4}) to the respective power supplies, a tedious and time-consuming process, especially when a rapid succession of survey experiments is to be performed. Online computer control and system monitoring is therefore highly desirable. Initial tests with the power supply control hardware in use at the UNILAC did not provide an adequate level of performance, making it necessary to design a new system. In terms of cost and labor effectiveness use of a commercially available microcomputer (DEC PDP 11/23) turned out to be the optimum choice, especially in view of existing minicomputer systems and expertise at GSI. This unit also offers sufficient computing power for eventual expansion to a stand alone system. This note does not present any new or unique schemes, however it does show that adherence to elementary electrical design rules makes this a routine project.

In the adopted scheme the sets of data calculated on the IBM 370 are transferred directly to a PDP 11/23 via a slow data link[1], usually prior to a run. Memory space in the microcomputer is sufficiently large to make online operation essentially unaffected by vagaries in performance of the computer center. The microcomputer sets the desired field parameters, monitors their values in the course of operation and executes corrections if necessary. The magnet currents are determined by measuring either the corresponding voltage drop over a series resistor or the voltage output of a gauss-meter. Switching from one measuring port to another is performed by a relay-multiplexer using relays with a low thermal offset voltage (≤ 15 µV) (CLARE HGJ2MT). The respective voltages (≤ 400 mV) are measured to an accuracy of 10µV by a digital-voltmeter (SOLARTRON 7055). The ten power supplies (BRUKER) are set by individual 16-bit digital to analog converters (BURR-BROWN DAC 72-CSB), driving the analog control inputs of the respective supplies. The overall stability of the DAC's is better than 150 µV over a 10 V output voltage range. Care has been taken to avoid ground-loops. All interconnections are isolated and each DAC has its separate isolated power supply. The relay-multiplexer, the DAC's and the digital voltmeter are interfaced to three 16-bit parallel I/O-interfaces of a PDP 11/23 microcomputer. The program in the microcomputer can select a monitor-voltage, can read out the digital voltmeter and can preset a desired output-voltage of a selected DAC. The program also performs precycling of the magnets, drives the power supplies to their desired values and monitors these values during the run. Installation of the complete system is currently in progress. It is expected to go into operation in mid-1980.

[1] K. Poppensieker et al., GSI-Jahresbericht 1978, GSI 79-11, p. 191



Calculation of a Dipole Magnet, Extending SHIP to a Mass Separator for Unslowed Fusion Reaction Products [G]

B.Thuma, H.Ewald, Uni Gießen
G.Münzenberg, S.Hofmann, F.Heßberger, GSI Darmstadt

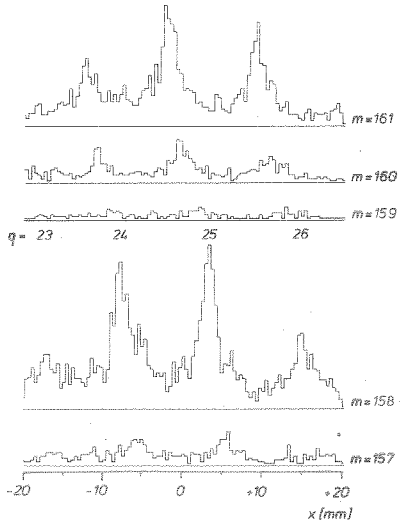
At the velocity filter SHIP presently most of the observed evaporation residues are identified by alpha spectroscopic methods. A device which can measure the mass number of these nuclei directly, as they are recoiling from the target, would be extremely useful.

The application of ionisation chambers is constrained to nuclei with specific energies of at least 1 MeV/u, and to experiments, where a spatial separation of different masses is not desired.

We have therefore investigated the possibilities of a deflection magnet coupled to the velocity filter in such a way, that focusing in angle and velocity is achieved for a certain mass over charge ratio.

A drawback of such a system is the charge multiplicity of the unslowed reaction products. Hence mass over charge ratios of different masses may become similar and cause overlays, a problem well known from recoil separators for fission fragments. In our case the observed mass range only covers few masses, so that this problem is less serious.

A sketch of the deflecting magnet in connection with SHIP is shown in figure 1. The velocity dispersion of the filter is cancelled by the magnet to get a velocity independent mass over charge dispersion. As the velocity dispersion of SHIP is quite modest due to the short electric deflecting condensers, the obtainable mass resolution is rather small. For focusing and correction of image aberrations a quadrupole doublet and multipoles are necessary.



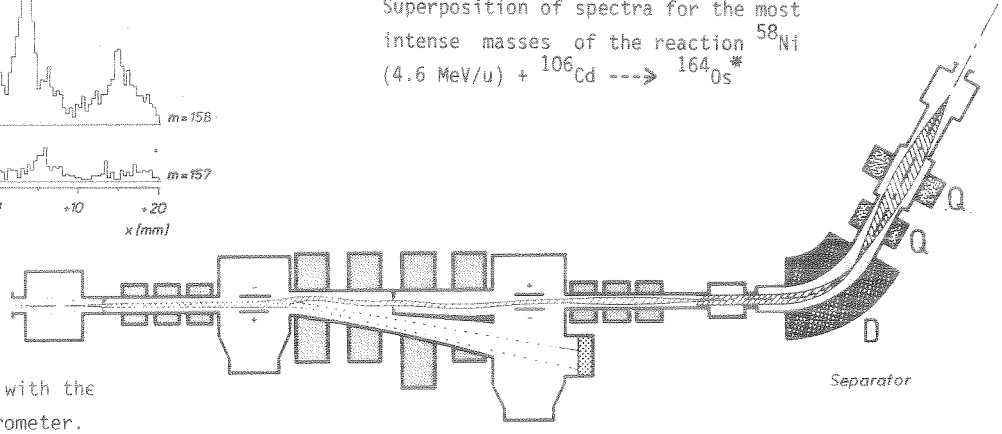


Fig.1 Velocity filter SHIP with the calculated DQQ spectrometer.

The calculations were done with the ion optical computer program GIOS (General Ion Optical Systems) /1/. They were carried out up to the third order. In combination with a Monte - Carlo - Program /2/ to calculate the characteristics of the evaporation residues after leaving the target (energy, charge, mass, position, angle) for a given reaction channel of a certain fusion reaction, it is possible to create realistic particle spectra in the focal plane of the spectrometer.

The recoil of the evaporation residues from evaporated neutrons, protons and/or alpha particles is taken into account using a special computer program /3/. Thus the creation and comparison of spectra for different reactions give a dependence of the line width from the reaction kinematics: An increasing projectile to target mass ratio, that means an evaporation residue angle distribution which is peaked more and more in foreward direction, implies a decrease of the line width and so an increase in mass resolution.

In figure 2 we generated a mass spectrum taking into account the partial cross sections for the generated evaporation residues by evaporation calculations /3/, creating the spectra for each isobar separately with the corresponding intensity. Now it is possible to see the overlap of neighbouring masses over the wanted mass lines for the considered fusion reaction.

The mass resolution moves between values of about 50 (Ni on Ni (2p,3n)) and about 200 (Xe on Fe (5n)). The transmission with the separator is reduced by a factor of two compared to the transmission of SHIP, if three charge states are regarded in the mass spectrum.

/1/ E.Kasseckert, T.Matsuo, H.Wollnik to be published
/2/ W.Faust GSI - report P - 4 - 78
/3/ W.Reisdorf private communication

Fig.2
Superposition of spectra for the most intense masses of the reaction ^{58}Ni (4.6 MeV/u) + ^{106}Cd ---> $^{164}Os^{*}$

Computer Simulation of the Motion of Heavy Ions Passing Through Gas Filled Systems [G]

J. Zienert, K. Güttner[+]
II. Phys. Institut, Universität Giessen

G. Münzenberg
GSI Darmstadt

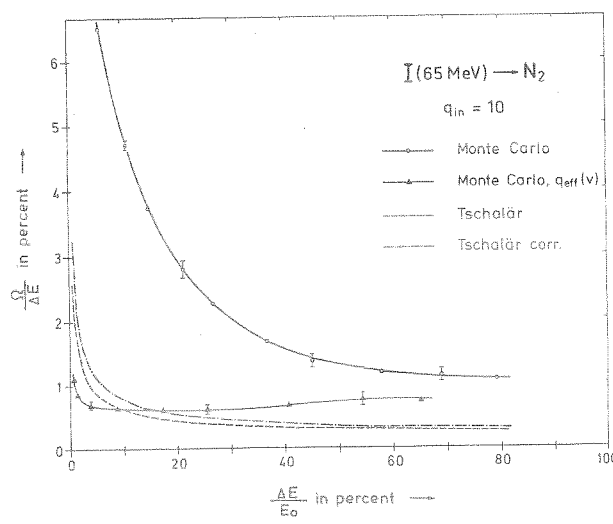
In the preceding two GSI-Annual Reports a computer program, based on a Monte Carlo method, has been described in detail. This program has been used to investigate the influence of a gas filling on the focusing properties of quadrupol systems. In the meantime some calculations concerning the energy straggling of charged particles in gas targets have been performed.

The energy straggling has been studied theoretically, for example, by Landau[1], Vavilov[2] (valid for energy loss ΔE much smaller than the primary-particle energy E), and by Tschalär[3] (straggling distributions calculated up to ΔE = 0,8·E for heavy particles). During the last few years also experimental data[4-6] have been published on the energy straggling of heavy ions in an energy range, where the charge of the ions is still greatly fluctuating while passing through matter. The experimental values exceed the theoretical predictions now and then several times. It has been suggested, that charge exchange of the ions gives a significant contribution to energy loss straggling causing a broadening of energy distribution. An explicit calculation of this energy straggling due to charge state fluctuations has been given by Vollmer[7].

In our Monte Carlo program the path of the particles in the gas is determined using theoretical formulae describing the processes of charge exchange, elastic nuclear scattering, and energy loss. Besides other information the energy loss of each particle in a gas target can be obtained and calculating a large number of particles also the energy loss distribution. In order to consider the charge state fluctuations the charge exchange for loss and capture of one or several electrons are necessary. Unfortunately these cross sections have been determined only for a few ion-target-combinations experimentally. Therefore the applicability of the present program is somewhat limited. Sometimes, however, approximation formulae can produce reasonable results.

The figure shows a comparison of different predictions for the energy straggling of I (65 MeV) in N_2 (up to energy losses of 80 %). The charge exchange cross sections used in the Monte Carlo calculations have been taken from Angert et al.[8]. Straggling also has been calculated for a velocity-dependent effective charge, that means without charge state fluctuations. For energy losses up to 20 percent only fluctuations of the charge give an additional contribution to the collision straggling. Furthermore theoretical values of Tschalär[3] and a curve calculated using Avdeichikov's[4] method of including shell corrections in Tschalär's theory are plotted. Energy straggling from Monte Carlo calculations taking into account fluctuations of the ion charge exceeds the theoretical predicted values several times. In this case straggling due to charge exchange seems to be dominating. For the ion-target-combination F in Ar considered too the energy loss straggling only increases by a factor of 1.2 - 1.5 due to the contribution of charge fluctuations.

[1] L. Landau, J. Phys. USSR 8 (1944) 201
[2] P.V. Vavilov, Zh. Eksperim. i. Teor. Fiz. 32 (1957) 920
[3] C. Tschalär, Nucl. Instr. and Meth. 61 (1968) 141 and 64 (1968) 237
[4] V.V. Avdeichikov et al., Nucl. Instr. and Meth. 118 (1974) 247 and 131 (1975) 61
[5] B. Efken et al., Nucl Instr. and Meth. 129 (1975) 219
[6] G. Frick et al., IEEE Trans. Nucl. Sci. 23 (1976) 1137
[7] O. Vollmer, Nucl. Instr. and Meth. 121 (1974) 373
[8] N. Angert et al., Phys. Lett. 27 A (1968) 28 and 621



Relative energy loss straggling (standard deviation) for I (65 MeV) versus energy loss in N_2-absorbers.

[+] now at KWU, Offenbach

PRELIMINARY TESTS FOR AN EXPERIMENT SEARCHING FOR SHORTLIVED ^{B} VERY HEAVY NUCLEI FROM TRANSFER REACTIONS

J. B. Wilhelmy+, Y. Civelekoglu, P. Glässel, D. v. Harrach, R. Männer, H. J. Specht
Universität Heidelberg

In addition to fusion reactions, transfer reactions in systems like U+U or U+Cm are a promising mechanism for the production of very heavy nuclei ($Z > 110$) in the ground state. The cross-section limits obtained so far, refer to lifetimes $\geq$1d for the standard chemical methods [1] or 10 - 100 ms for gas jet or fast chemical separation. An extension of the accessible range of lifetimes by 5 to 6 orders of magnitude towards shorter times can only be achieved with electronic methods or track detectors.

We have tested the feasibility of an experimental technique which combines both methods and which should have a sensitivity of 1nb or better for lifetimes >50ns. The basic idea is to implant the heavy transfer product in a dielectric track detector. Delayed fission will then give a characteristic T-track, i. e. 180^{o} fission fragment tracks starting from the end of the primary track. The lower life time limit is given by the time-of-flight of the heavy transfer product, the upper limit depends on the time of development of the track detector. An experiment using only track detectors does not seem to be feasible at present, since one T-track would have to be found among 10^{9} background tracks. At the highest reasonable track density of $10^{6}/cm^{2}$, an area of 10^{3} cm^{2} would have to be scanned, requiring 100 to 1000 man-days for usual scanning or the development of highly sophisticated automatic scanning techniques.
However, the combination of the dielectric track-detector with a time- and position-sensitive transmission detector allows to restrict the scan to the few areas, where a very heavy transfer product has been detected by the on-line measurement of a kinematic coincidence.
The sensitivity limit of this method depends on the selectivity of the kinematic analysis against the unwanted background of elastic scattering and prompt fissions. A high on-line suppression factor for the background is needed due to the limited count-rate capability of the data conversion and storage system. In a preliminary test, an on-line suppression factor of $2 \cdot 10^{-2}$ was achieved. The kinematical off-line analysis brings this factor down to 10^{-7}. Thus the proposed experiment seems to be feasible. At present the suitability of various dielectric track-detector materials is beeing tested.

+ Los Alamos Scientific Laboratory, N. M.

[1] M. Schädel, J.V. Kratz, H. Ahrens, W. Brüchle, G. Franz, H. Göggeler, I. Warnecke, G. Wirth, G. Hermann, N. Trautmann and M. Weis, Phys. Rev. Lett. 41 (1978) 496.

Development of the big position sensitive ionization chamber

G. Augustinski, H. Sann, A. Olmi[+]
GSI Darmstadt, [+]MPI Heidelberg

In the last years gas counters have shown their usability in nuclear reaction measurements, because of their size, flexibility and adoptability. Especially our position sensitive ionization chamber (1,2) is liked to be used in one particle inclusive measurements (3,4) and kinematical coincidences as well, because the detector allows the complete determination of the detected particle by determining: dE, E, Θ, Ø, t which thus allows the reconstruction of its mass, charge, energy and momentum and so the transformation to the CM-system. But there remained some problems. Due to the extreme dynamic variations for the charge and energy of the reaction products their range in the detector can easily vary by more than a factor 30 - for example, in the reaction U+Ca[5] it's necessary to detect under certain angles U-nuclei with 2 to 5 MeV/u and Ca-nuclei with 0.5 to 12 MeV/u. This provokes two problems in our old detector which has a depth of only 30 cm: It is impossible to select the presure in the detector in such a way that all elements are stopped in the chamber - necessary for the energy measurement and at the same moment get the optimal charge resolution which is reached when the ratio of the energy loss to the rest-energy is around 0.5. This let us to the construction of a new detector, on the old principles (1) which allows particle ranges of 120 cm instead of 30 cm. The setup is shown in fig. 1. By dividing the anode into 4 parts with the lengths of: 6, 6, 20, 84 cm it is possible to do multiple Z-determination, and to select for each event the best conditions for the charge determination. With this method the resolution for elastically scattered U atoms is determined to $(\Delta Z)/Z = 1.0$ (FWHM) at $E_u = 4.5$ MeV/u (fig. 2,3). The new ionization chamber is equally well suited for light ions, as is demonstrated in fig. 4. Here the EdE distribution for the charges from Deuterium up to Carbon is shown. The distribution was measured with the 86 MeV/u C^{12}-beam at Cern. The resolutions for the other parameters detected with the chamber are:
$\Delta E/E \leq 1$ %; $\Delta x/x \leq 2$ mm; $\Delta y/y \leq 1$ mm;
they are the same as the values measured with the small detector. Only the timing signal desired from the cathode is worse (~2 ns), because of the high cathode capacity. If a better timing is necessary we use a parallel plate avalanche detector in front of the ionization chamber.

[1] H. Sann et al., Nucl.Instr.&Meth. 124 (1975) 509
[2] U. Lynen et al., Nucl.Instr.&Meth. 162 (1979) 657
[3] A. Olmi et al., Phys.Rev.Lett. 44 (1980) 383
[4] D.v.Harrach et al., Phys.Rev.Lett. 42 (1979) 1728
[5] H. Sann et al., Proc.Int.Conf. Hirschegg 1978

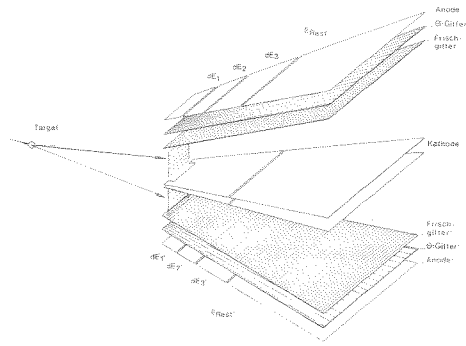


Fig. 1

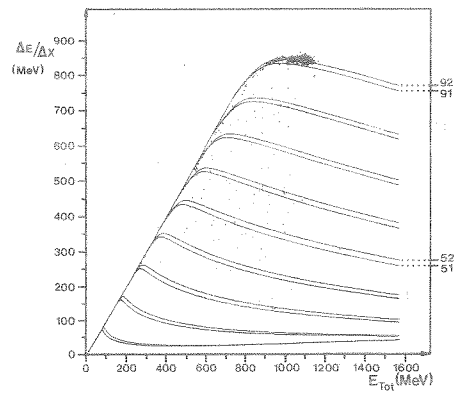


Fig. 2

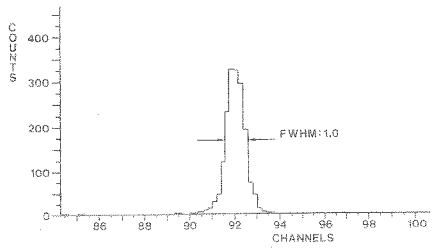


Fig. 3

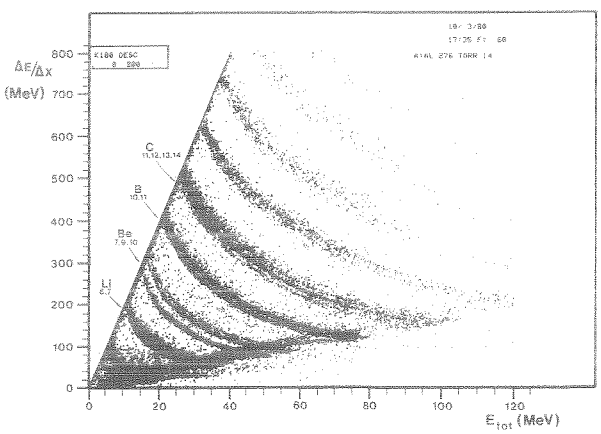


Fig. 4

Energy Loss of Very Heavy Ions in Si-Surface Barrier Detectors [B]

H. Essel, K. Hartel, P. Kienle, H.J. Körner, K.E. Rehm, P. Sperr, W. Wagner
Physik-Department, TU-München

Silicon detector telescopes are employed frequently to determine the charge of the reaction products in deeply inelastic collisions. This technique requires the knowledge of the energy loss of the detected particles in Si over the full energy range of interest. In experiments with lighter ($A \lesssim 40$) ions the tabulated curves of Northcliffe and Schilling [1] are used successfully for this purpose. In order to investigate the accuracy of these energy loss curves for very heavy ions we have measured the energy loss in Si for ^{64}Ni, ^{94}Zr, ^{110}Pd, ^{148}Sm, ^{170}Er, ^{181}Ta and ^{208}Pb ions in the energy range between 300 MeV and 1200 MeV. A ^{208}Pb beam was elastically scattered from thin self-supporting target foils, and the recoil particles were detected [2]. Pulse height defects in the Si surface barrier detectors were measured and taken into account in the determination of the energy loss curves. Fig. 1a shows data obtained with a 9.2 um thick Si ΔE transmission detector for the different particles. The comparison with the tabulated values shows that the measured energy loss is larger by ~ 30% than the tabulated values of Northcliffe and Schilling [1] (thin solid lines) and by ~ 10% if compared to the values calculated by Braune [3] (dashed lines).

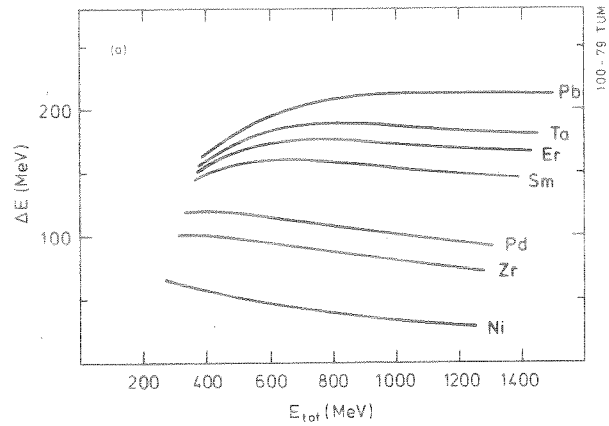


Fig. 1: a) Energy loss curves in Si for different ions as indicated in the figure.

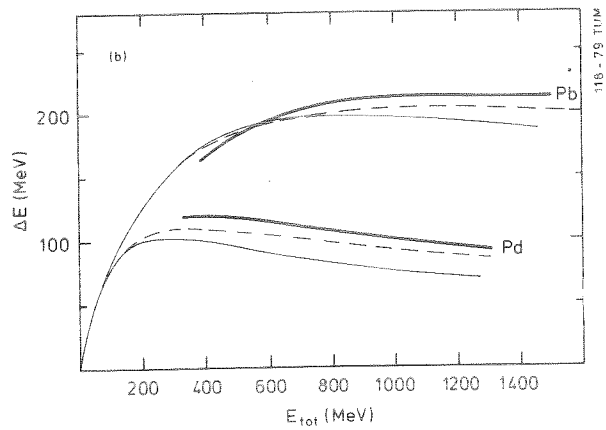


Fig. 1: b) Comparison of the measured energy loss for ^{208}Pb and ^{110}Pd ions with the predictions of Ref.1 (thin solid lines) and Ref. 3 (thin dashed lines).

[1] L.C. Northcliffe and R.F. Schilling, Nucl. Data Tables A7, 233 (1970)

[2] H. Essel et al., Subm. to Nucl. Instr. Meth.

[3] K. Braune, Staatsexamensarbeit MPI Heidelberg 1977

Rise Time Discrimination between Heavy Ions and α Particles with Semiconductor Detectors

T. Kitahara, H. Geissel, S. Hofmann, Y. Laichter, G. Münzenberg and P. Armbruster
GSI Darmstadt

The possibility of rise time discrimination between α particles and heavy ions having the same energy signals when implanted in a silicon surface barrier detector has been investigated. The method is based on the fact that due to larger specific energy loss of the heavy ions, their plasma effect will cause a larger enhancement of the pulse rise time compared to that of α particles [1]. The most significant differences in the rise time can be expected for rear side implantation into a detector whose thickness is comparable to the range of the α particles in silicon. In Fig. 1 we represent the block diagram of the electronic circuit used for the measurements of pulse shape discrimination. The GSI 109040 voltage sensitive preamplifier has been used for fast output of the pulses.

A mixed source of ^{239}Pu, ^{241}Am and ^{244}Cm was used as α emitter. The energetic ions of Ti, Pb and U were obtained from the low-energy line of the UNILAC and were further slowed down by Al foils to the energy region of the α particles as demonstrated in a typical energy spectrum in Fig. 2. Heavy ions and α particles were implanted simultaneously into the rear side of the detector. Representative results with U ions are shown in Fig. 3. The spectrum 3a has been obtained at 18 V operating voltage, corresponding to about 35 μm depletion depth of the 52 μm thick detector [2]. In this case the uranium ions are stopped in the dead layer and show long rise times and a wide rise time straggling. The α particles can be separated clearly, though their rise time straggling is also wide. In Fig. 3b the applied voltage is increased to 20 V and the detector is almost totally depleted. Rise time straggling decreases and the α lines are still separated clearly from those of the heavy ions. This is the optimum operating condition for rise time discrimination. The pulse height of the α lines is nearly independent of the applied voltage.

When the nominal 45 V is applied some rise time discrimination is still obtained as shown in Fig. 3c. The discrimination, however, is so weak that it cannot be used practically. As expected the rise time discrimination becomes worse when a thick detector is used. The results for Ti and Pb ions are similar to those of U. Cooling down the detectors to -20°C has no practical effect on rise time discrimination.

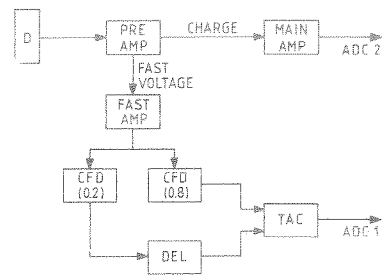


Fig. 1: Electronic setup

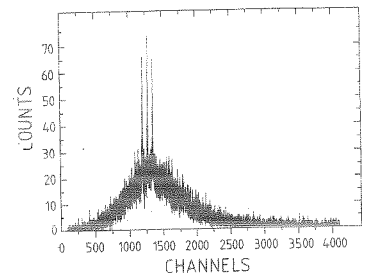


Fig. 2: Energy of attenuated U ions and ^{239}Pu, ^{241}Am, ^{244}Cm α particles.

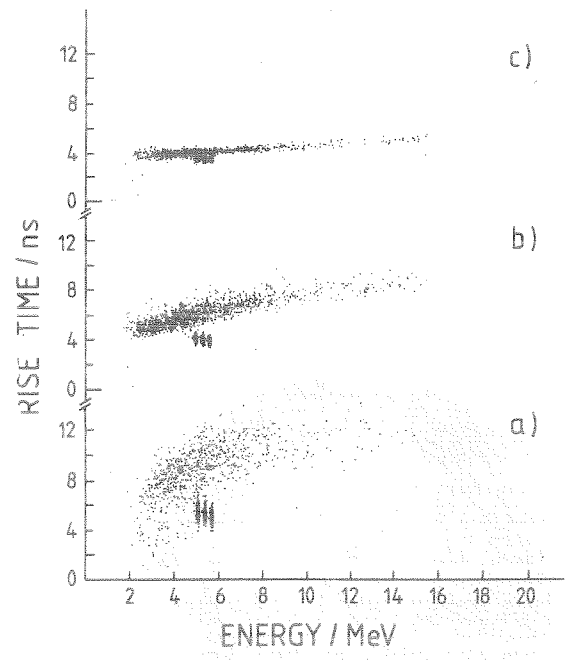


Fig. 3: Rise time versus energy of α particles and Uranium ions having the same pulse height for different detector voltages.
a) 18 V b) 28 V c) 45 V

[1] W. Seibt, K.E. Sundström and P.A. Tove, Nucl. Instr. and Meth. 113, 317 (1973)

[2] P.A. Tove and K. Falk, Nucl. Instr. and Meth. 29, 66 (1964)

A Parallel Plate Ring Counter

Y.T. Chu*, H.W. Daues, H. Sann
GSI Darmstadt

Binary reactions are completely determined by the measurement of 3 kinematic quantities: the detection of the time of flight difference Δt and of both scattering angles θ and ϕ of the two coincident fragments is particularly advantageous. It can easily be realized, for big solid angles, with two position sensitive parallel plate detectors. In order to optimize the position readout with respect to the symmetry axis of the scattering (beam axis), the detector system (fig. 1) is constructed in a ring geometry. The counter is subdivided in two equal halfs (fig. 1) and consists of 3 electrodes. At the back, the cathode consists of a printed circuit plate with a diameter of 30 cm. The conductive layer is subdivided in concentric rings 2.5 mm wide. These are interconnected by an LC-delay line (chip) for the θ_1; θ_2 position readout (fig. 2). Two hostaphan foils of 2 µ thickness are mounted in front of the cathode. The first foil, at a distance of 2 mm above the cathode is evaporated on both sides with a gold layer of 40 µg/cm^2 and serves as anode. Here the timing signals are collected. Above this central anode is mounted a second foil, which operates as a second cathode. So we have two parallel plate counters after each other, with multiplication zones on both sides of the central anode. Using a mask, 60 segments are evaporated onto the cathode foil in order to subdivide the azimuthal angular range. Two arrays of 30 segments each are connected via a coax-cable delay line (fig. 1). They deliver the azimuthal angles ϕ_1, ϕ_2 of the two coincident particles. This controls the coplanarity of the reaction products, and thus allows to

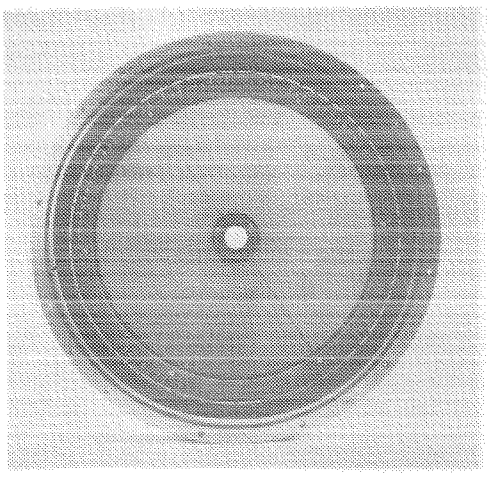


Fig. 1

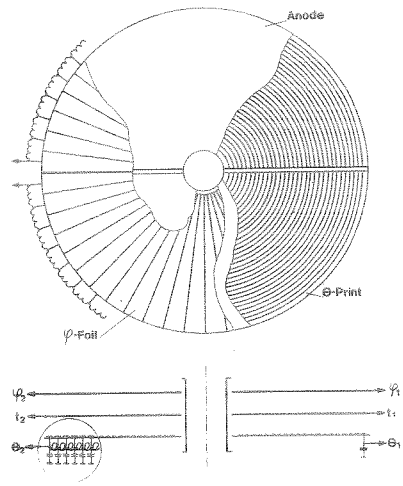


Fig. 2

suppress 3-body reactions. Constant sum of the delay times from both sides of each delay line provides the condition of detecting only one particle in one counter. Above the ϕ-cathode is mounted the window foil, which holds the pressure of the detector gas (10 Torr isobutylen).

A hole of 28 mm diameter in the center of the ring detector allows to extract the beam from the reaction chamber for coincidence measurements between binary fragments and x- or γ-rays. With this detector system we reached the following resolutions with 5 MeV α-particles:
1) for timing $\Delta t \simeq 570$ ps, and the internal delay of the timing signal is less then 1 ns over the whole detector surface without correction on the position dependences;
2) the position resolutions in both angles are only limited by the width of the readout strips or segments and were thus 2.5 mm in θ direction and 6^0 in ϕ-direction.
The counter was constructed for the measurement of fusion-fission reactions, using heavy projectiles like ^{208}Pb or ^{238}U on light target nuclei (e.g. ^{48}Ca). Under such conditions solid angles of more then 3π in the center of mass system can be obtained. Results, gained with this detector system are reported in separated communications in this annual report.

*Alexander von Humboldt-Fellow, on leave from Institute of Modern Physics, Academia Sinica, Lanshow, China.

Test and Performance of a Position Sensitive Parallel Plate Avalanche Counter

Ch. Schandera, C. Lauterbach, J. de Boer
Sektion Physik der Univ. München
H. Stelzer
GSI, Darmstadt

The experimental setup[1] used for the measurement of the circular polarization P_γ of gamma-rays following deep-inelastic reactions was changed in order to measure the dependence of P_γ on the scattering angle θ of the ejectiles. A scattering chamber was constructed in which two particle detectors can be moved independently at a distance of 25 cm from the target (Fig. 1). Two identical polarimeters are mounted close to the target on either side of the reaction plane. (Fig. 2)

The measurement of P_γ over a large range of scattering angles θ requires a particle detection system with large solid angles and a high counting rate capacity. We have built two dimentional position sensitive parallel plate avalanche counters (PPAC) with an active area of 5x16 cm^2 corresponding to an angular range of $\Delta\theta=33^\circ$ in the scattering plane (Fig. 3).

The PPAC's consist of 3 planes mounted parallel to each other at a distance of 1.6 mm. The cathode is divided into twelve 5 mm wide gold stripes evaporated on a printed circuit board. 80 gold wires (20 μ diameter) are spanned at 2 mm distance from each other and perpendicular to the stripes. The anode consists of a 60 μ g/cm^2 gold layer evaporated on a 2.5 μ mylar foil. The wires and stripes are connected by resistors and read out by the charge division method yielding the x- and y-coordinate of the event.

Masses and kinetic energies of the reaction products are determined by their scattering angle and their time of flight (TOF) relative to the bunched beam using a pair of PPAC's on opposite sides of the beam axis (Fig. 1). The microstructure of the beam is monitored measuring the TOF of the particles scattered from a gold target mounted 30 cm downstream from the main target using a small PPAC (active area 2 cm^2, gap size 1 mm[2] (Fig. 1)).

Test measurements using 4.7 MeV/amu ^{132}Xe + ^{138}Ba and 5.6 MeV/amu ^{86}Kr + ^{197}Au reactions yielded a time resolution of 150 ps for each counter. The position resolution is Δx=1.9 mm and Δy=5 mm. Correcting for the internal delay of the detectors, an overall mass resolution of 5 amu and a kinetic energy resolution of 20 MeV were found for the reaction 5.6 MeV/amu ^{86}Kr+^{197}Au.

(1) GSI - JB 1977; p. 49.

(2) The support by the GSI det. lab. is gratefully acknowledged.

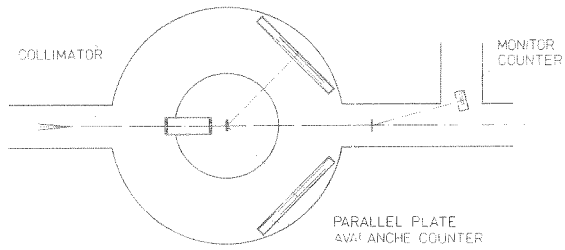


Fig. 1

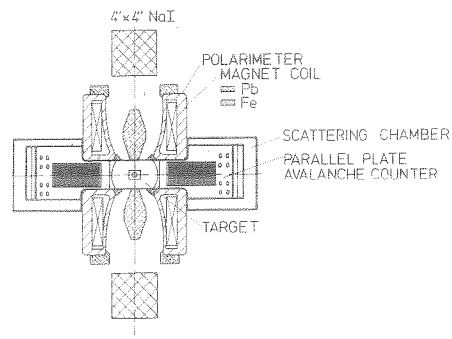


Fig. 2

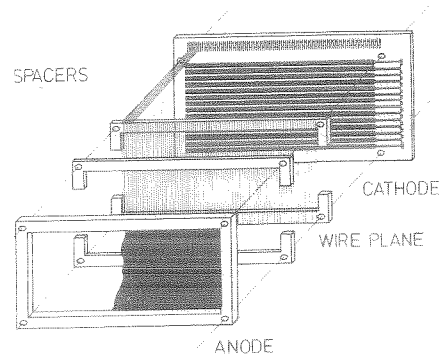


Fig. 3

New Detector System for the 5m Time-of-Flight Spectrometer [G]

U. Arlt, R. Bass, V.Hartmann, H. Noll, R.Renfordt+, K.Sapotta
Institut für Kernphysik der Universität Frankfurt am Main

The new detector system[1] was completed and installed at the time-of-flight spectrometer. For timing purposes it consists of a start detector (17x43 mm^2) and large-area stop detector (90x20 mm^2), both featuring isochronous 180^0 magnetic deflection of secondary electrons onto channel plates and position sensitivity in the scattering plane. The time resolution was measured during a test run with ^{40}Ar beam; the following results were obtained (FWHM): start detector against (200 mm^2) surface barrier counter (distance 10 cm) 200 ps, stop detector against surface barrier counter (distance 15 cm) 175 ps, start detector against stop detector (distance 4.45 m) 230 ps, left channel plate against right channel plate stop detector 175 ps. The latter measurement can be used conveniently to monitor the instrumental resolution of the stop detector during a run. The timing efficiency was approximately 97%. The position resolution of each detector was determined using suitably arranged slit systems, and values of < 0.7 mm and < 0.3 mm (FWHM) were obtained for the start and stop detector, respectively, with negligible nonlinearity in the position measurement. Fig.1 shows a position spectrum measured with the start detector in coincidence with a surface barrier detector placed about 10 cm behind the start detector. The slits had a distance of 3 mm and width of 0.3 mm and were located close to the surface barrier detector.

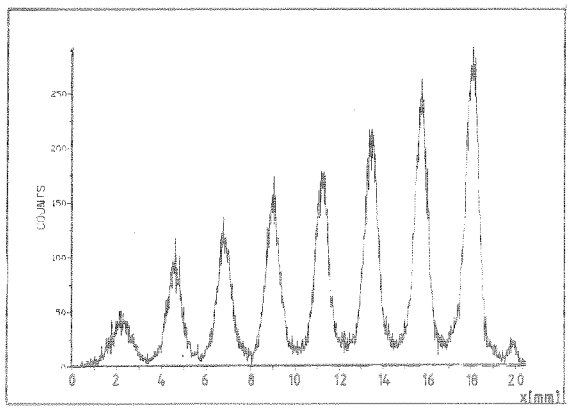


Fig.1: Position spectrum measured with the start detector

In connection with a third timing signal from the accelerator the start and stop detectors can be used to perform a double time-of-flight measurement, and hence to correct for the spread in beam energy. This technique makes use of the time structure of the beam at the accelerator exit and the 75 m flight path from the accelerator to the target position. An example, corresponding to comparatively poor adjustment of the accelerator, is given in Figs. 2 and 3. Figure 2 demostrates the correlation between the flight times accelerator - start detector and start detector - stop detector. Figure 3 shows time-of-flight spectra with (Δt=300 ps) and without (Δt=900 ps) correction for beam energy spread.

The stop detector is followed by an ionization chamber for ΔE and E measurements. It has an entrance window of 40 x 80 mm^2 area and is divided in two ΔE sections with lengths of 10 cm each and an (E-ΔE) section with 40 cm length. The energy resolution was measured as < 0.5 % with 4.8 MeV/u ^{40}Ar ions.

+Now at University of Marburg and LBL Berkeley

[1] R. Bass et al., GSI 79 - 11 (1979) p. 168

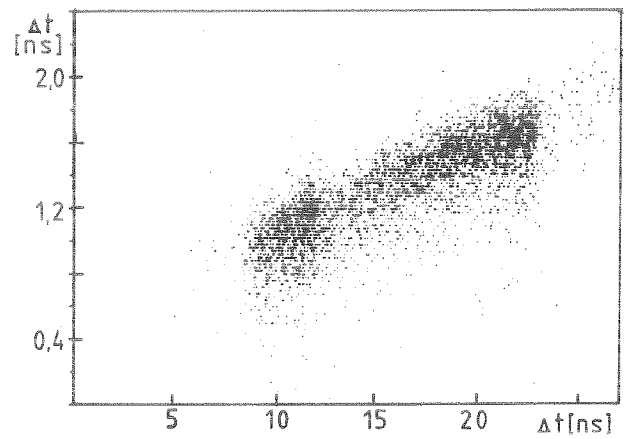


Fig. 2: Correlation between flight times UNILAC - start detector (abscissa)and start detector - stop detector(ordinate)

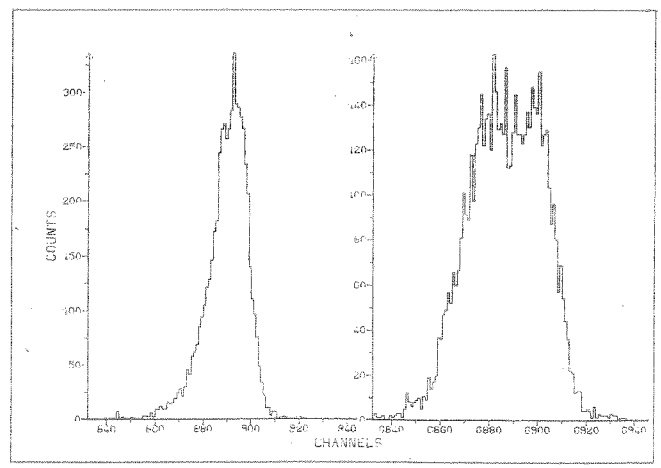


Fig. 3 Time-of-flight spectra with and without correction for beam energy spread (20 ps/channel)

G

A large-area scintillation stop detector for the magnetic spectrometer

F. Busch, W. Pfeffer, F. Pühlhofer
Fachbereich Physik der Universität Marburg

D. Schüll
GSI Darmstadt

In the magnetic spectrometer[1] at GSI the mass of the heavy reaction products to be analyzed is determined from their time-of-flight through the whole system. The identification of nuclei in the mass range A > 100 requires detectors with a time resolution in the sub-nanosecond region. Whereas this is easily achieved by the channel plate start detector[2] at the entrance of the spectrometer, the relatively slow timing signal obtained from the large ionization chamber used as focal plane detector severely limits the mass resolution. In order to overcome this difficulty a thin transmission-type stop detector has been constructed and inserted directly in front of the ionization chamber.

The new detector is basically a scintillation detector containing a thin plastic foil. This detection technique is well known, but it has never been applied to very large effective areas as required in our case (50·6 cm^2). Despite this size the thickness of the scintillator foil can be kept below 100 $\mu g/cm^2$, which is low enough not to affect the energy resolution of the focal plane detector. This could not be achieved by a large-area avalanche-counter.

The layout of our detector is shown schematically in fig. 1. The scintillator consists of a self-supporting 100 $\mu g/cm^2$ NE 111 foil. It is viewed by four 3" photomultiplier tubes mounted in a row close to the upper edge of the foil. The light collection is improved by a cylindrical reflector (radius 75 mm) mounted below the foil. In this configuration the total amount of light entering the photo tubes is almost independent of the vertical position of the emission point in the foil. The multipliers are operated with equal gains. Their anode signals are adjusted in time by cable delays and then mixed to a common signal which is fed into a standard constant-fraction trigger.

For 6 MeV/u Xe-ions the signal amplitude was found to be 50 times above the dark (single electron) pulses, the rise time is 3 ns. The total time resolution of the detector is 400-500 ps across the whole focal plane. This value gives a considerable improvement of the mass resolution of the magnetic spectrometer, which now is about $\Delta m/m = 1/400$ and almost independent of Z and energy. Fig. 2 shows a mass spectrum of quasielastic Xe-like products from reactions between 800 MeV ^{136}Xe ions and a ^{56}Fe target.

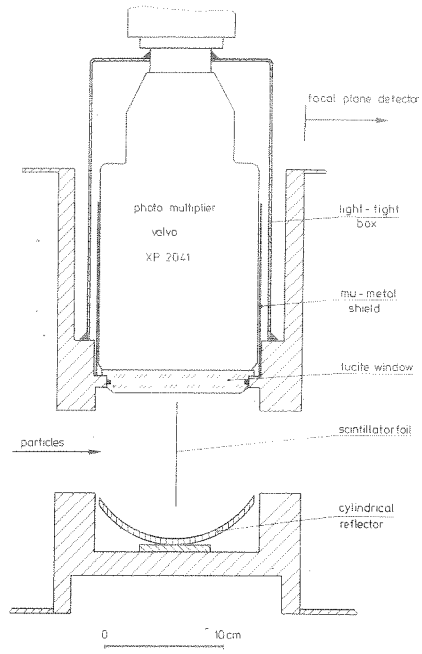


Fig. 1

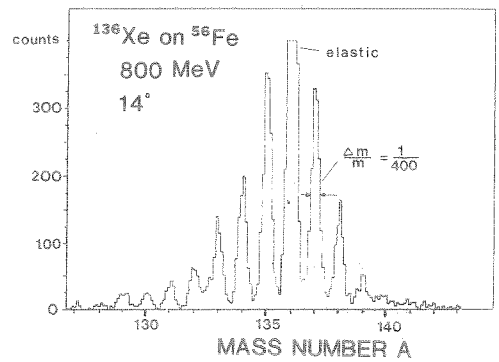


Fig. 2

[1] GSI-Jahresbericht 1977, GSI-J-1-78, p. 185
[2] GSI-Jahresbericht 1977, GSI-J-1-78, p. 186

G

Relation of Pulse Height and Absorbed Energy in Gas-Scintillation Heavy-Ion Detectors

J. Pannicke, M. Mutterer, K. Scheele, J.P. Theobald and P. Zöller
Institut für Kernphysik, Technische Hochschule Darmstadt

Preceding experiments[1] with gas scintillators on the relation between pulse height and absorbed energy have revealed linearity within a few percent between α particles and heavy ions of masses up to A = 136. We have performed more detailed linearity measurements with different scintillator gases, (Xe, Ar and Ar with different admixtures of N_2), using 40-Ar, 136-Xe and 208-Pb ions of 1.4 MeV/amu and 5.48 MeV 241-Am α particles.

The scintillation cell is a cylindrical chamber of 80 mm diameter viewed by a 40 mm diameter quartz-window photomultiplier. The chamber walls are covered with reflector material and an evaporated layer of p-TP wavelength shifter. A weak gas flow was maintained during the measurements; Xe gas was continously pumped through a rare gas purifier. The PM stability was controlled by an electronic peak stabilizer[2], with light pulses of a temperature stabilized LED as reference.

For all gases investigated, the scintillation pulse height per unit energy A/E (corrected for the energy loss in the 60 μg/cm^2 polypropylene window) was observed to be equal or higher for the heavy ions than for the

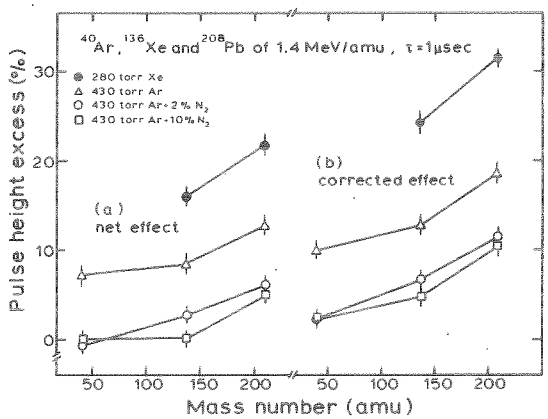


Fig.1 Pulse-height excess of the gas scintillator for heavy ions relative to α particles, versus the heavy-ions mass number.

α particles. In fig.1a, the measured relative pulse-height excess (PHE) for the heavy ions, defined by

$$PHE = (A_{HI}/A_\alpha)/(E_{HI}/E_\alpha)-1 ,$$

is plotted versus the heavy-ion mass number. Figure 1b shows PHE values corrected for (i) the energy loss by nuclear collisions, and for (ii) the small difference in light geometry for the α-particle and heavy-ion absorption. It is obvious, that the light yield increases with heavy-ion mass number and hence with ionization density for all the gases used. The pulse-height excess is up to 30% in pure Xe; admixtures of N_2 to Ar were found to reduce it with increasing N_2 concentration (fig. 2).

For the Ar-N_2 gases, the only small excess in light yield for the heavy ions is nearly compensated by the pulse-height defect due to nuclear stopping, resulting in a good linearity of pulse height and absorbed energy for charged particles of all masses (E ≈ 1.4 MeV/amu). It should be noted, however, that the pulse-height excess depends considerably on the main amplifier time constant; e.g. reducing τ from 1 μs (all values in fig. 1) to 0.25 μs decreases the PHE value for 136-Xe ions in pure Xe gas from 16 to 2%, and the corrected PHE value from 24 to 10%. This indicates, that the absorption of heavy ions induces another scintillation mechanism, with a longer decay time than the dominant molecular components. Experiments

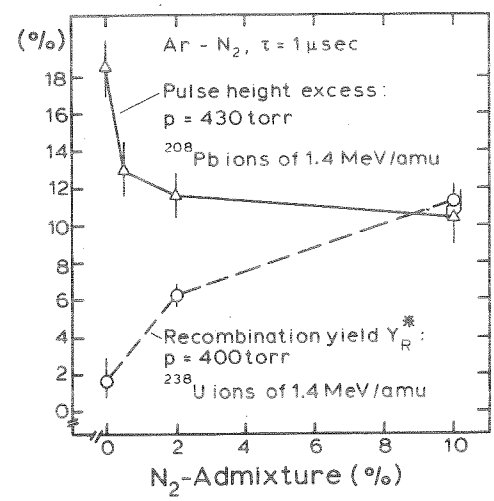


Fig.2 Pulse-height excess and recombination yield[3] $Y_R^* = Y_R/(1 + Y_R)$ in Ar-N_2 gas, versus the N_2 concentration.

on the luminescence due to electron-ion recombinations in the strongly ionized heavy-ion track[3] have shown, that columnar recombination can only partly explain the measured pulse-height excess. In fig. 2, both effects are plotted for the case of Ar-N_2, showing contradictory dependances on the N_2 concentration.

1. M. Mutterer at al., Nucl. Instr. Meth. 144, 159 (1977).

2. J. Pannicke, Diplomarbeit, IKDA, 1979

3. W. Spreng et al., this report.

G

Recombination Luminescence in Heavy-Ion Excited Gas Scintillations

W. Spreng, P. Brülls, H. Heckwolf, M. Mutterer, J. Pannicke and J.P. Theobald

Institut für Kernphysik, Technische Hochschule Darmstadt

In α-particle induced scintillations of noble gases, the luminescence which accompanies columnar recombination is known to contribute to the total light emission at gas pressures above several atmospheres [1]. In heavy-ion gas scintillators, this light emission process is expected to be important at much lower pressures because of the higher ionization densities involved.

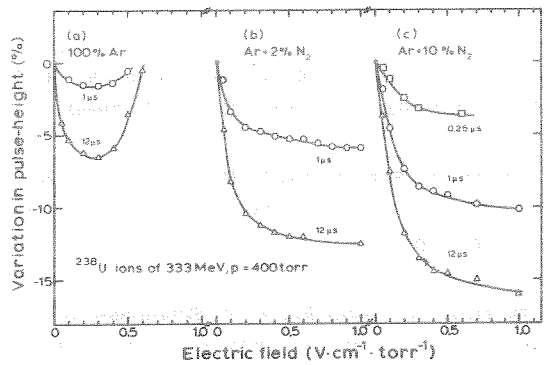


Fig.1 Electric field effect on the scintillation amplitude in Ar and Ar-N_2 gas mixtures.

We have investigated the luminescence due to columnar recombinations in Ar, Xe and Ar-N_2 and Xe-N_2 gas mixtures at pressures below 700 torr, using 238-U and 208-Pb ions of 1.4 MeV/amu. A gas cell was applied, where a narrow heavy-ion beam enters through a thin needle, between electrodes formed by a wire mash of 90% optical transmission. Figure 1 shows, as example, the measured variation in scintillation pulse height for Ar and Ar-N_2 gases with the electric field E applied perpenticular to the particles trace. Figure 2 demonstrates, for the case of Ar and Xe gas with admixtures of 2% N_2, that the reduction of the scintillation pulse height with E is closely related to an increasing charge collection at the positive electrode. For the noble-gas

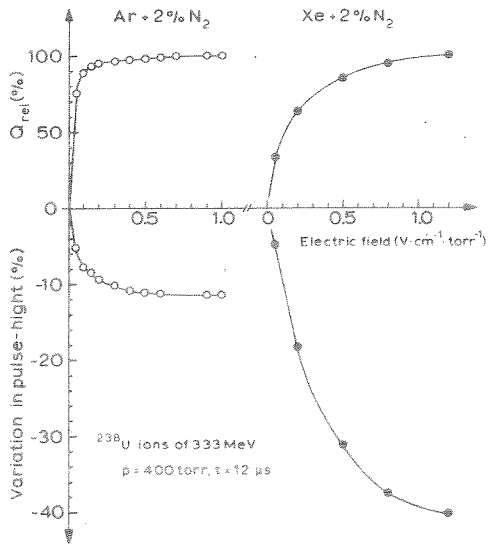


Fig.2 Variation of the scintillation and charge pulse-heights with the electric field.

nitrogene mixtures, both the scintillation and charge pulse heights saturate at fields of ~ 1 V/cm/torr, indicating a complete separation of electrons and ions in the ionized column. In the pure noble gases, the light amplitude increases again at fields $\gtrsim$ 0.5 V/cm/torr due to the secondary light emission induced by the electrons (electro-luminescence). The decay time of the recombination luminescence was observed to be in the order of serveral µs, which is generally much slower than the molecular scintillation components [2]. It is obvious, that the application of a weak electric field in heavy-ion gas-scintillation detectors considerably improves their high-rate capability.

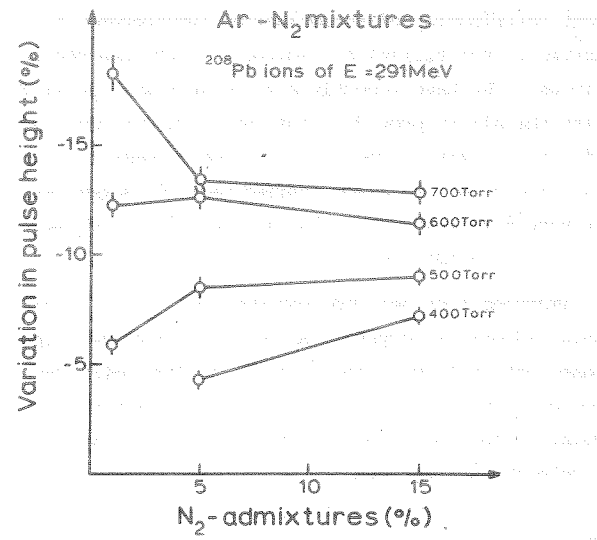


Fig.3 Recombination yield Y_R in Ar-N_2 gas mixtures at various pressures p, versus N_2 concentration.

The relative abundance of the recombination luminescence, determined from the yield $Y_R = [A(E=o) - A(E=1.o)]/A(E=o)$, measured at a main amplifier time constant of 12 µs, shows a characteristic dependence on the N_2 concentration and on pressure (fig. 3). It seems, that Y_R is also sensitive to the projectile mass, since Y_R values measured with 238-U and 208-Pb ions differ by up to 50%. However, small variations in gas purity might have influenced these results.

We plan further experiments on this subject, using an improved gas supply and mixer for gases at a high purity level.

1. S. Konno and T. Takahashi, Nucl. Instr. Meth. 150, 571 (1978).

2. M. Mutterer et al., IEEE Trans. Nucl. Sci. NS-26, 382 (1979).

G

A Solid-Xenon Scintillation Detector for Heavy Ions

H. Heckwolf, W. Spreng, M. Mutterer, J.P. Theobald, P. Zöller and J.C. van Staden[+]

Institut für Kernphysik, Technische Hochschule Darmstadt

To use condensed noble gases as scintillation detectors was proposed already more than 30 years ago[1], but has not been investigated in detail until now. However, much work has been devoted to studies of radiative decay mechanisms, showing that the light emission processes and the emission spectra are very similar to the gas phase. Decay constants of only a few ns and an important contribution of recombination luminescence were observed in scintillations excited by light charged particles[2]. We have recently started work with solid Xe, with the aim to provide a fast and luminous scintillator with an ionization medium sufficiently dense ($\rho = 3.6$ g/cm^3) to allow charged-particle spectroscopy at very high energies. First attempts with a detector of low light geometry were reported earlier[3].

An improved test detector was developed (fig. 1) in which a solid-Xe crystal can be grown from the liquid phase onto a 40 mm diameter suprasil disc which is cooled with liquid nitrogene by using a temperature regulator. The quartz-window photo multiplier, with p-TP wavelenght shifter evaporated onto its window, is separated from the cooled disc by a 2 cm wide high-vacuum gap.

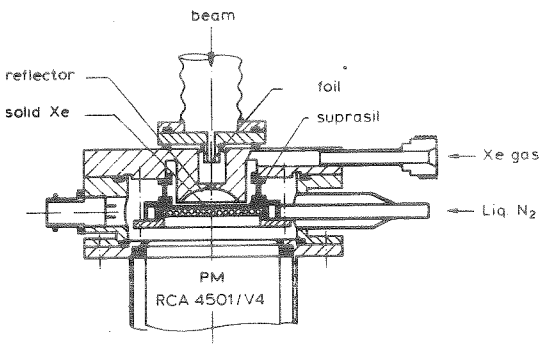


Fig.1 Test detector of a solid-Xe scintillator.

First measurements were performed with 5.48 MeV α particles of 241-Am. The observed scintillation pulses have a rise time of 2.5 ns, which is the limit of the PM, and a decay time of ~ 30 ns. The energy resolution dE/E obtained with a crystal of 2 mm thickness and at a temperature of ~ -150°C is 2.0% fwhm, compared to only 7% attained with gaseous Xenon[4]. This improvement is mainly due to the better light geometry, since the light yield of solid Xe was determined to be only 50% higher than that of Xe gas at 700 torr.

We plan to test the solid-Xe scintillator with UNILAC ions in order to assess the energy resolution, time resolution and counting rate capability at higher energies and ionization densities. An experimental set-up with improved gas purity and temperature control is under construction, which will also allow the growth of thicker crystals.

[+]CSIR, Pretoria, South Africa

1. J.A. Northrop and R. Nobles, Nucleonics 14, 36 1956); IRE Trans. Nucl. Sci. NS-5, 59 (1956).

2. S. Kubota, M. Hishida and A. Nohara, Nucl. Inst. Meth. 150, 561 (1978); S. Kubota et al., Phys. Rev. B17, 2762 (1978).

3. M. Mutterer, J. Pannicke, K.-P. Schelhaas, J.P. Theobald and J.C. van Staden, IEEE Trans. Nucl. Sci., NS-26, 382 (1979).

4. M. Mutterer, J.P. Theobald and K.-P. Schelhaas, Nucl. Instr. Meth. 144, 159 (1977).

G

Energy- and Time-Resolution Studies with Gas-Scintillation Heavy-Ion Detectors

M. Mutterer, P. Brülls, J. Pannicke, W. Spreng, J.P. Theobald and P. Wastyn
Institut für Kernphysik, Technische Hochschule Darmstadt

Previous experiments on the energy resolution capability of gas scintillation detectors have been performed with low-energy ions of 1.4 MeV/amu. The values obtained for the energy resolution (e.g. 1.6% fwhm for 136-Xe ions with 400 torr Xe as scintillator gas) and systematic studies of the light yields of various gases[1] indicate, that for the higher-energy ions available at the UNILAC, an energy resolution below the 1% level can be expected. Here, we report on the results obtained at a few-hours beam time with 8.1 MeV/amu 86-Kr.

The detector, consisting of a cylindrical gas chamber of 80 mm diameter, was tested in X2 by measuring projectile-like fragments scattered into an angle of 15° in the reaction of 8.1 MeV/amu 86-Kr ions on 89-Y. To assure complete absorption, 1 atm Xe (99.997% purity) was used as scintillator gas. The observed energy resolution was 0.7% for the elastically scattered 86-Kr ions (7.6 MeV/amu).

The ΔE and Z resolution was tested, using a gas filling of Ar + 2% N_2 at a pressure of 540 torr which results in an energy loss of ~ 30% of E. The rest energy E- ΔE was measured with a surface-barrier Si detector incorporated into the gas volume. Figure 1 shows the measured ΔE/E plot in the region of the quasi elastic events, figure 2 the corresponding Z representation. The ΔE resolution of the elastic peak was d(ΔE)/ΔE = 2.6%fwhm, the corresponding Z resolution ΔZ = 0.40 Z.

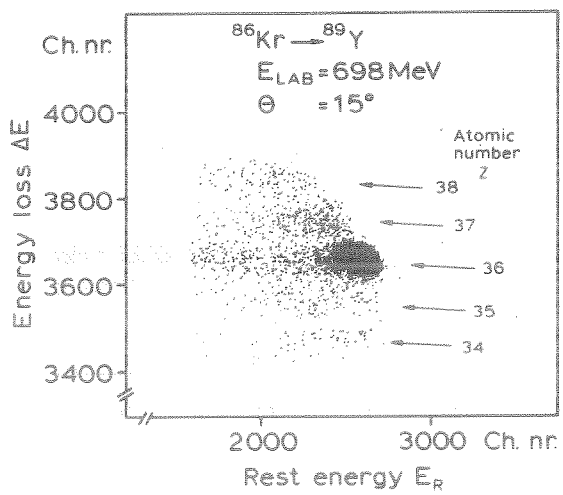


Fig.1 ΔE/E_R - plot of quasi elastic events in the reaction of 8.1 MeV/amu 86-Kr on 89-Y. Θ(LAB) = 15°.

The time resolution of the gas scintillator was measured with ions of 1.4 MeV/amu, using a fast secondary-electron time pick-off[2]. For ions of different masses, the different scintillation gases (Xe, Ar, Ar-N_2 in the range of pressure between 200 and 600 torr) have yielded resolutions dt in the order of 200 ps. With Ar gas with an admixture of 10% N_2, as example, which has the lowest light output, resolution was 250 ps with 208-Pb ions. This mixture, which has a fast scintillation decay of ≤ 30 ns at pressures above 400 torr, also allows high counting rates[1].

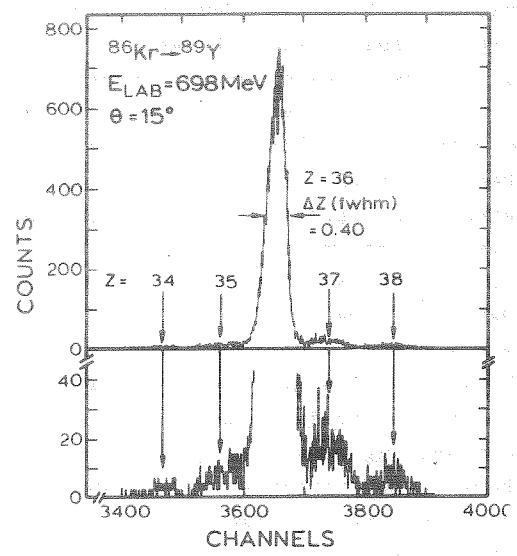


Fig.2 Z resolution, measured for 7.6 MeV/amu 86-Kr ions with an Ar-N_2 gas scintillator as ΔE detector.

1. M. Mutterer, J. Pannicke, K.-P. Schelhaas, J.P. Theobald and J.C. van Staden, IEEE Trans. Nucl. Sci. NS-26, 383 (1979).

2. P. Wastyn, M. Mutterer and J.P. Theobald, GSI - 79 - 11, 180 (1979).

Track profile measurements for ^{132}Xe tracks in nuclear track emulsions

N. Klein, E. Ganßauge, AG Hochenergiephysik, FB 13
P. Vater, Kernchemie, FB 14, Uni Marburg

In heavy ion research it is necessary to analyse the fragments resulting from heavy ion collisions. In order to perform kinematic calculations, the type and energy of the fragment, as well as the geometry of the interactive process, must be known.
At GSI, various types of nuclear track emulsions were irradiated with 8.5 MeV/u ^{132}Xe for the purpose of calibration. The tracks, which become visible in the emulsion following developing, appear different according to the type of emulsion[1]. Here, the rule applies, the more sensitive the emulsion, the wider the track.
The track width is a measure of the type of particle and its energy loss in the emulsion. For measurements of track profile, a profile measuring apparatus was constructed in Marburg[2]. The principle of the device consists in moving a rectangular slit stepwise across the track and viewing in the intermediate image plane of a microscope. The light absorption caused by the track is measured. With reference to the object plane (i.e. the track), the slit measures 0.3 times 10.5 µm[2]. The result of the measurement is a track profile, for which the width is a measure of the track width.

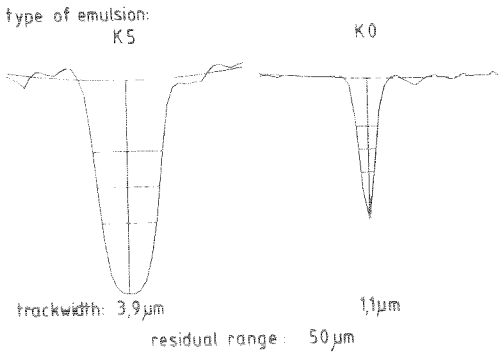


Fig. 1: Track profile for ^{132}Xe in K0 (right) and K5 (left) emulsions

Fig. 1 shows the track profile for ^{132}Xe in K5 and K0 emulsions, each taken at a residual range of 50 µm, i.e. 50 µm before the end of the track. Track width is here defined as the FWHM of the profile. In the K5 emulsion the Xe track is 3.5 times wider than in K0. This can be explained by the high sensitivity of the K5 emulsion; e.g. electrons (which in this case arise from the interactions between the Xe and the particles of the emulsion) give rise to tracks in K5, but not in K0.
Fig. 2 shows the track width for ^{132}Xe as a function of the residual range in K0 (+) and K5 (x) emulsions. With the help of these curves the emulsions can be calibrated, so that it is then possible to identify unknown fragments.

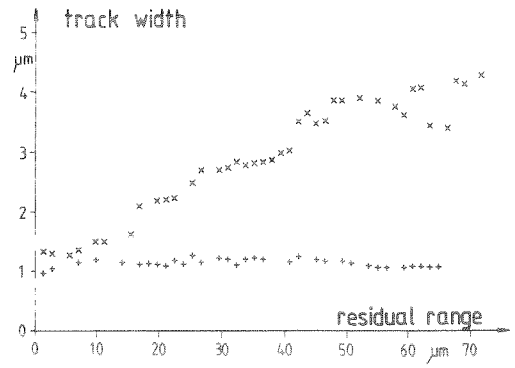


Fig. 2: Track width for ^{132}Xe vs. residual range in K0 (+) and K5 (x) emulsions

[1] N. Klein et al., GSI-79-11(1979)185
[2] N. Klein, Diplomarbeit, FB Physik, Universität Marburg, 1979, not published

Recording properties of plastic track detector CR-39 for Xe and Pb ions [B]

B. Grabez*, P. Vater and R. Brandt. Kernchemie, FB 14, Philipps-Universität Marburg

A new and promising solid state nuclear track detector based on plastic material and called CR-39 has recently been found[1]. In our work we have investigated its recording properties for ^{136}Xe and ^{208}Pb ions. Samples of CR-39 (produced by SGL Homalite, USA) were irradiated with 4.7 MeV/u ^{136}Xe and 8.5 MeV/u ^{208}Pb ions at GSI. Irradiated samples were etched at various temperatures, concentrations of NaOH and times. Fig. 1 presents mouths of Xe and Pb tracks after 2 h etching in 6.25M NaOH at 70 °C.

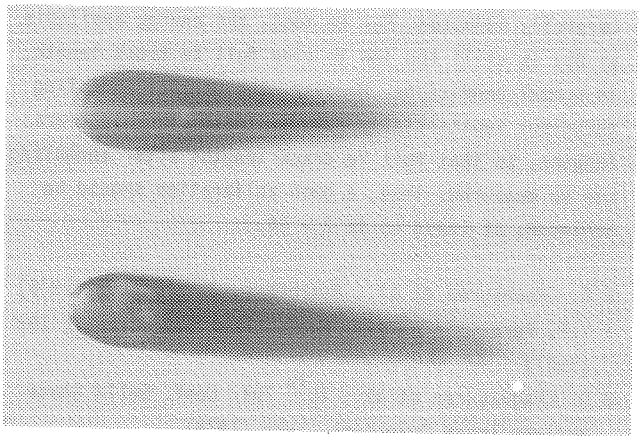


Fig. 1: Mouths of Xe (top) and Pb (below) tracks in CR-39 (entrance angle 45°)

For the bulk etch rate V_B we got values of (0.30±0.05)μm/h at 50 °C and (1.38±0.20)μm/h at 70 °C with 6.25M NaOH and (0.6±0.2)μm/h at 70 °C with 4M NaOH. The ranges of Xe and Pb ions are resp. (62.4±1.2)μm and (111.5 ±1.1)μm. The mean values (i.e. values for the fully etched tracks) of track etch rate V_T under etching conditions of 70 °C and 6.25M NaOH were found to be (21.2±1.0)μm/h (Xe) and (27.9±0.7)μm/h (Pb) and at 70 °C and 4M NaOH: (15.3±0.6)μm/h (Xe) and (22.2±0.6)μm/h (Pb). The sensitivity expressed as V_T/V_B decreases with decreasing temperature of etching. That is in agreement with results of ref.2 but in disagreement with results of ref.3 where temperature dependence of sensitivity was not observed.

During our work with CR-39 we made some observations about the so called "etch induction time" T_{ind} (time from start of etching to the appearence of visuable tracks[4]). We have noticed that the plastic detector CR-39 enables very good resolution of particles by their etch induction time. T_{ind} is shown in Fig. 2 as a function of Z^*/β (Z^* is the effective charge[5]) for some particles. It shows, that heavy target-like fragments and fission fragments are revealed after a very short etching time. However, when CR-39 is used in high-energy heavy ion reactions, such as (Pb + 84 MeV/u ^{12}C) -from CERN-SC-, we observe the projectile and projectile-like fragments only after a long etching time. Our results also show that T_{ind} depends on V_B, which depends on the temperature and concentration of etching solution[6]. T_{ind} seems to be an important and suitable parameter of CR-39 detectors.

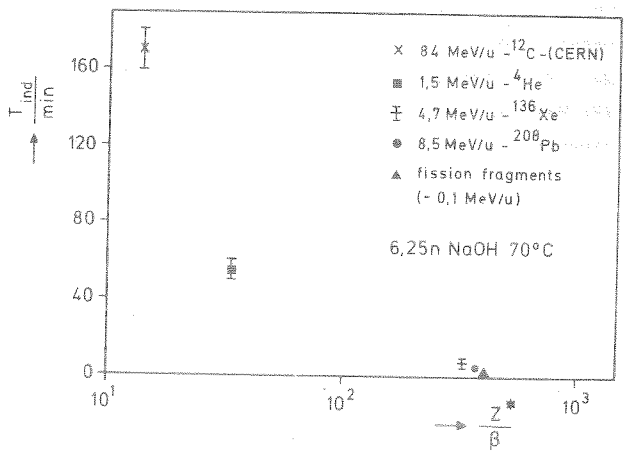


Fig. 2: Etch induction time T_{ind} as a function of Z^*/β

[1] B.G. Cartwright et al., NIM 153(1978)457
[2] E.V. Benton et al., 10th Intern. Conf. on SSNTD, Lyon, 1979 (Proc. in print)
[3] G. Somogyi et al., as 2)
[4] F.H. Ruddy et al., NIM 147(1977)25
[5] R.L. Fleischer et al., Nuclear tracks in Solids, Univ. of California Press (1975)24
[6] B. Grabez et al., to be published

*Visitor from the Institute of Physics, Belgrad

Study of heavy ion tracks in meteoritic crystals

C. Perron, P. Pellas
Laboratoire de Mineralogie du Museum, Paris, France
V.P. Perelygin, S.G. Stetsenko
Joint Institute for Nuclear Research, Dubna, USSR

The final aim of our study is to determine the abundance of the actinide element group in Galactic Cosmic Rays, by means of the nuclear tracks registered in meteoritic crystals during their exposure in interplanetary space. Apart from this problem - of major astrophysical interest - the study could possibly yield some information on the existence of Super Heavy Elements in Cosmic Rays (or, at least, a lower limit of their abundance). Previous studies[1,2] gave somewhat ambiguous results, so we are now tackling the problem on a new basis[3]. This essentially consists in partially annealing the tracks by a thermal treatment of the crystals, before performing the measurements. This technique has several marked advantages, but requires extensive and careful calibrations, which are being carried out by means of the heavy ions accelerated at GSI.

We started irradiations of meteoritic olivine - $(Fe,Mg)_2SiO_4$ - crystals at the end of 1979, and the experiments are still going on. These include measurements of track length distributions, and of track etch rate variations for various incident ions and thermal treatments. Preliminary results show that, for some annealing conditions, track length distributions may be quite broad, which would of course lead to a bad charge resolution. In order to reproducibly obtain narrow distributions, the experimental conditions have to be carefully adjusted. For Xe ions, the energy available at GSI is still too low to give full Xe track length, in normal conditions. However, the partial annealing technique substantially reduces total etchable track lengths, so that full Xe track lengths after annealing can be measured. Thus, a good calibration should be achieved, at least up to Z = 54.

1 O. Otgonsuren et al., Astrophys. J. 210, 258 (1976)
2 V.P. Perelygin et al., Nucl. Track Detection 1, 199 (1977)
3 D. Lhagvasuren et al., 10th Int. Conf. Solid State Nuclear Track Detectors, Lyon (1979)

Experimental Electronics Department (Elektronik/Experimente)

R. Albrecht, J. Dengler, J. Dusek, H. Hammal, H. Hardel, H.P. Liebold, K. Mömerzheim, K. Poppensieker, D. Quis, M. Richter, H.-G. Schmidt, R. Schulze, H. Spieler, H. Wahl, W. Wißmann

GSI Darmstadt

Activities in the Experimental Electronics Department span the whole range of electronics and instrumentation involved in experiments at the UNILAC. They can be broken down into three areas: 1) Detectors and signal processing, 2) the online computer system (hardware and software) and 3) control systems.

Detectors and Signal Processing

1. Nuclear Electronics Pool

About 200 Modules were added to the Nuclear Electronics Pool in this year. 50% of these are for long term equipment loans, reflecting the increasing number of experiments which have become so complex that mandatory dismantling of electronics after each run can not be justified. Fortunately, the growth of the pool has not been accompanied by a corresponding increase in repairs: on the contrary, the number of repairs has decreased by 30% with respect to last year. This is a direct result of our in-house repair policy, which enables us to analyze causes, implement corrective measures and which provides guidance in the procurement of new equipment. This approach has also paid off in the case of the ADC's for the on-line computer system, where the repair level has decreased to about 20% of its previous level, although the number of ADC's has been tripled.

Demand for our "standard" designs has not diminished: 100 charge sensitive preamplifiers were produced (total count 400) and about 220 high-rate photomultiplier bases were delivered. 150 of these are in use in the "plastic wall" detector at the Bevalac in Berkeley[1], the remainder - various versions for 10 different types of photomultiplier tubes - was destined for experiments at the UNILAC. Production and partial testing of these "production" items is handled by local shops, which means that the workload for GSI is considerably less than the production numbers indicate.

2. Research and Development Work

The following projects were pursued or completed in the last year:

- Eightfold Gate and Delay Generator: This single width NIM module contains eight individual channels providing continuously adjustable output pulse delay and width for each channel. The minimum input pulse width is 3 ns. Output delay and width can be adjusted independently between 50 ns and 10 µs in two switch selectable ranges.

- 8 x 8 Coincidence Unit: This 5/12 NIM module basically consists of eight eight-input AND/OR gates with parallel connected inputs and individual outputs. Each input of each individual gate may be operated in either the non-inverting or inverting mode or disabled, thereby providing AND and OR logic functions or combinations, e.g. coincidence + anticoincidence, at the individual outputs. Output timing matched to within 100 ps can be defined by a common output strobe. All inputs and outputs are negative NIM, minimum pulse width 10 ns.

- Test Pulse Generator: Primarily intended to provide a simple means of verifying performance of ADC's including gating functions in the online computer system, this unit furnishes a variable amplitude (0-10V into 50 Ω) flat top pulse together with positive NIM and negative NIM trigger outputs, which provide clean output pulses in both terminated and non-terminated operation. Repetition rate is continuously variable from 0 to 10^6 Hz. A pseudo-logarithmic control characteristic eliminates range switching. Readout is provided by a 5 digit frequency counter.

- Computer Aided Design of Subnanosecond Pulse Amplifiers: Digital computers offer the possibility of rigorously calculating the characteristics of wideband amplifier circuits without resorting to simplifying modeling procedures. The effects of stray reactances may be ascertained, critical points in a circuit can be located and a realistic prediction of the best possible response for a given set of devices in a specific amplifier configuration can be made. A set of dialogue oriented SPEAKEASY programs has been written, which - starting from either S-parameters or complex h-parameters - calculate magnitude and phase of the input impedance, input reflection coefficient, voltage gain, current gain, transconductance, transresistance and output impedance of various one and two stage feedback amplifier circuits. Despite the limited (mostly after hours) time put into this endeavor, it has already proved to be a very enlightening and time saving technique in practical design work, especially when compared to the time honored

methods of cut and try. First results as applied to a DC coupled 700 ps risetime linear amplifier have already been published[2].

- Use of silicon solar cells as heavy ion detectors[3] for applications not requiring the ultimate in performance has been investigated. Even uncoated cells invariably exhibit appreciable dead layers and poor charge collection. They nevertheless seem to offer a promising alternative for applications requiring a low cost detector with limited energy discrimination.

- In keeping with the current vogue in spherically shaped multi-detector arrays we are participating in both the Plastic Ball[1] and the GSI/Heidelberg Crystal Ball[4] projects. Work for the Crystal Ball includes tests of various photomultiplier tubes, design of the light pulser calibration system and the design of multiplicity trigger units. Participation in the Plastic Ball/Plastic Wall project involves a considerable amount of work in overall technical planning, definition of specifications and production. Long term tests of photomultiplier tubes have been conducted, 25 octal constant fraction discriminators have been produced, the high voltage distribution system has been designed and a low cost photomultiplier base has been designed and production of 700 bases has commenced.

Online Computer System

In 1979 84% of all experiments at GSI used a computer for online data acquisition of their experimental data. 88% of these experiments used the standard GSI online data acquisition system GOLDA.

Installation of 70 new ADC's has significantly decreased setup time for the experimentalists and has also dramatically increased reliability of all four PDP 11/45 data acquisition stations. All of the new ADC's are NIM packaged 13 bit Wilkinson type units, 35 of them with a 400 MHz clock(SILENA 7420/S) and 35 with 100MHz clocks SILENA 7421). The improvement in reliability can be attributed to the inherent reliability of the ADC's as ascertained by previous tests[5] and also to the fact that constant redistribution of ADC's with attendant plugging and unplugging of the data connectors is no longer necessary, since each computer is now equipped with a fixed complement of at least 20 ADC's.

The GOLDA computers are equipped with a DEC CA 11-C general purpose CAMAC interface. In list mode operation a hardware controlled scan mode is used, which originally involved a 25 µs interrupt interval at the end of each scan. This unnecessary dead time has been removed by hardware modifications within the CA 11-C. Readout time in scan mode is now 6µs per address with no additional overhead.

In addition to constructing data lists by direct memory access to the PDP-11, the CA 11-C also implements accumulation of up to eight "singles" spectra in a direct memory increment mode. These two modes interfere with one another on the CAMAC branch highway as well as on the PDP-11 UNIBUS, thereby increasing the dead time of each input channel. Moreover, only 32 K of 16 bit words are available for all eight singles spectra together. In order to remove these limitations we are planning to segregate the accumulation and storage of singles spectra from the computer by connecting each singles ADC directly to an individual incrementing memory module. These memory modules are CAMAC plug-ins with a separate front panel data port for connection to the ADC. The memory is only accessed by the computer for display purposes. During accumulation the combination ADC + memory is autonomous. A control module providing control functions and routing inputs capable of accessing two 16 K memory modules has been successfully tested with Nuclear Enterprises NE 9082 memory modules, each providing 16384 channels with 24 bits content per channel and operating with a memory cycle time of 1 µs.

Conversion of channel contents for a logarithmic spectrum display incurs about 5 times as much dead time as a linear spectrum display if calculated on the PDP-11. To avoid this time penalty a dedicated processor was designed which is accessed directly by the UNIBUS and calculates the logarithm of a 32 bit word in 450 ns, i.e. within one UNIBUS cycle. This unit has been fully tested and should be available by mid 1980.

A module capable of reading out the memory contents of a multichannel analyzer and transferring them via CAMAC to either the magnetic tape or the memory of the PDP-11 has been designed. This is useful when a multichannel analyzer is used as an adjunct or as an afterthought in experiments run on the online computer. Overall reliability and operating convenience is also improved over dedicated MCA tape controllers and tape drives. All GOLDA computers and Canberra MCA's have been equipped for this feature.

Two prototypes of a newly designed fast data link between a PDP-11 and an IBM /370-168 or 3032 computer via an IBM System /7 have been built and tested with two computers. One link will be connected via a parallel direct memory access (DR 11-B) to the UNIBUS and the other link will be connected via a cycle steal interface to an IBM System/7.

Data transmission is 16 bit parallel, half duplex. The connecting cable may be up to 400 m long. The hardware tranfer rate with a 200 m connecting cable is 560 kbyte/s.

To reduce the interrupt rate on the PDP-11 and the System /7 (and thereby the software overhead), an automatic pre-transfer of two 16 bit words of information is implemented in hardware (e.g. for the word count of the following main transfer and for the data source and destination identification).

The link allows bidirectional communication in half duplex mode. Parity check for each byte and a cyclical redundancy check (CRC) for the whole transfer controls the data transmission. A handshake mechanism observes the correct transfer of a 16 bit data word and the same word may be transmitted again up to nine times. This will eliminate intermittent data errors. Highly developed fast error detection and interruption is one of the main features of this link. Program malfunctions and hardware errors can be uniquely detected by the hardware.

Control Systems

A microcomputer based control system for the velocity separator SHIP was designed and has passed initial tests. This is described elsewhere in this report (H.J. Schött and K. Poppensieker: Microcomputer Control of the Velocity Separator SHIP).

A revamped and (so we hope) foolproof version of the sample changer control systems for production of nuclear track filters was designed. It should be completed by mid 1980.

[1] M.R. Maier et al.: IEEE Trans. Nucl. Sci. NS-27 (1980) 42

[2] H. Spieler: IEEE Trans. Nucl. Sci. NS-27 (1980) 302

[3] G. Siegert: Nucl. Instr. and Meth. 164 (1979) 437

[4] R. Simon et al.: GSI Jahresbericht 1978, p. 164
R. Simon et al.: Status of the Nat Crystal Ball project, in this annual report

[5] Albrecht et al.: GSI Jahresbericht 1978, p. 188

Microprocessor-Activities

G. Englert, W. Dehnhardt, H. Groß, T. Györffy, P. Hahne, A. Huber, W. Welzel, M. Wiemers, V. Zelba

GSI Darmstadt

Electronic-equipment for the control of an accelerator is mostly rather sophisticated because of the numerous parameters with their logical and timing interdependence. Using conventional design the specifications may not be met or only with unproportional high effort. The interfacing of such an equipment to a control-computer transfers all the equipment-specific problems to the interface-electronic and the handler- and operating-software. Using microprocessors at the frontend-electronic makes the design simpler and uniform yet allowing more intelligent and complex solutions. The same hardware may be used for various projects.

From the broad line of some 50 different types of uP we chose the 8 bit-type 8085 from INTEL. Besides of its striking technical features the wide acceptance in industry, the expanding line of interface-chips, the numerous second-sources and last not least the excellent software-support dominated in our decision.

To support and standardize the development and programming of uC-equipment for control-application an electrical and mechanical system had to be defined, regarding European-format for printed circuits, cardconnector, signalbus, memory-organisation, interrupt-handling, input/output-transfer, Camac-interfacing, monitor-software etc.

Especially the electrical standard was strongly influenced by demands for powerful programming and debugging aids resulting form experience with computer-control in recent years.

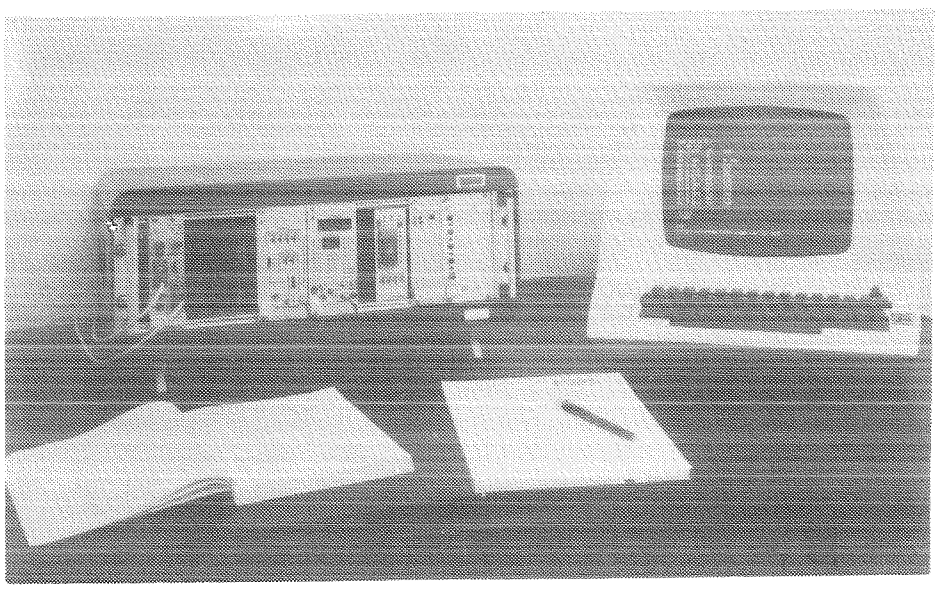
Finally all fundamental system- and user-cards were defined and developed.

The heart of the uC-System is the CPU-card carrying the 8085-processor, programstore (4 kB EPROM, 1 kB RAM), interruptlogic and hardware-timer. Together with suitable input/output-cards (e.g. serial, digital and analog) a complete data collection system may be formed. In addition a designer may apply monitor-and diagnostic-cards for debugging.
The monitor-card contains a comfortable supportprogram to relief the user from all standard input/output operations and shows some useful features e.g. address- and/or datacompare, breakpoints, single step, trace, incremental assembler and disassembler.

Besides of the above mentioned uC-moduls exist a few special function cards e.g. video interface, arithmetic processor, step motor controller, RAM- and EPROM-memory, programming card for PROM. An increasing number of cards is now used in the laboratories and for process control. Due to some external interest and not to bind internal capacity the production and sale of the GSI 85-Microcomputersystem was lincensed to a firm.

At the end of the reporting year the development of a prototype interface for coupling uP-based equipment to CAMAC has been finished.

It provides storage of process dependant data and parameters and allows asynchronous access from Camac and uP to shared data files.



Laboratory set of
GSI 85-µC-System

Computing Center

(H.Hultzsch)

Experiences with the computer concept

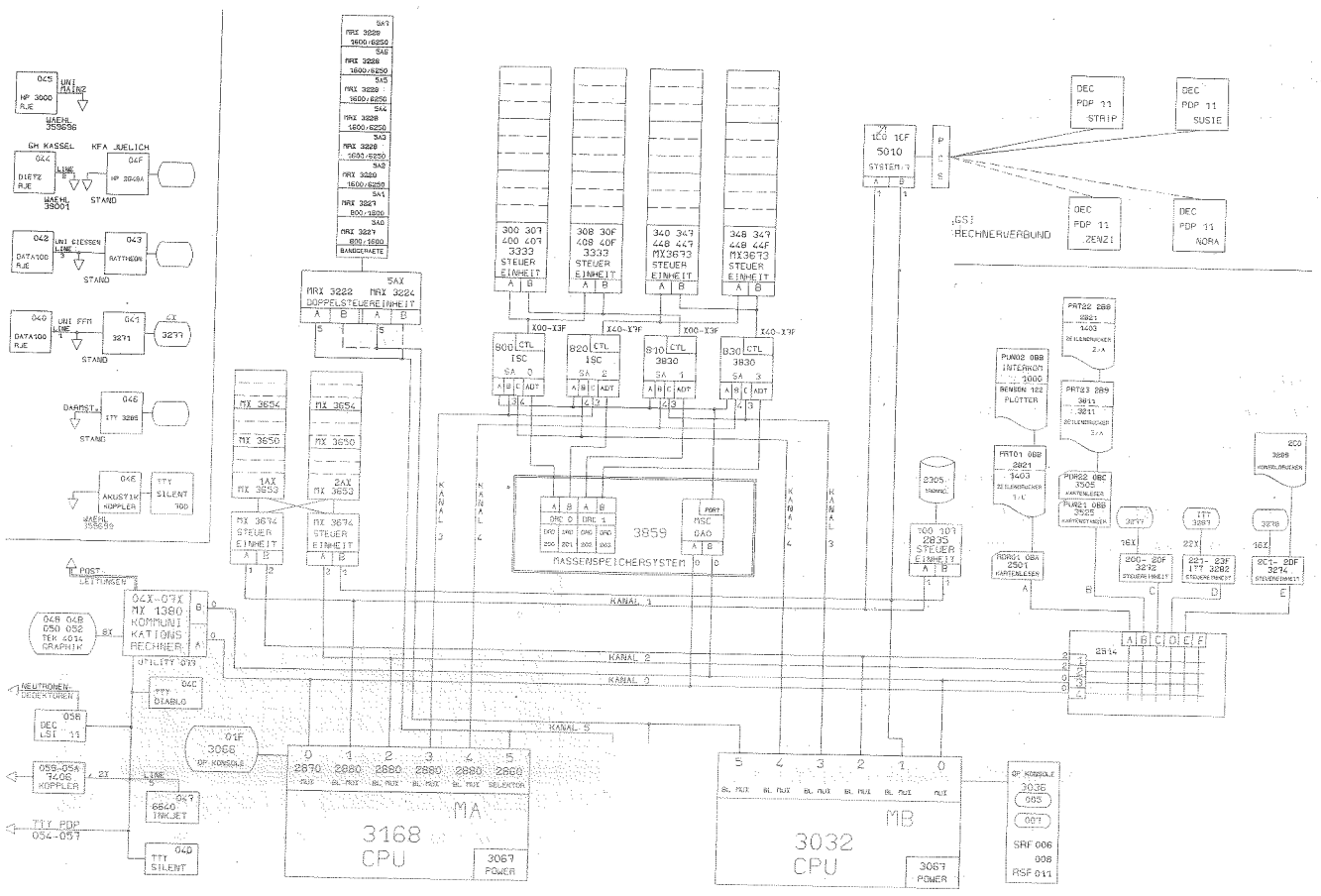
(H.Egger, S.Glückert, H.Hultzsch, J.Lowsky, G.Wohlrab)

Since January 1979 the computing load has been distributed to the two Central Processing Units, an IBM 3168 and an IBM 3032 both with 4 Megabytes of main storage. The two processors are run under identical software, the MVS (Multiple Virtual Storage) operating system. Both computers together are under control of the job entry subsystem JES3, which manages the common resources. The stipulated aims to be reached with the new computer concept were

- balancing of user groups with different performance characteristics,
- high availability for priority tasks, such as controlling experiments at the UNILAC,
- flexibility in case of errors on particular devices or in case of maintenance activities,
- data set integrity in storage and retrieval as well as CPU-independent access mechanisms and
- minimum manpower requirements for operations and system support.

Experiences from other installations such as DESY, CERN, KfK with application characteristics similar to those at GSI served as guidelines for the overall systems planning. The resulting computer configuration is shown in the drawing below.

In normal operations with both processors, batch as well as interactive applications are distributed to both computers. The experiment data analysis tasks with high main memory activity and intensive CPU-loading are run on the GLOBAL-processor together with the larger part of JES3, while other interactive applications are connected to the LOCAL-Processor. The LOCAL- and GLOBAL-Function of JES3 can easily be exchanged between the processors by Dynamic Systems Interchange. Batch also is run on both processors. Due to the tuning mechanisms of MVS with empirically determined tuning parameters the batch-load is dynamically pushed back when interactive applications claim the computer resources. In the symmetric system, the magnetic tapes and the direct access storage devices (magnetic disks and the Mass Storage System) in total are adressable from both computers continuously without any manual



Computing Center Systems-Configuration Overview

switching activity. Only the visual displays, the printing- and card-peripherals can be attached in groups to one of both computers; in normal operations the printers and the card-periphals are attached to the GLOBAL processor. The remote job entry and the remote interactive stations also can be connected to both processors by means of the switching capability of the telecommunication processor Memorex 1380. In normal operations remote job entry and graphics applications are connected to the GLOBAL processor, while all other interactive devices are linked to the LOCAL processor. Access to data stored on either magnetic disks or within the mass storage system is unrestricted from both processors. The Mass Storage System which stores most of the online data has become a critical component of the total system. Due to the data needed a breakdown of the Mass Storage System hurts certain applications, especially experiment data processing, as heavily as a total system outage, even if both processors are in full operation. Fortunately the Mass Storage System has proved to be a very reliable device with high availability since it was upgraded to model A2 with four data recording devices and two controllers for the mechanical parts.

In total the aims of the computer concept have been reached without any additional manpower need. The computer power supplied has been doubled; the response time in interactive as well as batch applications overall reached satisfactory values; experiments at the UNILAC could be supplied during longer periods of time with the necessary computing power for data logging and live analysis. The total system availability for priority tasks significantly grew to a satisfactory level.

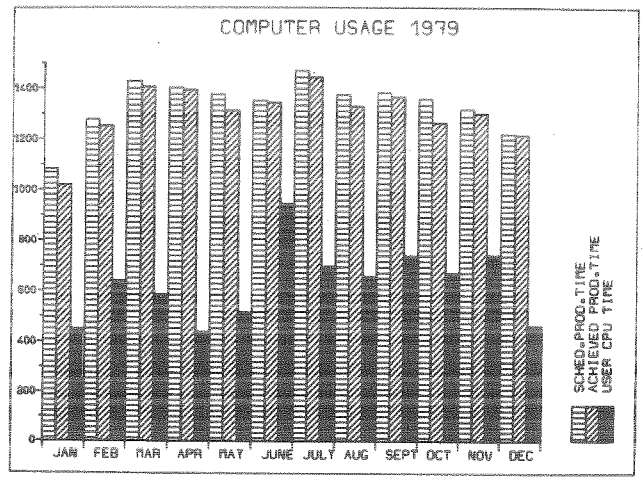
Nevertheless, the computing power available did not satisfy the growing demands, especially not in interactive applications and experiment data analysis.

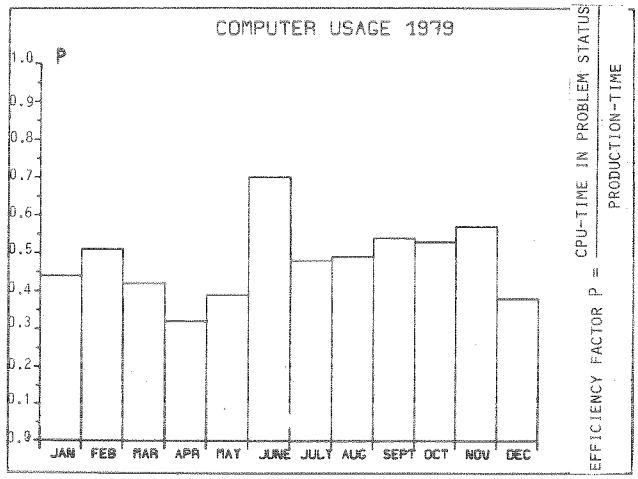
Operations and Service (H.Egger, S.Glückert)

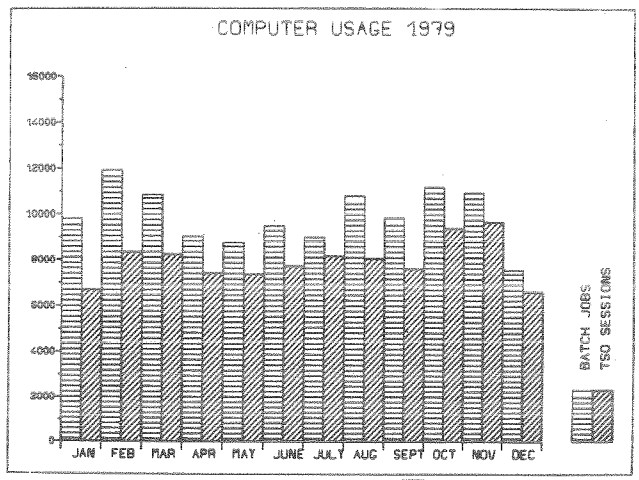
The computers are in operations almost continuously 24 hours a day, seven days a week. Every four weeks during UNILAC shutdown weeks, the Tuesday morning is reserved to run diagnostics on the total computer system allowing no user service. During other weeks hardware maintenance and software tests are scheduled at Tuesday and Friday morning with one processor out of user service, thus guaranteeing only half the computing power compared to normal operations.

The high stability and the modified schedule with computer service at one processor during maintenance periods created a much better computer availability. But the demand for computer service during those periods of limited service very often was higher than the power available. In order to avoid overload situations at one processor, the number of terminals was limited, allowing with preference only priority applications to be started.

The two processor system is operated with a very low number of seven operators. The communication to the total system mostly is handled through JES3. Only in the case of more complex error situations, commands have to be directed to the separate operating systems. Operation at night and during the weekend is without







Operating data of the Computers IBM 3168 and 3032

the attendance of operators, suffering the risk of interrupted computer service in case of an error which cannot be solved by the system itself. Fortunately, the experience of the last years shows that the system proves to be rather stable also during those unattended periods. Nevertheless, the presence of an operator is undispensable during periods when the computer system is run in on-line operations for data logging and live analysis from UNILAC-experiments.

After severe problems in the begin of 1979, the new processor for teleprocessing Memorex 1380 has become a powerful and reliable component of the total system, guaranteeing a very high flexibility of operations. Each device attached to this processor can be switched to each of the two main-computers dynamically, i.e. during full operations without any effect to other activities. By this means the device contributes to the balancing of user groups with different application characteristics between the two main computers.

Very successful in operations proved to be the concept with two separate data paths from each computer to each direct access storage device, i.e. magnetic disks and virtual disks in the mass storage system. During the daily peak load a very high total transfer rate is possible by distributing the stochastic load to the paths available at any moment. On the other hand in case of an error at a certain device, data transfer and computer operation is continuously enabled due to the availability of an alternate data path.

By the end of the year 1979 ca. 35.000 data sets were kept on line in the system. The total number of batch jobs run in 1979 was 119.200 and 95.359 TSO-sessions were started. Total computer usage, TSO-activity and CPU-efficiency are shown in the diagrams.

System Software (G. Wohlrab)

The operating system MVS (Multiple Virtual Systems), which is in use since 1974 was upgraded continuously. In an environment with steadily varying application characteristics generated by the users changing activities, MVS with the numerous self error-recovering software components proves to be the base of the high total computer system stability. At the end of 1979, computer operations were run under MVS Rel. 3.8, PUT 7907.

A new version of JES3 (Selectable Unit 26) was integrated into the system software in April 1979 offering better performance, a better operator's communication, a faster service in dynamic allocation ("fastpath") and a more reliable support for the mass storage system.

The teleprocessing software was replaced by TCAM10 in January 1979 reducing the system overhead and offering a faster service. TCAM10 was modified at GSI in order to allow dynamic activation and deactivation of terminals at each computer. In total 50 modifications specific to GSI-applications had to be integrated into the system software, twenty of which were reflecting to the JES3 job entry subsystem.

During the last quarter of 1979 preparations were made to run MVS/SE(System Extensions) and other software packages using the extended instruction set available on the IBM 3032 and 3168, offering enhanced switching capabilities of the hardware, adding 5 to 12 percent to the computing power available, especially during interactive load characteristics.

Service Programs (S.Glückert, G.Wohlrab)

Besides the software system for experiment data analysis SATAN (System to Analyse Tremendous Amounts of Nuclear data) and the support for the online Software GOLDA (GSI OnLine Data Acquisition) the following software was available at GSI computing systems:

FORTRAN-G Compiler	PL/I Optimizing Compiler
FORTRAN-H Compiler	PL/I Checkout Compiler
FORTRAN-H Enhanced Lib.	PL/I FORMAC Translator
FORTRAN Interact.Debug	PL-11 Compiler
FORTRAN-PL/I Transl.	SPEAKEASY Interpreter
WATFIV FORTRAN Comp.	VS-COBOL
SPITBOL Compiler	VS-ASSEMBLER
RUNOFF Textformatter	SSP Scientific Subr.Pack.
TSO Command Package	PLMATH Scient. Subr.Pack.
SPF Struct.Progr.Fac.	GSI Graphics Software
PCF Access Control	CPC Comp.Phys.Comm.Library
RACF Acc.Contr.Facil.	EISPACK Eigenvalue Subr.Pck.
Westingh.Fast Dump/Rest.	CA-Sort
Multiple Sys.Integr.Fac.	Omegamon

The languages mostly in use are FORTRAN and PL/I, with a continuously growing demand for PL/I from the user population. The software developped and supplied by the computing center such as SATAN is implemented in PL/I.

SPEAKEASY, a very simple but powerful interactive programming language, enjoys a growing popularity. Text processing with the SPF-Editor and the RUNOFF text formatter is increasingly demanded from scientists as well as from secretaries, since appropriate printing devices such as lower case printer chains, DIABLO typrewriters and an IBM 6640 ink jet printer are available.

Software-Development

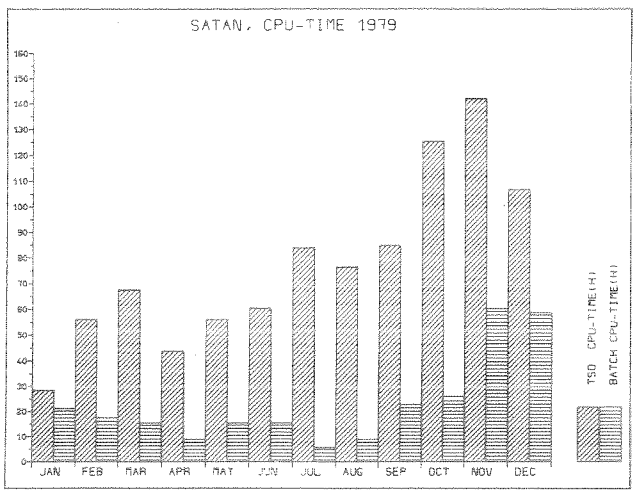
Experiment Data Processing (J. Lowsky)

The usage of the software system SATAN (System to Analyse Tremendous Amounts of Nucelar Data) which was developped at GSI, more than doubled during 1979, due to increasing requirements in experiment evaluation at GSI. The potentiality of this increase originated from the higher availability of computer resources and from the enhanced tuning mechanisms, guaranteeing special performance conditions for experiment data analysis tasks (see drawing). Especially the user frequency grew significantly for control of data capture and live analysis in the online modus. The software itself stabilized in its operating conditions by solving the former problems in data buffer management, synchronizing independent subtasks for control of the separate output to alphanumeric and graphic displays. Batch operations of SATAN are properly handled now in the case of a program error, an erroneous command or a timeout through a controlled breakdown, ensuring the storage of the already processed data.

Performance characteristics have been optimized by reducing the minimum working-set of SATAN significantly. This was mainly achieved by implementing dynamic load mechanisms and by diminishing the space needed for data handling.

The spectrum of functions of SATAN was expanded significantly. Some of these functions are:

- Processing of multiparameter experiments with a dynamic number of data stored in an event;
- several spectra can be shown on one display at one time;
- enhanced load-procedures;
- enhanced performance characteristics for trivial commands, such as "display".



SATAN usage in 1979

The flexibility in the interactive usage of SATAN also has been improved by allowing compilation of analysis-programs either in submitted batch or interactive modus selectively.

Computer Link (J.Lowsky, J.Lustig)

The maximum speed of data transmission between the experiment control computers (type PDP 11) and the computing center IBM computers has been raised to 180 KByte/sec by implementing a dual buffer management in the communication processor IBM System/7. The data transfer between PDP 11's and System/7 at one side and between IBM 3032 or 3168 and System/7 at the other side is asynchronously handled in independent memory areas.

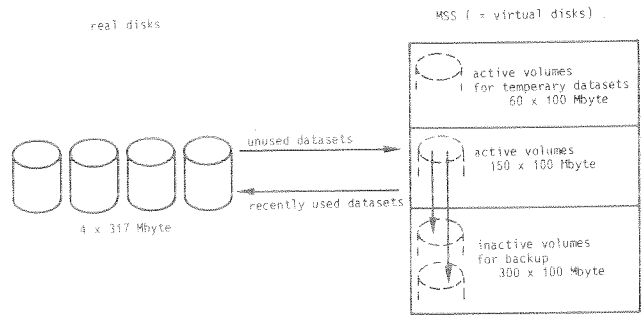
An enhanced error recovery has been implemented within the link software. In most cases transmission errors by occasional hardware malfunction are handled by the software without any perceivable effects in usage thus establishing a very high total stability of the link.

Usage of the central computers through the link for on-line data logging and live data analysis has encreased in 1979 to 470 hours.

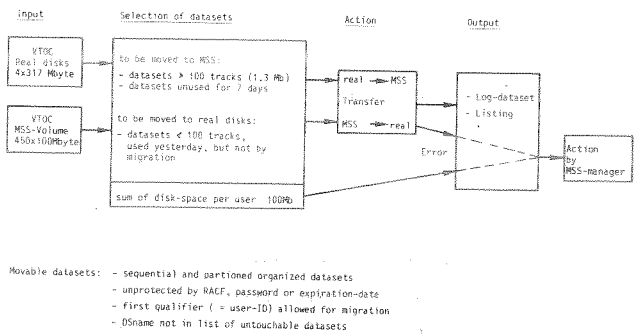
Data Migration (H. Döpke)

User data sets are stored either on four real disks (USER01,...,USER04) or on virtual disks within the mass storage system. Each user may have a maximum space of one personal virtual disk, i.e. 100 Megabytes of data; normally he shares a virtual disk with other users.

Due to the load mechanism of mass storage cartridges the access time to data stored in the mass storage system is much longer than the time needed to reach data stored in real disks. Therefore the GSI data migration system tries to store those data on real disks which carry the highest access probability. Based on the supposition that data accessed frequently during the past most probably will be used again in the very near future, a data migration run decides each night which data sets are stored on real disks and which will be moved to virtual disks within the mass storage system.



Dataset migration concept

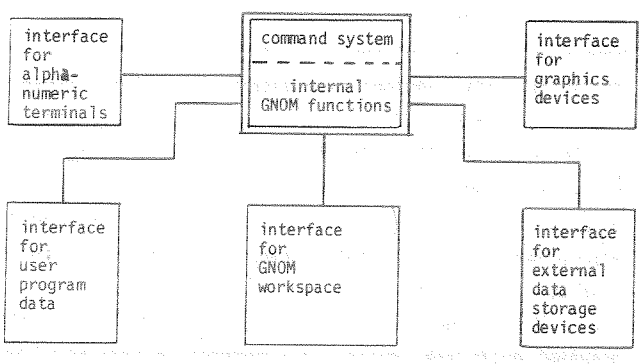


Dataset migration program scheme

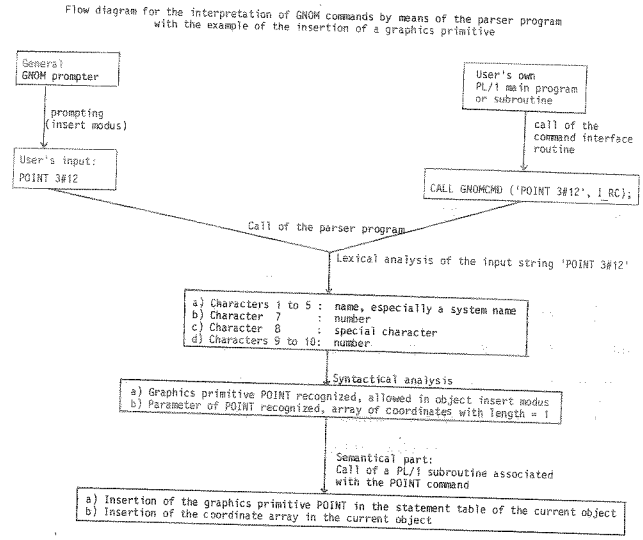
The data migration software developed at GSI, in use since 1977, has been modified extensively, aiming at higher stability and better performance. The decision which data sets have to be moved from real disks to virtual mass storage disks or vice versa is now made on base of information stored in the VTOC (Volume Table of Contents) available on each real or virtual disk. Earlier the SMF (System Management Facility) data have been used to prepare the information necessary to decide which data sets were to be moved in either direction. This modification was necessary since dynamic allocations, which are very frequently used at GSI, do not result in usable SMF data logging. The modification is based on a fast reading mechanism to reach the VTOC-data, which has been designed and implemented at GSI.

Graphics and Numeric Operations Method (I. Giese)

Interactivity, image objects enabling storage and retrieval, image structure and device independence were the aims and the motivation for designing and implementing the GNOM-software (Graphics and Numeric Operations Method). The project is run together with ZAM from KfA Jülich.



GNOM structure scheme



GNOM interpreter processing scheme

After first tests in the beginning of 1979 with some basic software components, a syntax structured command interpreter (parser) has been implemented and tested in the GNOM software environment. With this parser, calls of the GNOM command processor as well as graphic and numeric instructions to the GNOM software are effectively managed. The parser includes error detecting and prompting components.

Engineering and Technology

E. Malwitz, K. Blasche, W. Bleuel, H. Gaiser, K. Illert,
H. Kiesewetter, U. Kopf, H. Kraus, F. Nöhmeyer, K. Wilhelm
GSI Darmstadt

Engineering department

For several years the design of experimental facilities was the main point of all construction activities. This year design work concerning the UNILAC improvement program and the installation of two additional Alvarez cavities ranks with about 50 % above the design of experimental facilities with 40 %. The major tasks were:

Alvarez III/IV
Rf coupling loop and
Rf power lines for the Alvarez cavities
New large aperture injection beam line
Emittance measuring device
Test bench for high current ion sources and
High current beam diagnostic equipment
SIS accelerating cavity
Crystal ball detector system
Spherical vacuum chamber
Ion microscope
Oktopus spectrometer
Positron spectrometer
Mechanical chopper, collimators
Double actuator.

A large part of the Alvarez design work such as cavity design, cooling and vacuum casings was done by an external engineering office under control of GSI engineers who were responsible for the conceptual design. The rf transmission lines were conceived at GSI while detailed drawings and parts lists were prepared by the contractor.

Production engineering

In the production engineering department all tasks for the mechanical workshop are accepted and passed on either into GSI or external workshops. Coordination, expediting, and statistics are done routinely by means of a computer program. A large part of all production work - 185 orders with a total value of 412800 DM - was passed into other companies. Recently the department has started to prepare the programs for the new NC milling machine.

Workshops

The mechanical workshop has handled 726 tasks, the locksmith shop 449 and the development and experimental workshop 83 tasks. About 15 % of the workshop activities were required for small tasks that had to be performed immediately. For both, the accelerator and the experimental facilities about 50 % of the total capacity were used.

During a period of 5 months the work load on the machines was recorded in order to provide the data that were required by the administrative audit. They range between 15 % for tool grinders and 85 % for lathes and milling machines. When comparing these results to the work loads in production companies it must be taken into account that the workshops in a small research institute have got a lot of special tasks such as assembly und start up of prototypes and new equipment, disposition of tools and materials, design and production of fixtures, attachment appliances etc., instruction of apprentices and probationers, special service for accelerator repairs etc.

Alvarez cavities III and IV

Experience with the UNILAC has shown that the design of the Alvarez cavities can be simplified. In the new design the tank sections will be simply grinded by sand belt on the inner surfaces and then copper plated. Depth limitations of the plating bath containers restrict the length of each section to 2.6 m. Five sections are welded together for each Alvarez cavity. The weld seams are copper plated by means of a locally attached bath which covers a segment of the circumference. In the old design all tank sections were machined in order to taper the inner diameter and five sections were flange connected for each cavity. The end walls are now just 90 mm thick endplates that form both an rf and a pressure wall whereas before a thin rf wall was supported by a heavy spider and a casted bulk head. The new drift tubes consist of stainless steel parts that are assembled by argon arc welding and copper plated afterwards. In the original drift tube design all components were machined to close tolerances from OFHC copper and then were assembled by furnace braze and electron gun welding (Fig. 1). The new design helps to reduce considerably the total costs of the new Alvarez cavities.

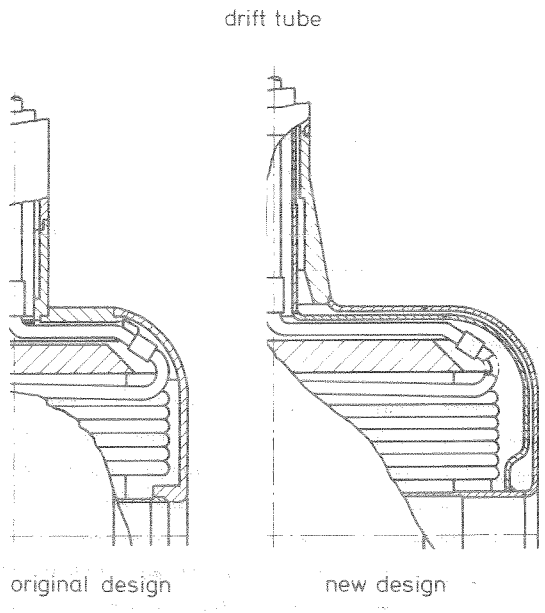


Fig. 1: Drift tube design for the original and the new Alvarez-accelerator

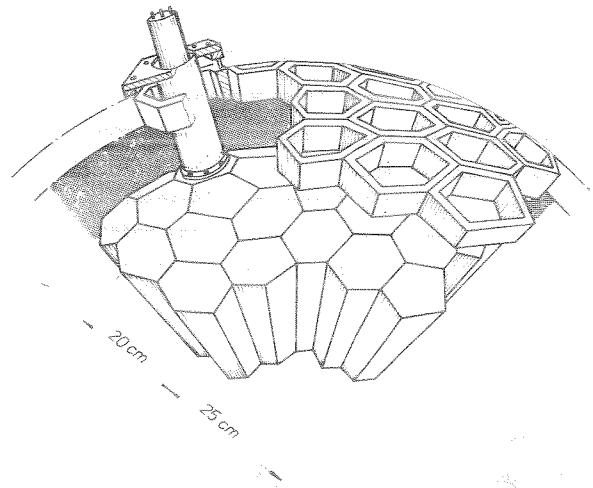


Fig. 2: Principle of the crystal-ball detector system

SIS accelerating cavity

The design of a prototype accelerating cavity is underway. In order to cool the ferrite material about 70 cooling disks have to be interleaved. Different design alternatives were studied and finally it was proposed to roll square copper tube into a spiral that will be soldered afterwards to form solid cooling plates. Recently the 70 cooling plates for the prototype cavity have been ordered.

Crystal ball detector system

The crystal ball is a detector system with close to 4π geometry to study the decay γ-radiation following heavy ion reactions. The detector has the shape of a spherical shell of NaJ with an inner free radius of 25 cm and an outer radius of 45 cm (see Fig. 2). This shell encloses the target chamber completely, and it is subdivided into 162 seperate counters of equal solid angle.

In order to perfectly tile the sphere the free gaps between neighbouring counters must be very small. On the other hand these gaps have to guarantee that the fragile counters do not touch and damage each other.

A large aluminium sphere of 6.5 cm thickness and an outer diameter of 138 cm is used to support and adjust the individual counters. It seemed impractical however, to start from a massive sphere (or two hemispheres, respectively) and have the necessary 162 pentagonal and hexagonal portholes pierced into it. Instead, the supporting frame is built from individual cells which are assembled into a spherical honeycomb structure. A prototype-cell is shown in Fig. 3.

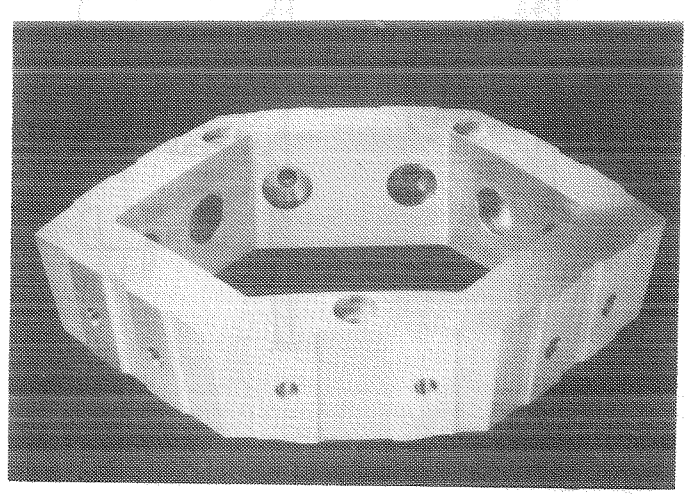


Fig. 3: One cell of the spherical honey comb structure

There exist 4 different types of cells in the total structure. These cells are cast aluminium and will be machined at GSI to the required tolerances on a computer-driven CNC mill. Five computer programs required for such a production have been developped.

A spherical vacuum chamber

For an experiment that was designed to detect neutrons from heavy ion reactions a spherical vacuum chamber with a diameter of 1000 mm and a wall thickness of only 3 mm was required. Two procedures for the production of the half shells were considered: Deep drawing of metal sheets and sandwich techniques using either fibre-glas-reinforced polyester or layers of Al/polyurethane/Al. The sandwich techniques seemed to be too

complicated and the deep drawing technique was finally preferred. A first trial with $AlMg_3$ failed and 3 mm thick sheets of the softer Al 99.5 % had to be used. The two half sheils are flange-connected. In order to reduce the amount of material that disturbs the neutron flux at first a special flange was designed. Since this flange was deformed when the chamber was under vacuum, it was finally replaced by a small conventional flange (Fig. 4).

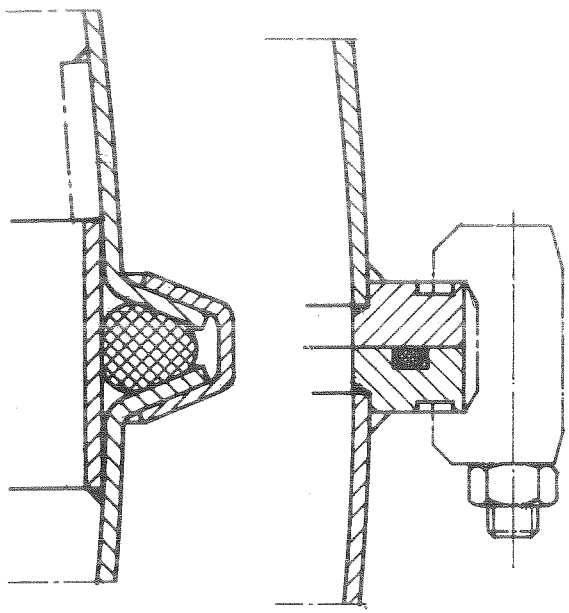


Fig. 4: Extraordinary light flange-connector on the left, normal flange-connector on the right

Mechanical beam chopper (Figs. 5, 6)

A mechanical chopper was designed that can be moved into beam position within the time interval of 15 ms between two pulses of the UNILAC beam. In this way beam intensity and pulse repetition frequency can be reduced for experiments. A light weight tantalum shutter mounted on a rotary shaft is used to chop the beam. For the shaft a vacuum tight "Ferrometic" rotary feedthrough is used. The ferromagnetic sealing fluid of this device shows much less friction than a gasket so that even at high rotation frequencies vacuum tightness without any abrasion of the sealing material is achieved. For the same reasons it was not possible to use a water tight gasket in the junction element between the rotating tubular shaft and the water pipes. Instead the junction is mounted vertically and the water that passes through the slots between pipes and shaft is collected in a water tight duct around the junction. A stepping motor is used to drive the chopper shaft. Since both the feedthrough and the water function element show low friction the motor torque is sufficiently strong to switch the shutter within 15 ms from the parking position into the beam position and vice versa.

Beam collimator (Fig. 7)

Many experiments require an exact control of the beam cross section at well defined beam tube positions. Therefore a low cost standard collimator was designed that can be mounted like a conflat flange with interior diameters of 100 mm or 150 mm due to its extremely flat structural design with a height of 30 mm. Around the cast-metal box that is made from stainless steel 4 micrometer screws and 4 current feed throughs can be mounted so that the collimator plates can be positioned exactly and collimator currents can be measured independently. At both sides of the movable plates additional collimators can be mounted in fixed positions. Water cooling of the collimator plates can be foreseen. The cast-metal box is a multi purpose element that can be also used when e.g. beam diagnostic equipment has to be positioned inside the beam tube.

Actuator combination on a CF/NW100 flange (Fig. 8)

Linear actuators are in use since many years especially for the mounting of beam diagnostic equipment. Now the actuator design was modified so that two actuator types can be installed on a single CF/NW100 flange. One actuator that is driven by a stepping motor has a travel of 245 mm and a positioning accuracy of 0.03 mm per step while the other air-operated actuator has a travel of 80 mm from the parking position into the beam position reaching an accuracy of 0.3 mm in both positions. Originally the new design was made for the foil stripper that was installed between the accelerator cavities. In this application 10 foils are mounted on the stepping motor actuator and a profile grid can be brought into position immediately in front of the foils by the air-operated actuator. Meanwhile the new actuator combination is often used when target stacks and beam diagnostic equipment have to be installed in close vicinity.

High power collimator plates (Fig. 9)

Presently high current ion sources are studied that yield up to 100 mA. In the test bench equipment for these ion sources collimator and screening plates are required which can stand a beam power up to 12.5 kW. Therfore collimator plates in sandwich technique were developed which have three elements: a copper cooling plate with cooling channels that are carefully optimized

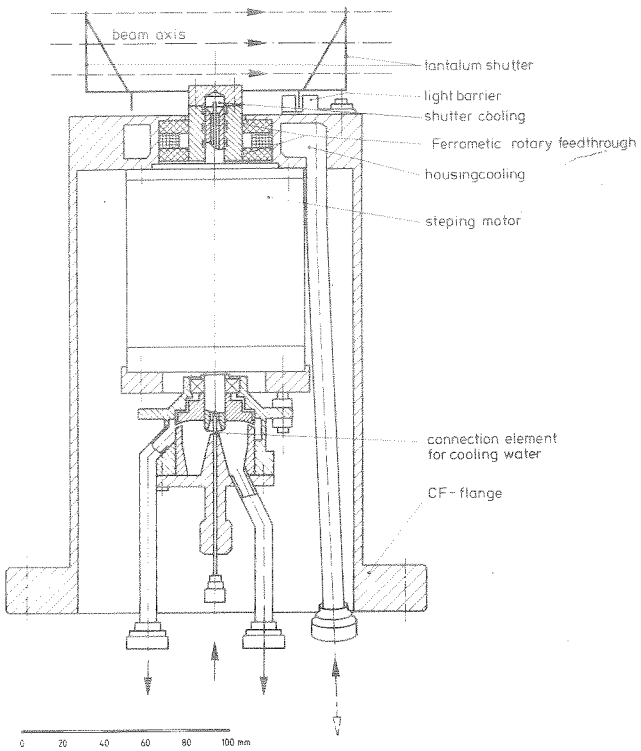


Fig. 5: Mechanical chopper cross section

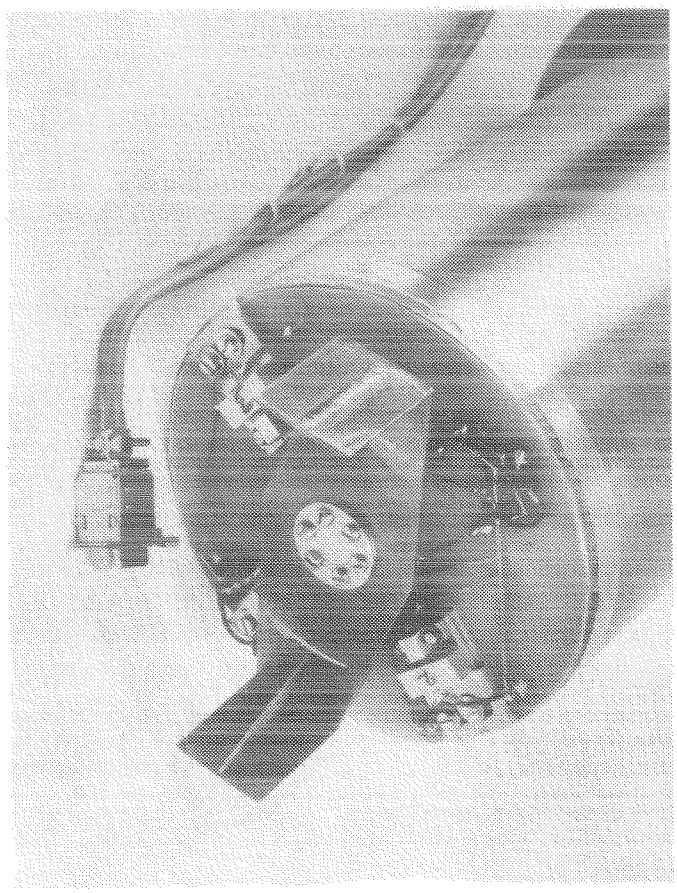


Fig. 6: Mechanical chopper with wing

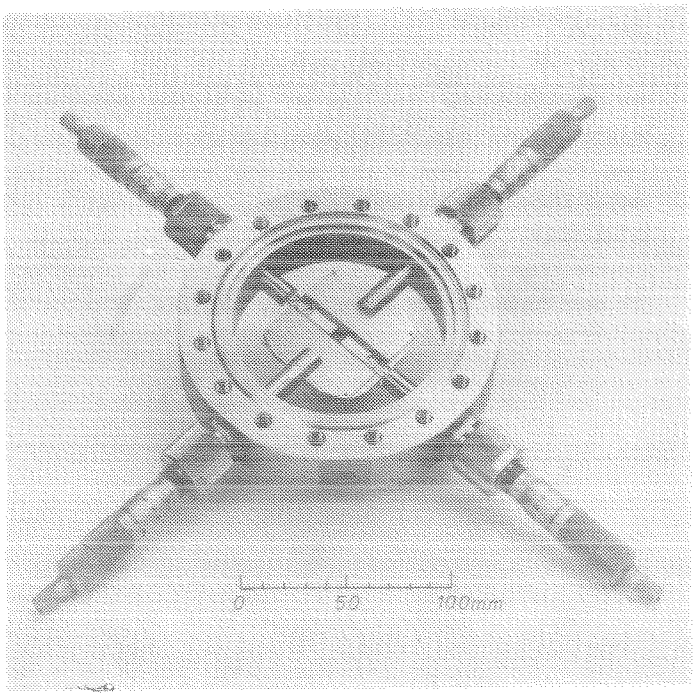


Fig. 7: Cross slot-collimator

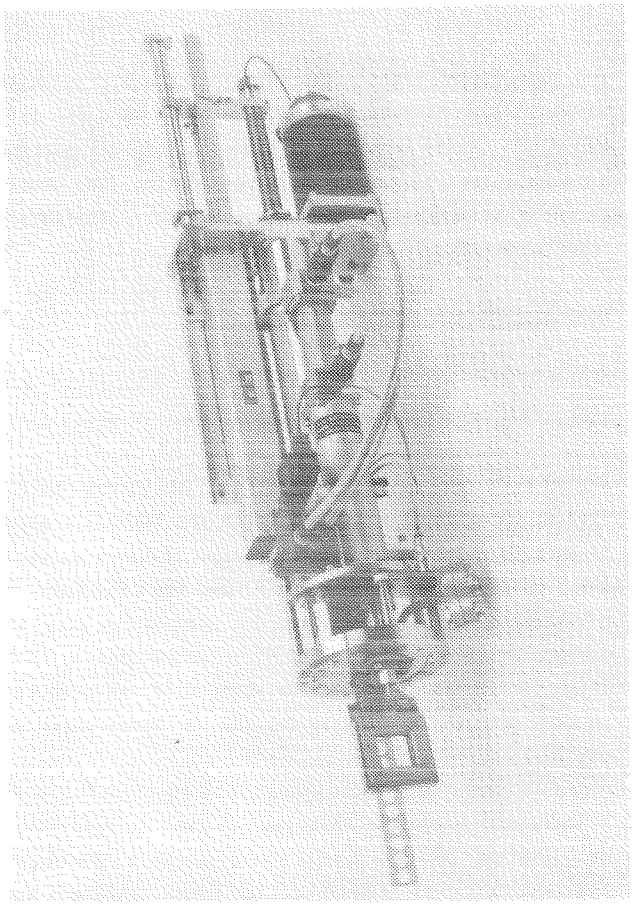


Fig. 8: Actuator combination on a CF/NW100 flange

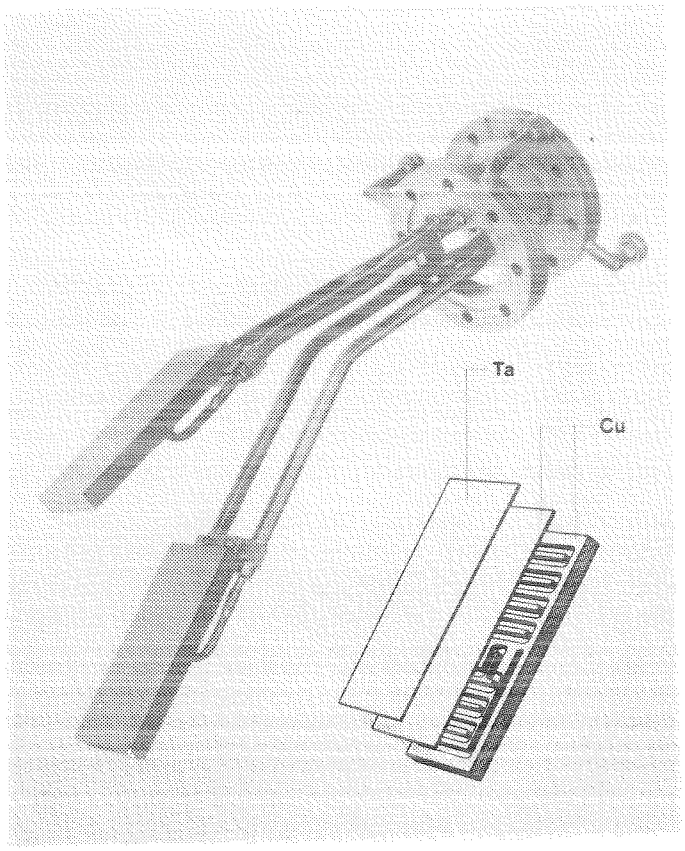


Fig. 9: High power collimator plates

with respect to cross section, length etc., an intermediate copper plate and a tantalum sheet on top. these layers are brazed together in a vaeuum furnace. Although the collimator plates strongly bend during the cooling process after brazing they can be easily straightened under pressure.

New machines and new techniques

Recently a NC mill was installed in the mechanical workshop. Althrough experts had warned that it would take a long time to train programmers on the new machine it was argued that the new mill which can be anyhow operated like a conventional mill is worth the extra investment of 30 % for the electronic control. After 4 weeks of test operation the programmer and the mechanic had established the programs that are needed for the production of 162 cells in the 4π-crystal ball detector (Fig. 3). It is expected that alone with the production of this detector the costs for the NC electronics will pay off.

A new acetylene cutter that can be used to copy complicated shapes by means of a photo-electric keying head has simplified the production of vacuum chambers where complicated pipe sockets had to be prepared on milling machines before.

The brazing furnace has been in repair for several months. At this occasion a gas dosing installation for nitrogen was mounted. Brazing under protective gas provides an improved reduction of metal oxides, a more uniform heating and cooling, and a shortening of brazing times. In addition metalization of aluminia ceramic requires a hydrogen atmosphere. Unfortinately the TUEV-controls for the operation with hydrogen gas are not yet finished.

Electroplating plant

Since it was decided to reuse the plating technique for the production of the new Alvarez cavities the large bath containers of the electroplating facility were restored. The copper plating process has the following steps:

1. Cleaning with solvents and steam jet
2. Electrolytic cleaning (anodic and cathodic)
3. Pickling in sulfuric acid (10 %)
4. Nickel plating
5. Pickling in sulfuric acid
6. Copper plating in copper sulphate electrolyte.

In the copper plating process that was used a few years ago for the UNILAC cavities nickel plating was done in a nickel sulphate electrolyte (Watt's Ni electrolyte). This nickel bath was modified by the addition of NiCl in order to improve the adhesive strength of the Ni/Cu in order to improve the adhesive strength of the Ni/Cu layers, since good results have been achieved in this electrolyte (Ni-strike bath) during the past years with small parts.

The five 2.7 m long sections of one Alvarez cavity are welded together with a circular seam after copper plating. The ring zones at the welding seams have to be copper plated afterwards in a locally attached bath which covers a segment of one fifth of the circuumference (Fig. 10, 11). This procedure will be tested in the near future at two short cavity sections.

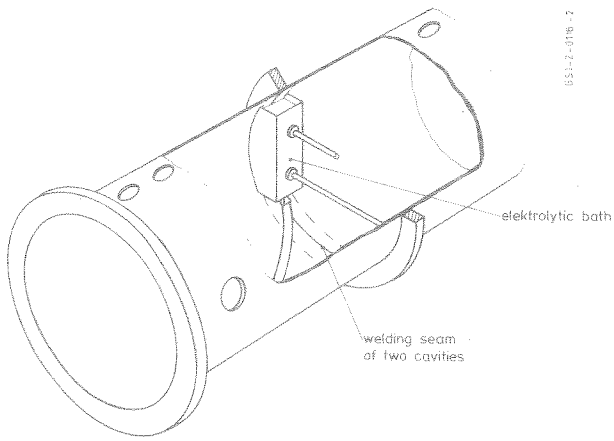


Fig. 10: Scheme of the copper plating process for the welding seams of the new Alvarez cavities

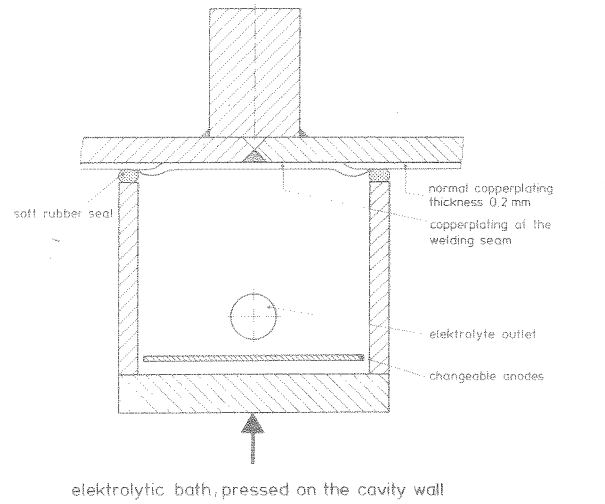


Fig. 11: Electrolyting bath for the copper plating of the welding seams

5. Accelerator

PAGE

5.1 UNILAC Performance and Ameliorations 210

5.2 Accelerator - Projects 215

Unilac-Operation

N. Angert, J. Klabunde, M. Müller, P. Strehl
GSI Darmstadt

The Unilac is operated with a new schedule since January 1979. Previously the machine run continuously except for two shut-down times of about six weeks each in spring and fall. Now, operation is interrupted every fourth week for maintenance purposes, and to some extend for accelerator development. This new schedule resulted in a decrease of the total operation time per year from 6620 in 1978 to 6360 in 1979 (s. table 1). The number of target hours, however, could be increased from 3050 to about 3400.

target time	3413 h	
parasitic target time		592 h
acc. development	284 h	
tuning time (exp. area incl.)	1086 h	
break down time	1124 h	
maintenance	453 h	
total operation time	6360 h	

Table 1: Unilac operation times in 1979

For more than 50 % of the total operation time lead and uranium beams have been accelerated. Fig. 1 indicates the shift of the required ions towards heavier elements, compared to 1978. Table 2 surveys the ion beams which have been accelerated till end of 1979. Fig. 2 shows the increasing interest in high energies. Less than 3 % of the operation time was scheduled for energies above 9,5 MeV/u in 1978, whereas in 1979 more than 10 % have been spent for these high energies.

The new operation schedule proved to be very useful. It is now possible to match the short term maintenance activities flexibly according to the performance of the machine. Nevertheless, the down time is still too high. About 70 % of this was due to rf and injector failures. As the Alvarez rf amplifiers are still far away from the design aim of 1.6 MW peak power alternate programs have been started to reach that goal. The measures for the suppression of rf leakage of the poststripper rf stages have been finished successfully after a three year lasting improvement program. Due to recent measurements of the injector beam parameters it was considered necessary to increase the acceptance of the injector beam line by a factor of three in order to increase beam currents and to reduce tuning times by computer aided optimisation. The control of the accelerator - exclusive of the rf - is now done only from the main control room via the computer.

Isotope	Poststripper charge state	Average Intensity (particles/s)	Energy (MeV/u)
^{40}Ar	10+	$9,4 \cdot 10^{12}$	
^{46}Ti	13+	$1,4 \cdot 10^{11}$	
^{48}Ti	13+	$1,2 \cdot 10^{12}$	
^{50}Ti	13+	$9,6 \cdot 10^{10}$	
^{56}Fe	14+	$2,8 \cdot 10^{12}$	
^{58}Ni	14+	$4,0 \cdot 10^{11}$	
^{65}Cu	15+	$2,5 \cdot 10^{11}$	
^{84}Kr	17+	$7,0 \cdot 10^{11}$	
^{86}Kr	17+	$2,0 \cdot 10^{11}$	
^{86}Kr	17+/30+	$1,0 \cdot 10^{10}$	13,1 (2.STR)
^{107}Ag	19+	$3,3 \cdot 10^{11}$	
^{129}Xe	21+	$7,0 \cdot 10^{11}$	
^{132}Xe	21+	$7,0 \cdot 10^{11}$	
^{136}Xe	21+	$2,4 \cdot 10^{11}$	
^{136}Xe	21+/44+	$1,0 \cdot 10^{10}$	11,5 (2.STR)
^{154}Sm	32+	$6,0 \cdot 10^{10}$	
^{183}W	34+	$5,0 \cdot 10^{9}$	
^{184}W	34+	$1,0 \cdot 10^{10}$	
^{208}Pb	36+	$4,4 \cdot 10^{10}$	
^{208}Pb	MC	$1,0 \cdot 10^{11}$	10,5 (2.STR)
^{209}Bi	37+	$8,0 \cdot 10^{10}$	
^{238}U	40+	$9,4 \cdot 10^{10}$	9,0
^{238}U	MC	$4,0 \cdot 10^{11}$	10,0 (2.STR)

MC: Multi Charge Operation; 2.STR: Second Stripper

Table 2: List of isotopes accelerated at the Unilac till end of 1979

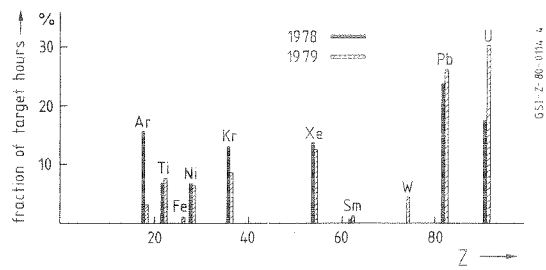


Fig. 1: Statistics of elements

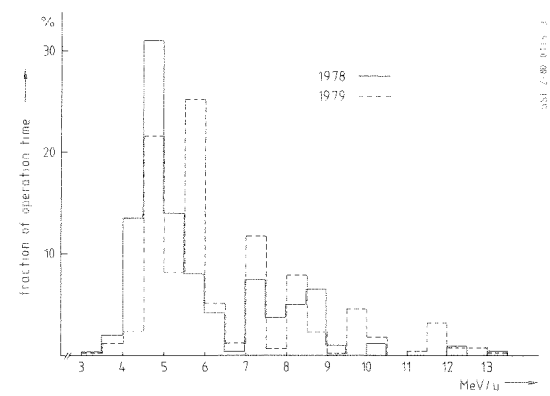


Fig. 2: Statistics of energies

Ion source development

PIG and ECR sources

H. Schulte
GSI Darmstadt

After some time of exclusive use of PIG sources for the production of highly charged ions for the Unilac plans were arising in the preceding year to replace this source in the long run by a more reliable one, which promised to give a more stable beam and to need less service. Therefore development work has shifted from PIG sources to ECR sources, though this activity does not seem to be a quick success.

With PIG sources only some more exotic tests were carried out. The production of alkali ion beams which was intended to be tried by sputtering of the respective halogenides did not yet lead to a useful method. The manufacture of sputtering electrodes was done by intense grinding a mixture of KCl and graphite in a ball mill and briquetting the resulting powder by high pressure (up to 15 t/cm^2) in a die. This technique produced good pieces of fine grained low resistance material which were then tried as sputtering electrodes. The results were poor and erratic.

Immediately after starting the source a good potassium beam was obtained without any sputtering voltage present but the intensity decreased rapidly in time. Increasing the sputtering voltage had little effect on the potassium output but around 100 V severe sparking occurred with temporary rise in K-beam current. When the source power (arc current) was increased a new outburst of potassium occurred and died away in a few minutes. The whole thing looks very much like KCl evaporation from the electrode surface whereas proper sputtering (at higher voltage) is prohibited by charge accumulation on the crystalites. If interest in alkali beams should prevail RF sputtering (a common method for insulators) could probably be a solution to this problem. Experiments in this direction were postponed due to lack of a suitable RF power supply. Difficulties with the low yield of tungsten sputtering (~ 1 μA W^{7+}) led to the idea to take advantage of chemical reactions. Remembering the volatility of WO_3 we tried an admixture of oxygen to the argon auxiliary gas. This caused a remarkable increase in tungsten output but there was no longer any clear dependence on sputtering voltage. The conclusion was that the tungsten did not originate from the sputtering electrode but from the tungsten PIG cathodes. In the next step we tried a PIG anode as normally used for gases without sputtering electrode and a variable argon/oxygen mixture as a discharge gas.

The finding is that the tungsten yield in the extracted beam rises with increasing oxygen content and reaches a maximum for pure oxygen operation. For optimizing W^{7+} a lower oxygen content in the gas is more favorable but the percentage was not exactly determined in these measurements. Even operating the source with air seems a good choice for producing W^{7+}.

For the planned ECR (Electron Cyclotron Resonance) source preliminary experiments were taken up with the production of metal vapor beams on the oven test bench. Calcium seemed a good candidate for the beginning because of its high vapor pressure. Since the delivery of the 14 GHz microwave generator (2 kW) was only expected for the end of the year, we tried to speed up experiments by use of a smaller 2.45 GHz magnetron unit. The main purpose of these experiments is to study the coupling of microwave power to a collimated beam of metal vapor running in good vacuum (< 10^{-6} Torr). The first experiments on calcium were rather disappointing in this sense, for it was only possible to ignite a discharge by the admission of auxiliary gas (He, Ne) to the chamber.

A cylindrical resonator surrounding the beam as well as a helical microwave launcher were tried with the same limited success. The frequent observation of luminous particles crossing the discharge then led us to suspect that only part of the calcium in the beam which was subliming from the solid phase, might be in an atomic state.

The change over to barium as a test substance, which can more readily be evaporated from the liquid phase, then took us a step nearer to our goal. With barium it was in fact possible to ignite a discharge in a column of metal vapor with a background pressure of less than 10^{-6} Torr. The use of barium brought the further advantage that ionized barium (blue resonance line, 4554 Å) can be easily distinguished from the excited neutral (green resonance line, 5535 Å), hence the advent of ion current in the Faraday cup is accompanied with the observation of a blue column of ionized barium following the magnetic field lines within a green diverging beam of neutral Ba.

Ion currents from the ECR discharge are still small (50 μA), but this result has been obtained with only 15 W of injected microwave power. On the other hand material consumption is excessive, amounting to several g/h of evaporated Ba to reach the beam density necessary for a discharge.

For not to delay the study of more basic processes too much by technological work on metal vapors it was decided to develop in parallel a simple one-stage ECR source for permanent gases only. Some informative measurements in this direction could be done on the "Micromafios" source during a short visit to R. Geller's laboratory in Grenoble. Xe^{6+} is easily obtained from this source though the currents in this experiment (25 μA Xe^{6+}) were somewhat small compared to our goal of 500 μA Xe^{6+}.

High Current Ion Source Development

Roderich Keller
GSI Darmstadt

Sources of typically 100 mA singly charged heavy ions are interesting at GSI for three reasons: at first, to yield reasonably high intensities of isotopes with low natural abundances without using enriched materials; secondly because a synchrotron for relativistic heavy ions would need much higher peak intensities than actually injected into the Unilac; and lastly for a heavy ion fusion project to be brought forward in the following years.

A scaled down version of the Culham "picket fence" reflex source[1], named ELSIRE (Einzel-Ladungs-Schwer-Ionen-Reflex-Entladung) was designed in the autumn of 1978. Tests began by 1979 and are still continued. The source body (see fig.1) consists of a cylindrical anode, lined with 12 permanent magnets. Axially, the discharge chamber is confined by two reflector electrodes, the one carrying a thermionic cathode and the other bearing the source outlet grid, part of an accel/decel extraction system.

For this source a completely new test stand had to be assembled,with efficiently cooled protection plates as beam powers up to 12.5 kW could be released on a few cm^2. For examinations of beam transport phenomena, a two meter drift space was inserted between the source and the 90^0 double focusing analyzer magnet. We intend to install a quadrupole triplet in the drift space; presently only the central part of the beam is passed through the analyzer, carrying about 20 % of the total current. During the first runs a 7-hole extraction system with 0.9 cm^2 total aperture area yielded up to 58 mA xenon ions within a Ø 50 mm wide Faraday cup at 400 mm distance from the source. The extraction system was shaped according to a design communicated us by the Berkeley Super Hilac group.

Source performance, however, suffered from the fact that the discharge power pulsing unit had to be used near its current limit of 80 A and frequently switched to the d.c. mode due to overload during sparks. Therefore at first a better cooled source was built, and also for the extraction a more rugged design with 7 holes and 0.5 cm^2 total aperture area was used, following design criteria of the Culham group[2]. Secondly, a new pulsing unit was designed and built at GSI, sustaining up to 500 A. This new unit worked very satisfactory.
The ion currents measured with a Ø 30 mm Faraday cup at 300 mm distance from the source are given in tab.1. The extraction voltage was 30 kV, duty factor 10 % at 50 Hz.

Element	Total Current mA (2 ms)	Relative Abundance % of particles 1+	2+
Ar	55	97	3
Kr	31	94	6
Xe	26	87	13
Hg	18	93	7

Table 1: Measured ion currents

For emittance measurements a pepper pot device was used; the sputtering marks on a copper target indicated the intensity distribution. Thus normalized emittances (about 70 %) of 0.016 mm mrad were found, leading to source brilliances of 115 A/(cm mrad)^2 for xenon and 140 for argon.
Further investigations concerned the cathode geometry and position. With the long-life duoplasmatron disc cathode[3] highest lifetimes, up to 10 h for argon, were obtained but, contrarily to operation with the duoplasmatron, the source plasma still hits the filaments as there is no axial magnetic field present in ELSIRE which could force the plasma towards the disc. With an additional coil around the cathode region, on the other hand, the discharge was extinguished at slightest field values (B ≈ 10 G).
Biasing the reflector electrodes still more negative than the cathode results in a good protection of the cathode insulators against vapour condensation as no discharge can then be struck between cathode and reflector, and the outcoming beam is not at all affected.

[1]A. Goede et al.: 8th Europ. Conf. on Controlled Fusion and Plasma Physics, Prague, 1977.
[2]J.R. Coupland et al.: Rev. Sci. Instr. 44, 1258 (1973).
[3]R. Keller: Radiation Effects 44, 201 (1979).

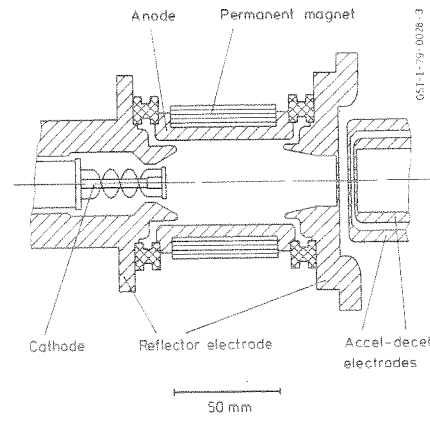


Fig. 1: Ion Source ELSIRE

300 kV Accelerator

M. Müller, B.H. Wolf
GSI Darmstadt

In 1979 experiments for the acceleration of higher ion currents (> 10 mA) were continued. From a Duoplasmatron ion source with expansion-cup and accel-decel extraction (- 30 kV) an ion beam goes through a quadrupole doublet (aperture 80 mm Ø) to the accelerating column.[1] The single gap geometry (5 cm) was changed to a five electrode geometry (30 cm). By that it was possible to reach voltages up to 200 kV without any conditioning, and currents up to 10 mA could be handled instead of 5 mA before. For higher currents (He 20 mA), however, only 95 kV could be reached without permanent sparking, since the beam load of the electrodes was too high for the potential defining resistors of the column (8 x 110 MΩ). A simple solution for a 3 kW-30 MΩ-resistor is a water-tube. We use 8 teflon tubes 180 mm in length and 6 x 1 mm Ø for the up- and down-streeming water, which are connected to the electrodes through stainless steel fittings (fig.1). The conductance of the water, circulating in a closed circuit with a heat exchanger, was controlled by a conductance meter and an ion-exchanger to a value of 20 µS cm^{-1}. Now it was possible to accelerate 26 mA He ions to 200 kV. For Neon 12 mA could be generated and accelerated. In this case the magnetic quadrupole lens reached here upper limit, so that it was not possible to get optimum beam matching for heavier ions. After a defect in one quadrupole coil an electrostatic quadrupole was constructed and tested (fig.2). With a pole-length of 200 mm and an aperture of 80 mm Ø the ion beam could be matched to the beam line with only 5 % of the accelerating voltage (6 kV for 300 kV). Naturally the quadrupole voltage is constant for different ion species. Till now we only used ion beams up to 2.5 mA. Experiments with higher currents whereby space charge effects should appear will be undertaken as soon as possible.

Besides the high current experiments ion implantation studies were made by several research groups, reports of which will be given in this volume separately. For this experiments about 30 different elements have been accelerated in 1979.[2]

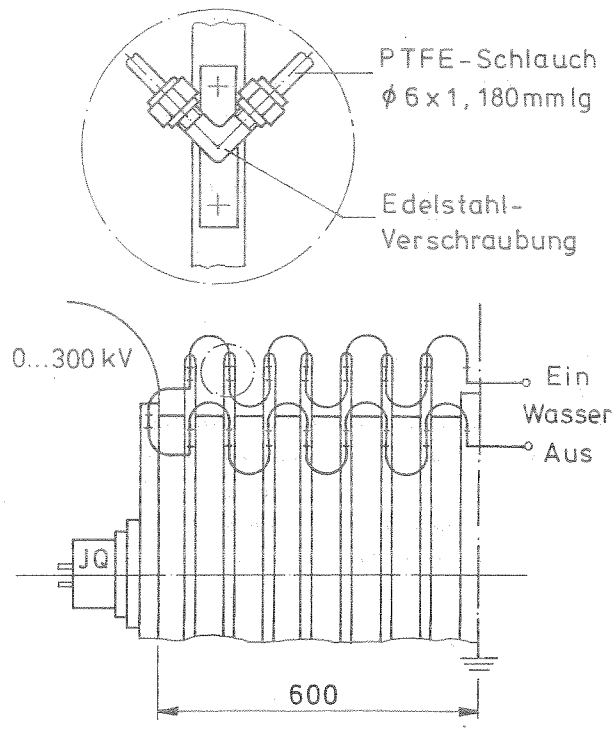


Fig. 1: Accelerating column with water resistor

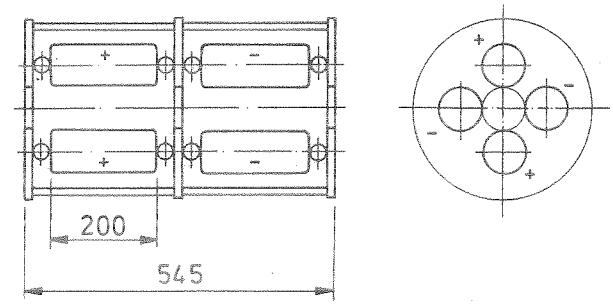


Fig. 2: Electrostatic quadrupole

[1] M. Müller, GSI report 79-11, p. 208 (1979)
[2] B. Wolf, GSI news 1-80 (1980)

Process-Control

M. Wiemers, F. Bock, R. Busch, A. Ehrich, B. Grasmück, I. Morrison, D. Rochna, E. Schaffner

GSI Darmstadt

Increasing consolidation of the computer supported operating of the UNILAC by use of the main control room facilities was enforced by integration of the ion-source control and surveillance to the pool of existing operating software as well as the operators became more and more familiar with the computer environment. The computer control initially restricted to the injection and the Wideröe-/Stripper-sector could be extended to the entry of the experimental hall as soon as corrections at the magnet system had been completed. For the experimental hall all beam diagnostics could be incorporated into computer control.

In detail the following problems have been handled:
ION SOURCES: The operating program controlling the ion sources has been redesigned satisfying the representation requests of the operator crew. Changes in the data transmission hardware made both injectors software compatible enabling the computer control of the second injector at the end of the year in report. Based on the basic modes nowadays a program is under development with automatic support of conventional ion source operating procedures, procedural switching on and off as well as igniting.

Under support of the completed graphic software and by the automatic periodic recording of ion source parameters now it's possible to display interactivly the behaviour of ion sources along the time.

GRAPHIC SOFTWARE: After completion of the plot software, supporting graphics built by standard CALCOMP-subroutine calls to be displayed and manipulated at Tektronix-CRT-terminals, now additional routines enable one-dimensional representation of up to 9 parameters in one figure. This graphic package could be applied successfully to the evaluation of the ion source data.

SYSTEM SOFTWARE: In parallel to the consolidation of the computer control considerable effort has been undertaken, to increase continuously stability of the computer network. Diagnostic facilities were improved adding a SIGMA 6/PDP11 system load demonstration program displayed via video-terminals in the main control room and at the local control areas. All the growing old PDP11/15 were substituted by PDP11/34 processors reducing electrical and mechanical problems and making possible virtual operating system software.

Bottle necks in the communication software appearing mainly under high traffic load led to changes and standardisation of the local handler structure (handler = user task for handling the local process interfaces).

Increasing demands for flexibility of the complete computer system request the construction of a new central data base. It's the aim of this development to remove dependency of operating and application software on process parameters and peripheral interfacing characteristics. In addition the total number of direct accesses to local handlers will be minimized, reducing the network load and making error handling easy for application software.

An extensive numerical subroutine package has been implemented on SIGMA 6 for use by application software and by evaluation routines.

ADDITIONAL IMPROVEMENTS: Main control room support now includes some improvements concerning automatic selection and positioning of the stripper foil, switching on/off most of the power supplies of the magnet system using the trackball and the magnet surveillance program, switching the inflection magnet according to the selection of the northern or southern injection beam line. In addition to the computer mode for faraday cup current measurement via amplifier the mode preferred by operators using magnetoelectric instruments now is supported too.

The program for recording charge and mass spectra has been extended to accumulate spectrum of current depending on any magnet of the beam line. A fit procedure improving the representation has been integrated too.

Finally the building up of a consistent and comprehensive software documentation has begun. A new editor (TED) available at the PDP11 level especially supports standardisation offering interactive text macros. This editor and a macro library (TOPS-11) were introduced to offer hints for structured and modular programming at the PDP11 assembler level.

SIS - An Accelerator Facility for Relativistic Heavy Ions

K. Blasche, D. Böhne, B. Franczak, B. Franzke, B. Langenbeck
GSI Darmstadt

In 1979 the GSI accelerator program for the next decade was defined and summarized in a study report[1].
This program will comprise

- The UNILAC up-grading by insertion of two more Alvarez cavities in order to boost the maximum energies from about 10 to 25 MeV/u.

- A new injector linear accelerator at the front end of the UNILAC that will accelerate high beam currents of about 10 mA of singly or doubly charged ions up to about 0.1 MeV/u in a low duty cycle (1Hz).

- A large synchrotron dubbed SIS that will provide high current ion beams in the extremely broad energy range from 20 MeV/u up to 14 GeV/u.

Fig. 1 presents a survey of the proposed GSI accelerator facilities. The SIS will play the dominant role in the whole program. In Fig. 2 the performance of the SIS in terms of intensity and energy is shown. It is clearly demonstrated that the installation of the high current injector linac will improve the beam intensities of the SIS by factors between 100 and 1000 in the full energy range. In this way even in the low energy range where is the domain of cyclotrons the intensity performance of these accelerators is achieved. Before defining the GSI program the world wide scene of heavy ion accelerators was thoroughly reviewed. Today three lines of development can be distinguished.

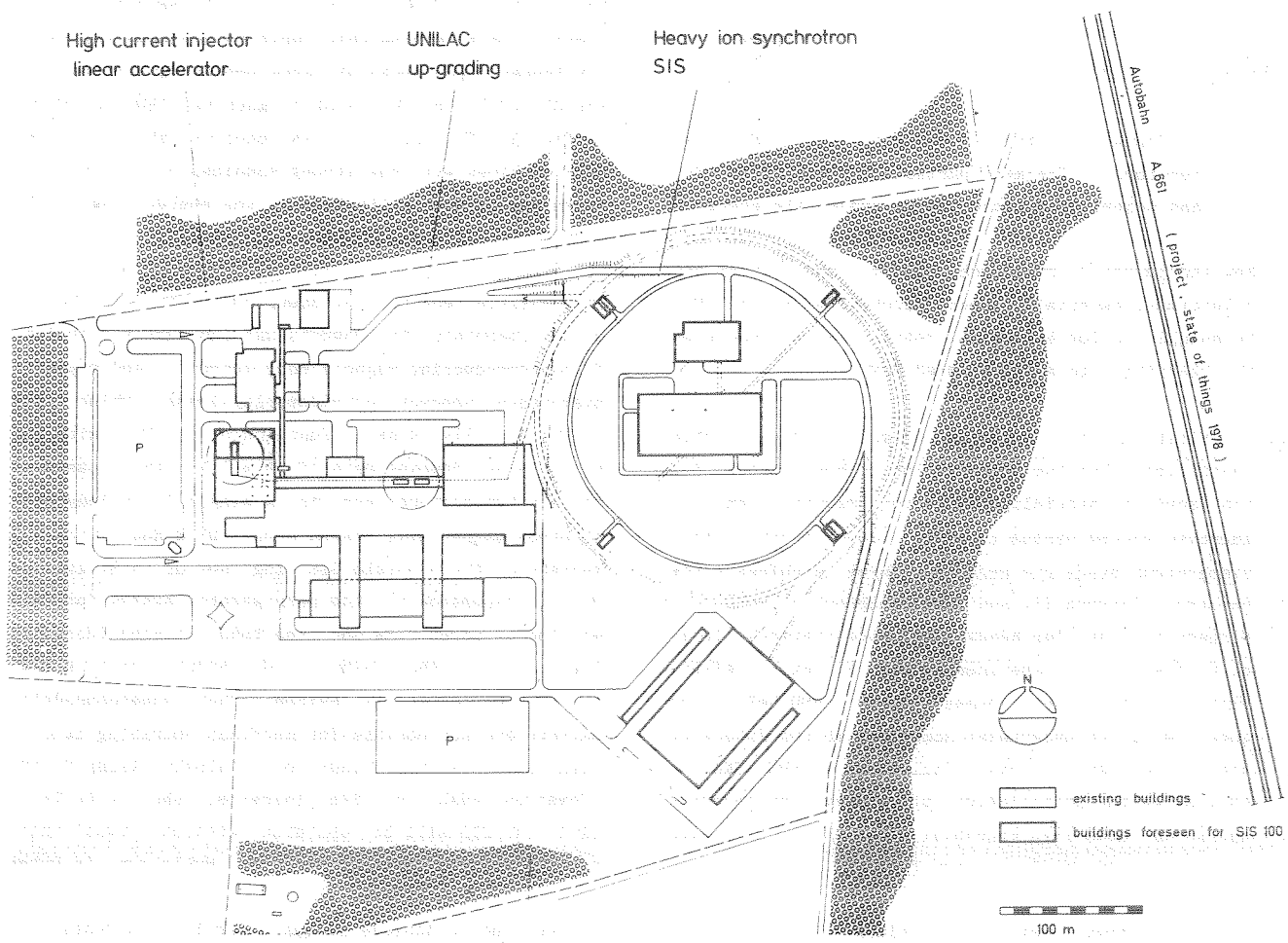


Fig. 1: The GSI accelerator program.

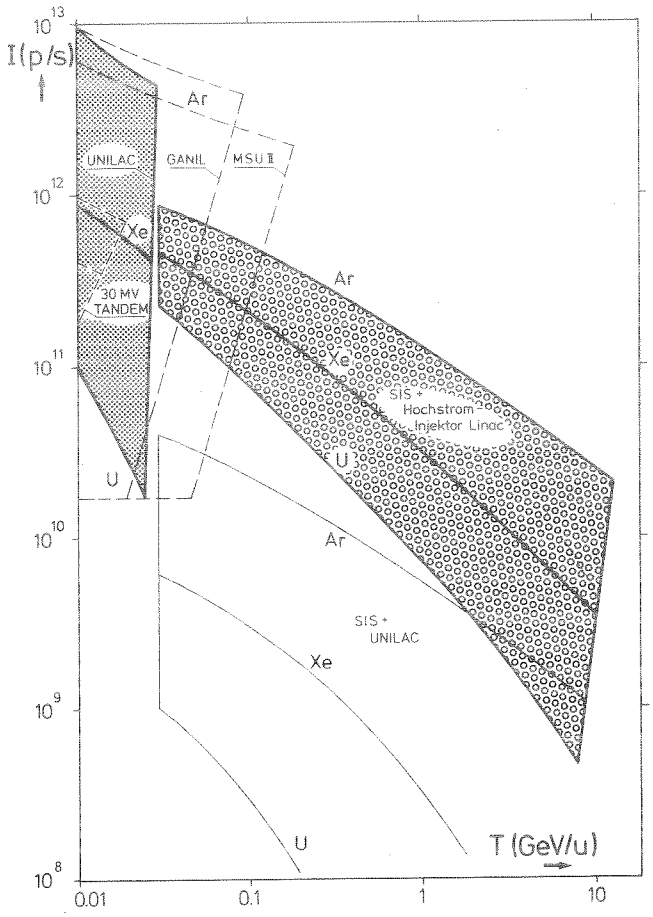


Fig. 2: Performance of the SIS and other heavy ion accelerators. The mean particle current of Ar, Xe, and U-ions is plotted versus projectile energy.

1. New and improved cyclotron, tandem, and linear accelerators, especially superconducting machines. For technical and for economical reasons maximum energies are restricted to a few hundred MeV/u.

2. Modification of existing high energy proton facilities. For the acceleration of heavy ions new ion sources, specialized injector machines and an improved vacuum system ($p = 10^{-10}$ Torr) in the first synchrotron stage are required. Three machines - the Bevatron, Saturne II, and the Synchrophasotron - are already in use for heavy ion acceleration. It is quite clear that experiments with extremely relativistic heavy ion beams - about 100 GeV/u or more - will be undertaken some day in the future at one of the large proton facilities - CERN, FNAL or BNL, since the installation of a heavy ion injector system is much less expensive than the construction of a very large dedicated new facility.

3. New high energy heavy ion accelerators are proposed for the energy range from 1 GeV/u to 20 GeV/u: the Numatron (Tokyo), SIS (Darmstadt), Venus (Berkeley), and the Nuklotron (Dubna). While the Numatron is a small synchrotron the other projected machines are all comparable in size to the CPS (CERN) or the AGS (Brookhaven).

At GSI the UNILAC is available as the first stage of a high energy heavy ion accelerator. Since the extension of the linear accelerator to energies of some 100 MeV/u as well as the construction of a heavy ion cyclotron are both expensive and energy consuming solutions, a synchrotron was preferred, which for a given maximum energy is less expensive, saves energy and delivers nevertheless comparable beam intensities when combined with a high current injector linac. The proposed maximum energy of 14 GeV/u is a significant step above the values of 2 and 3.5 GeV/u attained so far at the Bevalac and the Synchrophasotron. The SIS is planned as a strong focusing synchrotron with conventional magnets, whereas Venus is designed as a double ring colliding beam facility with superconducting magnets and the Nuklotron will make use of iron core magnets with superconducting coils. These differences need the following comments:

- A colliding beam facility operating at beam energies between 10 and 20 GeV/u will provide energies in the center of mass system that could be achieved for heavy ion target experiments at large proton facilities like the SPS (CERN) or the Isabelle machine (BNL) as shown in Fig. 3. Therefore it was concluded that colliding beam machines with the strong handicap of low reaction rates may be not attractive in the energy range up to 20 GeV/u.

- The possible reduction of power consumption in the SIS using superconducting magnets was thoroughly studied. In superconducting magnets eddy currents and magnetic hysteresis produce considerable losses which are plotted in Fig. 4 as a function of $\dot{B}$. Even with the rather slow ramping rate of $\dot{B} = 1$ T/s the losses at the 4 K temperature level in a single 1.2 m long synchrotron magnet will reach about 25 W and in the 130 magnets of the complete SIS ring sum up to 32 kW. The power consumption of the refrigerator system for this machine is about 2 MW and the total losses including the losses of the magnet power supply are more than 2.5 MW. Hence it is evident that superconducting magnets are appropriate for machines operating at constant field (storage rings) or at slowly rising fields (Tevatron, FNAL: 0.5 T/s; Isabelle, BNL: 0.02 T/s). Since the SIS will be operated without a small rapid cycling booster synchrotron (the Nuklotron in Dubna will get such a booster machine), a short ramping time is required to achieve adequate particle currents. It was therefore concluded that warm magnets are a good choice for this machine.

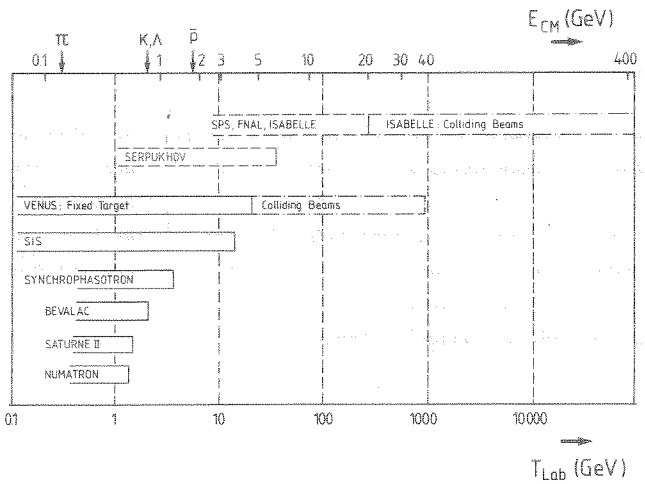


Fig. 3: Energy range of heavy ion accelerators and potential range of high energy proton machines for light ions with the charge to mass ratio q/A = 0.5.

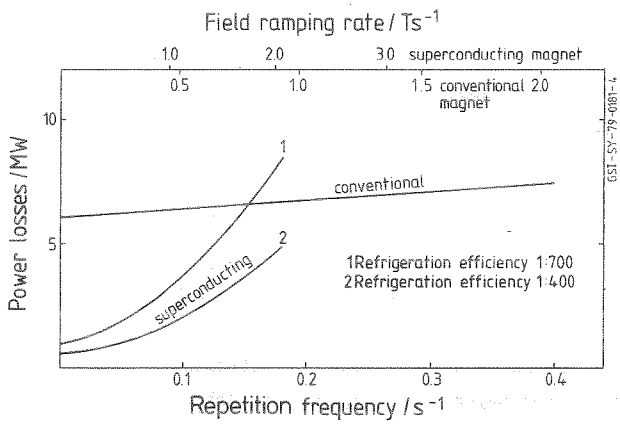


Fig. 4: Comparison of power losses in a superconducting and a normal conducting conventional bending magnet system for the SIS 100 (Extraction duty cycle D_E = 30 %).

In order to prepare the construction of the SIS three prototype programs for the design of the most important machine components are underway: the rf accelerating cavity with amplitude, frequency, and phase controls, a 6 m long section of the ultrahigh vacuum system operating at a pressure of 10^{-11} Torr and a magnet program with a prototype bending magnet, a pulsed power supply and the equipment for dynamic field measurements. These machine components play a prominent roll in the machine construction - they finally represent a financial volume of more than 50 MDM - and they need a long and careful technological development in order to optimize costs and performance. Since the tight time schedule of five years for the machine construction will leave no time for R & D activities, the prototype programs are an indispensable element in the present planning (Fig. 5). Finally one should emphasize that the time schedule for the machine construction was established on the basis of the personel development plan shown in Fig. 6. The validity of this time schedule strongly depends on the recruiting of the necessary personel.

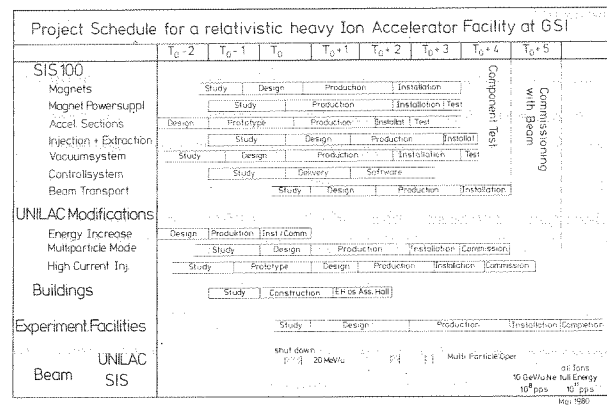


Fig. 5: Time schedule for the construction of SIS.

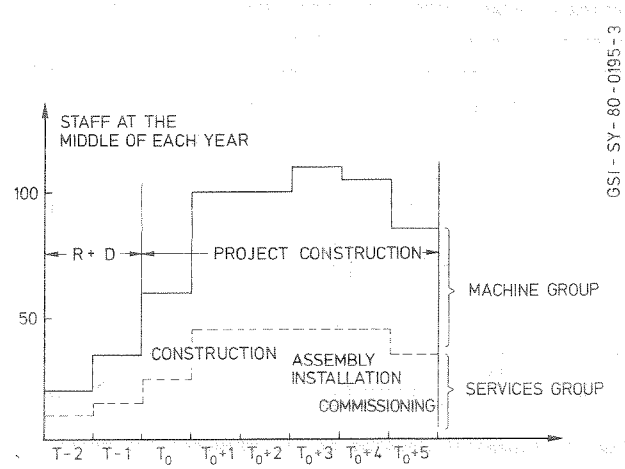


Fig. 6: Personel developmentplan for the construction of SIS.

[1] SIS - Eine Beschleunigeranlage für relativistische schwere Ionen.
GSI-Bericht 1979.

Injection System for the SIS

B. Franczak, R. Steiner
GSI Darmstadt

Contrary to proton injectors the UNILAC delivers long pulses (5 ms) at low currents. Therefore injection procedures with long injection times are necessary. Multi turn injection into the transverse (x,x')-phase space is limited according to the ratio of synchrotron acceptance to normalized beam emittance. The corresponding injection time for the SIS 100 is 150 μs. Therefore other more complicated procedures like storage into the longitudinal phase space, injection via stripper targets and intermediate storage rings were discussed.

At present only the least expensive multi turn injection is proposed (Fig. 1). In this scheme the ion beam is inflected into the synchrotron by inflector magnets IM and by an electrostatic septum ES. At the start of the injection process the closed orbit is displaced by kicker magnets KM and passes through the septum at a distance of about 80 mm from the unperturbed closed orbit. During the injection process the kicker field decreases steadily thus shifting the closed orbit into the centre of the vacuum chamber.

The optimum ramping time depends on the brightness distribution for the injected particle beams. Injection during a large number of turns would yield a high local brightness, since only the bright centre region of the injected beam is used. On the other hand a septum shadow will appear in the accumulated emittance of the beam after each turn thus reducing the average brightness.

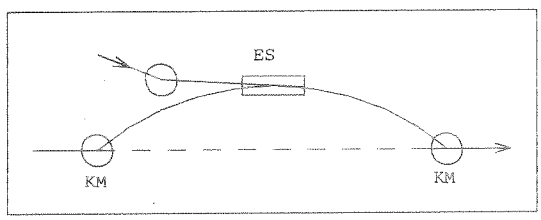


Fig. 1: Schematic drawing of the elements for multi turn injection.

Fig. 2 gives a plot of the closed orbit at the beginning of the injection process. Since the kicker magnets are seperated by about 1/2 of a betatron period, maximum displacement occurs in the septum while the closed orbit in the rest of the machine is scarcely perturbed.

The injection elements are designed for the maximum rigidities BxR=4.2 Tm and ExR=2.9x10^8 V (U^{41+} at 25 MeV/u). The kicker elements will be either small dipole magnets or correction coils on suitable bending magnets. When using kicker coils in dipole magnets they have to be installed at a distance of one betatron wavelength in order to compensate for the voltage that is induced into the main coils since in this case the required kicker fields have opposite signs. The kicker parameters are given in Table 1.

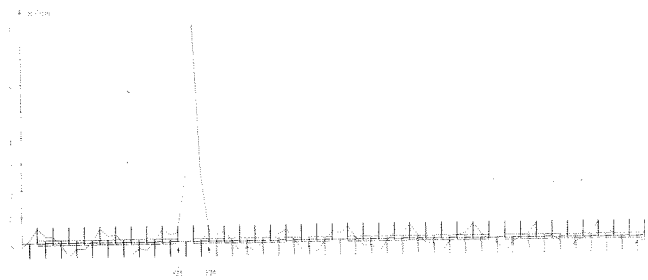


Fig. 2: Closed orbit at the start of injection for Q_H = 9.75

	dipole	correction coil
defelection angle	3 mrad	
magnet length	1	2.75 m
field	0.013	0.005 T
ramping rate	65	25 T/s
ampere turns	520	200 A

Table 1: Parameters for the injector kickers.

The parameters for the electrostatic septum and inflector magnet are listed in Table 2. The technical layout is shown in Fig. 3. The electrostatic septum has to be installed inside the UHV-chamber in an adjustable position. The magnetic septum can be mounted outside the UHV-system.

	ES		IM	
deflection angle	30	mrad	100	mrad
trajectory length	1.5	m	0.6	m
field	70	kV/cm	0.7	T
full aperture	30x55	mm^2	100x35	mm^2
septum width	< 0.1	mm	20	mm

Table 2: Parameters for the inflector system.



Fig. 3: Layout of the inflector system.

Extraction System for the SIS

B. Franczak, R. Steiner
GSI Darmstadt

Slow extraction

At present no definite decision concerning the maximum duty cycle required for experiments has been made. However, many experiments will need a duty cycle of at least 10 %. Therefore slow extraction during several thousand turns must be installed.

To employ the method of sextupole resonance extraction the betatron tunes must be shifted to $Q_H = 9.6\bar{6}$ or $Q_H = 11.3\bar{3}$ by adjustment of the machine quadrupoles and by additional correction quadrupoles. The extraction is controlled by sextupole magnets, which leave particles with small betatron amplitudes inside the stability region while particles outside the separatrix are driven with exponentially growing amplitudes towards the edge of the vacuum chamber (Fig. 1). The resonant particles are deflected out of the machine by means of an electrostatic septum and an additional magnetic septum a quarter betatron wavelength downstream. Increasing the strength of the sextupol magnets reduces the size of the stable region. Thus the whole beam can be extracted slowly. A control system has to stabilize the extracted current. The electrostatic septum is placed near a F quadrupole where the amplitude function has a maximum.

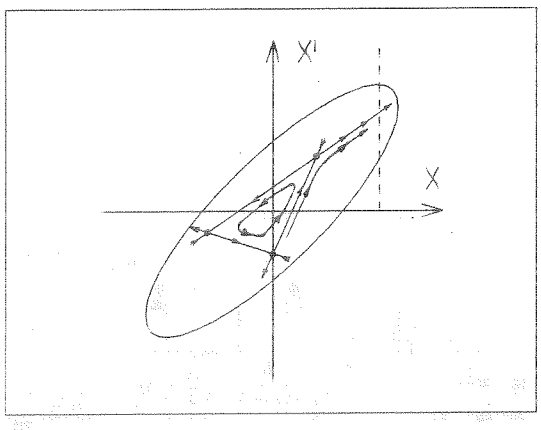


Fig. 1: Scheme of sextupole excited resonant extraction.
ellipse: horizontal acceptance
---> : movement of particles

Design parameters for these elements are listed below:

Bump kickers

deflection angle	2.5	mrad
ramping time	20-200	ms
magnetic rigidity	100	Txm
kick strengtn	0.25	Tm

Electrostatic septum

length	1	m
field (stregth)	100	kV/cm
deflection angle	0.33	mrad
voltage	300	kV

Magnetic septa	MS1	MS2/MS3	
septum width	5	22	mm
aperture	100x50	120x50	mm^2
length	1	1.5	m
magnetic field	0.5	1.2	T
current density	150	66	A/cm^2

Fast extraction

A fast extraction system will probably not be installed for initial operation of the SIS 100. However, space will be provided for an installation at a later time. For fast extraction the beam is first displaced just to the inner side of the leading septum magnet. A sudden kick then pushes the beam across the septum into the magnetic deflector field.

The fast kicker magnet can be installed a quarter wave length in front of the septum magnet 1 (Fig. 2). The kicker field will be raised in the time interval between two successive bunches in order to achieve extraction without particle losses. Assuming a bunch length of 180^o the rise time is about 70 ns at maximum energy. The required deflection angle is 1.1 mrad and the aperture 0.12x0.04 m^2. In the following table the kicker parameters are given:

number of kicker units	8	
length of one unit	0.3	m
magnetic field	0.046	T
current	1.5	kA
module voltage	33	kV

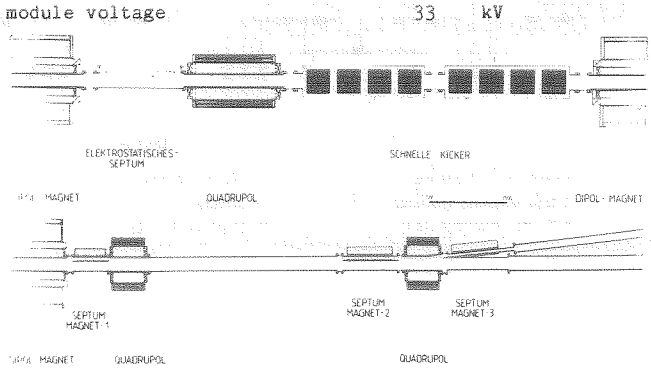


Fig. 2: Extraction for SIS 100.

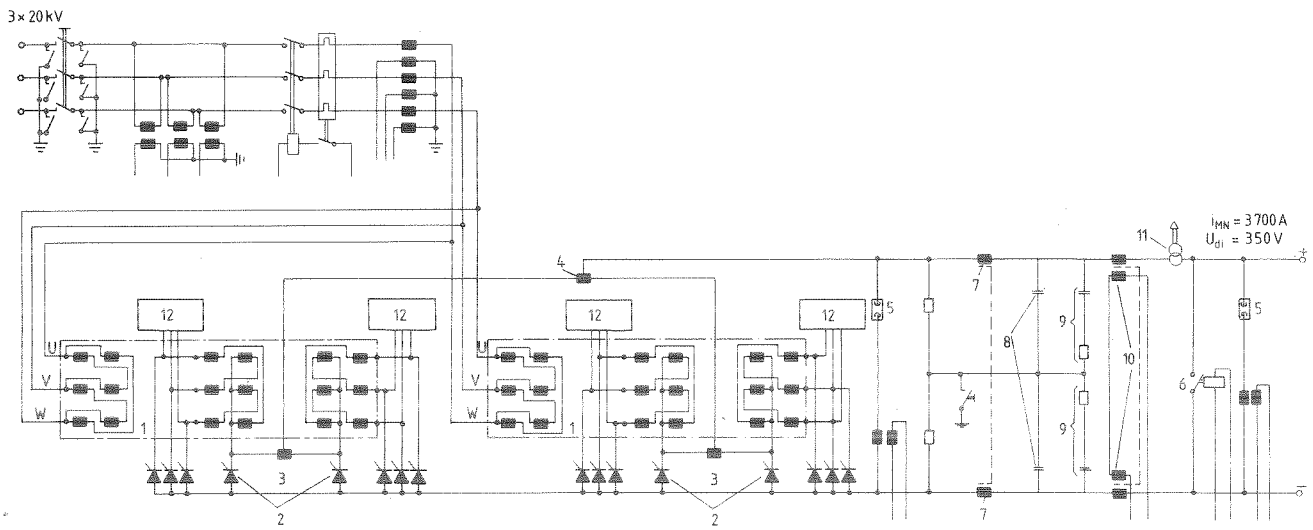
Test Power Supply for Two SIS Dipole Magnets

G. Breitenberger
GSI Darmstadt

A prototype dipole magnet for the SIS is under construction. For test measurements at this magnet a pulsed power supply is required. Furthermore, all 130 magnets of the SIS ring have to be compared in an acceptance test with one reference magnet. Therefore a power supply feeding two magnets in series was designed and specified. The design is based on the following parameters:

Inductance	L_M	= 38 mH
Resistance	R_M	= 12.4 mΩ
Nominal max. current	I_{MN}	= 3700 A
(pulsed and dc operation!)		
Min. current	I_{M1}	= 47 A
Maximum ripple		
(throughout the entire current range)		= $\pm$ 1x10^{-4}
Current rise time from I_{MI} to I_{MN}	t_{AN}	= 880 ms
Min. current rise time	t_{Amin}	= 590 ms

The transient periods before and after current rise will last 2x30 ms. With a linear current rise at t_{Amin} = 590 ms a maximum terminal voltage of 300 V is required; the equivalent open circuit voltage is 350 V. The test power supply will be connected to the existing 20 kV, 50 Hz supply mains which has a short circuit power of 234 MVA. A 12-pulse converter circuit is used in order to suppress the 5th and 7th harmonic frequencies on the mains current. Another advantage of the 12-pulse circuit is the smaller passive LC-filter and, consequently, the short transition times from constant to rising current and vice versa. Since the terminal voltage is rather low, a drainage coil circuitry will be used, which produce only half the thyristor losses of a bridge circuit. Moreover, free wheeling thyristors are used, which reduce the mains current by about 70 % when the test power supply is operated at the maximum constant current of 3700 A since the resistive voltage drop at maximum current is only 50 V. Two separated, identically constructed transformers with polygon circuitry on the primary side are used, while the secondary windings are connected in zigzag in order to guarantee the flux balance in the transformers with current carrying free-wheeling thyristors. The 12-puls dc-voltage with ripple frequencies of nx600 Hz is smoothed by means of a earth symmetrical passive LC-filter with attenuation network, which is followed by an active filter in order to reduce the ripple voltage at frequencies below 600 Hz.



Power part of the power supply

1 rectifier transformer
2 free wheeling thyristor
3 150 Hz - drainage coil
4 300 Hz - drainage coil
5 arrester
6 short circuit - breaker
7 smoothing choke
8 smoothing capacitor
9 attenuation
10 aktive filter
11 dc current transformer
12 ac attenuation

Amplitude, Frequency and Phase Control for the SIS Accelerating Cavities

M. Emmerling, K. Kaspar
GSI Darmstadt

The SIS accelerating cavities, which have to be tuned in the frequency range from 1 to 7.6 MHz, need precise amplitude, frequency and phase control. These controls are developed parallel with the cavity prototype program. In a first step amplitude and phase controls were built for a small test cavity that is used to study the properties of two ferrite disks by sweeping the frequency in real time. The second step will be the development of the controls for the synchrotron accelerating cavities where a higher precision will be required and cable lengths of more than 100 m have to be taken into account.

The amplitude control system makes use of a linear peak-type rectifier connected to the cavity gap by means of a broad band capacitive voltage divider in order to measure the amplitude independently of frequency. In the future it may be necessary to place the amplitude detector outside the synchrotron tunnel in order to protect it from radiation, which would require a different design. The rectified rf signal is compared to the reference signal in an AGC amplifier. The error signal is amplified, and adjusted to the frequency response of the regulation loop.

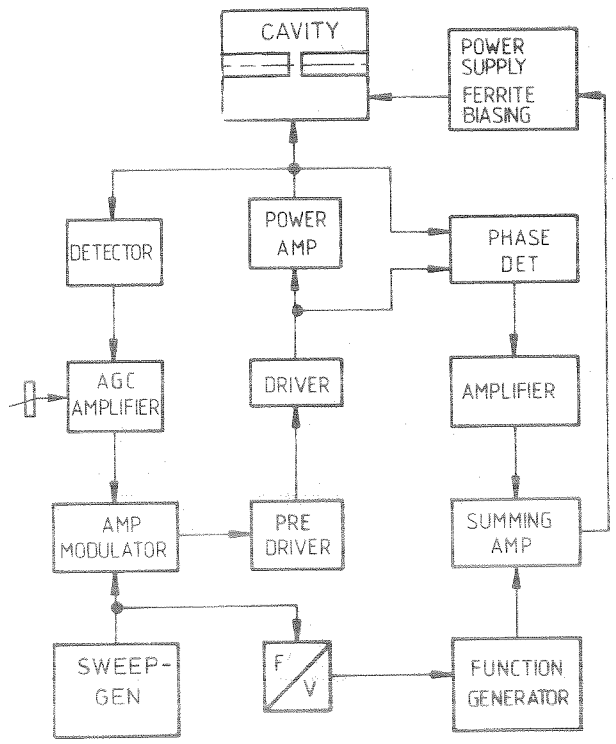
In the amplitude modulator - a balanced mixer followed by a broadband-amplifier-chip - the amplitude of the rf-signal is controlled.

The sweep generator also delivers the rf signal for the frequency and phase control loop. This signal passes via a buffer amplifier to a TTL 8:1 divider and a frequency to voltage converter where it is measured. This analog signal feeds a 5 step diode function generator that delivers the reference signal for the ferrite bias power supply. Without control loop only coarse control of the ferrite biasing current is possible. For precise control the phase difference between grid of the power amplifier and gap has to be regulated to 180°.

The final phase detector a digital circuit using ECL-components is being developed. In the meantime the phase is measured in a broadband 90° quadrature hybrid with two identical diodes at its outputs. The signal from the phase detector is used to correct the reference signal of the diode function generator.

So far the frequency/phase loop operates satisfactorily at small gap amplitudes. At high amplitudes a lot of difficulties arise. Due to resonances just above 7.6 MHz which are caused by the anode choke and other components of the power amplifier circuit harmonics of discrete frequencies in the range from 2.3 to 7.6 MHz disturb the rf current and consequently the ferrite biasing current. In addition, difficulties are caused by the variation of the loop gain with frequency which is due to a change of the cavity Q-value with frequency, the varying slope of the magnetization curve and the frequency dependent response of the phase discriminator.

In the test cavity where the Q-value variation is especially large the loop gain at 7.6 MHz is 4 times lower than at 1.5 MHz. Finally at high sweeping rates the tuning is disturbed at the lower turning point of the frequency range due to a special effect of high permeability ferrites. All these problems need further studies in order to improve the phase control loop.



Prototype of a Synchrotron Accelerating Station

K. Kaspar, M. Emmerling, A. Gasper
GSI Darmstadt

In the SIS synchrotron 12 ferrite-tuned accelerating cavities have to be installed around the machine in order to provide the rf accelerating voltage of 185 kV per revolution that is required for the 2 s machine cycle. To cover the energy ranges from 1.4 to 80 MeV/u respectively from 12 to 1400 MeV/u the frequency of the accelerating voltage has to be continuously swept from 1.0 to 7.6 MHz. Tuning ferrites that allow tuning over this broad frequency range use to have extremely high rf losses. So, about 50 kW of rf power have to be fed to each cavity to reach the needed accelerating voltage.

Fig. 1 shows a simplified cross-section of the cavity design chosen for the SIS. Two coaxial quarter-wave resonators are working in push-pull mode on one common accelerating gap. The resonators are each filled with a stack of ferrite rings interleaved with cooling discs. DC current windings around the ferrite stacks produce the dc magnetic bias field which controls the permeability of the ferrites and hence the resonant frequency of the cavity.

Many questions being of fundamental importance for the design of the cavities come from the ferrite material. There exists quite a series of phenomena which may seriously restrict the function of the accelerating system: non-linear ferrite behaviour, Q-loss-effect, time dependencies of the tuning characteristics, thermal instabilities etc. Part of these problems have been discussed in the 1978 annual report.

Most of these special effects do not show up in common commercial ferrite applications. The manufacturers themselves can not give enough support in measuring these effects. Which ferrite material may give the best results in a cavity, how can materials of different manufacturers be compared, where are principal material limitations, which are the actual data of each single ferrite ring, etc.? All these questions have to be answered by the designer of the cavity himself.

Considering the high number of cavities needed activities have been started about two years ago to develop the indispensable ferrite measuring equipment and to set up a prototype of one complete SIS accelerating station. A large portion of the planned devices could be assembled and put to work during the last year. Fig. 2 shows a photograph of the present state of the equipment.

The main part of the prototype station consists of a 150 kW power amplifier for the frequency range from 0.8 to 7.6 MHz. It has been described in the 1978 annual report. In the photograph only the 200 W predriver and the control unit of this amplifier are visible (right rack). The power amplifier itself is standing behind the racks, for lack of space and to insure the shortest rf-connection with the ferrite test-cavity standing in front. First difficulties with harmonic distortions of the output rf signal could be solved by moving the working point to class-A operation.

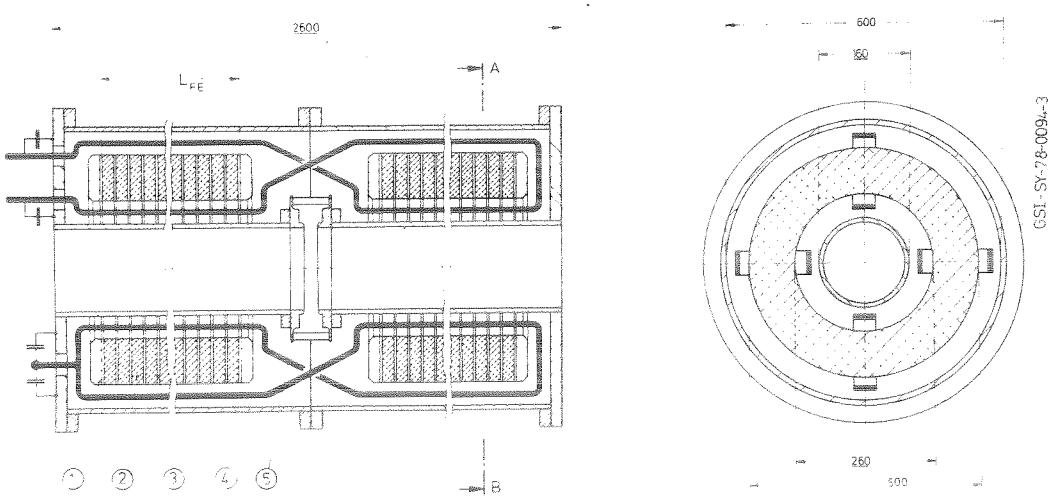


Fig. 1: Simplified cross-sections of the cavity design chosen for the SIS
(1) Ferrite support (2) Ferrite ring (3) Cooling disc
(4) Bias winding (5) Accelerating gap

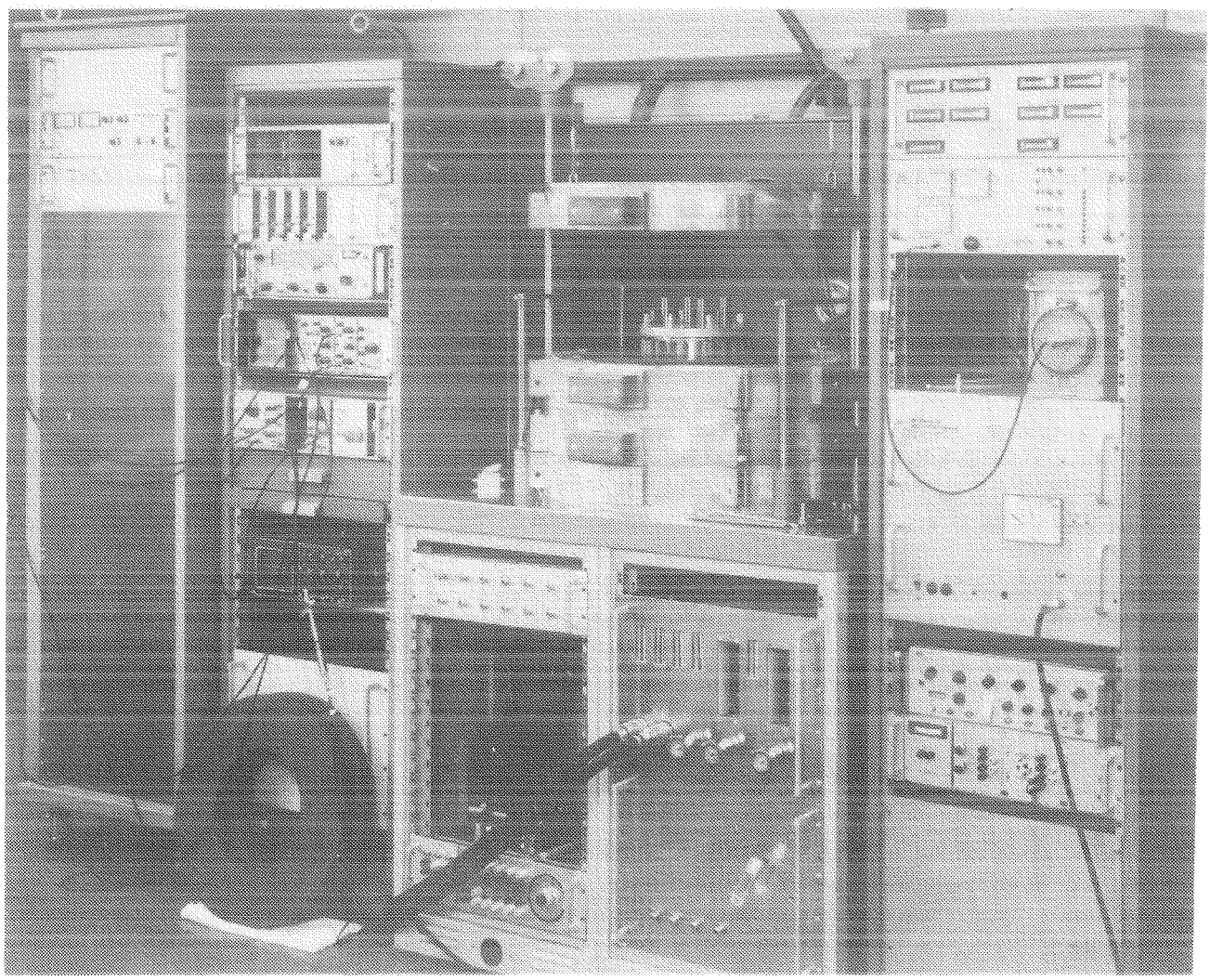


Fig. 2: View of the present state of the prototype accelerating station

The power amplifier is presently used to power the ferrite test-cavity standing between the racks. This cavity has been developped to measure the incremental permeability and the Q-value of individual ferrite rings. Details about the test-cavity are given in the next chapter. Since the ferrite data also depend on the rate of frequency tuning, it is intended to measure each ring under dynamic tuning conditions. The equipment used for amplitude and frequency control and the measuring equipment are assembled in the rack left of the test-cavity. The two ferrite rings standing in front of this rack give an impression of the size of these elements.

The rack standing on the left side contains the dc power supply for tuning the ferrites in the test-cavity and later in the prototype-cavity. It delivers up to 1200 A with about 5 V output voltage. The rise time from 0 to 1200 A is less than 1 ms in a resistive load.

The development of the prototype accelerating cavity has been stopped for several months in 1979. The reason was to wait for more reliable ferrite data from the measurements in the ferrite test-cavity. The construction of the cavity is being continued since fall 1979. The design will be very close to the principle shown in Fig. 1. However, six dc bias windings will be installed instead of four. This allows to realize and study various alternatives for the dc bias system.

In the beginning of 1980 all the ferrite rings and the cooling-discs for the prototype cavity have been ordered. It is expected that the delivery of these parts, the measurements on the individual ferrite rings and the assembly of the prototype cavity will be completed by about October 1980.

Test-Cavity for Single SIS 100 Ferrite Rings.

K. Kaspar, G. Stubenrauch
GSI Darmstadt

The permeability μ and the magnetic Q-value of a ferrite material are, besides the composition of the material, strongly dependent of the external conditions during production. Even with best control of all conditions relatively large tolerances of the data of each ferrite element have to be accepted. In an accelerating cavity (cf. last chapter) the aim is to obtain as close as possible the same frequency and tuning characteristics for the integral μ and Q-values of the two ferrite stacks. Ferrite rings with lower Q-values or other less favourable properties must be selected and assorted into less critical places in the ferrite stacks.

The ferrite test-cavity has been designed as a means of measuring the properties of individual ferrite rings under original conditions. A photograph of the test-cavity is shown in Fig. 2 of the previous chapter. The electrical equivalent circuit is explained in Fig. 1. The cross-section of the mechanical assembly is shown in Fig. 2.

Two ferrite rings and the indicated orientations of the rf and the dc windings are needed to exclude interference between the rf and the dc bias system. The two inductances L_1 and L_2 and the capacitors C_1 and C_2 are connected to form a parallel resonant circuit LC. The resonant frequency f_{HF} is set to the wanted values by means of C and the bias current I_{dc}. From a measurement of f_{HF}, C, the rf voltage U_{HF} and the rf current IH_F the wanted ferrite data $\mu(I_{DC},f_{HF},U_{HF})$ and $Q(I_{dc},f_{HF},U_{HF})$ can be calculated. The principle of measurements and their evaluation is standard for ferrites. What is special in the test-cavity is that close simulation of the working conditions inside an accelerating cavity is realized, as for rf and dc field-distribution, rf amplitude, rf power density, frequency tuning rate, and cooling of the ferrites. About 2 kW of rf power are needed for that purpose, more than 100 kW are available.

The measurements of U_{HF} are performed with oscilloscope probes or capacitive deviders. For the measurements of I_{HF} an rf current transformer has been developed. To avoid influences from the near bias-windings, the current transformer uses no ferrite core. The response of current versus frequency is surprisingly flat.

The test-cavity is presently used to study all kinds of properties of the few full size ferrite ring samples available. To obtain the desired high precision activities have been started to improve the rf contacts in the test-cavity and to reduce harmonic distortions of the I_{HF}-signal.

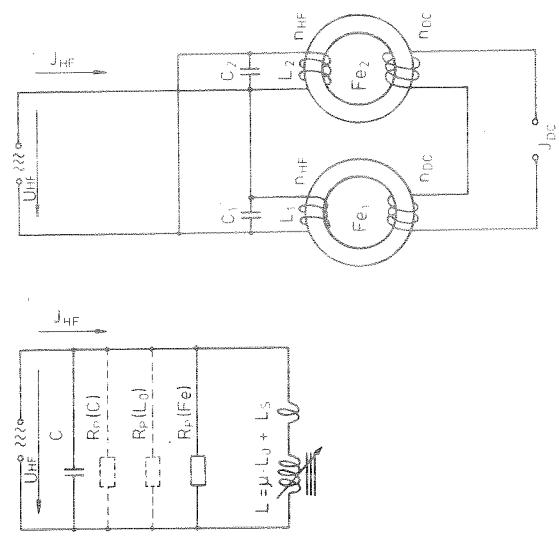


Fig. 1: Equivalent circuit of the test-cavity.

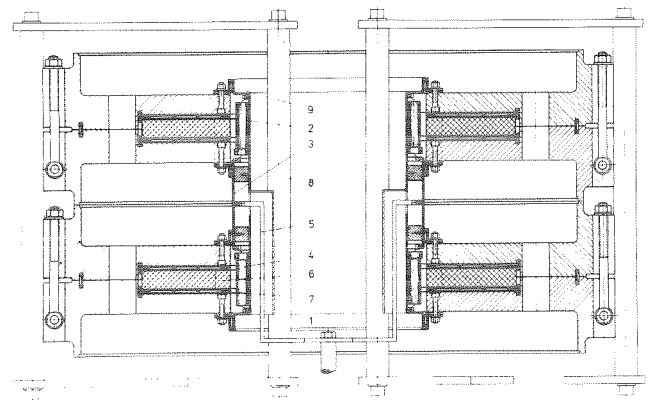


Fig. 2: Mechanical construction of the test-cavity.

1 Aluminium resonator-body	6 Ferrite ring
2 Connection ground-potential	7 Water-cooled discs
3 Connection HF-potential	8 Dc bias conductors
4 Capacitors	9 Contact springs
5 HF power lines	

When the about 800 ferrite rings for SIS 100 will be delivered each ring has to be measured individually in the test-cavity. An HP 9835A computer will be used to control and evaluate the measurements. The computer and all peripheral devices are already available and the software is being developed.

Charge Change Cross Sections for 1.4 MeV/u-Uranium in H_2 and N_2

B. Franzke
GSI Darmstadt

The wide range of extraction energies from 20 MeV/u up to 14 GeV/u is one of the most attractive features of the heavy ion synchrotron SIS[1]. Especially for energies below 100 MeV/u both low injection energy and low ionic charge state are required. Under these conditions the cross sections for change of ionic charge state by collisions between ions and residual gas molecules are very large, and, consequently, the average vacuum pressure in SIS has to be in the ultra-high vacuum range close to 1×10^{-11} mbar. Experimental cross section values for the worst case of U^{10+} at 1.4 MeV/u should help to improve calculations of the upper limit for the beam losses in SIS caused by charge changing processes[2].

With respect to the most abundant components of the residual gas spectrum in the UHV-range, H_2 and N_2 were selected for target molecules, N_2 representing also other heavier components as for instance O_2 or CO, which should deliver comparable cross sections.

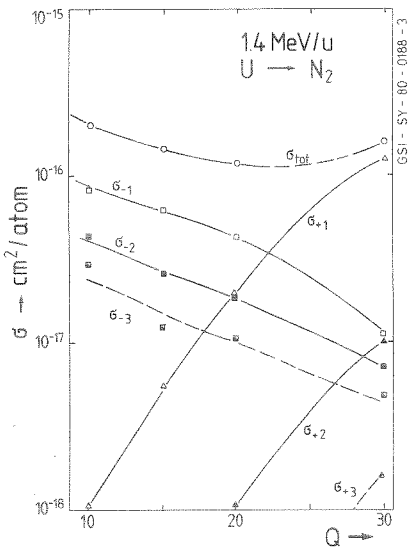


Fig. 1: Cross sections for electron capture, σ_{+n}, electron loss, σ_{-n}, and for change of charge state, σ_{tot}, of 1.4 MeV-Uranium in N_2 as functions of incident ionic charge state Q, n designing the number of electrons captured or removed in a single U - N_2 collision.

Charge state distributions formed under single collision condition in very thin targets (windowless gas cell) have been evaluated for cross section values. Fig. 1 illustrates the results for the systems U^Q in N_2, Q varying in the range +10 to +30. The cross sections for loss, σ_{-n}, where n designes the number of electrons removed from the ion in a single collision, decrease monotonously, whereas those for electron capture, σ_{+n}, increase very strongly with increasing incident charge state Q. The sum of all cross sections, σ_{tot}, passes through a minimum in the interval $20 < Q < 25$. A similar picture is found also for the systems U^Q in H_2 though the absolute cross section values as well as the fraction of multiple electron loss or capture processes are considerably lower.

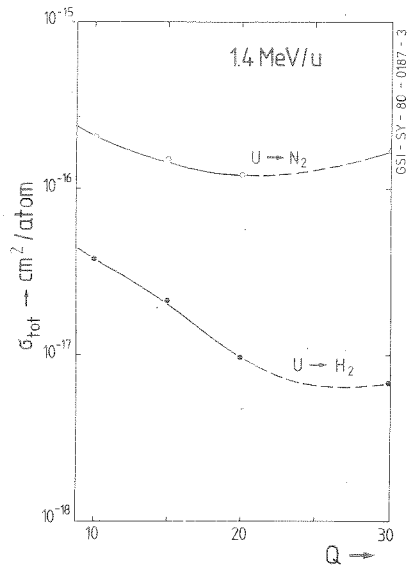


Fig. 2: Cross sections for change of charge state, σ_{tot}, of 1.4 MeV/u-Uranium in H_2 and N_2 as functions of incident ionic charge state Q.

In Fig. 2 the total cross sections, σ_{tot}, in H_2 and N_2 are plotted versus incident charge state Q. The ratio $R = \sigma_{tot}(N_2)/\sigma_{tot}(H_2)$ turnes out to be strongly dependent on Q, increasing from 5.3 at Q = +10 to 24.3 at Q = +30. In the latest measurements with U-ions at 10 MeV/u R-values between 66 for Q = +58 and 71 for Q = +68 have been found.

The experimental values for the system U in N_2 confirm the practical utility of the empirical cross section formula presented in the preceeding annual report[3].

[1] SIS/Eine Beschleunigeranlage für relativistische schwere Ionen, GSI-Darmstadt (1979).

[2] dto., p. C 47

[3] B. Franzke, W. Erb, GSI 79-11, 118(1979)

Test Program for an UHV-Section of the SIS

P. Finke, B. Franzke, A. Kritzer
GSI Darmstadt

There is a lot of experience with vacuum systems in the pressure range of 10^{-11} mbar especially in the ISR group at CERN. Nevertheless the new technique has to be introduced at GSI in order to provide a reliable vacuum system at moderate costs. As a first step in this direction we have decided to construct a test section of 9 m length containing all UHV-components of a half SIS focusing period (see Fig. 1):

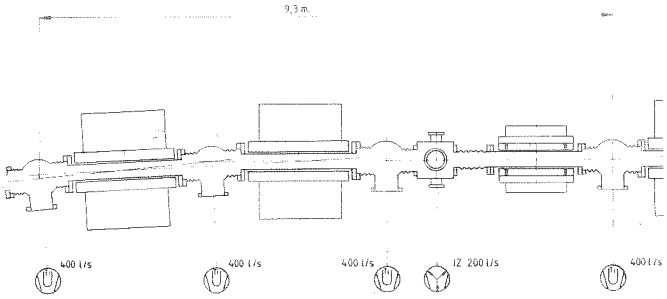


Fig. 1: UHV-prototype section.

The most important points of the test program will be the following:

1. Pretreatment of the stainless steel material used for chambers and flanges. At present glowing at 1100 °C in a vacuum furnace seems to be necessary to reduce outgassing rates.

2. Cleaning procedures for all UHV-components.

3. In situ-baking of UHV-systems: Dependance of total pressure and residual gas composition on temperature and duration of baking.

4. Test of UHV-components offered by industry:
   Pumps, metal-sealed valves and manometers for extreme low pressures.

5. Design of the UHV-system for SIS, concepts for operation, control and servicing.

Preliminary tests were carried out with short stainless steel tubes pumped by ion sputter pumps of the triode type. To obtain outgassing rates lower than 10^{-13} mbar ls^{-1} cm^{-2} all the material, as the pump body, the pumping elements, the tube and the flanges had been pretreated for one hour in a vacuum furnace at 1100 °C, to remove the hydrogen out of the bulk. As the material of the flanges must retain a sufficient hardness after this treatment, stainless steel 1.4429 seems to be a good compromise between price and mechanical properties.

The UHV teststand had an overall volume of 30 l and a surface of about 10^4 cm^2. The pumping speed installed was 100 l/s in the 10^{-10} mbar region. After a 24 h bakeout at 300 °C, an ultimate pressure of some 10^{-11} mbar could be reached. The measurement was done simultaneously by a modulated Bayard Alpart gauge and an extractor gauge. Mechanical forces coming from a temperature gradient in the flanges may cause leakage at the knifedges of the conflat sealings during bakeout. Therefore much care must been taken, to keep thermal gradients as low as possible in glow pretreated stainless steel during the heat up and cool down phase of the bakeout cycle.

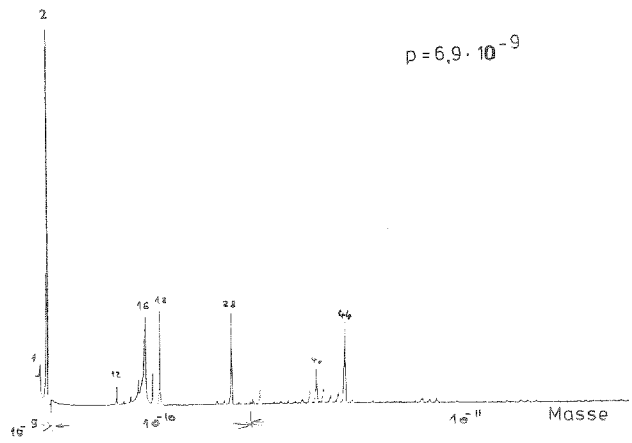


Fig. 2: Residual gas spektrum with variable gain of 10^{-9} - 10^{-11}.

Fig. 2 shows the spectrum of residual gas components in a 1.5 m long stainless steel chamber with ondulated, 0.4 mm thick walls. The hydrogen fraction of more than 90 % mainly diffuses out of the material which was not glowed before. The H_2-leakage can be reduced from about 1×10^{-12} mbar ls^{-1} cm^{-2} down to a value below 5×10^{-14} mbar ls^{-1} cm^{-2} by glowing the material at 1100 °C in the vacuum furnace [1].

[1] C. Benvenuti, CERN ISR Nr. Vienna 77
Production and measurement of extreme vacua.

RFQ Acceleration Structures

R. W. Müller
GSI Darmstadt

R.f. quadrupole (RFQ) structures materialize the ideas of several authors[1] to shape the accelerating r.f. fields in the gaps of a linac in such a manner that the transverse weakly defocusing effect of the accelerating and bunching fields is counterweighted by an alternating electric quadrupole gradient. About 1970, Kapchinskij and Teplyakov[2] made a new approach to this method, and since then it found growing interest and application in the low verlocity part of proton and deuton accelerators. For slow particles ($\beta < 1...5\ \%$) it offers the strongest technically possible focusing. Its application to heavy ion accelerators for extremely high currents (low energy part of a fusion ignitor) is therefore quite obvious. In a very favourable manner one can apply also the method of adiabatic bunching of a d.c. beam, without using a separate bunching device.

Application to very heavy ions in a low charge state, with its typically low working frequencies, 10 MHz or lower, demands for r.f. cavity designs which are different from those[2] used in the light ion case. Fig. 1 shows the cavity developped for this purpose[3], one cell of several cells which form an accelerator. In principle, it is a Wideroe type structure, optimized for having the best possible resonant restistance in the presence of a high capacitive load which is formed by the quadrupole system. A new feature is the nearly perfect flatness of the voltage distribution, and the good stability of the useful r.f. mode against geometric disturbations. In view of this stability a suspension device for the quad electrodes is used which recalls associations to drift tubes (fig. 2). This shape also contributes a little to a good "transit time factor" or accelerating potential amplitude at higher β, so that a mean effective acceleration voltage gradient of more than 0.5 MV/m can be reached. Details of these techniques are given in a GSI report[4], and have been established by model measurements and by numerical potential calculations in the meantime.

The theoretical models of the space charge effects limiting the ion beam current have been studied, partially extended, and evaluated. Mainly for checking them, but also to gain first experiences with RFQ structures, a proton model is built by a cooperation GSI-University of Frankfurt. It is a geometric 1:4 model of a 13.5 MHz high current injector conceived for UNILAC in the SIS injection mode[5]. Since all the voltages and currents are 1/100, and the r.f. powers 1/5000 of the original, the model will be of comparibly low cost. At the end of 1979, essential parts for the first cavity were ready, and the ion source was in a state of construction. The importance for the heavy ion ignited fusion technique is underlined by our planning a prototype accelerator for Xe^{1+} and Bi^{1+} ions, current of 50 to 200 mA, from a 350 kV injector, at a frequency of 6.8 MHz and an aperture of 4 cm. At still lower frequencies, and with higher r.f. voltage at a larger aperture, the currents might be even higher.

[1] Compiled by D. Boussard, in P. Lapostolle, A.L. Septier (ed.), Linear Accelerators. Amsterdam 1970, N.H. Publ. Co.

[2] I.M. Kapchinskij, V.A. Teplyakov, Prib. i Tekh. Eksp. 2 (1970), 19

[3] German patent application P 30 03 258.7.

[4] R.W. Müller, GSI report 79/7.

[5] Eine Beschleunigeranlage für schwere Ionen (SIS 100). GSI, May 1979, p.C 75.

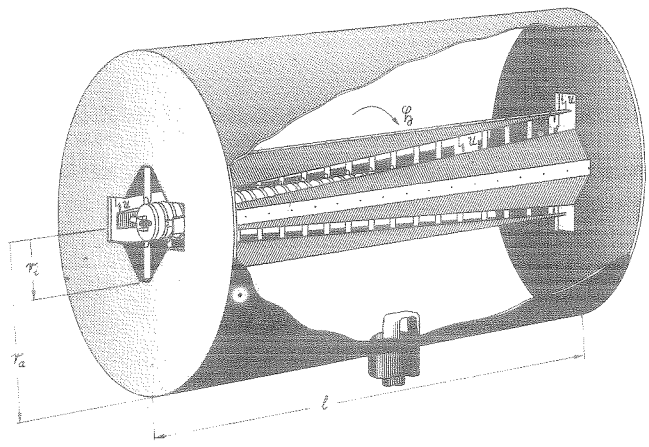


Fig. 1: RF Cavity for Heavy Ion RFQ Application

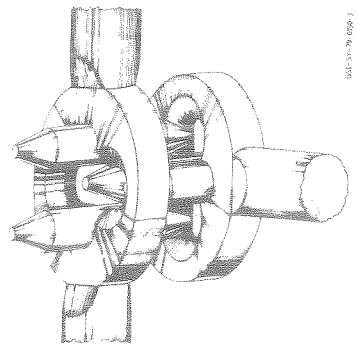


Fig. 2: RFQ Electrode Suspension

6. Annex

		PAGE
6.1	Scientific Activities Outside GSI	230
6.1.1	Publications	230
6.1.2	Conference Contributions	241
6.1.3	Seminars at other Instituts	254
6.1.4	Lectures and Courses	258
6.2	Scientific Activities Within GSI	259
6.2.1	Conferences and Seminars on Research Proposals	259
6.2.2	Seminars at GSI	260
6.2.3	GSI-Berichte (Reports)	263
6.2.4	Visiting Groups at GSI	264
6.3	Scientific Committees, Guests, and Staff	265
6.4	Author Index	268

6.1.1 Publications

R. Anholt, H.-H. Behncke, S. Hagmann, P. Armbruster, F. Folkmann and P.H. Mokler
K-Vacancy Production by 3.6 - 4.75- and 5.9 MeV/u ^{238}U Ions, Z. Physik A289, 349 (1979)

P. Armbruster and P. Kienle
Calibration of the Energy Transfer for Coulombionization by Heavy Ions, Z. Physik A291, 399 (1979)

S. Ayik
Dynamical Description of Dissipative Heavy-Ion Collisions in the Adiabatic Representation,
Z. Physik A292, 257 (1979)

H. Backe
Atomic Processes in Close Collisions of Very Heavy Ions with Atoms,
Trends in Physics, 4th General Conference of the European Physical Society, York, 25-29 Sept. 1978.
Ed. M.M. Woolfson. Bristol: Hilger, 1979, p. 445

H. Backe, F. Weik, P.A. Butler, V. Metag, J.B. Wilhelmy, D. Habs, G. Himmele and H.J. Specht
Direct Observation of Coulomb Fission of ^{238}U with ^{184}W Projectiles,
Phys. Rev. Letters 43, 1077 (1979)

H. Backe, E. Kankeleit
Positronenmessung bei SI Stößen, GSI-Nachrichten 11-79, 5 (1979)

A. Baran, A. Superson and K. Pomorski
New Estimates for the Parameters of the Modified Oscillator Potential of the Rare Earth Nuclei,
Accepted for Publication in Z. Physik A

A. Baran, K. Pomorski
New Modified Oscillator Potential for Nuclei in the Actinide Region,
Z. Physik A291, 175-178 (1979)

R. Bayer, J. Kowalski, R. Neumann, S. Noehte, H. Suhr, K. Winkler, G. zu Putlitz
Dye Laser Saturation Spectroscopy of the $2^3S_1 - 2^3P$ Transition in $^{6,7}Li^+$ Ions,
Z. Physik A292, 329 (1979)

H.-J. Becker, R. Brandt, H. Jungclas, T. Lund, D. Molzahn
A Low Background Spontaneous Fission Detection System, Nuclear Instr. and Methods 159, 75 (1979)

H.-J. Becker, T. Lund, R. Brandt
Upper Limits for the Production of Superheavy Elements in the Reaktion ^{136}Xe with $^{nat.}U$,
Radiochem. Acta 26, 15-19 (1979)

H.-H. Behncke, P. Armbruster, F. Folkmann, S. Hagmann, J.R. Macdonald and P.H. Mokler
Measurements of K-Shell Ionization with ^{132}Xe and ^{208}Pb Projectiles in the Energy Range of
1.4 - 5.9 MeV/u, Z. Physik A289, 333 (1979)

E. Bergmann, P. Bopp, J. Kowalski, F. Träger, G. zu Putlitz
Nuclear Charge Radius, Spin, Nuclear Moments of ^{45}Ca by Laserspectroscopy,
Z. Physik A292, 401 (1979)

M. Berlanger, A. Gobbi, F. Hanappe, U. Lynen, C. Ngô, A. Olmi, H. Sann, H. Stelzer, H. Richel and M.F. Rivet
Study of Fast Collective Mode in Deep Inelastic Reactions: Quantal Fluctuations,
Z. Physik A291, 133 (1979)

H.F. Beyer, R. Hippler and K.-H. Schartner
An Application of the Branching Ratio Method for Ion Impact Cross Section Measurements in the
Far Ultra-Violet, Z. Physik A289, 239 (1979)

H.F. Beyer, F. Folkmann and K.-H. Schartner
Few-electron States of Ne Produced by 1.4 MeV/u Heavy Ion Impact, J. de Physique 40, C1-17 (1979)

H.F. Beyer, R. Hippler and K.-H. Schartner
Multiple Ionization of Neon 2s- and 2p-Electrons Induced by Ion Atom Collisions,
Z. Physik A292, 353 (1979)

S. Bjørnholm
Kernstruktur bei hohen Drehimpulsen, Physikalische Blätter 34, 672 (1978)

R. Bock
Heavy Ion Collisions, Vol.1 (Editor), North Holland Publishing Company

J. Bonn, W. Klempt, R. Neugart, E.W. Otten and B. Schinzler
Hyperfine Structure and Isotope Shifts of Neutron-Rich $^{138-142}$Cs, Z. Physik A289, 227 (1979)

R. Brandt, P.A. Gottschalk, P. Vater
An Application of SSNTD to Nuclear Physics: Multiprong Events in Heavy Ion Reactions, due to Multiple Sequential Fission, Nuclear Instr. and Methods (in print)

R. Brandt, T. Lund, D. Molzahn, P. Vater H. Jungclas, A. Marinov (Marburg-Jerusalem)
An Application of SSNTD to Nuclear Physics: Search for Superheavy Elements,
Nuclear Instr. and Methods (in print)

R. Brandt
Overall Reviev of the Application of SSNTD in Nuclear Physics (Reviev),
Nuclear Instr. and Methods (in print)

R. Brandt
Gibt es überschwere Elemente?, UMSCHAU in Wissenschaft und Technik 79, 577-578 (1979)

R. Brandt. T. Lund, A. Marinov, D. Molzahn, G. Tress, P. Vater
Suche nach überschweren Elementen III: Heiße Salz-Sole Atlantis II (im Roten Meer),
GSI-Bericht 1978, GSI-79-11, S. 74

F. Busch, M.J. Canty, W. Pfeffer, B. Kohlmeyer, W. Schäfer, W.F.W. Schneider, H. Freiesleben, F. Pühlhofer
A Study of the Influence of Shell Effects in Nuclear Level Densities on the Decay of the Compound Nucleus ^{58}Ni, Z. Physik A290, 167 (1979)

M.J. Canty, P.A. Gottschalk, F. Pühlhofer
Shell Model Level Densities in Evaporation Calculations, Nuclear Physics A317, 495 (1979)

L.C. Carraz, G.T. Ewan, E. Hagberg, J.C. Hardy, B. Jonson, S. Mattson, H.L. Ravn, P. Tidemand-Petersson
A Precise Determination of the Excitation Energy of the Lowest T=3/2 State in ^{35}Ar,
Phys. Letters 85B, 212 (1979)

W. Cassing and H. Friedrich
A Quantal Description of DIC Including Radial Dissipation and Diffusion of Energy,
Contribution to the International Workshop VIII, Hirschegg, Austria, Jan.1980, (in press)

W. Cassing and H. Friedrich
On the Quantum Mechanical Description of Scattering by a Dissipative and Diffusive Scattering Centre, Z. Physik A291, 339 (1979)

W. Cassing and H. Friedrich
Quantal Fluctuations in Inelastic Heavy-Ion Collisions,
Contribution to the International Conference on Nuclear Physics, Berkeley, 1980 (to be published)

W. Cassing and H. Friedrich
Quantal Phenomena in the Double Differential Cross Section $d^2\sigma/d\theta dE$ for DIC, (to be published 1980)

M. Dakowski, P. Doll, A. Gobbi, G. Rudolf, H. Sann, R. Bock, U. Lynen and A. Olmi
Structure Effects in Dissipative Collisions, Phys. Letters 90B, 379 (1980)

C. Détraz, D. Guillemaud, G. Huber, R. Klapisch, M. Langevin, F. Naulin, C. Thibault, L.C. Carraz, F. Touchard
Beta Decay of $^{27-32}$Na and their Descendants, Phys. Rev. C19, 164 (1979)

M. Diebel and U. Mosel
Inclusion of Pairing into Strutinsky-type Cranking Calculations, Z. Physik A293, 53 (1979)

H.D. Dohmann and R. Mann
High Precision Measurement of the Lifetime of the $^3P_2$ and $^4P_{5/2}$-States in $Ar^{16+}$and Ar^{15+},
J. de Physique 40, C1-218 (1979)

H.D. Dohmann and R. Mann
Measurement of the Lifetime of the $^3P_2$ and $^4P_{5/2}$-States in Ar^{16+} and Ar^{15+},
Z. Physik A291, 15 (1979)

K. Dorenburg, M. Gladisch, G. zu Putlitz
Hyperfine Structure Density Shift Coefficients for K, Rb and Cs at High Buffer Gas Densities,
Z. Physik A289, 145 (1979)

K. Dorenburg, M. Gladisch, D. Herlach, W. Mansel, H. Metz, H. Orth, G. zu Putlitz, A. Seeger, W. Wahl, M. Wigand
Trapping by Vacancies and Mobility of Positive Muons in Neutron-Irradiated Aluminium, Z. Physik B31, 165 (1978)

B. Eichler, H. Gäggeler-Koch and H. Gäggeler
Thermochromatography of Carrier-free Elements: Polonium in Copper Columns, Radiochem. Acta 26, 193 (1979)

H. Emling
B(E2)-Values of High Spin States in ^{158}Dy, in Interacting Bosons in Nuclear Physics, ed. by F. Iachello, Plenum Publ. Company, 1979

M. Epherre, G. Audi, C. Thibault, R. Klapisch, G. Huber, F. Touchard, W. Wollnik
Direct Measurements of the Masses of Rubidium and Cesium Isotopes far from Stability, Phys. Rev. C19, 1504 (1979)

H. Essel, K. Hartel, W. Henning, P. Kienle, H.J. Körner, K.E. Rehm, P. Sperr, W. Wagner, H. Spieler
Charge and Mass Transfer in the Reaction ^{136}Xe + ^{208}Pb at Energies Close to the Coulomb Barrier, Z. Physik A289, 265 (1979)

H. Essel, K. Hartel, P. Kienle, H.J. Körner, K.E. Rehm, P. Sperr, W. Wagner
Neutron Rich Nucleon Flow in Central Heavy Ion Collisions, Phys. Letters 81B, 161 (1979)

R.A. Esterlund, P. Patzelt, U. Reus, A.M. Habbestad Wätzig, W. Wätzig and W. Westmeier
Determination of Mass Yields and Angular Distributions at Various Bombarding Energies for the Systems ^{132}Xe + nat Fe and ^{86}Kr + ^{103}Rh, GSI-Report, GSI-79-11, p. 19 (1979)

R.A. Esterlund, W. Westmeier, A.M. Habbestad Wätzig, U. Reus and P. Patzelt
Mass Yields from the System ^{132}Xe + nat Fe at E_{lab} < 940 MeV, Verhandl. DPG (VI), 14, 747 (1979), Physik Verlag Weinheim, 1979

G.T. Ewan, E. Hagberg, P.G. Hansen, B. Jonson, S. Mattsson, G. Nyman, E. Roeckl, D. Schardt, P. Tidemand-Petersson
Ratios of Beta-Delayed Particle Branches and the Role of the Fluctuation Function, Phys. Letters 84B, 173 (1979)

Y. Eyal, G. Rudolf, I. Rode and H. Stelzer
Evidence for Statistical Equilibrium of the Fragment Isobaric Distributions in Strongly Damped Collisions of ^{86}Kr with ^{166}Er, Phys. Rev. Letters 42/1, 826 (1979)

Y. Eyal, A. Gavron, I. Tserruya, Z. Fraenkel, Y. Eisen, S. Wald, R. Bass, G.R. Gould, G. Kreyling, R. Renfordt, K. Stelzer, R. Zitzmann, A. Gobbi, U. Lynen, H. Stelzer, I. Rode and R. Bock
Neutron Emission in Deep Inelastic Collisions Induced by ^{86}Kr on ^{166}Er at 5.7, 7.0 and 7.9 MeV/n Phys. Rev. 21 1377 (1980)

R. Faß, P. Lemmertz, H. Wollnik, D. Schardt, K. Wien, D. Hirdes, H. Jungclas, G.M. Gowdy, R. Kirchner, O. Klepper, W. Reisdorf, E. Roeckl, P. Tidemand-Petersson
Suche nach neutronenarmen Thallium-Isotopen, GSI-Bericht, GSI-79-11, S. 66

W. Faust, P. Armbruster, S. Hofmann, G. Münzenberg, H. Ewald and K. Güttner
Atomic Collision Induced Projectile Excitation - Its Application to Identification of Heavy Ion Fusion Products, Journal of Radioanalytical Chemistry, 55, 175 (1979)

W. Faust, G. Münzenberg, S. Hofmann, W. Reisdorf, K.-H. Schmidt, P. Armbruster and K. Güttner
The Efficiency of the Velocity Filter SHIP for Unslowed Evaporation Residues, Nuclear Instr. and Methods 166, 397 (1979)

H. Ferber, H. Folger, H. Kasten, G.K. Wolf, W.J. Lorenz, H. Schweickert, H. Folger
The Influence of Ion Implantation on the Corrosion Behaviour of Iron in Acid Solution, Corr. Science 20, 117 (1980)

G. Fiedler, U. Steinhauser, T. Rautenberg, R. Haag and P.A. Gottschalk
Glass Detectors for Heavy Ions, Nuclear Instr. and Methods (in print) spring 1980

B.E. Fischer and R. Spohr
Heavy Ion Microlithography - A New Tool to Generate and Investigate Submicroscopic Structures, Nuclear Instr. and Methods 168, 241-246 (1980)

J. Fleckner, U. Mosel, P. Ring and H.-J. Mang
Self-consistent Calculation of Rotational States in the Rare Earth Region with an Effective Ground State Interaction, Nuclear Physics A331, 288 (1979)

H. Folger and U. Richter
Explosively Clad Uranium Targets, Nuclear Instr. and Methods 167, 85 (1979)

G.N. Fowler, N. Stelte and R.M. Weiner
Condensates and Bose-Einstein Correlations, Nuclear Physics A319, 349 (1979)

G. Franz, J.V. Kratz, W. Brüchle, H. Folger, B. Haefner
Sub-Coulomb Transfer and Fission in Collisions of ^{129}Xe, ^{132}Xe and ^{136}Xe with ^{238}U,
Z. Physik A291, 167 (1979)

H. Freiesleben, K.D. Hildenbrand, F. Pühlhofer, W.F.W. Schneider, R. Bock, D. v.Harrach and H.J. Specht
The Reaction ^{238}U + ^{238}U at 7.42 MeV/u, Z. Physik A292, 171 (1979)

E.M. Friedländer and R.M. Weiner
Evidence from Very Large Transverse Momenta of a Change with Temperature of Velocity of Sound in Hadronic Matter, Phys. Rev. Letters 43, 15 (1979)

H. Frischkorn, K.O. Groeneveld, S. Schumann, R. Latz, G. Reichhardt, J. Schader, R. Mann and W. Kronast
Possible Evidence for Heavy Ion Induced Collective Electron Emission from Solids,
Phys. Letters 76A 155 (1980)

H. Gäggeler, A.S. Iljinov, G.S. Popeko, W. Seidel, G.M. Ter-Akopian and S.P. Tretyakova
A Study of Fusion Reactions Between $^{206,207}Pb$ Nuclei and ^{40}Ar Ions Near the Coulomb Barrier,
Z. Physik A289, 415 (1979)

H. Gäggeler, H. Ahrens, N. Trautmann, M. Zendel, D. Hirdes, H. Jungclas, E. Georg, P. Lemmertz
Kontinuierliche Abtrennung des Quecksilbers in der Gasphase, GSI-Bericht, GSI-79-11, S. 156

M. Gladisch, D. Herlach, H. Metz, H. Orth, G. zu Putlitz, A. Seeger, H. Teichler, W. Wahl and M. Wigand
Muon Spin Rotation in Superconductors, Hyperfine Interactions 6, 109 (1979)

P. Glässel, D. v.Harrach, Y. Civelekoglu, R. Männer, H.J. Specht, J.B. Wilhelmy, H. Freiesleben, K.D. Hildenbrand
Three-Particle Exclusive Measurements of the Reactions ^{238}U + ^{238}U and ^{238}U + ^{246}Cm,
Phys. Rev. Letters 43, 1483 (1979)

A. Gobbi and W. Nörenberg
Dissipative Collisions, in 'Heavy Ion Collisions' Vol.2, ed. by R. Bock, North Holland Publishing Company, Amsterdam

P.A. Gottschalk, P. Vater, H.J. Becker, R. Brandt, G. Grawert, G. Fiedler, R. Haag and T. Rautenberg
Direct Evidence for Multiple Sequential Fission in the Interaction of ^{208}Pb and ^{238}U with Uranium,
Phys. Rev. Letters 42, 359 (1979)

K.O. Groeneveld
Molecular Break-Up in Heavy Ion Collisions, IEEE Trans. Nucl. Sci NS26, 1033 (1979)

K.O. Groeneveld, H.J. Frischkorn, S.Schumann D. Gemmell, P.J. Cooney, E.P. Kanter, W.J. Pietsch
The Structure of Molecular Ions Studied with Fast (MeV) Heavy Projectiles,
Proceedings of the XIV. European Conference on Molecular Spectroscopy (EUCMOS)
Frankfurt/M 1979, p. 19

E. Grosse
Determination of B(E2)-Values between High Spin States from Coulomb Excitation and (HI,xn)-Reactions,
Proc. of the Argonne Conference on High Spin Phenomena, Argonne Nat. Lab. 1979, ANL/PHY-79-4

D. Habs, F.S. Stephens and R.M. Diamond
A Proposal for a Crystal-Ball Detector System, Lawrence Berkeley Lab. Report Publ. - 5020

E. Hagberg, P.G. Hansen, P. Hornshøj, B. Jonson, S. Mattsson, P. Tidemand-Petersson
Alphy Decay of Neutron-Deficient Mercury Isotopes and their Daughters,
Nuclear Physics A318, 29 (1979)

E. Hagberg, J.C. Hardy, B. Jonson, S. Mattsson, P. Tidemand-Petersson
The Superallowed Decay of ^{35}Ar: A Persistent Anomaly, Nuclear Physics A313, 276 (1979)

S. Hagmann, P. Armbruster, G. Kraft, P.H. Mokler and H.J. Stein
Inner-Shell X-Ray Production in Adiabatic Iodine - Z_2 Collisions with $Z_1+Z_2>100$,
Z. Physik A290, 25 (1979)

D. Hahn, G. Terlecki and Werner Scheid
Theory of Molecular Collective Excitation in the Scattering of Identical Nuclei,
Nuclear Physics A325, 283-304 (1979)

L. Handschug, H. Backe, H. Bokemeyer
A Kinematic Doppler Correction Method for High Resolution In-Beam Conversion Electron Spectroscopy after (HI,xn)-Reactions, Nuclear Instr. and Methods 161, 117 (1979)

D. v.Harrach, P. Gläßsel, Y. Civelekoglu, R. Männer and H.J. Specht
Angular Momentum Transfer in Deeply Inelastic Collisions from Exclusive Sequential-Fission Experiments, Phys. Rev. Letters 42, 1728 (1979)

D. v.Harrach and H.J. Specht
A Square Meter Position Sensitive Parallel Plate Detector for Heavy Ions,
Nuclear Instr. and Methods 164, 477 (1979)

H. Hartung and B. Fricke
Prediction of the Azimuth Angle Dependence of the Quasimolecular Anisotropy in Heavy Ion Collision,
Physical Letters 71A, 335 (1979)

H. Hartung, B. Fricke, T. Morović, W.-D. Sepp and A. Rosén
Interpretation of the Anisotropy of M MO Radiation in Slow I on Au Collisions,
J. de Physique B12, 2193 (1979)

U. Heinz, W. Greiner and W. Scheid
Equation of State for Hot Nuclear Matter, J. de Physique G Nuclear Physics Vol.5, No.10, 1383-1404 (1979)

H. Heitmann, P. Hansen, K. Witter, R. Spohr
Influence of Nuclear Tracks on the Coercivity of Single Crystalline $(Gd,Bi)_3$ $(Fe,Ga)_5$ O_{12} LPE Garnet Films, J. Magn. Magn. Mat. 10, 97-99 (1979)

D. Herlach, W. Decker, M. Gladisch, W. Mansel, H. Metz, H. Orth, G. zu Putlitz, A. Seeger, W. Wahl, M. Wigand
The Investigation of Defects in Neutron-Irridated Monocrystalline Al and Nb with Positive Muons,
Proc. 5th International Conference Positron Annihilation, p. 767 (Japan 1979)

D. Herlach, W. Decker, M. Gladisch, W. Mansel, H. Metz, H. Orth, G. zu Putlitz, A. Seeger, W. Wahl, M. Wigand
The Study of Defects with Positive Muons in Neutron-Irridated Single Crystals of Al and Nb,
Hyperfine Interactions 6, 323 (1979)

D.L. Hillis, J.D. Garrett, O. Christensen, B. Fernandez, G.B. Hagemann, B. Herskind, B.B. Back and F. Folkmann
Gamma-Ray Multiplicity Studies for ^{40}Ar and ^{86}Kr Induced Reactions leading to Er Compound Nuclei at Limiting Angular Momenta, Nuclear Physics A325, 216 (1979)

D. Hirdes, H. Jungclas, T. Lund, D. Molzahn, R. Brandt
On the Evidence of High-Energy Alpha Emitters (E>10.6 MeV) in Monazite,
Le Journal de Physique-Lettres 40, L-97 (1979)

D. Hirdes, H. Jungclas, R. Brandt, P. Lemmertz, R. Faß, H. Wollnik
Suche nach Spontanspaltern in der Reaktion nat.U + ^{238}U,
GSI-Bericht 1978 (Marburg-Gießen Gas-Jet Kollaboration), GSI-79-11, S. 71

S. Hofmann, W. Faust, G. Münzenberg, W. Reisdorf, P. Armbruster, K. Güttner and H. Ewald
Alpha Decay Studies of Very Neutron Deficient Isotopes of Hf, Ta, W and Re,
Z. Physik A291, 53 (1979)

A.V. Ignatyuk, I.N. Mikhailov, L.H. Molina, R.G. Nazmitdinov, K. Pomorski
The Shape of the Heated Fast-Rotating Nuclei Reports of JINR, Dubna, USSR, No. P4-12398 and P4-12399, submitted to Nuclear Physics A

E. Kankeleit
Positrons from Heavy Ion Collisions, Nuclear Interactions, Conference Canberra, 28 Aug.-1. Sept. 1978. Ed. by B.A. Robson, Canberra, Austr. Acad. Sci., Berlin, Heidelberg, New York: Springer 1979, p. 306 (Lecture Notes in Physics 92)

E.P. Kanter, P.J. Cooney, D.S. Gemmell, K.O. Groeneveld, W.J. Pietsch, A.J. Ratkowske, Z. Vager, B.J. Zabransky
The Role of Excited Electronic States in the Interaction of Fast (MeV) Molecular Ions with Solids and Gases, Phys. Rev. A20, 834-854 (1979)

H.A. Khan, K. Raschid, R. Akbar, G. Hussain, P. Vater, P.A. Gottschalk, R. Brandt (PINSTECH-Marburg Kollaboration)
First Indication of Double Sequential Fission in the Interaction (7.4 MeV/u ^{208}Pb + ^{208}Pb), GSI-Bericht 1978, GSI-79-11, S. 33

H.A. Khan, K. Raschid, R. Akbar, G. Hussain, P. Vater, P.A. Gottschalk, R. Brandt (PINSTECH-Marburg)
First Indication of Multiple Sequential Fission in the Interaction of 7.38 MeV/nucleon Pb on Pb, Nuclear Instr. and Methods (in print)

H.A. Khan, P. Vater, R. Brandt,
Multiprong Fission Events Produced by 1477 MeV ^{208}Pb in Natural Uranium, Nuclear Tracks (in print)

H.A. Khan, G. Tress, P. Vater, R. Brandt
Some Registration Properties of Muscovite Mica Track Detectors Used in Heavy Ion Reaction Studies, Nuclear Tracks (submitted to)

J. Kirsch, W. Betz, B. Müller, J. Reinhardt, G. Soff
K-MO-Radiation in Heavy Ion Collisions, Abstracts of Invited and Contributed Papers, The VIth International Seminar on Ion-Atom Collisions, Tokai-mura, Japan, 1979, p. 79

J. Kirsch, W. Betz, J. Reinhardt, B. Müller, W. Greiner, G. Soff
The Impact Paramater Dependence of the Pb + Pb K-MO Spectrum, Z. Physik A292, 227 (1979)

J. Kirsch, W. Betz, B. Müller, W. Greiner, G. Soff
Theory of Quasimolecular Radiative Phenomena in Heavy Ion Collisions, Proceedings of the XVIIth International Winter Meeting on Nuclear Physics, Bormio, Italy, 1979, p. 95

W. Klempt, J. Bonn and R. Neugart
Nuclear Moments and Charge Radii of Neutron-Rich Rb Isotopes by Fast Beam Laser Spectroscopy, Physical Letters 82B, 47 (1979)

U. Klingbeil, J. Kowalski, F. Träger, H.B. Wiegemann, G. zu Putlitz
Atomic Beam Saturation and Resonance Fluorescence Spectroscopy in the Weak Calcium Intercombination Line, Sov. Journ. Quant. El. 5, 1716 (1978)

U. Klingbeil, J. Kowalski, F. Träger, H.B. Wiegemann, G. zu Putlitz
Isotope Shift and Hyperfine Structure of ^{43}Ca by Laser Spectroscopy, Z. Physik A290, 143 (1979)

U. Klingbeil, J. Kowalski, F. Träger, H.B. Wiegemann, G. zu Putlitz
Saturation-Dips in the Weak Calcium Intercombination Line, Appl. Phys. 17, 199 (1978)

J. Kowalski, R. Neumann, H. Suhr, K. Winkler, G. zu Putlitz
Doppler-Free Two-Photon Laser Spectroscopy in Lithium, Sov. Journ. Quant. El. 5, 1713 (1978)

J. Kowalski, F. Träger, S. Weißhaar, H.B. Wiegemann, G. zu Putlitz
Nuclear Charge Distribution of ^{41}Ca, Z, Physik A290, 345 (1979)

J. Kowalski, R. Neumann, F. Träger, G. zu Putlitz
Dye Laser Saturation Spectroscopy with Beams of Atoms and Ions, in: Laser Spectroscopy IV, p. 539, Ed. H. Walther, K.W. Rothe, Springer Verlag, Berlin, Heidelberg, New York 1979

J. Kowalski, R. Neumann, H. Suhr, K. Winkler, G. zu Putlitz
Two-Photon Intracavity Dye Laser Spectroscopy of the 4S and 3D Term in $^{6,7}Li$, Z. Physik A287, 247 (1978)

C. Kozhuharov, P. Kienle, E. Berdermann, H. Bokemeyer, J.S. Greenberg, Y. Nakayama, P.Vincent, H. Backe, L. Handschug and E. Kankeleit
Positrons from 1.4 GeV Uranium-Atom Collisions, Phys. Rev. Letters 42, 376 (1979)

J.V. Kratz, W. Brüchle, G. Franz, M. Schädel, I. Warnecke, G. Wirth, M. Weis
Study of the N/Z Ratios of Light and Heavy Fragments from Collisions of ^{129}Xe, and ^{136}Xe with ^{197}Au Near the Interaction Barrier, Nuclear Physics A332, 477 (1979)

J. Kunz and U. Mosel
Patterns for Collective Rotations in Heavy Nuclei, Nuclear Physics A323, 271 (1979)

R. Lucas, J. Poitou, J.V. Kratz, G. Wirth
Study of the Heavy Products from ^{84}Kr + ^{238}U Collisions at 522 MeV, Z. Physik A290, 327 (1979)

Ch. Lukner
Mechanisms for the Production of Negative Ions in Sputtering Sources, Nuclear Instr. and Methods 167, 249 (1979)

T. Lund, H.-J. Becker, H. Jungclas, D. Molzahn, P. Vater, R. Brandt
Are there Superheavy Elements in the Meteorite Allende?, J. Inorganic Nucl. Chem. Letters 15, 413-416 (1979)

T. Lund, R. Brandt, H. Jungclas, D. Molzahn, P. Vater
Suche nach überschweren Elementen I: im Meteoriten Allende, GSI-Bericht 1978, GSI-79-11, S. 72

T. Lund, R. Brandt, H. Jungclas, D. Molzahn, P. Vater
Suche nach überschweren Elementen II: Reaktion (Pb + U), GSI-Bericht 1978, GSI-79-11, S. 73

U. Lynen, H. Stelzer, A. Gobbi, R. Bock, H. Sann and A. Olmi
Large Area Two Dimensional Position Sensitive Detectors, Nuclear Instr. and Methods 162, 657 (1979)

R. Mann and F. Folkmann
Selective Electron Capture Effects at Highly Ionized Ne Target Atom After 1.4 MeV/u Heavy Ion Impact, J. de Physique 40, C1-236 (1979)

V. Maruhn-Rezwani, N. Grün and W. Scheid
Numerical Solution of the Time-Dependent Schrödinger Equation and Application to H^+-H,
Phys. Rev. Letters 43, 512-515 (1979)

D. Marx, F. Nickel, G. Münzenberg, K. Güttner, H. Ewald, W. Faust, S. Hofmann, H.J. Schött and W. Thalheimer
A Rotating Target Wheel with Thin Targets for Heavy Ion Beams of High Current Densities,
Nuclear Instr. and Methods 163, 15 (1979)

D. Marx, F. Nickel, W. Thalheimer
Rotating Sandwich Targets of Isotopically Enriched Lead for High Intensity Heavy Ion Beams,
Nuclear Instr. and Methods 167, 152 (1979)

H. Metz, H. Orth, G. zu Putlitz, A. Seeger, H. Teichler, J. Vetter, W. Wahl, M. Wigand, K. Dorenburg, M. Gladisch, D. Herlach
Muon Location and Mobility in High-Purity Metals, Hyperfine Interactions 6, 271 (1979)

W.G. Meyer, H.H. Gutbrod, Ch. Lukner and A. Sandoval
Correlations Between Slow and Fast Fragments in Relativistic Nuclear Collisions,
LBL-Report 9151 (1979), Phys. Rev. C (in print)

W.E. Meyerhoff, D.L. Clark, Ch. Stoller, E. Morenzoni, W. Wölfli, F. Folkmann, P. Vincent, P.H. Mokler, P. Armbruster
Molecular-Orbital X-Rays from 1 GeV ^{208}Pb + ^{208}Pb and ^{209}Bi + ^{209}Bi Collisions,
Phys. Letters 70A, 303 (1979)

D. Molzahn, R. Brandt, R. Helmbold, H. Jungclas, P. Vater (Kernchemie-Geowissenschaften)
On the Evidence of "Giant" Halos, Nuclear Tracks (in press)

U. Mosel
Influence of Dissipative and Conservative Properties on Heavy Ion Fusion,
Phys. Rev. C19, 2167 (1979)

A. Müller, Ch. Achenbach and E. Salzborn
Dependence of Charge Transfer Between Atoms and Highly Charged Ions on the Ionization Potential of the Atoms, Phys. Letters 70A, 410 (1979)

A. Müller and E. Salzborn
Production of Isotope-Resolved Beams of Highly Charged Xenon Ions,
Nuclear Instr. and Methods 164, 607 (1979)

G. Münzenberg, W. Faust, S. Hofmann, H.J. Schött and K. Güttner
A High Voltage Deflection Condenser Operated under High Vacuum Conditions,
Nuclear Instr. and Methods 166, 391 (1979)

G. Münzenberg, W. Faust, S. Hofmann, P. Armbruster, K. Güttner and H. Ewald
The Velocity Filter SHIP, a Separator of Unslowed Heavy Ion Fusion Products,
Nuclear Instr. and Methods 161, 65 (1979)

M. Mutterer, J. Pannicke, K.-P. Schelhaas, J.P. Theobald and J.C. van Staden
Noble-Gas Scintillation Counters for the Detection of Energetic Heavy Ions,
IEEE Trans. Nucl. Sci. NS-26, 382 (1979)

F. Nickel, W. Hartmann, D. Marx
Preparation of Isotopically Enriched Targets and of Thin Metal Foils with High Melting Temperature
Using an Electron Gun, Nuclear Instr. and Methods 167, 175 (1979)

H. Nienstädt, D. Gawlik, G. zu Putlitz, H.G. Weber
Cross Section for the Resonant Charge Exchange Cs^{+} + Cs at Thermal Energies,
Z. Physik A288, 109 (1978)

W. Nörenberg
Dissipative Heavy-Ion Collisions: A New Source of Information about Nuclear Dynamics,
Trends in Physics, (The Institute of Physics, London, 1979) p. 399

W. Nörenberg and C. Riedel
Entrance-Channel Coherence in Dissipative Heavy-Ion Collisions and Compound-Nucleus Formation,
Z. Physik A290, 335 (1979)

A. Olmi, U. Lynen, J.B. Natowitz, M. Dakowski, P. Doll, A. Gobbi, H. Sann, H. Stelzer, R. Bock
and D. Pelte
Projectile Splitting at 12.1 MeV/u, Phys. Rev. Letters 44, 383 (1980)

H. Otto, P. Peuser, G. Nyman, E. Roeckl
Determination of Q_{β} Values from Endpoint Energies of Beta Spectra, Nuclear Instr. and Methods 166,
509 (1979)

J.Y. Park, W. Scheid, W. Greiner
Theory of Nucleon Transfer in the Dynamical Two-center Shell Model, Phys. Rev. C20, 188 (1979)

J. Pedersen
Yrast Traps, 4th EPS Gen Conference (1979)

P. Peuser, H. Otto, M. Weis, G. Nyman, E. Roeckl, J. Bonn, L. von Reisky, C. Spath
Half-Lives, Neutron-Emission Probabilities and Fission Yields of Neutron-Rich Rubidium Isotopes
in the Mass Region A = 96 to A = 100, Z. Physik A289, 219 (1979)

P. Peuser, H. Otto, N. Kaffrell, G. Nyman, E. Roeckl
Total β-Decays Energies and the Mass-Energy Surface of Very Neutron-Rich Nuclei Near Mass 100,
Nuclear Physics A332, 95 (1979)

A. Płochocki, G.M. Gowdy, R. Kirchner, O. Klepper, W. Reisdorf, E. Roeckl, P. Tidemand-Petersson,
J. Zylicz, U.J. Schrewe, R. Kantus, R.D. von Dincklage, W.D. Schmidt-Ott
Masses of Very Neutron Deficient Nuclei in the Tin Region
Nuclear Physics A332, 29 (1979)

J. Poitou, R. Lucas, J.V. Kratz, W. Brüchle, H. Gäggeler, M. Schädel, G. Wirth
Second Moments of N/Z-Distributions in Damped Collisions of ^{132}Xe with ^{197}Au,
Phys. Letters 88B, 69 (1979)

K. Pomorski and K. Dietrich
Derivation of a Proximity Interaction Between Nuclei from the Hartree-Fock Functional with Skyrme
Interaction, submitted to Z. Physik A

K. Pomorski and H. Hofmann
On the Dynamics of Fission as a Dissipative Process, submitted to Nuclear Physics A

G. zu Putlitz, G. Siegert
Expeditionen ins Innere der Atome (Schwerionenforschung bei der GSI),
Bild der Wissenschaft, 16. Jahrg., Heft 12, S. 154 (1979)

K.E. Rehm
The Time Dependence of the Variances of Charge and Mass Distributions in Deep Inelastic Collisions,
Phys. Letters 86B, 260 (1979)

K.E. Rehm, H. Essel, K. Hartel, P. Kienle, H.J. Körner, P. Sperr, W. Wagner
The Time Evolution of the Equilibration Process in ^{208}Pb + ^{110}Pd Collisions,
Phys. Letters 86B, 256 (1979)

K.E. Rehm, H. Essel, K. Hartel, P. Kienle H.J. Körner, R.E. Segel, P. Sperr. W. Wagner
Time Scales for Charge Equilibration in Heavy Ion Collisions, Z. Physik A293, 119 (1979)

J. Reinhardt, B. Müller, W. Greiner, G. Soff
Delta Electrons: An Atomic Clock for Deep Inelastic Collisions, Z. Physik A292, 211 (1979)

J. Reinhardt, B. Müller, W. Greiner, G. Soff
Role of Multistep Processes in Heavy-Ion Inner-Shell Excitations, Phys. Rev. Letters 43, 1307 (1979)

J. Reinhardt, B. Müller, W. Greiner, G. Soff
Theory of Positron Production in Heavy Ion Collisions, Proceedings of the XVII International Winter Meeting on Nuclear Physics, Bormio, Italy, 1979

J. Reinhardt, V. Oberacker, B. Müller, W. Greiner, G. Soff
Theory of Positron Production in Heavy Ion Collisions, Proceedings Predeal International School, Heavy Ion Physics, 1978, Romania, Ed. A. Berinde, V. Ceausescu, I.A. Dorobantu, p. 69 (1979)

H.-W. Reist, D.E. Casperson, A.B. Denison, P.O. Egan, V.W. Hughes, F.G. Mariam, G. zu Putlitz, P.A. Sounder, P.A. Thompson, J. Vetter
Development of a Low-Momentum "Surface" Muon Beam for LAMPF,
Nuclear Instr. and Methods 153, 61 (1978)

U. Reus, W. Westmeier and I. Warnecke
Gamma-Ray Catalog, GSI-Report 1979, GSI-79-2, GSI Darmstadt

U. Reus, W. Westmeier und I. Warnecke
Aufstellung und laufende Korrektur eines Gamma-Katalogs, GSI-Report 1979, GSI-79-11, p. 54

U. Reus und P. Patzelt
Massenausbeuten aus der Reaktion $^{56}Fe + {}^{197}Au$ bei $E_{lab} < 538$ MeV, Verhandl. DPG (VI) 14, 747 (1979), Physik Verlag Weinheim, 1979

C. Riedel, G. Wolschin and W. Nörenberg
Relaxation Times in Dissipative Heavy Ion Collisions, Z. Physik A290, 47 (1979)

C. Riedel, R. Spohr
Statistical Properties of Etched Nuclear Tracks, I. Analytical Theory and Computer Simulation, Radiation Effects 42, 69-75 (1979)

C. Riedel and W. Nörenberg
Theoretical Estimates for the Production of Transuranium Elements in Heavy Ion Collisions, Z. Physik A290, 385 (1979)

C. Riedel, R. Spohr
Möglichkeiten und Grenzen bei der Herstellung von Kernspurfiltern aus Glimmer, Ber. der Bunsenges. Phys. Chem. 83, 1165-1168 (1979)

A. Rosén and B. Fricke
Electronic Structure of UF_5, Chem. Phys. Letters 61, 75 (1979)

A. Rosén, B. Fricke, T. Morović and D.E. Ellis
Relativistic Molecular Calculations of Superheavy Molecules, J. de Physique C4, 218 (1979)

G. Rudolf, A. Gobbi, H. Stelzer, U. Lynen, A. Olmi, H. Sann, R.G. Stokstad and D. Pelte
Energy Loss and Nucleon Exchange in the Reaction of ^{86}Kr with ^{166}Er,
Nuclear Physics A330, 243 (1979)

A. Sandoval, H.H. Gutbrod, W.G. Meyer, A.M. Poskanzer, R. Stock, J. Gosset, J.C. Jourdain, Ch. King, G. King, Ch. Lukner, N. Van Sen, G.D. Westfall and K.L. Wolf
Spectra of p, d, t from Relativistic Nuclear Collisions, LBL-Report 8771 (1979), submitted to Phys. Rev. C

D. Schardt. R. Kirchner, O. Klepper, W. Reisdorf, E. Roeckl, P. Tidemand-Petersson, G.T. Ewan, E. Hagberg, B. Jonson, S. Mattsson, G. Nyman
Alpha Decay Studies of Tellurium, Iodine, Xenon and Cesium Isotopes,
Nuclear Physics A326, 65 (1979)

K.-H. Schmidt, W. Faust, G. Münzenberg, H.-G. Clerc, W. Lang, K. Pielenz, D. Vermeulen, H. Wohlfarth, H. Ewald, K. Güttner
Alpha Decay Properties of New Protactinium Isotopes, Nuclear Physics A318, 253 (1979)

U.J. Schrewe, A.J. Hautojärvi, W.-D. Schmidt-Ott, H. Jungclas, D. Hirdes
Messung von Energie und Halbwertszeit von neutronenarmen Isotopen beim Beschuß von Y mit ^{84}Kr, Jahresbericht 1978, GSI-79-11, S. 62

S. Schumann, I.A. Sellin, R. Mann, H.J. Frischkorn, D. Rosich, Gy. Szabó, K.O. Groeneveld
Delayed Coincidence Auger Electron Lifetime Measurement, J. de Physique 40, C1-221 (1979)

S. Schumann, K.O. Groeneveld, G. Nolte and B. Fricke
Equilibrium K-shell Excitation of Highly Ionized Neon, Z. Physik A289, 245 (1979)

R.S. Simon, R.M. Diamond, Y. El Masri, J.O. Newton, P. Sawa and F.S. Stephens
Shell Effects at High Spin in the γContinuum from Te Evaporation Residues,
Nuclear Physics A313, 209 (1979)

G. Soff, B. Müller, W. Greiner
Delta-electron Spectroscopy of Superheavy Quasiatoms, Proceedings Predeal International School,
Heavy Ion physics, 1978, Romania, Ed. A. Berinde, V. Ceausescu, I.A. Dorobantu, p. 931 (1979)

G.Soff, W. Greiner, W. Betz, B. Müller
Electrons in Superheavy Quasimolecules, Phys. Rev. A20, 169 (1979)

G. Soff, J. Reinhardt, W. Betz, J. Kirsch, K.-H. Wietschorke, V. Oberacker, B. Müller, W. Greiner
Multiple Coulomb Excitation of Electron Configurations in Superheavy Quasimolecules,
XIth International Conference on the Physics of Electronic and Atomic Collisions, Kyoto, Japan,
1979, p. 696

G. Soff, W. Betz, J. Kirsch, V. Oberacker, J. Reinhardt, K.-H. Wietschorke, B. Müller, W. Greiner
New Phenomena of Atomic Physics in Collisions of Very Heavy Ions, Proceedings Predeal International
School, Heavy Ion Physics, 1978, Romania, Ed. A. Berinde, V. Ceausescu, I.A. Dorobantu, p. 889(1979)

G. Soff, J. Reinhardt, W. Betz, J. Kirsch, B. Müller and W. Greiner
Theory of Inner-Shell Vacancy Formation in Superheavy Quasimolecules, Abstracts of Invited and
Contributed Papers, The VIth International Seminar on Ion-Atom Collisions, Tokai-mura, Japan,
1979, p. 69

G. Soff, J. Reinhardt, B. Müller, W. Greiner
Delta-electron Emission in Deep-Inelastic Heavy Ion Collisions, Phys. Rev. Letters 43, 1981 (1979)

R. Stock
Nuclear Reactions Between Relativistic Heavy Ions, in Heavy Ion Collisions, Ed. R. Bock,
p. 607 (1979)

R. Stock
Reactions of Relativistic Heavy Ions, Nukleonika 24, 165 (1979)

Ch. Stoller, E. Morenzoni, W. Wölfli, W.E. Meyerhoff, F. Folkmann, P. Vincent, P.H. Mokler,
P. Armbruster
MO X-Ray Angular Distributions from 1 GeV $^{208}Pb + ^{208}Pb$, submitted to Z. Physik A

E.M. Szanto, A. Szanto de Toledo, H.V. Klapdor, M. Diebel, J. Fleckner and U. Mosel
Backbending in ^{22}Ne, Phys. Rev. Letters 42, 622 (1979)

T. Tanabe, M. Dakowski, R. Bock, A. Gobbi, H. Sann, H. Stelzer, U. Lynen, A. Olmi and D. Pelte
The Pb-Pb Collisions, Nuclear Physics (in print)

G. Tress, P. Vater, D. Hirdes, R. Brandt, B. Genswürger, R. Spohr(Marburg-GSI)
Some Properties of Nuclear Track Microfilters in Mica, Nuclear Tracks (in print)

G. Tress, P. Vater, R. Brandt, B. Genswürger, R. Spohr
Kernspur-Mikrofilter aus Glimmer: Herstellung und Eigenschaften, GSI-Bericht 1978, GSI-79-11,S.136

P. Vater, P.A. Gottschalk, R. Brandt, G. Grawert(Kernchemie-Kernphysik Marburg)
Multiple Sequentielle Kernspaltung in der Reaktion ^{238}U + 7.5 MeV/u ^{238}U,
GSI-Bericht 1978, GSI-79-11, S. 34

P. Vater, G. Tress, R. Brandt, B. Genswürger, R. Spohr(Marburg-GSI)
Nuclear Track Microfilters Made of Mica, Nuclear Instr. and Methods (in print)

D. Vermeulen, H.-G. Clerc, W. Lang, K.-H. Schmidt, G. Münzenberg
212 Th, a New Isotope, Inst. für Kernphysik, TH Darmstadt, IKDA 79/16, Sept. 1979

P. Vincent and J.S. Greenberg
Collision Broadening of Continuum Radiation from Ni + Ni Collisions,
J. Phys. B, Atom. Molec. Phys. 12, L641 (1979)

W. Wätzig
A Direct Method for Background Subtraction in Gamma-Ray Spectra, Proc. Conf. on Computers in Activation Analysis and Gammy-Ray Spectroscopy, Mayaguez, Puerto Rico, April 30 - May 4, 1978, CONF-780421, Technical Information Center / U.S. Department of Energy, 1979

W. Wätzig and W. Westmeier
Determination of the Average FWHM in Background-free Spectra, Nuclear Instr. and Methods 159, 547-551 (1979)

W. Wätzig
Beiträge zur kernsystematischen Untersuchung deformierter Übergangskerne durch Studium des Zerfalls von Tl-188 und Tl-190, Dissertation, Universität Marburg, Dez. 1979

W. Wätzig und P. Patzelt
Untergrundsubstraktion in Gamma-Spektren Analysen, Verhandl. DPG (VI) 14, 713 (1979), Physik Verlag Weinheim, 1979

P. Wastyn, H. Genz, M. Mutterer, A. Richter, G. Schrieder, J.C. van Staden and J.P. Theobald
Elastic Scattering of ^{40}Ca at E_{lab} = 191, 236 and 272 MeV, Nuclear Physics A320, 433 (1979), South African Journal of Physics 1, 224 (1978)

P. Wastyn, H. Feldmeier, F. Beck, M. Dworzecka, H. Genz, M. Mutterer, A. Richter, G. Schrieder and J.P. Theobald
Strongly Damped Collisions in the ^{40}Ar + ^{40}Ca System, Nuclear Physics A332, 455 (1979)

R. Weiner
Hot Spots - A "Common Market" of Nuclear and Elementary Particle Physics, Proceedings of the International Workshop on Reaction Models for Continuous Spectra of Light Particles, Ed. J. Ernst, Institut für Strahlen- und Kernphysik Bonn, S. 129 (1979)

W. Westmeier, W. Wätzig und P. Patzelt
ALFUN und ALFWHM, Computerprogramme zur Auswertung komplexer Alpha-Spektren, Verhandl. DPG (VI) 14, 714 (1979), Physik Verlag Weinheim, 1979

W. Westmeier und P. Patzelt
Reichweitenrechnungen für schwere Ionen in beliebiger fester Materie, Verhandl. DPG (VI) 14, 741 (1979), Physik Verlag Weinheim, 1979

W. Westmeier
Detection Probabilities Using Surface Barrier Detectors for Alpha-Decay-Chain Members, Nuclear Instr. and Methods 163, 593-595 (1979)

K.-H. Wietschorke, B. Müller, W. Greiner, G. Soff
Self-Consistent Determination of Critical Two-Centre Distances, J. de Physique B12, L31 (1979)

K.L. Wolf, H.H. Gutbrod, W.G. Meyer, A.M. Poskanzer, A. Sandoval, R. Stock, J. Gosset, Ch. King, G. King, N. Van Sen and G.D. Westfall
Pion Production in the ^{40}Ar + ^{40}Ca Reaction at 1.05 GeV/A, Phys. Rev. Letters 42, 1448 (1979)

G.K. Wolf
Ionenbeschuß als Methode in der Korrosionsforschung und Verhütung, Werkstoffe und Korrosion 30, 853 (1979)

G. Wolschin
Shape Relaxation in Heavy Ion Collisions
Phys. Lett. 88B (1979) 35

G. Wolschin
Angular Momentum Transport in Heavy Ion Collisions
Nucl. Phys. A316 (1979) 146

6.1.2 Conference Contributions
(Alphabetical order of Conference-Towns)

Microcircuit Engineering '79 - Microstructure Fabrication, Aachen, September 1979

B.E. Fischer, R. Spohr:
Heavy Ion Lithography

IV International Conference on Ion Beam Analysis, Aarhus, Dänemark, June 1979

B.E. Fischer, R. Spohr:
Heavy Ion Microlithography - A New Tool to Generate and Investigate Submicroscopic Structures

Symposium on High Spin Phenomena in Nuclei, Argonne, USA, March 1979

S. Bjørnholm, J. Borggreen, O. Christensen, A. Del Doppo, B. Herskind, J. Pedersen, G. Sletten, F. Folkmann, R.S. Simon:
Determination of the Excitation Energy of High Spin Isomers

H. Bohn, T. Faestermann, F. v. Feilitzsch, P. Kienle, A. W. Sunyar, H. Emling, P. Fuchs, E. Grosse, D. Schwalm, H.J. Wollersheim:
High Spin States in Neutron Rich Rare Earth Nuclei

E. Grosse:
Determination of B(E2)-values between High Spin States from Coulomb Excitation and (HI,xn)-Reactions

G.B. Hagemann:
Entry Region Studies by Means of Sum Spectrometer and Multiplicity Techniques

Workshop on γ-Ray Spectroscopy, Beekbergen, Holland, November 1979

R. S. Simon:
Energy Correlations - a New Approach to study the γ-Continuum following Heavy-Ion Reactions

Symposium on Ultrarelativistic Heavy Ion Reactions, Berkeley, USA, May 1979

R. Weiner
Evidence for a Change of Sound Velocity in Hadronic Matter

DPG Frühjahrstagung, Berlin, März 1979

E. Berdermann, H. Bokemeyer, F. Bosch, M. Clemente, F. Güttner, P. Kienle, Ch. Kozhuharov, H. Krimm, B. Martin, B. Povh, K. Traxel, Th. Walcher:
Spektroskopie von hochenergetischen δ-Elektronen an schweren Stoßsystemen

H.F. Beyer, R. Mann, F. Folkmann, K.-H. Schartner:
Spektroskopie von langsamen hochionisierten Atomen erzeugt beim 1,4 MeV/u Schwerionenstoß

H. Bohn, H. Brum, T. Faestermann, P. Kienle, C. Kozhuharov, V. Zacek:
Stoßparameterabhängigkeit der K-Schalen Ionisation für asymmetrische Schwerionen-Stoßsysteme

J. Bonn, W. Klempt, R. Neugart, E.W. Otten, B. Schnizler, K.P.C. Spath, D. Weskott:
Laserspektroskopie am schnellen Atomstrahl zur Bestimmung von Hfs und Isotopieverschiebung neutronenreicher Rb und Cs-Isotope

H.D. Dohmann, R. Mann, H. Pfeng:
Lebensdauermessungen von Zwei- und Dreielektronenzuständen in Ar durch hochauflösende Röntgen- und Augerelektronenspektroskopie

G. Henkel, A. Müller, W. Seim, E. Salzborn:
Vergleichende Untersuchungen des Ladungstransfers bei Stößen mehrfach geladener Ionen mit H_2 und He

G. Huber, F. Touchard, S. Büttgenbach, C. Thibault, R. Klapisch, S. Liberman, J. Pinard, H.T. Duong, P. Juncar, J. L. Vialle, P. Jacquinot, A. Pesnelle:
Untersuchung der D_2 Linie kurzlebiger Caesium- und Rubidium Isotope

J. Kirsch, J. Reinhardt, G. Soff, B. Müller, W. Greiner:
Theorie der quasimolekularen Röntgenstrahlung in mittelschweren und schweren Systemen

D. Liesen, P. Armbruster, H.-H. Behncke, S. Hagmann, P.H. Mokler, H. Schmidt-Böcking, R. Schuch:
Inner-Schalen-Anregung in sehr schweren Stoßsystemen

R. Mann, F. Folkmann, H.F. Beyer:
Selektiver Elektroneneinfang in äußere Schalen von hochionisierten N und Ne Ar

V. Maruhn-Rezwani, N. Grün, W. Scheid:
Numerische Lösung der Schrödinger-Gleichung für H^+-H-Stöße

A. Müller, Ch. Achenbach, K. Miethe, E. Salzborn:
Abhängigkeit des Elektroneneinfangs hochgeladener Ionen vom Ionisationspotential des Targets bei langsamen Ion-Atom-Stößen

H. Schmidt-Böcking, K. Strebing, W. Lichtenberg, R. Schuch, G. Nolte, R. Anholt, P. Vincent:
Impact Parameter Dependence of Quasimolecular K Radiation from 90 MeV Ni + Ni Collisions

P. Vincent, H. Bokemeyer, H. Emling, E. Grosse, D. Schwalm, J.S. Greenberg:
Selective Observation of X-ray Transitions in the Pb + Pb Quasimolecule

18. Hauptversammlung der Gesellschaft Deutscher Chemiker, Berlin, September 1979

J.V. Kratz:
Kernchemische Untersuchungen zum Mechanismus von Schwerionenreaktionen

G. Tress, P. Vater, R. Brandt, B. Genswürger, R. Spohr:
Kernspur-Mikrofilter aus Glimmer

Symposium on Deep Inelastic and Fusion Reactions with Heavy Ions, Berlin, October 1979

U. Mosel, M. Diebel:
Yrast-Line Limitations on Heavy Ion Fusion Reactions

W. Nörenberg:
Transport Theory and Doorway Configuration in Dissipative Heavy-Ion Collisions

H. Oeschler, H. Freiesleben:
Fusion-Fission Type Collisions

F. Pühlhofer
Pre-equilibrium Emission in Heavy-Ion Induced Fusion Reactions

K.E. Rehm, H. Essel, P. Sperr, K. Hartel, P. Kienle, H.J. Körner, R. E. Segel, W. Wagner
Deep Inelastic Collisions at Energies Close to the Coulomb Barrier

N. Stelte:
Hot Spots in Inclusive Reactions

Institute of Physics Conference on Nuclear Structure and Elementary Particle Physics, Birmingham, England, March 1979

D. Schwalm:
γ-Spectroscopic Studies of Nuclei at High Angular Momenta

H.J. Specht:
Fission Phenomena in Deep Inelastic Collisions

International Winter Meeting on Nuclear Physics, Bormio, Italien, January 1979

H. Backe:
Positron Production in Heavy Ion Collisions

T. Faestermann:
High Spin States in Neutron Rich Deformed Nuclei

E. Grosse:
Determination of B(E2)-Values of High Spin States in Deformed Nuclei

R.S. Simon:
Physics with the Crystal Ball

World Conference of the International Nuclear Target Development Society, Boston, USA, October 1979

H. Folger, J. Klemm:
Rolling of Sensitive Target Foils being Coated with Evaporated Metal Layers

Symposium on Heavy Ion Physics from 10 to 200 MeV/U, Brookhaven, USA, July 1979

P. Glässel, D. v. Harrach, Y. Civelekoglu, R. Männer, H.J. Specht, J.B. Wilhelmy, H. Freiesleben, K.D. Hildenbrand:
Fission Properties of Trans-Fermium Nuclei produced in Deep Inelastic Collisions

P. Glässel, D. v. Harrach, H.J. Specht:
Experiences with Large-area Position-sensitive Heavy-Ion Detectors

Physique des Ion Lourds et de la Fission, Bruxelles, Belgien, December 1979

E. Roeckl:
Production of Exotic Nuclei by Heavy-Ion Reactions

European Conference on Surface Science, Cambridge, United Kingdom, March 1979

A. Rosén, P. Grundevik. T. Morović:
Molecular Cluster Calculations for the Analysis of Chemisorption

Atomic and Molecular Processes in Constrolled Thermonuclear Fusion, Château de Bonad, France, August 1979

A. Müller:
Charge Transfer and Electron Impact Ionization of Mulitply Charged Ions

SRC-Meeting, Daresbury, United Kingdom, March 1979

P. Armbruster:
Experiments with "SHIP"

J.D. Garrett, B. Herskind:
In-Beam Spectroscopy on Very High Spin States

F. Pühlhofer:
The GSI Magnetic Spectrometer - Concept and Planned Experiments

Study Weekend on the Study of Nuclei Far from Stability, Daresbury, United Kingdom, September 1979

E. Roeckl:
Studies with the GSI On-Line Separator

Jahrestagung der Bunsengesellschaft, Düsseldorf, Mai 1979

C. Riedel, R. Spohr:
Möglichkeiten und Grenzen bei der Herstellung und Anwendung von Kernspurfiltern aus Glimmer

6th International Conference on Atomic Masses, East Lansing, USA, September 1979

A. Płochocki, G.M. Gowdy, R. Kirchner, O. Klepper, W. Reisdorf, E. Roeckl, P. Tidemand-Petersson, J. Zylicz, U. Schrewe, R. Kantus, R. v. Dincklage, W. Schmidt-Ott:
Masses of Very Neutron-Deficient Nuclides in the Tin Region

E. Roeckl:
Alpha Decay of Neutron-Deficient Isotopes Studied at GSI Darmstadt

K.H. Schmidt, D. Vermeulen:
Mutual Support of Magicities

Third German-Israeli Minerva Physics Symposium, Ein Bokek, Israel, February 1979

W. Nörenberg:
Deeply Inelastic Collisions as a Dissipative Process

D. Schwalm:
High Spin States - Experimental

IX. European Conference on Physics and Chemistry of Complex Nuclear Reactions, Engelberg, Schweiz, September 1979

T. Lund, R. Brandt, D. Molzahn, G. Tress, P. Vater:
Superheavy Elements in Hot Brines?

H.J. Specht:
Fission Isomers and Fission Barriers - the present Situation

XIV European Congress on Molecular Spectroscopy, Frankfurt/M, September 1979

P. Grundevik, A. Rosén, B. Fricke, T. Morović, W.D. Sepp:
Non-Relativistic and Relativistic Molecular Calculations for the Chalcogen Hexafluorides: SF_6, SeF_6, TeF_6 and PoF_6

Seminar über spezielle Fragen der Kernphysik, Frankfurt/M, November 1979

G. Soff:
Bestandsaufnahme der Schwerionen-Atomphysik

Frühjahrstagung der DPG, Arbeitsgemeinschaft Kernphysik, Gent, Belgien, March 1979

U. Arlt, R. Bass, C.R. Gould, V. Hartmann, R. Renfordt, K. Sapotta, K. Stelzer, G. Kreyling:
Neutronenemission bei Fusionsreaktionen mit schweren Ionen

P. Armbruster:
Inner Shell X-Ray Production in Very Heavy Collision Systems and Spectroscopy of Superheavy Atomic Systems

H. Backe, H. Bokemeyer, Y. Gono, E. Kankeleit, L. Richter, P. Senger, P. Vincent, F. Weik, R. Willwater:
Messung von Positronenspektren nach Schwerionenstößen

A. Bałanda, H. Bokemeyer, E. Grosse, Y. Nakayama, L. Handschug, H. Backe:
Determination of the Electron Conversion Coefficients for Transitions between the High-Spin States of ^{158}Dy

A. Bałanda, H. Emling, F. Folkmann, E. Grosse, R. Piercey, D. Schwalm, R.S. Simon, H.J. Wollersheim, D. Evers:
Lifetimes of High-Spin States in ^{238}U from the Dopplershift

R. Bass, U. Arlt, V. Hartmann, R. Renfordt, K. Sapotta:
Interpretation korrelierter Massen-, Ladungs- und Energieverteilung bei der Streuung von ^{40}Ar an ^{208}Pb

E. Berdermann, H. Bokemeyer, F. Bosch, M. Clemente, S. Güttner, P. Kienle, C. Kozhuharov, H. Krimm, B. Martin, B. Povh, K. Traxel, Th. Walcher:
δ-Electrons from Very Heavy Collision Systems

M. Berlanger, A. Gobbi, F. Hanappe, U. Lynen, C. Ngô, A. Olmi, H. Sann, H. Stelzer, H. Richel, M.F. Rivet:
Fast Collective Mode in Deep Inelastic Collisions: Quantal Fluctuations

H. Bohn, T. Faestermann, F. v. Feilitzsch, P. Kienle, H. Emling, P. Fuchs, E. Grosse, D. Schwalm, H. J. Wollersheim:
High Spin States in Neutron Rich Rare Earth Nuclei

J. Bonn, W. Klempt, R. Neugart, E.W. Otten, B. Schinzler, K.P.C. Spath, D. Weskott:
Nuclear Moments and Charge Radii of Neutron-Rich Rb and Cs-Isotopes by Laser-Spectroscopy

W. Brüchle, H. Gäggeler, J.V. Kratz, M. Schädel, G. Wirth, G. Herrmann, M. Weis, R. Lucas, J. Poitou:
Correlated Mass and Charge Transfer in Damped Collisions of Xe + Au

W. Brüchle:
Search for Superheavy Elements in the $^{238}U + ^{238}U$ Reaction

Y. Civekoglu, P. Glässel, D. v. Harrach, R. Männer, D. Pelte, H. Sann, H.J. Specht:
Fission Phenomena in Deep Inelastic Collisions

Y. Civelekoglu, P. Glässel, D. v. Harrach, R. Männer, D. Pelte, H.J. Specht:
Charge Dependence of Angular Momentum Transfer in Deep Inelastic Collisions

Y. Civelekoglu, P. Glässel, D. v. Harrach, R. Männer, J. Wilhelmy, H.J. Specht:
Three Particle Events from ^{238}U at 7.5 MeV/A

P.J. Cooney, E.P. Kantor, D.S. Gemmell, K.O. Groeneveld, Z. Vager, B.J. Zabransky:
Collision-Induced Dissociation of MeV H_2^+ and HeH^+ in Atomic and Nuclear Gases

M. Diebel, U. Mosel:
Miscroscopic-Macroscopic Calculations of Low-Spin States of sd-Shell Nuclei

P. Doll, A. Gobbi, H. Stelzer, R. Bock, U. Lynen, J.B. Natowitz, A. Olmi, H. Sann, D. Pelte, G. Rudolf:
A Mass Drift Towards Asymmetry in Deep Inelastic Collisions at High Energies

H. Emling, P. Fuchs, E. Grosse, J. Idzko, D. Schwalm, R.S. Simon, H.J. Wollersheim:
Determination of B(E2)-Values in ^{238}U from a Multiple Coulomb Excitation Experiment

H. Emling, P. Fuchs, E. Grosse, D. Schwalm, R.S. Simon, H.J. Wollersheim, D. Pelte, R. Wagner:
The Structure of the Stable Dy-Isotopes at High Angular Momenta

H. Essel, K. Hartel, P. Kienle, H.J. Körner, K. E. Rehm, R. E. Segel, P. Sperr, R. Wagner:
Strong Dependence of the Nucleon Transfer on the Mass Asymmetry in the Entrance Channel

R. A. Esterlund, W. Westmeier, A.M. Habbestad Wätzig, U. Reus, P. Patzelt:
Mass Yields from the System $^{132}Xe + ^{nat}Fe$ at $E_{lab} = 940$ MeV

B. E. Fischer, B. Genswürger, R. Spohr:
Heavy-Ion Micro-Lithography - A New Tool to Generate and Investigate Submicroscopic Structures

J. Fleckner, U. Mosel, P. Ring, H.J. Mang:
Selfconsistent Skyrme-Type Caluclation of Rotational States in Rare Earth Nuclei

P. A. Gottschalk, P. Vater, R. Brandt, G. Grawert, G. Fiedler, R. Haag, T. Rautenberg:
Multiple Sequential Fission in the Interaction of 7.5 MeV/amu and 9.02 MeV/amu U+U

G. M. Gowdy, G. Huber, R. Kirchner, O. Klepper, W. Reisdorf, E. Roeckl, P. Tidemand-Petersson, L. Alquist:
A Comparative Study of Excitation Functions for the Reactions $^{99, 100, 102}Ru$ $(^{86}Kr, xn)$ Hg

G.M. Gowdy, R. Kirchner, O. Klepper, W. Reisdorf, E. Roeckl, P. Tidemand-Petersson, J.L. Wood, G. Nyman, N. Kaffrell, K. Schneeweiß:
Levels in the Even Te Isotopes Populated in the Decays of Very Light I Isotopes

K.O. Groeneveld:
Heavy Ion Induced Electron Emission From Molecular Systems

S. Hofmann, W. Faust, T. Kitahara, G. Münzenberg, W. Reisdorf, P. Armbruster, K. Güttner, B. Thuma:
Alpha Decay Studies of Very Neutron Deficient Isotopes of Hf, Ta, W, and Re

G. Huber, F. Touchard, S. Büttgenbach, C. Thibault, R. Klapisch, S. Liberman, J. Pinard, H.T. Duong, P. Juncar, J.L. Vialle, P. Jacquinot, A. Pesnelle:
Laserspectroscopy on Isotopes of Rubidium and Cesium

J. Idzko, K. Stelzer, F. Rauch, Th. Elze, H.J. Wollersheim, H. Emling, P. Fuchs, E. Grosse, D. Schwalm:
Multiple Coulomb Excitation of $^{194, 196}Pt$ with ^{208}Pb Ions

E.P. Kanter, P.J. Cooney, D. S. Gemmell, K.O. Groeneveld, W. J. Pietsch, A. J. Ratkowsky, Z. Vager, B.J. Zabransky:
Angeregte elektronische Zustände bei der Wechselwirkung von energetischen (MeV) Molekülen mit Festkörpern und Gasen

R. Keller:
A Versatile Liquid Argon Detector for Fragments from High Energy Heavy Ion Reactions in the 40-200 MeV/A Energy Domain

J. Kirsch, W. Betz, J. Reinhardt, K. Wietschorke, B. Müller, W. Greiner, G. Soff:
Spectroscopy of Electronic States in Superheavy Systems

I.König, W. König, F.W. Richter, K.O. Groeneveld, I.A. Sellin:
Einfluß der Projektilladung $(H^+, H_2^+, He^{n+}, C^{n+}, Kr^{n+})$ auf die Ioneninduzierte Elektronenemission im Bereich $\bar{v}_e \approx \bar{v}_{ion}$

O.Klepper, K.H. Burkard, W. Hüller, R. Kirchner, W. Reisdorf, E. Roeckl:
Release Times and Separation Efficiencies of the GSI On-Line Mass Separator

H. Lehr, W. v. Oertzen, W. Bohne, K. Grabisch, H. Morgenstern, F. Pühlhofer:
Study of Fusion of ^{20}Ne with ^{12}C and ^{26}Mg

H.D. Lemke, B. Ziegler, M. Arnould, M. Mutterer, J.P. Theobald:
Absolute Photofission Cross Section of ^{209}Bi Measured with Monoenergetic Gamma Radiation between 40 and 65 MeV

T. Lund, H. Jungclas, D. Molzahn, P. Vater, R. Brandt:
Production of SHE and Transplutonium Actinides in the Reaction between ^{208}Pb and ^{238}U

W.G. Meyer:
A Study of the Reaction Mechanism in Relativistic Heavy Ion Collisions

D. Molzahn, T. Lund, R. Brandt, H. Jungclas, P. Vater:
Gegenwärtiger Stand der Suche nach überschweren Elementen im Meteoriten Allende und Erzschlamm aus dem Atlantis II-Tief

G. Münzenberg, W. Faust, S. Hofmann, T. Kitahara, W. Reisdorf, K.H. Schmidt, P. Armbruster, K. Güttner, B. Thuma:
Report on the Synthesis of Neutron Deficient Fm Isotopes in the Reactions ^{40}Ar + $^{208, 209}Pb$

H. Oeschler, J.P. Coffin, P. Engelstein, B. Heusch, P. Wagner, H. Freiesleben, K.D. Hildenbrand:
Limits of Compound Nucleus Fission in Medium-Mass Nuclei

J. Park, W. Greiner, W. Scheid:
Nucleon Transfer in the Dynamical Two-Center Shell Model

J. Reinhardt, G. Soff, B. Müller, W. Greiner:
Positron Production in Quasimolecular Collisions of Very Heavy Ions

U. Reus, P. Patzelt:
Massenausbeuten aus der Reaktion ^{56}Fe + ^{197}Au bei E_{lab} = 538 MeV

C. Riedel, W. Nörenberg:
Entrance-Channel Coherence in Dissipative Heavy-Ion Collisions

G. Rudolf, A. Gobbi, U. Lynen, A. Olmi, H. Sann, H. Stelzer:
Unfolding of Positive and Negative Angle Scattering in Dissipative Collisions

A. Sandoval:
Multiple Production and Exclusive Charged Particle Measurements of Relativistic Heavy Ion Central Collisions

H. Sann, S. Bjørnholm, R. Bock, P. Doll, A. Gobbi, D. Habs, U. Lynen, V. Metag, A. Olmi, D. Pelte, H.J. Specht, H. Stelzer:
Low Energy Fission in the Reaction U+Ca

K. Sapotta, R. Bass, J.v. Czarnecki, V. Hartmann, D. Kästner, R. Renfordt, R. Zitzmann:
Experimentelle Untersuchung einer Quadrupol-Anordnung für Flugzeitexperimente mit schweren Ionen

P. Schlüter, G. Soff, W. Greiner:
Conversion Coefficients for Internal Pair Creation

W.F.W. Schneider, F. Pühlhofer, H. Freiesleben, B. Heusch, C. Volant, B. Kohlmeyer, W. Pfeffer:
Evaporation Residues from Fusion of 5.9 MeV/u ^{84}Kr with ^{27}Al

D. Schüll, F. Pühlhofer, B. Langenbeck, K. Blasche, W. Pfeffer, F. Busch, Th. Walcher:
A Magnetic Spectrometer for Heavy Ions

R.G. Stokstad, K.D. Hildenbrand, J.V. Kratz, G. Wirth, W. Reisdorf, R. Lucas, J. Poitou:
Fusion of ^{40}Ar and $^{144, 148, 154}Sm$ below the Barrier

B. Thuma, K. Güttner, S. Hofmann, W. Faust, T. Kitahara, G. Münzenberg, H.J. Schött, P. Armbruster:
A New Position and Time Correlation Method for Implanted α or p Active Nuclei

P. Tidemand-Petersson:
Beta-Delayed Particle Spectroscopy as a Source of Information on Nuclear Properties

A. Szanto de Toledo, M. Scharder, E. M. Szanto, H. V. Klapdor, U. Mosel:
The Use of Critical Angular Momentum Effects in the Spectroscopy of High Spin States in the $A \lesssim 30$ Region

G. Tress, P. Vater, R. Brandt, B. Genswürger, R. Spohr:
Hitze-, Säure- und Lösungsmittel-beständige Mikrosiebe aus Glimmer

D. Vermeulen, H.G. Clerc, W. Land, K.H. Schmidt, W. Faust, G. Münzenberg, W. Reisdorf:
Production Cross Sections for Th-isotopes near the N=126 Shell in Ar-induced Fusion Reactions

W. Wätzig, P. Patzelt:
Untergrundsubtraktion in Gamma-Spektren Analysen

P. Wastyn, M. Mutterer, A. Koldobski, J. Pannicke, K. Scheele, J.P. Theobald:
A Multiparameter Heavy-Ion Detection System

P. Wastyn, H. Feldmeier, F. Beck, M. Dworzecka, H. Genz, M. Mutterer, A. Richter, G. Schrieder, J.P. Theobald:
Strongly Damped Collisions in the ^{40}Ar + ^{40}Ca System

W. Westmeier, P. Patzelt:
Reichweitenrechnungen für schwere Ionen in beliebiger fester Materie.

W. Westmeier, W. Wätzig, P. Patzelt:
ALFUN und ALFWHM, Computerprogramme zur Auswertung komplexer Alpha-Spektren

R. Wolf, U. Mosel, S. Pieper:
Application of the Ingoing Wave Boundary Condition to $^{16}O + ^{16}O$ and $^{12}C + ^{12}C$ Scattering

G. Wolschin, C. Riedel, W. Nörenberg:
Relaxation Processes in Heavy-Ion Collisions

E. Wüst, U. Mosel, P.G. Zint:
Change of Central Density and Surface Diffuseness with Rotation

Symposium on Blood Rheology, Glasgow, Great Britain, September 1979

H. Kiesewetter, K. Mussler, P. Teitel, U. Dauer, H. Schmid-Schönbein, R. Spohr:
New Methods for the Measurement of Red Cell Deformation Ability

Workshop on Nuclear Spectroscopy of Fission Products, Grenoble, France, May 1979

R. Kirchner, E. Roeckl:
The FEBIAD Ion Source

P. Peuser, H. Otto, G. Nyman, E. Roeckl:
Decay Properties of Neutron-Rich Isotopes of Rubidium (Z=37) Through Technetium (Z=43) and the Mass-Energy Surface around A=100

8th International Conference on Atomic Collision in Solids, Hamilton, Canada, August 1979

K.O. Groeneveld, S. Schumann, Gy. Szabó:
Heavy Ion Induces Secondary Electron Emission

Seminar über neuere Heidelberg-Frankfurt-Darmstadt Ergebnisse, Heidelberg, Mai 1979

G. Soff:
Theorie der K - Schalenanregung in sehr schweren Systemen

International Workshop VII on Gross Properties of Nuclei and Nuclear Excitations, Hirschegg, Austria, January 1979

S. Ayik, W. Nörenberg:
Generalized Fokker-Planck Equation of Dissipative Heavy-Ion Collisions

G. Huber, F. Touchard, S. Büttgenbach, C. Thibault, R. Klapisch, S. Liberman, J. Pinard, H.T. Duong, P. Jungcar, J.L. Vialle, P. Jacquinot, A. Pesnelle:
Nuclear Shape and Magnetic Moments in the Sodium and Caseium Region from Laser Spectroscopy

E. Kankeleit:
HI-Positron Production, New Results and a Pedestrian Analysis

W. Nörenberg, C. Riedel:
Entrance-channel Coherence in Dissipative Heavy-Ion Collisions and Compound-Nucleus Formation

E.W. Otten:
Optical Methods Probing Nuclear Structures off Stability

K. Pomorski:
Cranking Model Estimate of the Collective Inertia for the Mass Asymmetry made at and after the Scission Configurations

W. Reisdorf:
Heavy-Ion Induced Fusion Reactions and the Production of Exotic Nuclei

D. Schardt, G.M. Gowdy, R. Kirchner, O. Klepper, W. Reisdorf, E. Roeckl, P. Tidemand-Petersson, G. T. Ewan, E. Hagberg, P.G. Hansen, B. Jonson, S. Mattsson, G. Nyman:
Trans-Tin Alpha Decay

K.H. Schmidt:
Fission Barriers of Heavy Nuclei

G. Wirth, W. Brüchle, H. Gäggeler, J.V. Kratz, M. Schädel, I. Warnecke, G. Herrmann, M. Weis, R. Lucas, J. Poitou:
Correlations between Masses and Charges in Damped Collisions of Xe+Au

G. Wolschin:
Shape Relaxation and Angular-Momentum Dissipation in Heavy-Ion Collisions

ACS-Meeting, Honolulu, Hawaii, April 1979

H. Gäggeler:
Production of Heavy Elements in Damped Collisions of ^{238}U with ^{238}U

Adriatic Europhysics Study Conference on Statistical Properties of Nuclei, Hvar, Jugoslavia, October 1979

S. Ayik:
Transport Theory of Heavy-Ion Collisions in the Adiabatic Representation

Third ASTM - Euratom Symposium on Reactor Dosimetry, Ispra (Italy), October 1979

M. Debeauvais, J. Tripier, F. Amoudry:
Detecteurs Solides de traces et leur utilisation en dosimetrie neutronique

International Symposium on Physics and Chemistry of Fission, Jülich, May 1979

A. Baran, K. Pomorski, S.E. Larsson, P. Möller, S.G. Nilsson, J. Randrup, A. Lukasiak, A. Sobiczewski:
Dynamical Calculations of the Spontaneous-fission Half-lives

H.G. Clerc, W. Lang, H. Wohlfarth, H. Schrader, K.H. Schmidt:
Detailed Study of the Nuclide Yields in $^{235}U(n_{th},f)$ and their Relation to the Properties of the Scission Configuration and the Dynamics of the Fission Process

G. Fiedler, R. Haag, T. Rautenberg, P.A. Gottschalk, P. Vater, H.J. Becker, R. Brandt, G. Grawert:
On the Sequential Nature of Multifragment Reactions Induced by Heavy Ions

D.v.Harrach, P. Glässel, Y. Civelekoglu, R. Männer, H.J. Specht, J.B. Wilhelmy, H. Freiesleben, K.D. Hildenbrand:
Fission Properties of Very Heavy Nuclei Produced in Deep Inelastic Collisions

K.H. Schmidt, W. Faust, G. Münzenberg, W. Reisdorf, H.G. Clerc, D. Vermeulen, W. Lang:
Experimental Determination of Fission Probabilities for Proton Rich Nuclei near the N=126 Shell

EPS Topical Conference on Large Amplitude Collective Nuclear Motion, Keszthely, Hungary, June 1979

S. Ayik:
Dynamical Description of Dissipative Heavy-Ion Collisions in the Adiabatic Representation

H. Feiesleben:
A New Type of Strongly Damped Collisions

W. Nörenberg, C. Riedel:
Initial correlations and Transport Theory of Dissipative Heavy-Ion Collisions

Workshop on Very Stable Nuclear Systems, Kornö

P. Armbruster:
Cold Fragmentation of ^{234}U

XIth International Conference on the Physics of Electronic and Atomic Collisions, Kyoto, Japan, September 1979

H.F. Beyer, K.H. Schartner, F. Folkmann:
X-Ray Spectroscopy of Highly Excited Recoil Ions

H.F. Beyer, K.H. Schartner, R. Hippler:
Ion Impact Ionization of Both 2s-Electrons of Neon

H.F. Beyer, R. Mann, F. Folkmann, K.H. Schartner:
Selective Electron Capture by Highly Charged Very Slow Ions: I. Method

M. Eckhardt, K.H. Schartner, H.F. Beyer:
Electron Impact Ionization of 2s- and 2p-Electrons of Neon

B. Fricke, W.d. Sepp, T. Morovic, A. Rosen:
An Improved Calculation of the $2p_\pi$ - $2p_\sigma$ Rotational Coupling

C. Kozhuharov, P. Kienle, E. Berdermann, H. Bokemeyer, J.S. Greenberg, Y. Nakayama, P. Vincent, H. Backe, L. Handschug, E. Kankeleit:
Charge Number and Scattering Angle Dependence of the Positron Production in Very Heavy Ion Atom Collisions

W.N. Lennard, I.V. Mitchell, P.H. Mokler, G.C. Ball:
Projectile Charge State Dependence of K X-Ray Production in Heavy Ion-Atom Single Collisions

D. Liesen:
Intermediate and Superheavy Atomic Collision Systems: Experiments at the UNILAC

R. Mann, H.F. Beyer, K.H. Schartner, F. Folkmann:
Selective Electron Capture by Highly Charged Very Slow Ions: II. Spectroscopic Results

V. Maruhn-Rezwani, N. Grün, W. Scheid:
A Numberical Solution of the Schrödinger Equation for Atomic Collisions

P.H. Mokler, W.N. Lennard, I.V. Mitchell:
Linear Polarization Measurement for Quasimolecular K Radiation

E. Salzborn, A. Müller:
Electron Capture by Multi-Charged Ions Colliding with Multi-Electron Targets

W.A. Schönfeld, P.H. Mokler:
Projectile L-Subshell differentiation in 1.4 MeV/u Pb → Z2 Collisions

Ch. Stoller, E. Morenzoni, W. Wölfli, W.E. Meyerhoff, E. Folkmann, P. Vincent, P.H. Mokler, P. Armbruster:
Mo X-Ray Angular Distributions from 1 GeV ^{208}Pb + ^{208}Pb and ^{209}Bi + ^{209}Bi Collisions

P. Vincent, D. Schwalm, H. Bokemeyer, H. Emling, E. Grosse, J.S. Greenberg:
Selective Observation of Continuum Radiation from the Pb + Pb Quasimolecule

10th International Conference on Solid State Nuclear Track Detectors, Lyon, France, July 1979

M. Debeauvais, S. Jokic, J. Tripier:
Etude à l'aide du Makrofol des interactions U sur U et Pb à des énergies supérieures à 7 MeV/UMA

B.E. Fischer, B. Genswürger, R. Spohr:
Density Micromapping and Micromachining of Surfaces by Means of Heavy Ion Lithography

R. Haag, G. Fiedler, T. Rautenberg, P.A. Gottschlak, G. Grawert:
Coincidence Measurements of Heavy Ion Reaction Products via Solid State Nuclear Track Detectors

H.A. Khan, P. Vater, R. Brandt:
Multiprong Fission Events Produced by 1477 MeV ^{208}Pb

C. Riedel, R. Spohr:
Multiple Hole Probabilities and Areal Dispersions of Etched Nuclear Tracks and their Consequences for Practical Applications

M. Schäfer, R. Facius, H. Bücker:
Response of Bacillus subtilis Spores to Heavy Ion Irradiation Using Cellulose Nitrate Detectors

P. Vater, G. Tress, R. Branst, B. Genswürger, R. Spohr:
Properties of Microfilters Made of Mica

Nordic Symposium on Nuclear Physics, Lysekil, Schweden, August 1979

P. Armbruster:
Fusion of N = 126 Nuclei and Recent Experiments with the Separator "SHIP"

D.v. Harrach:
Fission Phenomena in Deep Inelastic Collisions

G. Huber:
Laserspectroscopy in Nuclear Physics

P. Tidemand-Peterson, G. Nyman, G. Gowdy, R. Kirchner, O. Klepper, A. Płochocki, W. Reisdorf, E. Roeckl, D. Schardt, J. Zylicz:
Studies of Very Neutron-Deficient Nuclides with $50 \leq Z \leq 56$

D. Vermeulen, H.G. Clerc, W. Lang, K.H. Schmidt, W. Reisdorf, G. Münzenberg:
Shell Strengths and their Influence on the Survival of Heavy Evaporation Residues

H.J. Wollersheim:
Structure of the Stable Dy-Isotopes at High Angular Momenta

12th Summer School on Nuclear Physics, Mikołajki, Poland, September 1979

K.D. Hildenbrand:
Compound Nucleus Fission at High Angular Momenta in the Reaction $^{132}Xe + ^{30}Si$

E. Kankeleit:
Collisional Quasiatoms, Facts and Speculations

G. Münzenberg, P. Armbruster, W. Faust, S. Hofmann, F. P. Hessberger, W. Reisdorf, W. Schneider, H.J. Schött, B. Thuma, K. Güttner, H. Ewald, H.G. Clerc, D. Vermeulen:
Investigation of Evaporation Residues from Heavy Ion Fusion with the Velocity Filter SHIP at GSI Darmstadt

W. Reisdorf:
Low Energy Heavy Ion Induced Fusion: Probability of Fusion and of Survival to Fission

1979 Linear Accelerator Conference, Montauk, USA, September 1979

R.W. Müller:
Work on R.F. Quadrupole Focusing Structures at GSI

1. Deutsch-Sowjetisches Laserseminar, Moskau, UDSSR, December 1979

G. Huber:
High Resolution Spectroscopy of Radioactive Alcalies

International Conference on Magnetism, München, September 1979

H. Heitmann, P. Hansen, R. Spohr, K. Witter:
Properties of Magneto-optic $(Gd, Bi)_3 (Fe, Ga)_5 O_{12}$ Films Irradiated with High-Energy Heavy Ions

Nagoya Seminar on Atomic Processes in Fusion Plasmas, Magoya,Japan, September 1979

E. Salzborn:
Atomic Collisions in Fusion Plasmas Involving Multiply Charged Ions

Hemorheology et Pathologie Symposium European, Nancy, France, October 1979

H. Kiesewetter, U. Dauer, K. Mussler, H. Schmid-Schönbein, R. Spohr:
Rigidity Measurements in Individual Red Cells

International Symposium on Future Directions in Studies of Nuclei far from Stability, Nashville, USA, September 1979

E. Roeckl:
Recent Experiments at the GSI On-Line Separator

W. Scheid, W. Greiner:
Theory of Nuclear Molecules

Gordon Research Conference "Nuclear Chemistry", New London, USA, June 1979

H. Emling:
The Collectivity of Stable Dysprosium Nuclei at High Spin

E. Roeckl:
Decay of Very Neutron-Deficient Isotopes Close to the Proton Drip Line in the Trans-Tin Region

International Spring School on the Development and Applications of Solid State Nuclear Track Detectors, Pinstech, Rawalpindi, Pakistan, March 1979

R. Brandt:
Overall Review of the Applications of SSNTD in Nuclear Physics

R. Brandt, P.A. Gottschalk, P. Vater:
An Application of SSNTD to Nuclear Physics: Multiprong Events in Heavy Ion Reactions, due to Multiple Sequential Fission

R. Brandt:
An Application of SSNTD to Nuclear Physics: Search for Superheavy Elements

G. Fiedler, U. Steinhauser, T. Rautenberg, R. Haag, P.A. Gottschalk:
Glass Detectors for Heavy Ions

K. Rashid, H.A. Khan, P. Vater, R. Brandt, G. Hussain, R.A. Akber:
First Indication of Multiple Sequential Fission in the Interaction of 7.38 MeV/nucleon Pb on Pb

R. Spohr:
Nuclear Track Research Activities at GSI

J. Tripier, M. Debeauvais:
Detector of Heavy Cosmic Rays aboard Cosmos 936

P. Vater, G. Tress, R. Brandt, B. Genswürger, R. Spohr:
Nuclear Track Microfilters Made of Mica

Journées de Tandem, Orsay, France, Januar 1979

P. Armbruster:
Tendances actuelles de la physique atomique auprès des accélérateurs

XI. EGAS Conference, Paris, Juli 1979

H.F. Beyer, R. Mann, K.H. Schartner, F. Folkmann:
Spectroscopic Investigation of Highly Charged Very Slow Recoil Ions

K.P.C. Spath, J. Bonn, W. Klempt, R. Neugart, B. Schinzler:
High Resolution Laser Spectroscopy of Neutron-Rich Rb and Cs-Isotopes in a Fast Atomic Beam

4th International Conference on Laser Spectroscopy, Rottach-Egern, 1979

H.J. Kluge, R. Neugart, E.W. Otten:
Laser Spectroscopy of Short-Lived Isotopes in Fast Atomic Beams and Resonance Cells

S. Liberman, J. Pinard, H.T. Duong, P. Juncar, J.L. Vialle, P. Pillet, P. Jacquinot, G. Huber, F. Touchard, S. Büttgenbach, C. Thibault, R. Klapisch, A. Pesnelle:
Hyperfine Spectroscopy of Radioactive Alcali Isotopes

International Symposium on Continuum Spectra of Heavy Ion Reactions, San Antonio, USA, December 1979

U. Arlt, R. Bass, J.v. Czarnecki, V. Hartmann, R. Renfordt, K. Sapotta, R. Zitzmann:
Scattering and Transfer in ^{40}Ar + ^{208}Pb Collisions at 236 MeV

R. Bass:
Coupling Between Mass and Energy Transport in Inelastic Nucleus-Nucleus Collisions

M. Dakowski, P. Doll, A. Gobbi, U. Lynen, A. Olmi, G. Rudolf, H. Sann, R. Bock:
Nuclear Structure Information in Dissipative Collisions

H. Freiesleben, P.R. Christensen, O. Hansen, O. Nathan, F. Videbaek, H.C. Britt, S. v.d. Werf:
Angular Momentum Transfer in Deep Inelastic Collisions of ^{86}Kr + ^{154}Sm at $E_{lab} \approx 1.3$ and ≈ 1.7 Times the Coulomb Barrier

W. Nörenberg:
Transport Theories of Dissipative Heavy-Ion Collisions: Survey and Recent Developments

K.E. Rehm, H. Essel, P. Sperr, K. Hartel, P. Kienle, H.J. Körner, R.E. Segel, W. Wagner:
Deep Inelastic Collisions at Energies Close to the Coulomb Barrier

H.J. Specht:
Fission Phenomena in Deep Inelastic Collisions

IEEE Nuclear Science Symposium, San Francisco, USA, October 1979

H. Spieler:
A DC Coupled Subnanosecond Linear Pulse Amplifier

M. Mutterer, J. Pannicke, K. Scheele, W. Spreng, J.P. Theobald, P. Wastyn:
A Multiparameter Gas-Scintillation Counter for Heavy Charged Particles

Topical Conference on Computerized Data-Acquisition Systems in Particle and Nuclear Physics, Santa Fee, USA, May 1979

R. Chestnut, B. Grasmück, R. Hadsell, E. Krieger, W. Lebershausen, J. Lowski, W. Plappert, M. Richter, H. Rother, O. Siart, R. Thieme:
The GSI Data-Acquisition System (EDAS)

Expertentreffen der Kernphysiker, Schleching, März 1979

J.V. Kratz:
N/Z-Äquilibrierung in der Kernspaltung und in gedämpften Schwerionen-Stößen

H.J. Specht: Spaltung

Summer Institute on Nucleus-Nucleus Interactions, Seattle, USA, August 1979

U. Mosel:
Yrast-Line Limitations to Fusion

Symposium on Atomic Spectroscopy, Tucson, USA, 1979

E.W. Otten:
Laserspectroscopy on Radioactive Atoms - Exploring Nuclear Structure off Stability

Spore Group Meeting at the 6th International Congress of Radiation Research, Tokyo, Japan, May 1979

M. Schäfer, R. Facius, H. Bücker:
Observation of Long Ranging Radial Inactivation Efficiency of Heavy Ions on Spores of Bacillus Subtilis

VIth International Seminar on Ion-Atom Collisions, Tokai-mura, Japan, September 1979

H. Backe, W. Bonin, W. Engelhardt, E. Kankeleit, M. Mutterer, P. Senger, F. Weik, R. Willwater, V. Metag, J.B. Wilhelmy:
Positron Production in Heavy Ion Collisions

H.F. Beyer, F. Folkmann, R. Mann, K.H. Schartner:
Selective Electron Capture into Slow Highly Ionized Recoil Atoms Produced in Heavy Ion-Atom Collisions

G. Soff:
Delta-Electrons from Heavy Ion Atom Collisions

2. Symposium über Synthetische Membranen in Wissenschaft und Technik, Tübingen, September 1979

G. Tress, P. Vater, R. Brandt:
Einige Eigenschaften von Kernspur-Mikrofiltern aus Glimmer

P. Vater, G. Tress, R. Brandt:
Properties of Microfilters Made of Mica

International School of Physics Enrico Fermi, Varenna, Italien, July 1979

A. Gobbi:
The Evolution of Dissipative Collisions

M. Dakowski:
Structure Effects in Dissipative Collisions

G. Wolschin:
Approaching Equilibrium in Heavy-Ion Collisions

Meeting of the American Physical Society, Washington, USA, April 1979

E. Hagberg, J.C. Hardy, L.C. Carraz, P.G. Hansen, B. Jonson, S. Mattson, H.L. Ravn, P. Tidemand-Petersson, G. T. Ewan:
A Precise Determination of the Excitation Energy of the Lowest T=3/2 State in ^{35}Ar

6.1.3 Seminars at other Instituts

P. Armbruster Univ. Marburg 1.2.1979	Hochenergieschwerionenexperimente ($E/_U$ > 20 MeV/u) in der Atomphysik
P. Armbruster Univ. Gießen 12.2.1979	Intermediäre, superschwere atomare Stoßsysteme - Experimente am UNILAC
P. Armbruster Univ. Groningen 3.5.1979	Experiments on Superheavy Nuclear and Atomic Systems
P. Armbruster Leningrad, UDSSR 4.6.1979	Atomic Physics Experiments at the UNILAC
P. Armbruster Nowosibirsk, UDSSR 20.6.1979	Experiments on Superheavy Atomic Collision Systems
P. Armbruster Eriwan, UDSSR 26.6.1979	Experimental News from UNILAC
P. Armbruster Dubna, UDSSR 28.6.1979	Experiments Concerning SHE at UNILAC
P. Armbruster Univ. Dortmund 3.7.1979	Atomstoßexperimente schwerer Systeme - Spektroskopie superschwerer Systeme
P. Armbruster CEN Bordeaux-Gradignan, France 20.7.1979	Etudes de la Fusion des Ions Lourds au Sépérateur "SHIP"
S. Ayik Univ. München July 1979	Statistical Description of the Heavy-Ion Collisions in the Adiabatic Representation
S. Ayik TH Darmstadt December 1979	The Time-Dependent Hartree-Fock Theory and the Statistical Treatment of the Two-Body Collisions
H. Backe Univ. Mainz January 1979	Atomphysikalische Prozesse beim Stoß sehr schwerer Ionen mit Atomen
H. Backe Univ. Basel 31.5.1979	Positronenerzeugung beim Schwerionenstoß
H. Backe Seattle, USA 14.9.1979	Atomic Processes in Close Collisions of Very Heavy Ions with Atoms
H.F. Beyer Univ. Gießen 25. 1. 1979	Röntgenspektroskopie an leichten Targetionen nach 1.4 MeV/u Schwerionenbeschuß
H.F. Beyer Univ. Bielefeld 26.10.1979	Selektiver Elektroneneinfang in hochionisierte langsame Atome, erzeugt beim 1.4 MeV/u Schwerionenbeschuß
H.F. Beyer HMI Berlin 7.11.1979	Spektroskopische Untersuchungen hochionisierter langsamer Atome
R. Bock KfK Karlsruhe 9.1.1979	Thermonukleare Fusion durch Trägheitseinschluß mit schweren Ionen
Siemens, Erlangen 14.1.1979	" " " "
Univ. Marburg 17.1.1979	" " " "
Univ. München 22.1.1979	" " " "
Univ. Gießen 18.6.1979	" " " "
TH Darmstadt 19.7.1979	" " " "
H. Bohn Seattle, USA 20.3.1979	Special Topics in Heavy Ion Research at GSI and Munich
H. Bohn ILL Grenoble France 5.12.1979	High Spin States in Neutron Rich Rare Earth Nuclei
H. Bokemeyer HMI Berlin 22.5.1979	Elektronen- und Positronenemission in Stößen sehr schweren Ionen
H. Bokemeyer Ibaragi, Japan 11.9.1979	Positron Creation in very Heavy Ion Collisions
H. Bokemeyer Tokyo, Japan 10.9.1979	Positron Creation in very Heavy Ion Collisions
H. Bokemeyer Fukuoka, Japan 14.9.1979	Pair Production from 1.4 GeV U-Atom Collision and Related Topics
R. Brandt Univ. Heidelberg 28.6.1979	Suche nach überschweren Elementen
R. Brandt Univ. Freiburg 12.12.1979	Können wir SHE nachweisen?
R. Brandt BMFT Bonn 16.10.1979	SHE im Atlantis-II-Schlamm?
R. Brandt NUKEM, Hanau 24.10.1979	Kernspur-Mikrofilter aus Glimmer
B.E. Fischer Univ. Bochum 15.1.1979	Schwere Ionen für Mikroskopie und zur Erzeugung von Mikrostrukturen
B. Fricke Grenoble, France January 1979	Relativistic Calculations of Molecules
B. Fricke Berlin June 1979	Ab Initio-Rechnungen in Atomen und Molekülen
H. Gäggeler Dubna, UDSSR 21.3.1979	Search for Superheavy Elements in Damped Collisions of ^{238}U with ^{238}U

H. Gäggeler Tokai, Japan 27.3.1979	Very Heavy Element Production Studies at GSI
P. Glässel Argonne, USA July 1979 East Lansing, USA July 1979 Berkeley, USA August 1979 Stanford, USA August 1979	Fission Properties of Trans-Fermium Nuclei Produced in Deep Inelastic Collisions
A. Gobbi Univ. Frankfurt September 1979	Kernstruktur-Effekte in tief-inelastischen Stößen
A. Gobbi Oak Ridge, USA November 1979	Nuclear Structure Information in Dissipative Collisions
G.M. Gowdy TU München February 1979	Gamma-Ray and Particles Decays of Very Neutron-Deficient Nuclei in the Trans-Tin Region
E. Grosse Univ. Louvai la Neuve, Belgium February 1979	In Beam Gamma Spectroscopy Experiments at GSI
E. Grosse Stony Brook, USA March 1979	On the Collectivity of Deformed Nuclei at High Spins
E. Grosse Copenhagen, Denmark, Nov. 1979	Multiple Coulomb Excitation of Heavy Deformed Nuclei with ^{208}Pb Beams
E. Grosse TU und LMU München November 1979	Coulombanregung von Hochspin-zuständen in schweren Kernen
E. Grosse TH Darmstadt December 1979	Multiple Coulombanregung von Schweren Deformierten Kernen
D.v.Harrach Copenhagen, Denmark	Fission Phenomena in Deep Inelastic Collisions
G. Huber Univ. Mainz May 1979	Hyperonische Kerne
G. Huber Univ. Mainz June 1979	Möglichkeiten und experimentelle Ansätze zum Bau von Röntgenlasern und von nuklear gepumpten Lasern
E. Kankeleit Univ. Konstanz 6.2.1979	Experimente an überschweren Quasiatomen
E. Kankeleit Ein Bokek, Israel 21.2.1979	Positron Experiments
E. Kankeleit NBI Copenhagen, Denmark 21.5.1979	Experiments on Superheavy Quasiatoms
E. Kankeleit Univ. Aachen 22. 10. 1979	Suche nach Superkritischen Coulombfeldern bei SI Stößen
P. Kienle Univ. Hamburg January 1979	Neue Entwicklungen in der Schwerionenphysik
P. Kienle Univ. Bordéaux February 1979	On the Superconducting, Sectorzyklotron "SUSE"
P. Kienle Erice, Italy April 1979	Central Collisions of Heavy Ions at Bombarding Energies Close to the Coulombbarrier
P. Kienle Erice, Italy April 1979	Experiments Related to Quantum Electrodynamics of Strong Fields
P. Kienle TU München May 1979	Neue Entwicklungen in der Schwerionenphysik
P. Kienle Bay. Akademie d. Wissenschaften July 1979	Supraleitendes Sektorzyklotron "SUSE"
P. Kienle MPI f. Kernphysik Heidelberg December 1979	Das Supraleitende Sektorzyklotron "SUSE" für München
R. Kirchner Univ. Mainz December 1979	On-line Massentrennung am UNILAC
H.J. Körner Groningen December 1979	Multinucleon Transfer in Heavy Ion Reactions
H.J. Körner Argonne, USA December 1979	Time Scales for Equilibration Processes in Heavy Ion Reactions
H.J. Körner Univ. Amsterdam December 1979	Multinucleon Transfer in Heavy Ion Reactions
C. Kozhuharov Univ. München 20.1.1979	δ-Strahlen aus Schwerionen-Stößen
J.V. Kratz Frankfurt 29.11.1979	Neuere Ergebnisse der Chemiegruppe: Superschwere Kerne, Coulombspaltung, und N/Z-Gleichgewicht
J.V. Kratz Univ. Bern 14.6.1979	Radiochemische Untersuchungen von Schwerionenreaktionen
D. Liesen HMI Berlin 6.6.1979	Innerschalenanregung sehr schwerer Stoßsysteme
D. Liesen Univ. Bonn 26.11.1979	Innerschalenanregung in Schwerionenstößen
D. Liesen Univ. Gießen 20.12.1979	Experimente zur Röntgenspektroskopie intermediärer, superschwerer Stoßsysteme
T. Lund Oak Ridge, USA 23.2.1979	Search for SHE in Nature and Reactions
T. Lund St. Louis, USA 27.2.1979	Search for SHE in Meteorites and Hot Brines

T. Lund Upton, USA 1.3.1979	Search for SHE in Nature and Reactions
T. Lund Oslo, Norway 3.7.1979	Search for SHE
R. Mann Univ. Gießen May 1979	Augerelektronenspektroskopie hochionisierter Targetatome nach Schwerioneneinschuß
R. Mann Univ. Bochum January 1979	Augerelektronenspektroskopie mit Schwerionen
P.H. Mokler Univ. Bochum 23.11.1979	Gibt es für die Innerschalen-ionisation beim Schwerionen-stoß Skalierungsgesetze?
P.H. Mokler TH Darmstadt 30.11.1979	Röntgenexperimente zu super-schweren quasimolekularen Stoßsystemen
T. Morović Bochum July 1979	Korrelationsdiagramme und die Schwerionenstreuung
T. Morović Regensburg December 1979	Atomphysikalische Aspekte der niederenergetischen Ion-Atom-Streuung
U. Mosel TH Darmstadt January 1979	Leichte Atomkerne bei hohen Drehimpulsen
U. Mosel Brookhaven, USA August 1979	The Role of the Yrast Line in Heavy Ion Fusion Reactions
U. Mosel Livermore, USA August 1979	Yrast Line Effects in Fusion Reactions
A. Müller Gießen 18.1.1979	Elektronenstoßionisation von Ionen
A. Müller Moskau, UDSSR 22.5.1979	On Charge Transfer and Electron Impact Ionization of Multiply Charged Ions
A. Müller Moskau, UDSSR 23.5.1979	Atomic Collision Processes Involving Highly Charged Ions
A. Müller Leningrad, UDSSR 30.5.1979	Latest Results of Cross Section Measurements with Multiply Charged Ions: Electron Capture and Electron Impact Ionization
A. Müller Dubna, UDSSR 13.6.1979	A Review on the Production of Highly Charged Ions and their Application in Collision Experiments
A. Müller Gießen 12.11.1979	Ionisation von Ionen durch Elektronenstoß
W. Nörenberg TU München 16.2.1979	Dissipative Schwerionenstöße
W. Nörenberg Copenhagen, Denmark, 26.3.1979	Transport Theory of Dissipative Heavy-Ion Collisions
W. Nörenberg Copenhagen, Denmark, 12.3.1979	Initial Correlations and the Dynamical Potential in Heavy-Ion Collisions
W. Nörenberg TH Darmstadt 9.11.1979	Relaxationsphänomene in Schwerionenstößen
W. Nörenberg Univ. Gießen 27.4.1979	Relaxationsphänomene in dissipativen Schwerionenstößen
W. Nörenberg Oak Ridge, USA 7.12.1979	Transport Theory and Doorway Confirguration in Dissipative Heavy-Ion Collisions
G. zu Putlitz Reading 4.4.1979	Lasers in Heidelberg
G. zu Putlitz Daresbury, U.K. 5.2.1979	The Nuclear Charge Radii of Odd and Even Calcium Nuclei
G. zu Putlitz Darmstadt 11.5.1979	Neues von den einfachsten myonischen Atomen
G. zu Putlitz Dubna, UDSSR 18.6.1979	SIS - Eine neue Beschleuniger-anlage für die GSI
G. zu Putlitz Engelberg, Switzerland, 26.9.1979	Report from GSI
G. zu Putlitz Darmstadt 2.11.1979	Moleküle - dauerhafte oder auch nur vorübergehende Verbindung zweier Atome
G. zu Putlitz Moskau, UDSSR 3.12.1979	Nuclear Charge Radii of Calcium Isotopes by Dye Laser Spectroscopy
F. Pühlhofer Daresbury, U.K. March 1979	The Magnetic Spectrometer at GSI - Concept and Plans for Experiments
A. Richter Saclay March 1979	Elastic and Deep-Inelastic Collisions in the System $^{40}Ar + ^{40}Ca$
M. Richter Argonne, USA April 1979	The GSI Data-Acquisition System
E. Roeckl Berkeley, USA June 1979	Decay of Very Neutron-Deficient Isotopes Close to the Proton Drip Line in the Trans-Tin Region
H. Sann Straßburg 14.6.1979	Low Energy Fission in the Superheavy Mass Region
H. Sann Saclay 28.8.1979	Un syncrotron a GSI
E. Salzborn 22.5.1979 Univ. Bonn 1.6.1979 Univ. Bielefeld 25.6.1979 MPI Heidelberg	Erzeugung und Umladung hochgeladener Schwerionen " " " " " "
E. Schneider Tokyo, Japan May 1979	A Comparison of the Inactivation of Dry and Wet Yeast Cells by Accelerated Heavy Ions of Very High LET
F. Schöpfer Lüttich, Belgien October 1979	Inactivation of Dried Yeast Cells by Heavy Ions

D. Schüll KFA Jülich 29.5.1979	Der GSI-Magnetspektrograph
D. Schüll KFK Karlsruhe 25.9.1979	Schwerionenspektrometer
D. Schüll Gent, Belgien March 1979	A Magnetic Spectrometer for Heavy Ions
D. Schwalm Groningen 1.3.1979	Multiple Coulomb Excitation with ^{208}Pb-Ions
D. Schwalm Utrecht 2.3.1979	Multiple Coulomb Excitation with ^{208}Pb-Ions
D. Schwalm Nashville, USA 14.3.1979	Coulomb Excitation with ^{208}Pb
D. Schwalm Straßburg, France 24.4.1979	γ-Spectroscopy of High Spin States
D. Schwalm HMI Berlin 2.5.1979	γ-Spektroskopie von Hochspinzuständen mit sehr schweren Ionen am Beispiel der Dy-Isotope
D. Schwalm MPI Heidelberg 31.5.1979	Der Dopplereffekt in der Kernphysik
D. Schwalm Gießen 5.7.1979	γ-Spektroskopie von Hochspinzuständen - die Dy-Isotope
R.S. Simon Heidelberg 22.2.1979	Messung der totalen γ-Energie nach Coulomb-Anregung
R.S. Simon München 31.5.1979	NaJ-Kristallkugel
R.S. Simon Orsay, France 15.11.1979	Rotation Alignment in Actinide Nuclei
R.S. Simon Bordéaux, France 23.11.1979	Evidence for Superdeformation in Nuclei at High Angular Momentum
H. Spieler Argonne, USA 2.10.1979	A Front-End View of Data-Acquisition at GSI
R. Spohr TH Darmstadt 3.5.1979	Einige Anwendungen der Kernspurtechnik
R. Spohr Köln 28.5.1979	Anwendungen der Kernspurtechnik am Beispiel ausgewählter Forschungsaktivitäten bei der GSI
R. Spohr Univ. Frankfurt 31.5.1979	Anwendungen der Kernspurtechnik am Beispiel ausgewählter Forschungsaktivitäten bei der GSI
R. Stock Univ. Heidelberg Jan. 1979	Kompression von Kernmaterie
Univ. Hamburg Apr. 1979	Relativistische Kernphysik
Univ. Frankfurt Feb. 1979	Hochenergie-Schwerionenreaktionen
J.P. Theobald Gent, Belgien 22.6.1979	Heavy-Ion Scattering
J.P. Theobald Leningrad, UDSSR 10.10.1979	Theory and Experiments on Heavy Ion Scattering
J.P. Theobald Leningrad, UDSSR 12.10.1979	Multiparameter Detectors for Heavy Charged Particles
P. Tidemand-Petersson Aarhus, Denmark January 1979	Determination of Nuclear Lifetimes by Particle X-Ray Coincidence Measurements
P. Vater TH Darmstadt 18.1.1979	Kernphysikalische Experimente mit Hilfe von SSNTD
K.J. Weber Tokyo, Japan May 1979	Effect of Radiation on Transcription of Ribosomal RNA in Yeast Cells
K.J. Weber Jülich October 1979	Ribosomal RNA-Synthesis in Dried Yeast Cells After Exposure to Heavy Ions
R. Weiner Irvine, USA May 1979	Hot Spots in Particle and Nuclear Physics
R. Weiner Univ. of Maryland USA, June 1979	New Results on Hot Spots in Nuclear Physics
R. Weiner FU Berlin October 1979	Hot Spots - Ein "gemeinsamer Markt" in Elementarteilchen- und Kernphysik
W. Westmeier KFA Jülich 24.9.1979	Zur Bestimmung der Wirkungsquerschnitte alpha-aktiver Produkte der Spallation von ^{232}Th mit 600-MeV Protonen
H.J. Wollersheim Univ. Frankfurt	Die Struktur der stabilen Dy-Isotope bei hohen Drehimpulsen
G. Wolschin TH München 13.2.1979	Drehimpulstransport in Schwerionenreaktionen
G. Wolschin Univ. Mainz 23.5.1979	Relaxationsprozesse in Schwerionenreaktionen
G. Wolschin Dubna, UDSSR 7.6.1979	Macroscopic Description of Low-Energy Heavy-Ion Collisions
G. Wolschin Straßburg 5.7.1979	Relaxation Processes in Heavy-Ion Collisions
G. Wolschin HMI Berlin 5.12.1979	Tiefinelastische Schwerionenreaktionen
J. Zylicz Univ. Mainz May 1979	Masses of Nuclides very far from Beta Stability
J. Zylicz Univ. Marburg July 1979	Masses of Nuclides far from Stability and Search for Proton Radioactivity
J. Zylicz Brookhaven, USA September 1979	Masses of Nuclides far from Stability and Search for Proton Radioactivity

6.1.4 Lectures and Courses

Lectures:

G. Herrmann	Kernchemie I + II (Universität Mainz)
H. Hultzsch	Datenverarbeitung im physikalischen Experiment (Universität Mainz)
J. Klabunde	Physik für Elektrotechniker (Fachhochschule Darmstadt)
K.P. Lieb P.H. Mokler	Kern- und Atomphysik mit schweren Ionen (Universität Köln)
D. Liesen	Physik für Maschinenbauer (Fachhochschule Darmstadt)
G. zu Putlitz	Atomphysik (Universität Heidelberg)
G. zu Putlitz	Atomphysik mit schweren Ionen (Universität Heidelberg)
G. Soff	Relativistische Quantenmechanik (Universität Frankfurt/M)
G. Soff	Quantenelektrodynamik (Universität Frankfurt/M)
G. Soff	Ergänzungen zur Mechanik I (Universität Frankfurt/M)
R. Stock	Großforschung - Struktur und Ziele (Universität Marburg)

Courses:

G. Herrmann	Kernchemisches Praktikum I + II (Universität Mainz)
R. Keller	Seminar über Ionenquellen (Fachhochschule Wiesbaden-Rüsselsheim)
W. Neuwirth M. Kleber P.H. Mokler M. Dost	Oberseminar über Stoßprozesse (Universität Köln)
R. Stock	Hochenergie-Schwerionenphysik

6.2.1 Conferences and Seminars on Research Proposals

19.1.	Workshop on Physics with the Crystal Ball	
31.1.	Research Seminar	Nuclear Track Technique
14.2.	Research Seminar	Quasi-Elastic and Deep Inealstic Collisions
21.3.	Research Seminar	Atomic Spectroscopy
4.5.	Computer Workshop	
9.5.	Research Seminar	Atomic Reactions
6.6.	Research Seminar	Atomic Physics
14.11.	Research Seminar	Nuclear and Atomic Physics
17.12.	Anniversary Ceremonies - 10 Years GSI	

6.2.2 Seminars at GSI

08.01.	H. Breuer Maryland (USA)	Studium der Ladungs- und Massenverteilung bei tiefinelastischen Reaktionen von Fe auf Bi und Ho bei 300-500 MeV
16.01.	P.Kleinheinz Jülich	High Spin Spectroscopy Related to the Double Shell Closure at ^{146}Gd
17.01.	H. Oeschler Strasbourg (Frankreich)	Grenzen der Compoundkernspaltung bei mittelschweren Kernen
29.01.	G. Westfall Berkeley (USA)	Production of exotic nuclei from fragmentation of ^{40}Ar and ^{48}Ca at 200 MeV/A incident energy
30.01.	K.P. Lieb Köln	Zum Zeitverlauf von YRAST-Kaskaden in mittelschweren Kernen
31.01.	C.H. Stoller Zürich (Schweiz)	Quasi molekulare Röntgenstrahlung bei Schwerionenkollisionen
05.02.	J. Merdinger Strasbourg (Frankreich)	High Spin Structure of Rare Earth Nuclei
05.02.	I. Lindgren Göteborg (Schweden)	Atomic-beam Experiments on Short-Lived Nuclei at ISOLDE, CERN
06.02	J.P.Blaser Villigen (Schweiz)	Das Schweizerische Institut für Nuklearforschung: Anlagen, Forschungsprogramm, Pläne
07.02.	P. Mokler GSI	Polarisationsmessung der Quasi-molekularen Strahlung, Ergebnisse aus Chalk River
13.02.	G.A. Voss Hamburg	PETRA
21.02.	G. Kraft GSI	Medizinische Anwendungen hochenergetischer Ionen
28.02.	G. Siegert GSI	Detektoren zur Bestimmung von Energie und Kernladung von Spaltprodukten
06.03.	Y. van der Meulen Yorktown Heights, (USA)	The IBM Research Program
06.03.	P. Doll GSI	Untersuchungen von Schwerionenreaktionen bei 20 MeV/u am 88" Zyklotron u. bei 200 MeV/u am Bevalac
13.03.	M. Faessler Genf (Schweiz)	Die Reaktion von Kernmaterie auf hochenergetische Hadronen
14.03	C. Pomorski Lublin (Polen)	Dynamical Calculation of the Spontaneous Fission Halflife for Even and Odd-Even Nuclei
16.03.	E. Roeckl, S. Hofmann GSI	Exotische Kerne am Massenseparator; Exotische Kerne am Geschwindigkeitsfilter
20.03.	W. Bleuel GSI	Lötttechniken in der GSI
20.03.	W.G. Meyer GSI/LBL	Target Fragmentation in Relativistic Nuclear Collisions
22.03.	A. Sandoval Uni. Marburg	Pion Production in Relativistic Nuclear Collisions
27.03.	Y.-K. Kim Illinois (USA)	Inertial Confinement Fusion by Heavy Ions
03.04.	C. Toepffer Johannesburg (Südafrika)	Quadrupolriesenresonanzen im ^{12}C-^{12}C System
10.04.	H. Aufhaus Uni. Mainz	Aufbau und Einsatz eines Array-Prozessors am Institut für Kernphysik der Universität Mainz
24.04.	R. Stock GSI	Kompression von Kernmaterie
25.04.	R. Piercey GSI	Lebensdauermessungen an ^{238}U mit der Doppler-Shift-Attenuation-Methode
02.05.	C. Riedel GSI	Statistische Fluktuationen in in tiefinelastischen Reaktionen
08.05.	K. Schadewaldt Heidelberg	Eine interaktive Version des SPITBOL-Compilers
08.05.	W. Greiner Frankfurt	Quantenelektrodynamid der starken Felder u. überschwere Quasimoleküle - die fundamentalen Probleme der niederenergetischen Schwerionenforschung
10.05.	R. Stock GSI	Physik der Hadron-Hadron Streuung
10.05.	A. Daneels Genf (Schweiz)	Structured Design Benefits to a Process Control Software Project

15.05.	R. Stock GSI	Relativistische Kinematik
15.05.	W. Brandt München	Positronenfieber
16.05.	J.A. Maruhn GSI	Massenverteilung in der Fragmentations-Theorie
21.05.	H.Kähler IBM	Die Version 2 des Betriebssystems MVS/SE
22.05.	R. Cusson Durham (USA)	Array - Processing Techniques
23.05.	G.M. Ter-Akopian Dubna (UDSSR)	Recent Results in the Search for Superheavy Elements in Nature
28.05.	E. Breuer GSI	Methoden der Datenfernübertragung
29.05.	D. Böhne GSI	Eine Beschleuniger-Anlage für relativistische Schwere Ionen
30.05.	P. Glässel Uni Heidelberg	Spalteigenschaften von Kernen an den Grenzen der Stabilität
31.05.	C. Riedel GSI	Relativistische Kinematik II
05.06.	Th. Hänsch Stanford (USA)	Hochauflösende Laser-Spektroskopie
06.06.	G.E.Brown, Stony Brook (USA)	The Little Bag
06.06.	E. Murnick Murray Hill (USA)	Laser Lamb Shift Spectroscopy on High Z Heavy Ions
07.06.	H. Emling GSI	Kaskadenmodelle
11.06.	H. Rafelski GSI	Die Graphik-Systeme beim CERN
12.06.	C. Rolfs Münster	Neuere Untersuchungen zur nuklearen Astrophysik
13.06.	R. Stock GSI	Kaskadenmodelle II
13.06.	M. Hass, Israel	Atomic Polarization Effects and Nuclear Magnetic Moments
18.06.	M. Steitz GSI	Behandlung untergliederter Dateien in PL/1
18.06.	S. Glückert GSI	Vielfach-Genauigkeit in FORTRAN
19.06.	M. Dost Köln	K-Schalenionisation und Compoundkernanregung
20.06.	P. Vincent GSI	Selective Observation of Continuum X-Rays from Pd+Pd Collisions
20.06.	C.Kozhuharov GSI	δ-Elektronen-Emission in Schwerionenstößen
28.06.	H.Freiesleben GSI	Thermodynamik I
28.06.	R. Burke Argonne, (USA)	Heavy Ion Fusion at ANL
03.07.	H. Ströbele Heidelberg	Auswertung von Bildern der Streamer- und Blasenkammer
03.07.	J. Knoll Heidelberg	Dynamische u. statistische Aspekte hochenergetischer Kernreaktionen
06.07.	W. Johnson Cambridge (USA)	Applications of the Rel. Random Phase Approx. to the Determination of the Transition Probabilities
10.07.	J. Forster Chalk River Kanada	Time Evolution Studies of Heavy Ion Induced Fission
11.07.	N. Stolterfoth Berlin	Anregung und Zerfall ausgerichteter Zustände bei energiereichen Ion-Atom-Stößen
12.07.	H. Sann GSI	Relat. Termodynamik II
17.07.	R. Sizmann München	Solare Energienutzung
27.08.	W. Kutschera Argonne (USA)	Nachweis von Radioisotopen mit Tandem-Beschleunigern
27.08.	W.Schimmerling Berkeley (USA)	Neutron Production in Relativistic Nuclear Interactions
28.08.	Jean, Camplan Orsay (Frankreich)	Status Report on the Orsay Separator Development
11.09.	W. Cassing	Quantenfluktuationen in tiefunelastischen Reaktionen
18.09.	G.Holzwarth Siegen	Bemerkungen zur Fluiddynamik für Kerne
18.09.	M. Kleber Köln	Bindung, Polarisation und Rückstoß im asymmetrischen Atomstoß
09.10.	Y. Yariv Rehovot, (Israel)	Microscopic Cascade Calculations for Relativistic Nuclear Reactions
09.10.	A.A.Ogloblin Moskau (UDSSR)	Report from the Kurchatov Institute (Nuclear Reaction Experiments and Accelerator Plans)
17.10.	F. Bosch GSI	Neue Messungen zur stoßparameterabhängigen 1 sσ - Ionisation im Bereich $[133 \leq Z_1 + Z_2 \leq 178]$
23.10.	P.Ambruster GSI	Untersuchungen zur Fusion im Massengebiet N=126 - mögliche Rückschlüsse auf das Gebiet der überschweren Elemente um N=184
24.10.	M. Dakowski	Structure Effects in Dissipative Collisions
29.10.	Dr. Silver Oxford (England)	Some Measurements in Helium-like Ions
30.10.	M. Lefort Orsay (Frankreich)	Present Status of Ganil Construction. Plans for Experimental Equipment
31.10.	P. Hess Uni Frankfurt	Theorie der Spektren schwerer Kerne im Rahmen kollektiver Kernmodelle

31.10.	K. Pomorski Lublin (Polen)	Application of a Fokker-Planck Equation to the Fission Dynamics
06.11.	E. Werner Hannover	On the Strutinsky Shell Corrections in the Lead Region
07.11.	M. Richter GSI	GOLDA's Zukunft
13.11.	M.Deutschmann Aachen	Die Übergangsstrahlung und ihre Anwendung zur Identifizierung geladener Teilchen hoher Energien
15.11.	H. Krappe Berlin	Vergleich von Modellen für die Fusion
19.11.	A. Urnov	Highly charged Ions and X-Ray Spectroscopy of high temperature Plasma
20.11.	J. Hüfner Heidelberg	Einige einfache Konzepte in der Streuung Schwerer Ionen bei hohen Energien
20.11.	R. Hagedorn Genf (Schweiz)	Vom Kerngas zur Hadronenmaterie
27.11.	W. Weise Regensburg	Pion-Kondensation in dichter Materie und präkritisches Verhalten in Kernen
28.11.	K. Blasche GSI	Schwerionenbeschleuniger der 80er Jahre bei GSI und anderswo
04.12.	J. Hüfner Heidelberg	Einige einfache Konzepte in der Streuung schwerer Ionen bei hohen Energien
04.12.	J. Maruhn Frankfurt	Systematisches Studium kollektiver Potentialflächen
05.12.	S. Humphries Albuquerque (USA)	High Current Pulsed Linear Ion Accelerators
11.12.	K.H.Beckurts Jülich	Wohin geht die Kernenergie
12.12.	R. Männer Jülich	Überlegungen zu Struktur und Einsatz eines flexiblen Multiprozessor-Systems
14.12.	R.A.Broglia	Nuclear Collective Motion Probed in Heavy-Ion Collisions
18.12.	H.Kleinpoppen Bielefeld	Winkelkorrelationen und Spin-Effekte in atomaren Stoßprozessen
19.12.	R.O.Bangerter Danville (USA)	Inertial Fusion Option: Photons, Electrons and Ions
19.12.	S. Ayik GSI	Time-dependent Hartree-Fock theory and statistical treatment of two-body collisions
19.12.	J.Klabunde P.Strehl GSI	UNILAC 79/80

6.2.3 GSI-Berichte (Reports)

79 - 1 P. Brix
Anfänge und Fortschritte der Schwerionenforschung.
Festvortrag zum 70. Geburtstag von Christoph Schmelzer am 17.11.1978

79 - 2 U. Reus, W. Westmeier, I. Warnecke
Gamma-Ray-Catalog

79 - 3 R. Bock, A. Gobbi, H. Sann, H. Stelzer, U. Lynen, A. Olmi
Large Area Two Dimensional Position Sensitive Detectors

79 - 4 H. Bokemeyer
Atomic Physics with Heavy Ions

79 - 5 W. Nörenberg
Transport Theory of Dissipative Heavy Ion Collisions

79 - 6 H.F. Beyer
Röntgenspektroskopie an leichten Targetionen nach 1,4 MeV/amu Schwerionenbeschuß

79 - 7 R.W. Müller
Layout of a High-Intensity Linac for very Heavy Ions with R.F. Quadrupole Focusing

79 - 8 M. Schädel
Radiochemische Messungen der Bildungsquerschnitte von Aktinidenisotopen in der Reaktion von ^{238}U-Ionen mit ^{238}U

79 - 9 H. Stöcker
Zur Untersuchung stark komprimierter und hochangeregter Kernmaterie in relativistischen Schwerionenstößen

79 - 10 W.E. Frahn
Closed-Form Description of Heavy-Ion Transfer Reactions Based on Distorted-Waves Theory

79 - 11 Jahresbericht 1978

79 - 12 A.A. Ogloblin
The Problem of the Neutron Nuclei: Why they can Exist and how to Look for them

79 - 13 P. Strehl. J. Klabunde, V. Schaa, H. Vilhjalm H. Vilhjalmsson, D. Wilms
Das Phasensondenmeßsystem am UNILAC
Sondendimensionierung und Signalauswertung

Ansprachen anläßlich der Amtsübergabe von Herrn Prof. Dr. Christoph Schmelzer, wiss.-techn. Geschäftsführer der GSI in den Jahren 1971-1978 an Herrn Prof. Dr. Gisbert zu Putlitz am 15.9.1978

GSI 1969 - 1979
Schritte zur Gründung der GSI
Rede des Aufsichtsratsvorsitzenden der GSI, Ministerialdirigent Dr. Josef Rembser, anläßlich der Verabschiedung von Prof. Dr. Ch. Schmelzer als wiss.-techn. Geschäftsführer der GSI am 15.9.1978

6.2.4 Visiting Groups at GSI

19.01.	Berufsbildungsschule, Mainz	19	Personen
26.01.	Fr. Ebert Gymnasium, Mühlheim	11	"
21.02.	GID und GSI	15	"
21.02.	Georg Büchner Schule, Darmstadt	15	"
5.03.	Schülerpraktikanten	10	"
19.03.	Berufsförderungswerk, Frankfurt	23	"
19.03.	Fachhochschule, Rüsselsheim	20	"
22.03.	Physik-Kurs, Gesamtschule Groß-Bieberau	12	"
23.03.	Physikalisches Institut, HD	40	"
24.04.	SPD-Fraktion des Ortsbeirates Wixhausen	17	"
28.04.	Fa. Pittler AG, Langen	22	"
15.05.	Physikstudenten, Würzburg	24	"
16.05.	Fa. Klein, Schanzlin und Becker	18	"
16.05.	Americain High School, Bad Kreuznach	9	"
17.05.	Kantschule, Rüsselsheim	20	"
18.05.	Gymnasiale Oberstufe	25	"
12.06.	VDE Hamburg	18	"
12.06.	Akademischer Verein, Darmstadt	12	"
27.06.	Amerik. Hochschulpräsidenten	10	"
27.06.	Physikstudenten, Heidelberg	140	"
5.07.	Kerntechnische Gesellschaft, Karlsruhe	16	"
5.07.	Kernchemie, Mainz	25	"
11.07.	Studienstiftler, Humangenetik	6	"
11.07.	Kernphysik, Marburg	31	"
16.07.	Kernforschungszentrum, Karlsruhe	10	Personen
17.07.	Physikstudenten, TU München	57	"
7.08.	Armed Forces Communications and Electronics Association	50	"
3.10.	Fa. BBC, Mannheim	5	"
4.10.	Fernmeldeamt, Wiesbaden	6	"
29.10.	Fachhochschule Wiesbaden	11	"
30.10.	Städt. Krankenanstalten, Mannheim	27	"
31.10.	KfK und Interatom	26	"
1.11.	Fachhochschule Rüsselsheim	20	"
5.11.	Fachbereich Elektrotechnik, TH Darmstadt	8	"
6.11.	Physikkurs, Hilda-Gymnasium, Koblenz	23	"
8.11.	Fachhochschule Würzburg/ Schweinfurt	19	"
13.11.	Physikkurs, Justus-Liebig-Schule,Darmstadt	18	"
23.11.	Inst. für Physikal. Chemie, Heidelberg	13	"
23.11.	Fa. Siemens, Frankfurt	30	"
28.11.	Fachhochschule, Darmstadt, Maschinenbau	21	"
30.11.	Kernphysikstudenten, Karlsruhe	10	"
10.12.	Physikstudenten, TU München	13	"
19.12.	Studentenverbindung, Rheinpfalz	10	"
20.12.	Physik-Kurs, Freiherr vom Stein-Schule, Frankfurt	33	"
		968	Personen

6.3. Scientific Committees, Directorate and Personnel

Scientific Council

Prof. P. Brix (Heidelberg, Chairman), Prof. P. v. Brentano (Köln), Dr. R. Gremmelmaier (Erlangen), Dr. H. A. Grunder (Berkeley), Dr. W. Hilger (Hoechst), Prof. H. W. Levi (Berlin), Prof. K. H. Lieser (Darmstadt), Prof. B. Povh (Heidelberg), Prof. E. Schopper (Frankfurt), Prof. G. Stöcklin (Jülich), Prof. E. Werner (Hannover)

Program Advisory Committee

Prof. E. W. Otten (Mainz, Chairman), Prof. P. Armbruster (GSI), Dr. K. Blasche (GSI), Prof. R. Bock (GSI), Dr. D. Böhne (GSI), Prof. H. Ewald (Gießen), Dr. A. Gobbi (GSI), Prof. W. Greiner (Frankfurt), Prof. G. Herrmann (GSI), Prof. E. Kankeleit (Darmstadt), Prof. P. Kienle (München), Dr. J. V. Kratz (GSI), Dr. P. Mokler (GSI), Prof. W. Nörenberg (Heidelberg), Prof. W. v. Oertzen (Berlin), Dr. E. Roeckl (GSI), Dr. D. Schwalm (GSI), Prof. H. J. Specht (Heidelberg), Prof. G. K. Wolf (Heidelberg)

Scientific Directorate

Prof. G. zu Putlitz (Chairman, Scientific and Technical Managing Director), H. O. Schuff (Administrative Managing Director), Prof. P. Armbruster, Prof. R. Bock, Dr. D. Böhne, Prof. G. Herrmann

Scientific and Technical Division Leaders

Prof. P. Armbruster, Prof. R. Bock, Dr. D. Böhne, Prof. G. Herrmann, Prof. W. Nörenberg, Dr. D. Schwalm

Scientific Committee

Dr. D. Schwalm (Chairman), Dipl.Chem. H. Ahrens, Dr. N. Angert, Dr. K. Blasche, Ing. grad. K. H. Burkard, Dr. A. Gobbi, Dr. H. Hultzsch, Dr. J. Klabunde, Dr. G. Kraft, Dr. J. V. Kratz, Dr. D. Liesen, Dr. P. Mokler, Dr. H. Prange, Prof. G. zu Putlitz, Dr. W. Reisdorf, Dr. M. Richter, Ing. grad. D. Wilms

Scientific Guests and Consultants

Y. Avishai (Israel), S. Ayik (Turkey), A. Balanda (Poland), M. Charifi (Iran), Y. T. Chu (People's Rep. China), R. Cusson (USA), M. Dakowski (Poland), S. Dhawan (India), K. Dietrich (FRG), R. Ferguson (USA), G. Gowdy (USA), J. Greenberg (USA), W. Greiner (FRG), M. Gyulassy (USA), R. Hahn (USA), M. Hass (Israel), G. Holzwarth (FRG), J. Hüfner (FRG), K. Hulet (USA), S. Ito (Japan), T. Kitahara (Japan), M. Kleber (FRG), C. Kozhuharov (stateless), R. Kulessa (Poland), Y. Laichter (Israel), H. Liesem (FRG), R. Lougheed (USA), U. Lynen (FRG), D. Maor (Israel), S. Matsuki (Japan), J. McGrory (USA), A. Merchant (Great Britain), W. Meyer (USA), U. Mosel (FRG), M. Moshinsky (Mexico), J. Nitschke (USA), J. Nyman (Sweden), P. Oblozinsky (Czechoslovakia), R. Piercey (USA), A. Plochocki (Poland), J. Poitou (France), S. Polikanov ([USSR] Denmark), G. Prete (Italy), F. Pühlhofer (FRG), C. Riedel (FRG), R. Santo (FRG), A. Schett (Austria), Ch. Schmelzer (FRG), R. Schule (FRG), J. Schweppe (USA), W. C. Shen (People's Rep. China), A. Shergin (USSR), T. Sikkeland (Norway), G. Soff (FRG), H. Stock (FRG), H. Stöcker (FRG), P. Tidemand-Petersson (Denmark), P. Vincent (USA), H. Wieman (USA), G. Wolschin (FRG), J. Wood (USA), E. C. Wu (People's Rep. China), H. Yadav (India), Y. Yariv (Israel), J. Zylicz (Poland).

Scientific Personnel

H. H. Ahrens, J. Ahrens, R. Albrecht, N. Angert, P. Armbruster, H. Beyer, K. Blasche, R. Bock, D. Böhne, H. Bokemeyer, F. Bosch, G. Breitenberger, W. Brüchle, L. Dahl, H. D. Dohmann, P. Doll, J. Dusek, H. Egger, H. Emling, M. Emmerling, J. G. Festag, P. Finke, B. Fischer, H. A. Folger, B. Franczak, B. Franzke, H. J. Freiesleben, P. Fuchs, H. Gäggeler, H. Geissel, I. Giese, J. Glatz, S. Glückert, A. Gobbi, E. Grosse, U. Grundinger, H. Gutbrod, T. Gyoerffy, H. Günter, D. Hartwig, G. Herrmann, F. P. Hessberger, K. Hildenbrand, S. Hofmann, A. Huber, G. Huber, H. Hultzsch, G. Hutter, W. Jacoby, K. Kaspar, H. J. Keller, R. Keller, M. Khaouli, R. Kirchner, J. Klabunde, O. Klepper, G. Kraft, J. V. Kratz, B. Langenbeck, H. D. Liesen, J. Lowsky, H. J. Lustig, R. Mann, D. Marx, P. H. Mokler, M. Müller, R. Müller, G. Münzenberg, F. Nickel, W. Nörenberg, K. Poppensieker, H. Prange, G. zu Putlitz, H. Rafelski, W. Reisdorf, M. Richter, E. Roeckl, C. Sahm, H. J. Sann, M. Schädel, E. Schaffner, K. H. Schmidt, W. Schneider, D. Schüll, H. Schulte, R. Schulze, D. Schwalm, O. Siart, G. Siegert, R. S. Simon, H. Spieler, R. Spohr, R. Steiner, H. Stelzer, H. J. Stock, R. Stock, P. Strehl, H. Ströbele, J. Struckmeier, K. Sümmerer, H. Trautmann, G. Ulm, F. Weik, W. Weizel, M. Wiemers, K. Winkelmann, G. Wirth, G. Wohlrab, B. Wolf, H. Wollersheim, V. Zelba.

Technical and Administrative Staff

F. Achenbach, J. Alt, L. Appel, K. Arnold, G. Augustinski, E. Babinsky, A. Bach, G. Baumann, E. Bayersdorf, H. J. Beeskow, E. Benz, G. P. Benz, H. J. Benz, W. Bergsträsser, L. Bernhardt, H. Bingel, H. Blaschke, W. Bleuel, H. Blinn, F. Blumert, W. Bock, P. Borisch, I. Bormet, R. Bormet, J. Bossler, W. Bourgeois, W. Brenger, E. Breuer, H. Britz, N. Brunner, C. Bruske, D. Bruske, K. H. Burkard, H. G. Burkhard, R. Christmann, H. Dächert, H. Damm, H. W. Daues, J. R. Dengler, G. Dick, I. M. Diedrich, R. Diehl, H. Döpke, R. Döring, H. Dünkel, R. Dünkel, O. Eberhardt, H. Eckhardt, K. A. Ehrich, M. F. Eick, G. Eisold, E. Eitel, H. Emig, W. Enders, G. Englert, U. Ernst, H. Fischer, G. Fliss, M. Fradj, O. Frank, P. W. Frank, G. R. Freiwald, P. Freudenberger, E. Fritsch, G. Fröse, R. Gärtner, H. Gaiser, K. D. Ganser, A. Gasper, M. Gassner, H. Gebhardt, B. Genswürger, I. Georg, E. Gerbig, O. Gerhardt, H. Gilbert, W. Gockel, M. G. Göttmann, V. G. Gomez, K. Graf, B. Grasmück, H. Grein, G. Grill, D. Grimm, G. Grimm, H. Grösch, J. Grösser, G. Grom, H. Gross, J. Gross, W. Gutowski, K. H. Haag, E. Häcker, B. Häfner

D. Hager, R. v. Hagen, W. Hahn, P. Hahne, P. Hahnel, H. Hammal, E. Hammann, E. Hanel, H. Hardel, O. Hartmann, W. Hartmann, W. Hartmann, M. Hartung, T. Heinbüchner, K. Heinz, I. Heipke, D. Held, H. Heller, H. Helms, H. Hewig, J. Hey, R. Hill, F. Himmelmann, C. Hoffmann, K. D. Hoffmann, N. Hofmann, L. Horas, H. Horneff, A. L. Hotop, R. Hotz, W. v. d. Hoya, W. Huber, W. Hüller, G. Ickert, W. Ille, K. Illert, H. Jakobi, S. Jansen, G. K. Jöst, L. Kabey, R. Kaiser, H. J. Kalawsky, E. Kammer, W. Kappel, F. Keil, H. L. Kempf, H. R. Kiesewetter, N. Kischnick, A. Kissler, G. Klappich, H. Klecker, H. Klemm, J. Klemm, G. L. Klinger, K. Klingler, P. Klink, F. P. Klinke, R. Kluber, K. D. Knapp, U. Kniess, W. Köthe, K. Kohl, U. Kopf, H. Kraus, K. R. Kress, W. Kreuzer, H. Krichbaum, A. Kritzer, C. Kröh, L. Krueger, G. Kube, M. K. Kucharczyk, H. Kühn, J. Kühtz, K. Küper, W. Kunz, H. P. Kurz, R. Kutschka, E. Labinsky, H. Lameli, H. Langendorf, G. Langer, H. Larem, B. Lasitschka, K. D. Leible, G. Leidel, E. Leiser, H. Leiser, W. Leiser, G. Lenz, H. Leonhardt, H. P. Liebold, L. Liebschwager, G. Lingk, F. List, A. Lörcher, D. Loos, A. Lorenz, W. Losert, M. Ludwig, S. Lüttges, D. Macina, H. Mader, K. H. Mader, E. Magnussen, E. Malwitz, I. Malwitz, H.G. Manns, H.G. Martens, W. Marx, R. Matheis, K.H. Matthöfer, R. Mayr, H. Meder, H. Meister, D. Metzger, S. Metzger, W. Meufels, G. Micsa, A. Mittelstädter, E. Mitz, K. Möller, K. Mömerzheim, L. Molnar, A. Morhardt, I. Morrison, T. Mrugalla, C. H. Mühle, A. Müller, B. Müller, E. Nagel, K. H. Neff, W. Neuhäuser, A. Nicklas, G. Niemann, D. Nitsch, R. Norcia, W. Österreich, G. Olscha, G. Pabst, J. Palm, F. Peldzinski, H. Peter, K. Petrich, E. Pfaff, E. L. Pfaff, K. L. Pfaff, R. Pfeiffer, E. Pfeng, P. Pfitzenmeier, A. Poppe, I. Poppert, W. Quick, D. Quis, M. Rack, E. Rass, U. Regenfuß, W. Rehm, H. Reining, H. Riesner, D. Rochna, C. Röder, D. Röder, H. Röder, W. Rösch, R. Rulfs, W. Salzer, B. Schabelsky, H. W. Schäffer, F. Schäffer, B. Schätzke, H. Schiemann, G. Schill, E. Schimpf, D. Schmalz, G. Schmelig, H. G. Schmidt, W. Schmidt, L. Schmiedler, R. Schmitt, K. Schneider, K. Schneider, N. Schneider, H. J. Schött, W. Schorstein, W. Schue, I. Schüler, H. Schütz, H. O. Schuff, R. Schumann, G. Schunk, W. Schuth R. Schwarz, V. Schwarz, R. Schwedhelm, G. Schweipert, U. Seckert, S. Selent, R. Sigmund, H. Sitta, G. Sobainsky, H. Spengler, S. Sperling, W. Spiess, H. Spika, A. Stagno, M. Steitz, E. Stenger, J. Störmer, U. Stork, W. Stork, I. Strehl, G. Stubenrauch, E. Sturm, A.Suderleith, K. Süßbrich, D. Svrcina, W. Thalheimer, A. Theis, R. Thieme, H. Thomas, E. Thurau, H. Valter, E. Veith, H. Vilhjalmsson, W. Vinzenz, H. Vogel, U. Vogel, I. Vogeley, D. Vogt, R. Vrtal, V. Wagner, H. Wahl, K. Waitz, G. Wannemacher, I. H. Warsow, R. Weber, W. Weber, P. W. Weinreuter, L. Weiss, D. Wendt, E. Werkmann, D. Werner, W. Weyrich, G. Wilde, K. Wilhelm, S. Wilhelm, D. Wilms, H. Wirth, W. Wissing, W. Wissmann, H. Wörner, G. Wolf, H. Ziegler, A. Ziem, E. Zilch, A. Zschau, K. Zweig.

6.4 Author Index

Abul- Naga, N. 69
Achenbach, Ch. 118
Albrecht, R. 162, 193
Alquist, L. 31, 51
Angert, N. 210
Armbruster, P. 6, 55, 56, 59, 104, 106, 107, 108, 120, 122, 123, 124, 181
Artl, U. 21, 22, 23, 24, 184
Augustinski, G. 164, 179
Ayik, S. 85, 86
Baba, C. 50
Backe, H. 4, 101, 168
Balanda, A. 41, 102, 161
Baltschukat, K. 150
Bangert, D. 15, 20
Bangert, U. 144
Bass, R. 21, 22, 23, 24, 184
Beck, F. 3, 11, 79
Becker, R. 119
Beckmann, R. 33
Beeskow, H.J. 161, 164
Beier, G. 18, 19
Berdermann, E. 100, 103
Bergmann, E. 52
Bethge, K. 102, 160, 161
Betz, W. 131, 132
Beyer, H.F. 111, 114, 115, 167
Bimbot, R. 120
Björnholm, S. 9, 48, 49, 50
Björnstad, T. 35
Blasche, K. 202, 215
Bleuel, W. 202
Bock, F. 214
Bock, R. 9, 10, 13, 166
Böhne, D. 215
de Boer, J. 183
Bohn, H. 43
Bond, P. 2
Bokemeyer, H. 100, 102, 105, 161
Bonin, W. 101, 168
Bonn, J. 173
Bopp, P. 52
Borggreen, J. 48, 49
Bosch, F. 100, 103, 106, 107, 108, 109, 112
Brandt, R. 33, 51, 64, 65, 158, 191
Brannigan, J.P. 38
Breitenberger, G. 220
von Brentano, P. 117
Breskin, A. 24
Britt, H.C. 18, 19, 25
Brüchle, W. 5, 27, 28, 29, 60, 63, 121
Brügger, M. 174
Brülls, P. 187, 189
Bruske, C. 169
Buchwald, G. 84, 92
Buck, P. 78
Bücker, H. 150
Busch, F. 2, 3, 20, 185
Busch, R. 214
Burkard, K.H. 169, 170, 171
Butler, P.A. 4
Cassing, W. 75
Chandra, H. 67
Christensen, O. 48, 49, 50
Christensen, P.R. 2, 25
Chu, Y.T. 9, 10, 164, 182
Civelekoglu, Y. 30, 178
Clemente, M. 100, 103
Clerc, H.G. 6, 8, 125
Cole, J.D. 58
Csernai, L.P. 91, 92
Cusson, R. Y. 83, 84, 88, 89, 91, 92
Dakowski, M. 13, 24
Dauer, U. 151
Daues, H.W. 164, 182
Debeauvais, M. 34
Degheidi, A.R. 82
Dehmelt, G. 117
Dehnhardt, W. 196
Delic, G. 3
Del Zoppo, A. 48, 49
Dengler, J. 193
Depta, K. 82
Dersch, G. 31, 51
Diebel, M. 66, 67
Dietrich, K. 71
Dohmann, H.D. 116
Doll, P. 13, 24, 164
Dorsch, C. 52
Dusek, J. 193
Ehrich, A. 214
Elze, Th.W. 44, 46
Emling, H. 39, 40, 41, 42, 43, 44, 45, 46, 47, 105
Emmerling, M. 221, 222
Engelhardt, W. 101
Englert, G. 196
Eriksen, D. 35
Essel, H. 16, 17, 18, 180
Esterlund, R.A. 26
Euler, R. 135
Ewald, H. 176
Facius, R. 150
Faestermann, T. 43
Faß, R. 31, 51, 57, 64
Faust, W. 55, 56
v. Feilitzsch, F. 43

Feldmeier, H. 11, 78, 79
Ferber, H. 145
Ferguson, R.L. 63
Fiedler, G. 32
Finke, P. 226
Fischer, B.E. 155
Flaig, H.J. 167
Fleury, A. 120
Folger, H. 5, 39, 102, 121, 146, 161
Folkmann, F. 25, 48, 49, 50, 104, 114, 115
Fraenkel, Z. 24
Franczak, B. 215, 218, 219
Franzke, B. 215, 225, 226
Frauendorf, S. 68
Freiesleben, H. 2, 14, 15, 20, 25, 30, 166
Freyhardt, H.C. 143
Fricke, B. 135, 136
Friedrich, H. 75
Friedlander, G. 5
Frischkorn, H.J. 142
Fröbich, P. 21
Frodl, R. 119
Fuchs, P. 40, 42, 43, 45, 46, 47,
Gäggeler, H. 27, 28, 29, 60, 61, 62, 63, 154
Gäggeler-Koch, H. 27, 29
Gaiser, H. 202
Ganßauge, E. 190
Gasper, A. 222
Gardes, D. 120
Geaga, J.V. 38
Geißel, H. 120, 122, 123, 124
Gembalies, D. 60
Genz, H. 3, 11
v. Gerdtell, L. 117
Gerhard, A. 157
Georgiadis, A. 117
Ghiorso, A. 63
Glässel, P. 30, 178
Glas, D. 67
Gobbi, A. 9, 10, 13, 14, 24, 164, 166
Gönnenwein, F. 6
Gosset, J. 37
Gottschalk, P.A. 32, 33
Gowdy, G. M. 54, 57, 58
Grabez, B. 191
Gräf, H. 162
Graebner, G. 92, 93
Graeger, V. 143
Grasmück, B. 214
Grawert, G. 33
Greenberg, J.S. 102, 105, 161
Grein, H. 102, 161
Greiner, W. 69, 70, 82, 83, 84, 88, 89, 90, 91, 92, 93, 97, 98, 128, 129, 130, 131, 132, 133, 134, 137, 138
Greulich, N. 154
Groeneveld, K.O. 142
Groß, H. 196
Grosse, E. 9, 10, 39, 40, 41, 42, 43, 44, 45, 46, 47, 105
Grün, N. 127
Gruppe, A. 102, 161
Günther, C. 45
Güttner, F. 100, 103
Güttner, K. 55, 56, 177
Gutbrod, H.H. 36, 37, 163
Guirguis, J. 70
Györffy, T. 196
Haag, R. 32
Habs, D. 4, 162
Haefner, B. 5, 61
Hagebø, E. 35
Hagmann, S. 107
Hahn, J. 82, 83
Hahn, R.L. 63
Hahne, P. 196
Haldorsen, I. 35
Halperin, J. 65
Hamilton, H.J. 47
Hammal, H. 193
Hansen, O. 2, 25
Hansen, P. 140
Hardel, H. 193
v. Harrach, 30, 178
Harris, J. W. 38
Hass, M. 41
Hartel, K. 16, 17, 18, 19, 180
Hartmann, V. 21, 22, 23, 184
Heckwolf, H. 187, 188
Heinz, U. 98, 132
Heitmann, H. 140
Herr, W. 141, 144
Herrmann, G. 60, 63, 165
Herskind, B. 48, 49, 50
Hess, P.O. 69
Hessberger, F. 8, 55, 56, 59, 176
Hickmann, U. 154
Hildenbrand, K.D. 14, 164, 166
Himmele, G. 4
Hirdes, D. 31, 51, 64, 158
Hopf, H. 18, 19
Hofmann, S. 55, 56, 59, 80, 92, 176, 181
Huber, A. 196
Huber, G. 172
Hubert, F. 120
Hübel, H. 45

Hüller, W. 169, 170, 171
Hulet, E.K. 63
Hultzsch, H. 197
Idzko, J. 44, 45, 46
Illert, K. 202
Ito, S. 102, 161
Jaeschke, E. 162
Jokic, S. 34
Jüttner, F. 173
Jungclas, H. 31, 51, 64
Kaffrell, N. 39, 46
Kankeleit, E. 101, 168
Kaspar, K. 221, 222, 224
Kassen, F. 31, 51, 64
Kasten, H. 146
Keim, H.J. 165
Keller, J. 8
Keller, R. 212
Kester, P. 118
Ketelle, B.H. 65
Kiefer, J. 147, 148, 149
Kienle, P. 16, 17, 18, 19, 43, 100, 103, 180
Kiesewetter, H. 151, 202
King, Ch. 36, 37
King, G. 36, 37
Kirchner, R. 54, 57, 169, 170, 171
Kirsch, J. 131, 132
Kitahara, T. 55, 56, 120, 122, 123, 181
Klabunde, J. 210
Kleber, M. 126
Klein, G. 29
Klein, H. 119
Klein, N. 190
Kleinrahm, A. 45
Klempt, W. 173
Klepper, O. 54, 57, 169, 170, 171
Knitz, U. 165
Koenig, W. 100, 103
Könnecke, R. 70
Körner, H.J. 16, 17, 18, 19, 180
Kopf, U. 202
Kowalski, J. 52
Kozhuharov, C. 100, 103
Kraft, G. 147, 148
Kratz, J.V. 5, 7, 27, 28, 29, 60, 63, 121
Kraus, H. 202
Kreisler, P. 160
Kreyling, G. 24
Kritzer, A. 226
Kronast, W. 142
Kruse, H. 92
Kühl, T. 173
Külzer, H. 141
Kulessa, R. 39, 40, 41
Kumbartzki, G.J. 41
Laichter, Y. 122, 123, 124, 181
Lang, W. 8
Langenbeck, B. 215
Latz, R. 142
Lauterbach, C. 183
Lemmertz, P. 31, 51, 64
Liebold, H.P. 193
Lieder, R.M. 48, 50
Liesem, H. 148, 149
Liesen, D. 106, 107, 108, 109, 110, 112
Lindenzweig, W. 54
Lougheed, R.W. 63
Lucas, R. 7, 28, 29
Ludwig, M. 164
Lund, T. 35, 64, 65
Lustig, H.J. 83
Lynen, U. 9, 10, 13, 14, 24, 164
Männer, R. 30, 178
Maier, M.R. 163
Malwitz, E. 202
Mann, R. 111, 114, 115, 116
Mantri, A.N. 66
Margetan, F. 69
Maor, D. 106, 108, 110, 112
Marinow, A. 65, 166
Maruhn, J.A. 69, 70, 82, 83, 84, 88, 89, 90, 91, 92, 93
Maruhn-Rezwani, V. 127
Martin, B. 100, 103
Marx, D. 159, 172
Matsuki, S. 161
Mayer, W. 18, 19
Mazumdar, A.K. 174
Metag, V. 4, 101, 162
Meyer, W.G. 36, 37
Meyerhof, W.E. 104
Mietke, K. 118
Mömerzheim, K. 193
Mokler, P.H. 104, 106, 107, 108, 109, 110, 112, 113
Molzahn, D. 35, 64, 65
Morenzoni, E. 10, 104
Morovic, T. 135, 136
Morrison, I. 214
Mosel, U. 66, 67
Müller, A. 98, 118, 119
Müller, B. 92, 98, 129, 130, 131, 132, 133, 134, 138
Müller, K.H. 87
Müller, M. 210, 213
Müller, R.W. 227
Müller, W. 9, 10, 164

Müller, U. 132
Münzenberg, G. 8, 55, 56, 59, 176, 177, 181
Mussler, K. 151
Mutterer, M. 6, 11, 101, 186, 187, 188, 189
Nathan, O. 2, 25
Neugart, R. 173
Nguyen, V.S. 36, 37
Nickel, F. 159
Nitschke, J.M. 63
Nöhmeyer, F. 202
Nörenberg, W. 72, 73, 81
Noll, H. 21, 22, 23, 184
Nyman, G. 54
Olmi, A. 9, 10, 13, 14, 164, 179
Otten, E.W. 173
Ower, H. 44, 45, 46, 47
Pannicke, J. 186, 187, 189
Patzelt, P. 26
Patzner, W. 168
Pedersen, J. 48, 49, 50
Peitz, H. 131, 132
Pellas, P. 192
Pelte, D. 41, 162
Perelygin, U.P. 192
Perron, C. 192
Peter, J. 163
Peuser, P. 60, 165
Pfeffer, W. 20, 185
Pfeng, E. 111, 116
Piercey, R. 44, 47
Pinkston, W. T. 92
Piotrowski, A. 54
Plasil, F. 2
Plochocki, A. 54, 57
Poitou, J. 7, 28, 29
Pomorski, K. 71, 80
Poppensieker, K. 175, 193
Poskanzer, A.M. 36, 37, 163
Potzel, W. 103
Povh, B. 100, 103
Pühlhofer, F. 2, 3, 20, 25, 185
zu Putlitz, G. 52
Quade, U. 6
Quis, D. 193
Ramayya, A.V. 47
Rase, S. 149
Rehm, K.E. 16, 17, 18, 19, 180
Reichhardt, G. 142
Reinhardt, J. 128, 130, 132, 133, 134, 137
Reisdorf, W. 7, 8, 54, 55, 56, 57, 59, 71
Renfordt, P. 21, 22, 23, 24, 184
Repnow, R. 162
de Reus, T. 132
Reus, U. 26, 53
Richter, A. 3, 11
Richter, M. 193
Riedel, C. 27, 72, 73, 74, 81, 156
Riedel, M. 97
Riedinger, L.L. 58
Rinn, K. 118
Ritter, H.G. 163
Rochna, D. 214
Roeckl, E. 54, 57, 171
Rosen, A. 135, 136
Rosenberg, L.J. 38
Rosner, R. 110
Rudolf, G. 13
Rudolph, K. 6
Sandoval, A. 36, 37, 38
Dann, H. 9, 10, 13, 14, 24, 164 179, 182
Sahm, C.C. 8, 125
Salzborn, E. 118, 119
Sapotta, K. 21, 22, 23, 184
Santo, R. 164
Schader, J. 142
Schädel, M. 27, 28, 29, 60, 63
Schäfer, M. 150
Schäfer, W. 138
Schaffner, E. 214
Schandera, Ch. 183
Schardt, D. 54, 57
Scharmann, A. 167
Schartner, K.H. 167
Scheele, K. 186
Scheid, W. 127
Schemp, A. 157
Schimpf, E. 62
Schinzler, W. 173
Schmid-Schönbein, H. 151
Schmidt-Böcking, H. 106, 107, 108, 110
Schmidt, G. 98
Schmidt, H.G. 193
Schmidt, K.H. 8, 59, 125
Schmidt, R. 77
Schmitt, C. 8
Schneider, E. 147, 148, 149
Schneider, W. 162
Schneider, W. F. 166
Schönfeldt, W.A. 109, 112
Schöpfer, F. 147
Schött, H.J. 55, 56, 59, 175
Schorstein, W. 60
Schrader, H. 6
Schrewe, U. J. 57
Schrieder, G. 3, 11

Schroeder, L.S. 38
Schuch, R. 106, 107, 108, 109, 110
Schüll, D. 2, 3, 20, 185
Schule, R. 102, 161
Schulte, H. 8, 125, 211
Schultz, R. 161
Schulze, R. 193
Schumann, S. 142
Schwalm, D. 9, 10, 39, 40, 41, 42, 43, 44, 45, 46, 47, 102, 105, 161, 162
Schweppe, J. 102, 161
Seiler-Clark, G. 41
Seim, W. 118
Seiwert, M. 69
Senger, P. 101, 168
Sepp, W.D. 135, 136
Serre, C. 35
Sharfir, N.H. 123
Shen, W.C. 2, 3, 20
Shergin, A.P. 111
Simon, R.S. 40, 48, 49, 50, 68, 162
Sletten, G. 48, 49, 50
Soff, G. 128, 129, 130, 132, 133, 134, 137
Soffel, M. 98
Sørensen, S.P. 2
Spath, K. 173
Specht, H.J. 4, 30, 162, 178
Speidel, K.H. 41
Sperr, P. 16, 17, 18, 19, 180
Spieler, H. 193
Spitz, W. 167
Spohr, R. 140, 151, 155, 156, 158
Spreng, W. 187, 188, 189
Stachel, J. 39
van Staden, J.C. 188
Stelte, N. 94, 95, 96
Stelzer, H.E. 38, 163, 183
Stelzer, K. 24, 44, 46
Steiner, R. 161, 218, 219
Stetsenko, S.G. 192
Stock, R. 36, 37, 38, 163
Stöcker, H. 83, 84, 88, 89, 90, 91, 92, 93, 138
Stokstad, R.G. 7
Stoller, Ch. 104
Stoughton, R.W. 65
Sträter, H.D. 117
Strehl, P. 210
Stubenrauch, G. 224
Sümmerer, K. 29, 60, 61
Subramanian, P.R. 92
Terlecki, G. 127
Tharun, U. 165
Theis, J. 92, 132
Theobald, J.P. 6, 11, 186, 187, 188, 189
Thiel, K. 141, 144
Thuma, B. 55, 56, 59, 176
Tidemand-Peterson, P. 54, 57
Tietsch, W. 160
Tittel, G. 60, 63
Trautmann, N. 46, 47, 60, 63, 102, 154, 165, 174
Trautner, N. 25
Träger, F. 52
Tress, G. 65, 158
Tripier, J. 34
Tserruya, I. 24
Tsertos, H. 100, 103
Uhlig, M. 82
Ulbrich, R. 32
Ulm, G. 172
Unterseer, K. 126
Varga, P. 119
Vasak, D. 92
Vater, P. 33, 65, 158, 190, 191
Vermeulen, D. 8, 59, 125
Viang, C.L. 2
Videbaek, F. 2, 25
Viehböck, F.P. 119
Vincent, P. 102, 104, 105, 161
Wätzig, W. 26
Wagner, H. 174
Wagner, W. 16, 17, 18, 19, 103, 180
Wahl, H. 193
Walcher, Th. 100, 103
Walcher, W. 174
Wald, S. 24
Waldschmidt, M. 102, 161
Warczak, A. 113
Warnecke, I. 53
Warwick, A.I. 163
Wastyn, P. 3, 11, 189
Weber, J. 6
Weber, K.J. 148
Weber, W. 62
Weik, F. 4, 101, 163, 168
Weiner, R. 94, 95
Weis, M. 27, 29
Weiter, M. 162
Welzel, W. 196
Wendt, K. 173
van der Werf, S. Y. 25
Westfall, G.D. 37
Westmeier, W. 26, 53
Weström, M. 95

Wiemann, H.	163
Wiemers, M.	196, 214
Wietscherke, K.H.	128, 129, 132
Wilhelm, K.	202
Wilhelmy, J.B.	4, 30, 101, 107, 178
Willwater, R.	101
Winter, H.	119
Wirkner-Bott, I.	118
Wirth, G.	7, 27, 28, 29, 60, 62, 63, 165
Wißmann, W.	193
Wölfli, W.	10, 104
Wolf, B.H.	213
Wolf, G.K.	145, 146
Wolf, K.L.	36, 37, 38
Wollersheim, H.J.	40, 41, 42, 43, 44, 45, 46, 47, 107
Wollnik, H.	31, 51, 64
Wolschin, G.	72, 74, 76, 77
Wood, J.S.	57, 58
Wu, E.C.	14
Zelba, V.	196
Zganjar, E.F.	58
Ziegenhain, K.H.	82
Ziemert, J.	177
Zöller, P.	186, 188
Zylicz, J.	54, 57

FRONTCOVER

Doppler-corrected γ-spectrum resulting from Coulombexcitation of ^{248}Cm with 5.3 MeV/u ^{208}Pb-ions. The ground state band of ^{248}Cm was populated up to spin 28^+ (tentativeley 30^+). The de-excitation γ-rays from the I → I-2 decays are labelled by the spin I of the initial state and the deduced transition energies are quoted in keV with the error of the least significant digit given in parenthesis (see report on page 47).